Title
Hyper-fidelity depletion in pebble bed reactors

Author
Robert, Yves Eric Maxime

Publication Date
2023

Peer reviewed|Thesis/dissertation

Hyper-Fidelity Depletion in Pebble Bed Reactors

By

Yves Eric Maxime Robert

A dissertation submitted in partial satisfaction of the

requirements for the degree of

Doctor of Philosophy

in

Engineering – Nuclear Engineering

in the

Graduate Division

of the

University of California, Berkeley

Committee in charge:

Professor Massimiliano Fratoni, Chair
Professor Per Peterson
Associate Professor Zeyu Zheng

Summer 2023

Hyper-Fidelity Depletion in Pebble Bed Reactors

Abstract

Hyper-Fidelity Depletion in Pebble Bed Reactors

By

Yves Eric Maxime Robert

Doctor of Philosophy in Engineering – Nuclear Engineering

University of California, Berkeley

Professor Massimiliano Fratoni, Chair

Interest in pebble bed reactors (PBRs) has surged in the past decade, given distinct unique designs and potential for inherently safe operation. Nevertheless, accurately modeling and simulating the behavior of PBRs, especially determining the flux spectrum distribution and pebble trajectories, remains an intricate task due to methodological challenges and extensive computational demands. In contrast with methods using spectral zones that aggregate pebbles over large core regions, this research proposes a novel approach called hyper-fidelity depletion (HxF), in which each pebble's history is individually tracked.

The dedicated HxF tool, a Python-based wrapper code, follows this approach. It uses the Cerberus/Serpent 2 interface at its core, which allows to finely control the simulation of a PBR operation in a time-dependent iterative manner. Running the HxF tool for an extended period, the equilibrium state of a core can be determined. Serpent 2 embeds numerous features that make the geometry modeling simple and the neutron transport processes accurate and efficient. In addition, the integration of domain decomposition ensures the feasibility of individual pebble depletion without prohibitive memory requirements. The time for obtaining a full-scale equilibrium core from scratch is on the order of magnitude of days on an average cluster, which, while not considered fast for design exploration or optimization, makes it acceptably short.

The motion and fuel handling components are synchronized with depletion within the HxF tool. Successive positions are determined either through a streamlined discrete motion sequence or by integrating granular data from a discrete element method (DEM) simulation. DEM uses a spring-dashpot model to represent mechanical interactions between pebbles and is coupled to an innovative looping method, drastically saving computational time. These positions are then communicated to Serpent 2. Pebbles undergo discharge, discard, re-insertion, and fresh fuel introduction throughout depletion. Comprehensive pebble-wise data such as position, nuclide concentrations, detector (power, flux), burnup, decay heat, activity, or passes can be tracked and saved. The discrete motion approach offers efficiency in the simulation process and faster computation times. Though effective, it has limitations in addressing complex geometries and

varying pebble velocities. The DEM instead provides more precise pebble trajectories, which is especially important for more geometries with fueling and defueling chutes with the price of increased computational demand.

A preliminary exploration of the thermal-hydraulics is also provided by incorporating thermal-hydraulics coupling into HxF using the GeN-Foam solver through the Serpent 2/OpenFOAM multiphysics interface. A porous media solver and a pioneering double-heterogeneous power model enabled a better understanding of the interplay between temperature, density distributions, and neutronics within the PBR core. In particular, accounting for thermal distributions in determining accurate core behavior is essential. As temperature varies, so does the core reactivity, thus emphasizing the need for this coupling in the HxF tool.

These capabilities were applied to the generic FHR (gFHR), a benchmark model made by Kairos Power. First, a comparison is performed between the equilibrium state obtained with HxF using discrete motion and the one with the company's house code KPACS. While both tools presented satisfactory results for the equilibrium core, HxF provided a more acute understanding of parameter distributions within the core and their temporal variations. Then, using a DEM with the gFHR and a more realistic geometry, HxF displayed enhanced accuracy in depicting pebble trajectories and velocity profiles, especially when confronted with complex geometries like fueling and defueling chutes.

The HxF method's adaptable design showcases remarkable versatility, making it suitable for various applications. It can explore slow transients, diverse fueling strategies, waste management insights, fuel performance analyses, and non-proliferation evaluations. Furthermore, the rich data generated by HxF is a valuable resource for training machine learning algorithms, enabling accurate predictions and operational assessments.

Critical areas for future development include adjusting the carbon-to-heavy metal (C/HM) ratio, enhancing the discard threshold, and improving depletion through dedicated, dynamic predictor/corrector methods. Additionally, enhancements in thermal-hydraulics modeling and addressing compatibility issues with Serpent 2 and Cerberus are essential to unlock HxF's full potential.

By better simulating PBRs operations, the community can better understand their behavior, optimize their design, explore new possibilities and ideas, and predict future operation conditions.

To my parents

Contents

Table of Figures

Table of Tables

Acknowledgments

I wish to express my gratitude to all the institutions that have nurtured my education and experience, especially the University of California, Berkeley nuclear engineering department. I reserve particular thanks to the mentors in France, Switzerland, Finland, and the United States who have generously shared their knowledge, shaping me both as a researcher and a person.

Special acknowledgment is due to Dr. Emmanuel Léger, whose guidance during my internship at LBNL ignited my passion for research and without whom I would probably not have had my chance in the United States. I am indebted to Professor Haruko Murakami Wainwright for her support during my internship application process. My profound appreciation and admiration extend to Professor Massimiliano Fratoni, who selected me for a fascinating project and whose exceptional mentorship, teaching, and human qualities have been a guiding light throughout my Ph.D. journey. It has been a privilege to learn and grow under his supervision.

I am immensely grateful for the great friendships forged along this path. A distinctive thanks to Clara, Jaewon, Lorenzo, Matthew, and Tatiana; their emotional support, shared laughter, talent, and human values have been a continuous source of inspiration to me. Thanks also to my housemates, cohort, and research group members, such as Faisal, Inhyung, Kenji, and Ludovic, for the stimulating discussions and shared joy. From my home country, I offer heartfelt thanks to my friends Raphael and Alexandre from INSA Lyon, who have been great companions, and to Nicolas and Alexandre, who have unwaveringly supported me along the way.

Above all, my deepest gratitude is reserved for my family: my brothers and sisters, Aurélie, Francis, Sylvain, Marie-Aude, and their significant others, as well as my nieces and nephew, Clara, Alyzée, and Clément. They form the core of who I am today, and I am filled with endless love for them. Lastly, my enduring thanks and dedication go to my parents, whose unimaginable support since birth has been my foundation. This thesis is for them, for all they deserve, and more. Their pride fuels my determination, and I strive every day to honor them.

Chapter 1
Introduction

1.1 PBRs features and operation

Pebble bed reactors (PBRs) and their unique attributes have recently drawn attention from the nuclear community. Introduced in the mid-20th century, PBRs were pursued in South Africa and the United States, and some demonstration plants have been operating in Germany and China. The United States is today seeing renewed interest in modular PBRs design, with private companies leading the development of future demonstration plants.

PBRs are a high-temperature thermal reactor design, either cooled with gas or molten salt. They employ TRISO (for TRIstructural-ISOtropic) particles, which are micro-sized structures renowned for their resilience under high irradiation, mechanical stress, and temperatures, thanks to the multiple layers in which the fuel is enclosed. PBRs use graphite pebbles to encase these particles, providing additional containment, neutron moderation, and excellent thermal properties. Each coolant type offers a set of operational characteristics, thermal efficiency, and safety features, which influence the design of the reactors.

PBRs operate using continuous refueling, where fuel pebbles traverse the core over time, consuming fuel and getting removed for inspection once reaching the end of the core. A multipass operation is often adopted to maximize fuel utilization, enhance safety, and simplify operation.

Development

The development of PBRs was first conceptualized during the mid-20th century at Oak Ridge National Laboratory (ORNL) [1]. The PBR design uses inherent safety features and has the ability to operate at higher temperatures than typical reactors, aiming to create a safer and more efficient nuclear reactor.

Germany pioneered PBR technology by developing the Arbeitsgemeinschaft Versuchsreaktor (AVR), a small 46 MW_{th} experimental reactor operational from 1967 to 1988. Throughout its two decades of operation, the AVR demonstrated the potential and viability of the pebble bed principle, providing valuable lessons for future projects [2, 3]. The subsequent Thorium High-Temperature Reactor (THTR-300), also in Germany, faced various operational and technical challenges. These included mechanical issues, higher-than-expected fuel failure rates, and escalating costs. Despite its innovative design and goal to use thorium fuel, the THTR-300 was closed prematurely in 1989 after just a few years of operation [4]. In South Africa, an ambitious program was launched in the late 1990s by Eskom, the national electricity provider, to develop a commercially viable PBR. The Pebble Bed Modular Reactor (PBMR) project was envisioned as a scalable and exportable solution for electricity generation. However, despite significant advancements and publications regarding its design [5, 6], the project was defunded in 2010 [7].

Meanwhile, China has emerged as a global leader in PBR development, building on the lessons from German and South African experiences. The HTR-10, a 10 MW_{th} experimental reactor, has been operating successfully since 2003, allowing Chinese engineers to gather invaluable operational data and lessons to improve their design [8]. More recently, in 2022, China achieved a significant milestone by commissioning the HTR-PM with a dual-module high-temperature gas-cooled reactor, with each module driving a steam turbine to generate a combined output of 210 MW_e [9, 10]. These developments in China represent steps toward the global commercial application of PBR technology.

In the United States, interest in modular PBRs has resent in the past few years [11]. Several private companies, supported by investors and the US Department of Energy (DOE), are designing and constructing demonstration plants in the next decade. X-energy, founded in 2009, is developing an 80 MW_e helium-cooled PBR design called Xe-100 [12] expected to be deployed by 2030. Another key company is Kairos Power, which aims to build the first Fluoride-salt-cooled High-temperature Reactor (FHR). Using molten salts as a coolant and fuel in a nuclear reactor was first proposed and tested in the 1960s with the Molten Salt Reactor Experiment (MSRE) at ORNL [13]. The FHR design was later proposed, combining PBRs with a liquid fluoride salt coolant. Early work was mainly done by ORNL and the University of California, Berkeley [14, 15, 16, 17, 18]. However, other national laboratories and universities joined the global effort. Kairos Power builds on these recent developments to build its KP-FHR design. Their first iteration, the Hermes small-scale reactor of 35 MW_{th}, is planned to end construction by 2026 in Oak Ridge before larger power subsequent iterations.

TRISO particles

TRISO particles are multi-layered spherical particles specially designed to withstand extensive amounts of irradiation while effectively containing fission products, even under high temperatures and mechanical stress [19, 20]. The safety attributes of the TRISO fuel particles are remarkable. TRISO fuel particles typically measure around a millimeter in diameter. They contain a fuel kernel at their core, as described in Figure 1-1, encased within a succession of three types of layers, each having a distinct role.

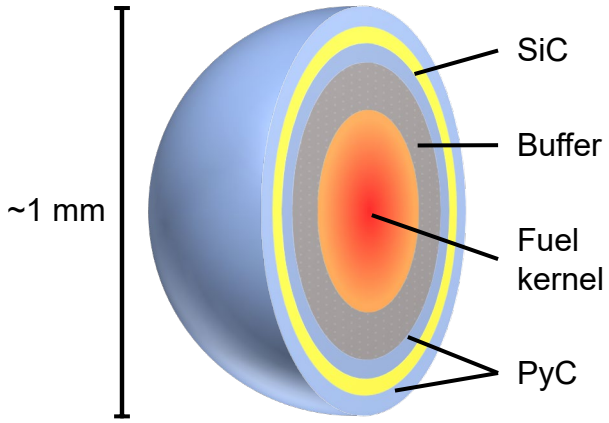

Figure 1-1: TRISO particle layers representation.

The first one, directly encompassing the fuel kernel, is a porous carbon buffer layer. This layer acts as a shock absorber, accommodating the fuel kernel's expansion as it heats up during operation. It also serves as an initial barrier to releasing fission gases, capturing and retaining fission products from the fuel kernel. Next, a dense pyrolytic carbon (IPyC) layer consisting of a compact, isotropic carbon layer holds a structural role. It also serves as a containment barrier for fission products, preventing their outward migration. The outermost layer comprises silicon carbide (SiC), a ceramic material known for its excellent heat resistance and mechanical strength. It plays a role in maintaining the integrity of the fuel particle under irradiation and high temperatures beyond 1,600°C [21]. It also serves as an additional barrier to radiation and the release of fission products and protects the layers from corrosion. Finally, the TRISO particle is covered by an outer pyrolytic carbon (OPyC) layer. This layer offers additional structural support to the SiC layer and is the last line of defense of the structure. It also provides additional protection to the particle against mechanical and chemical damage.

Fuel is typically enriched with between 9% to 20% in ^{235}U and mainly comes into two forms: UO_2 and UCO. While UO_2 is more traditionally used, understood, and less complex, UCO provides better fission product retention due to the high solubility of certain metallic fission products and thermal conductivity. The amoeba effect is also mitigated by the presence of carbon atoms, reducing the risk of CO buildup from excess oxygen atoms of the UO_2, which is the cause of high pressures within the TRISO and, ultimately, higher failure rates [22].

Graphite pebbles

PBRs utilize a distinctive fuel design, shown in Figure 1-2, where TRISO fuel particles are enclosed within 3-6 cm-diameter graphite pebbles. These spherical fuel pebbles comprise two to three distinct zones: the outer shell, the TRISO-bearing matrix, and in the case of FHRs, a graphite core.

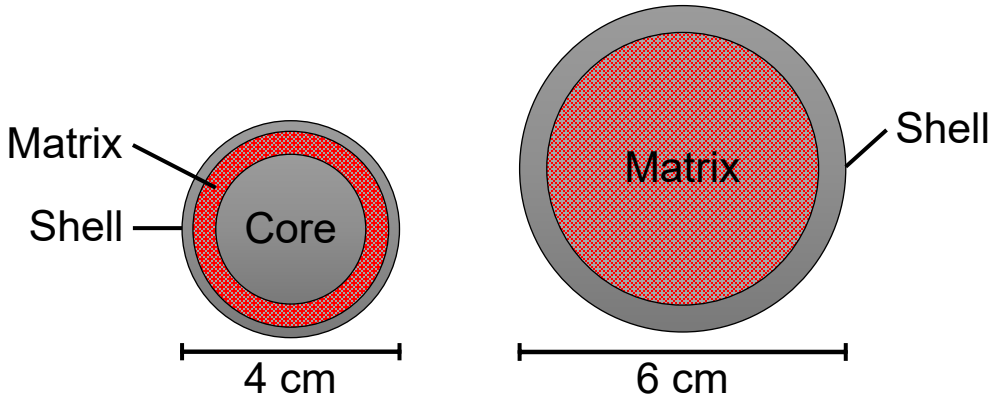

Figure 1-2: Typical FHR (left) and HTGR (right) pebbles.

The outer shell of the pebble, which is made of pure nuclear graphite, functions as a barrier, providing additional containment for fission products. This shell does not contain TRISO particles and is engineered to achieve this protective role and maintain the pebble's structural integrity. The

key region of the pebble, known as the matrix zone, contains thousands of TRISO particles dispersed throughout its volume. In FHRs, the graphite pebbles contain a third zone in the form of a pure low-density graphite core. This core is free of TRISO particles and is present to ensure the buoyancy of pebbles within the molten salt coolant.

The graphite in these pebbles serves dual functions. On the one hand, it moderates the neutrons generated by fission reactions, making the neutron spectrum thermal and ensuring efficient fuel consumption. On the other hand, graphite's high thermal conductivity allows distributing of heat uniformly, mitigating the risk of localized temperature peaks that could lead to fuel damage while providing significant heat capacity.

Pebbles offer significant inherent safety features. In an accident scenario, their excellent thermal properties help prevent an excessive rise in core temperature, and the generated decay heat can be effectively dissipated, even without active cooling. Powers and temperatures typically decrease thanks to negative reactivity feedback, mitigating the risk of core meltdown accidents [23]. Moreover, the pebble design represents another barrier, in addition to TRISO layers, to releasing fission products. Even under severe accident conditions, the structural integrity of the graphite matrix and the pebble's spherical shape further mitigate the risk of fission product release. In addition, pebbles can contain multiple compositions (uranium/thorium, burnable poisons, pure graphite), allowing for flexibility of use and possibly fuel breeding [24].

Coolant

PBRs are typically cooled with either helium in the case of High-Temperature Gas-cooled Reactors (HTGRs) or a molten salt such as FLiBe in Fluoride-cooled High-temperature Reactors (FHRs). These coolants shape the operational characteristics, thermal efficiency, safety features, and potential applications of the reactors. Each one provides advantages and challenges that influence the reactor's design and performance.

In HTGRs, helium is an inert noble gas, not impacted by radiation, transparent to neutrons, and carries excellent thermal properties for a gas. Nevertheless, operating pressures for helium in HTGRs typically range between 70-100 bar to increase its cooling efficiency and reduce the size of these reactors. Still, the size of these reactors is large, and the power density is small, typically less than 10 W/cm^3. That low density, associated with the significant pressure, directly impacts the reactor's footprint and construction costs. The primary circuit in HTGRs can reach temperatures as high as 950°C, permitting efficient conversion to electricity through steam and gas thermodynamic cycles and enabling high-temperature industrial processes, such as hydrogen production and cogeneration [25]. The fuel often reaches temperatures around 1200°C due to helium's relatively low cooling efficiency. Finally, helium's inert nature prevents it from causing corrosion to reactor components, and its transparency to neutrons ensures excellent neutron economy.

On the other hand, FLiBe is used in FHRs. FLiBe is a fluoride molten salt of the form 2LiF-BeF_2 that operates at near-atmospheric pressures thanks to its high boiling point of 1,430°C and low freezing point of 459°C. Therefore, FHRs operate between 600°C and 700°C. FLiBe's low operating pressure decreases the construction cost and mechanical stress on the reactor vessel and

associated systems. This factor, coupled with its high boiling point that greatly exceeds operational temperatures, provides a large safety margin to prevent coolant from boiling even under abnormal conditions.

Moreover, FLiBe's thermal capacity and good heat transfer properties are excellent, leading to fuel temperatures between 850-950°C during normal operation. FLiBe's ability to absorb and disperse heat and its capability for dissolving fission products minimizes the risk of radioactive release. In addition, thanks to these thermal properties, smaller pebbles with more surface area per unit volume can be used, which increases the overall power density while ensuring relative thermal homogeneity in the fuel. However, handling and managing FLiBe is more complex and challenging due to its corrosive nature and highly toxic beryllium content. In addition, FLiBe has a non-negligible absorption cross section and adds, to some extent, moderation to the reactor, which impacts the neutronics compared to helium.

Operation

In contrast with most reactors' traditional batch fueling mode of operation with static fuel elements, PBRs use continuous refueling, as represented in Figure 1-3.

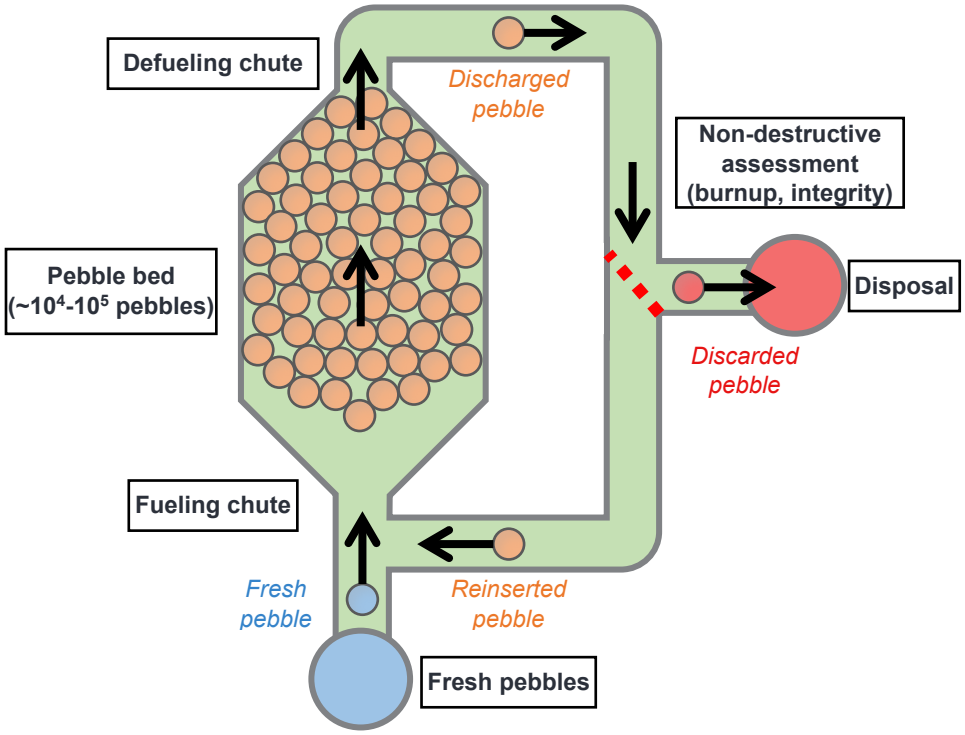

Figure 1-3: Schematic view of MEDUL PBR operation (FHR case).

PBRs are characterized by a core filled with 10^4-10^5 fuel pebbles arranged in a packed bed. These pebbles are gradually inserted from one end of the reactor core and slowly evolve, driven by the coolant and either gravity (in HTGRs) or buoyancy (FHRs). Pebbles slowly traverse the core a few centimeters daily, experiencing a neutron flux and consuming their fuel. Once a pebble

reaches the bottom of the core, it is discharged and inspected using non-destructive assessment techniques after a cooling period of a few days. These include gamma spectroscopy, which allows the detection of gamma-emitting fission products such as ^{137}Cs to estimate burnup [26], or visual inspection to check for potential surface defects. This inspection ensures that only pebbles in proper mechanical condition and with sufficient remaining uranium content are returned to the core for another pass. Pebbles that can sustain another pass are reinserted, and others are discarded. PBRs nowadays typically use a multi-pass operation (MEDUL, "mehfachdurchlauf" in German), where pebbles circulate through the core multiple times before disposal, as opposed to the Once through Then Out (OTTO) scheme. This MEDUL operation offers high fuel utilization, a key advantage of PBRs, but requires a more sophisticated fuel handling system. By continuously introducing fresh fuel pebbles while removing burned ones, PBRs can stay critical and operate with minimal excess reactivity, simplifying operations and enhancing safety. The continuous refueling approach also eliminates the need for shutdowns to refuel, which is typical in conventional nuclear reactors, thereby increasing the reactor's availability and capacity factor. MEDUL operation leads to diverse burnup levels dispersed within the pebble bed.

After a start-up and run-in phase, pebbles continue circulating, fuel is consumed, fresh pebbles are inserted, used ones are discarded under constant operational conditions, and the pebble bed gradually evolves to an equilibrium state. The global core parameters achieve this quasi-steady state operation.

Modular designs can be applied to PBRs, turning them into Small Modular Reactors (SMRs). This approach capitalizes on the cost efficiency of mass production, thereby reducing the associated investment risks. [27, 28].

1.2 Simulation And Modeling of PBR Operations and Depletion

Identified challenges

As described in the previous subsection, PBRs are characterized by unique structural and operational features. These features create substantial challenges for accurate simulation and modeling:

1. Non-self-determined neutron spectrum and pebble mixing: In PBRs, the neutron spectrum in each fuel pebble is not self-determined but depends on many neighboring pebbles over large distances, each containing considerably different fuel compositions. This phenomenon is due to the relatively small size of fuel elements in relation to the long diffusion length of neutrons in graphite. In other words, neutrons born in one pebble are likely to be absorbed in another pebble, with possibly different composition. Moreover, the continuous refueling and recirculation of pebbles lead to the random mixing of pebbles at different burnup levels, inducing significant fuel composition differences between adjacent pebbles. This influence between the pebbles over large distances with possibly different burnups makes it challenging to accurately calculate the neutron cross sections within an

individual pebble, as it requires knowledge of the fuel composition distribution throughout the pebble bed. Therefore, an infinitely reflected single pebble cannot accurately represent the behavior of the core.

2. Fuel elements double-heterogeneity and structure: Having TRISO particles within pebbles makes the "double-heterogeneous" nature of the fuel elements. In particular, strong spatial self-shielding occurs at the fuel kernel level, which needs to be accounted for correctly. Conventional deterministic methods, typically optimized for homogenized or single heterogeneous models, face considerable challenges when dealing with this complex fuel structure and typically use correction factors to account for it.
3. Pebble motion: Each pebble follows a unique set of trajectories within the core and experiences different neutron spectra with time. In addition, the pebble bed packing has slight variations with time, even at equilibrium. Therefore, accurate motion modeling is needed for neutronics to be informed with positions.
4. Fuel handling: Accurately accounting for the reinsertion of pebbles, discarding spent pebbles, and introducing fresh fuel pebbles is critical. It also involves tracking the number of passes and manipulating the data between depletion steps, adding further complexity to the problem. In addition, the presence of moderator pebbles must be possible. Indeed, inserting pebbles fully containing graphite controls the carbon-to-heavy metal ratio. It leads to the simultaneous simulation of at least two types of pebbles and possible changes in the number of moderator pebbles to adjust the moderation in the core.
5. Thermal behavior and reactivity feedback: Like the burnup, the power production of individual pebbles differs significantly, depending on their content and reactivity. Associated with the coolant temperature gradient between the inlet and outlet, it leads to significant differences in pebble materials temperatures within the core and complex spatial temperature profiles. This thermal behavior, a byproduct of each pebble's neutronic characteristics and resulting fission power level, reciprocally influences the neutronics through reactivity feedback, mainly due to significant differences in fuel temperatures between fuel pebbles with higher reactivity versus lower reactivity. Accurately simulating the core's complete thermal-hydraulic behavior and fuel temperature distribution is crucial for predicting the equilibrium state, operational margins, and fuel performance.
6. Substantial computational resource requirements: The unique history, trajectory, and evolution of a large number of pebbles necessitate complex and large-scale multi-physics simulations. Consequently, simple iterative processes are inadequate, and motion, depletion, and thermal-hydraulic calculations can become computationally intensive.
7. Lack of experimental validation: Experimental validation data for PBR simulations is scarce, making it difficult to verify and validate the models used in simulations. Even if such data were available, PBRs essentially function as "black boxes," and the amount of in-core data that can be measured (and therefore quantities that can be verified) is limited.
8.

Traditional approaches

The typical approach to address the depletion challenge for long-term operation in PBRs is using spectral zones or macrozones. Such a method divides a PBR core into large zones (multiple pebble diameters wide) and assumes that the fuel composition, thus the neutron spectrum, in these macrozones is uniform. This assumption is supported by the non-self-determined nature of the neutron spectrum within a pebble. Therefore, starting from an initial guess composition for each zone, cross sections are generated, and depletion is performed based on possible tracks pebbles follow through the different spectral zones. The data, contingent on the location, is then used to deplete the fuel and update the composition in each spectral zone within an iterative process until a stable equilibrium state is achieved.

The macrozones technique was initially applied in VSOP [29] in 1980 as part of the German HTR program. VSOP is a time-dependent tool in which few-group cross-sections are determined within each macrozone based on the current time step compositions, and motion is replicated with the transfer of fuel compositions between zones at each time step, with the capability of simulating out-of-equilibrium conditions. Later, other codes used the same method to simulate PBRs operation or to find equilibrium. While other codes such as ZIRKUS [30] and PANGU [31] used the same time-dependent approach while improving the cross sections determination process, BATAN-MPASS [32] and PEBBED [33, 34] were developed to be dedicated to the search for equilibrium through iterative processes. All codes relied on deterministic tools to calculate the flux distribution within the core and have the added capability of being coupled with thermal hydraulics.

In recent times, however, the spectral zones method has been re-explored, substituting the deterministic solver with a Monte Carlo transport code. In 2008, Fratoni coupled the stochastic transport code MCNP [35] with the depletion code ORIGEN2 [36] to carry out coarse mesh burnup calculations in the design of PB-AHTR, an early pebble-bed FHR design [37, 38]. An iterative search was developed to determine the equilibrium composition for multiple pass operations using the macrozones approach. Cisneros expanded on this concept in 2013, integrating the multiple burnup states method [39]. The idea of macrozones is still leveraged, but rather than adopting a uniform composition within the zone, it utilizes a mix of pebbles with different compositions grouped based on the burnup level.

Recent advancements saw Kairos Power publish equilibrium concentrations for their generic FHR design (gFHR) in 2021, using their in-house code KPACS [40]. Similarly to VSOP, KPACS is a time-dependent tool that employs the macrozones method, but it resolves transport and depletion with the Monte Carlo code Serpent 2 rather than a deterministic approach.

Other methods chose to reduce the core's geometry to a simplified representation while retaining the double-heterogeneity of the fuel pebbles. Unit cell approaches represent the core as one or multiple pebble compositions, infinitely reflected. On the other hand, ORNL proposed to use a slice approach in which a two-dimensional core slice (including the reflector) zoned in rings is used with TRITON, coupled with a tri-dimensional SCALE transport calculation with zone-averaged compositions, until convergence [41].

Most of these methods are generally considered reliable while being computationally efficient. However, they do have certain limitations. Foremost, they primarily target the equilibrium core composition and have limited capacity to model transition phases, such as the transition from initial critical loading to equilibrium. Additionally, as mentioned before, their true accuracy cannot be validated due to the lack of available experimental data. Their data represents an average behavior, often missing details about distributions and outliers, such as pebbles with burnup far beyond the set nominal limit.

1.3 Hyper-fidelity depletion

With the new interest in developing PBRs comes a need for a better understanding of their operations, more accurate and detailed distributions in the core, and a way to increase confidence in the previously mentioned methods. In addition, as more detailed simulations will be needed in the future, flexibility in implementing the tools is critical.

In parallel, the computing landscape has changed significantly in the last decade. Computing resources are more easily accessible, with more efficient processors and memory commonly available in universities, laboratories, and companies. In addition, parallel computing, in which multiple processors (CPU) and multiple computers (nodes) work together to solve the same problem, has drastically increased, and codes are designed to ensure their compatibility and efficiency. In particular, in neutronics, each neutron history can be assumed independent from other simulated neutrons, making the parallelization of Monte Carlo parallel codes simple and efficient. That explains why they gained interest in large-scale depletion calculations, such as MCNP, OpenMC [42], Serpent 2 [43], Griffin [44], and KENO-VI [45]. Specifically, these codes improve efficiency and add features that facilitate modeling PBRs.

In that context, it is possible to push the boundaries of simulation by proposing a higher resolution, named hyper-fidelity depletion (HxF). This technique transcends the concept of spectral macrozones and, instead, tracks every single pebble in full-scale explicit geometry simulations individually in position, composition, and temperature while minimizing the assumptions made during simulations and keeping calculations within acceptable resources. HxF requires neutronics fine-resolution calculations for determining power distribution and effective cross-sections, thermal-hydraulic simulations for establishing temperature distribution, and dynamic modeling for reconstructing pebble motion. In order to achieve that goal, transport must model the core, pebbles, and TRISO particles explicitly, and each pebble must contain a unique fuel composition that evolves independently from the others. Temperature distributions within the core must be modeled, given the power distribution obtained during transport calculations. Between time steps, pebbles must move based on simplified or more detailed motion models. Finally, the insertion of fresh fuel, discarding of used fuel, and pebbles recirculation has to be accounted for. To that end, a Python-based tool (referred to as “HxF”) is developed based on the communication between the Cerberus interface library and Serpent 2, a discrete element method (DEM), and a porous media solver. It provides a highly accurate, time-dependent, flexible framework to run heavy full-scale depletion calculations on commonly available computing

resources in reasonable amounts of time. Eventually, HxF will be able to be used for key PBR core design functions such as finding equilibrium and fine-tuning the adequate fuel-to-moderator ratio and discard threshold.

This thesis describes the work done to develop the HxF approach and tool, its implementation, the tools used, and the numerous possibilities it opens through multiple applications. First, Chapter 2 provides an overview of the framework and describes the tools used in the HxF. Chapter 3 focuses on the individual depletion of pebbles and the choice of Serpent 2 for that task, including a performance study and applications to a static PBR model. Chapter 5 describes the work performed to integrate the thermal aspects into the simulation, and Chapter 6 wraps the depletion, motion, and thermal components with an application to the generic FHR (gFHR) model. Finally, although this thesis primarily focuses on searching for an equilibrium core, Chapter 7 provides an overview of the applications made possible by using HxF.

Chapter 2

HxF tool components

The simulation of PBRs poses numerous challenges due to their uniquely dynamic nature and the complexity of their fuel elements and their operation. PBRs consist of spherical graphite fuel elements, known as pebbles containing micro-sized TRISO fuel-coated particles. These pebbles are cooled by helium in HTGRs or molten salt in FHRs. Pebbles are continuously discharged from the core, assessed for their condition, and either reinserted for another pass or discarded. Additionally, fresh fuel pebbles are inserted to maintain criticality. This continuous online refueling and MEDUL operation offer advantages such as improved fuel burnup, low excess reactivity, and increased plant availability.

However, accurate modeling of PBRs is challenging due to factors like the number of pebbles ($\sim 10^5$-10^6), the double heterogeneity of the fuel, and the non-self-determined flux spectra resulting from graphite moderation associated with the small size of fuel elements (3-6 cm-diameter). The multi-pass nature of PBR cores introduces further complexities. Pebbles with diverse compositions and burnup values can be located adjacent, and complex pebble inventory handling needs to be accounted for.

Existing simulation tools often rely on simplified geometries or make assumptions about pebble zoning, which limits their flexibility, accuracy, and applicability. In contrast, the HxF approach takes advantage of recent advancements in tools and computing capabilities to accurately track the history of every pebble individually, avoiding common assumptions. The HxF approach incorporates the discrete element method (DEM) for realistic pebble motion, Monte Carlo neutron transport for precise power distribution and burnup calculations, and a thermal-hydraulic model to determine temperature distribution. By leveraging these techniques, HxF can be used for benchmarking, identifying outlier pebbles accurately, and providing high-fidelity input data for models such as fuel performance, waste management, and source term analysis.

This Chapter summarizes the Python-based dedicated HxF code [46], which aims to integrate the Monte Carlo code Serpent 2.2.0 [43], DEM-obtained pebbles positions evolution, and temperature calculations through a porous media solver. The HxF tool relies on the Cerberus Python library [47], which is part of the Kraken reactor analysis framework, and facilitates the communication of critical information with Serpent.

2.1 Overview of tools used

Neutronics

For neutron transport and burnup calculations, the latest version of HxF relies on a modified version of the Monte Carlo code Serpent 2 (version 2.0) selected for a range of features that

facilitate modeling and simulations of PBRs [48]. It uses delta-tracking, handles explicit stochastic geometry for pebbles and TRISO particles, uses a cartesian search mesh to speed up the transport calculation, tallies pebble-wise reactions with an irregular lattice detector, performs parallel computing with domain decomposition (DD) to reduce memory usage and applies automated materials division to create individual pebble materials efficiently and easily. Materials temperatures and distributions can be linked to an OpenFOAM [49] mesh through the multiphysics interface with TMS treatment.

Recently, an enhanced specific burnable division algorithm for pebble bed objects was implemented, reducing the initialization time from tens of minutes to seconds. The version also embeds a source-code modification which provides a more flexible way of defining domains for each material zone by reading a text file with domain indices. These features are essential for achieving HxF in large-scale PBRs. Chapter 3 provides a more detailed overview of the Serpent 2 capabilities and an application to a full-scale static model.

Motion

The HxF tool provides two motion modes: discrete motion and DEM. In discrete motion mode, pebbles are moved based on a simplified pattern of channel motion. In DEM mode, the tool explicitly resolves mechanical interactions between pebbles and the core walls, using a contact force model that considers normal and tangential forces and rolling friction.

Regardless of the simulation mode, each pebble in HxF is assigned a unique index that remains unchanged throughout its history. The tool's motion component can automatically detect discharged and reinserted pebbles and appropriately mark them. In Serpent 2, the number of pebbles within the core remains constant throughout the simulation. However, pebbles can be selectively excluded from the transport calculation. Therefore, a constant number of pebbles and fuel materials is initialized and maintained throughout the simulation, even if the pebble inventory varies. Furthermore, when a pebble is discharged, its fuel kernel composition can be replaced with that of a fresh fuel pebble of the same index, thus reducing the number of materials to create.

To simulate the operation of PBRs over multiple passes, the HxF tool incorporates a novel motion looping method. This method leverages the cyclic behavior of the pebble bed and assumes that pebbles follow similar trajectories across passes. Chapter 4 details the discrete motion approach, the DEM method used, the looping component, and applications on the generic FHR (gFHR) model provided by Kairos Power.

Thermal-hydraulics

In PBRs, temperatures vary significantly within the coolant, pebbles, and TRISO materials, spanning hundreds of Kelvins. These temperature distributions are influenced by the core's neutronics behavior, which is, in turn, influenced by the individual power distribution through various reactivity feedback mechanisms. The material densities are also sensitive to temperature changes and actively contribute to the overall neutronics behavior. An iterative process is required to capture this interdependence between neutronics and thermal-hydraulics. This can be done using Computational Fluid Dynamics (CFD) [50, 51]. However, performing multiple CFD calculations

at every time step is prohibitively expensive. Therefore, the porous media approach is employed, which provides reasonably accurate temperature distributions for neutronics while maintaining acceptable computing times.

The HxF tool leverages the compatibility between Serpent 2 and OpenFOAM through the multiphysics interface. Specifically, it utilizes the GeN-Foam library [52], based on OpenFOAM and designed explicitly to study advanced reactors. GeN-Foam employs volume-averaged Navier-Stokes equations and incorporates terms such as porosity, tortuosity, and sink/source terms to account for fluid behavior in porous media.

In the case of PBRs, the active region is treated as a homogeneous porous medium with a cell-wise power density distribution to approximate the thermal-hydraulic behavior of the core. A double-heterogeneous model has been recently implemented to calculate temperature profiles in pebbles [53], considering the convective boundary conditions between the coolant and pebble surfaces within cells of comparable size to the pebble size. The cell-wise pebble power densities obtained from Serpent 2 are used to calculate the average matrix temperature in a cell. In contrast, considering its layers' power and thermal properties, the average fuel temperature of a representative TRISO particle within the pebble is determined. A description of the power model used in HxF, of the coupling between Serpent and GeN-Foam, and applications are available in Chapter 5.

Interface through Cerberus [54]

The HxF tool incorporates Cerberus as its foundation. Cerberus is the multiphysics driver for VTT (Technical Research Centre of Finland) tools and enables real-time monitoring and control of simulations through socket communication between Python and Serpent. This integration allows on-the-fly interaction between the two, communicating input and output variables within Serpent via Python signals. Collaborative efforts between VTT and the University of California, Berkeley have further enhanced Cerberus to support PBR simulations and, more specifically, the HxF approach [54]. The Serpent/Cerberus interface embeds the following capabilities:

- Communication of current depletion step information such as core power, neutron population, burnup, and depletion time.
- Sending and receiving individual or arrays of divided materials' isotopic compositions, burnups (in MWd/kg_{HM}), volumes, and domains.
- Calculation of materials' atomic and mass densities, burnup (%FIMA), activity, and decay heat.
- Pebble bed information update, including pebbles' positions and radii, automatically modifies the cartesian search mesh accordingly.
- Depletion control, enabling adjustments of the time step, toggling the burnable status of materials, resetting materials to their original (fresh) nuclide compositions, generating a separate binary restart file for all current burnable materials, performing depletion or decay of individual materials, and switching the depletion mode (burnup, decay, activation).

These features enable HxF to finely control the simulation while leveraging the excellent Serpent 2 performances and options previously discussed. More comprehensive lists of monitored and controlled quantities are provided in Table 2-1 and Table 2-2.

Table 2-1: List of Serpent 2 output (monitoring) variables in Cerberus.

Output variable (*sss_ov*)	**Quantity**	**Application in HxF**
DET_<detector name> [_rel_unc]	Tallies/Uncertainty	In-core/Out-of core detectors, pebble-wise quantities
ANA_KEFF [_rel_unc]	Multiplication factor/Uncertainty	Follow equilibrium, criticality
CONV_RATIO [_rel_unc]	Conversion ratio/Uncertainty	Follow equilibrium, breeding
norm_<normalization quantity>	Power, flux, fission rate, …	Check current simulation conditions
inventory	List of followed nuclides	Get followed nuclides names
burnup/burn_time	Total burnup (MWd/kg_{HM}), time	Check current depletion step
time_from_burnup/ burnup_from_time	Time, Total burnup (MWd/kg_{HM})	Convert from one quantity to another from last transport step (output)
pbed_<pbed object>_xyzr/xyz/r/ universe	1D array of positions, radii, universes	Get current pebbles/TRISO positions, radii, universes
materials	Material names list	Get list of all simulation materials
material_<material name>_adens/ mdens/burnable/burnup/fima/ volume/<ZAI>/activity/ decayheat/domain	Material atomic density, mass density, burnable nature Boolean, burnup (MWd/kg_{HM}/%FIMA), volume, inventory nuclide concentration, activity, decay heat, domain for DD	Monitor current material information, including divided zones (fuel in pebbles)
composition_<material name>_nuclides/zai/ adens/original/inventory	Material nuclides names list, ZAI list, concentrations, original concentrations, inventory concentrations	Monitor current material nuclide-wise information
material_div_<parent name>_adens/mdens/burnable/burnup/ fima/ volume/<ZAI>/activity/ decayheat/domain	1D array of divided material atomic densities, mass densities, burnable nature Booleans, burnups (MWd/kg_{HM}/%FIMA), volumes, activity, decay heat, domain for DD	Monitor all divided materials (all fuel materials in pebbles) from a parent material (fuel) at once
composition_div<parent name>_adens	1D array of all divided materials nuclides concentrations	Monitor all compositions of divided material (all fuel materials in pebbles) at once

Table 2-2: List of Serpent 2 input (control) variables in Cerberus.

Input variable (*sss_iv*)	**Quantity**	**Application in HxF**
neutrons_per_cycle/ active_cycles	Active neutrons population	Change neutron population dynamically between steps
plot_geometry	Plotting Boolean	1: re-plot modified geometry (after pebble motion)
write_restart	Writing integer	-1: add current compositions binary restart file in binary restart file >0: store current compositions in binary restart file with integer suffix in name
norm_<normalization quantity>	Power, power density, flux, fission rate, …	Control current simulation conditions (change power)
burn_time	Time	Change current depletion time (after decay)
time_from_burnup/ burnup_from_time	Time, Total burnup (MWd/kg_{HM})	Convert from one quantity to another from last transport step (input)
burn_type	Burnup mode	1: Depletion mode 2: Decay mode 3: Activation mode
pbed_<pbed object>_xyzr/xyz/ r	1D array of positions, radii	Change current pebbles/TRISO positions (pebble motion), radii (0: ghost pebble)
material_<material name>_ burnable/burnup/volume/ <ZAI>/domain	Burnable nature Boolean, burnup (MWd/kg_{HM}), volume, inventory nuclide concentration, domain for DD	Update current material information, including divided zones (fuel in pebbles)
material_<material name> _decay/burn	Decay/depletion time	Decay or burn individual material
material_<material name>_reset	Reset Boolean	Reset composition to original one (fresh fuel)
composition_<material name> _adens	Material nuclides concentrations list	Update current material nuclide-wise concentrations
material_div_<parent name>_ burnable/burnup/volume/ <ZAI>/domain	1D arrays of burnable nature Booleans, burnups), volumes, inventory nuclide concentrations, domains for DD	Update all divided materials (all fuel materials in pebbles) from a parent material (fuel) at once
material_div_<parent name>_reset	1D array of reset Booleans	Reset some of the divided materials at once (all discarded pebbles)

Cerberus also embeds functions to communicate other actions to Serpent 2:

- *initialize()*: Start Serpent 2, read input files, create geometries, and load materials and cross sections.
- *solve():* Run one transport calculation with current materials.

- *advance_to_time(time step)*: Run one transport calculation and deplete (or decay) materials.
- *correct()*: Run one transport calculation and apply corrector depletion step.

By allowing on-the-fly modifications and choosing when to solve for transport and depletion, Cerberus holds excellent potential for complex calculations. In particular, the recent pebble bed reactor-specific additions, such as pebble position modification, divided materials monitoring, and control, make HxF simpler and more accessible.

2.2 HxF Framework

The HxF tool incorporates the capabilities and methods previously discussed. Figure 2-1 provides an overview of the general framework in the case of a search for equilibrium.

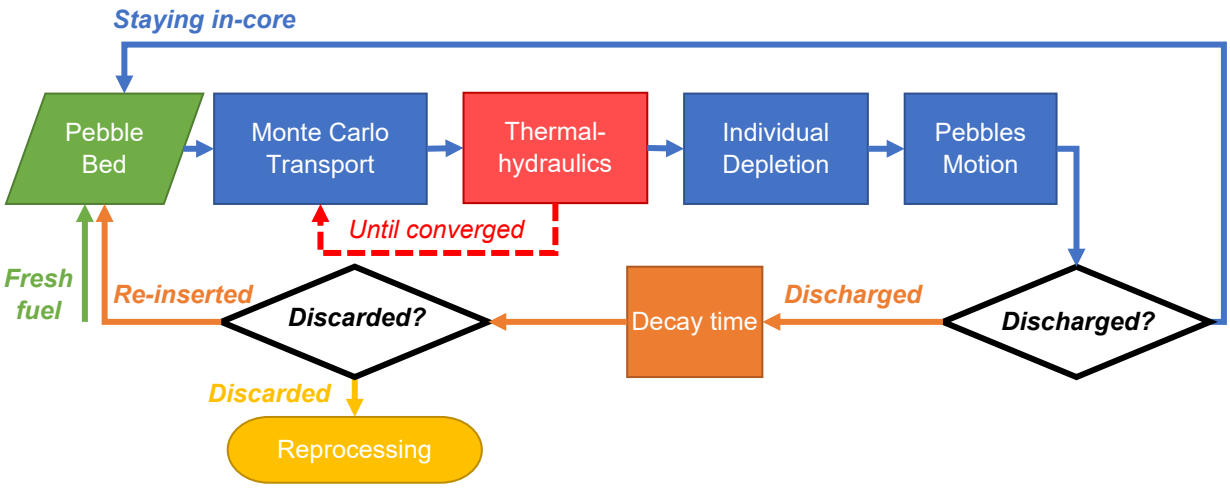

Figure 2-1: HxF tool global framework.

The script starts with reading a dedicated input and performing various actions in place of Serpent, including inventory management, domains and pebble-wise detectors creation, restart path configuration, pebble bed position file creation, materials volume calculation, and initialization of pebble pass numbers and residence times.

Starting from an initial composition distribution using a binary restart file, the pebble bed geometry and materials are created in Serpent 2 and distributed across parallel domains. In the case of thermally coupled simulations, the OpenFOAM mesh is read, and materials' temperatures and densities are initialized with default values. Then, for a given time step, the code starts with performing a transport calculation to obtain transmutation cross-sections, flux, and power distributions. If the GeN-Foam library is utilized, the mesh power distribution is output by Serpent 2, and a thermal-hydraulics simulation is done to obtain updated materials' temperature and density distributions, which are then fed back into the system. This iterative process continues until

convergence is reached between the transport and thermal-hydraulics calculations.

Next, materials are depleted for a duration corresponding to the motion step. Burnt pebbles move either through discrete motion or following the DEM motion, wherein their positions within Serpent 2 are modified. If necessary, the looping method can also be applied, and pebble residence times are updated accordingly. During the motion step, if pebbles are detected to have recirculated, they are marked as "discharged". If desired, a decay step is applied only to the discharged pebbles to simulate the cooling-off period before testing, and their number of passes is incremented. At this stage, HxF receives information from Serpent on various fields of interest for monitoring the reactor's operation, such as tallies data, fuel inventory, burnup, multiplication factor, decay heat, and activities. Based on a set threshold on one of the extracted fields, pebbles beyond the limit are marked as "discarded." The fuel composition of discarded pebbles is then reset to their fresh compositions. HxF offers the capability to save in-core, discharged, and discarded data as text or binary files, and it includes plotting features for visualizing statistical distributions, 1D profiles, 2D slices, and 3D views of the extracted fields of interest. This process is iterated as many times as needed to achieve an equilibrium step.

In addition, HxF offers several additional features and capabilities:

- An initial equilibrium guess calculator determines the restart file based on the desired threshold, expected residence time, and number of passes.
- The ability to restart a calculation from stored data if needed.
- A restart file processor for reading and manipulating Serpent binary materials files.
- A separate Cerberus-based decay tool to evaluate long-term decay heat and activity, nuclide-wise, for every discarded pebble.
- The generation of gamma emission spectra from pebble compositions using a dedicated feature.
- The flexibility to vary powers, thresholds, and neutron populations between steps enabling the simulation of slow transients and faster convergence.
- An adaptable threshold option in which the discard threshold is modified based on a target quantity (e.g., multiplication factor equal to 1) and gradient descent.
- Handling multiple types of pebbles, including pure graphite or multiple fuel types, each with its own threshold.
- Advanced tracking features, such as cumulative detector data (e.g., fluence) throughout the entire history or during the last pass, can be easily implemented in HxF.

2.3 Conclusions

Tracking individual pebbles in a PBR core in terms of their composition, trajectory, and temperature as they evolve is possible. Indeed, the ad hoc HxF methodology has been specifically

implemented, leveraging state-of-the-art codes and methods interconnected through the Cerberus Python library to accurately and efficiently simulate PBRs. Through Cerberus's recent improvements, the developed HxF tool embeds high-fidelity explicit transport, porous media thermal-hydraulics, individual pebble depletion, pebble motion, fuel handling, and out-of-core decay processes. In addition, extra features, such as restart capabilities, equilibrium guess, gamma spectrum generation, advanced tracking, and long-term decay behavior, make HxF a highly flexible, versatile, and efficient tool to obtain the most accurate results possible in PBRs depletion calculations.

Chapter 3
Individual pebbles depletion

As stated in Chapter 1, some high-fidelity PBRs simulations are required to verify the existing, lower-fidelity approaches and provide more accurate data for the input of other models, such as fuel performance, waste management, or source term. In addition, they are needed for capturing outliers and determining the envelope behavior during operation. The HxF approach addresses these requirements by individually tracking each core pebble's composition, position, and temperature.

In particular, central to the methodology and the ad hoc HxF Python tool, the transport and depletion of individual fuel compositions in PBRs present significant challenges. The double-heterogeneous geometry renders deterministic methods impracticable for such a problem. Monte Carlo methods are hence preferred. In addition, the small size of the fuel kernel within TRISO particles typically leads to poor statistical uncertainties and the need for larger simulated neutron populations. Furthermore, the complete data of the tens to hundreds of thousands of pebbles in the core, each containing hundreds of nuclides, must be kept in memory during the simulation, which generates significant constraints on the simulation.

With the increase in computing power, the development of advanced simulation methods, and the increasing use of parallelization, overcoming these challenges is possible. Monte Carlo methods are particularly compatible with these complex geometries when solving transport calculations without making constraining or strong approximations on the problem. However, although, in theory, they can be used for individual pebbles depletion, they suffer from significant CPU time and Random Access Memory (RAM) space requirements. These limitations are generally insurmountable unless supercomputing types of resources are available. Nevertheless, the Monte Carlo code Serpent (version 2.1.32 at the beginning of the project) [43] provides a unique set of features, such as the compatibility with OpenFOAM and the recent Cerberus interface, in addition to others that can be used to lower CPU time and limit RAM requirements.

This Chapter first discusses the choice of the Monte Carlo transport and depletion code Serpent 2 as the primary neutronics tool of the HxF approach and its key features. Then, a quantification of Serpent 2 PBR simulation performances shows its computational requirement for PBR cores as large as half-million pebbles. Finally, results from an example model are presented and compared to those obtained with a spectral zone approach using two different mesh resolutions.

3.1 Neutronics tool: Serpent 2 features [48, 55]

Modeling PBRs is generally computationally demanding due to the number of fuel pebbles and TRISO particles and their multi-layered structure. Nevertheless, the Serpent 2 code includes numerous features that facilitate at the same time PBR modeling and large-scale burnup simulations. The explicit stochastic geometry feature [56] allows us to easily define the location of pebbles and TRISO particles within pebbles using pre-generated location points, thus, not

needing an unrealistic lattice structure. Combining a cartesian search mesh overlaid on the geometry and the Woodcock delta-tracking method [57], Serpent significantly reduces simulation times compared to other Monte Carlo codes that rely on surface-tracking rather than delta-tracking. This is a substantial advantage in models with many surfaces within a short distance, as in the combination of pebbles/TRISO particles. Serpent 2 natively handles depletion within the code, minimizing unnecessary communication time with other burnup codes. There are multiple choices regarding the burnup scheme, including predictor/corrector methods and several modes available for handling predictor/corrector steps.

To reduce the memory and time required to create numerous materials, Serpent 2 applies an efficient automated materials division method that generates a unique material for all regions with the same initial composition that is then replicated using a recursive algorithm. After the initial setup, each material is treated independently. Once again, this feature is well-suited to quickly create a full pebble bed core model with individual pebble materials. As common to any Monte Carlo code, Serpent 2 can leverage parallel computing using OpenMP (an efficient way to use multiple cores within a given computer or cluster node) and MPI (message passing interface, which allows for using multiple computers/nodes simultaneously). Typically, multi-core, single-node calculations are prohibitive in terms of RAM and time required for extensive depletion calculations, and multi-node suffer from extended communication time between nodes and the need to replicate geometry and material data (thus using memory) on each node. To reduce RAM requirements when using multiple nodes, Serpent 2 employs domain decomposition. Burnable materials are divided based on chosen parameters (location or associated indices) to decompose the core in domains, each corresponding to a given MPI task. Each task uses a fraction of the neutrons batch for each cycle, and only contains the corresponding domain's materials, limiting the information to store in memory. The drawback of this decomposition is an increased communication time between nodes. Indeed, when a neutron collides in another domain than the one it was in, an interface communicates between the two domains. This phenomenon is particularly impactful in graphite-moderated systems because the considerable neutron diffusion length makes domain crossing more frequent. Finally, in Serpent 2, reaction rates, flux, and other significant quantities can be easily determined for individual pebbles relying on the same tools used for regular lattice geometries. To the best of the author’s knowledge, no other tool provides such a comprehensive list of features making individual depletion possible, hence justifying the use of Serpent 2 as part of HxF.

Optimization modes and options

Serpent 2.1.32 contains diverse options implemented to adapt the simulation conditions to the calculation requirements. In particular, a set of options can be collectively changed through what is called *optimization modes* in order to adapt to the scale of a specific problem [58]. This set of options is beneficial for burnup calculations since memory usage can become a limiting factor. This is particularly true for PBRs, where the number of materials is significant. An overview of the optimization capabilities that Serpent 2 provides can be found in Table 3-1. Four different modes are available, with the corresponding options enabled or disabled.

Table 3-1: Summary of the optimization modes for Serpent 2 (adapted from [58])[1].

Mode	Description	σ reconstruction, unionized grid	Σ pre-calculation	Spectrum collapse	Group constant generation
4	Fastest, highest RAM	ON	ON	ON	ON
3	Fast, high RAM, bad scaling	OFF	ON	ON	ON
2	Slow, low RAM	ON	OFF	ON	OFF
1	Slowest, lowest RAM	OFF	OFF	OFF	OFF

Reconstructed microscopic cross-sections: this option is linked to the use of a unionized energy grid. Each nuclide has cross-section points for specific energies based on the available data for the given nuclide. Therefore, when a neutron is within a material, Serpent needs to search for the energy points for each of its nuclides. This CPU-intensive process can be avoided using a unionized energy grid. When this option is enabled, before the first transport step, Serpent gathers the energy points of all nuclides in a material and creates a unique energy grid with these points. Therefore, only one grid search must be achieved when a neutron enters a material. This method saves CPU time, but the total memory requirements are increased because the overall energy grid is more extensive and becomes significant when many nuclides are present in a material (during burnup, for example). Memory requirements can be reduced by deleting points out of energy limits or by thinning the unionized energy grid by merging energy points close to each other within a relative tolerance. In the scope of this work, the default energy grid is used.

Precalculated macroscopic cross-sections: instead of calculating materials macroscopic cross-sections by summing the nuclides cross-sections on-the-fly, Serpent can precalculate them. Indeed, these values do not depend on transport data; therefore, they can be stored in memory before running the transport calculation. This could benefit the simulation time since this step is done once per transport step but has a detrimental effect on memory because of the storage of a large amount of data per burnable material in memory.

Spectrum-collapse in burnup mode: once transport has been achieved and when applying burnup, it is necessary to calculate one-group microscopic cross-sections for each burnable material. To this end, reaction rates can be directly tallied by Serpent through the transport process. However, this method is slow. Alternatively, a fine group flux spectrum can be used to collapse multigroup cross-sections and obtain it:

[1] The description column corresponds to the usually observed behavior for water-cooled reactors, and not what the options produce in the case of PBRs.

$$\overline{\sigma_{\mathrm{I,r}}} = \frac{\Sigma_{\mathrm{g}} \sigma_{\mathrm{i,r}}^{\mathrm{g}} \phi_{\mathrm{g}}}{\Sigma_{\mathrm{g}} \phi_{\mathrm{g}}} \qquad (1)$$

Where $\overline{\sigma_{\mathrm{I,r}}}$ is the calculated one-group cross-section for isotope i and the reaction of interest r, $\sigma_{i,r}^{g}$ is the energy group g cross-section and ϕ_g is the group g flux value. This option mainly affects the simulation time. Indeed, this option was developed to increase the performance when using higher optimization modes for a few burnable materials. However, this benefit could be balanced by the processing time needed for collapsing the cross sections when using the option with more materials.

Group constants generation: specified universes can be spatially homogenized to produce group constants, available in the output files of Serpent. This option needs to be manually turned off as there is no direct need for HxF to calculate group constants. Turning off this option induces a negligible memory increase but saves CPU time, avoiding unnecessary data processing.

Cases are simulated with the four optimization modes, and memory and CPU time requirements are compared in the subsequent sections.

Burnable materials and depletion

After each transport step, the evolution of the compositions in each pebble must be calculated. This application uses a predictor (constant extrapolation)/corrector (linear interpolation) method. A 10 MWd/kg burnup step with constant power is applied to compare the simulation behavior between the different cases.

Using multiple burnable materials can become a lengthy process to initialize the geometry and the materials themselves, but it also requires significant RAM. Once more, it is particularly problematic when this number is high (multiple thousands) and, in practice, becomes impossible. To eliminate this problem, Serpent uses the fact that usually, burnable materials have the same geometry (pin, particle, assembly, pebble with *pbed*, …) and the same initial composition. In this case, it is possible to create a lattice of cells filled with the same material and to process it uniformly. Then, the code applies an automated division routine to independently generate materials with different evolutions and compositions throughout the burnup cycles. Each burnable material, divided from the parent *{mat_name}*, is created with the name *{mat_name}z{index}* with the initial composition. Usually performed by applying a recursive algorithm, this process drastically reduces the initial materials processing time[2]. In addition, the amount of RAM needed for this process is reduced, and this benefit is further reinforced when the number of burnable materials is substantial. In practice, the cells are separated into depletion zones and subzones. The first drawback of this method is that volumes must be defined, but this can be done manually (in

[2] In Serpent 2.1.32, used in this section, the burnable materials division specially defined for *pbed* objects was not implemented. Starting from 2.2.0, the time was reduced to few seconds thanks to the new feature.

Serpent or, later, in Cerberus) or using a built-in Monte Carlo routine in Serpent. Most importantly, all depletion zones (pebbles) must have the same initial composition and geometry. However, that limitation can be overcome by using the restart capability of Serpent.

Parallelization and domain decomposition

Monte Carlo simulations in neutronics are easily parallelizable because of the neutrality of neutrons. Therefore, each particle's history can be run independently without affecting the others. Three important concepts can be used in Serpent 2.

OpenMP: Calculations can be parallelized between the cores of a given computer. This is done in Serpent with OpenMP [59], which yields a very high efficiency in that the time spent for parallelization and synchronization of the information is low, almost dividing the transport time by the number of cores (threads) used. The other advantage of this type of parallelization is the fact that within a computer, all cores have access to a shared memory in which the geometry, cross-sections, and materials are stored. The benefits of internal parallelization in Serpent are insufficient for extensive burnup calculations like full PBR cores, as shown in the following sections.

MPI: Another way to parallelize is to use multiple computers (or nodes within a cluster) and synchronize their execution and processing steps. With large clusters, this solution has been increasingly used and helpful. MPI [60], coupled in a hybrid approach with OpenMP, is used to this end. However, there are two major intrinsic differences between OpenMP and MPI: first, the information passing and synchronization between nodes takes more time, meaning the simulation time is generally not divided by the number of nodes used; the second is that the geometry, materials, and cross-sections need to be stored on each node individually. Transport time can be saved using this capability by itself, but not RAM.

Domain Decomposition: In order to save memory using MPI, it is necessary to use domain decomposition. Recently developed in Serpent, this capability decomposes the divided burnable materials into separate domains, each corresponding to an MPI node. A representation of domain decomposition within a typical PBR is given in Figure 3-1. This option divides the burnable material memory requirements by the number of MPI tasks. In this manner, in a given domain (and node), the neutrons are evolving in a particular region. However, nodes must communicate to account for neutrons going from one domain to another. An interface sends the neutrons to the corresponding entering node instead of leaking out of the system. This process affects the parallelization efficiency and increases the transport time. If the neutrons diffusion length is significant relative to the dimensions of the domain, the detrimental impact on the CPU time is high.

Consequently, while the impact is relatively low in thermal light water reactors, it becomes more critical in carbon-moderated systems. Although this effect has a non-negligible impact on the simulation time, this option drastically reduces the memory needed for materials. Several spatial options to divide the core into domains are available. For the performance analysis, the decomposition is made based on the index of the pebbles, resulting in axial pebble layers. This method prevents unreasonable amounts of communication between the nodes.

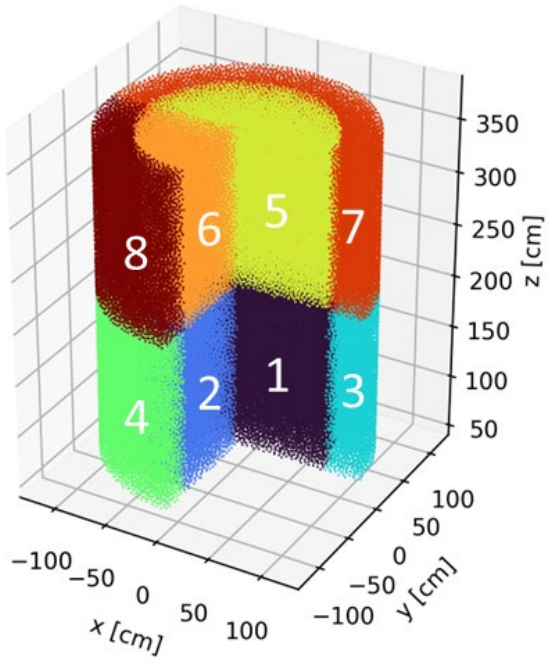

Figure 3-1: Cut view of a typical PBR, divided into 8 domains with 2 axial zones, 2 radial zones, and 2 sectors.

Other features

Other features of Serpent 2 make the tool attractive for HxF. Lattice detectors, calculating reaction rates over each lattice element, have been compatible with explicit pebble bed geometry division. This considerably simplifies the definition of these tallies by the user. In addition, the restart capability allows for reading a list of different compositions from a binary file, thus replacing the initial compositions used when dividing burnable materials. Serpent 2 is also compatible with OpenFOAM [49], making thermal-hydraulics and thermomechanical coupling possible. Finally, starting from version 2.2.0, Serpent 2 embeds full compatibility with Cerberus, drastically increasing its flexibility and possibilities.

3.2 Evaluation of Serpent 2 Capabilities [48]

This section aims to investigate if the depletion of individual pebbles in Serpent 2 is feasible regarding memory and computing time using average computational resources. Therefore, simplified static pebble bed models of diverse sizes and numbers of pebbles are modeled, and the performance (CPU time and RAM) of Serpent 2 is quantified with different sets of options.

Core model

A reference model, assumed to be cylindrical, is chosen as the standard core. Its parameters are summarized in Table 3-2, and a representation of the Serpent 2 model is shown in Figure 3-2. The core has a height-to-diameter aspect ratio of 1.2 and is surrounded by a graphite reflector 1 m

thick. The space between pebbles is filled with FLiBe ^{7}Li- enriched lithium (10 ppm of ^{6}Li). Each pebble has a diameter of 3 cm and consists of three concentric spherical zones: a central graphite core, an external graphite shell, and in between a layer of TRISO particles mixed in a graphite matrix. The TRISO particles are 810 μm in diameter, contain 10 w%-enriched $UC_{0.5}O_{1.5,}$ and are arranged in a simple cubic lattice. Pebbles are disposed according to a face-centered cubic lattice for which sphere centers are externally calculated and input to Serpent. The bed is static, meaning pebble motion is not considered at this proof-of-concept stage. In addition, no reactivity control is modeled. Temperature is assumed to be uniform across all materials (900 K). Each pebble in the core is tracked individually for depletion. The fuel composition within an individual pebble is assumed to be uniform.

Table 3-2: Reference core parameters.

Component	Parameter	Value
Core	Total Power	178.8 MW
	Number of pebbles	354,306
	Temperature	900 K
	Active height	250 cm
	Active radius	105 cm
	Reflector thickness	100 cm
Pebbles	Lattice structure	Face Centered Cubic
	Lattice pitch	2.275 cm
	Graphite core radius	1.251 cm
	Graphite core density	1.594 g/cm^3
	Fuel layer outer radius	1.4 cm
	Graphite matrix density	1.704 g/cm^3
	Pebble outer radius	1.5 cm
	Graphite shell density	1.750 g/cm^3
TRISO particles	Lattice structure	Simple Cubic
	Lattice pitch	0.0886 cm
	Fuel radius	0.02 cm
	Fuel form	$UO_{1.5}C_{0.5}$
	Fuel enrichment	10 wt%
	Fuel density	10.500 g/cm^3
	Buffer outer radius	0.03 cm
	Buffer density	1.050 g/cm^3
	IPyC outer radius	0.0335 cm
	IPyC density	1.900 g/cm^3
	SiC outer radius	0.0370 cm
	SiC density	3.180 g/cm^3
	OPyC outer radius	0.0405 cm
	OPyC density	1.900 g/cm^3
FLiBe	Li-6 concentration	10 ppm
	Density	1.963 g/cm^3

In order to investigate the impact of the number of pebbles on the computing performance, the

number of materials within the core is varied by changing the number of pebbles Np – each pebble being treated as a unique material – within the core. Therefore, the core's dimensions were changed, modifying this number and, thus, the required computing resources. The model does not include partial pebbles to keep an integer number of pebbles (this number varies from 1,028 to 510,022). For simplicity, pebbles were assumed to be distributed according to a regular lattice. However, their positions were pre-determined and stored in a file for use with the *pbed* command. Such an assumption has no impact on the results of this study and could be replicated with any pebble distribution. The TRISO particles were modeled in a simple cubic lattice.

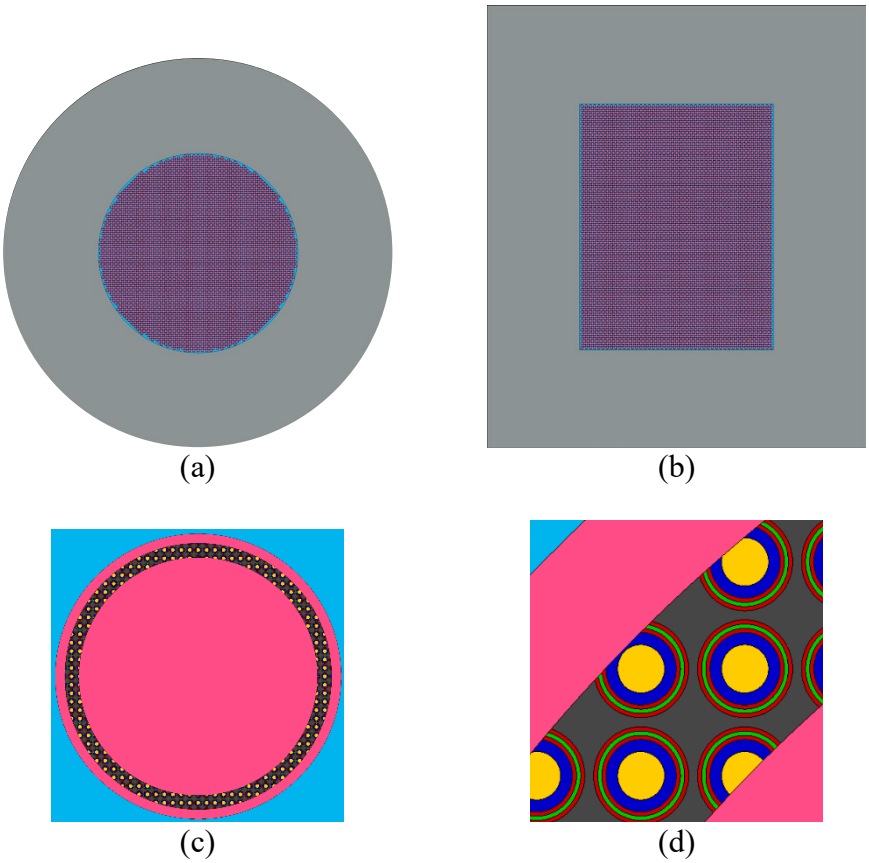

Figure 3-2: Horizontal (a) and vertical (b) cross section of the core model; cross section of a pebble (c) and detail of the TRISO particles layer (d).

Although HxF is expected to be computationally demanding, the work is constrained upfront to determine its feasibility by relying on available resources without appealing to a supercomputer. The following results come from calculations that used the Berkelium cluster of the Nuclear Engineering Department at the University of California, Berkeley. The cluster includes 12 nodes

(AMD Opteron Processor 6172, 2.1 GHz) with 94 GB of memory and 48 cores[3]. Domain decomposition was implemented to divide the burnable materials into axial layers.

Memory requirements

A key limiting factor when running burnup calculations is memory usage. The allocated RAM is decomposed into four categories:

- The fuel mainly dominates materials properties and compositions because each pebble has a unique burnable material.
- Microscopic cross-sections loaded from a library.
- Results, which are mainly detectors for PBRs and (if calculated) macroscopic cross-sections.
- Miscellaneous.

Multiple cases with varying numbers of pebbles were run with each optimization mode. Clear relationships between memory usage and the number of pebbles can be drawn. Materials, results, and miscellaneous memories vary linearly with the number of burnable materials, whereas the cross-section calculations memory usage is constant. The coefficients vary significantly from one optimization mode to another, as reported in Table 3-3.

Table 3-3: Memory usage for each optimization mode.

Opt.	Materials (MB)	Cross sections (MB)	Results (MB)	Miscellaneous (MB)	Total (MB)
1	$2.2 + 0.471N_p$	4897	$1.7 + 1.1 \times 10^{-3} N_p$	$2007 + 2.6 \times 10^{-3} N_p$	$6908 + 0.475N_p$
2	$2.5 + 0.502N_p$	6960	$1.7 + 1.1 \times 10^{-3} N_p$	$1995 + 3.2 \times 10^{-3} N_p$	$8959 + 0.506N_p$
3	$245 + 65.35 N_p$	7340	$1.6 + 1.2 \times 10^{-3} N_p$	$2004 + 2.6 \times 10^{-3} N_p$	$9591 + 65.35N_p$
4	$62.7 + 16.59N_p$	6833	$3.0 + 1.1 \times 10^{-3} N_p$	$2003 + 3.3 \times 10^{-3} N_p$	$8901 + 16.59N_p$

Table 3-4 shows values for the case of a small (50,000 pebbles) and a large (500,000 pebbles) core, as well as for the case of set resources (90 GB) on a single node. Memory with optimization modes 1 and 2 is considerably lower than with optimization modes 3 and 4, where the requirements for simulating PBRs on a single node are prohibitively high. The slight difference between optimization 1 and 2 is relatively low and would allow for around 15,000 more pebbles with the first mode.

The number of 90 GB nodes required to run reference cases when using domain decomposition is also given. It is interesting to observe that 500,000 pebble core simulations become possible

[3] The cluster nodes are considered low-performance, and the obtained CPU times are considered as order of magnitude estimates for verifying the feasibility of individual depletion, and not a fine quantification of the performances with nowadays performances.

when using clusters with more than 3 nodes in optimization modes 1 and 2. Instead, 50,000 pebble geometries can be handled with modes 1, 2, and 4, whereas optimization 3, because of its large memory per material, is still impractical. Therefore, the time requirements were not explored for this latter one. The importance of domain decomposition is also demonstrated here. Materials being the main data stored in memory when simulating large cores, using domain decomposition roughly multiplies the maximum number of pebbles that the number of nodes used can simulate.

Table 3-4: Memory limitations and requirements for each optimization mode with 50,000 and 500,000 pebbles.

Opt.	RAM/node for 50,000 pebbles (GB)	RAM/node for 500,000 pebbles (GB)	Max. number of pebbles with 90 GB and 1 node	Nodes needed for 50,000 pebbles with DD	Nodes needed for 500,000 pebbles with DD
1	31	244	174,899	1	3
2	34	262	160,106	1	3
3	3,277	32,684	1,230	37	364
4	838	8,302	4,889	10	93

Another key point is the low memory taken by detectors, which means numerous detectors can be included in the calculation without impacting the number of nodes needed. Lastly, it is possible to determine the minimum number of nodes to use, given the RAM per node. For instance, Figure 3-3 shows that 10 nodes with 32 GB of RAM are sufficient to manage 500,000 burnable materials independently.

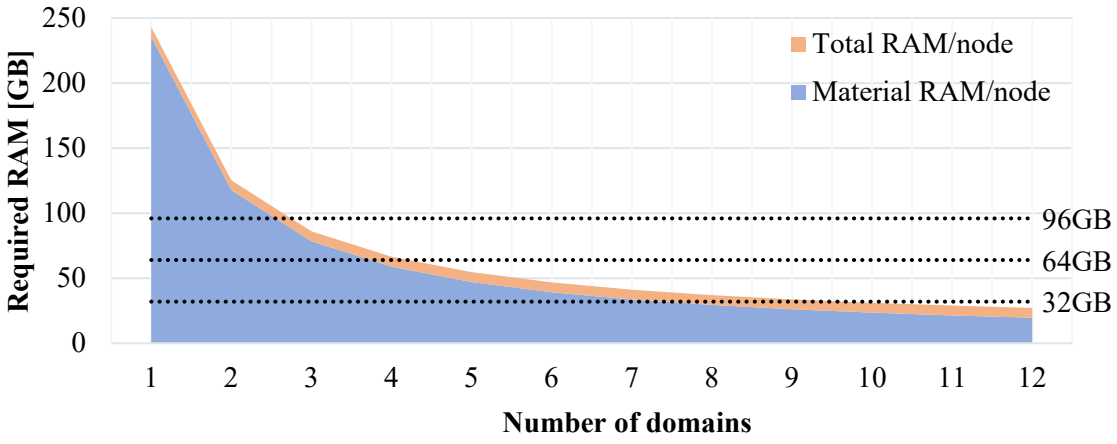

Figure 3-3: Required RAM with domain decomposition (500,000 pebbles, optimization 1).

CPU time

Simulation time also represents an important problem in full-core Monte Carlo simulations. Therefore, this section compares the time taken with each optimization mode of interest. The number of particles per cycle for each core size was determined after a convergence analysis to ensure the results' accuracy and the simulation duration's realistic nature. Each case was run with

100 inactive cycles, 1000 active cycles, and 300,000 particles per cycle, which is considered fully converged. Then, the fission source convergence was determined when the difference between the converged Shannon entropy and all successive inactive cycles' Shannon entropy was low enough ($<10^{-3}$). Next, the threshold on the relative error for the multiplication factor estimator was set to 30 pcm for active cycles, and the maximum relative error on the pebbles flux detector was set at 2%. These three parameters determined the approximate number of particles needed to ensure convergence (Table 3-5).

The different processes that Serpent goes through during simulations can be grouped into four categories:

- Initialization time (IT) taken before starting transport, including geometry creation, nuclides data loading, and materials creation.
- Processing time (PT) after each transport cycle handling data.
- Transport time (TT) which includes active and inactive cycle simulations.
- Burnup time (BT) taken to solve Bateman equations, burn materials, and calculate new compositions.

This analysis considered a single burnup step with a predictor/corrector burnup scheme. In such a case, three steps occur. At zero burnup, a first predictor step is run and uses initial compositions to determine the flux and macroscopic cross sections, followed by a 10 MWd/kg depletion calculation to determine the next cycle's initial composition. In the following transport step, the corrector uses this composition to calculate the new cross-sections, and a linear interpolation is applied between the two steps to approximate the next initial composition. Finally, a second predictor is applied as the last transport step. Therefore, when running such a burnup scheme, the CPU time per burnup step can be determined by the sum of the predictor and the corrector steps.

If a simulation uses a number N_{bu} of burnup steps, the initialization process is done only once, whereas the rest of the processes are repeated N_{bu} times. The wall clock time required for a single node and optimization modes 1, 2, and 4 are summarized by category in Table 3-5. As stated above, this table only considers the first predictor and corrector steps for PT, TT, and BT. For each of these categories, the time of the first predictor was added to the time of the corrector in order to obtain an approximated CPU time per burnup step. The fourth optimization mode was run until the memory exceeded 90 GB. This table shows that the processing time with optimization mode 4 is much longer, likely due to the considerable number of macroscopic cross-section calculations, and makes this mode highly impractical for PBRs. Even if it is described as the fastest option set for transport, the transport step is slower than the two other modes for a given number of depletion zones.

The time taken for initiating the calculation is similar to optimization 1 to 2. Regarding the dependence on the number of burnup steps, the second mode is generally slightly faster than the first one but of the same order of magnitude, with maximum savings of 3%, due to less processing. The initialization time seems negligible compared to the rest of the processes, especially as N_{bu}

increases. With the two first modes, transport time remains the main contributor, always taking at least 75% of the combined time per step. This contribution decreases with N_p, while the processing and burnup steps have increasing roles with larger cores. In particular, the time taken to burn materials becomes more important, taking up to a fifth of the simulation duration per step with 100,720 pebbles, whereas the processing time increase is less steep.

Table 3-5: Simulation time (in minutes) by category on a single node with varying numbers of pebbles for optimization modes 1, 2 and 4.

N_p	Particles/cycle	Optimization	IT	PT	TT	BT	Total
1028	5000	1	1.1	0.4	4.0	0.3	$1.1 + 4.7N_{bu}$
		2	1.4	0.1	3.9	0.3	$1.4 + 4.2N_{bu}$
		4	1.5	7.6	4.2	5.1	$1.5 + 16.8N_{bu}$
2018	10000	1	1.2	0.5	10.4	0.5	$1.2 + 11.4N_{bu}$
		2	1.5	0.2	10.4	0.5	$1.5 + 11.1N_{bu}$
		4	1.8	14.7	11.9	9.0	$1.8 + 35.6N_{bu}$
5086	20000	1	1.2	0.7	28.6	1.3	$1.2 + 30.6N_{bu}$
		2	1.4	0.4	28.0	1.3	$1.4 + 29.7N_{bu}$
		4	2.9	56.3	32.5	38.9	$2.9 + 127.7N_{bu}$
9788	20000	1	1.4	0.9	35.9	2.4	$1.4 + 39.2N_{bu}$
		2	1.6	0.7	35.5	2.4	$1.6 + 38.6N_{bu}$
19448	20000	1	1.7	1.9	41.6	4.7	$1.7 + 48.2N_{bu}$
		2	2.0	1.8	43.3	4.8	$2 + 49.8N_{bu}$
50764	20000	1	3.1	4.3	54.5	13.1	$3.1 + 71.8N_{bu}$
		2	3.4	3.9	53.1	12.7	$3.4 + 69.7N_{bu}$
100720	35000	1	8.6	9.9	102.9	26.0	$8.6 + 138.8N_{bu}$
		2	9.3	9.1	101.7	25.7	$9.3 + 136.6N_{bu}$

As previously concluded, memory represents the limiting factor when not using multiple MPI nodes along with domain decomposition. Therefore, cases with more than 100,000 pebbles were only run with the whole cluster of 12 nodes. MPI alone does not enable larger cores simulations; domain decomposition is used by default. The results are compiled in Table 3-5. Optimization mode 2 still has a lower processing time. However, transport becomes slower than the other mode (up to 40%).

Another critical information conveyed by the two tables is that although parallelization between cluster nodes does allow for simulating larger cores through domain decomposition, the benefits on CPU time are far from being perfectly efficient. Indeed, the time required for initializing is on the same order of magnitude with and without parallelization, and the time per burnup step is only divided by a factor ranging from 2 to 3, far from the factor 12 that could have been ideally reached. This comes from two elements of the parallelization: the communication time with MPI with more than 2 hours spent on MPI waiting and synchronization tasks for 510,022 pebbles, and the time taken to interface between domains when the neutrons cross a domain boundary, further increased by their large diffusion length in graphite.

It can also be observed that the initialization roughly varies quadratically, and although 500,000 pebbles (geometry and materials) can be created in about 3 hours, 1 million pebbles are created in 12 hours, and it takes more than a day to create 1.5 million pebbles[4]. In addition, the N_{bu}-dependent time approximately indicates a linear behavior, only multiplying the time for 500,000 pebbles by two when simulating a 1 million pebble core.

Table 3-6: Simulation time (in minutes) by category on 12 nodes with domain decomposition and varying numbers of pebbles for optimization modes 1, 2

Np	Particles/cycle	Optimization	IT	PT	TT	BT	Total
2018	10000	1	1.5	0.4	4.5	0.1	$1.5 + 5N_{bu}$
		2	1.7	0.1	5.5	0.1	$1.7 + 5.6N_{bu}$
5086	20000	1	1.5	0.6	10.8	0.2	$1.5 + 11.6N_{bu}$
		2	1.7	0.2	12.7	0.2	$1.7 + 13.1N_{bu}$
9788	20000	1	1.6	0.8	12.9	0.3	$1.6 + 14N_{bu}$
		2	1.7	0.3	17.8	0.3	$1.7 + 18.4N_{bu}$
19448	20000	1	1.7	1.3	16.0	0.6	$1.7 + 17.8N_{bu}$
		2	1.8	0.6	20.9	0.5	$1.8 + 22N_{bu}$
50764	20000	1	2.3	2.9	25.1	1.3	$2.3 + 29.4N_{bu}$
		2	2.5	1.5	29.0	1.4	$2.5 + 31.9N_{bu}$
100720	35000	1	7.0	5.6	44.7	2.6	$7 + 52.9N_{bu}$
		2	7.0	3.3	60.6	2.7	$7 + 66.6N_{bu}$
204786	50000	1	30.5	12.1	86.4	4.8	$30.5 + 103.2N_{bu}$
		2	34.2	7.1	111.2	6.7	$34.2 + 125N_{bu}$
510022	75000	1	188.5	31.6	176.3	12.9	$188.5 + 220.8N_{bu}$
		2	185.0	18.8	247.5	14.3	$185 + 280.6N_{bu}$

Finally, simulation times varying the number of burnup steps N_{bu} is calculated for three core sizes: 50,764, 100,720, and 510,022 pebbles. The approximated times without the last predictor steps are shown in Approximated simulation times (in hours) for optimization modes 1 and 2, varying the number of pebbles and the number of burnup step, with and without domain decomposition. Although using a single node for a model up to 100,000 pebbles with 10 burnup steps in less than a day is feasible, this time drops to less than 10 hours with 12 nodes and domain decomposition. Moreover, this table shows that burnup calculations with an entire 500,000 pebble core can be achieved in less than 2 days of calculation with regular resources.

Therefore, using domain decomposition, which drastically reduces the RAM requirements, the burnup calculations with full-scale pebble bed reactors timescale is on the order of days. Therefore,

[4] This time was obtained with Serpent 2.1.32. In Serpent 2.2.0, a specific pebble bed initialization was implemented, reducing the materials division time, mainly responsible for this large initialization time, to seconds.

individual depletion is deemed to be feasible.

Table 3-7: Approximated simulation times (in hours) for optimization modes 1 and 2, varying the number of pebbles and the number of burnup step, with and without domain decomposition.

N_p	Optimization	# nodes	N_{bu}		
			1	**5**	**10**
50764	1	1	1.2	6.0	12.0
	2	1	1.2	5.9	11.7
	1 w/ DD	12	0.5	2.5	4.9
	2 w/ DD	12	0.6	2.7	5.4
100720	1	1	2.5	11.7	23.3
	2	1	2.4	11.5	22.9
	1 w/ DD	12	1.0	4.5	8.9
	2 w/ DD	12	1.2	5.7	11.2
510022	1 w/ DD	12	6.8	21.5	39.9
	2 w/ DD	12	7.8	26.5	49.9

3.3 Results and comparison with coarse meshes [55]

Proven that individual pebble depletion is achievable, this section presents data obtained from the reference simplified example. The purpose is to verify that the obtained data from this analysis is physical and to demonstrate the type of information that HxF can provide that is otherwise unattainable using the coarse mesh approximation. This comparison is performed, once again, on a static case.

Test case and assumptions

The same model as the reference case is used to compare the HxF method with the macrozone method. In the latter case, two different subdivisions are considered: a 3x3 coarse mesh and a finer 10x10 mesh (Figure 3-4). In both cases, the radial regions assume equal cross-sectional area, and the axial regions equal length.

The data presented below were obtained using the model described in the performance study, tracking depletion for 354,306 stationary pebbles. In addition, multiple lattice detectors were set up to tally the individual pebbles' thermal, fast, total flux, and fission rate. The pebbles' local burnups and all isotope concentrations were calculated within Serpent and compiled in output files, increasing the simulation time. The code is slightly modified to make domain decomposition compatible with the burnup output file creation by creating separate output files for each domain. This feature has been added in Serpent version 1.32 for binary restart files.

Transport calculations were run with 75,000 neutrons per cycle, 1,000 active and 100 inactive cycles at each step, ensuring uncertainties below 2% for the flux detector and 6% for the power in each pebble. Regarding the depletion calculation, the predictor/corrector method with constant extrapolation and linear interpolation is chosen. Ten burnup steps were used: 0, 1, 5, 10, 20, 30,

40, 50, 60, 70, and 80 MWd/kg$_{HM}$. Given the static, unrealistic nature of the pebble bed, these values are chosen arbitrarily. For comparison, the entire burnup calculation is performed using the coarse 3x3 mesh model and the finer 10x10 mesh model. All cases were run with the ENDF/B-VII library [61].

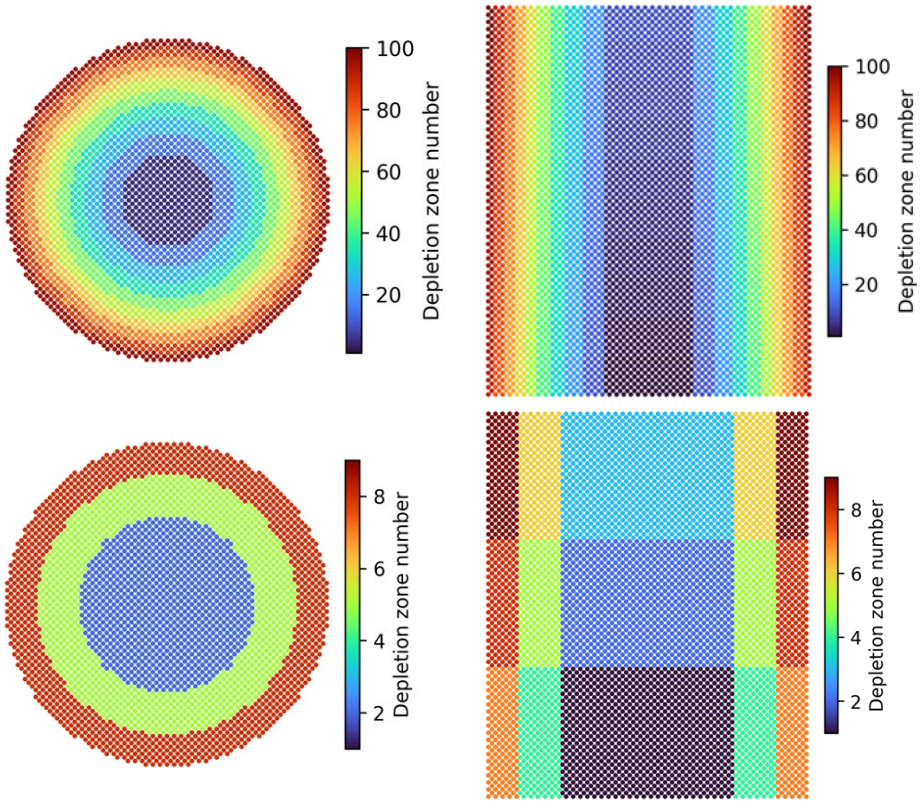

Figure 3-4: Core spectral regions XY (left) and YZ (right) views with a 10x10 mesh (top) and a 3x3 mesh (bottom).

For this example, HxF required around 23 GB of RAM on each of the 12 nodes, 65% being memory needed to store the domain materials and 20% to store cross sections. The simulation was completed in 60.4 hours[5], of which 55.8 hours were used for the transport calculation and the remaining split between creating the geometry and materials (1.5 hours) and data processing (1.9 hours). The domain decomposition adds to the time required for communication among nodes by MPI. This additional time is included within the transport time, which accounts for 32.7 hours[6]. The CPU usage represents 30% of the total capacity of the nodes. Due to the complex geometry of many materials, the delta tracking efficiency ranges from 30% to 40%. Another time-consuming

[5] This time can be reduced by turning off the reproducibility among OpenMP tasks, using private scoring buffer and results arrays, and using the fission source passing.

[6] Using more neutrons per cycles with less cycles increases the CPU usage.

step is the output writing as, for the scope of this study, the concentrations of all isotopes included in each fuel material were written into an output file for all burnup steps, along with the local burnups, total densities, and initial fissile materials. The total storage needed for this simulation is 41 GB, with the depletion output files requiring 4 GB each (except for the first with fewer isotopes, taking only 100 MB), representing 11 kB per material. Each detector file is 100 MB. The size of the rest of the files is minimal and does not impact storage. In order to process the large amount of data generated through HxF, a function library is developed in Python 3. This library uses the input pebble bed position file and links it to the pebble-wise output files to process the data. Its capabilities include representing the core in 1, 2, or 3-dimensional plots and providing information about the output data.

Results

Figure 3-5 shows the thermal neutron flux (E < 0.1 eV) distribution as a function of core average burnup. The thermal flux peaks at the core center with fresh fuel, becoming more evenly distributed as fuel is consumed. High values near the reflector are instead present throughout.

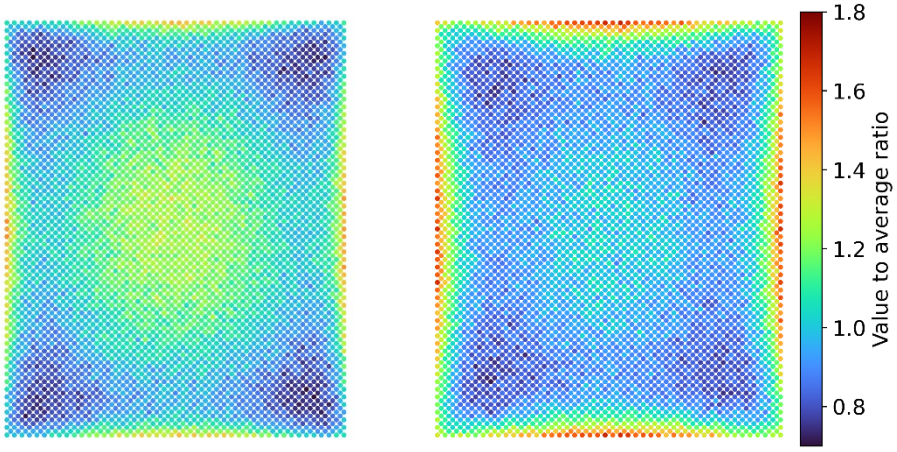

Figure 3-5: YZ view of the thermal neutron flux (in neutrons $cm^{-2}s^{-1}$) at 0 MWd/kg_{HM} (left) and at 80 MWd/kg_{HM} (right) core average burnup. Values are represented relative to their average values, $3.92x10^{13}$ $n/cm^2.s$ and $5.43x10^{13}$ $n/cm^2.s$, respectively.

The evolution of the radial fission profile with burnup is displayed in Figure 3-6, along with the evolution of the ^{235}U density profile. At low average burnups, the fission profile always peaks at the center and the edges of the core, whereas at higher burnups, the peak at the edge disappears. Indeed, once enough fissions happen, the fuel at the edge of the pebble bed becomes too depleted to yield a large number of fissions. The cylindrical geometry of the core makes the fission rate still peak at the center, even if the depletion was higher in this region during the cycle. The area next to the reflector is the zone where the ^{235}U generates the lowest number of fissions.

The neutron flux and power distribution behaviors appear to be as expected. Although this does not constitute a formal verification of the hyper-fidelity methodology, it provides confidence that the approach functions as expected.

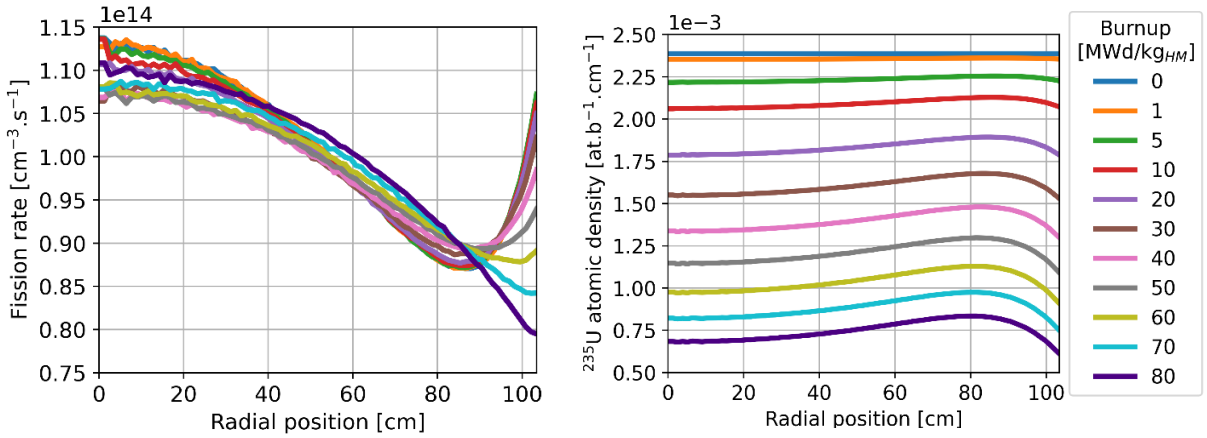

Figure 3-6: Radial average fission rate (left) and ^{235}U concentration (right) as a function of distance from the core center and core average burnup.

One of the central added values of HxF is the possibility of generating information on the distribution of quantities of interest in addition to average values. For example, Figure 3-7 shows the radial and axial distributions of the average burnup and the variation between minimum and maximum burnup at the corresponding location. Of interest is how the range of the burnup distribution for a given position widens with time. The burnup peaking factor, defined as the ratio between the maximum pebble burnup and the core average burnup, monotonically decreases from 1.498 at 1 MWd/kg$_{HM}$ to 1.275 at 80 MWd/kg$_{HM}$. To reduce statistical uncertainty, minimum and maximum values were assumed to be the average of the ten lowest and highest values, respectively.

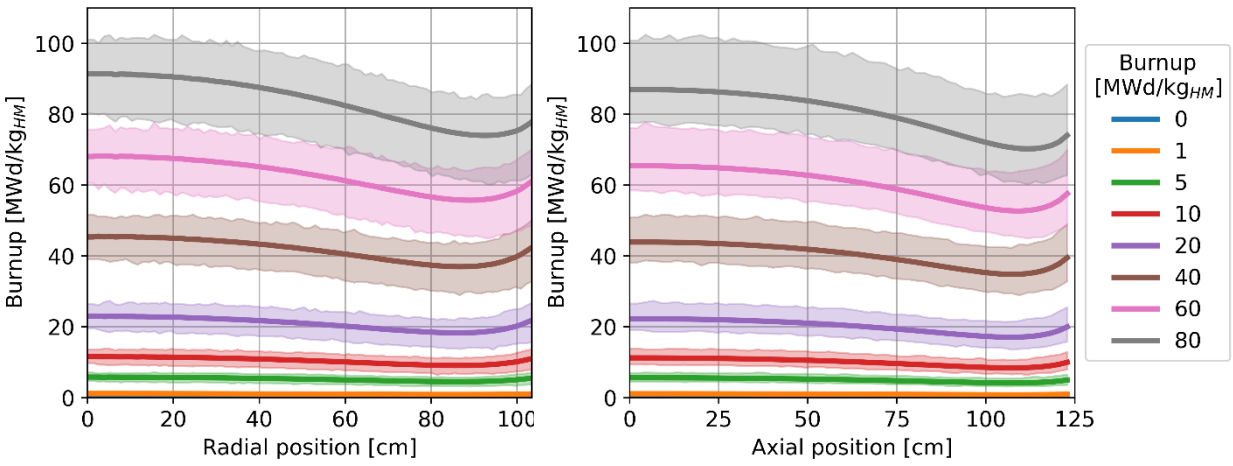

Figure 3-7: Radial and axial burnup distribution as a function of core average burnup. The solid line represents the average burnup, and the area represents the range between the minimum and the maximum burnup at the corresponding position.

Detailed burnup distributions at 80 MWd/kg$_{HM}$ are shown in Figure 3-8. Like thermal flux, the

burnup peaks at the center with low burnup regions at the corners due to leakage. Again, the edges have a slightly higher burnup than the region further from the reflector due to backscattered neutrons.

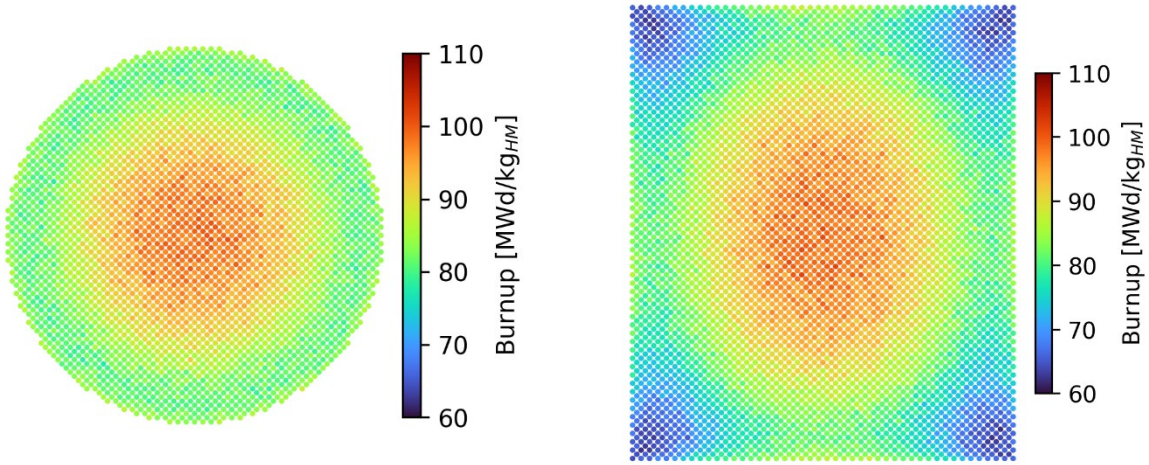

Figure 3-8: Horizontal (left) and axial (right) pebble burnup distributions at an average core burnup of 80 MWd/kg$_{HM}$.

Figure 3-9 shows the number of occurrences for each burnup value when the core average burnup is 80 MWd/kg$_{HM}$. The distribution is highly peaked around the core average value; half of the pebbles display a burnup between 74.5 MWd/kg$_{HM}$ and 85.2 MWd/kg$_{HM}$, whereas a small fraction (less than 4%) of the pebbles have a burnup higher than 95 MWd/kg$_{HM}$. A secondary peak can be observed at around 65 MWd/kg$_{HM}$. It corresponds to the pebbles at the edges of the bed next to the reflector.

It should be noted that the results provided in this section are pertinent to a static bed and are expected to differ from systems with continuous refueling.

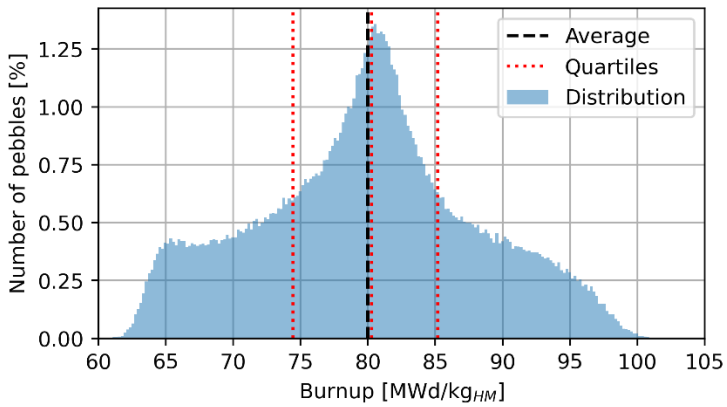

Figure 3-9: Number of pebbles as a function of burnup at a core average burnup of 80 MWd/kg$_{HM}$ (0.2 MWd/kg$_{HM}$ wide bins).

HxF vs. coarse mesh

This section compares HxF to classical spectral zone methods, where depletion is performed by averaging data of multiple pebbles and assuming uniform fluxes within coarse regions. Two options are compared, a 3x3 mesh and a 10x10 mesh. Table 3-8 compares the required computational resources for the different methods. As expected, hyper-fidelity requires longer computing times (four to five times longer) and larger memory (about three times), whereas minor differences were observed between the two coarse mesh models. It should be noted that the data in that table were obtained using the same number of histories for all Serpent calculations, and the difference in time could be potentially more significant if the comparison were to be done, setting the same maximum statistical uncertainty for each case.

Table 3-8: Comparison of time and memory requirements for the full-core calculation between the 3x3 coarse mesh, the 10x10 finer mesh, and HxF.

Parameter	Spectral zones 3x3	Spectral zones 10x10	Hyper-fidelity
Initiation time (min)	2.7	2.4	88.3
Data processing time (min)	3.6	13.5	114.4
Transport cycles time (min)	704	956	3,299
Burnup cycles time (min)	0.2	0.5	60.5
Total time (min)	712	974	3,574
Memory size (MB)	7,413	7,645	22,750

The evolution of the multiplication factor for both macrozones cases is compared against the hyper-fidelity case in Figure 3-10. The 10x10 provides closer results with a maximum difference of around 100 pcm, whereas the 3x3 mesh over-predicts k_{eff} by as much as 300 pcm.

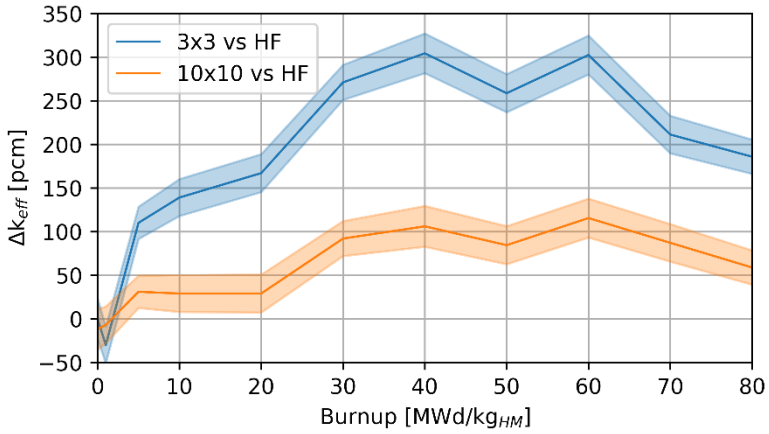

Figure 3-10: Absolute difference in multiplication factor between the 3x3 and 10x10 meshes and the hyper-fidelity calculation. The shaded areas represent the uncertainties from the Monte Carlo simulations.

Figure 3-11 shows the axial burnup distribution obtained using the macrozones method.

Qualitatively, the trend resembles that obtained using individual pebble depletion (Figure 3-8), confirming that the spectral zones approach is sufficient to capture average behaviors. Nevertheless, they cannot provide proper distribution behavior, particularly when using a small number of zones, e.g., in the 3x3 case. Figure 3-12 shows the burnup distribution within the core at the end of the considered time frame. Although both mesh structures reproduce the overall shape of the distribution well, the range of burnup values is impacted, especially for the 3x3 mesh. The lowest pebble burnup is 60.8 MWd/kg$_{HM}$ for the HxF; it becomes 64.7 MWd/kg$_{HM}$ for the 10x10 mesh and 71.8 MWd/kg$_{HM}$ for the 3x3. Similarly, the maximum burnup is 102.0 MWd/kg$_{HM}$ for the hyper-fidelity and 93.4 MWd/kg$_{HM}$ for the coarsest mesh, and 97.1 MWd/kg$_{HM}$ for the finer. This shows how the macrozones approach reduces the range by averaging burnups with surrounding regions. Furthermore, the number of pebbles having a high burnup value is significantly higher than those from the HxF calculation.

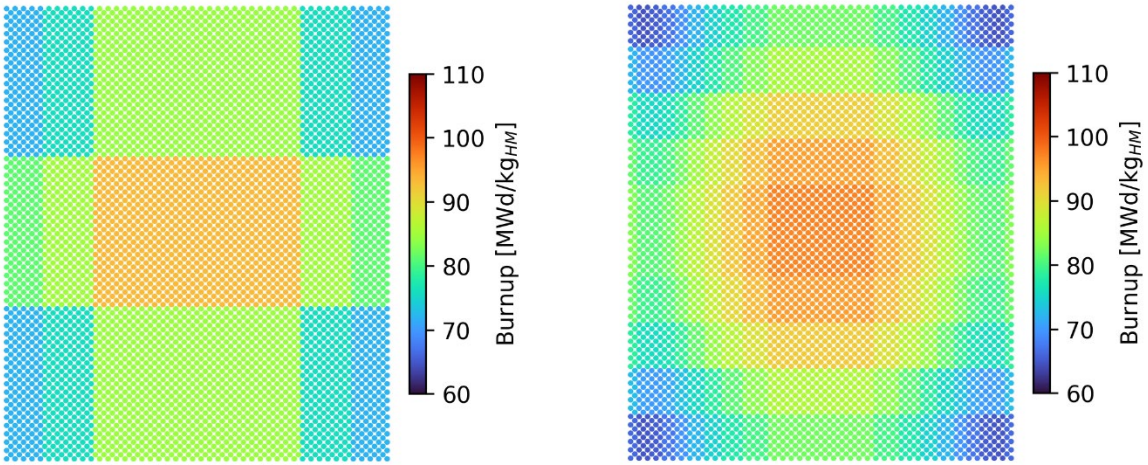

Figure 3-11: Axial burnup (MWd/kg$_{HM}$) distribution at a core average burnup of 80 MWd/kg$_{HM}$ for the 3×3 mesh (left) and the 10×10 mesh (right).

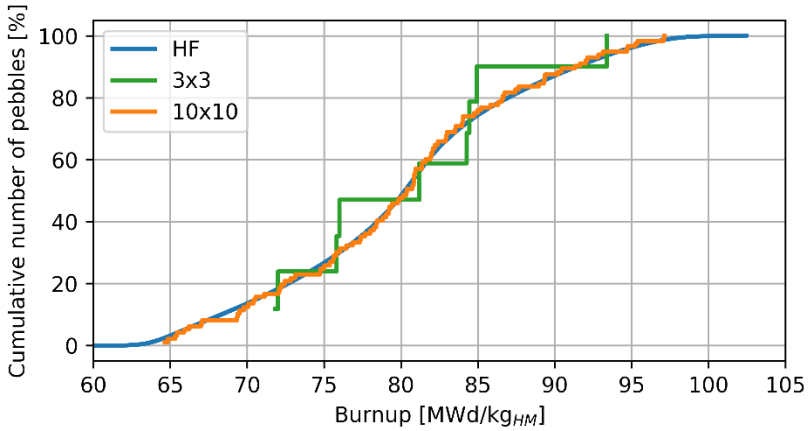

Figure 3-12: Pebbles burnup cumulative distribution comparison between HxF, the 3x3 mesh, and the 10x10 mesh at a core average burnup of 80 MWd/kg$_{HM}$.

Figure 3-13 compares the average burnup value as a function of the radial position in the core at two axial positions: midplane and close to the reflector. Once again, the shapes of the profiles are similar between the three calculations, but the local values are not well captured using the coarse mesh. For instance, in the 3x3 mesh, there is no slight burnup increase next to the reflector, and in the 10x10 case, such peak is around 3 MWd/kg$_{HM}$ lower than with the HxF.

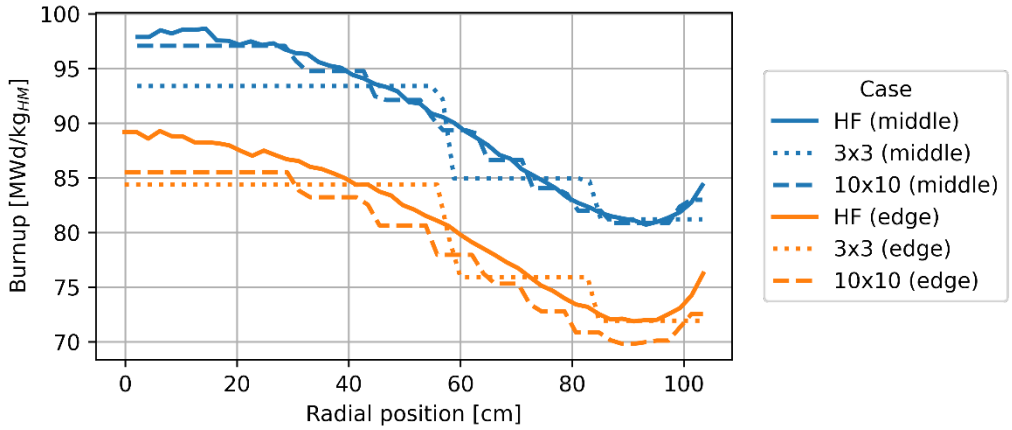

Figure 3-13: Comparison of the radial burnup distribution between individual pebble depletion, 3x3 mesh, and 10x10 mesh at the axial center of the core and at an axial distance of 80 cm, at an average core average burnup of 80 MWd/kg.

Not capturing the local (extreme) values ultimately leads to wrong peaking factor values. Figure 3-14 compares peaking factors evolutions with core average burnup for the three cases. The burnup peaking factor is largely underestimated when using uniform flux zones. From the power peaking factor point-of-view, it displays correct agreement at the beginning of the cycle but deviates at a burnup of 5 MWd/kg$_{HM}$. Table 3-9 summarizes key values at the end of the simulated cycle.

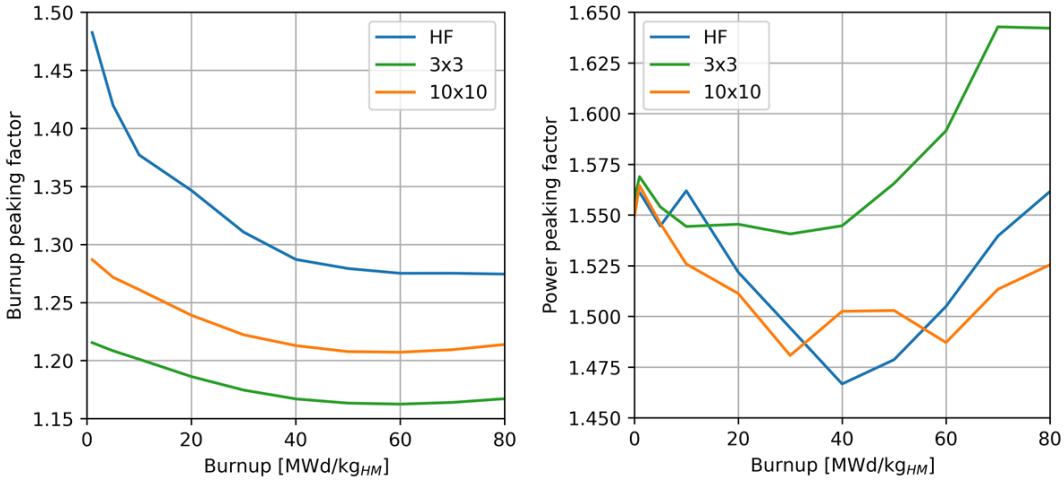

Figure 3-14: Burnup (left) and power (right) peaking factors evolutions comparison between hyper-fidelity, 3x3 mesh, and 10x10 mesh.

Table 3-9: Value of key parameters at a core average burnup of 80 MWd/kg_{HM}.

Quantity	Spectral zones 3x3	Spectral zones 10x10	Hyper-fidelity
Minimum burnup (MWd/kg)	71.8	64.7	60.8
Maximum burnup (MWd/kg)	93.4	97.1	102.0
Burnup peaking factor	1.17	1.21	1.27
Power peaking factor	1.64	1.52	1.56

3.4 Conclusions

This Chapter demonstrates that it is feasible to simulate the depletion of PBRs by individually depleting each pebble in a static core. Such calculations are made possible by features implemented in the Monte Carlo code Serpent 2, among which domain decomposition is the most relevant for burnup calculations. It is shown that depleting up to half-million pebbles does not require employing a supercomputer, but it is feasible using a modest computing cluster. The approach demonstrated here—referred to as HxF—represents a substantial leap compared to current methodologies based on grouping pebbles into macro spectral zones. As expected, depleting each pebble individually requires longer computational times (on the order of days); therefore, it is not foreseen to be used for scoping calculations but rather for confirmatory calculations as validation cases for lower fidelity methods and detailed analysis of selected designs.

One of the major features of HxF is the capability to generate a detailed distribution of quantities of interest, which is not available with macro spectral zones methods. Pebble by pebble power, burnup, fission products distributions, and many more can be used for fuel performance models, fuel handling and storage strategy, and other analysis for which average data are insufficient. A comparison of the result from the spectral zones method against hyper-fidelity is also made. It confirms that the average trend predicted by macro spectral zones, even when coarse, is reasonable, but peaking factors are largely misrepresented. Furthermore, using individual pebble depletion opens the possibility to model transition scenarios, such as from initial core configuration to equilibrium, with great accuracy.

This work focused on demonstrating the feasibility of depleting pebbles individually, and a proof of concept is provided using a static bed, an ordered lattice for pebbles, and a uniform temperature distribution. This represents a first step towards hyper-fidelity, to which motion should be added to account for the dynamic operational behavior of PBRs.

Chapter 4
Pebbles motion

The individual depletion performance study results indicate that a full-scale individual depletion in PBRs is technically possible with Serpent 2, using commonly available resources and within acceptable timeframes. In order to achieve this, parallelization, domain decomposition, and automated division of materials are employed. A second important part of the HxF approach is to model pebbles' motion within the core accurately. Indeed, moving pebbles enables continuous refueling, which allows the core to stay critical without significant excess reactivity. In addition, pebbles experience a variety of flux spectra, which leads to more uniform profiles than static depletion, thus yielding lower peaking factors. Finally, it allows pebble discharge and discarding tests, which allows replacing used fuel with fresh fuel during the simulation.

This Chapter, therefore, covers the pebble motion aspect of HxF. Two different methods are employed. The first is referred to as discrete motion. Such a model assumes an ordered bed with fixed pebble positions within which pebbles move in straight lines from one set position to another. Discrete motion was first directly implemented within Serpent 2 version 2.1.32 source code, and starting from version 2.2.0 and the compatibility of Serpent with Cerberus was instead implemented within the dedicated HxF Python tool. The second approach is to use HxF coupled with a discrete elements method (DEM), where mechanical interactions between the pebbles, walls, and fluid (one-way coupling) are computed to obtain the evolution of the pebble bed with time. Although DEM studies for PBRs have been performed in the past [62, 63] and coupling Monte Carlo and DEM has been explored [50], direct coupling with depletion has not been explored thus far.

First, a thorough description of the discrete motion approach with direct implementation of the technique within Serpent 2’s source code is provided. It is followed with an application to demonstrate the method's feasibility using a small-scale FHR with a flat velocity profile and the range of results that can be extracted from it. Then, a full-scale application showcases the extended data obtainable with HxF on an HTGR model. On the other hand, the theory and implementation of HxF with DEM is presented. This section describes the DEM solver for motion using the GPU-based physics modeling Project Chrono [64]. The method is used to model an HTR-10-based core by demonstrating an approach to equilibrium.

4.1 Discrete motion approach [65, 66]

Discrete element models (DEMs) have been applied to PBRs to determine the trajectory of each pebble during its lifetime [67, 68, 69, 70, 63, 71, 72]. For example, OpenFOAM and its DEM solver particleFoam have been used for simple applications in PBRs [68]. In addition, Serpent embeds an internal coupling with OpenFOAM allowing for reading OpenFOAM-formatted files and exchanging information (e.g., temperature, density) on-the-fly. However, two limitations make this approach challenging. First, although the communication interface between OpenFOAM and

Serpent can be leveraged, changing the pebble bed configuration cannot be done in the current state of the latter code. The cartesian search mesh, necessary for Serpent to explicitly model pebbles, must be updated when the position of the pebbles is changed. However, the search mesh is static in Serpent 2, and modifying this behavior would require extensive development efforts and profound modifications of the source code structure. In addition, it would be necessary to exit the code at every motion step, modify the input, and rerun Serpent. This process results in significant computational time for re-creating the geometry and materials and importing the saved compositions, in addition to increasing the complexity of the procedure. Second, although the OpenFOAM DEM solver has been used in the past for simulating the core loading [50], it has not been used with pebble recirculation. Overall, the implementation of this solver is not advanced enough and does not include the necessary features to make a full-scale pebble bed recirculate for multiple passes.

For these reasons, the initial coupling of pebble motion and depletion is implemented, assuming a simplified motion model that leaves the search mesh static by keeping the pebble positions unchanged throughout the simulation (Figure 4-1). The motion is then represented by moving pebbles' compositions from one position to another. A routine was added to the Serpent 2 (version 2.1.32) source code that moves compositions and accounts for discarding depleted pebbles and inserting fresh ones. It is assumed that pebbles move in straight lines, upward or downward, according to the type of PBR represented.

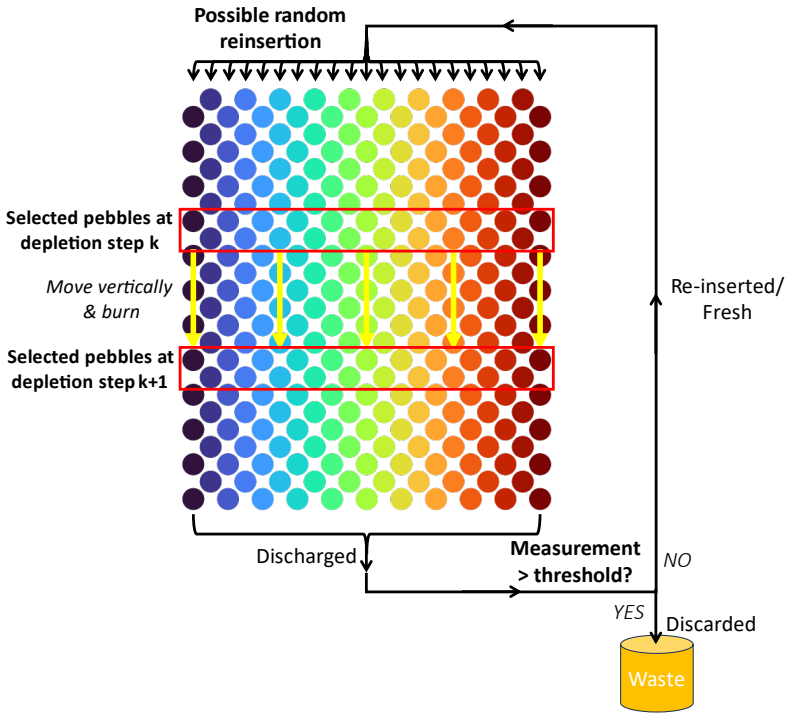

Figure 4-1: Schematic representation of the discrete motion approach (downward motion case). Colors represent possible trajectories and domains used for the simulation.

Implementation

The discrete motion feature in Serpent has two main components: the composition shuffling and the pebbles' recirculation handling. Changing the domain of pebbles was also examined. For this implementation, some simplifications needed to be done, as explained below.

A simplified illustrative example of a discrete motion step with a two-dimensional PBR and nine compositions is shown in Figure 4-2 (the direction of pebbles is only an example and can be changed as needed). In this example, pebbles 1 to 6 move down by one vertical slot after one step. Pebbles 7, 8, and 9 are tested for burnup: 7 and 9 are reinserted at the other extremity in a randomly selected trajectory; 8 is discarded, and its composition is replaced with fresh fuel concentrations while keeping the same index to reduce the number of materials to initialize in Serpent. The pebble positions are fixed, and compositions move downward in a discrete way. Bottom pebbles recirculate and are tested for burnup. Pebbles are reinserted in a random position at the top — pebbles changing trajectory change domain and their data must be communicated between the domains.

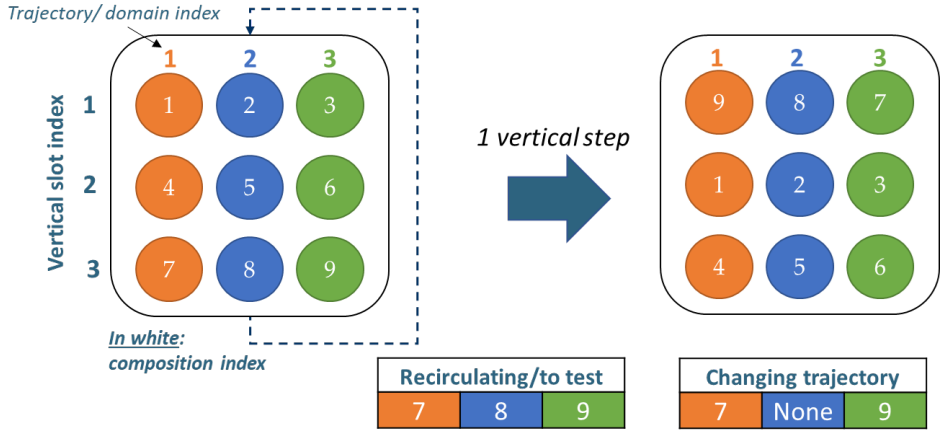

Figure 4-2: Example of discrete motion for a two-dimensional PBR. Composition IDs are shown in white.

Compositions shuffling

The capabilities of reading and modifying compositions in Serpent 2 were implemented as follows. When using the automized division of materials that Serpent applies to create the pebbles from the input pebble bed file, the parent fuel material is divided into identifiable zones, each having a specific ID number corresponding to a specific composition. These composition IDs are sorted in the same order as how the positions are defined in the explicit stochastic geometry and are stored in the ID vector $I^{(0)}$. The routine was modified so that at any step k>0, Serpent reads the current ID order $I^{(k-1)}$ in which compositions are and the new ID order $I^{(k)}$ in which compositions should be, and calculates a transition operator $T^{(k)}$ with the following equation:

$$I^{(k)} = T^{(k)} I^{(k-1)} \qquad (2)$$

Then, a new list of fuel materials is created from the current one based on the transition operator. This method can be applied to any reactor or geometry as long as the zone numbering is managed correctly. For this application, compositions are vertically shuffled at each step, replicating an upward or downward motion based on the type of PBR.

Pebbles recirculation handling

Most PBRs are envisioned to apply a MEDUL fuel management scheme, meaning when a pebble reaches one end of the core, it must be discharged, tested for burnup, if needed, replaced by fresh fuel, and reinserted at the other end. Therefore, it is necessary to account for pebble recirculation to represent this operation accurately. Discrete motion reproduces such behavior by assigning the composition of a recirculating (or a fresh fuel composition) to a pebble ID located at the other extremity of the core. The position of the pebble can be pre-determined or, as more common, be randomly chosen.

The newly developed capability for pebble recirculation tracks the number of passes and tests pebbles against a preset discarding criterion. Options for this criterion include a maximum burnup value, a maximum quantity of a set isotope (e.g., ^{137}Cs), or a maximum number of passes the pebble can go through the core (these different options are not all realistic but instead include criteria that have been used in other tools and benchmarks). The composition of discarded pebbles is stored in a separate data file for used-fuel characterization.

Pebbles changing domain

One key enabling feature for HxF is Serpent's domain decomposition method for burnup. In order to reduce memory requirements, Serpent splits the volumes to burn into multiple zones (domains) and distributes them among the computing nodes. Domains are continuous (cuboids, cylinders, or wedges), and material information is not shared across domains. In practice, this method results in a division of the memory requirement, largely dominated by materials data, by the number of domains used. Still, when discrete motion is applied, it occurs that materials move from one domain into another. To overcome this issue, data of materials that change domain are stored in an external file that is then read to populate the target domain. This process increases computing time by roughly 40% due to the communication between domains during transport when a neutron coming from a domain interacts with a material in another domain and data processing. Nevertheless, the benefits of domain decomposition in terms of drastic memory reduction greatly overshadow the additional time.

Simplifications

At this stage, the methodology illustrated above includes some simplifications. In addition to limiting pebbles to only occupy set positions, it is typically assumed that pebbles move as vertical channels without cross-mixing [34, 37, 73]. Furthermore, changes in the core geometry, such as the conic regions typically found in PBRs, are not considered. These limitations are not intrinsic to the discrete motion model but would require significant changes to the method; therefore, it was decided to address them in future work employing DEM. Although it is possible to maintain a more realistic pebbles distribution in the core, they are typically arranged in a regular lattice. This simplifies the generation of motion sequences without significantly affecting the expected results

due to the large neutron diffusion length in the system.

Application to a small-scale case

Test case model

A simplified small-scale FHR case, shown in Figure 4-3, is created to prove the feasibility of the discrete motion based on the individual depletion approach. The core consists of a thermally homogeneous reflected cylinder containing the pebble bed. This pebble bed is modeled as an FCC lattice of graphite pebbles, all containing the TRISO fuel, initially fresh. In addition, random initial ^{137}Cs concentrations are assigned to each pebble, ranging from 0 to the threshold value. This initialization step avoids a batch-like refueling behavior, as a uniform bed would similarly accumulate burnup regardless of the pebbles' history, and pebbles would all be discarded and simultaneously replaced, repeating this phenomenon for each refueling cycle. Instead, pebbles are gradually replaced, even if they are fresh. The impact of virtual ^{137}Cs concentrations on the overall neutronics of the core is assumed to be negligible. Essential information about the core geometry and materials is summarized in Table 4-1. Using HALEU-level enrichment, such a small core cannot be critical. However, it serves as a proof of concept, and a more realistic application is made in Chapter 6.1.

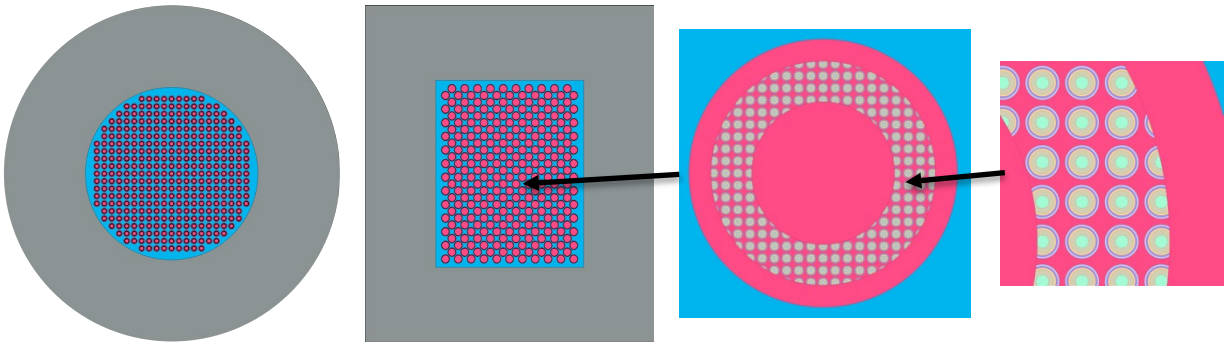

Figure 4-3: Core geometry representation: (a) cross-sectional view, (b) longitudinal view, (c) pebble model and (d) TRISO particles lattice.

The simulation is computed for 300 burnup steps with a time step of 4.75 days. For every burnup step, pebbles uniformly move vertically by two slots, each spaced by 4.551 cm. Therefore, the pebble bed has a flat velocity profile, and the operation is equivalent to 46 complete core passes. Each step uses a constant extrapolation and linear interpolation as predictor/corrector method and runs the history of 20,000 neutrons during 1000 active and 200 inactive cycles, respectively. This number was chosen to ensure the convergence of the fission source and results. Given the small scale of the simulation, an arbitrary ^{137}Cs concentration threshold of 3.0625×10^{-5} at/b.cm is applied. Therefore, if a pebble's ^{137}Cs concentration is higher than this limit when recirculating, it is discarded, stored as waste, and replaced by a pebble with a fresh composition (and a zero ^{137}Cs concentration).

Table 4-1. Core geometry and materials parameters.

Core (cylinder)	
Total Power	5.41 MW
Number of pebbles	4,849
Temperature	900 K
Height	62.5 cm
Radius (active)	26.25 cm
Reflector thickness	25 cm

Pebbles	
Lattice structure	FCC (characteristic length = 2.275 cm)
Layers	Central graphite, fuel+matrix, graphite shell
Layers Radii (cm)	1.25, 1.4, 1.5

TRISO particles	
Lattice structure	SC (characteristic length = 0.0886 cm)
Layers	Fuel, buffer, in. PyC, SiC, out. PyC, matrix
Layers Radii (cm)	0.02, 0.03, 0.0335, 0.0370, 0.0405
Form	$UO_{1.5}C_{0.5}$
Enrichment	19.9 wt-%
Density	10.5 g/cm^3

Results

The results shown in this section demonstrate the high-fidelity depletion method with discrete motion.

Core-wise parameters evolution

The evolution of global operation-related parameters is crucial for design purposes and can be extracted. The behavior of the core with time is shown in Figure 4-4 through the evolution of the effective multiplication factor, conversion ratio, and power peaking factors. It is important to note that such a small core, even though filled with fresh fuel, is not a critical configuration and that the order of magnitude of the values shown here is not representative of a real, full-scale core.

^{135}Xe buildup first results in a steep decrease in the effective multiplication factor and an increase in the conversion ratio. However, the peaking factor does not drastically change because this buildup simultaneously happens in all pebbles. After this drop, the multiplication factor keeps decreasing until it reaches a steady state after around 140 effective full-power days (EFPD). This evolution indicates that the core is approaching equilibrium. Two competing factors play a role in this phenomenon.

On the one hand, pebbles that were assigned a high ^{137}Cs concentration at the beginning of the operation are quickly discarded when recirculating. These pebbles are then replaced by fresh, more reactive fuel. This phenomenon is purely caused by the core initialization method used. On the other hand, the core, initially fresh and with reactivity at its maximum, sees the fuel in its pebbles being consumed, fission products accumulating, and fissile materials being depleted. Therefore, the reactivity tends to decrease. However, since a fuel utilization threshold is applied, fresh pebbles replace the most burnt pebbles, and the multiplication factor stabilizes to a value of 0.46284 ± 31 pcm after 140 EPFD.

The power peaking factor stays relatively constant, with an average value of 1.207 ± 0.013 and

values ranging between 1.182 and 1.284. The maximum value can be found at t=290 days, where the maximum pebble power is 6.3% higher than the average maximum pebble power and is located at the edge of the core.

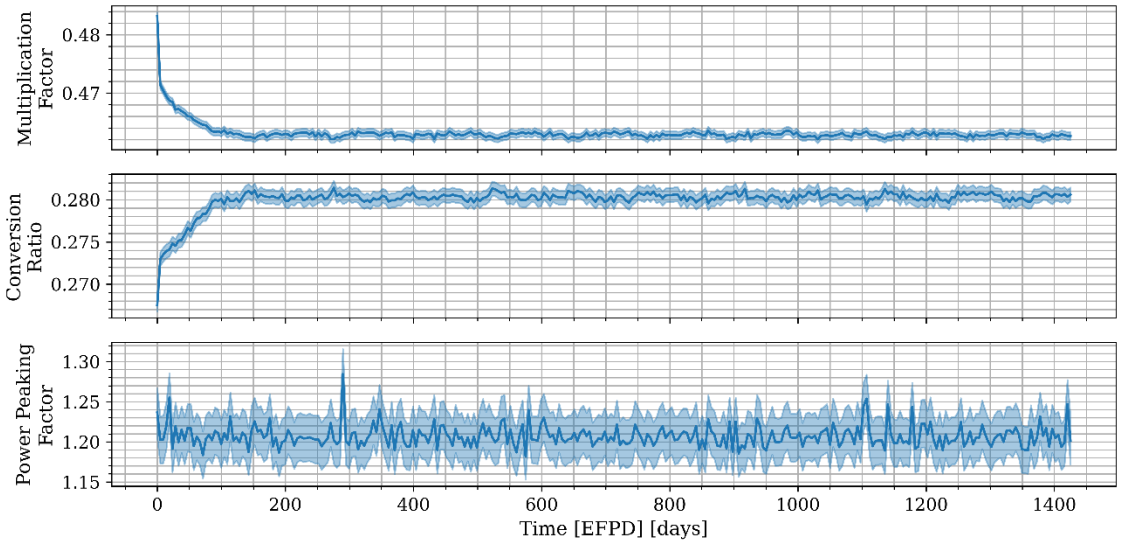

Figure 4-4: Evolution of core-wise parameters factor with time: multiplication factor (top), conversion ratio (middle) and power peaking factor (bottom). Each curve is plotted with its corresponding error (3σ).

Flux distribution

Pebble-wise data is available as well, providing valuable information about the operation. For instance, the flux distribution is shown in Figure 4-5 for thermal (E < 1.86 eV), epithermal (1.86 eV < E < 0.1 MeV), and fast (E >1 MeV) energies at the last step for t=1425 days. The thermal flux distribution logically replicates the behavior found in the static depletion calculation (Chapter 3.3). Because of the relatively small size of the reactor compared to the large diffusion length of neutrons in graphite, they primarily tend to reach the reflector, which moderates them. After probable scattering events, they re-enter the core with less energy and are more likely to react with pebbles at the edges of the core. This explains the large thermal flux found around this peripheral region. Then, since the geometry of the reactor is cylindrical, the neutrons are more densely concentrated at the center of the core and preferentially leak from the corners, leading to higher central values and lower values at the corner of the cylinder. The epithermal and fast fluxes show purely geometric distributions, where values decrease as they are further from the cylindrical core center. The orders of magnitude of the flux values show a rather hard spectrum for an FHR. The presence of higher neutron energies than commonly found in PBRs is caused by the small number of pebbles within the core.

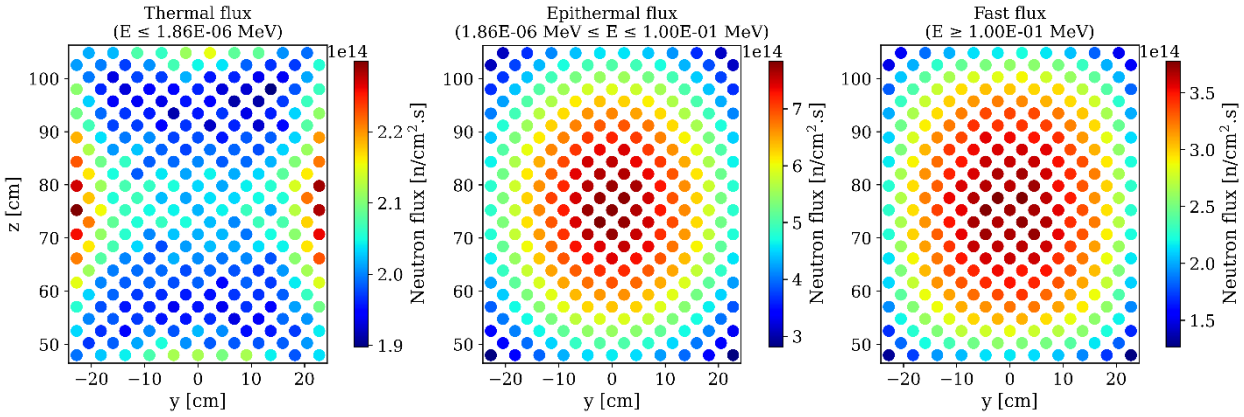

Figure 4-5: Cross-sectional thermal (left), epithermal (center) and fast (right) flux distribution at x=0 cm and t=1425 days.

Evolution of the power and burnup distributions

Radial and axial core-averaged profiles are obtained by averaging values at the same radial or axial distances over the core for pebble-wise burnups and power densities. This process is repeated for each burnup step after equilibrium (t > 140 days). Then, profiles are averaged to produce representative equilibrium profiles, shown in Figure 4-6. It also provides information about data noise at equilibrium due to pebble motion.

As the thermal flux distribution suggested, the radial profile shows peaked powers at the edge of the core, slightly higher values at the center, and lower values in between. The radial and axial peaking factors on the average profile are 1.07 and 1.04, respectively, with standard deviations ranging from 2.25 to 4.75 MWd/kg, showing that they are not strongly peaked and do not drastically vary with time. Regarding pebbles' burnup, the radial profile is flat with a peaking factor of 1.02 but has high standard deviations of around 6 MWd/kg over the whole core. Both are caused by the random recirculation process, leading to fresh pebbles neighboring used pebbles at any time of the cycle, flattening the average profile but producing strong variations in the pebbles' spatial distribution. The axial profile shows substantial variations with the same order of magnitude for the same reasons. However, it increases from top to bottom (peaking factor of 1.27) due to the nature of the recirculation: in this FHR, fresh pebbles are inserted from the bottom, hence decreasing the average burnup, and pebbles accumulate burnup as they move up the core, explaining increasing values. The step-like variations observed in this plot are due to the FCC lattice approximating the pebble bed geometry. The low threshold applied on a small core and the effect of averaging cause the low values for the burnup profile. In fact, the maximum burnup values are found to be around 20 MWd/kg, as described in the next section.

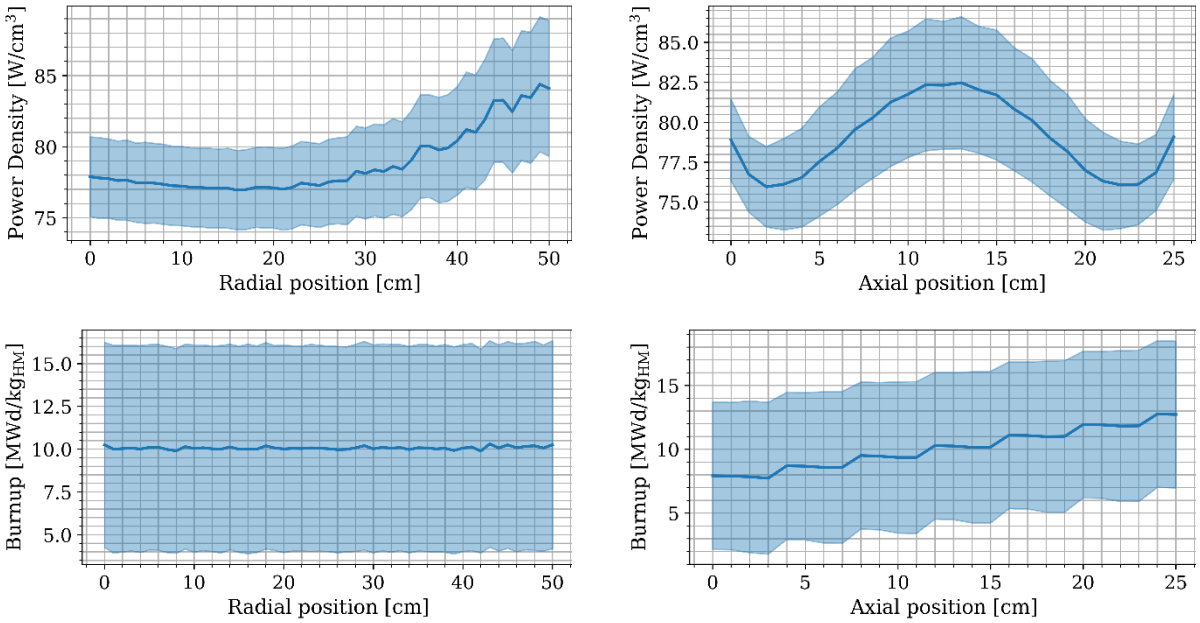

Figure 4-6: Radial (left) and axial (right) power density (top) and burnup (bottom) average profiles and standard deviation at equilibrium (t > 140 days).

Another way to analyze the core content with time is to study the statistical distribution of key parameters. For instance, the burnup distribution in Figure 4-7 indicates that pebbles are close to uniformly distributed. There are slightly more fresh pebbles caused by the burnup step size used in this application. Some pebbles have higher burnups than 20 MWd/kg, close to the applied threshold in practice. Indeed, if a pebble's burnup value is slightly below the threshold value when recirculating, it goes through an extra pass, and its burnup increases before being discarded.

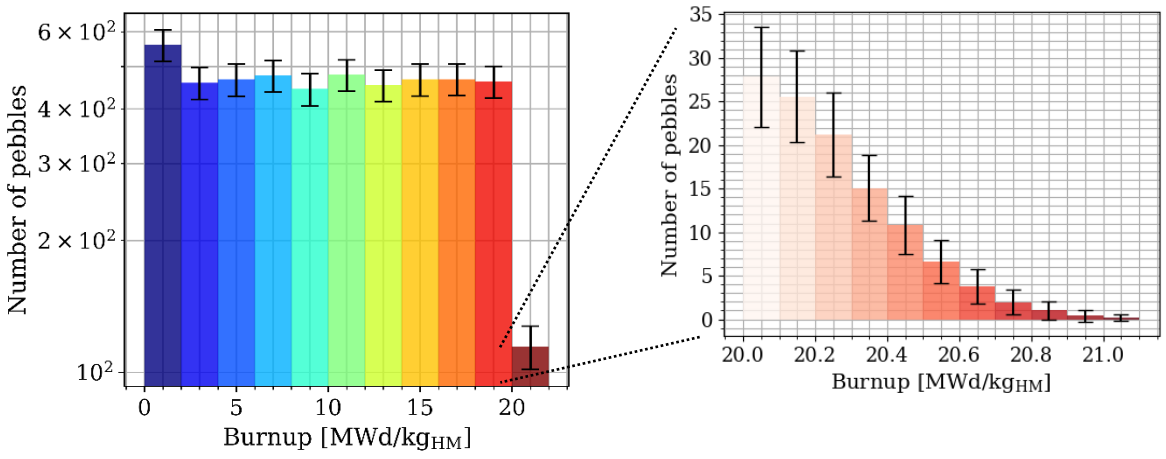

Figure 4-7: Pebble's burnup statistical distribution in the core and standard deviation at equilibrium (t > 140 days). Pebbles with higher burnups than 20 MWd/kg$_{HM}$ are more finely shown in the right chart.

Discarded pebbles content

Finally, discarded pebbles data is analyzed by studying their statistical distributions. Pebbles inserted once equilibrium is reached are considered, and the rest of discarded pebbles are neglected. Each pebble went through 4 passes before being discarded and had a residence time in the core of 123.5 days. This uniform residence time reflects the simplified case used in this study: simple geometry, flat velocity profile, small number of pebbles, and arbitrary threshold value. The ^{137}Cs to burnup ratio for each discarded pebble is calculated and shows a strong correlation between the two parameters, with an average value of 1.53e-06 ± 2.34e-10 $\frac{\text{at/b.cm}}{\text{MWd/kg}_{\text{HM}}}$. Therefore, a threshold of 3.0625×10^{-5} at/b.cm corresponds to a burnup threshold of 20.016 ± 0.003 MWd/kg$_{HM}$.

Figure 4-8 shows a set of relevant parameters for fuel utilization (burnup value, ^{235}U, ^{239}Pu, and ^{137}Cs concentrations), waste management with high activity fission products [74] (^{144}Ce, ^{137}Cs, and ^{90}Sr), or fuel performance with abundant fission products applying pressure in TRISO particles [75] (Xe and Kr total concentrations).

It can be observed that most parameters have a similar distribution to burnup. Maximum concentrations are reported. Representative waste pebbles can be extracted from such plots for feeding other models. For example, burnup values range from 20.22 to 22.13 MWd/kg, with a maximum value of 6.02% higher than the average burnup found in discarded pebbles. This difference is expected to be more significant when full-scale cores with higher accumulated burnup per pass and burnup thresholds are studied using this approach.

4.2 Application of discrete motion to a full-scale HTGR [65]

The capabilities of HxF with discrete motion are demonstrated by determining the equilibrium composition for a full-scale HTGR core. The model, depicted in Figure 4-9, incorporates typical geometry, dimensions, and material compositions based on the PBMR–400 design. Cycles and thermal-hydraulic parameters are arbitrarily assumed. Table 4-2 provides dimensions, materials, and other data. Although certain parameters are sourced from design documentation [76], it is important to note that this study serves as a demonstration of HxF capabilities and does not aim to establish a benchmark solution. To match the assumptions made for discrete motion, the geometry is simplified with a fully cylindrical active region surrounded by 90 cm-thick axial and radial reflectors and a 100 cm-radius inner graphite reflector. The resulting 1100 cm-high, 85 cm-wide pebble bed contains 451,360 pebbles. At the top of the bed is a 50 cm-high He-filled space. Pebbles are distributed in a face-centered cubic (FCC) lattice. The fuel is in the form of 9.8 wt%-enriched UO_2 kernels contained in a simple cubic lattice of 15,000 TRISO particles without clipping. The fuel temperature is set at 1,200 K, whereas the rest of the materials are assumed to have a uniform temperature of 900 K. Although the methodology can use a velocity profile, a flat profile is assumed for simplicity, meaning that pebbles belonging to the same row move with the same velocity.

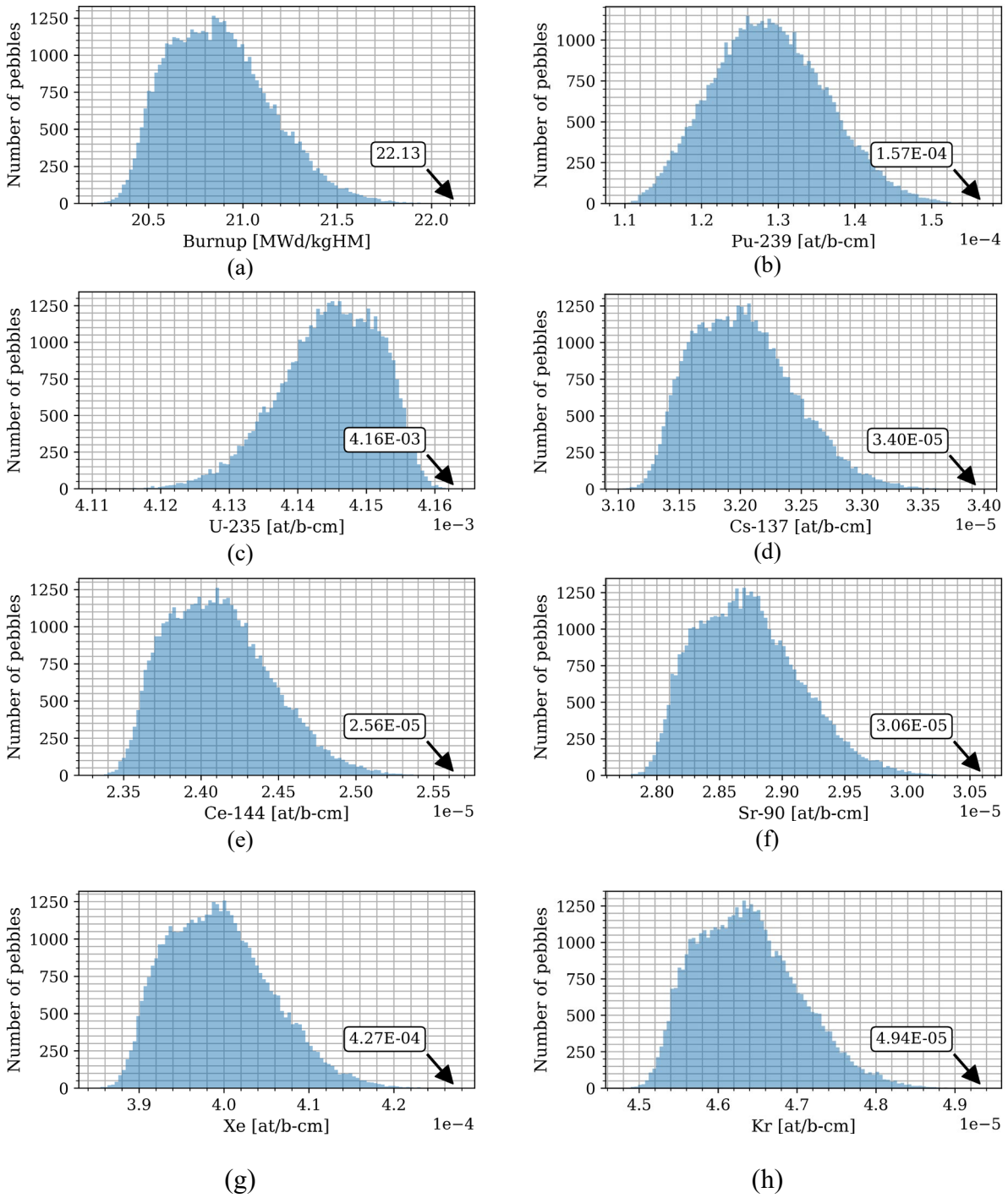

Figure 4-8: Statistical pebbles distribution for (a) discard burnup, (b) discard ^{239}Pu, (c) ^{235}U, (d) ^{137}Cs, (e) ^{144}Ce, (f) ^{90}Sr, (g) total Xe, and (h) total Kr concentrations respectively.

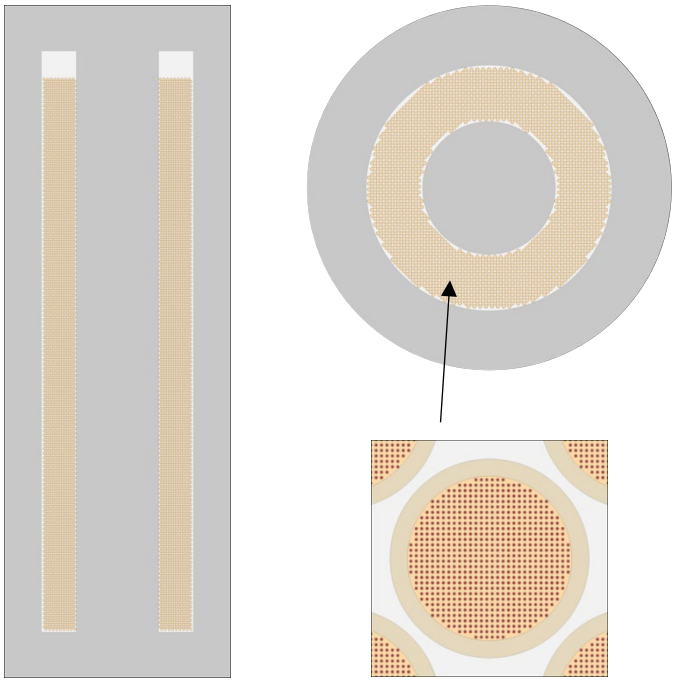

Figure 4-9: Test case model vertical (left) and horizontal (top right) cross section and pebble model (bottom right).

Motion sequence

As aforementioned, the shuffling of the compositions is based on a pre-determined series of ID lists reproducing the motion of the pebbles. The motion sequence is relatively simple since the bed is arranged in an FCC lattice. The bed at step k is represented as a matrix $M^{(k)}$ in which each row corresponds to axially aligned pebbles, and each column corresponds to radially aligned pebbles. With this representation, the matrix element $m_{i,j}^{(k)}$ corresponds to the composition at the slot of respective row and column indices i and j, at step k. Every two consecutive rows in the FCC lattice are labeled with the same index. The matrix is sorted in ascending index order, and a downward shift of compositions is applied from one step to the next. The magnitude n of the vertical shift (i.e., the number of rows by which compositions are shifted) depends on the selected size for the burnup step. Therefore, if the overall matrix of the bed is of size (N_r, N_c), the top $N_r - n$ rows are shifted downward, and the bottom n rows are moved to the top of the bed. Assuming the first pebble out is the first in and radial insertion is not controlled, the recirculated pebbles maintain the same stratification but are randomly reassigned to a column. The correlation between two consecutive steps can then be represented as follows (where $i = 0$ is the bottom row):

$$m_{i,j}^{(k)} = \begin{cases} m_{i+n,j}^{(k-1)} & \forall i \in \{1, N_r - n\}, \forall j \in \{1, N_c\}, \forall k > 0 \\ m_{i-N_r+n,j'}^{(k-1)} & \forall i \in \{N_r - n + 1, N_r\}, \forall j' \in \{1, N_c\}, \forall j \in \{1, N_c\}, \forall k > 0 \end{cases} \quad (3)$$

Table 4-2: Test case parameters [76].

Component		Parameter	Value
Core		Total Power	400 MWth
		Active height	1100 cm
		Total core height	1150 cm
		Inner reflector radius	100 cm
		Active radius	185 cm
		Outer reflector thickness	90 cm
		Non-fuel temperature	900K
Pebbles	Bed	Number of pebbles	451,360
		Packing fraction	61.0%
		Layout	FCC
		Pitch	3.115 cm
		Uniform pebbles velocity	10.87 cm/day
		Discharge rate	4514 pebbles/day
	Matrix/Shell	Graphite density	1.704 g/cm^3
		Graphite shell density	1.750 g/cm^3
		Pebble outer radius	3.0 cm

Component		Parameter	Value
TRISO	Lattice	Layout	SC
		Number of TRISO	15,000
		Packing fraction	9.1%
		Pitch	0.0804 cm
	Fuel	Outer radius	0.02 cm
		Form	UO_2
		Enrichment	9.8 wt%
		Temperature	1200 K
		Density	10.4 g/cm^3
	Buffer	Outer radius	0.03 cm
		Density	1.050 g/cm^3
	IPyC	Outer radius	0.0335 cm
		Density	1.900 g/cm^3
	SiC	Outer radius	0.0370 cm
		Density	3.180 g/cm^3
	OPyC	Outer radius	0.0405 cm
		Density	1.900 g/cm^3

The new state $M^{(k)}$ is then converted into the $I^{(k)}$ vector and written to a step-dependent file which the Serpent discrete motion routine uses:

$$I^{(k)} = \mathrm{vec}\left(M^{(k)}\right), \forall k \quad (4)$$

Additionally, the slots which contain recirculating compositions (i.e., of the n last rows) are stored in a recirculation file for assessment against the discharge criterion. It is to be noted that the motion sequence does not perform discharge and refueling. The Serpent 2 shuffling routine entirely handles this process. The motion sequence can be changed based on the specific geometry

and flow direction, and it uses indices generated with any external method, regardless of complexity.

The test described here assumes N_r=124 rows, and N_c=3640 columns (or trajectories). An initial motion step of n=61 is set to accelerate convergency towards the equilibrium core. Then, finer motion steps of n=11 are applied. Such a step corresponds to a shift of 96.5 cm. That means 8.9% of the bed is recirculated at each step, and given the pebble velocity, each burnup step lasts 8.9 effective full power days.

Computational setup

Along with the described sequence and between each motion step, a transport and depletion calculation is run by Serpent to determine the neutron population distribution, interactions with core materials, and resulting changes in compositions. The ENDF/B-VII.0 nuclear data library [61] is loaded once at the beginning of the simulation and stored throughout, obviating the need for reloading. Drawing from insights gained in Chapter 3.2, domain decomposition and pebble-wise automated burnable materials division are employed. These options facilitate the definition of a unique parent fresh fuel material, which is then efficiently subdivided into individual zones per material. This approach simplifies the input process, reduces simulation and memory requirements, and streamlines the overall computational workflow.

Additionally, Serpent optimization mode 1 is applied, utilizing a non-unionized energy grid and performing on-the-fly cross-section calculations through the direct tally approach. This choice further mitigates memory demands, enhancing computational efficiency. Starting from an initial random fuel composition, coarse steps are applied with 10^6 inactive and 10^7 active neutrons. Once a first equilibrium is obtained with this high uncertainty, large motion step sequence, a new simulation with 10^7 inactive and 10^8 active neutrons is run. Seventy full passes are simulated, each corresponding to 100 days, and the discarding criterion for pebbles is based on ^{137}Cs concentration, whose threshold value is set at 2.2238x10^{-4} mol/pebble, which roughly corresponds to a desired threshold value of 92 MWd/kg$_{HM}$. No predictor/corrector scheme is used in this study. Instead, a non-iterative depletion method is applied.

Results

This section illustrates some results obtained using HxF with discrete motion for the HTGR test case. In particular, it discusses the convergency to equilibrium and analyzes the equilibrium parameters for in-core and discarded pebbles.

Statistical considerations

Determining the convergence criteria is essential when searching for equilibrium in a PBR. Two different metrics were used in this work. First, the evolution of global parameters, such as the multiplication factor k_{eff} and the conversion ratio (CR), indicate the reactor's overall state. In this context, the equilibrium state is determined when these parameters have consistent trends with the fine motion step for three complete core cycles. Figure 4-10 shows how these two parameters have similar behaviors.

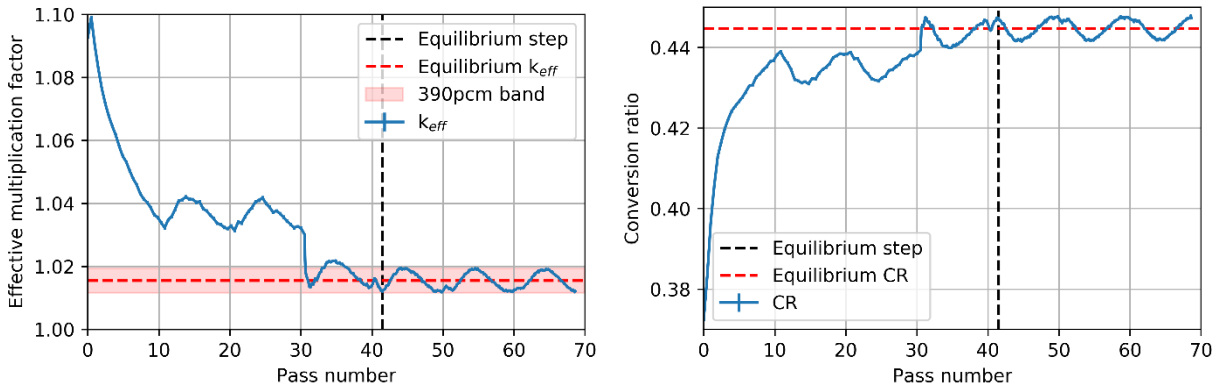

Figure 4-10: Evolution of global core parameters as a function of passes: multiplication factor (left) and CR (right).

A first oscillatory trend is observed from 10 to about 30 passes. Oscillations result from motion steps substantially larger than the diffusion length of neutrons in the core. This first simulation stage with large burnup is beneficial to decrease the computing time to reach equilibrium. Then, a drastic reduction in the burnup step was applied, resulting in smaller motion steps. As soon as this step size reduction happened, the multiplication factor dropped by around 1500 pcm, and the CR increased by 7×10^{-3}. This trend is explained by the lower number of fresh pebbles inserted into the core. Although some oscillatory behavior remains, the core is considered in an equilibrium state when the multiplication factor stays within a band of ±390 pcm, that is, after 42 passes. Oscillations are most likely caused by the dynamic nature of PBRs operation with pebbles motion. However, they can be influenced by the statistical uncertainty of the transport processes and the discrete nature of depletion calculations with batches of fresh pebbles inserted and used pebbles discarded. Every simulated step after this is regarded as an equilibrium state with a different configuration. In the results presented below, equilibrium average values refer to the average of a given quantity over 297 states (corresponding to 27 passes), whereas representative values for a single state refer to the last equilibrium state simulated. The average equilibrium multiplication factor and CR are 1.01554 ± 18 pcm and 0.44472 ± 14 pcm, respectively.

Further evidence of achieved equilibrium is sought by analyzing discarded pebbles. Figure 4-11 shows the evolution of the number of discarded pebbles (thus, of the inserted fresh pebbles) as a function of the total number of passes simulated. The value oscillates around 4,088 pebbles per step, between 3,640 and 4,566, corresponding to about 410 to 515 pebbles/day. Once again, these variations are interpreted as small enough to assume an equilibrium state. The increase of the discarded pebbles at around 50 passes matches the one of the multiplication factor previously observed. Figure 4-11 also shows the average burnup per pass and how this value, after reaching equilibrium, remains almost constant at around 9.85 MWd/kg_{HM}.

Overall, it is to be observed that the criteria set to determine equilibrium are arbitrary. Given the stochastic nature of PBRs, a core at equilibrium will always present an oscillatory behavior; therefore, it will have to be the responsibility of the modelers to apply their best judgment in determining acceptable criteria for equilibrium.

In terms of computational requirements, after a 36.9-minute initialization, the average transport process time for the initial depletion steps is 2.3 minutes, whereas for subsequent more accurate steps it increases to 19.6 minutes. The burnup and data processing times are relatively shorter, taking 1.2 and 1.1 minutes, respectively. The overall simulation time, conducted on 20 2.1 GHz Intel Xeon Gold 6230 nodes, amounts to 148 hours. Each node is allocated 18.7 GB of memory, with the majority utilized for domain materials data (55.7%), cross sections (25.2%), and calculated and tallied results (9.0%). The remaining memory corresponds to miscellaneous data.

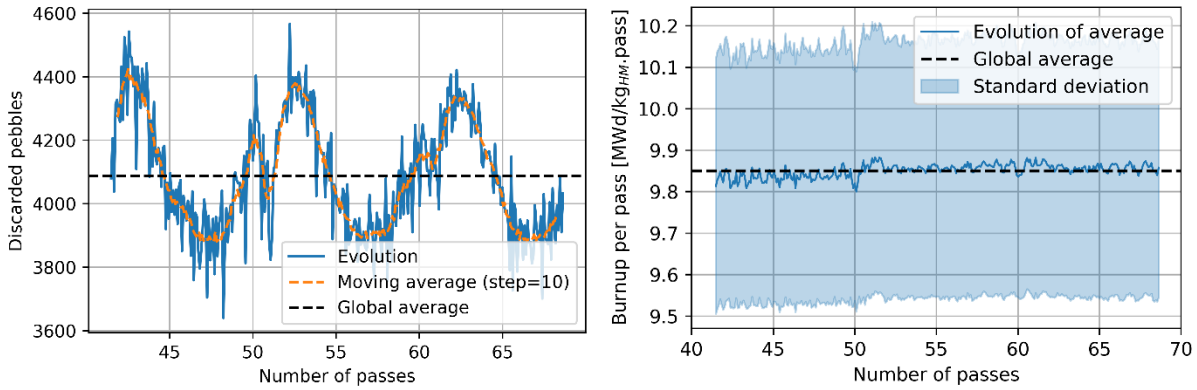

Figure 4-11: Evolution of global discarded pebbles parameters as a function of passes: number of discarded pebbles (left) and average discarded pebbles burnup, normalized by the number of passes (right).

Performing Monte Carlo calculations in large-scale models requires quantifying statistical uncertainties. First, the multiplication factor is not a limiting factor for the test case. The maximum statistical uncertainty obtained during fine steps is 22 pcm, which is small compared to the parameter variations. The main reason for simulating many neutron histories lies in the statistical uncertainty of pebble-wise detectors, such as the flux and power tallies. The highest values are found in pebble-wise power tallies due to the small size of the TRISO particles in which fissions are scored. The results are summarized in Table 4-3. Most pebbles (95%) have less than 6% uncertainty on the neutron flux and less than 12% on power.

Nevertheless, as Figure 4-12 suggests, the highest uncertainties are, as one can expect, at the bottom of the core, where there is the lowest number of neutron/nuclide interactions. This zone corresponds to where the fuel is the most burned and ready to be discharged, which results in lower power production. In addition, as the histogram shows more clearly, the fraction of pebbles having a high uncertainty in power and flux is small.

The statistical uncertainty could have a more significant impact on extreme, maximum, and minimum values. For example, when calculating the pebble power peaking factor, it is impossible to establish to what extent the value for maximum power is a real outlier or a statistical artifact. Nevertheless, Figure 4-13 shows that the pebble peaking factor only changes by roughly 5% when calculated using as peak the single highest power value and when using as peak the average 100 highest values. The same is true for neutron flux.

Table 4-3: Summary of statistical uncertainties in pebble-wise detectors.

Detector	Average	Standard Deviation	Minimum	Median	75% Percentile	95% Percentile	Maximum
Thermal flux (E<1.86 eV)	2.3%	0.9%	1.0%	2.0%	2.7%	4.3%	6.7%
Epithermal flux (1.86 eV < E < 0.1 MeV)	2.5%	0.9%	1.1%	2.1%	2.9%	4.5%	8.6%
Fast flux (E>0.1 MeV)	3.4%	1.2%	1.5%	3.0%	3.9%	5.9%	12.8%
Power	7.4%	2.1%	3.1%	6.7%	8.3%	12.0%	22.9%

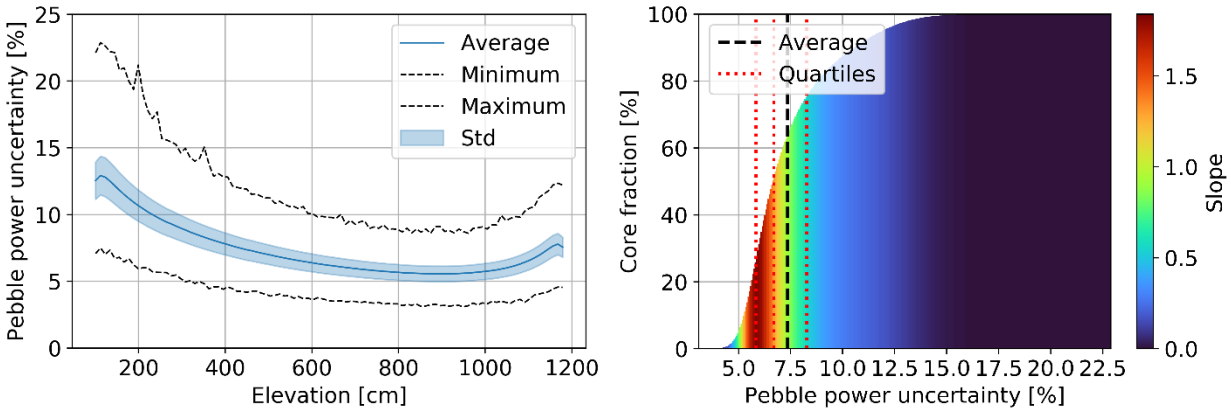

Figure 4-12: Axial profile (left) and cumulative statistical distribution (right) of the pebble-wise power statistical uncertainty.

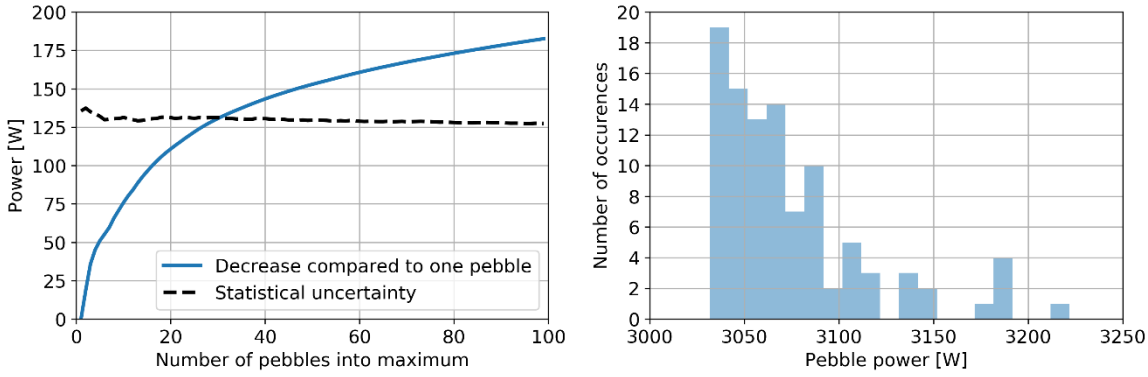

Figure 4-13: Evolution of the maximum power and its associated statistical uncertainty at equilibrium as a function of the number of values averaged to obtain this maximum power (left) and maximum 100 pebble-wise powers found at equilibrium (right).

In-core equilibrium data

The following subsections summarize the distribution of key in-core parameters at equilibrium, such as neutron flux, burnup, and power. It is essential to understand that the data depends highly on how many times pebbles went through the core. In fact, as the discard criterion is based on the content of ^{137}Cs in the pebble, the number of passes varies depending on the individual history. Table 4-4 provides the count of pebbles in the core over multiple equilibrium representations grouped by pass number. Pebbles are almost evenly distributed between 1 and 9 passes, each accounting for around 10% of the core. Pebbles at the 10^{th} pass, instead, make up 8.2% of the total inventory, and an 11^{th} pass is highly improbable. This suggests that pebbles are mostly discarded after 9 and 10 passes, and very few go through the core for 11 passes. Additional discussion on this matter is provided later on concerning discharge burnup.

Table 4-4: Average in-core pebble inventory over multiple equilibrium states.

Pass number	Average number of pebbles	Pebbles fraction [%]
1	46,152	10.2
2	46,206	10.2
3	46,264	10.2
4	46,224	10.2
5	46,076	10.2
6	45,892	10.2
7	45,802	10.1
8	45,811	10.1
9	45,889	10.2
10	37,031	8.2
11	14	3E-03
Total	**451360**	**100.0**

Neutron flux

Figure 4-14, Figure 4-15, Figure 4-16, and Figure 4-17 show the spatial distribution of thermal (E<1.86 eV) and fast (E>0.1 MeV) neutrons in the equilibrium core. As expected, the thermal flux peaks near the radial reflector and toward the top of the core. Indeed, neutrons are thermalized by the reflector, and once they re-enter the core, they do not travel long distances before being absorbed. In addition, the hollow-cylindrical nature of the core leads to a geometrical peak around the axial and radial centers of the bed while leading to neutron leakage around the corners. However, since pebbles are inserted from the top and discharged at the bottom and due to the large accumulated burnup per pass, pebbles experience a more significant flux, both thermal and fast, towards the top of the core.

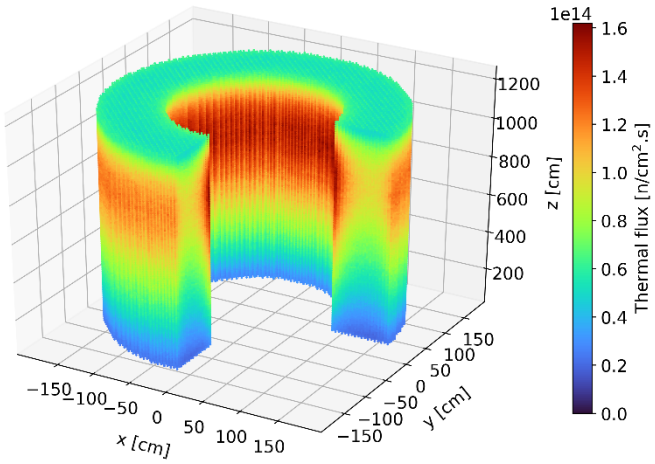

Figure 4-14: Thermal neutron (<1.86 eV) flux in each pebble in the core at a representative equilibrium step.

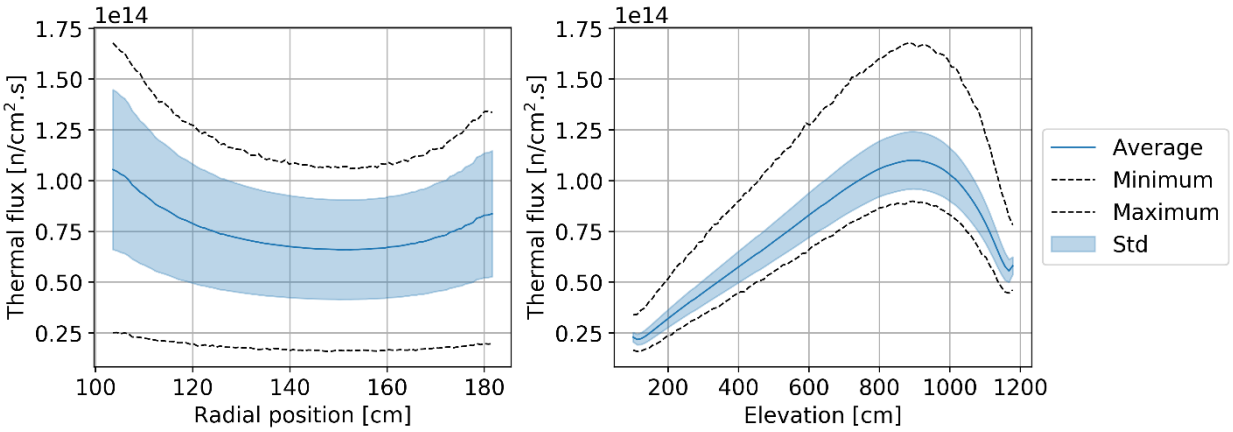

Figure 4-15: Radial (left) and axial (right) average thermal neutron (<1.86 eV) flux profiles at equilibrium.

Two observations can be made regarding the statistical distribution of the thermal flux per pass in the core at equilibrium, shown in Figure 4-18. Please note that in this plot and all other plots in this section showing per pass information, pass 11 does not appear because the sample size is too small to be visible. On the one hand, the thermal flux distribution is similar regardless of the pass number. On the other hand, the distribution shows clear flux peaks at around 0.2, 0.6, and 1.0 x 10^{14} n/cm^2.s.

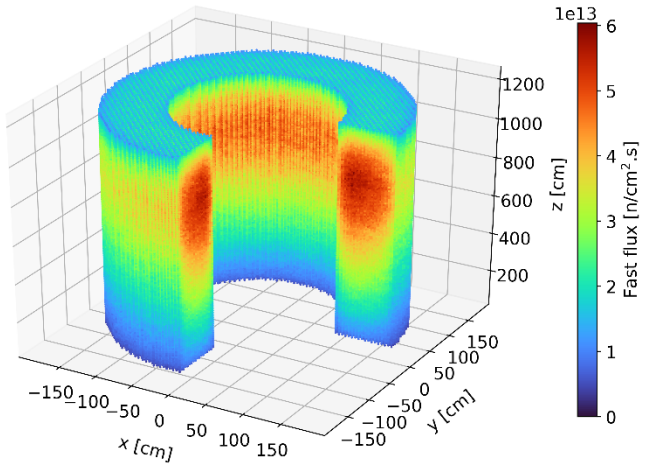

Figure 4-16: Fast neutron (>0.1 MeV) flux in each pebble in the core at a representative equilibrium state.

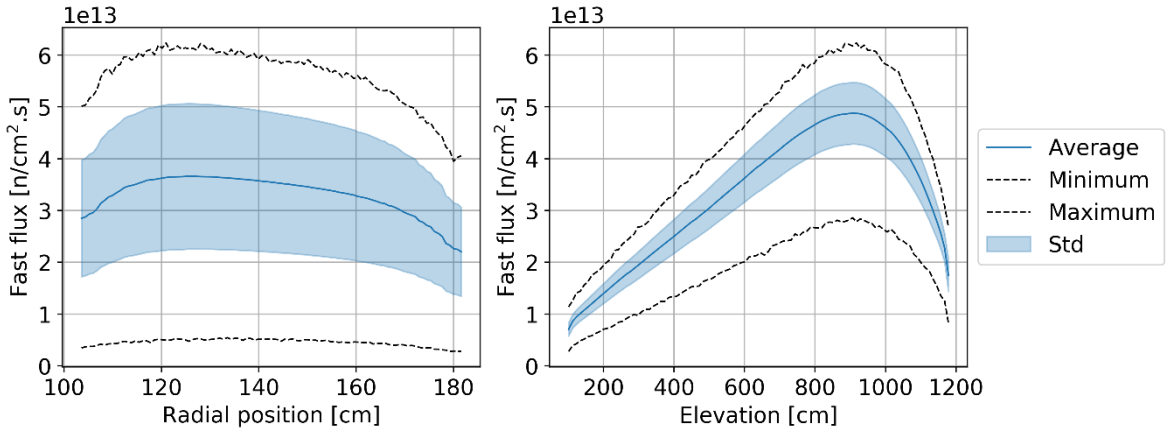

Figure 4-17: Radial (left) and axial (right) average fast neutron (>0.1 MeV) flux profiles at equilibrium.

Each of these peaks can be linked to identifiable core regions and is noticeable in Figure 4-14. The low peak corresponds to the bottom region of the core, with the most burned fuel and thermal leakage; pebbles with the median peak value are found at the top of the core and directly above the low peak region; the highest peak (which also has the highest value) corresponds to the central region where pebbles are sufficiently far from the reflector. Finally, a few pebbles at the core's top inner and outer edges experience the highest values. The same distribution for fast neutrons (Figure 4-19) shows that the maximum values slightly decrease with the number of passes.

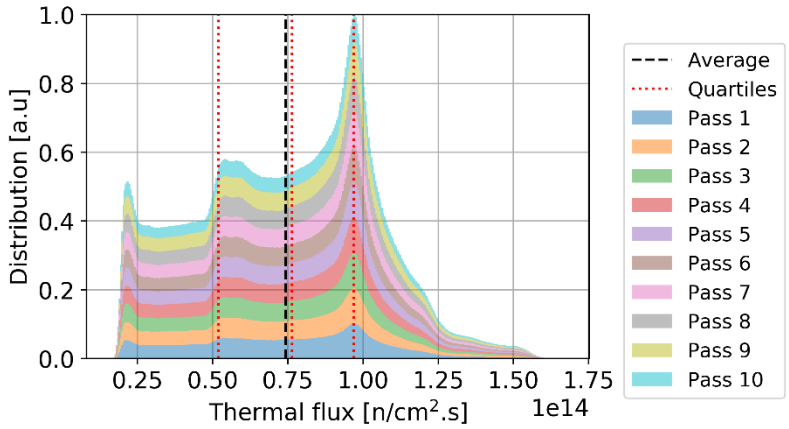

Figure 4-18: Cumulative thermal flux statistical distribution per pass over all equilibrium states, normalized over the maximum count (the envelope of the stack represents the global distribution).

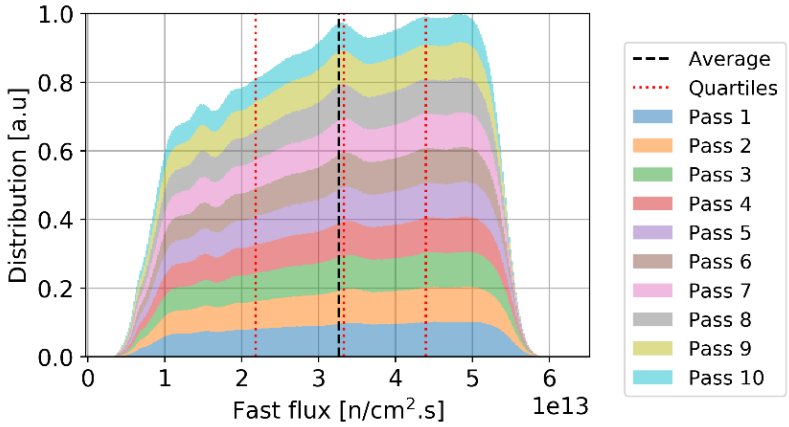

Figure 4-19: Cumulative fast flux statistical distribution per pass over all equilibrium states, normalized over the maximum count (the envelope of the stack represents the global distribution).

Fuel utilization

Figure 4-20 illustrates the spatial in-core distribution of burnup. The radial profile shows small peaks around the edges due to pebbles accumulating burnup more rapidly when closer to the reflector, particularly during the first four passes (Table 4-5). As pebbles are reinserted in a random radial location, the radial burnup profiles flatten with the number of passes. The axial burnup profile shows a monotonic increase behavior as pebbles descend through the core and accumulate burnup. The step-like behavior, noticeable mostly for pebbles in the first few passes, is artificial. It is caused by the discrete motion, moving less than $1/11^{th}$ of the core active height at each step. In any case, this artifact does not impact the trend and disappears as pebbles are randomly reinserted in different radial positions.

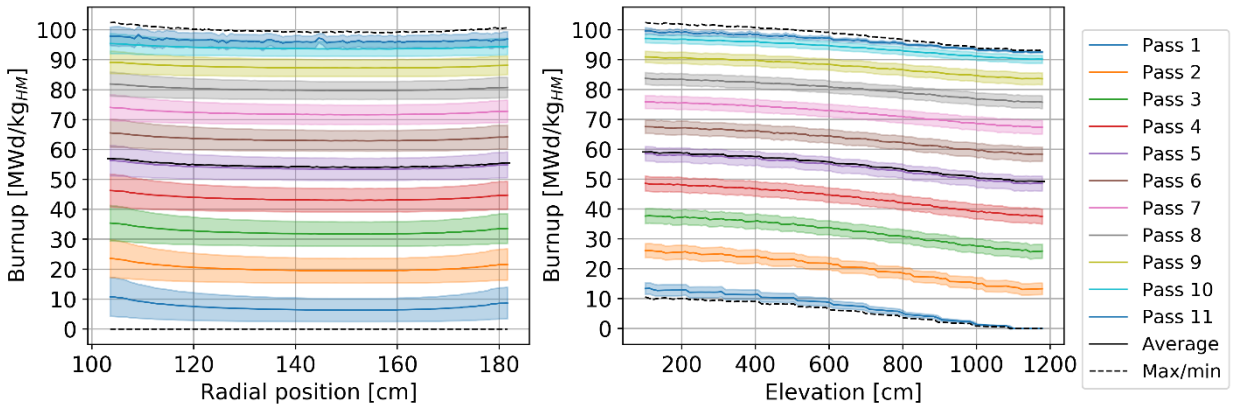

Figure 4-20: Radial (left) and axial (right) burnup profile per pass at equilibrium.

Figure 4-21 and Table 4-5 provide statistical data on burnup as a function of the number of passes. Two phenomena are worth noticing. First, the burnup distribution of pebbles during the first pass shows two anomalies: the large peak at zero burnup representing the fresh pebbles inserted in the core and the artificial multi-peak behavior due to the discrete motion approach. Second, the two peaks in the cumulative distribution at each pass result from each pass's discrete nature (real in this case) through the core. In other words, pebbles with different numbers of passes have overlapping burnups, which, when cumulated, generate patterns that are hard to attribute to a pass number if one does not have access to pass-dependent data.

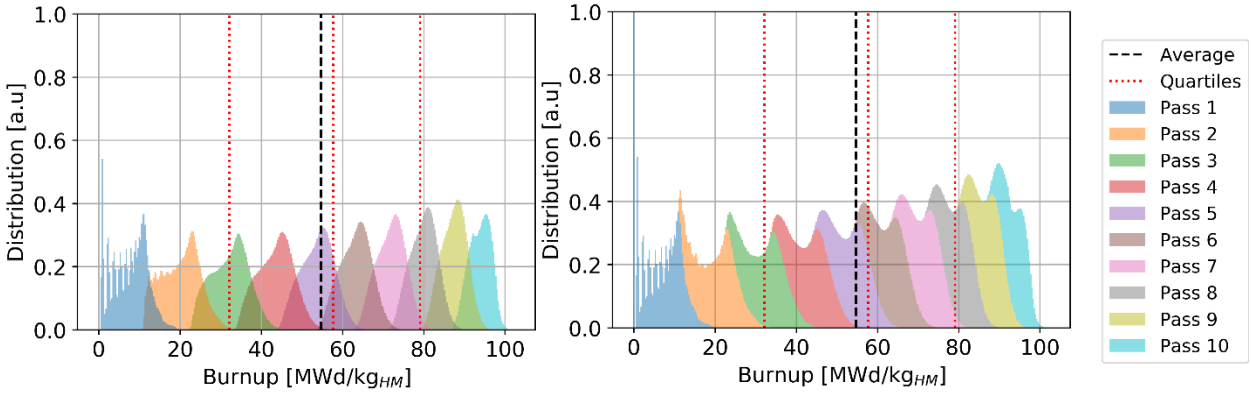

Figure 4-21: Burnup statistical distribution per pass over all equilibrium states, individual pass (left), and cumulative (right), normalized over the maximum count.

Power

Power production in each pebble is a critical in-core metric as high power production in a zone of the core leads to hot spots, resulting in lower thermal margins for both fuel and coolant temperatures and increased thermal stress on structural materials and reflectors. Figure 4-22 and Figure 4-23 illustrate the spatial distribution of power per pebble in the core at equilibrium. The radial and axial profiles show similar shapes to the thermal neutron flux, yielding a roughly constant peaking factor. At every pass, power decreases, in line with what was shown for burnup.

On average, at the end of life, a pebble generates half of the power produced during the first pass (Table 4-6). The first four passes account for half of the total core power (202 MW), pass five to eight for 37% (145 MW), and the last two for 13% (53 MW).

Table 4-5: Burnup statistics as a function of the number of passes.

Pass number	1	2	3	4	5	6	7	8	9	10	Core
Avg. cumulative (MWd/kg$_{HM}$)	7.2	20.3	32.5	43.7	54	63.5	72.1	80.2	87.6	94	54.7
Std (MWd/kg$_{HM}$)	4.6	4.7	4.5	4.3	4	3.8	3.5	3.3	3	2.6	3.9
Avg. increment (MWd/kg$_{HM}$)	7.2*	13.1	12.2	11.2	10.3	9.4	8.7	8.0	7.5	6.3	9.5
Minimum (MWd/kg$_{HM}$)	0	10.1	21.5	32.6	42.7	52.2	61.4	69.9	77.5	84.8	0.0
Maximum (MWd/kg$_{HM}$)	20.9	37.8	51.2	62.6	73.1	80.7	87.9	94.7	100.5	102.5	102.5
Range (MWd/kg$_{HM}$)	20.9	27.7	29.7	30	30.3	28.5	26.5	24.8	22.9	17.7	102.5
Peaking factor	2.90	1.86	1.58	1.43	1.35	1.27	1.22	1.18	1.15	1.09	1.87

** The first pass average increment only shows the average burnup, whereas values for other passes correspond to the average burnup difference.*

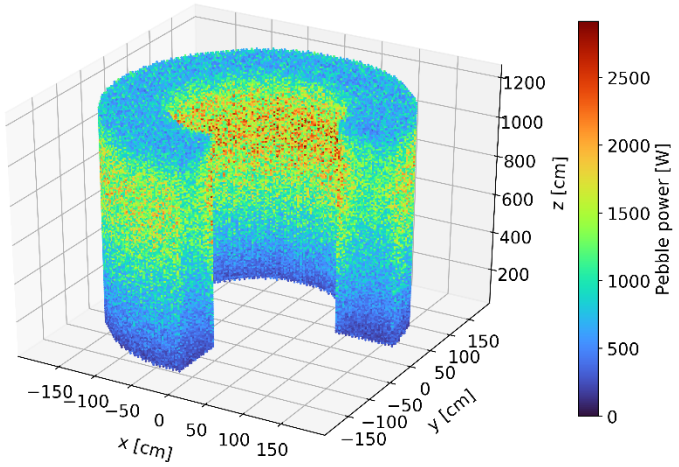

Figure 4-22: Power per pebble in the core at a representative equilibrium state.

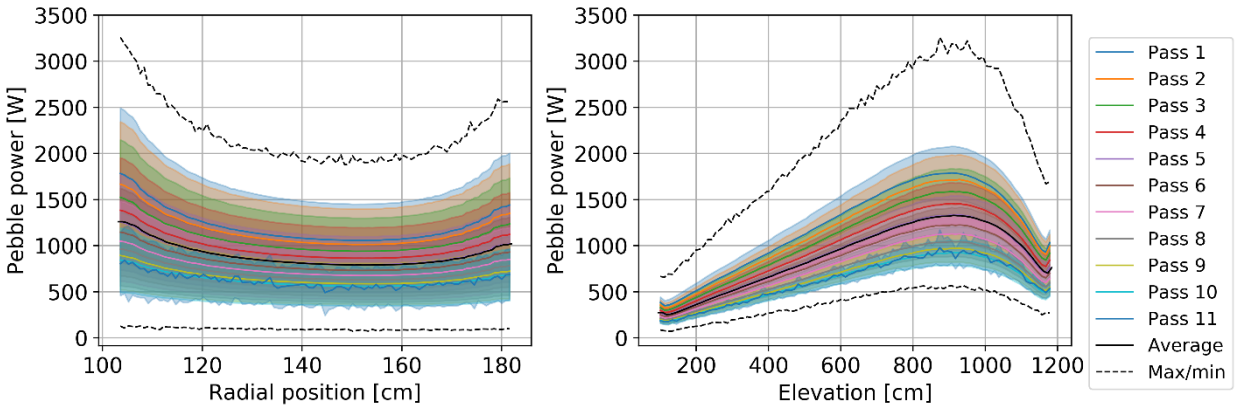

Figure 4-23: Radial (left) and axial (right) pebble power distribution per pass at equilibrium.

The statistical distribution of pebble power for each pass (Figure 4-24) shows three peaks representing distinct thermal flux regions, as seen above. It becomes closer to a uniform distribution due, once again, to the random radial re-insertion process.

Finally, it is observed that the peak power per pebble in the core is 3259 W, corresponding to 217 mW per TRISO particle and 28.82 MW/m^3. This information is particularly relevant to assessing fuel performance. This work assumes a fixed uniform temperature distribution, but in the future, coupling with a thermal-hydraulic model will be implemented to determine the implication of a detailed pebble-by-pebble power distribution.

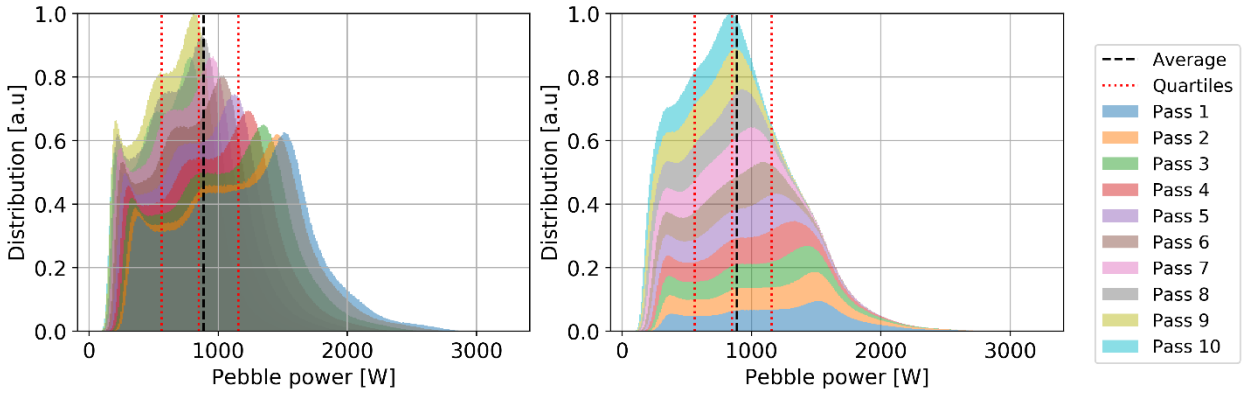

Figure 4-24: Pebble power statistical distribution per pass at equilibrium, individual pass (left), and cumulative (right), normalized over the maximum count.

Table 4-6: Pebble power statistics as a function of the number of passes.

Pass number	1	2	3	4	5	6	7	8	9	10	Core
Average (W)	1204	1146	1059	970	889	817	753	698	650	618	886
Std (W)	493	475	440	403	369	338	311	288	267	253	366
Minimum (W)	165	131	121	123	106	100	88	83	74	74	74
Maximum (W)	3259	3064	2899	2666	2420	2250	2101	1915	1810	1684	3259
Range (W)	3094	2933	2778	2543	2313	2150	2013	1831	1736	1610	3185
Peaking factor	2.71	2.67	2.74	2.75	2.72	2.75	2.79	2.74	2.78	2.72	3.68
Core power fraction (%)	13.9%	13.2%	12.2%	11.2%	10.2%	9.4%	8.6%	8.0%	7.5%	5.7%	100.0%

Data for individual pebbles

A unique capability of HxF is the possibility to pinpoint the history of every single pebble providing further insights. For example, data are presented for four pebbles to understand why they were discarded after four different passes. Their history in terms of burnup, power, and spatial position is shown in Figure 4-25. The pebble discharged after eight passes travel mostly close to the inner reflector; therefore, it experiences larger flux/power and accumulates burnup more rapidly. At the opposite extreme, the pebble discharged after 11 travels further away from the reflector and, from pass five on, moves increasingly into the lower power region. Notably,

although pebbles discarded after 8 or 9 passes accumulated a burnup of about 92 MWd/kg$_{HM}$, the other two reached about 101 MWd/kg$_{HM}$, in line with an extra pass.

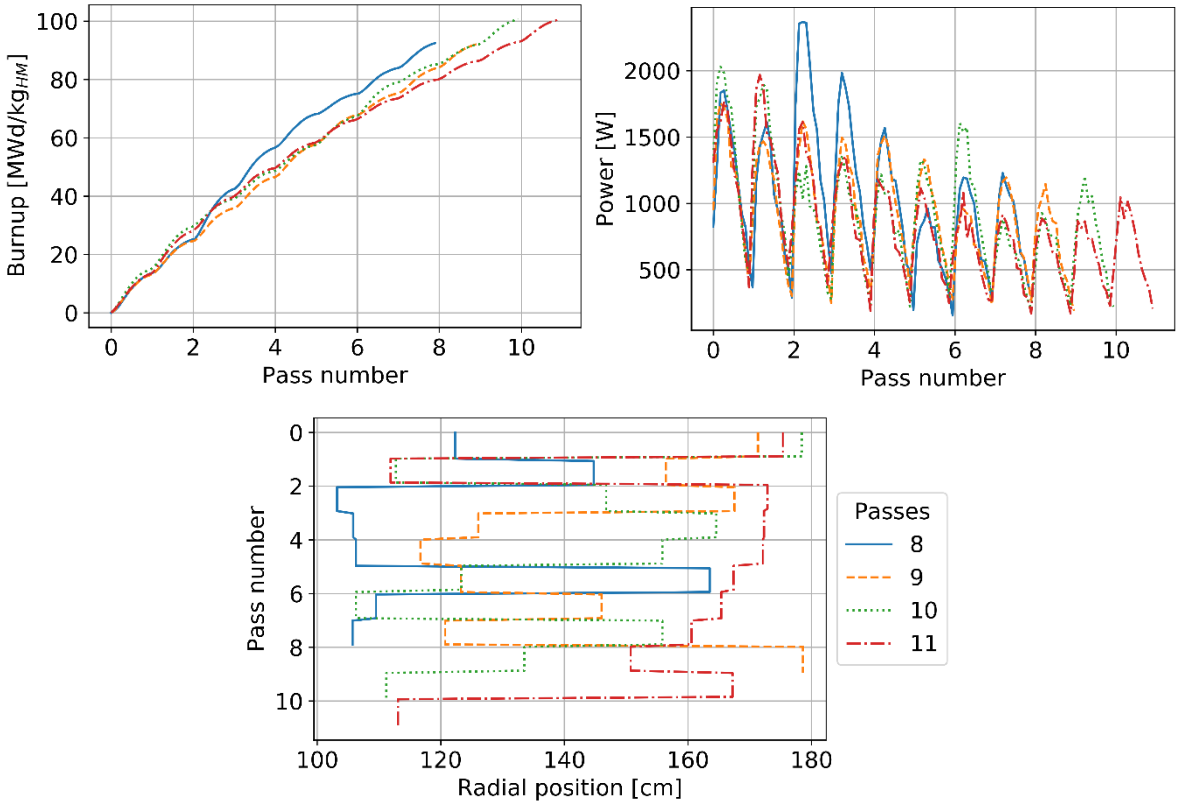

Figure 4-25: Burnup (top left), power (top right), and radial position (bottom) evolution of selected pebbles being discharged after 8, 9, 10, and 11 passes.

Used fuel data

In addition to high-fidelity in-core data, HxF can be used to collect data on used fuel. First of all, some considerations can be made on the discharge burnup. As explained in the methodology, ^{137}Cs concentration is used as a surrogate for burnup, and pebbles are discharged based on a set threshold.[7] The discharged pebbles data confirmed the linear relation between burnup and Cs (Figure 4-26). The set threshold of 2.2238x10^{-4} mol/pebble corresponds, on average, to a burnup threshold of 92.5 +/- 0.15 MWd/kg$_{HM}$ (ranging from 92.0 to 93.3 MWd/kg$_{HM}$).

[7] In real operation, the threshold can be varied in order to maintain criticality in the PBR.

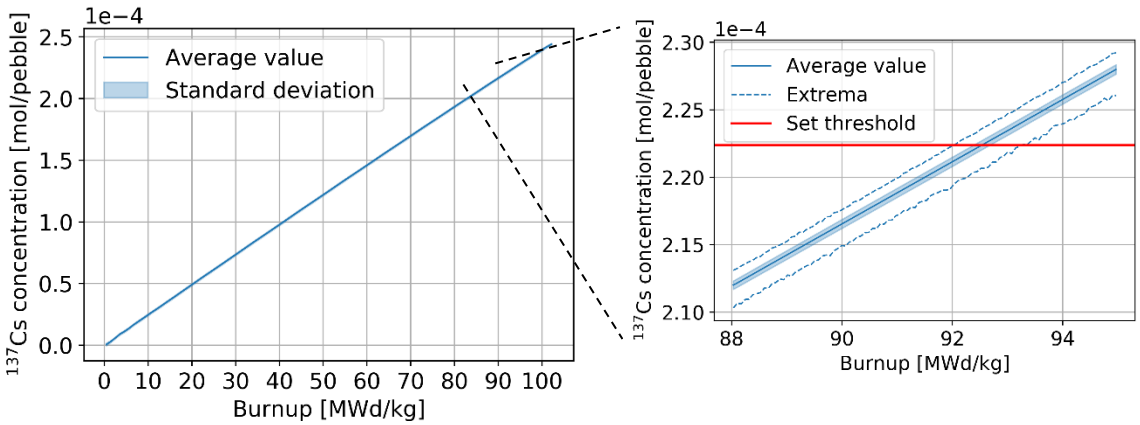

Figure 4-26: ^{137}Cs in a pebble as a function of burnup.

The ^{137}Cs threshold represents the minimum value a pebble must contain to be discarded when it is assessed for burnup. Most pebbles are discarded with larger concentrations/burnups, as the assessment occurs only after a complete pass. Table 4-7 summarizes the pebble inventory and burnup information, separated by the number of passes after which the pebbles were discarded. It can be observed that the substantial majority of pebbles (99.96%) go through the core 9 and 10 times, the average number of passes is 9.8, and the average discarded burnup is 96.5 MWd/kg$_{HM}$, which is 4% higher than the threshold (understanding this shift is essential when determining the threshold value). An extremely small number of pebbles (0.03%) go through the core for 11 passes and typically reach higher burnup levels or are discarded only after 8 and tend to reach lower burnups. In both extreme cases, the obtained burnup ranges are relatively narrow. The statistical distribution of burnup in used pebbles (Figure 4-27) shows the threshold cut around 92.5 MWd/kg$_{HM}$ (with the abovementioned uncertainty) and two peaks corresponding to discharge after nine or ten passes.

Table 4-7: Discarded pebbles inventory and burnup at equilibrium.

Pass number	**8**	**9**	**10**	**11**	**Global**
Fraction (%)	0.005%	19.55%	80.41%	0.03%	100%
Avg. discarded burnup (MWd/kg$_{HM}$)	92.9	93.7	97.1	99.5	96.5
Std (MWd/kg$_{HM}$)	0.5	1.0	1.4	0.9	1.9
Minimum burnup (MWd/kg$_{HM}$)	92.3	92.2	92.6	97.7	92.2
Maximum burnup (MWd/kg$_{HM}$)	94.9	100.7	102.7	102.3	102.7
Burnup range (MWd/kg$_{HM}$)	2.6	8.5	10.1	4.6	10.5

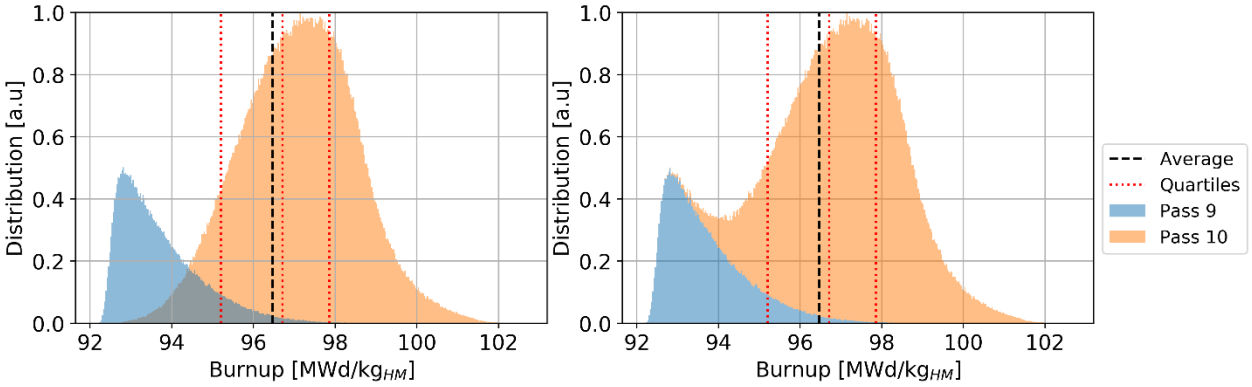

Figure 4-27: Discarded pebbles burnup statistical distributions per pass, individual pass (left) and cumulative (right).

Information about each nuclide can also be obtained. Figure 4-28 shows a few selected examples (the data are collected at discharge with no decay time).

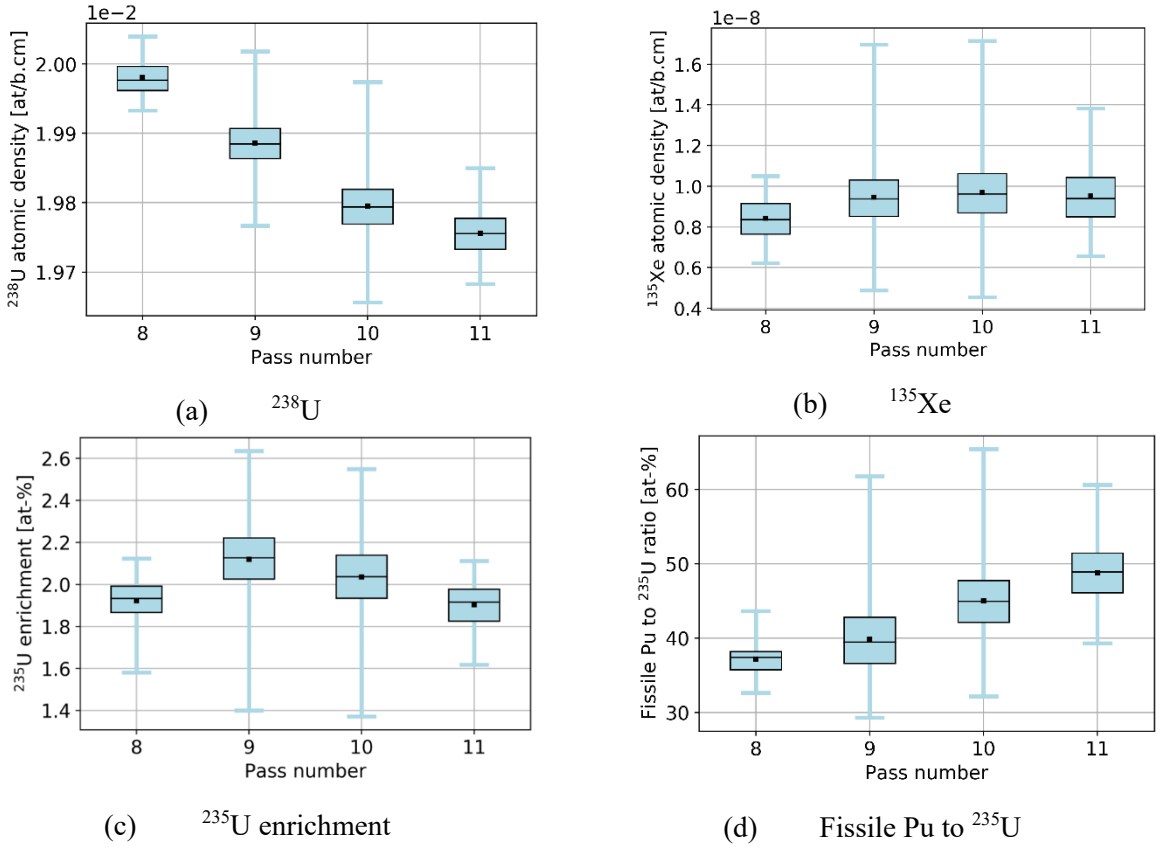

Figure 4-28: Statistical distributions of isotopic concentrations in discarded pebbles, per pass, for important fuel utilization-related quantities.

The concentration of ^{238}U monotonically decreases with the number of passes as expected, whereas the fissile isotopes of Pu (^{239}Pu and ^{241}Pu), fission product ^{135}Xe, and ^{235}U exhibit more

complex behaviors. This is due to the diversity of neutron spectra a pebble can experience during its lifetime, depending on the location and, thus, on the trajectories in the core. As previously shown, the pebbles discharged after eight passes are exceptional cases in which the pebbles are mainly located near the reflectors and experience a softer spectrum (Figure 4-29). Similarly, a softer spectrum leads to a more efficient consumption of ^{235}U and destruction of ^{135}Xe.

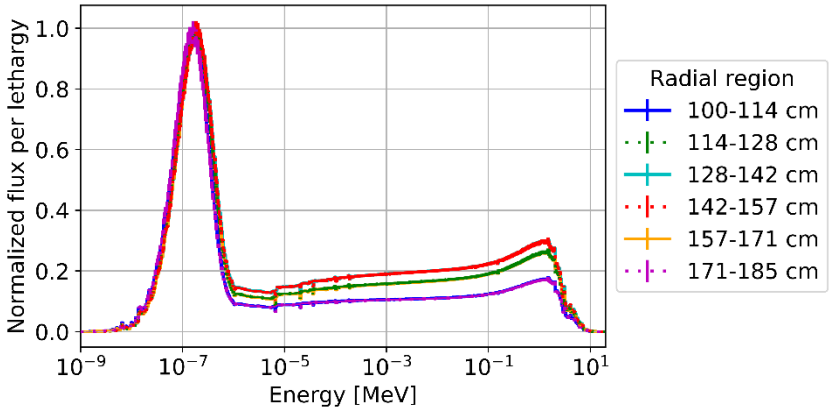

Figure 4-29: Neutron flux spectrum at equilibrium in six different radial zones.

4.3 Discrete Element Method approach

Building on the previous accomplishments and using the compatibility between Serpent 2 and Cerberus, we aim to represent pebble motion more accurately. However, determining the pebbles' trajectory is a challenging task due to the number of pebbles to track, the complex geometry in which they evolve (cones, fueling/defueling chutes), the complex physics of slowly evolving granular flow, and the pebbles' recirculation. In order to properly incorporate the pebble motion within HxF, it is necessary to determine the exact position of each individual pebble and avoid any overlap between fuel elements. Reduced order modeling and trajectory inputs are thus not viable for this type of analysis.

Therefore, Discrete Element Method (DEM) is chosen to simulate the pebbles flow. The DEM approach lies in computing the forces in each pebble using Newton's law, modeling pebbles as soft spheres with a high spring constant to resolve the pebble/pebble and wall/pebble interactions over very short time steps. Although heavy, DEM calculations are highly parallelizable due to the short interaction range between pebbles [77]. In practice, it is challenging to validate DEM results. However, previous comparisons in PBR settings were applied, and the results were encouraging [73, 78].

Various codes were developed in order to perform DEM calculations efficiently. In practice, positions from any DEM tool can be imported by HxF. Among them, LAMPPS [79] has been widely used over the years for PBRs simulations [71, 80, 81]. LIGGGHTS [82] extends LAMPPS capabilities by allowing for DEM/CFD coupling [67]. As mentioned above, OpenFOAM also contains a DEM solver named particleFoam and has been used for simple applications in PBRs

[68]. CHRONO::GPU, a solver from the Project CHRONO framework [64], is a highly parallelizable GPU-based DEM that also has been used for 3D PBR applications [83]. The GPU implementation makes the DEM performance scale linearly with the number of simulated pebbles, and its high modularity makes it an ideal tool for implementing pebbles recirculation as needed. Therefore, this last code is chosen for the rest of this work.

In a DEM calculation involving n_p pebbles, the velocity $\overrightarrow{v_i}$ for a given pebble index *i* of mass m_i and radius r_i is subject to gravity, normal and tangential forces ($\overrightarrow{F_n}$ *and* $\overrightarrow{F_t}$, respectively) as well as the forces exerted by walls $\overrightarrow{F_w}$ with its surroundings and is given by Newton's second law of motion:

$$m_i \frac{d\overrightarrow{v_i}}{dt} = m_i \vec{g} + \sum_{j=1}^{n_p}\left(\overrightarrow{F_{n,\,J\to\imath}} + \overrightarrow{F_{t,\,J\to\imath}}\right) + \overrightarrow{F_{w\to\imath}} \quad (5)$$

Similarly, the angular velocity $\overrightarrow{\omega_i}$ takes the rotational forces into account and are computed from the conservation of angular momentum:

$$I_i \frac{d\overrightarrow{\omega_i}}{dt} = \sum_{j=1}^{n_p}\left(\vec{r_i} \times \overrightarrow{F_{t,\,J\to\imath}} + \overrightarrow{M_{r,\,J\to\imath}}\right) \quad (6)$$

$\overrightarrow{M_r}$ is the rolling friction momentum. The normal and tangential forces are determined using a spring-dashpot model, and materials constants are computed using a Hertzian contact model. Once positions are obtained from the DEM, they can be imported into the HxF tool. Each depletion step corresponds to a set of positions, which are applied using Cerberus to communicate with Serpent.

Application to HTR-10 model

The example used for this demonstration is the HTR-10 research reactor, shown in Figure 4-30. Geometry and materials are based on the 3D HTR-10 benchmark model [84, 70, 85], thoroughly described in [86]. The core consists of a vessel surrounded by a graphite reflector and carbon bricks (pure and boronated). Control rod borings, KLAK channels, and coolant channels within the reflector are explicitly modeled, whereas the hot coolant flow borings are homogenized with the bottom reflector. The vessel, filled with pebbles and helium, is a 90 cm-radius and 221.818 cm-high cylinder, above a 29.61° conus which links the cylinder with a defueling chute (25 cm-radius, 221.236 cm height). The 31,275 pebbles loaded in the core have a radius of 3 cm, and 57% contain 17 wt%-enriched UO_2 (10.4 g/cm^3) fuel encapsulated into 8,355 TRISO particles of 455 µm radius. The rest of the pebbles consist of pure graphite. Each non-fuel material is assumed to have a uniform temperature of 900 K while the fuel is at 1200 K.

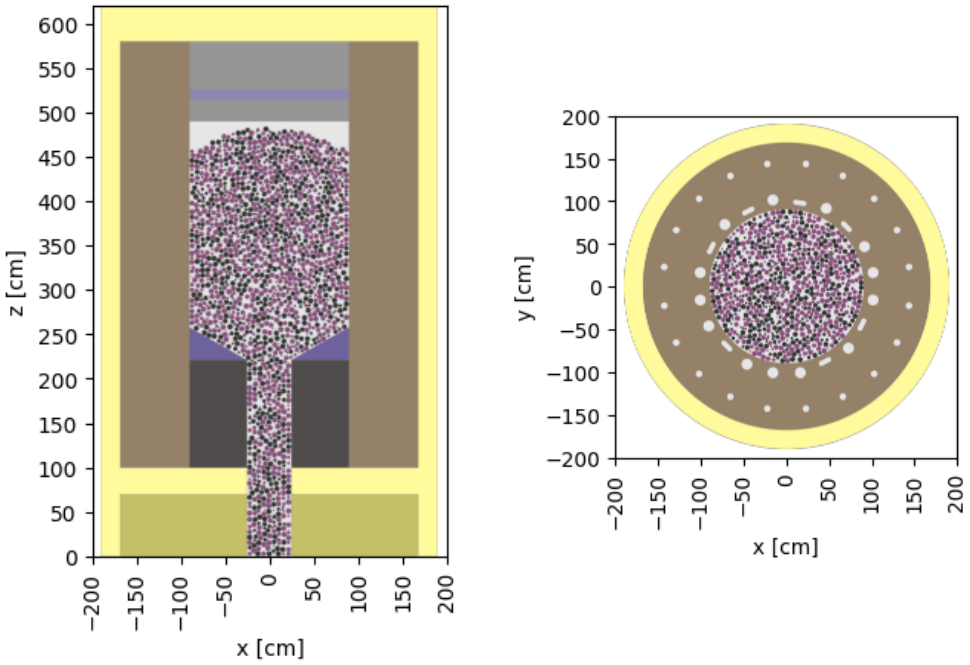

Figure 4-30: Serpent test case model, transverse (left) and longitudinal (right) views.

Serpent transport steps were run with $2x10^7$ active and $4x10^6$ inactive neutrons. These parameters ensure the fission source convergence, average statistical uncertainties of 1.2% for the pebble-wise flux and 4.2% for the pebble-wise power, and a multiplication factor statistical uncertainty below 30 pcm. Pebbles are divided into separate depletion zones with the Serpent 2 automated material division routine.

Discrete Element Method simulation

Simulation parameters

The calculation is performed with CHRONO::GPU using the parameters listed in Table 4-8. The very short time steps (50 μs) requirements for the DEM results to be valid make the use of realistic times (of the order of days) in the simulation infeasible. Instead, the slowly evolving pebble bed, which undergoes only a few axial centimeters of movement per day, is leveraged to derive quasi-static settled states that can summarize the evolution of the pebbles. In other words, it is unnecessary to simulate perfectly continuous recirculation from the DEM side, and the assumption of discrete drainage and settling steps in the core is not expected to affect the accuracy of the simulation in any manner.

Table 4-8: Discrete elements method parameters.

Parameter	Value
Total number of pebbles	31,275
Pebbles radius	3 cm
Pebbles density	1828.19 kg/m^3
Insertion speed	-3 m/s
Converged porosity passes	2
Total simulated passes	6.5
Step size	5% drainage (1564 pebbles)

Parameter	Value
Settling condition	v<0.25 m/s
DEM step size	50 µs
Youngs modulus	1 GPa
Poisson ratio	0.3
Coefficient of restitution	0.6
Sliding coefficient	0.7
Rolling coefficient	0.01

To efficiently produce the trajectories, a two-step process was applied. First, the core is filled with 31,275 pebbles, using the entire vessel radius as possible insertion positions, and no drainage is applied. This first filling step allows the desired number of pebbles to be obtained quickly. Then, for each drainage step, a total of 5% of the core is drained from the bottom end of the vessel, corresponding to 1,350 pebbles, and re-inserted at the top of the core (Figure 4-31). This time, the insertion is within a 10 cm radius, corresponding to the insertion pipe size in the HTR-10. This process is carried out over multiple steps to avoid overlapping of re-inserted pebbles. Once the correct number of re-inserted pebbles is reached, the tool waits for the entire pebble bed to settle (based on the pebble velocities). The settled state corresponds to a proper snapshot of the pebble bed, ready to be used by Serpent. As the first filled pebble bed does not describe a realistic configuration, several passes are simulated before the porosity is fully converged. Therefore, the initial two complete passes (40 steps) were excluded from the usable data. Subsequently, twelve additional passes were simulated to obtain the required settled state trajectories.

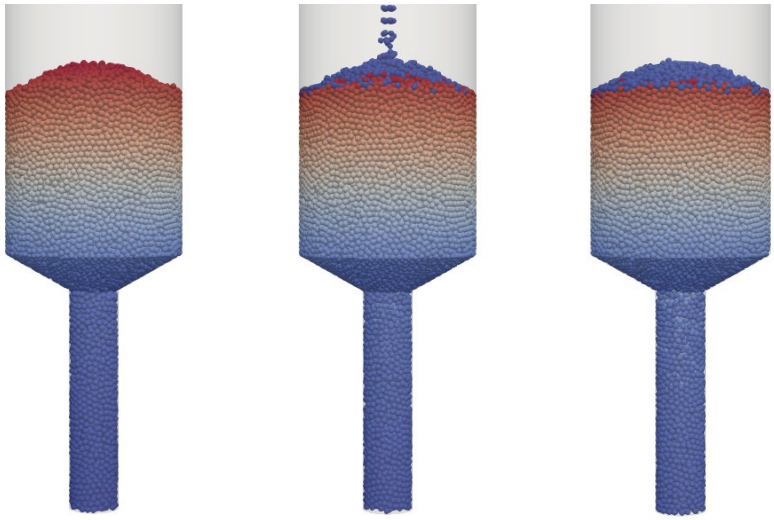

(1) (2) (3)

Figure 4-31: Evolution between two depletion steps. (1) Initial settled bed (2) Drainage step (3) Bed settling to next state. The colors correspond to the initial pebble elevation.

Trajectories Looping

DEM calculations on GPU are highly resource-demanding tasks, especially with the number of granular elements PBRs simulations require. However, the circulation of pebbles within a core is essentially cyclic, and a few complete passes are sufficient to capture the dynamic behavior of the pebble bed and typical trajectories. Therefore, a novel looping method was implemented and used for this study. Once the last DEM step is reached, the created routine uses the initial DEM step positions to create the subsequent steps, assuming the cyclic conditions are verified. As a given pebble's position at the first and last DEM steps are different, the positions of the initial step are re-ordered to match the last as well as possible.

The re-indexing is obtained from an optimization problem minimizing the radial and axial errors made by the matching process with equal weights. To reduce the optimization cost, the problem is broken down into multiple smaller ones, corresponding to radial and axial zones (in this case, 5 and 10, respectively). Once the optimal solution is found, the obtained indexing can be applied for a new complete set of DEM steps, using the second step for the following motion step until reaching the last one once again.

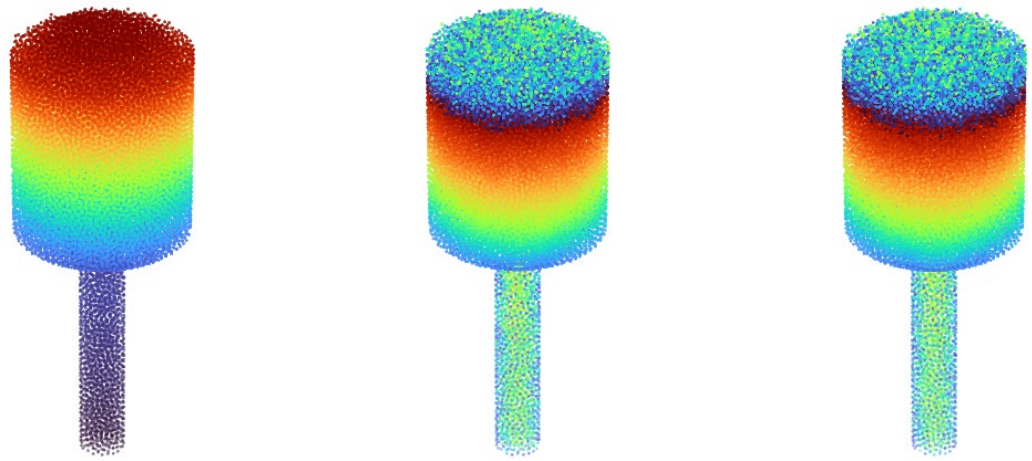

(a) First DEM step (b) Last DEM step (c) Looped DEM step

Figure 4-32: Looping method example on the HTR-10 after 6 short motion steps. Colors correspond to the pebble ID.

This looping approach can be used as often as needed and allows indefinite cycling through the DEM results, saving considerable simulation time. Distributions of errors made once when the looping routine is applied shown in Figure 4-33 indicate that very few pebbles moved by more than one pebble diameter (<0.01%) or one pebble radius (<0.75%), and most pebbles (>90%) moved by less than a quarter of diameter. Therefore, this method is not expected to significantly impact the simulation results while virtually allowing unlimited simulated passes. The total number of simulated passes for the simulation is 25 (not using the 2 passes for porosity

convergence), which required 5 looping steps.

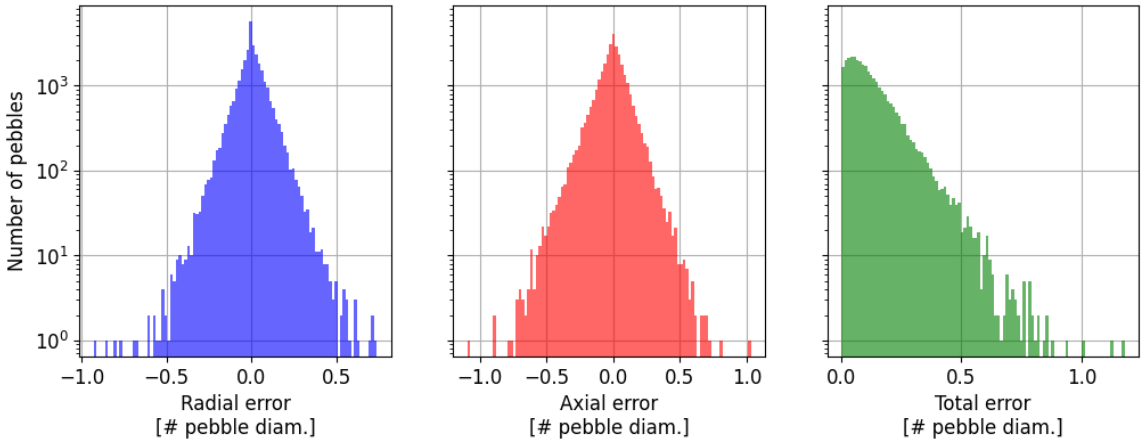

Figure 4-33: Distributions for the radial (left), axial (middle), and total (right) errors caused by the looping method as numbers of pebble diameters.

Caution must be exercised when utilizing this motion looping method in HxF. Sufficient DEM positions are required to capture comprehensive pebble behavior and trajectories within the core and to prevent pebbles from becoming stuck due to the looping process.

Simulation setup

Once the positions have been obtained, they must be communicated to Serpent 2 for each burnup step. The step length sets the speed of the pebble bed in the simulation. Here, a 5% drainage is applied every 12.5 days. This process is handled with the new HxF tool, a wrapper for hyper-fidelity depletion based on the Python interface for Serpent 2 coupled calculations called Cerberus [47], along with the pebble bed development branch of Serpent 2.2.0. Cerberus handles signals for sending and receiving data between Serpent 2 and Python, which makes the on-the-fly update of the pebble bed configuration possible. That includes modifying the position of the pebbles, each pebble's content, or the depletion routine itself. HxF handles the communication with Serpent transport, individual pebbles depletion, motion, discharge, discard, and replacement. In addition, information on in-core, discharged, and discarded data is stored at each time step.

For this study case, positions are directly read from the DEM output to update the pebble bed configuration accordingly at each time step. Discharged pebbles are automatically detected, and a decay step of 3 days is applied, corresponding to a cooling period before assessing their mechanical integrity and fuel content. Discharged pebbles are then tested against a discarding criterion, which is here a maximum ^{137}Cs pebble content. This threshold is set to a pebble content of 2.74 g, corresponding to a burnup of 72 MWd/kg$_{HM}$, corresponding to a guess to obtain a critical core. Pebbles with ^{137}Cs content above this value are discarded. The number of pebbles in the core is kept constant by replacing each discarded pebble with a fresh composition pebble. Therefore, the subsequent transport step has new pebbles positions, with contents from pebbles staying in-core, re-inserted, and freshly inserted. For convenience, a summary of the HxF simulation parameters is

shown in Table 4-9.

Table 4-9: HxF simulation and main operational parameters.

Parameter	Value
Thermal power	10 MW
Threshold ^{137}Cs pebble content	2.74 g (72 MWd/kg$_{HM}$)
Active neutrons per step	2x10^{7}
Inactive neutrons per step	4x10^{6}
Burnup step	12.5 days
Pebbles circulation rate	125 pebbles/day
Fuel fraction	57%
Fuel enrichment	17%
Total number of passes	25
Applied decay step	3 days

Results

Approach to Equilibrium

The reactor equilibrium is defined as the state where global parameters only vary due to the pebble bed motion, resulting in slight oscillations caused by the local changes. It can be observed from different quantities, and Figure 4-34 shows three of them: the multiplication factor, the average in-core burnup, and the average discharge burnup. Starting from an entirely fresh core in which the ^{137}Cs concentrations were randomly assigned between 0 and the threshold value, the reactor reaches equilibrium after around 18 passes. Indeed, once the core is in a steady state, the parameters stay within narrow bands of constant size, which all describe equilibrium snapshots. Those can be individually analyzed or merged in the case of global parameters to obtain overall operational parameters.

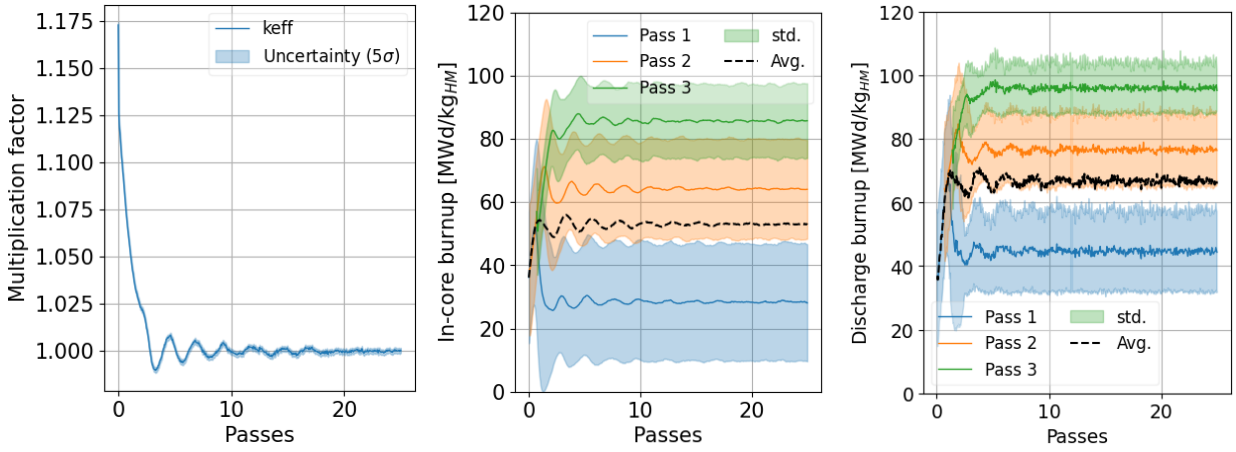

Figure 4-34: Evolution of the core multiplication factor (left), pebbles average burnups per pass, in-core (middle), and discharged (right) as a function of the number of simulated passes.

Equilibrium Core

At equilibrium, pebbles in the core are unevenly distributed, with 1-pass (42.3%), 2-pass (39.4%), and 3-pass (18.3%) pebbles. The average equilibrium multiplication factor over these snapshots is 0.99983 ± 5 pcm, with a standard variation of 46 pcm. This is also the case for in-core burnup data, which stabilizes at 29.09 ± 2.46, 63.63 ± 2.08, and 84.44 ± 1.47 MWd/kg$_{HM}$ for 1, 2 and 3 pass pebbles, respectively (with 19.16, 16.25, and 11.68 MWd/kg$_{HM}$ of standard deviation), and for discharged burnup data at 45.16 ± 1.79, 76.39 ± 1.53, and 95.38 ± 1.00 MWd/kg$_{HM}$ (with 13.66, 12.07 and 8.05 MWd/kg$_{HM}$ of standard deviation).

Spatial distributions for a representative snapshot in Figure 4-35 and global equilibrium profiles per pass in Figure 4-36 provide further insights into the in-core content. As one could expect, thermal flux is highest at the center and close to the reflector and shows a decrease in the corners of the conic zone or the pebble dome formed at the top. It becomes negligible at the bottom of the defueling chute. The fast flux distribution describes similar behaviors, but the reflector does not have as significant an impact as thermal flux. Burnup is influenced by the number of passes, current elevation in the reactor, and the path the pebble takes. Indeed, burnup depends on the flux distributions discussed above and the significant residence time variations depending on whether the pebble flows directly through the radial center or closer to the reflector. The axial burnup profile clearly shows that at 250 cm, where a considerable increase can be noticed, or by the radial profile, which increases closer to the reflector due to the longer times spent by pebbles taking that path. The power distribution, mainly resulting from the thermal flux and burnup, still increases towards the radial center and has the identifiable cone where the power stagnates.

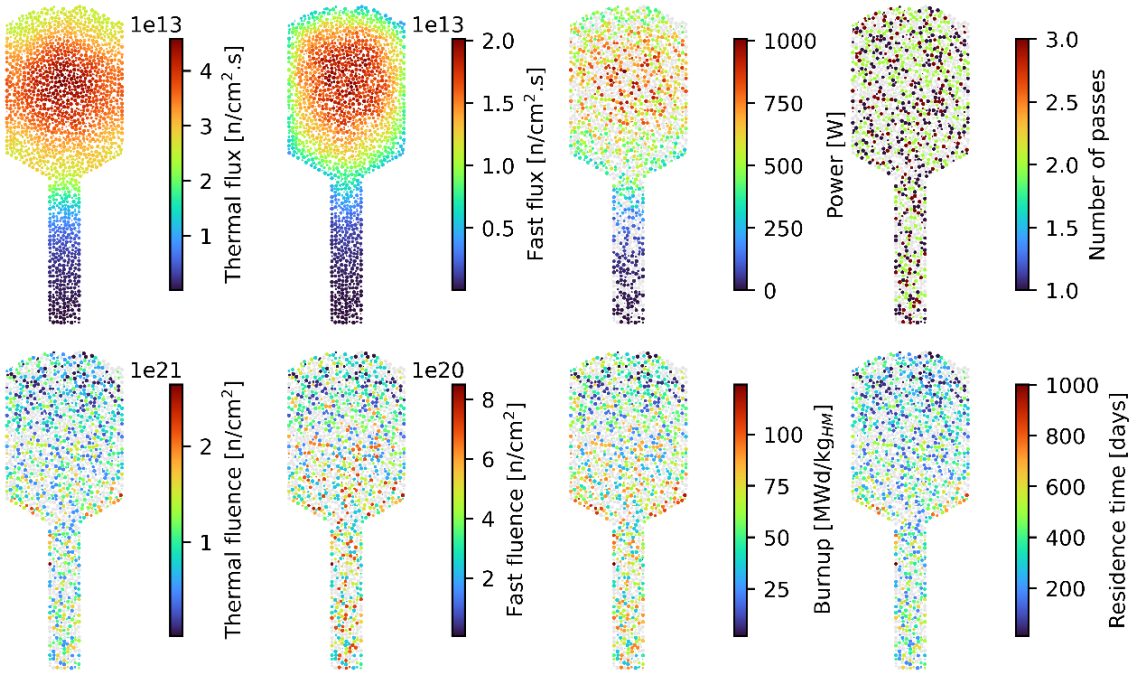

Figure 4-35: Slices of representative equilibrium snapshot with key pebble-wise parameters.

The resulting peaking factors further indicate heterogeneity in the core: 2.63 for the burnup, 3.27 for the residence time, and 1.72 for the power. The defueling chute only accounts for 1.4% of the total power production, and only 0.3% is produced below z=150 cm. The rest is produced in the conic region (3.9%), the upper pebble dome (2.5%), and mainly in the cylindrical region (92.2%). Therefore, the lower part of the defueling chute can be taken as a decaying region for future discharged pebbles.

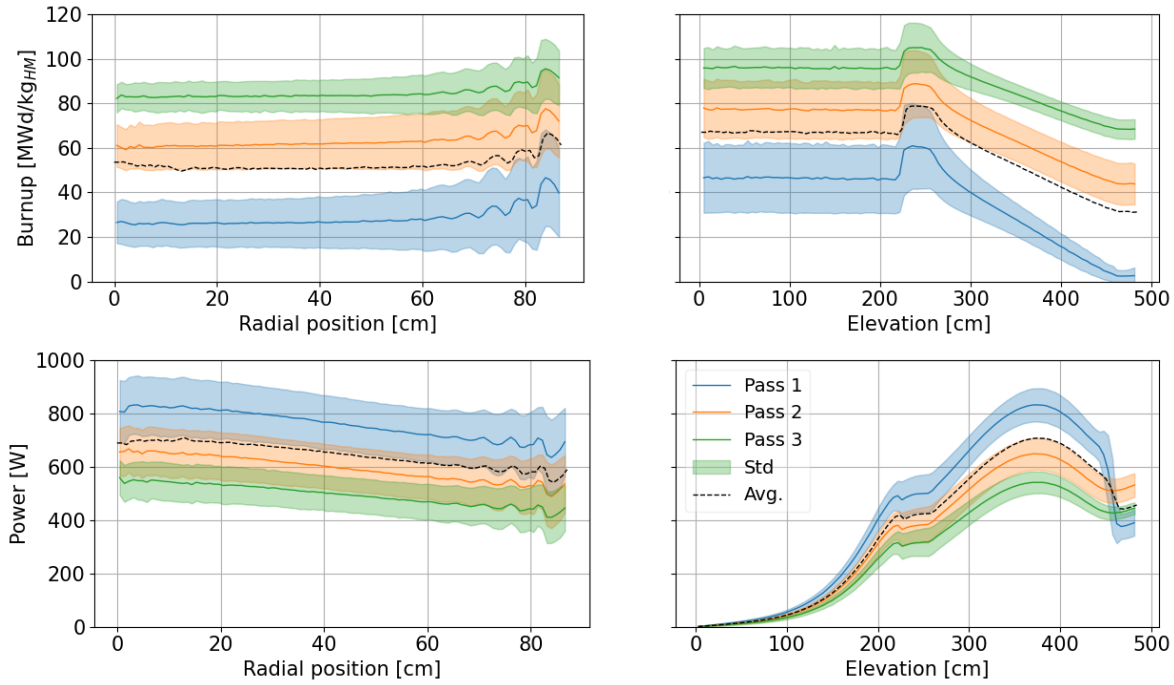

Figure 4-36: Aggregated equilibrium profiles for pebble-wise burnups (top) and powers (bottom). Radial profiles (left) are obtained for the cylindrical region of the core, whereas axial profiles (right) correspond to the entire core.

Discharged and Discarded Pebble Contents

HxF also enables the recording of comprehensive information on pebbles discharged from the core, such as cumulative or current-pass burnups, fluences, isotopic concentrations, and average radial path. This data is key for fuel performance or waste management models, for which the output depends on pebble content and history. For instance, the discharged burnup, thermal fluence, and fast fluence distributions discriminated by pass are shown in Figure 4-37.

For instance, the discharged burnup spans 31.8 to 96.4 MWd/kg$_{HM}$ for pebbles after 1 pass, which significantly overlaps with the second pass (60.4 to 124.3 MWd/kg$_{HM}$) and, to some extent, third-pass pebbles (84.8 to 128.4 MWd/ kg$_{HM}$). Therefore, burnup measurement alone cannot differentiate the number of passes through the HTR-10 core. This observation is the same for thermal fluence, whereas fast fluence has three apparent and non-overlapping distributions. The large minimum calculated burnup shows that pebbles are significantly consumed at each pass.

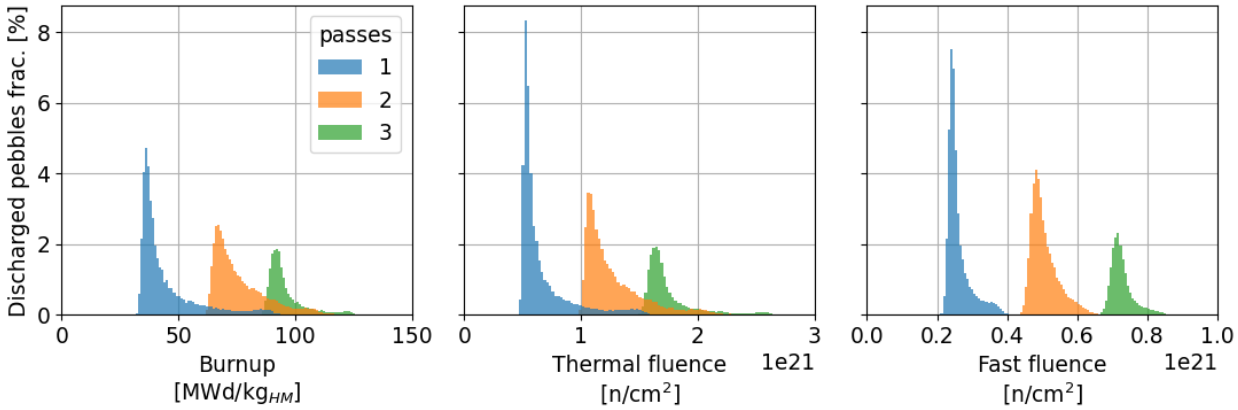

Figure 4-37: Statistical distributions of discharge burnup (left), thermal fluence (middle), and fast fluence (right) at equilibrium.

Looking at the discarded content (Figure 4-38), all discharged pebbles at pass 3 are discarded, which coincides with the discharged range being higher than the threshold value. On the contrary, very few pebbles are discarded after their first pass. Once again, overlaps are found between the three passes for burnup and thermal fluence, not for the fast. The average discarded burnup is 89.3 MWd/kg$_{HM}$, which is 24% higher than the set threshold. This is caused by the fact that pebbles can recirculate with values slightly below the threshold and thus experience an additional pass and a significant burnup accumulation per pass.

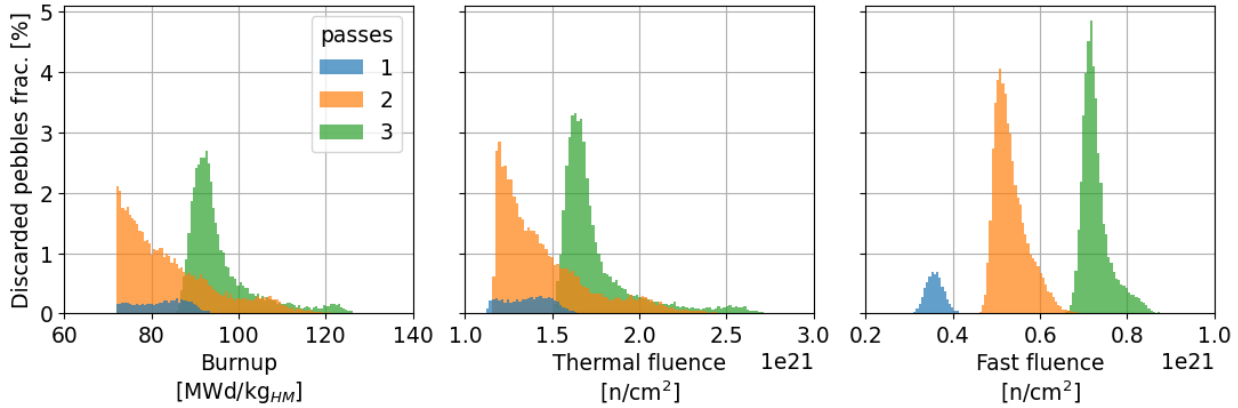

Figure 4-38: Statistical distributions of discarded burnup (left), thermal fluence (middle), and fast fluence (right) at equilibrium.

4.4 Conclusions

The integration of motion and fuel handling to the simulation of PBRs operation represents a considerable enhancement to the fidelity of the simulation, given the dynamic behavior of these reactors. Indeed, an approach to equilibrium can be achieved, and parameter distributions are much

closer to what is expected in PBRs. The motion component can be simulated with two different methods.

The first, discrete motion, was initially implemented directly within the Serpent 2 source code before being outsourced to the HxF tool with Cerberus. In discrete motion, pebble motion is represented using an ordered bed and fixed positions through which fuel elements move. The approach is agnostic to the direction of pebble motion, thus, compatible with any type of PBR. The current simplifications assume no radial motion, uniform axial pebble speed, and uniform core dimensions. However, discrete motion could be further developed to allow for a radial shift, to vary pebble speed for modeling phenomena such as wall effects, and to incorporate core regions of different dimensions, such as defueling conic regions. Nevertheless, these aspects are better addressed using DEM. Keeping the discrete motion approach simpler provides a relatively less demanding alternative to the couple DEM/Serpent in computing time and model creation.

A demonstration of the capabilities of HxF with discrete motion was provided using a full-scale HTGR model. More specifically, an approach to equilibrium was performed, which shows that HxF provides unique insight into PBR fuel, producing information on statistical distributions rather than average values only, as obtained by traditional methods that rely on spectral zoning for depletion. Knowledge of the distribution, minimum/maximum values, and number of occurrences for parameters such as pebble power and fission product concentration are key data when assessing reactor performance in normal and off-normal conditions. They can significantly reinforce confidence in the safety case of PBRs. Furthermore, the data generated does not represent a single equilibrium state but multiple of them (297 in this case), partially addressing the issue that PBRs can assume different configurations even when at equilibrium.

Then, DEM is employed in place of discrete motion for a more realistic representation of pebbles' trajectories. Solving for mechanical interactions between the pebbles and their surroundings, DEM supplies more granular data on the pebble motion. For each depletion step, a unique set of positions is computed from a new quasi-static core state produced by recirculating a batch of pebbles. These positions are communicated to the Python HxF tool, which, in turn, transfers the information to Serpent 2. The DEM tool used is the GPU::CHRONO module of Project Chrono. The discrete element model results are cycled through a novel looping routine, saving considerable computing resources while providing accurate results. HxF is used to obtain and analyze the equilibrium state of the study case through the extraction of in-core, discharged, and discarded pebble-wise parameters. In exchange for a higher computational cost, DEM yields more accurate velocity profiles and enables greater flexibility in terms of geometry. This approach avoids relying on extra assumptions, such as creating lattices of pebbles or predefined flow channels.

Regardless of the motion mode, fuel handling is part of the HxF tool, in which discharged pebbles are identified, and used pebbles above a set threshold are removed and replaced with fresh fuel, hence enabling MEDUL operation. It is worth noting that results obtained so far correspond to isothermal materials, in which pebble power is assumed not to impact the initial temperature guess of each material. However, thermal distributions and the associated reactivity feedback might influence the equilibrium core and overall parameters.

Chapter 5
Thermal-hydraulics

In Chapter 1, large-scale individual depletion alone was studied. Chapter 2 added motion and fuel handling to the simulations to replicate the dynamic nature of PBRs operation. However, applications so far are made with isothermal materials. Therefore, the thermal-hydraulics aspect is the last component to include in a comprehensive high-fidelity tool for PBRs simulation.

In a MEDUL equilibrium core, pebbles with highly diverse compositions and burnup values can be located next to each other. In the same way, individual pebbles' power productions significantly differ. Moreover, pebbles typically accumulate 10-20 MWd/kg$_{HM}$ per pass [37, 87], resulting in substantial spatial variations, steep thermal gradients within the core, and complex temperature profiles. The thermal behavior of the core, produced by the individual pebbles' powers, can, in turn, influence the neutronics. In addition, high fuel temperatures can impact fuel performance and operational margins and thus need to be quantified.

However, simulating the complete thermal-hydraulics behavior of the core, given the considerable number of pebbles, is computationally demanding. Therefore, a standard approach to solve this problem is to use the porous media approximation and couple it with a simplified neutronics model [40, 50, 88, 89]. This approximation eliminates the geometric dependencies in the pebble bed by assuming a diluted medium with volume-averaged effective properties, where pebbles and coolant are diluted. Then, Navier Stokes and heat transfer equations are applied to the coolant flow to determine its temperature. A drag coefficient is computed to approximate the pressure drop through the core without an explicit geometric description of the bed. The porous media solver is then locally coupled with a heterogeneous power source and on dedicated heat transfer models, which, in turn, computes other materials' temperatures.

In this Chapter, the thermal aspects of PBRs are discussed. In particular, thermal coupling is applied between transport on an equilibrium core with a porous media solver to obtain the core's thermal profile and quantify the impact on neutronics. The methodology is described and demonstrated for a static snapshot of the equilibrium HTR-10 core obtained with HxF and DEM in Chapter 4.3. The coupling is externally performed using the porous media solver from GeN-Foam [52] in an iterative process using a novel double-heterogeneous power structure developed for that purpose.

5.1 Thermal coupling description [53]

Porous media approximation and GeN-Foam

GeN-Foam, an OpenFOAM-based library, compiles solvers, correlations, and methods tailored to advanced reactors. Given its purpose and the high compatibility of OpenFOAM with Serpent, it is particularly well suited to this type of work and is used in this study. GeN-Foam thermal-hydraulics sub-solvers include capabilities for porous medium simulations on an

unstructured mesh. Porous-medium equations are obtained from volume-averaging Navier-Stokes equations. The result is a set of equations that resembles the original equations with the addition of 1) a porosity term to describe the fact that only a fraction of the domain is occupied by the fluid(s), 2) a tortuosity term to correct the diffusion coefficient; and 3) sink/source terms to describe pressure drops and heat exchange with the unresolved sub-scale structures. Sub-scale structures are modeled using dedicated models that determine solids temperatures in each mesh cell. Porous-medium equations revert back to standard Navier-Stokes equations in clear-fluid regions, which allows combining porous-medium and standard CFD equations in the same simulations.

In HxF, the entire active region is treated as a homogeneous porous medium in terms of physical properties with a cell-wise power density distribution, which provides an acceptable approximation of the coolant's thermal-hydraulics behavior. Boundary conditions are applied on the core inlet and outlet on pressure, temperature, and coolant flow rate. In the case of the HTR-10, these conditions are summarized in Figure 5-1. The outlet pressure is set to the nominal pressure, considering that the pressure drop in the core is not expected to be drastic. At the walls, a "no-sleep" condition is set. A first coolant temperature educated guess (700K here) and a uniform power density is set, to initialize the coupled calculation.

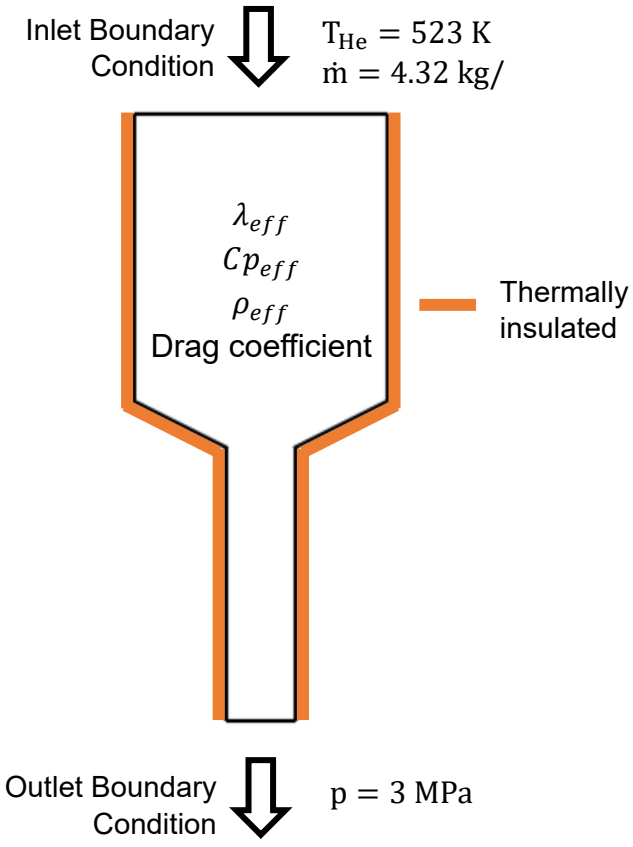

Figure 5-1: Thermal boundary conditions of the GeN-Foam model [19].

In order to update the mesh-wise coolant temperatures, GeN-Foam computes non-dimensional

quantities from correlations, such as the Reynolds (Re), Prandtl (Pr), Nusselt (Nu) numbers, which are in turn used to calculate the heat transfer coefficient and drag coefficient C_D. In HTGR, the heat transfer coefficient in porous media is typically calculated from the Wakao correlation [20]:

$$\mathrm{Nu} = 2 + 1.1\mathrm{Re}^{0.6}\mathrm{Pr}^{0.33} \qquad (7)$$

For the computation of Re, the hydraulic diameter D_H is calculated from the pebble bed porosity ϵ as:

$$\mathrm{D_H} = \frac{\epsilon}{1-\epsilon} 2\mathrm{R_P} \quad (8)$$

From the hydraulic side, the pressure drop within the pebble bed is calculated from the drag coefficient. The KTA correlation is commonly used [21]:

$$\mathrm{C_D} = \frac{320}{\frac{\mathrm{Re}}{1-\epsilon}} + \frac{6}{\left(\frac{\mathrm{Re}}{1-\epsilon}\right)^{0.1}} \quad (9)$$

Pebble and heat conductance power models

As a sub-scale power model, described in Figure 5-2, a new steady-state model has been implemented in GeN-Foam for double-heterogeneous spherical geometries. The pebble temperature profile is calculated given the surrounding coolant temperature. This way, TRISO particle temperature profiles are determined at every location of the pebble fuel matrix from the corresponding matrix temperature.

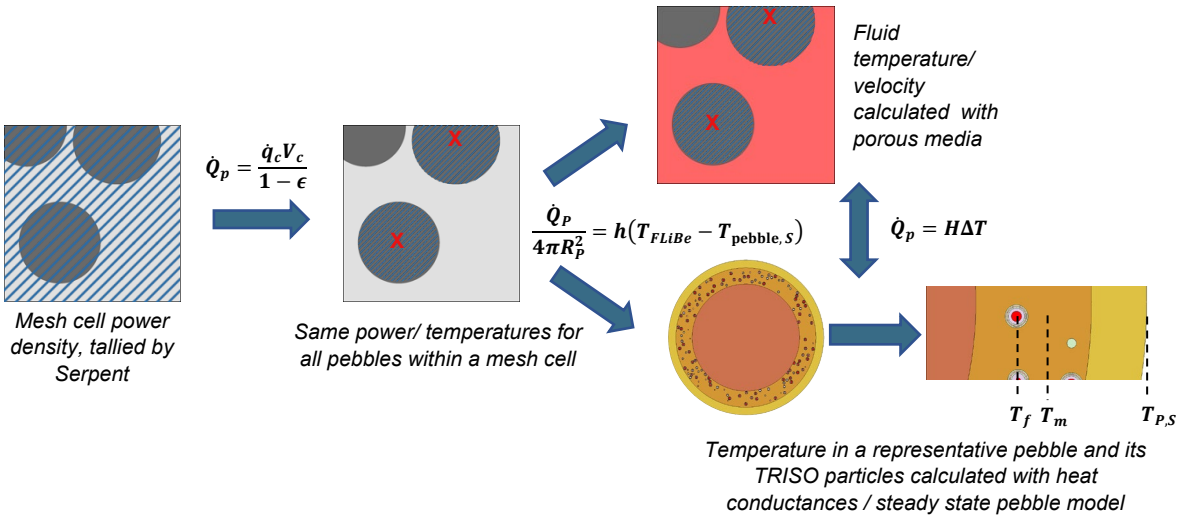

Figure 5-2: Processes involved during thermal coupling in GeN-Foam and double heterogeneous model.

First, the coolant and pebble surface (T_F and $T_{P,S}$) are linked through convection boundary

conditions:

$$\frac{\dot{Q}_P}{4\pi R_P^2} = h\left(T_F - T_{P,S}\right) \quad (10)$$

$\dot{Q}_P$ is the representative pebble power in a cell, R_P is the pebble's outer radius, and h is the heat transfer coefficient determined by GeN-Foam's porous media solver. The pebble power is calculated from the tallied cell-wise power density $\dot{q}_C$, the cell volume V_C, and the medium porosity ϵ, assumed constant, as:

$$\dot{Q}_P = \frac{\dot{q}_C V_C}{1-\epsilon} \quad (11)$$

Once obtained, the pebble surface temperature is used to determine the average matrix temperature $\bar{T}_m$:

$$\bar{T}_m = T_{P,S} + \frac{\dot{Q}_P}{4\pi}\left[\frac{1}{\lambda_s}\left(\frac{1}{R_m} - \frac{1}{R_P}\right) + \frac{R_m^2 - \frac{3}{5}\times\frac{R_m^5 - R_c^5}{R_m^3 - R_c^3}}{2\left(R_m^3 - R_c^3\right)\lambda_{eff}} + \frac{R_c^3\left(\frac{1}{R_m} - \frac{3R_m^2 - R_c^2}{2R_m^3 - R_c^3}\right)}{\left(R_m^3 - R_c^3\right)\lambda_{eff}}\right] \quad (12)$$

where λ_s and λ_{eff} are the shell and the effective matrix layer conductivities, respectively, and R_m R_c are the pebble matrix layer and core outer radii. The effective thermal conductivity of the matrix layer is set to 15 W/m.K [40]. However, it is worth noting that a wide range of conductivities can be used [89].

TRISO particles are uniformly dispersed in the pebble matrix. The surface temperature of an average TRISO particle is equal to the average pebble matrix temperature, as obtained above. From the matrix surface temperature at a location r, the corresponding fuel surface temperature $T_{f,S}$is determined with:

$$T_{f,S}(r) = T_m(r) + \frac{\dot{Q}_T}{4\pi}\sum_{i=1}^{4}\frac{1}{k_i}\left(\frac{1}{R_{i,in}} - \frac{1}{R_{i,out}}\right) \quad (13)$$

$\dot{Q}_T$ is the average power of a TRISO particle in the pebble, taking into account the TRISO packing fraction in the matrix. Each of the four outer layers i of the TRISO particle (buffer, inner PyC, SiC, and outer PyC) is taken into account with its thermal conductivity k_i and inner and outer radii $R_{i,in}$ and $R_{i,out}$. Therefore, the average fuel temperature $\bar{T}_f$ in each cell can be calculated from the fuel volume V_f as:

$$\bar{T}_f(r) = T_{f,S}(r) + \frac{\dot{Q}_T}{15 k_f V_f} \quad (14)$$

Another important metric to quantify is the maximum (inner) temperature reached in the fuel:

$$T_{f,\max}(r) = T_{f,S}(r) + \frac{\dot{Q}_T}{6 k_f V_f} \quad (15)$$

To illustrate the derived equations, Figure 5-3 provides a temperature profile within an HTR-10 pebble and its representative TRISO particle with the average matrix temperature as a boundary condition.

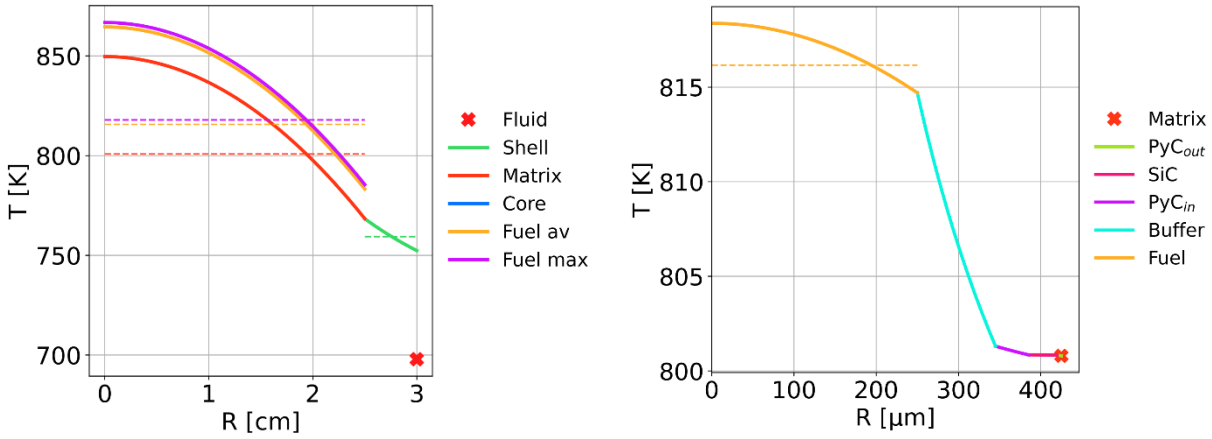

Figure 5-3: Temperature profiles in a representative pebble (634 W) and its representative TRISO particles (76 mW) calculated from the pebble power model.

The assumption of a thermal steady state is expected to hold for each HxF depletion step. Indeed, the pebble bed only evolves by a few centimeters a day, and the power profile varies slowly in space and time. However, another double heterogeneous model, applicable to any geometry, was further implemented and is compatible with transient simulations. The model is based on a series of heat conductances in different layers of the double heterogeneous structure. A more detailed description of the two models is provided in Appendix A.

Serpent/GeN-Foam coupling

Serpent can externally be coupled with a thermal solver. To this end, the Serpent multi-physics interface feature [90] is leveraged to communicate easily with OpenFOAM solvers [49]. In this mode of operation, materials' temperatures can be read directly from OpenFOAM and treated on-the-fly during transport simulations with the target motion sampling (TMS) method [91]. When a neutron-material interaction is sampled, the target velocity based on the material temperature in the mesh cell corresponding to the interaction location is accounted for. The rejection sampling routine considers temperatures as well. Although this enables cell-wise and material-wise temperatures to be imported in Serpent, this feature affects the computational performance of the transport simulation.

The coupling between neutronics and thermal-hydraulics works as Figure 5-4 describes. To start the calculation, the Serpent simulation is initialized, geometry and materials are created, and cross sections are imported. At that point, Serpent reads the unstructured mesh representing the active core in OpenFOAM which spatially links the two codes. The first transport step is run with the default benchmark temperatures. Since Serpent imports the unstructured mesh information, it automatically tallies cell-wise power densities. When transport ends, Serpent waits, and

OpenFOAM is run with the obtained power densities, determining the corresponding cell-wise temperatures from correlations and the pebble thermal model. The new temperatures are then communicated to Serpent, which will utilize them for a new transport step with TMS. After each transport iteration, tallied powers are relaxed in order to account for previous iterations following the equation:

$$\dot{q}_C^{(n)} = \dot{q}_C^{(n-1)} - \frac{\dot{q}_C^{(n-1)} - \dot{q}_{C,S}^{(n)}}{n} \quad (16)$$

where $\dot{q}_C^{(n)}$ is the power density passed to OpenFOAM at iteration n in a cell, and $\dot{q}_{C,S}^{(n)}$ is the corresponding tallied value during the Serpent transport step.

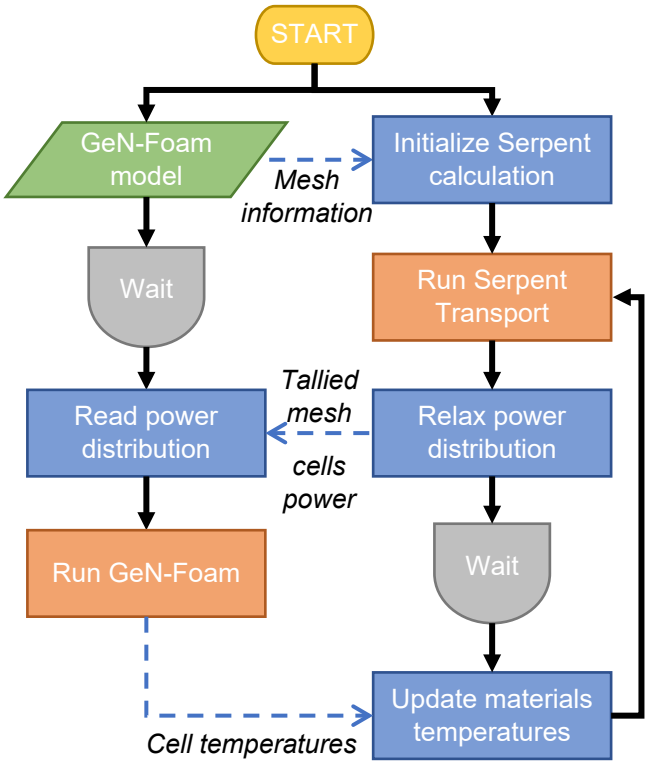

Figure 5-4: Serpent/GeN-Foam coupling flowchart. Solid lines show the process direction; dashed lines show the information exchange between tools.

5.2 Application to HTR-10 equilibrium snapshot

Mesh

An iterative Serpent/GeN-Foam loop is performed on the HTR-10 equilibrium core obtained in Chapter 4.3 to demonstrate the thermal coupling process and quantify its impact. To that end, an OpenFOAM mesh corresponding to the active core region must be created. As stated above, the mesh does not contain any pebbles. Instead, the GeN-Foam geometry is assumed to be uniform,

but the power density in each mesh cell corresponds to the corresponding tallied value in Serpent. Thus, the mesh should capture as finely the power distribution as possible. However, an overly fine mesh might led to instabilities and divergence of the solution, in addition to making the calculation slower. With the idea that thermal coupling should eventually be applied at each depletion step in HxF in mind, a tradeoff between the mesh resolution and computational time must be found.

In order to determine the mesh size, a sensitivity study is performed. To that end, a coarse, an intermediate, and a fine meshes are created, changing the number/size of the cells and the viscous layer. No viscous layer is modeled in the coarsest mesh, whereas three 1 cm-thick external layers are added to better capture the profiles at the edges of the core for the intermediate and fine mesh. The three meshes are represented in Figure 5-5**,** and their characteristics are summarized in Table 5-1**.** Each mesh is decomposed into 20 domains, each corresponding to a parallel task on a computer node. Thermal properties for the coolant and pebble materials are extracted from temperature-dependent correlations in [18]. The density of the coolant is also updated as a function of the pressure, using a perfect gas approximation. The remaining thermal properties are computed at the nominal pressure and are then assumed independent of the pressure. The meshed geometry and inlet, outlet, and wall patches are generated with SALOME (v2019). It is then exported in the UNIV format, which is, in turn, converted into an OpenFOAM-compatible format through the *ideasUnvToFoam* [17] command.

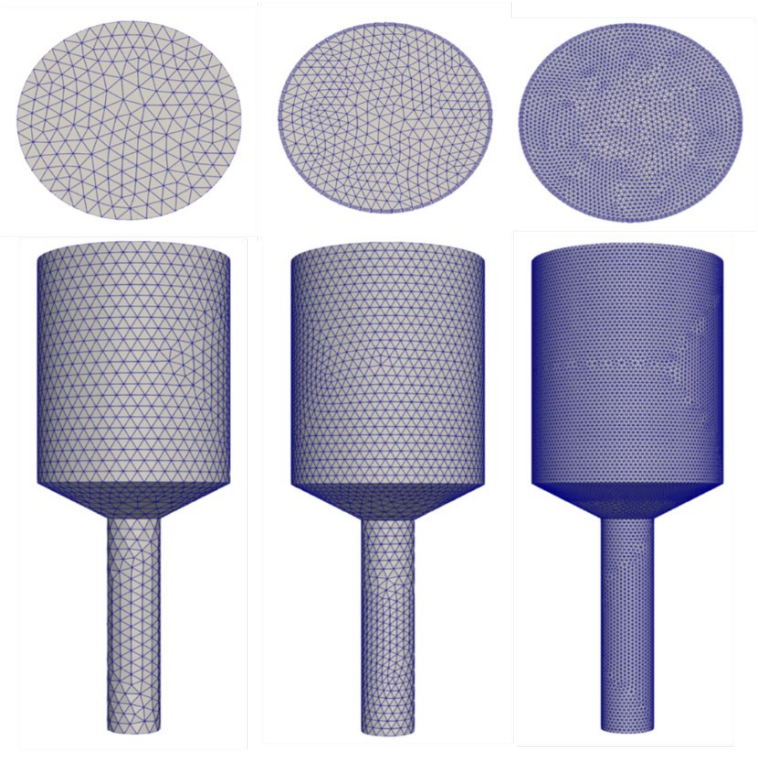

Figure 5-5: Coarse (left), intermediate (middle), and fine (right) meshes.

Table 5-1: Main characteristics of the meshes.

Mesh	Coarse	Intermediate	Fine
Number of cells	18,830	47,277	370,970
Viscous Layer	No	Yes, 3 cm thick with 3 layers	Yes, 3 cm thick with 3 layers
Computational time	-	90 s	500 s

GeN-Foam does not converge with the coarse mesh, thus not being a viable solution. On the other hand, the finest mesh's results are not drastically different from the intermediate mesh, with only a 1.5% overall variation, while being more than 5 times slower. In addition, it is more constraining from the neutronics side due to the need for more neutron histories to simulate, to obtain the same statistical uncertainties. Therefore, this sensitivity study brings confidence to using the intermediate mesh. It contains 47,277 tetrahedral cells, with a viscous layer of 3 cm thickness containing three internal regular layers along the wall of the vessel. The average size of the rest of the cells roughly corresponds to the size of a pebble. The thermal solver takes less than 2 minutes before temperatures converge with the described configuration.

Convergence

Each thermal iteration simulates 5 seconds. In order to determine if the coupling converged, the temperatures, powers, and multiplication factors are analyzed. As Figure 5-6 shows, very few iterations are needed. Indeed, starting from the second iteration, the quantities of interest stabilize between steps, with all fields undergoing a relative variation of less than 0.5% (convergence criterion).

The initial estimate of 700K for all materials represents an underestimation. Once thermally converged, the standard deviation on the change is low. Being the hottest element in the core, the fuel's most significant temperature variation occurs, with an initial iteration causing an average temperature change of up to +22%. In the same way, power converges quickly but has a higher standard deviation on the difference between steps because of the Serpent statistical uncertainty.

On the neutronics side, given negative temperature reactivity coefficients, the coupling decreases the multiplication factor. In the first iteration, before introducing the temperatures field from the thermal solver, both uncoupled and coupled k_{eff} are similar. Once the temperature field

is updated for the coupled model, the multiplication factor stabilizes around 0.95814 ± 27 pcm[8]. In contrast, the uncoupled case yields a value of 0.95368 ± 27 pcm, representing a non-negligible difference (-446 pcm). The following results are all taken at thermal equilibrium.

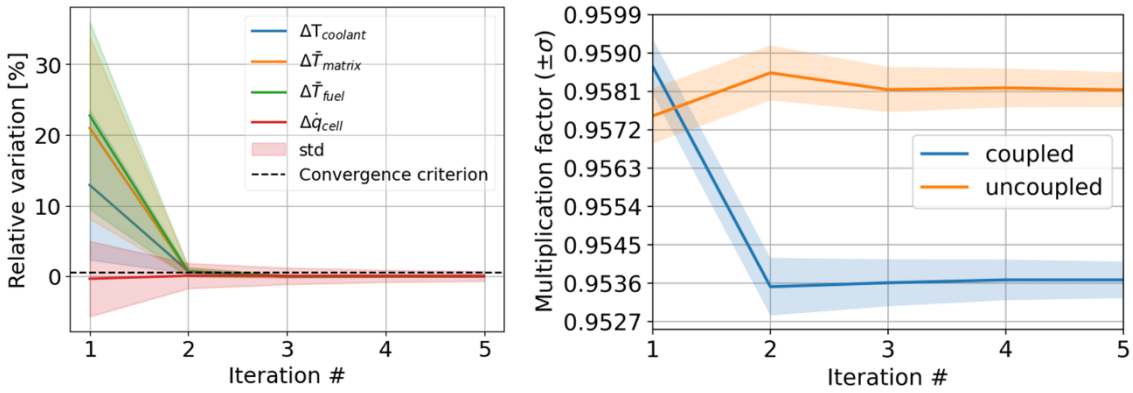

Figure 5-6: Thermal convergence (left) and neutronic convergence (right).

Hydraulic modeling

The resulting helium flow is analyzed to verify the physical behavior of the core. In a pebble bed, the pressure drop is given by the Ergun formula [24]:

$$\Delta P = \frac{150 L \mu}{D_p^2} \frac{(1-\epsilon)^2}{\epsilon^3} U + \frac{1.75 L \rho}{D_p} \frac{1-\epsilon}{\epsilon^3} U^2 \quad (17)$$

where L is the height of the bed, ϵ the porosity, μ, and ρ respectively, the dynamic viscosity and density of the coolant, D_p the diameter of the pebble, and U, the magnitude of the coolant velocity. In the active region, the pressure drop is 0.09 bar, the average velocity is 2.06 m/s, the average Reynolds number is 4,900, and the average Nusselt number is 122. It is worth noting that in this simulation, the outlet orifices at the cone are not modeled, taking the end of the defueling chute as the outlet. This does not reflect the reality, where the coolant enters from the top of the core (mainly) and the defueling chute and flows out from the cone orifices. This leads to mainly wrong cooling characteristics in the defueling chute. However, since almost no power is generated by pebbles in this core region, it should not affect the study results.

Temperatures and power distribution

The obtained temperatures and power results are summarized for the entire core for fuel

[8] This subcritical, thus unrealistic multiplication factor is due to the conditions taken for the discard threshold, but are not expected to affect the conclusion of this study.

pebbles in Table 5-2. The minimum values for each temperature field are close to each other and to the inlet temperature due to the low power of certain pebbles at the top of the reactor. Minimum power is reached in certain pebbles at the bottom of the defueling chute; where the flux is near zero, and the burnup tends to be higher.

Table 5-2: Summary of temperature and power within the core at thermal equilibrium.

Parameter	Minimum	Maximum	Average	Peaking factor
$\mathbf{T_{He}}$ **(K) (coolant)**	523.1	952.4	742.2 ± 131.4	1.28
$\mathbf{\overline{T}_m}$ **(K) (average matrix)**	528.6	1058.3	793.5 ± 127.6	1.33
$\mathbf{\overline{T}_f}$ **(K) (average fuel)**	529.5	1086.9	804.3 ± 128.0	1.35
$\mathbf{T_{f,max}}$ **(K) (maximum fuel)**	529.7	1091.0	805.9 ± 128.2	1.35
$\dot{Q}_p$ **(W)**[9]	0	1073.1	560.6 ± 181.5	1.91

The spatial temperature distributions in Figure 5-7 exhibit a temperature peak at the center of the active zone for the radial profile, with a slight reflector effect on the sides. Regarding the axial profile, pebbles are linearly heated with elevation until reaching the conic region and the defueling chute, where the temperature becomes constant due to the absence of power production. However, pebbles evolve downwards, and the temperature gap between the coolant and the pebble remains constant, even if the powers vary with the elevation. In other words, their powers do not significantly affect pebble temperatures.

[9] For power distributions, graphite pebbles powers are zero values and thus are not considered.

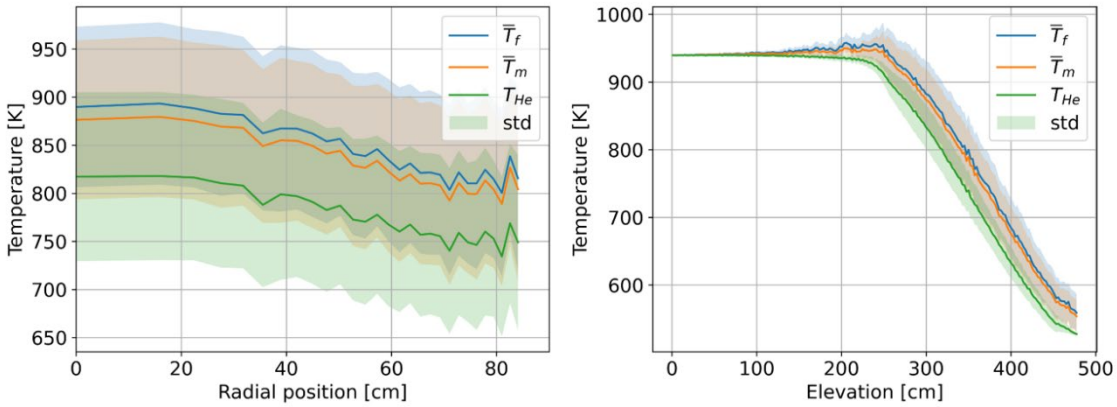

Figure 5-7: Radial[10] (left) and axial (right) temperature profiles for the fuel matrix and coolant.

The impact of coupling on pebble powers is also evaluated. The obtained statistical distribution and the relative difference between the cases with and without coupling are provided in Figure 5-8. The power distribution is characterized by a Gaussian-like component, representing the active region, while the defueling chute produces a lot of low-power pebbles. When applying the coupling, some pebble powers vary by more than 20% in the active region. However, 75% of the pebbles have a relative power variation of no more than +/- 3%, meaning that the thermal coupling has no global influence but a noticeable localized effect. For instance, pebbles experiencing the highest positive relative variation are located at the top of the reactor, where a colder coolant influences pebbles ($T_{He} = 523$ K). On the other hand, pebbles with the highest negative relative variation are located at the cone, where the coolant temperature is close to maximum.

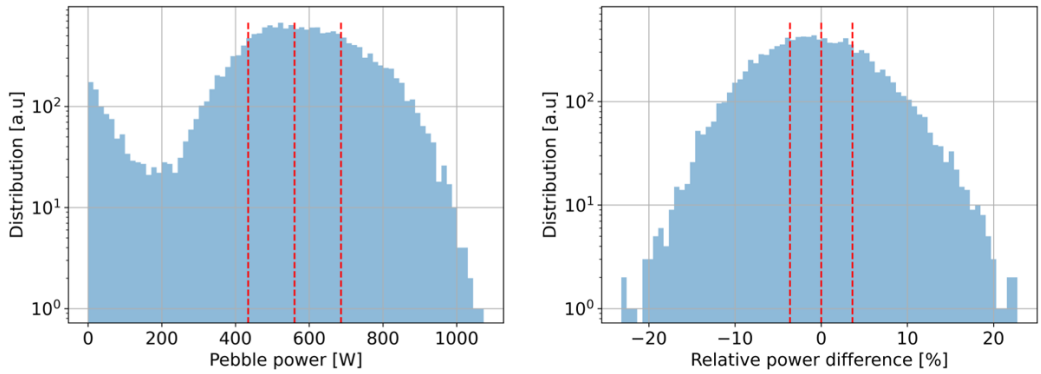

Figure 5-8: Pebble power distribution within the entire core after coupling (left) and relative

[10] Radial profiles are provided only for the active region and ignores the defueling chute.

pebble power variation between the uncoupled and the coupled model in the active region (right).

The pebble power profiles in Figure 5-9 and the relative variation between the uncoupled and coupled model corroborate that observation. Most pebbles do not experience any change in power, especially radially. To further analyze the trends in the PBR, this plot is associated with Figure 5-10, which shows a two-dimensional longitudinal slice representation with temperatures and powers. The most powerful pebbles are located at the center of the active zone. The reflector has a visible impact on the radial power by flattening the profile even if the small size of the reactor still leads to substantial leakage, reducing this effect.

Regarding axial evolution, the power of the pebble is also at its maximum at the center of the active core. Then, it decreases until a slight increase around z=210 cm, corresponding to the middle of the conic region, where pebbles are surrounded with reflector material. For the rest of the defueling chute, the exponential decrease related to the power decay is noticeable. Significant variations are observed in the defueling chute where pebbles are close to no power. The first top half experiences a positive relative difference in the active region due to a colder coolant than the uncoupled model. Then, the relative variation decreases linearly and exhibits a negative variation related to higher coolant temperatures than the guess. This phenomenon highlights the effect of the coolant temperature around the pebble on its power through its important influence on the fuel temperature.

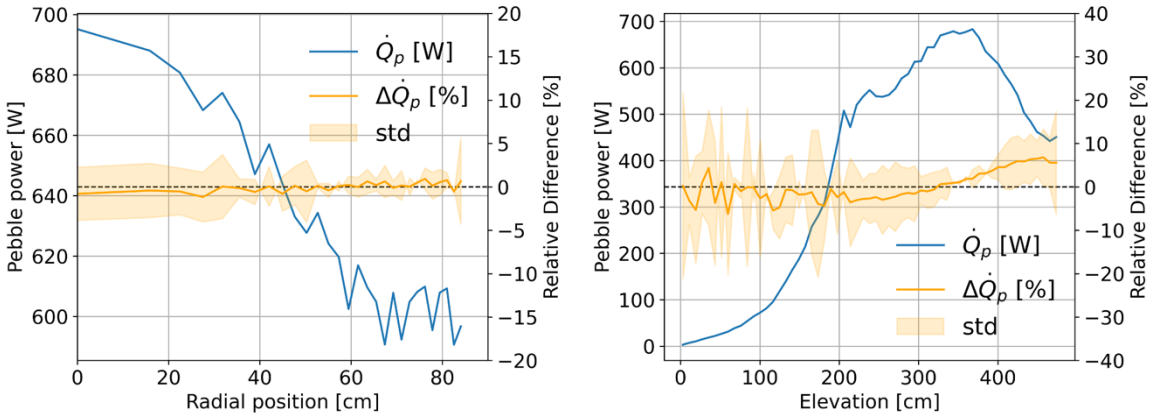

Figure 5-9: Radial (left) and axial (right) impact of thermal coupling on pebbles power.

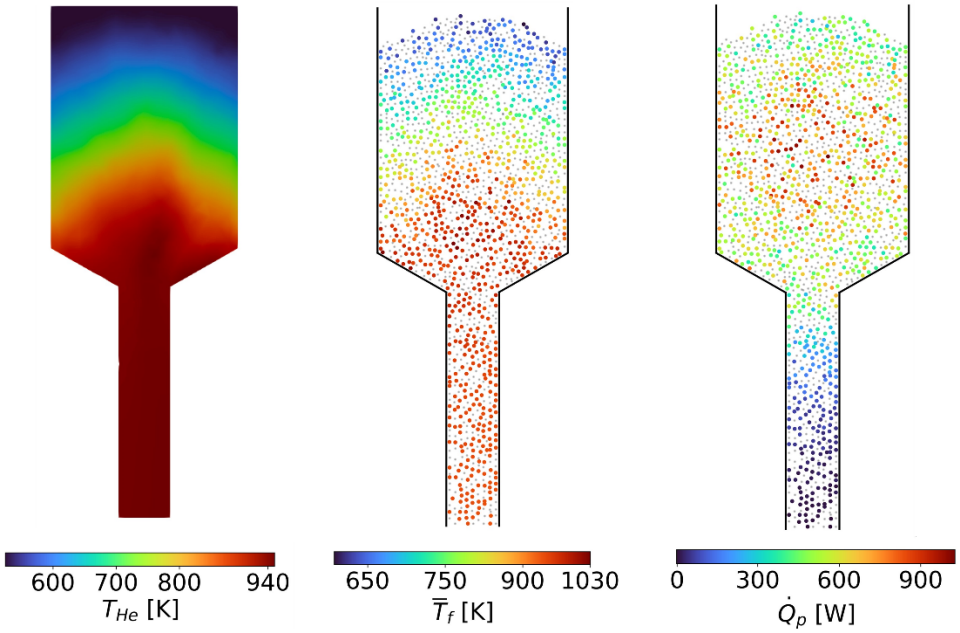

Figure 5-10: Longitudinal view of the HTR-10 converged thermal and power parameters. Graphite pebbles are represented in grey for fuel temperature and power.

The relative influence of the powers and coolant temperatures on fuel temperature can be seen in Figure 5-11. The fuel temperature in a pebble, communicated to Serpent 2, is almost independent of its own power production and is primarily influenced by the surrounding coolant temperature. Indeed, the fuel temperature's trend is roughly horizontal. This phenomenon is explained by equation (10). Indeed, HTGRs, particularly the HTR-10, have a low power density and use large pebbles. Although helium does not allow for high heat transfer coefficients, the temperature difference between coolant and pebble surface is low, even for the most powerful pebbles. Still, while the highest coolant temperatures are found in the defueling chute, the maximum fuel temperatures (910 K) are located slightly higher in the conic region, where power production is non-zero. This shows that the influence of power, while limited, is non-negligible.

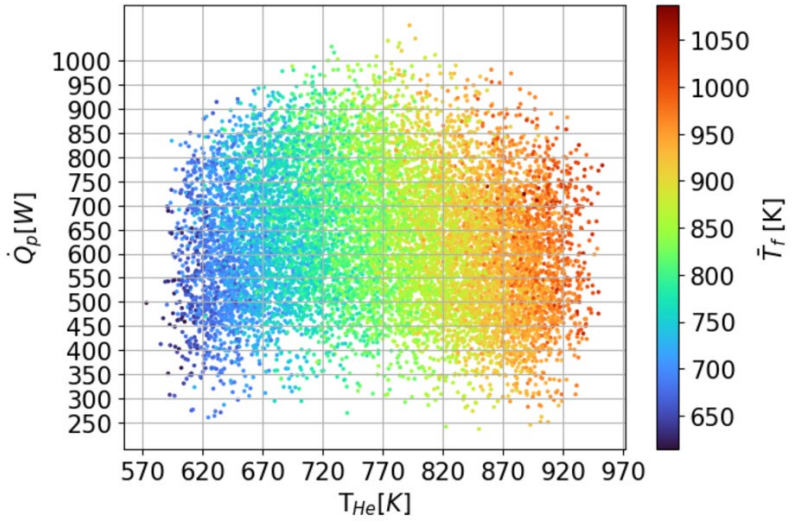

Figure 5-11: Influence of the pebble power and the coolant temperature on its fuel temperature in the active core.

Pebbles with the highest fuel temperature ($\bar{T}_f > 1000\ K$) are usually associated with a coolant temperature between 900 K and 940 K. As Figure 5-12 suggests, the 2% hottest pebbles ($\bar{T}_f > 1000\ K$) are mainly located in the conic region and bottom part of the active core. Indeed, pebbles are still producing power in this high temperature coolant area. In contrast, in the defueling chute, there is only decay heat, thus leading to constant temperatures.

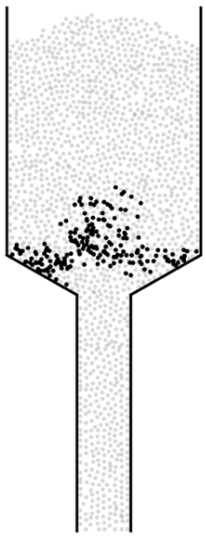

Figure 5-12: Representation of the 2% of fuel pebbles with the highest fuel temperature.

Thermal influence on neutronics

At thermal equilibrium, temperatures differ from the set initial guess. Given reactivity coefficients, it is expected to observe a difference in the neutronic behavior of the core. Therefore, it is worth evaluating the impact of coupling on the computed multiplication factor. In particular, coupled components are individually turned on or off to isolate their effects on the simulation, such as the coolant temperature and density, the graphite matrix temperature, and the fuel temperature. The explored combinations are summarized in Table 5-3. The first three couplings can be compared with the fourth (fully thermally coupled case) to obtain the individual coupling reactivity contribution. The last case, where coolant density is also determined and coupled, evaluates the simulation's worth accounting for densities.

Table 5-3: Summary of the different coupling combinations.

Field	Uncoupled	Matrix/Coolant Coupled	Fuel/Coolant Coupled	Fuel/Matrix Coupled	Temp. Coupled	Temp./Density Coupled
Fuel Temp.	x	x	√	√	√	√
Matrix Temp.	x	√	x	√	√	√
Coolant Temp.	x	√	√	x	√	√
Coolant Density	x	x	x	x	x	√

The reactivity differences with the uncoupled case for each combination are provided in Figure 5-13. The fuel temperature primarily influences the multiplication factor, with the highest difference between the initial guess and the converged value. Coolant and matrix temperatures coupling also result in a slight decrease in k_{eff}. When communicating the computed coolant density to Serpent 2, which is lower than the one associated with the initial coolant temperature guess, the multiplication factor further decreases. The density of the coolant (helium) does not significantly impact the multiplication factor, with results within uncertainty.

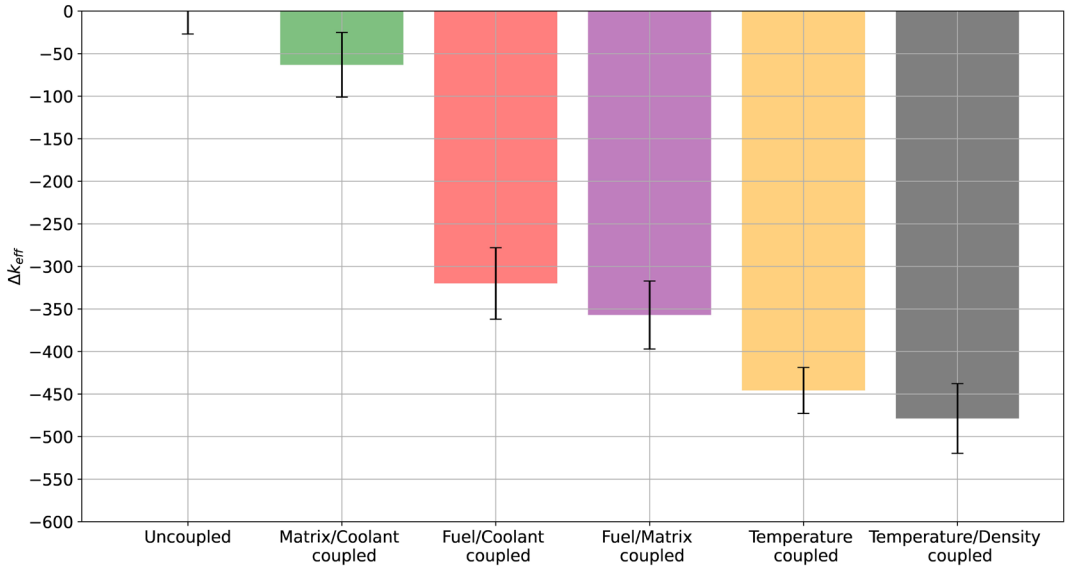

Figure 5-13: Effect of thermal coupling on the HTR-10 multiplication factor (in pcm) for different coupling combinations.

5.3 Conclusions

The thermal-hydraulics coupling with neutronics, which is the last key component of HxF, is implemented with GeN-Foam and adds a new layer of accuracy. We leverage the compatibility between Serpent 2 and OpenFOAM and use the porous media solver associated with a novel double-heterogeneous power model to represent the pebbles. Through an external process loop and using the Serpent multiphysics interface, an iterative process is applied in order to have transport power distribution and porous media temperatures communicate and influence each other. For a given depletion step, a thermal steady state assumption is made, given the slow evolution of the pebble bed and the simulated time taken to converge (in the order of seconds). The porous media approach is faster than CFD and is expected to yield acceptable results from the neutronics perspective.

The capability is demonstrated on a static HTR-10 equilibrium state obtained with HxF and DEM motion. Coupling GeN-Foam and Serpent 2 affects the multiplication factor. The difference between the initial temperature and the accurate distributions made by coupling, is non-negligible, which leads to a 446 pcm decrease in k_{eff}. The detailed power and temperature distributions provide insights into the pebble behavior and depict a strong dependence between the coolant temperature and the rest of the materials. The presence of the conic region and defueling chutes profoundly shape the thermal-hydraulics behavior of the core. In addition, accounting for all temperatures and coolant density distributions is important for increasing the accuracy of HxF.

This method is embedded into the HxF tool and can be used during a search for equilibrium. While it has been implemented for GeN-Foam, transitioning to another thermal-hydraulics code (e.g., CFD or Pronghorn [89, 92]) is possible. In addition, it can be used for transient simulations,

such as power excursions or accident scenarios, particularly for partial or total loss of coolant. In this work, the packing fraction in each mesh cell is assumed to be constant. However, the porosity of the pebble bed can considerably change in the core, specifically close to the walls. Therefore, local packing fraction calculators based on Voronoi cells and Monte Carlo simulations are currently being explored. In parallel, the development of a porosity-dependent porous media solver is pursued.

Chapter 6
Application of HxF to the generic FHR model

Previous chapters extensively cover the development and individual components of the HxF approach and dedicated tool. Indeed, individual transport and depletion, pebble motion, and thermal-hydraulics are all key components when accurately simulating the operation of PBRs. This Chapter is dedicated to applying HxF on a large-scale model, the generic FHR (gFHR). The reactor, shown in Figure 6-1, was specifically created as a standard for benchmarking analyses in FHR reactors research. The gFHR represents a full-scale FHR inspired by Kairos Power's global design but incorporates several simplifications. Among others, the gFHR vessel consists of a simplified geometry. Its active region is entirely cylindrical (309.47 cm-high, 120 cm-radius), without conic zones or fueling/defueling chutes, and is entirely enclosed in a 60-cm-thick graphite reflector which reduces neutron leakage. The reflector is radially surrounded by a stainless-steel core barrel, a downcomer, and a stainless-steel vessel of 5 cm, 2 cm, and 4 cm thickness. The core and downcomer are filled with the ^{7}Li-enriched FLiBe coolant (50 ppm ^{6}Li). In the core, 4 cm-diameter pebbles are dispersed with a packing fraction of approximately 60%. In the gFHR model, pebble motion is simplified as well. The pebble bed is assumed to evolve in slug flow, with individual pebbles having a purely vertical trajectory when moving up in the core. In addition, the motion is assumed to be uniform in the whole core. Both assumptions result in a constant velocity profile in space (radially flat) and time (steady). The core is also assumed to be mostly isothermal, with all materials at 900K, apart from the fuel set at 959K. More details on gFHR parameters are summarized on the Kairos Power website [93].

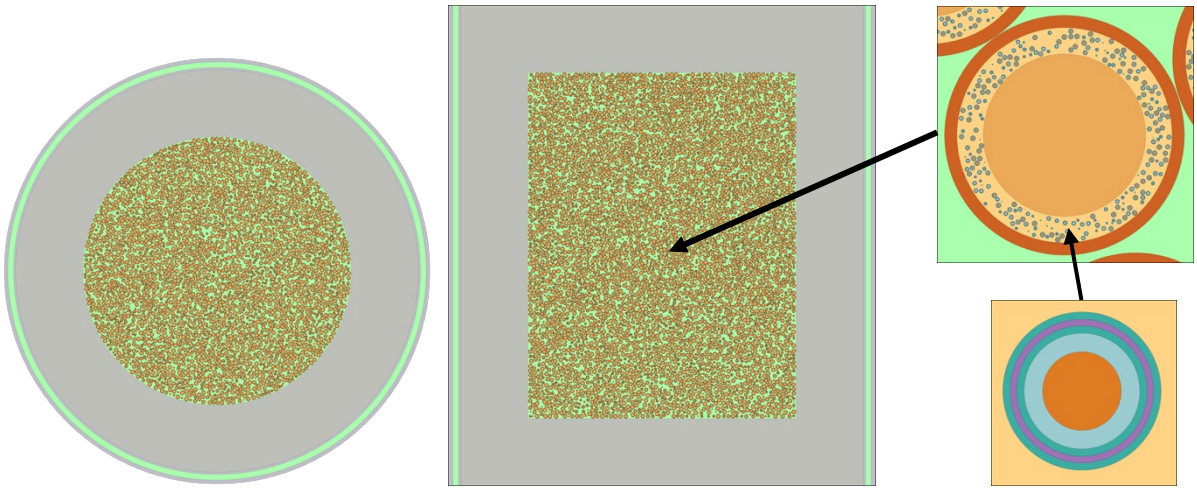

Figure 6-1: gFHR Serpent 2 model employed by Kairos Power with horizontal (left) and vertical (middle) cross sections and pebble (top right) and TRISO geometries (bottom right).

These simplifications were introduced for ease of simulation with various codes, including Kairos Power's proprietary code, KPACS (Kairos Power Advanced Core Simulator). KPACS is a tool developed by Kairos Power for designing their future FHRs, allowing for in-depth analysis of the core with multiple physics considerations [40]. Specifically tailored for pebble bed reactors, KPACS uses the macrozones approximation, dividing the core into spectral zones containing a large number of pebbles with uniform neutron flux and composition based on pass number. This approximation is based on the assumption of slowly spatially varying neutron spectra within the zones, supported by their relative size to the neutrons' diffusion length. This approach is similar to VSOP [29], but KPACS uses higher fidelity neutronics, with continuous Monte Carlo neutron transport and explicit modeling through Serpent 2 rather than a deterministic approach.

The tool uses externally informed initial pebble positions and motion, includes fuel insertion and discarding with a criterion based on passes, and allows for the presence of multiple fuel types and moderating pebbles in the same core. Users can specify different temperatures for each zone, informed by external Computational Fluid Dynamics (CFD) or porous media solvers. With its time-dependent implementation, KPACS enables the determination of the core equilibrium state, simulation of core startup, study of the running-in phase, and computation of reactivity feedback coefficients. The macrozones approach is particularly well-fitted for rapid iterations and parameter exploration. Likewise, the multi-physics capabilities and Monte Carlo method used for neutronics make it quite well-fitted for accurate simulations.

In the context of the gFHR, KPACS has been used to provide benchmarking results for this simplified case. The cylindrical core is divided into 10 axial and 4 radial macrozones. Each macrozone consists of 8 subzones corresponding to different pass numbers, ranging from fresh pebbles to last-pass pebbles. As mentioned earlier, the motion is constrained to a flat and vertical direction, meaning that compositions simply move upward from one zone to another. The equilibrium state is determined by running KPACS for a sufficient duration until reaching convergence. HxF providing higher fidelity, can be used to verify the behavior of KPACS by comparing the results of the same study for the two codes. Therefore, a comparison between HxF with discrete motion and KPACS is made to highlight the verification potential of HxF. Then, the results of HxF with discrete motion are compared with those obtained with DEM when keeping the same geometry and adding fueling and defueling chutes. Finally, thermal coupling is applied, and the impacts on the equilibrium are discussed.

6.1 Verification of KPACS against hyper-fidelity depletion and discrete motion

To compare results between KPACS and HxF, the discrete motion approach is employed as the chosen motion method to couple with Serpent 2. Therefore, once initialized, the pebble bed configuration remains unchanged throughout the simulation. To replicate trajectories, the fuel composition order is shuffled between each step, making materials move while maintaining a stationary pebble bed. This method is particularly well suited to the gFHR operation, in which a flat upward pebbles velocity profile is assumed. In this study, pebbles are assumed to be organized

as an FCC lattice, as represented in Figure 6-2, to simplify the motion sequence further. The packing fraction is set to be as close as possible to the original one while structuring the pebbles, resulting in an obtained packing of 60.072% (lattice pitch of 2.98 cm) — 0.3% higher than the model used by Kairos Power. Although this slight difference is not expected to impact the core equilibrium significantly, it must be considered when comparing global parameters obtained using the two methods, such as the multiplication factor or conversion ratio.

Nevertheless, the reorganization of pebbles into a lattice arrangement is not anticipated to produce substantial changes that would alter the conclusions drawn in this study. Indeed, the large neutron diffusion length in the reactor is expected to make it reasonably agnostic to how a uniformly packed bed is arranged. The rest of the parameters are conserved, including the TRISO particle configuration in each pebble.

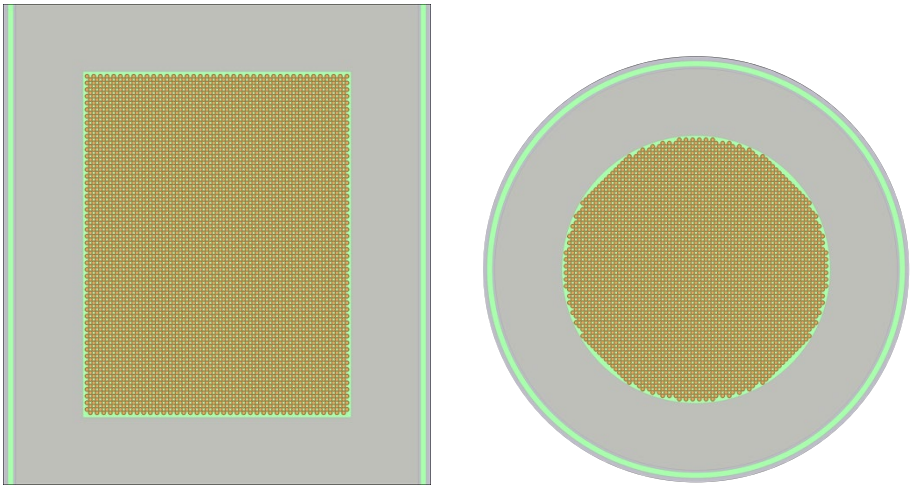

Figure 6-2: gFHR Serpent 2 model used by HxF with discrete motion horizontal (left) and vertical (right) cross sections.

In discrete motion, pebbles see their compositions shuffled between each step. Given the simulation conditions described above, the motion is purely vertical and flat. When pebbles reach the upper end of the core, their compositions are transferred to the bottom, the number of passes is incremented, and recirculated pebbles are randomly re-arranged to accurately replicate the stochastic nature of re-insertion. Recirculating pebbles also go through a discarding test. To maintain consistency with Kairos Power, pebbles that have passed through the core eight times are discarded, regardless of their burnup. The number of pebbles in the core, and thus the configuration, remains constant by replacing discarded compositions with fresh ones. Discharged and discarded pebbles' information is stored for subsequent processing. The depletion length and motion step size are related and depend on the velocity of the set pebble bed. In this simulation, each depletion step corresponds to a duration of 7.68 days. Therefore, the motion step size is 36.5 cm, equivalent to six FCC rows, accounting for 11.8% of the core's recirculation.

For this work, an initial guess for equilibrium compositions is obtained from a simplified reflected pebble model, for which compositions were interpolated as a function of burnup. Burnups

and numbers of passes are assumed to be uniformly distributed in the core. These initial compositions are imported into Serpent with the binary restart capability. An educated guess drastically decreases the number of steps to convergence. Then, multiple transport and depletion steps are applied, interspersed with motion steps. From the transport side, in order to accelerate convergence, 3 full cycles are simulated with a lower number of neutrons ($2x10^6$ active and $2x10^5$ inactive neutrons), followed by higher accuracy cycles until convergence ($5x10^7$ active and $5x10^6$ inactive neutrons). No predictor/corrector scheme is used, as it requires special treatments for inserted fresh pebbles.

Equilibrium results

This section presents key results derived from applying HxF with discrete motion on the gFHR core. We focus first on the progression toward equilibrium and then on an in-depth examination of the equilibrium state itself via spatial and statistical distributions. The content and histories of discarded pebbles, highlighting outliers, are also presented.

Approach to equilibrium

Defining equilibrium in Pebble Bed Reactors (PBRs) poses challenges. Kairos Power employed the convergence of the multiplication factor (k_{eff}) and conversion ratio (CR) as indicators that the core's global parameters have reached a steady state. Similarly, the criterion for HxF convergence to an equilibrium core is set when the multiplication factor demonstrates minimal oscillations for a cycle or more. Figure 6-3 shows the evolution for both parameters. The initial composition distribution guess of the fuel, which overestimates k_{eff} and CR, dictated initial values, although it only impacts the time to convergence and not the equilibrium itself. After an initial convergence with a non-converged fission source until 24 passes, the multiplication factor (k_{eff}) largely stabilizes after 34 passes, averaging 1.02112 ± 19 pcm, and remains within a standard deviation of 29 pcm. A parallel trend is observed for the conversion ratio (CR), with a standard deviation of 28 pcm around an average of 0.42357 ± 15 pcm. Subsequent core states, representing 11 passes, are considered equilibrium, with the observed oscillations attributed to pebble motion.

It is important to note that the multiplication factor derived from Serpent by HxF represents the value immediately post pebbles motion and fresh fuel insertion before the depletion steps. Therefore, considering that the entirely fresh fuel does not contain strongly absorbing fission products like ^{135}Xe, the accuracy of the depicted k_{eff} factor is influenced by the chosen step size (which is, in practice, the size of the inserted batch of fresh fuel). However, the sensitivity of the multiplication factor to the step size is considerably reduced post-depletion.

Figure 6-4 summarizes a sensitivity study conducted on the step size. It reveals that a reduction in step size effectively decreases the multiplication factor prior to depletion, whereas, conversely, the parameter remains relatively constant post-depletion. This suggests that an 11.8% core motion step sufficiently replicates the overall operation of the PBR well while also optimizing computational time. Given the rapid accumulation of strong absorbers, it is reasonable to infer that the keff estimation would align more closely with the post-depletion value rather than by averaging the two values and even less by taking the prior depletion value.

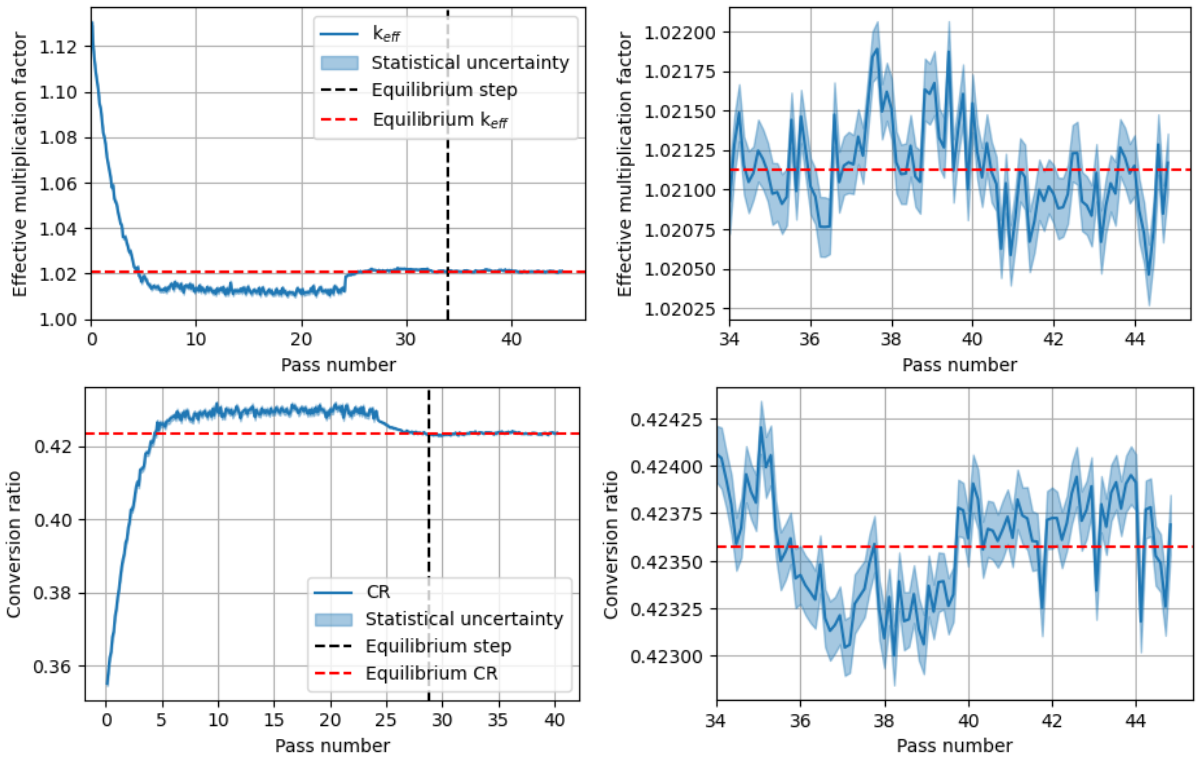

Figure 6-3: Progression towards equilibrium from the multiplication factor (top) and conversion ratio (bottom) perspectives. The right plots represent the equilibrium steps only.

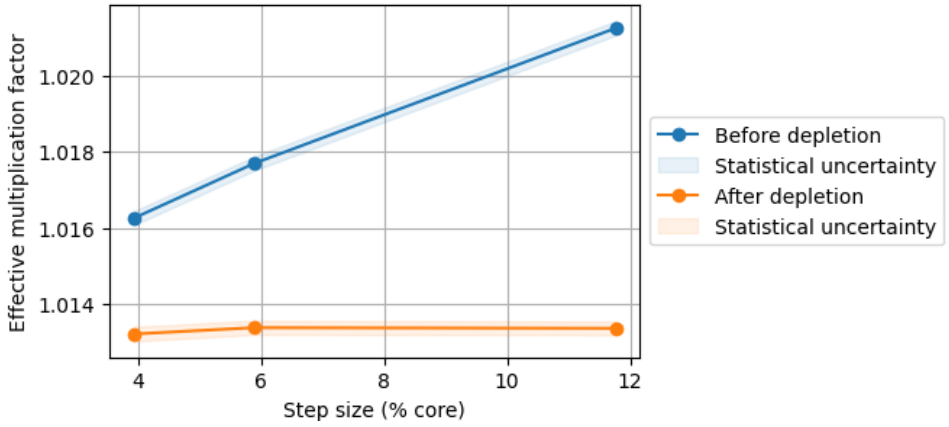

Figure 6-4: Impact of step size (expressed as a percentage of the core moved per step) on the multiplication factor.

Equilibrium core

Tallied fields

The instantaneously tallied data supplies insights into the individual experiences of pebbles as they traverse the core. Each pebble includes two types of neutron flux (thermal with E<1.86 eV

and fast with E>0.1 MeV) and the corresponding pebble powers. Figure 6-5 shows typical distributions for a representative equilibrium step and their average over all equilibrium steps. Once the system reaches equilibrium, the fluxes describe relatively steady distributions, as indicated by the similarity between the snapshot and averaged data, while the power shows more differences. This discrepancy is a consequence of the varying residence times among pebbles and their neighbors due to the MEDUL mode of operation in the gFHR. The uncertainties for the thermal fluxes average 2.9%, 3.8% for the fast fluxes, and 7.9% for the powers.

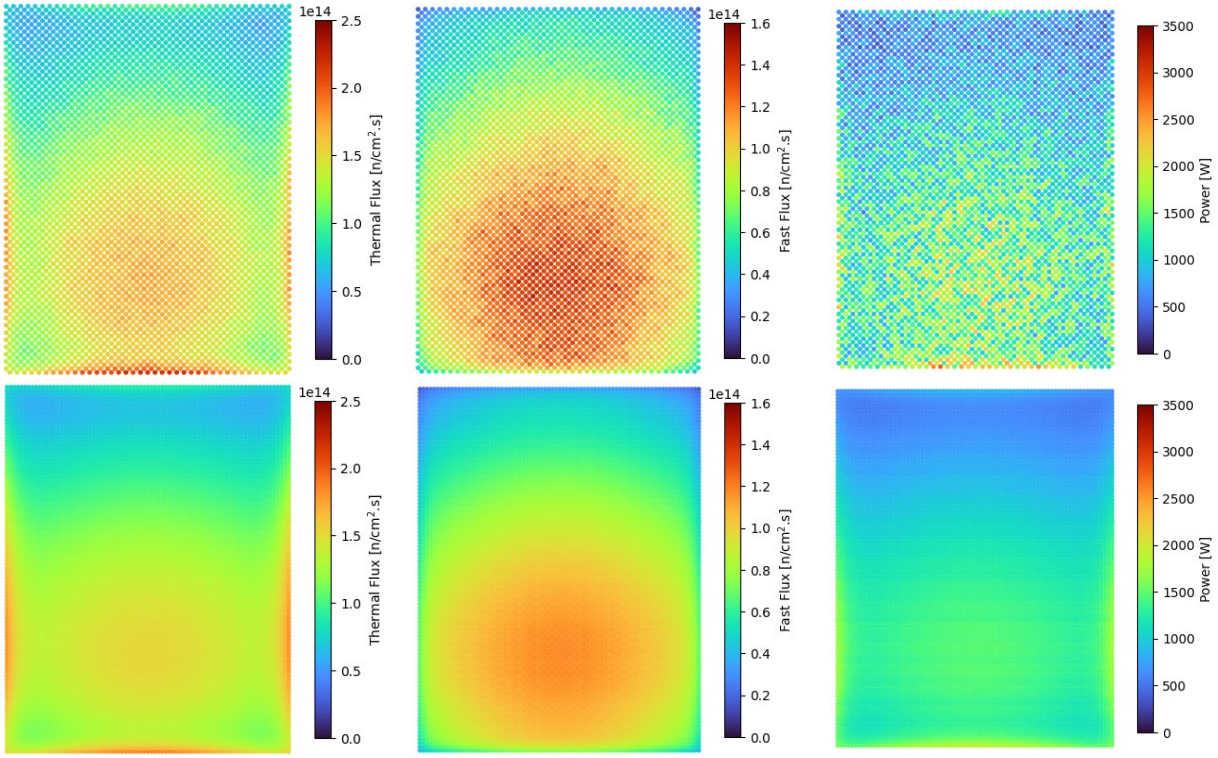

Figure 6-5: Longitudinal slice of the gFHR core at a representative equilibrium step (top) and averaged over all equilibrium steps (bottom).

The observed patterns in this simplified model align with expectations and findings from previous studies [65]. To further analyze data, one-dimensional spatial profiles averaged over all equilibrium steps are presented in Figure 6-6, Figure 6-7, and Figure 6-8. The thermal flux and power, despite the power's dependency on the pass number, display similar behavior due to the thermal spectrum in the core. On average, their values peak near the axial center for all pass numbers and near the reflector for power and thermal flux. This can be attributed to the interaction of the reflected thermalized neutrons with the fuel in that region.

Conversely, fluxes and power diminish towards the corners due to higher neutron leakage from the cylinder. Additionally, a downward shift is observed, resulting from the upward motion of pebbles. It can be explained by the fact that the fuel at the bottom of the core for a given pass number tends to be less utilized than at the top. This behavior is observed on one-dimensional profiles, where thermal flux and power have peaks at high radial distances, at the highest and

lowest elevations (fast fluxes do not), and at an axial peak below the center.

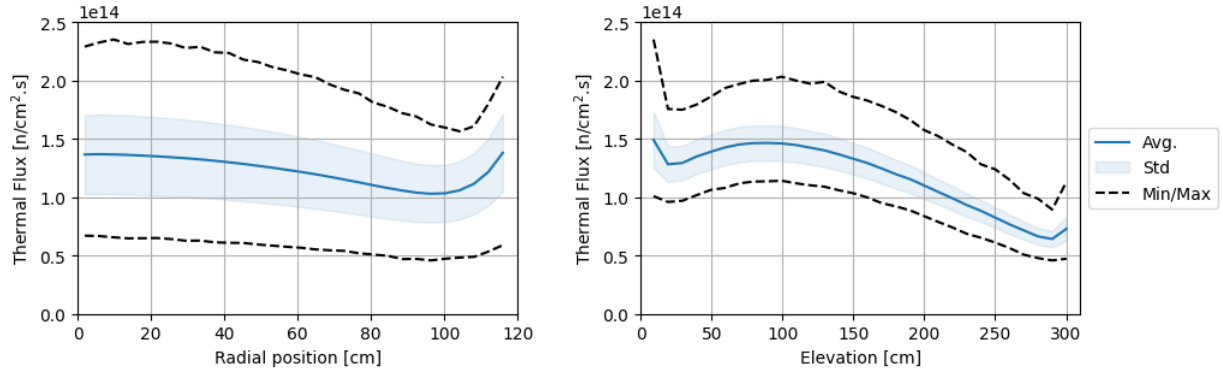

Figure 6-6: Radial (left) and axial (right) average thermal neutron (<1.86 eV) flux profiles at equilibrium.

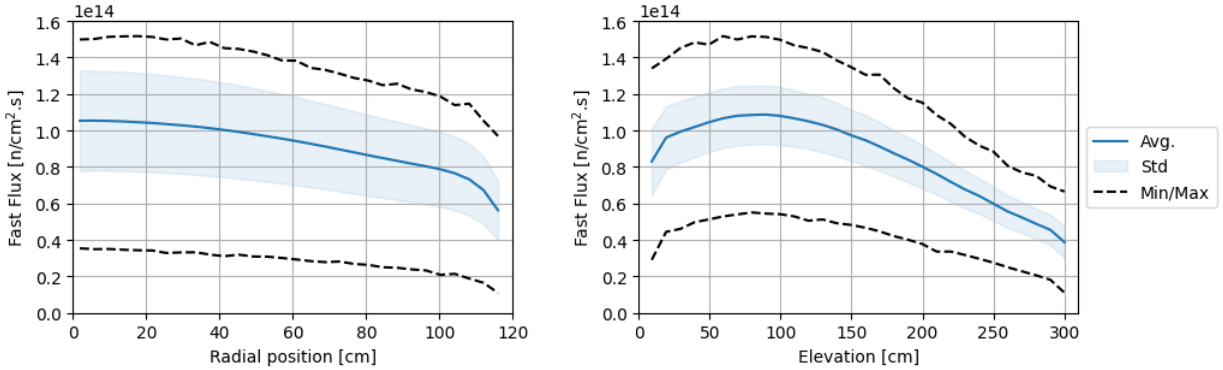

Figure 6-7: Radial (left) and axial (right) average fast neutron (>0.1 MeV) flux profiles at equilibrium.

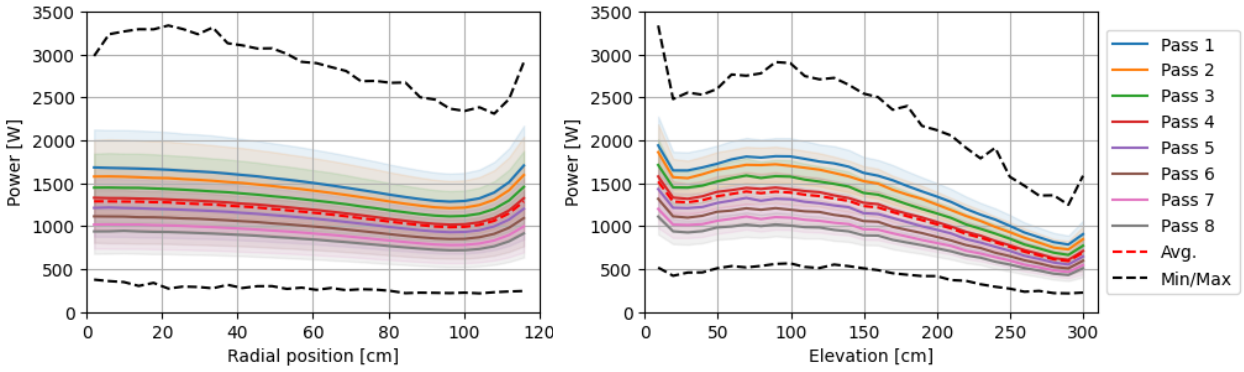

Figure 6-8: Radial (left) and axial (right) pebble power distribution per pass at equilibrium.

Power profiles are differentiated based on the number of passes the pebbles have gone through the core, and the corresponding statistical distributions per pass are depicted in Figure 6-9. Both

indicate that pebble powers decrease as the number of passes increases, as the fuel is progressively used and generates less power. However, given the even distribution of pebbles in the number of passes in the gFHR operation, the power profile shape, primarily dependent on the thermal flux profile, remains relatively constant. The average shift in power per pass remains quite stable (-92 ± 14 W/pass). The power distribution also broadens as the number of passes increases, indicating once again that the pebble's power output progressively decreases over its lifetime.

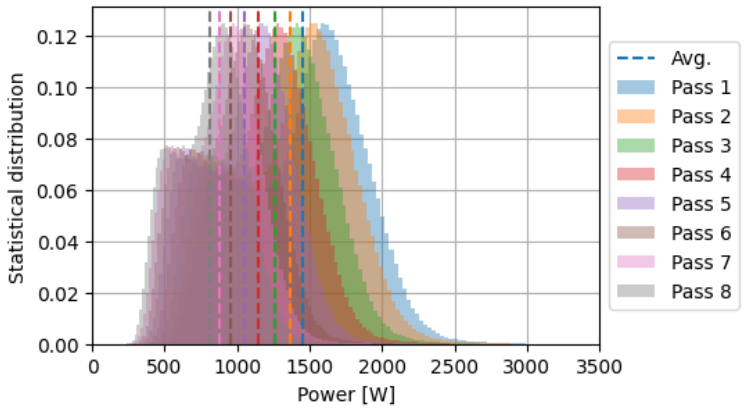

Figure 6-9: Pebble power statistical distribution per pass over all equilibrium states, normalized over the total count.

The substantial difference between the minimum, average, and maximum values for the three tallied quantities indicates the presence of outlier pebble histories, which will be examined in a later subsection. This disparity results in high peaking factors of 2.00, 1.79, and 2.99 for the thermal flux, fast flux, and pebble powers, respectively.

Then, cumulative results provide a broader understanding of gFHR's overall behavior. By integrating fluxes over the residence times, fluences can be obtained. Similarly, the burnup is proportional to the accumulated energy throughout the pebbles' history. Similar to the analysis of tallied data, cumulative quantities can be analyzed to gain insights into the behavior of the gFHR. Burnup and thermal fluence both provide cycle information and capture the history of the fuel, while fast fluence is an important parameter to estimate the radiation damage on the pebbles. Spatial distributions per pass are displayed in Figure 6-10, Figure 6-11, and Figure 6-12, with corresponding statistical distributions depicted in Figure 6-13.

All three parameters exhibit similar spatial behavior with nearly flat radial profiles. Over time, these profiles become more uniform due to pebbles' random radial re-insertion positions. Axially, the quantities increase almost linearly, accumulating slightly faster at the bottom of the core (where the flux is highest) compared to the top. However, the standard deviations increase with the number of passes, indicating a wide range of possible trajectories that pebbles may take throughout their history. The average burnup is 10.2%FIMA, while the maximum value found in the core is 20.2%FIMA, resulting in a peaking factor of 1.98.

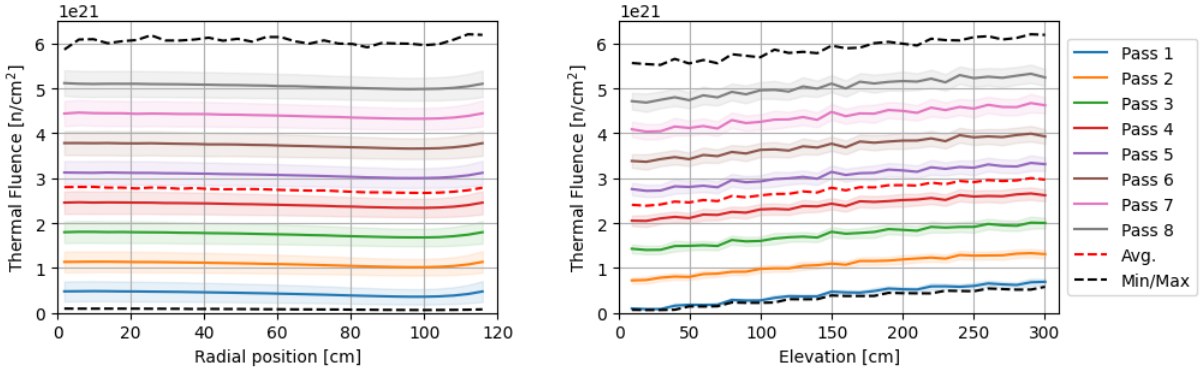

Figure 6-10: Radial (left) and axial (right) average thermal neutron (E<1.86 eV) fluence profiles at equilibrium.

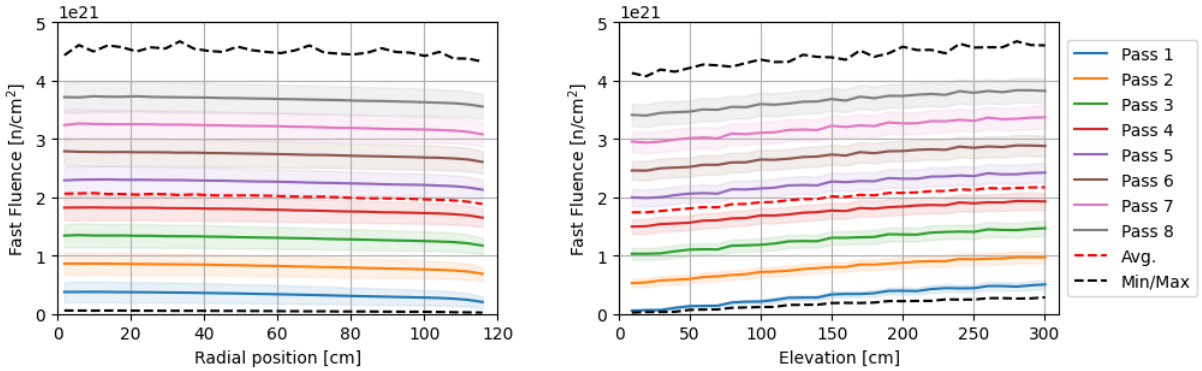

Figure 6-11: Radial (left) and axial (right) average fast neutron (E>0.1 MeV) fluence profiles at equilibrium.

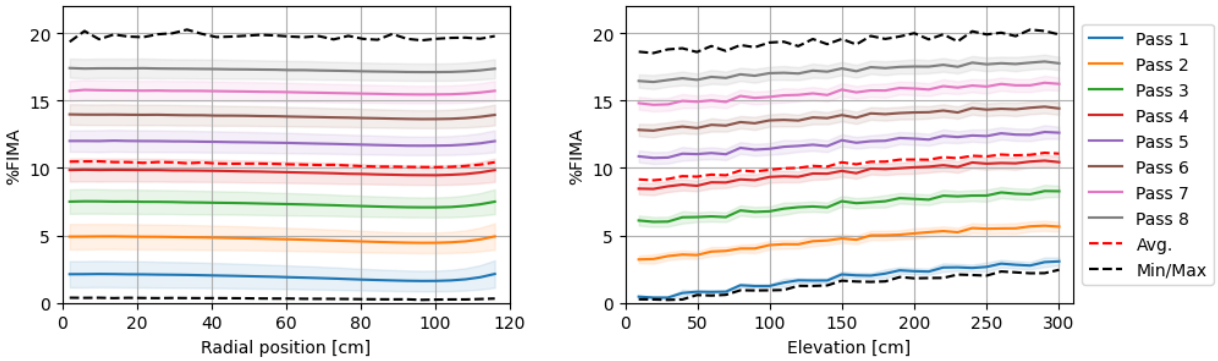

Figure 6-12: Radial (left) and axial (right) burnup (in %FIMA) profiles at equilibrium.

Similar to previous research [65], the distributions gradually align closer to Gaussian distributions and become less reliant on the initial fuel insertion over time. It is worth noting that there is an overlap between values corresponding to subsequent numbers of passes. This overlap becomes more prominent at higher numbers of passes due to the widening range of burnup values.

For instance, pebbles with three different pass numbers may overlap around 15.5%FIMA. This implies that one cannot identify with certainty the number of passes a pebble has made by only estimating its burnup through gamma spectroscopy and ^{137}Cs concentration determination through the 662.1 keV peak intensity, as is typically done in PBRs. Furthermore, as the discarding criterion for the benchmark case is based on the number of passes rather than the burnup value or ^{137}Cs content, the core behavior may not be entirely realistic. In fact, setting a measurable threshold for the pebbles would alter the distributions of the number of passes and high-burnup pebble content, which would likely impact the overall behavior of the core during steady operation.

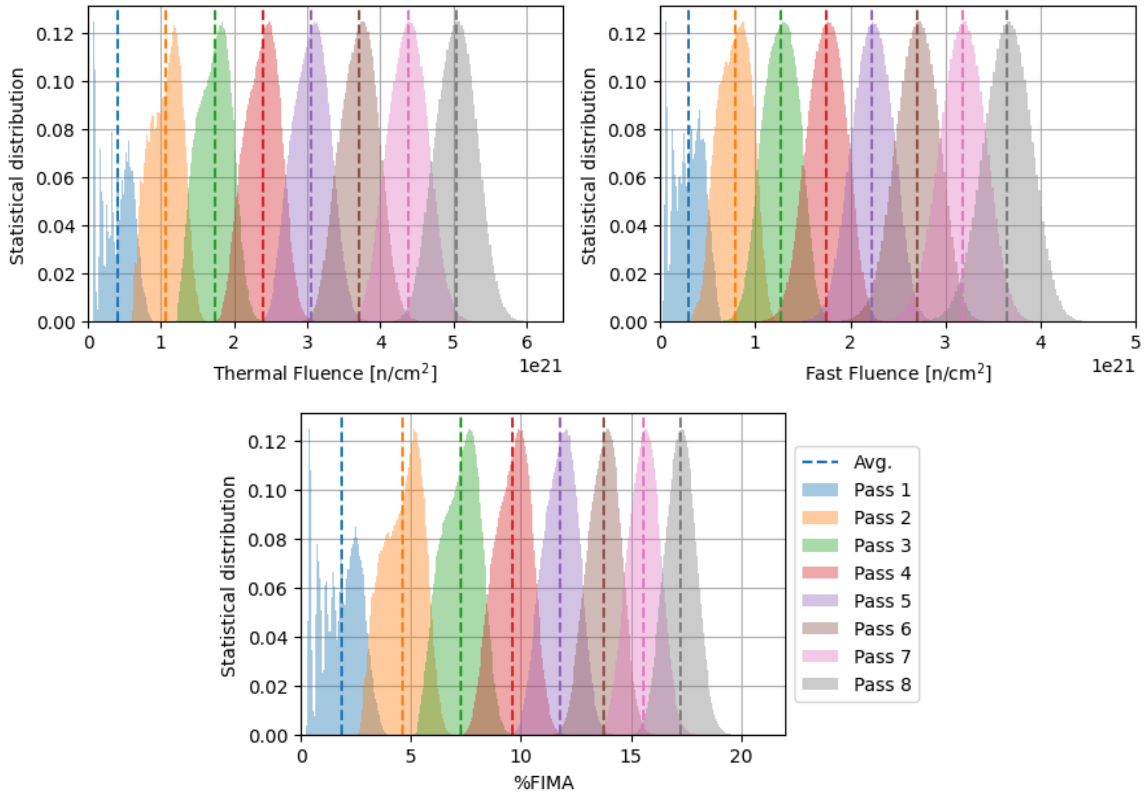

Figure 6-13: Pebbles thermal (top left) and fast (top right) fluences, and burnup (in %FIMA, bottom) statistical distributions over all equilibrium states, normalized over the total count.

Discharged and discarded pebbles content

The HxF tool allows recording the content for every discharged pebble, including discarded ones. In this study, considering the pass-dependent discarding criterion, the content of pebbles discharged at pass 8 corresponds exactly to the discarded content. Figure 6-14, Figure 6-15, and Figure 6-16 present the statistical distributions of cumulative quantities per pass, along with a more detailed view of the discarded contents. Both thermal and fast fluences demonstrate consistent increases per pass ($6.61 \times 10^{20} \pm 0.02$ n/cm².pass and $4.78 \times 10^{20} \pm 0.04$ n/cm².pass, respectively) due to the constant experienced fluxes throughout the pebbles' histories regardless of their burnups, as the fluxes depend solely on the overall core configuration at equilibrium. On the other hand, the burnup shift decreases from 2.75 %FIMA at the first pass to 1.6 %FIMA at the last pass.

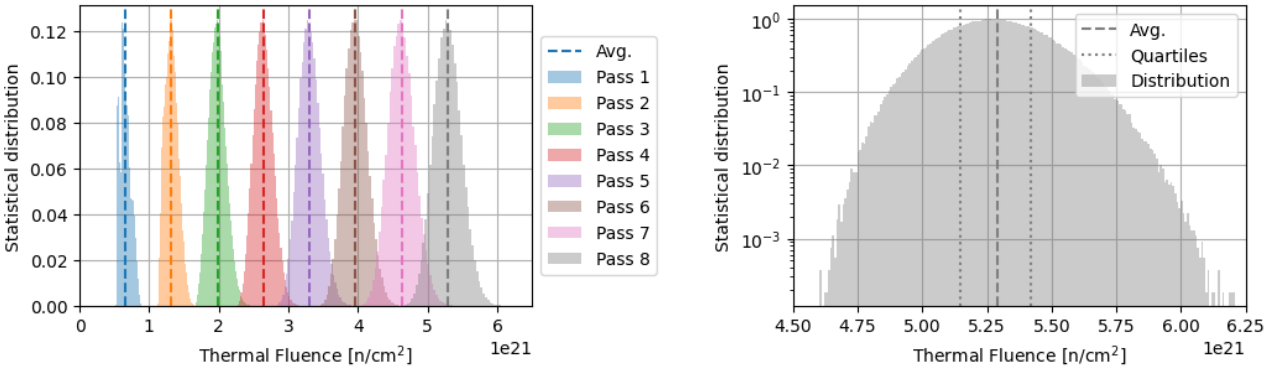

Figure 6-14: Pebbles thermal fluence statistical distribution over all discharged (left) and isolated discarded (right) pebbles at equilibrium, normalized over the total count.

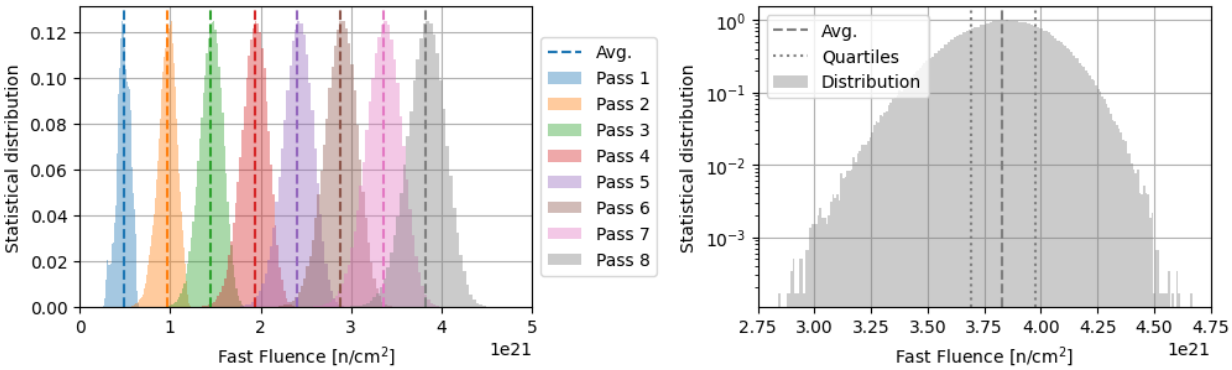

Figure 6-15: Pebbles fast fluence statistical distribution over all discharged (left) and isolated discarded (right) pebbles at equilibrium, normalized over the total count.

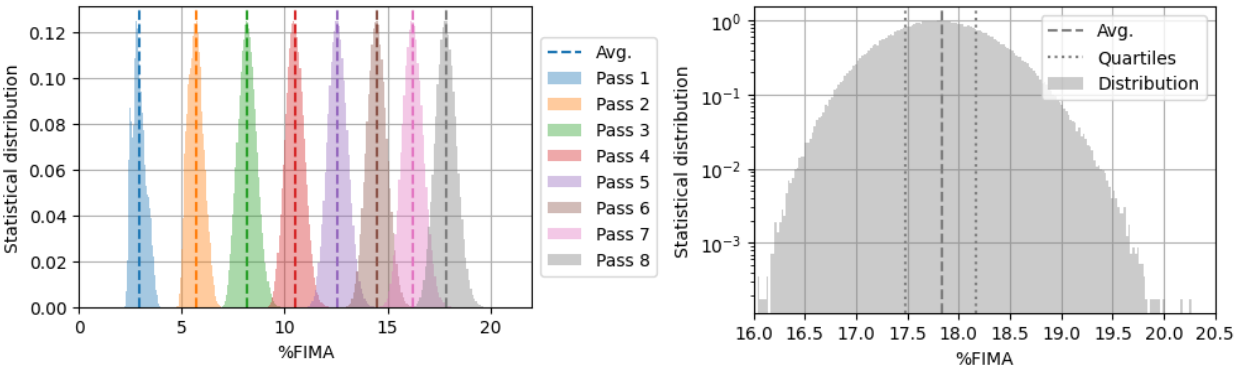

Figure 6-16: Pebbles burnup statistical distribution over all discharged (left) and isolated discarded (right) pebbles at equilibrium, normalized over the total count.

The maximum discarded fast fluence recorded is 4.67×10^{21} n/cm², significantly higher than the average value of 3.83×10^{21} n/cm². This maximum value can be utilized as an input for fuel performance models. The discarded pebbles exhibit burnup ranging from 16.0% to 20.3 %FIMA, with an average of 17.8%FIMA. Once again, the wide range of burnup values arises from pebbles,

with pass 8 discarded regardless of their burnup levels. Comprehensive minimum, average, and maximum pebble discharger content and information are given in Appendix C.

Trajectory analysis

One of the advantages of using HxF is the capability to track pebbles individually throughout their lifetimes and record their histories. By compiling and analyzing the complete pebble histories obtained during equilibrium, one can extract the minimum, maximum, and average pebble history for quantities of interest, as depicted in Figure 6-17. The average radial distance covered by pebbles after 8 passes ranges from 36.4 cm to 111.6 cm, with a mean value of 78.6 cm. This disparity in radial distance greatly influences which conditions pebbles experience. As mentioned earlier, the thermal flux experienced during a pass remains relatively constant on average, while the pebble power decreases over time due to increased burnup. This reasoning is, however, put in perspective for cases with shear stress using DEM methods to obtain the pebble trajectories in Chapter 6.2.

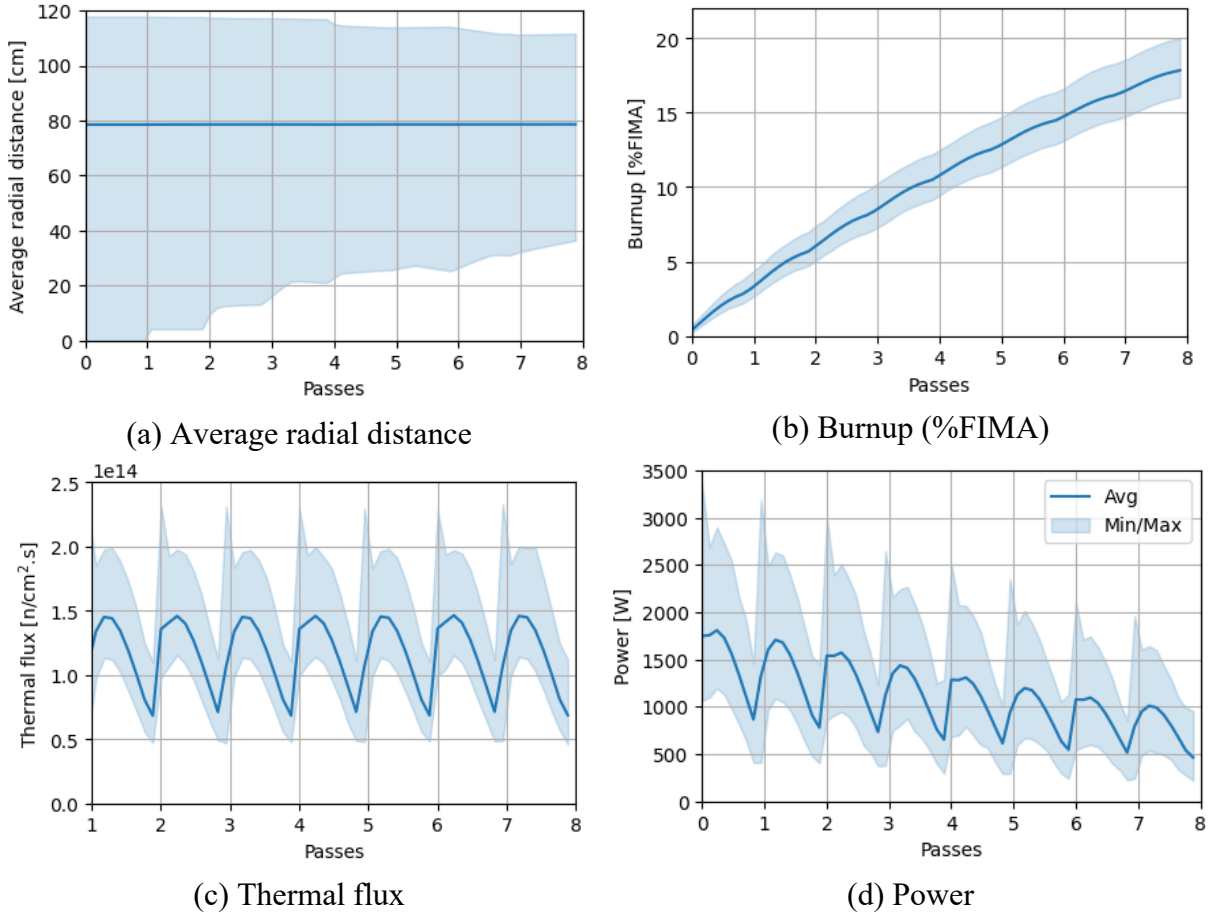

(a) Average radial distance

(b) Burnup (%FIMA)

(c) Thermal flux

(d) Power

Figure 6-17: Envelope and average pebbles histories at equilibrium for key parameters.

When examining the pebbles with the highest (>19.5%FIMA) and lowest (<16.5%FIMA) discarded burnup levels, as shown in Figure 6-18, it is clear that the former category predominantly circulates in the intermediate radial region, neither close to the reflector nor to the core center. In

this region, the pebbles are exposed to a lower thermal flux, resulting in lower power generation. In contrast, the highest burnups are produced by pebbles that predominantly reside near the center of the core throughout their history, where the flux and power levels are highest. This is particularly notable at the bottom of the core, near the bottom reflector, where the flux and power reach their peak values when inserted at the center while remaining low elsewhere. It is important to note that this behavior is influenced by the simplified geometry used in the gFHR. In a more realistic geometry, fueling and defueling chutes may be located at both axial ends of the core, significantly reducing this effect and altering the shape of the core.

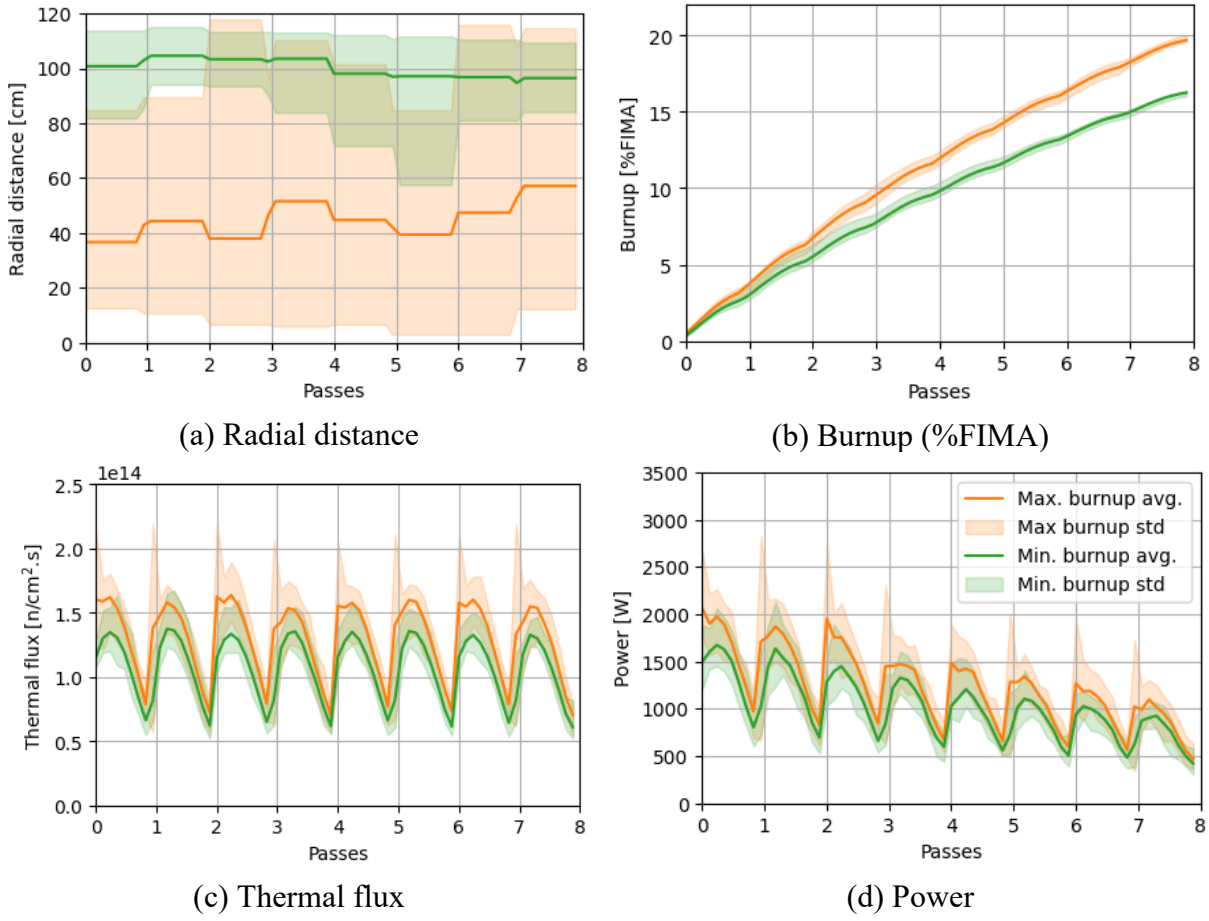

(a) Radial distance

(b) Burnup (%FIMA)

(c) Thermal flux

(d) Power

Figure 6-18: Histories for the 20 highest and 20 lowest discard burnup pebbles at equilibrium.

Comparison with KPACS results

The comparative analysis of the KPACS results and those procured from HxF is performed. A global parameter comparison is conducted, followed by a more local analysis. In particular, pebble-wise and macrozone-wise power distributions and isotopic concentrations are studied, as well as multiple reactivity coefficients.

Global core parameters

As mentioned above, HxF can provide multiplication factors before and after depletion stages.

The 0.3% discrepancy in the count of pebbles between the dispersed pebble bed and the lattice version causes an overestimation of multiplication factors and an underestimation of conversion ratios. For this comparison, a correction factor corresponding to this difference is thus applied. The comparative data of these two parameters, as shown in Table 6-1, illustrates that the KPACS-derived multiplication factor differs by -455 pcm and +307 pcm from the HxF results before and after depletion, respectively. While these discrepancies might seem large, it is noteworthy that the KPACS results fall within the range of the HxF values. For the conversion ratio, the difference is between -52 pcm and -806 pcm, which is higher than for the multiplication factor. This could be attributed to potential disparities in isotopic concentrations within the core, a topic further explored in a subsequent subsection.

Table 6-1: Comparison between the corrected multiplication factor obtained with HxF with those with KPACS.

Case	Multiplication factor	Conversion ratio
HxF (before depletion)	1.01794 ± 19 pcm	0.42225 ± 15 pcm
HxF (after depletion)	1.01021 ± 18 pcm	0.42546 ± 15 pcm
KPACS	1.01331 ± 13 pcm	0.42203 ± 11 pcm

The reactivity coefficients derived from the two methodologies are also compared. Following the methodology prescribed in [40], temperatures and densities variations are applied to the reference case to calculate the following reactivity coefficients: coolant temperature (CTC), fuel temperature (FTC), moderator temperature (MTC), reflector temperature (RTC), and coolant void (VC). Results in Table 6-2 show similar orders of magnitude and signs between the two methodologies. The FTC and VC values are in good agreement, whereas KPACS underestimates the magnitude of the CTC, MTC, and RTC.

Table 6-2: Comparison between the reactivity coefficients obtained with HxF with those with KPACS.

Case	|Δ|	Multiplication factor	HxF reactivity coefficient	KPACS reactivity coefficient	Difference
Ref	-	1.021124 ± 18 pcm	-	-	-
CTC*	100K	1.018537 ± 18 pcm	-2.59 ± 0.33 pcm/K	-1.20 ± 0.12 pcm/K	54%
FTC	100K	1.016536 ± 19 pcm	-4.59 ± 0.26 pcm/K	-4.56 ± 0.12 pcm/K	1%
MTC	100K	1.018345 ± 19 pcm	-2.78 ± 0.26 pcm/K	-0.40 ± 0.12 pcm/K	86%
RTC	100K	1.021691 ± 19 pcm	0.57 ± 0.26 pcm/K	0.92 ± 0.12 pcm/K	62%
VC	2.5%	1.022263 ± 19 pcm	-45.56 ± 10.61 pcm/%	-48.19 ± 9.05 pcm/%	-6%

* The coolant density was adjusted accordingly.

Power distributions

A comparative analysis of spatial power distributions, derived from HxF and KPACS methodologies, is illustrated in Figure 6-19. The radial profiles exhibit slight differences, with a maximum observed relative difference on average profiles of 3.5%. Nevertheless, a higher standard deviation indicates the presence of more extreme pebble power values in pebble power values across all core locations. KPACS tends to produce slightly higher values in the core, except

for peripheral regions, where powers are lower than HxF. This discrepancy may be attributable to the side reflector's reduced influence in KPACS.

A stronger contrast between the profiles is observed axially, highlighting the primary difference between the two methodologies. KPACS underestimates pebble power at the bottom of the gFHR by 14% while conversely overestimating power at the top by an identical margin. This variability is largely due to the dilution of compositions and fluxes in macrozones methods; pebbles within the same region, even if they have an identical number of passes, can still have substantial burnup differences and experience diverse fluxes depending on their proximity to a reflector, a corner, or the core's center.

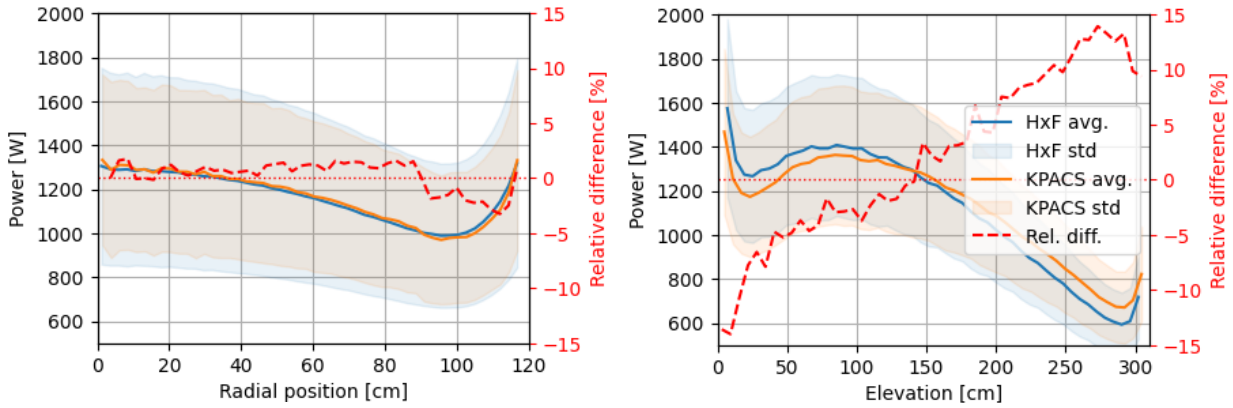

Figure 6-19: Comparison between radial (left) and axial (right) equilibrium power profiles obtained with HxF and KPACS.

The obtained statistical power distribution difference is represented in Figure 6-20. As inferred, pebble powers with the KPACS tool range from 320 to 2730W, a significantly narrower range than the one obtained through HxF (215 to 3340W). This observation, associated with the overrepresentation of values around the average (1115W) between 775 and 1475W, strengthens the argument that dilution plays a significant role in the equilibrium core distributions.

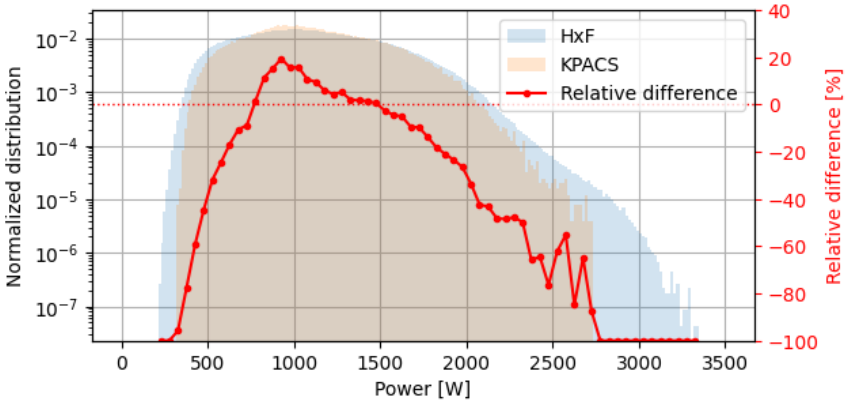

Figure 6-20: Comparison between equilibrium statistical power distributions obtained with HxF and KPACS.

Zone-wise spatial differences based on the number of passes are presented in Figure 6-21, where the observed phenomena are consistent with earlier observations. Radially, the results do not drastically change, except near the reflector, where the power difference value decreases. Axially, the difference is negative for low elevations and becomes positive at the top of the core. Axially, power differences are negative at lower elevations and gradually turn positive towards the core's top. This diagram further emphasizes that these observations remain consistent across each pass, implying that the number of passes does not significantly influence the disparity in results between the two tools.

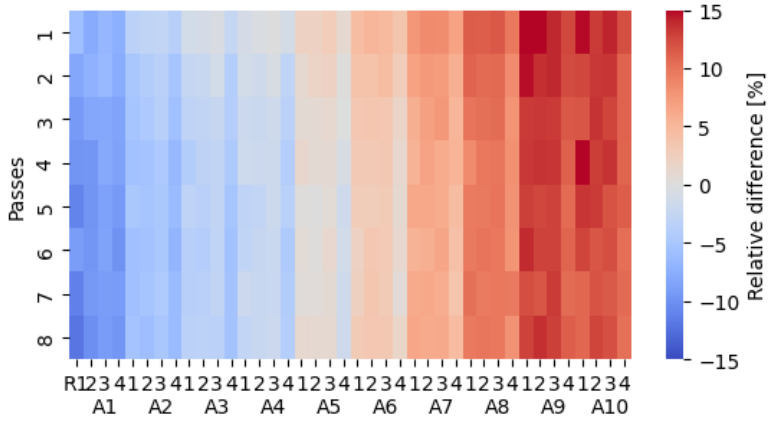

Figure 6-21: Zone-wise (axial — A and radial — R) relative difference between pass-dependent powers obtained with KPACS and HxF.

Another important aspect of benchmarking is peaking factors. Since both methods allow individual tallying of pebble power, zoning is not required. The power peaking factor derived from KPACS is 2.44, representing an 18.6% decrease compared to the HxF value obtained in Section IV.B, corroborating the observations made in this subsection.

Zone-wise compositions and burnup

The exploration of compositions and burnup can offer additional comparative insights. However, it is worth noting that KPACS only determines zone-wise values for these parameters. Therefore, a comparison with both individual and zone-averaged HxF values is made. The statistical distribution in Figure 6-22 suggests, in line with previous observations, that KPACS may not capture outlier values as effectively as HxF. Indeed, while the burnup distributions are notably similar below 18%FIMA (with a more discrete distribution in KPACS), the remainder of the values are absent in KPACS. While this discrepancy affects local parameters and outlier values, it is unlikely to impact the global equilibrium significantly, and this prediction is in line with the observations. Averaging HxF results over KPACS-defined macrozones brings the distributions closer to each other. The burnup peaking factor derived from KPACS is 1.748, 11.82% lower than the HxF value. However, when considering the zoned HxF data, the peaking factor value becomes 1.757, differing from KPACS's by only 0.51% and thus indicating a much closer match.

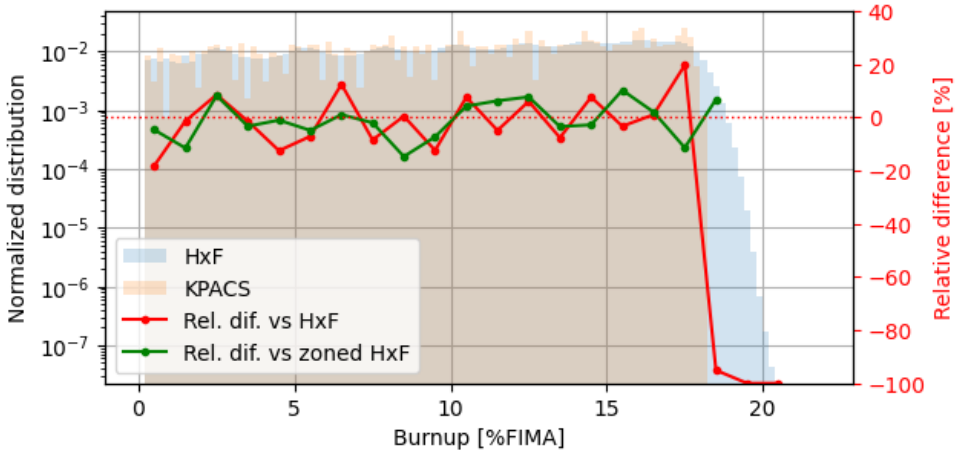

Figure 6-22: Comparison between equilibrium statistical burnup distributions obtained with HxF (zoned and not zoned) and KPACS.

Analyzing the absolute zone-by-zone differences in Figure 6-23, this minor global difference is observed across all pebble cycles and core regions. Indeed, radial and axial positions do not substantially influence this difference, and the number of passes only induces a slight trend towards burnup underestimation by less than 0.15%FIMA. At discard, the average burnup value in KPACS is 17.6, which is only a 0.2% deviation from the HxF value.

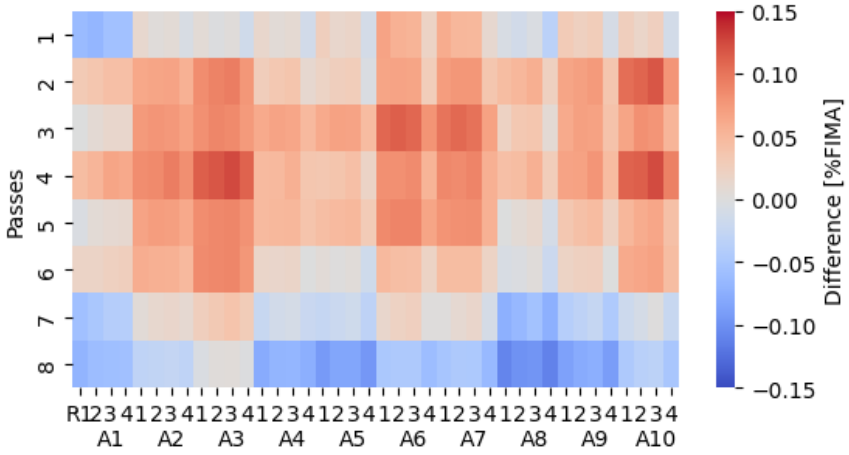

Figure 6-23: Zone-wise (axial — A and radial — R) absolute difference between pass-dependent burnups obtained with KPACS and HxF.

Regarding atomic densities of key nuclides, Figure 6-24 shows the difference between the two approaches for the highest axial zone. KPACS appears to have a higher ^{235}U fission rate than HxF, while ^{238}U is consumed less, and the plutonium vector and americium are generated less. This suggests that, on average, the spectrum is more thermal in KPACS than in HxF. Some fission products, such as ^{137}Cs and ^{90}Sr, are in close agreement between the two simulations, whereas others, like ^{131}I, which has a larger half-life, are underestimated by KPACS. This is attributable to

the more significant amount of fissions and reduced breeding. The ^{135}Xe concentration is underestimated at the top of the core, possibly due to the higher power in KPACS, leading to a higher transmutation rate of this fission product.

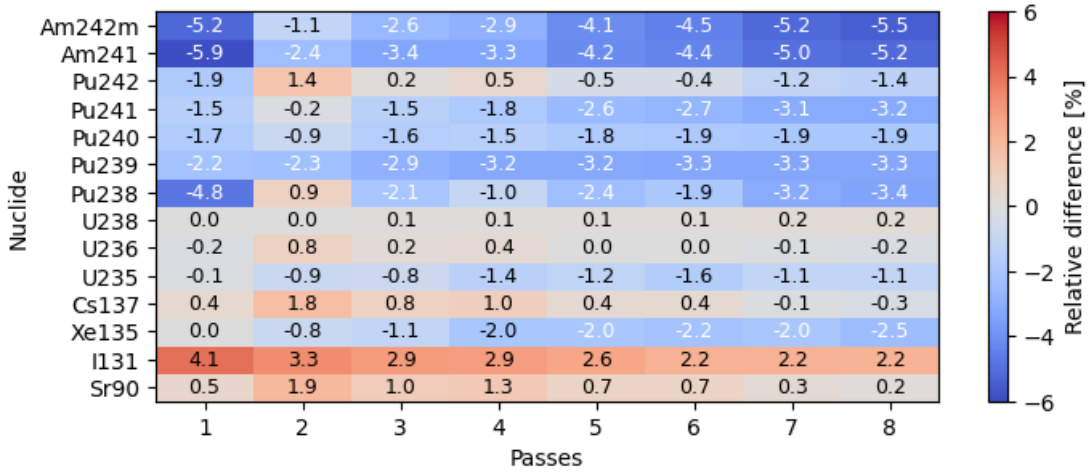

Figure 6-24: Pass-dependent top axial zone atomic concentrations differences between KPACS and HxF for key nuclides.

Examining the most significant discrepancies among fission products in Figure 6-25, the majority is negative, which implies that fewer fission products are produced due to the decreased amount of ^{235}U atoms undergoing fission. In particular, the Pm/Sm chain includes 5 of the 7 isotopes with the highest difference. Specifically, ^{149}Sm has an average difference across passes, radial and axial zones of -35%, reaching -45% to -50% for passes 6, 7 and 8. For a more comprehensive comparison with KPACS content, Appendix C provides more information about discharged pebbles information.

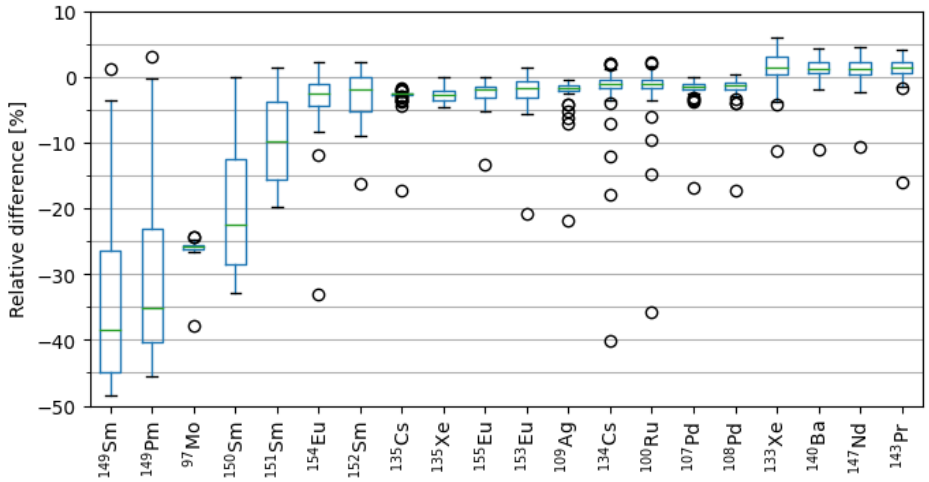

Figure 6-25: Atomic concentration differences between KPACS and HxF for the 20 most different nuclides.

6.2 Comparison between discrete motion and Discrete Elements Method

Discrete motion is particularly appropriate when applied to the gFHR benchmark model. Indeed, the velocity profile is assumed flat, with no wall effect and shear forces. In addition, the purely cylindrical geometry of the gFHR simplifies the sequence motion once the pebble bed is structured as an FCC lattice. However, residence time variability is expected, even in simplified geometry. Spatial pebbles' self-shielding effects and outliers might be altered.

Therefore, this section aims to compare the core behavior between the obtained results with discrete motion and those obtained with DEM. To that end, two new simulations are performed; first, with the same cylindrical geometry but replacing pebbles positions with DEM results; second, more realistic geometries containing fueling and defueling chutes linked to the active region through conic areas.

Compared models

The three models used for this comparison are represented for comparison in Figure 6-26. The first model is the one used in the earlier study. The second conserves the same geometry, materials, and roughly the same number of pebbles (taking the number used in KPACS). However, positions are obtained through a DEM calculation with parameters summarized in Table 6-3 and the method described in Chapter 4.3. Comparably, the third model uses DEM-obtained positions with the same parameters and number of pebbles, and the same materials as the other two models but has a modified geometry. A fueling and a defueling chute, both 50 cm large and 50 cm high, are connected to the active region through cones with a 120º slope. To better capture the pebble motion, the drainage step is set to 6% of the pebble inventory, and to make a one-to-one comparison, the DEM step was changed to the closest possible step to this value, 3.8 days (5.9%). Given the large time scales of the phenomena, the gravity is inverted to approximate the pebbles' buoyancy for both simulations.

Motion comparison

Given that the pebbles are not dispersed or structured in a lattice with some pitch with discrete motion, the active region is not filled with pebbles anymore and is packed more at the top of the core. To compare the packing among the three cases, a tailored Monte Carlo method is employed. The method involves generating a substantial number of uniformly distributed points within the geometry. Each sample is evaluated to check for potential collisions with the pebbles present in the core. The core is then divided into radial and axial regions for analysis. The packing fraction in a given zone corresponds to the fraction of detected collisions over the total number of samples in that zone. Results are shown in Figure 6-27 and Figure 6-28. The estimated total packing fractions of 60.07%, 59.88%, and 56.23% show overall that the DEM tends to yield lower values and that the presence of a defueling chute strongly affects them. The obtained local packing profiles highlight differences between the three cases. In the discrete motion case, the radial packing is irregular due to the pebbles being structured. The axial packing is relatively uniform,

except close to the reflector, which quickly drops to zero since some space is modeled between the pebbles and the side reflector. For the DEM cases, the axial and radial packing fractions tend to be more regular in the active region but with strong oscillation exceeding 70% packing towards the walls, showing the effects of shear stress. In the full DEM model, the different geometrical zones are identifiable in the axial profile. In the active region (from 104.85 cm to 384.32 cm), contrary to the two other cases, the axial packing is not roughly constant and decreases with the elevation. This can be attributed to the presence of the defueling chute in the model.

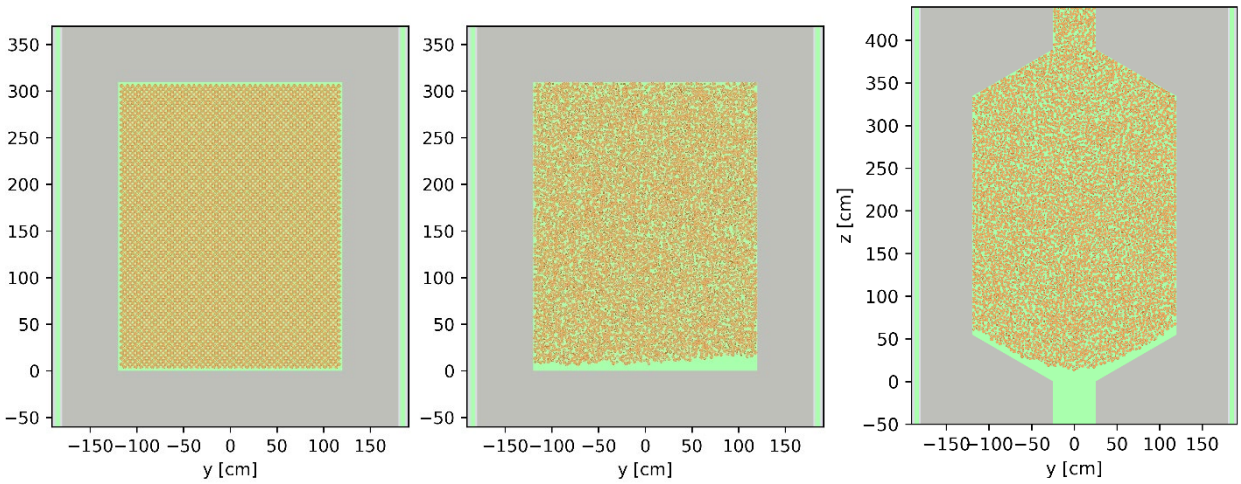

Figure 6-26: Serpent models for the discrete motion (left), cylindrical DEM (center), and full DEM (right) version of the gFHR.

Table 6-3: Discrete elements method parameters [83].

Parameter	Value
Total number of pebbles	250,190
Pebbles radius	2 cm
Pebbles density	1745 kg/m^3
Insertion speed	-2 m/s
Converged porosity passes	2
Total simulated passes	10
Step size	6% drainage (15,011 pebbles)

Parameter	Value
Settling condition	v<0.4 m/s
DEM step size	25 µs
Youngs modulus	8 GPa
Poisson ratio	0.12
Coefficient of restitution	0.6
Sliding coefficient	0.3
Rolling coefficient	0.1

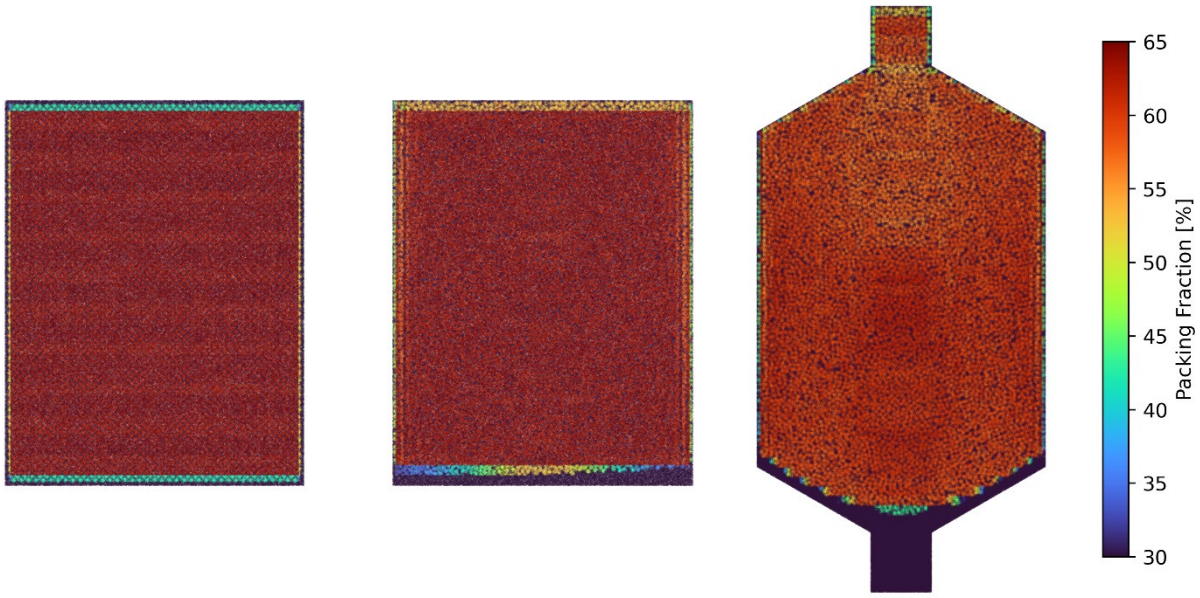

Figure 6-27: Packing fractions in a representative equilibrium slice for the discrete motion (left), cylindrical DEM (center), and full DEM (right) version of the gFHR.

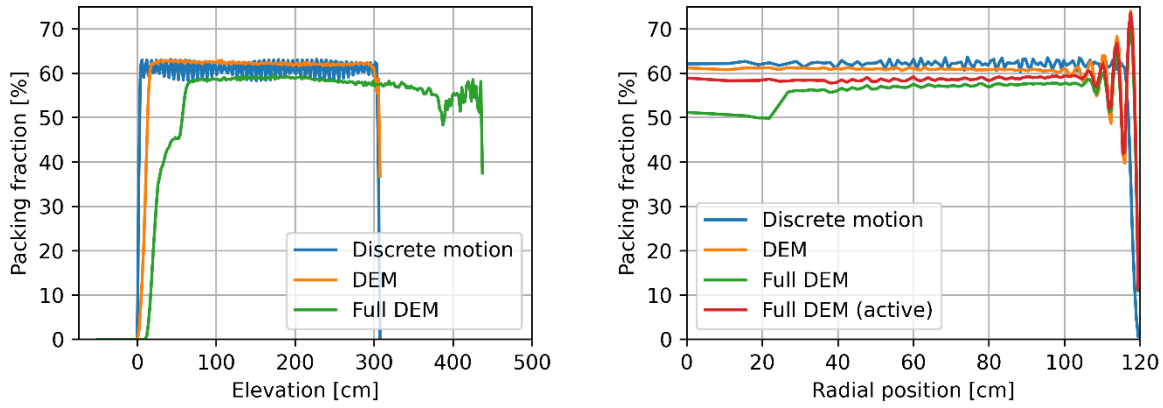

Figure 6-28: Axial (left) and radial (right) local pebbles packing fractions.

Similarly, pebble trajectories and residence times are compared in Figure 6-29. Pebble positions are compiled over all the motion steps, residence times are calculated, and all trajectories, from insertion to discharge, are extracted. The two first models are similar and show clear axial demarcations indicating the motion steps. The pebbles flow as radial channels with extremely low cross-mixing. However, the wall effect in the DEM model results in higher residence times towards the reflector (33% higher than at the center). This phenomenon is much more pronounced in the model with the defueling chutes. Indeed, the shear stress associated with the longer path length of pebbles close to the reflector than pebbles in the central region leads to residence times reaching up to 140 days. Therefore, current pass burnups accumulated in pebbles with these trajectories are expected to be more significant.

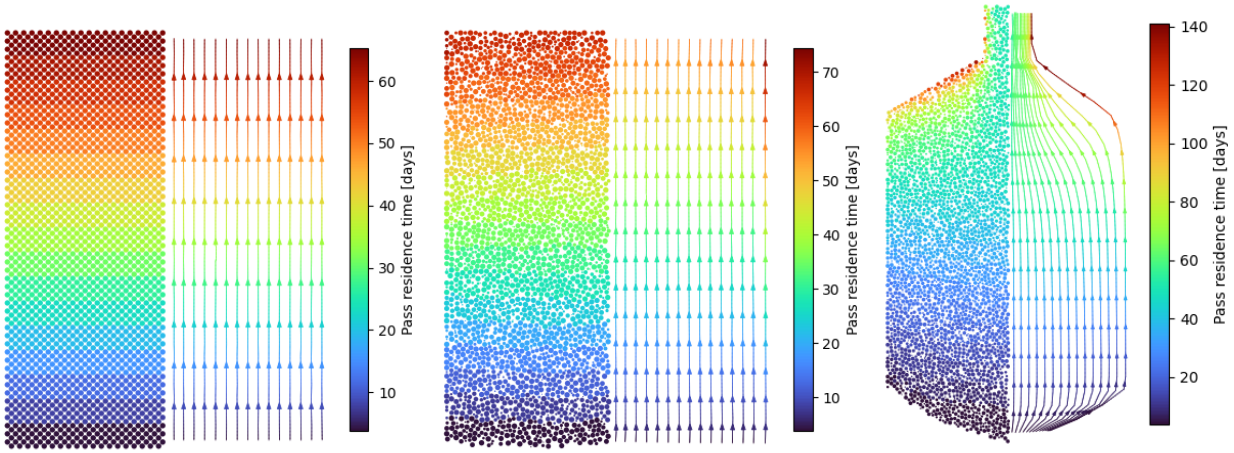

Figure 6-29: Average pebble trajectories and residence time during the current pebble pass in a representative equilibrium slice for the discrete motion (left), cylindrical DEM (center), and full DEM (right) version of the gFHR.

Equilibrium comparison

The three cores are run to equilibrium under the same conditions as in Chapter 6.1. The obtained multiplication factors are summarized in Table 6-4 and indicate that using the DEM increases them.

Table 6-4: Equilibrium multiplication factor comparison (before depletion) between the three models.

Case	Multiplication factor	Uncertainty (pcm)	Standard deviation (pcm)	Difference (pcm)
Discrete motion	1.01516	18	32	-
DEM	1.01797	19	22	+ 281
Full DEM	1.02345	19	34	+829

*Corrected from 1.01833, given a 0.3% higher number of pebbles

Then the three model's pebble-wise parameters are compared. A summary of the peaking factors found for each parameter is compiled in Table 6-5. First, the thermal flux is represented as two-dimensional slices in Figure 6-30 and as spatial profiles in Figure 6-31. The DEM and the discrete motion gFHR models have the same average flux radial profile. Axially, the results obtained with the DEM are shifted upwards with an increase in thermal flux towards the center of the core as well as at the top. The maximum values, hence the peaking factors, are higher in the discrete motion model. The different packings within the core mainly cause these differences. The closer proximity of the pebble bed to the bottom reflector in the discrete motion case produces higher thermal fluxes in that region, which then leads to more fuel consumption and less flux for

higher elevations. When adding the fueling and defueling chutes, several phenomena occur. First, the effect of the bottom reflector is less intense in the central region because of the presence of the fueling chute.

Similarly, the top of the core has a near-zero flux region in which pebbles simply decay. Overall, it results in higher axial flux gradients and flatter radial flux profiles, especially for the maximum values. Therefore, peaking factors are lower.

Table 6-5: Peaking factors for key depletion parameters and for each gFHR-based model.

	Discrete motion	DEM	Full DEM	Full DEM (active region)
Thermal flux	1.95	1.80	1.66	1.55
Fast flux	1.80	1.74	1.84	1.70
Pebble powers	2.95	2.65	2.48	2.30
Burnup	1.97	1.97	2.09	2.10
Thermal fluence	2.35	2.36	2.55	2.59
Fast fluence	2.30	2.28	2.16	2.18

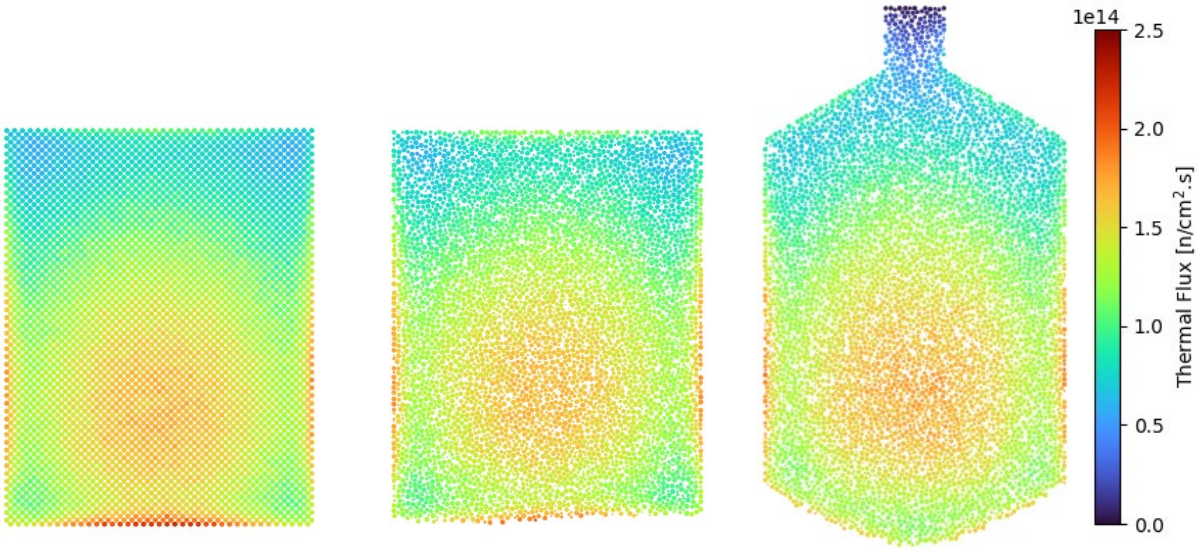

Figure 6-30: Thermal (E<1.86 eV) flux in a representative equilibrium slice for the discrete motion (left), cylindrical DEM (center), and full DEM (right) version of the gFHR.

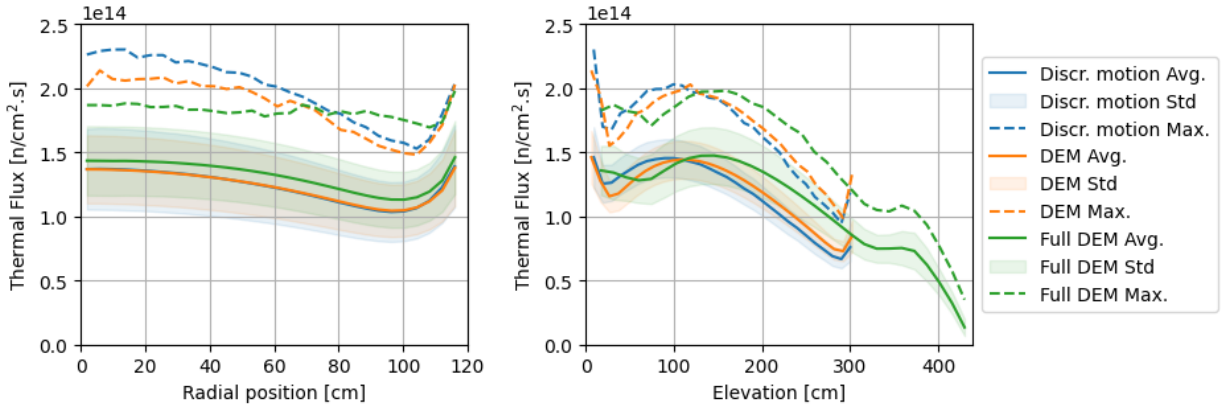

Figure 6-31: Thermal (E<1.86 eV) flux radial (left) and axial (right) profiles comparison between the three gFHR-based models. The radial profile for the full DEM model corresponds to the active region only.

Fast fluxes, shown in Figure 6-32 and Figure 6-33, have roughly the same average and maximum radial profile. However, once again, the axial peak is reached higher with the DEM than with discrete motion, although peaking factors are also similar. The change in geometry and packing does not significantly impact the fast neutrons, which travel long distances.

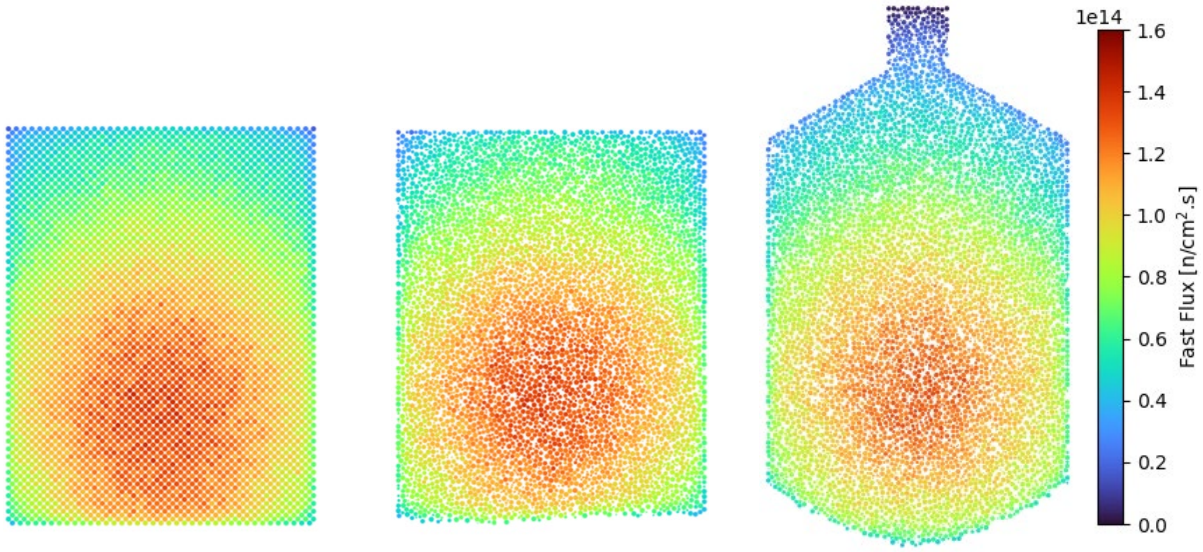

Figure 6-32: Fast (E>0.1 MeV) flux in a representative equilibrium slice for the discrete motion (left), cylindrical DEM (center), and full DEM (right) version of the gFHR.

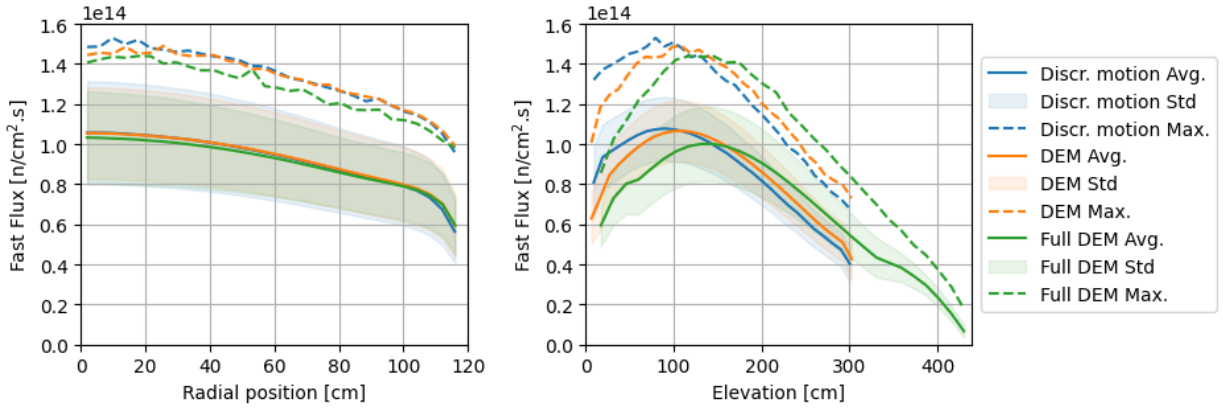

Figure 6-33: Fast (E>0.1 MeV) flux radial (left) and axial (right) profiles comparison between the three gFHR-based models. The radial profile for the full DEM model corresponds to the active region only.

The resulting power profiles are compiled in Figure 6-34, where, once again, the discrete motion case has a larger peaking factor than the two others. Indeed, powers follow the same trends as thermal fluxes.

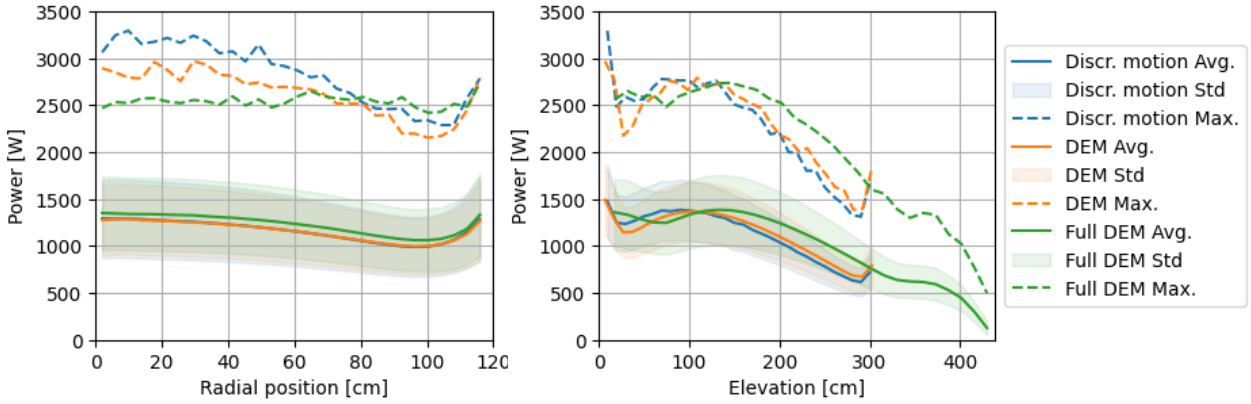

Figure 6-34: Pebble powers radial (left) and axial (right) profiles comparison between the three gFHR-based models. The radial profile for the full DEM model corresponds to the active region only.

Regarding cumulative parameters, the example of burnup is taken, but the same conclusions apply to the thermal and fast fluences. Trends in the burnup accumulated during a single pass result from the insertion burnup, the flux distribution, and the residence time. Therefore, as Figure 6-35 suggests, high-elevation pebbles at the center and close to the reflector in the cylindrical models tend to have accumulated more burnup during their current pass. A slight difference is observed near the edge, where the wall effect increases the residence times and, thus, the maximum burnups. However, this difference is negligible on average and only affects the maximum values for small numbers of passes. The full DEM model with fueling and defueling chutes has a different behavior.

The radial profile is almost flat, and although the average profile is lower, outlier pebbles have much larger burnup values.

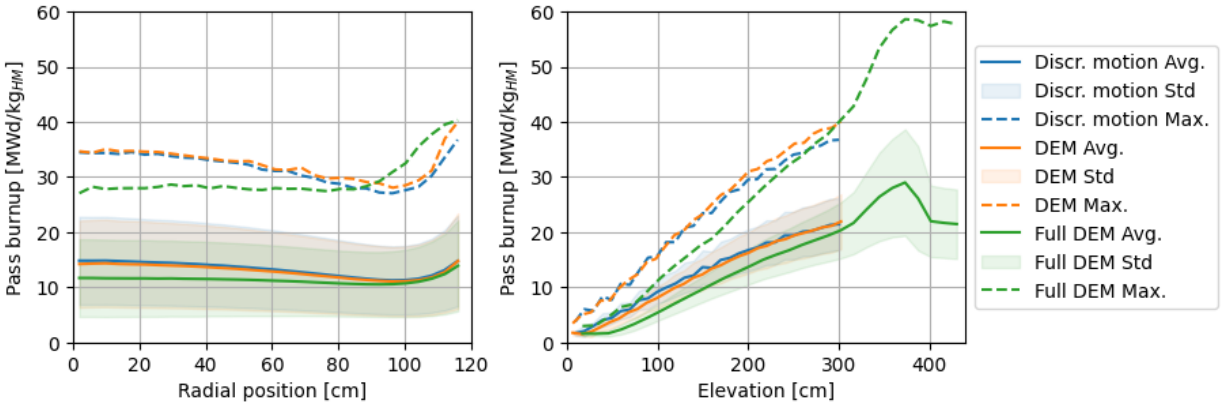

Figure 6-35: Pebbles current pass burnup radial (left) and axial (right) profiles comparison between the three gFHR-based models. The radial profile for the full DEM model corresponds to the active region only.

Looking at the cumulated burnups, the discrete motion and simple DEM models are almost identical, with the same shapes and peaking factors. It means that the higher residence time at the edges of the core does not drastically change pebbles compositions. The three average burnups are 97.8, 97.9, and 98.9 MWd/kg$_{HM}$, respectively. However, as Figure 6-36 and Figure 6-37 suggest, clear differences are to be noted. The high residence time towards the wall, especially in the defueling conic region of the full DEM model, leads to higher maximum fuel utilization. Therefore, in that case, the maximum is 206.8 MWd/kg$_{HM}$, much larger than 192.8 MWd/kg$_{HM}$ obtained for the two other models. This translates to a longer tail towards higher burnup values for each pass in the statistical distributions.

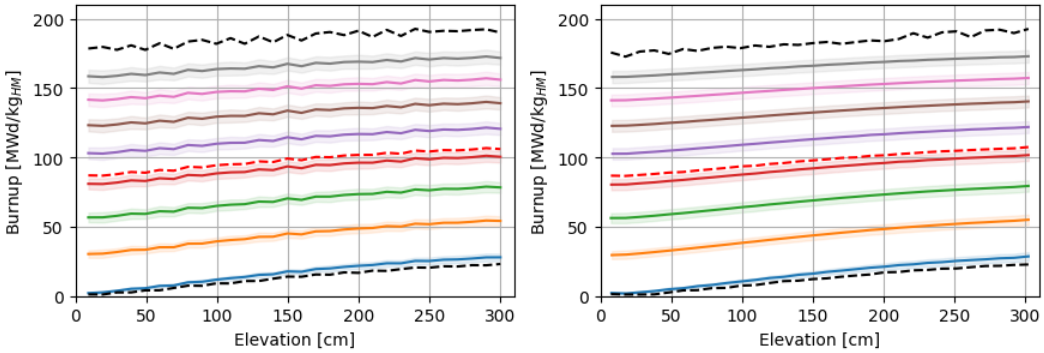

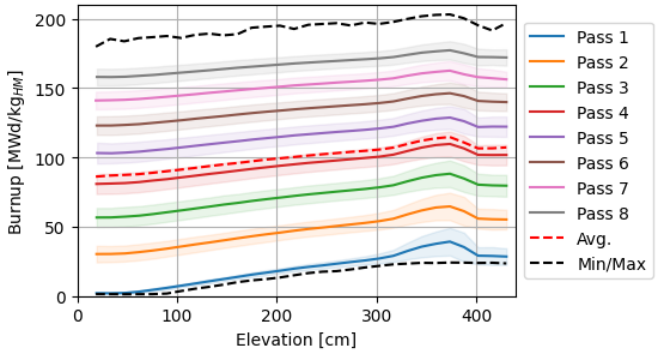

Figure 6-36: Burnup axial profile per pass for the discrete motion (top left), cylindrical DEM (top right), and full DEM (bottom) version of the gFHR.

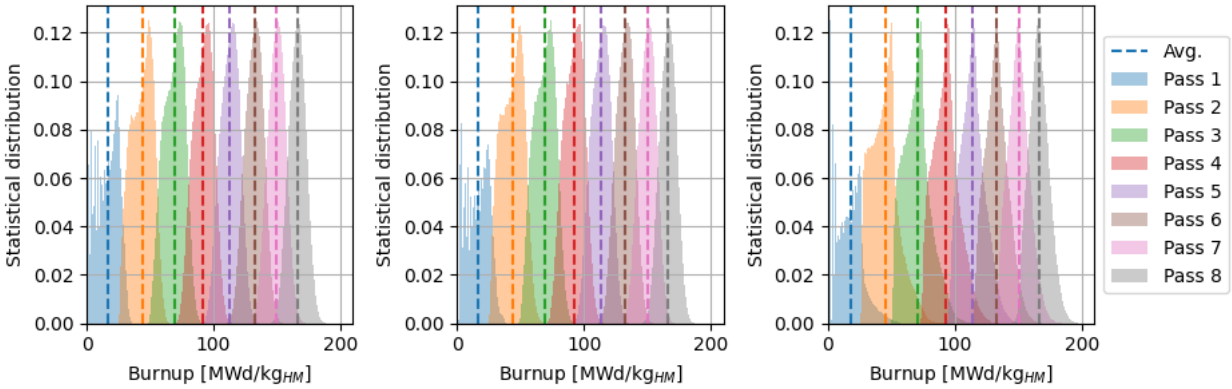

Figure 6-37: In-core burnup statistical distributions per pass for the discrete motion (left), cylindrical DEM (center), and full DEM (right) version of the gFHR.

These effects are even more noticeable in Figure 6-38 and Figure 6-39. The discharged burnups are similar between the discrete motion and the DEM cases, except for the first pass, where a few pebbles have a higher burnup and correspond to the ones that evolved at the very edge of the core. The effect then vanishes with passes due to the diversity of trajectories when recirculating. When focusing on the discarded content, the difference is not notable anymore. On the other hand, the larger tail is also visible in both the overall discharged and discarded contents of the full model, which also leads to larger overlaps between passes.

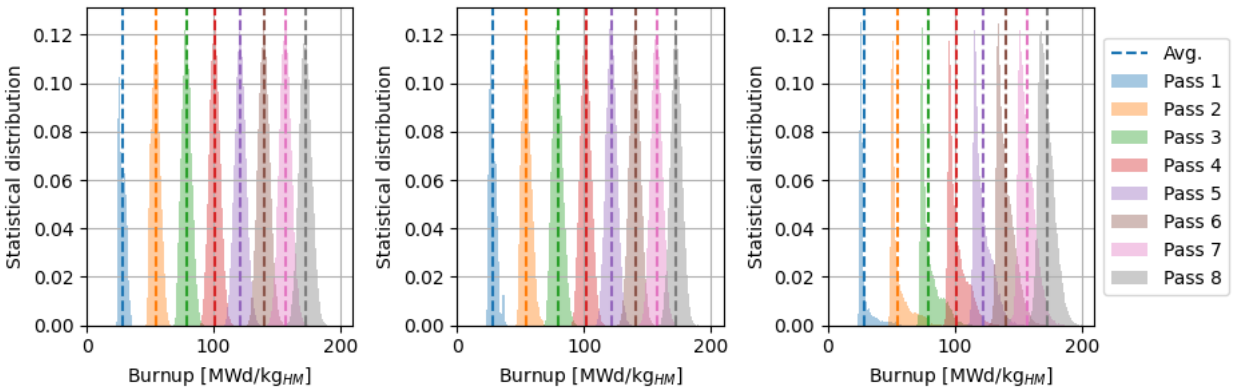

Figure 6-38: Discharged burnup statistical distributions per pass for the discrete motion (left), cylindrical DEM (center), and full DEM (right) version of the gFHR.

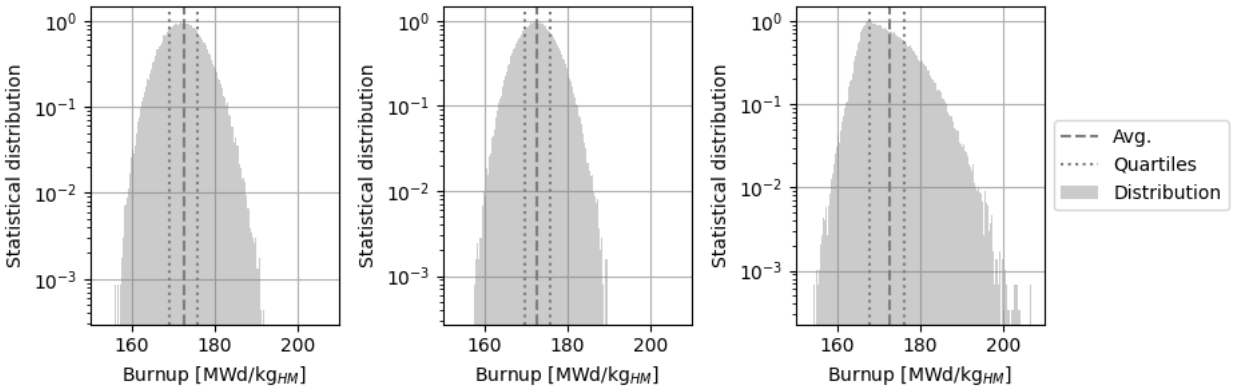

Figure 6-39: Discarded burnup statistical distributions per pass for the discrete motion (left), cylindrical DEM (center), and full DEM (right) version of the gFHR.

6.3 Thermal coupling on a static case

Thermal coupling effects are explored on the obtained gFHR equilibrium with discrete motion, using the same methodology as Chapter 5. Therefore, iterations between Serpent 2 and GeN-Foam are performed, with communications of power densities tallied by Serpent 2 and the material's temperatures and densities computed by GeN-Foam. The two codes use a common mesh, containing roughly one pebble per mesh cell, as Figure 6-40 shows. GeN-Foam applies a porous media/steady state pebble power model coupling to determine the thermal quantities. The initial temperature guess is taken at 900K.

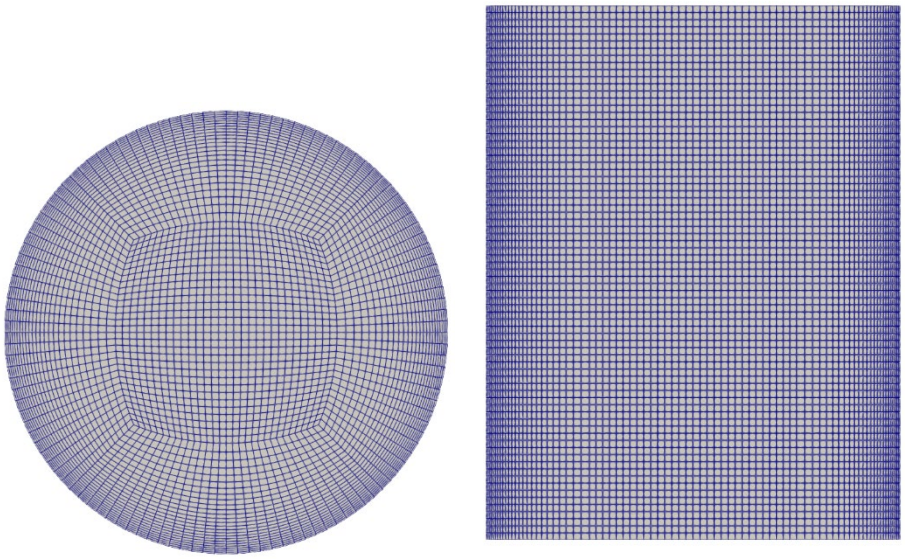

Figure 6-40: Cross-sectional (left) and longitudinal (right) gFHR Serpent 2/GeN-Foam common mesh.

Coupled iterations

Each iteration yields statistical uncertainties on tallied powers of 7.2% on average. As previously shown and as suggested by Figure 6-41, the powers, coolant, matrix, and fuel temperatures converge after two iterations only, meaning that thermal equilibrium is reached. The biggest change is in the average temperature of the fuel, which varies up to 10% during the first iteration. The isothermal temperature assumed in the benchmark, significantly differs from the determined fuel temperatures. As expected, the transport simulation time is impacted. Each iteration is, on average, 59% slower than without TMS.

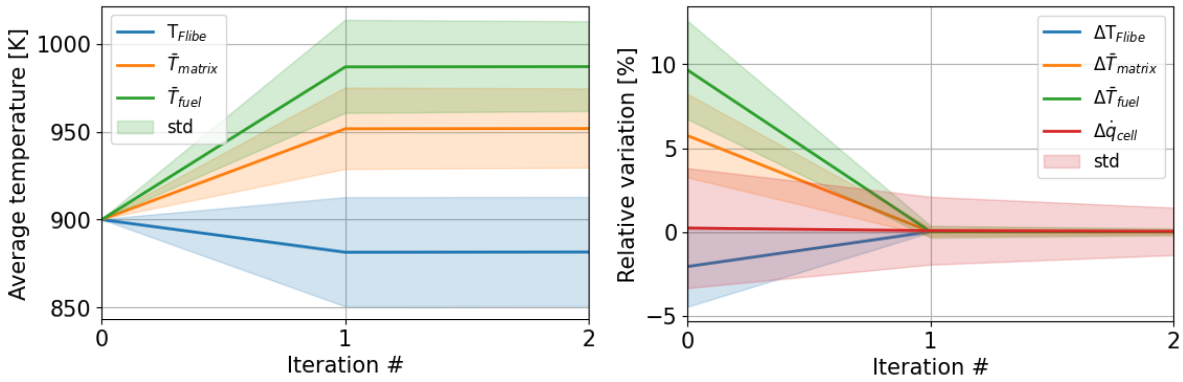

Figure 6-41: Evolution of the variation between iterations for pebble power and materials temperatures.

The impact on neutronics can also be quantified. To this end, the same iterations without coupling were run to have an accurate reference for comparison. First, the multiplication factor decreases once accurate temperatures (coupling) are applied, compared to the isothermal case, as

Figure 6-42 shows. Once again, a small number of iterations is enough to reach convergence. Without coupling, the obtained multiplication factor is 1.01223 ± 4 pcm.

In contrast, the converged coupled case's value equals 1.00758 ± 5 pcm. This non-negligible difference of -465 pcm is due to the global negative temperature coefficient of the reactor and the overall underestimated fuel temperature in the isothermal case. The thermal aspects will be discussed in the following sub-section in more detail.

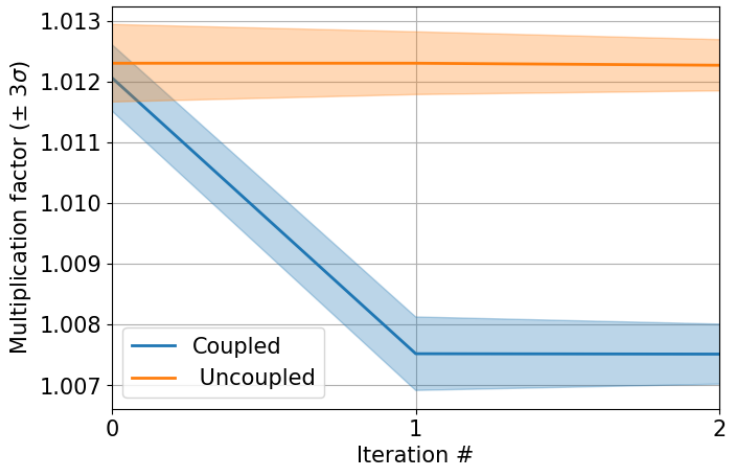

Figure 6-42: Evolution of the multiplication factor with iterations, with and without thermal coupling.

Regarding power, pebbles experience significant differences once the temperature variation is considered, ranging from -30% to 55% (Figure 6-43). Nevertheless, three-quarters of the pebbles show a variation of 7% in absolute value or less, the final uncertainty on power tallies being estimated between 1 and 3%. Thus, there is an impact on the individual pebbles, which cannot be neglected.

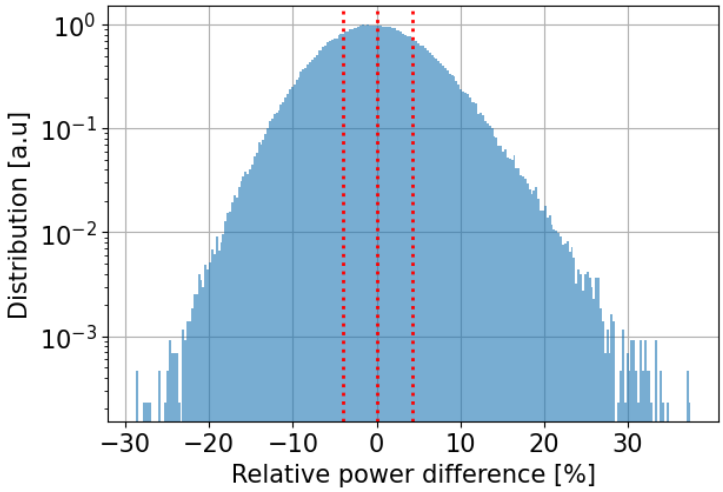

Figure 6-43: Statistical distribution of the impact of thermal coupling on pebbles power.

However, as Figure 6-44 suggests, no strong spatial trend is noticeable except a slight increase in power at the bottom of the core due to the coolant and graphite temperatures decrease. That being said, the strongest discrepancies are observed at the upper corner of the core. Power production in these regions is relatively lower than in other regions due to the overall higher burnup and lower thermal flux (higher neutrons leakage at corners).

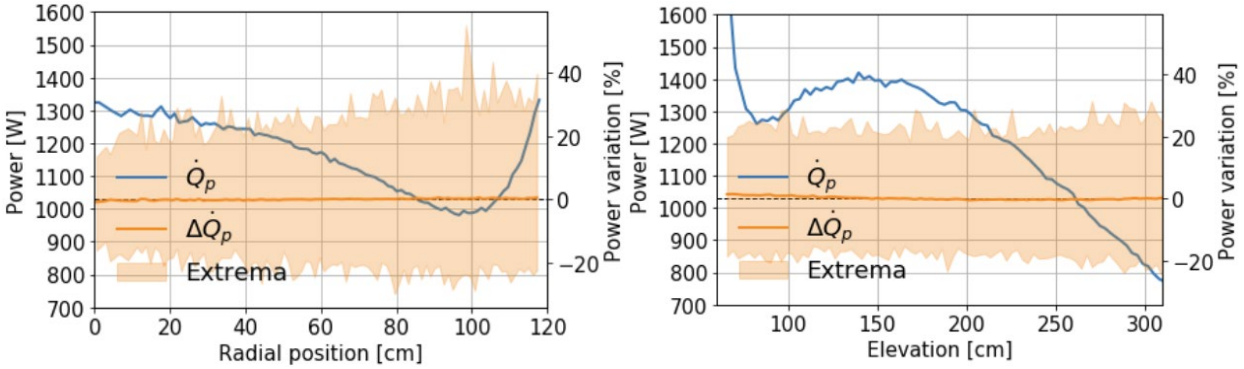

Figure 6-44: radial and axial impact of thermal coupling on pebbles power.

Thermal analysis

This sub-section discusses the thermal aspects of the obtained results. Converged temperatures and powers are summarized in Table 6-6 and spatially shown as a longitudinal slice in Figure 6-45 and, in the case of temperatures, as spatial profiles in Figure 6-46. Pebble-related parameters are only extracted for cells in which pebbles are found in the core, and average and extreme values are calculated accordingly, whereas the fluid temperature and corresponding values account for all cells. Although uncertainties and differences in the nature of the two methods used (based on spectral zones and HxF), these results are similar to the ones obtained by Kairos Power.

Table 6-6: Converged thermal and power parameters in the core.

	Minimum	Maximum	Average	Peaking factor
T_F (K)	823.2	947.5	880.6 ± 31.9	1.076
$\overline{T}_m$ (K)	852	1022.4	951.9 ± 21.9	1.075
$\overline{T}_f$ (K)	865.2	1094.4	987.1 ± 24.7	1.109
$T_{f,max}$ (K)	866.9	1103.3	991.5 ± 25.3	1.113
$\dot{Q}_p$ (W)	248.2	3161.4	1115.6 ± 390.8	2.834

Fuel temperatures are more directly impacted by power production than the rest, with fuel kernels being the origin of this power. Flibe flowing into the core influences its temperature distribution by the energy accumulated below any location. The matrix temperature is impacted by both the power production and the fluid temperature around. The core's radial center and very edges contain the most powerful pebbles, resulting in higher fuel, matrix, and coolant temperatures.

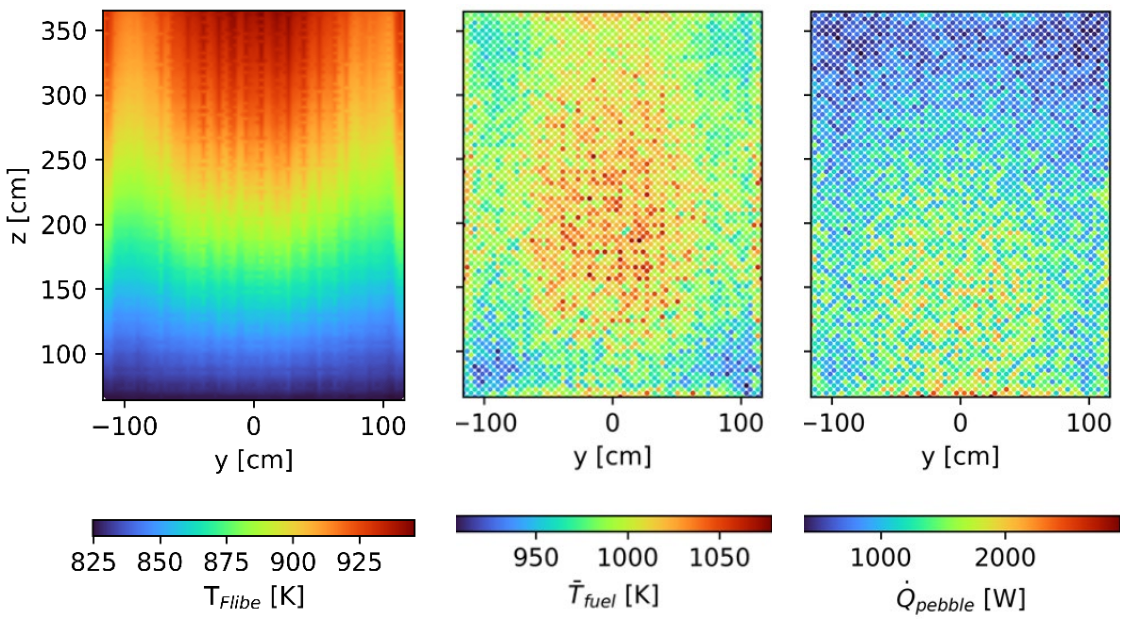

Figure 6-45: Longitudinal view of the gFHR converged thermal and power parameters.

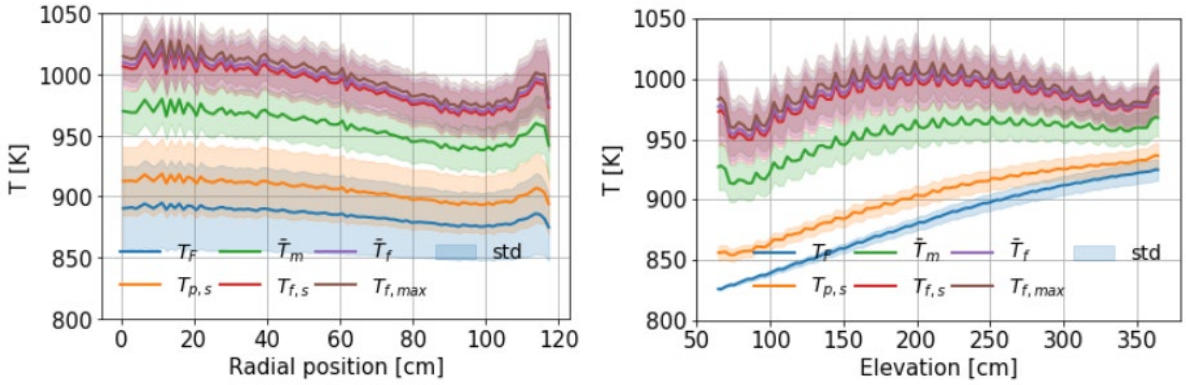

Figure 6-46: Radial and axial temperature profiles in the coolant, pebble, and TRISO particles.

The fluid temperature clearly shows the structured lattice used in this case study, with axial thermal stripes of hot Flibe where pebbles are located and colder Flibe elsewhere. The highest fuel temperatures ($T_{f,max}$>1085 K) are all found in pebbles close to the radial edge and at the axial center of the core. That zone is where the power produced is high, due to the presence of the reflector and the intermediary burnup, whereas the coolant temperature is around the average value. To some extent, the central and lower regions at the radial core center exhibit the same behavior, where all the fuel with $T_{f,max}$>1060K are located beside the previously described region. In general, the influence of power production and coolant temperature on the fuel can be observed in Figure 6-47. Matrix temperatures are similar with $\bar{T}_m$>1020 K at the axial center close the reflector. However, the other hottest matrix materials ($\bar{T}_m$>1000 K) are located at the radial core

center but around the axial center and the top of the core. This difference between fuel and matrix behaviors shows the more substantial influence of the fluid temperature on the matrix.

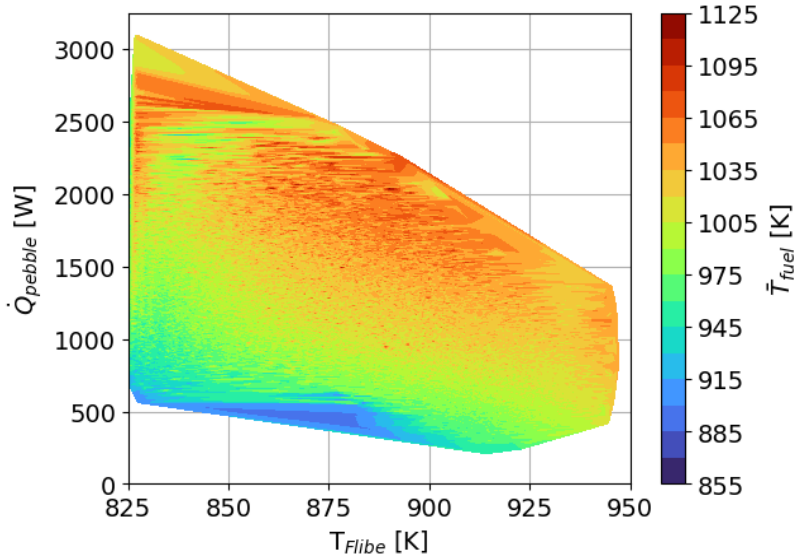

Figure 6-47: Influence of pebble power and coolant temperature on fuel temperature.

The detailed temperature profiles in each pebble can also be determined. Two example pebbles were extracted and shown in Figure 6-48. The first is located at the center top of the core (R=48 cm and Z=355 cm) and has a fuel temperature close to the average value ($\bar{T}_f$=989 K). Its power is 646 W, and the fluid temperature is 931 K. The second is the hottest pebble ($T_{f,max}$=1103 K) and is located at the axial center of the core, close to the reflector (R=114 cm and Z=173 cm). It is in contact with 879 K FLiBe and produces 2366 W. While trends are similar, the steepness of the profiles is significantly higher for the second pebble than the first. Nevertheless, the significant difference between fuel temperature and matrix temperature is caused by the low conductivity of the TRISO buffer. The maximum fuel temperature pebble information (composition, power, temperatures) can be used as a bounding case input for fuel performance models.

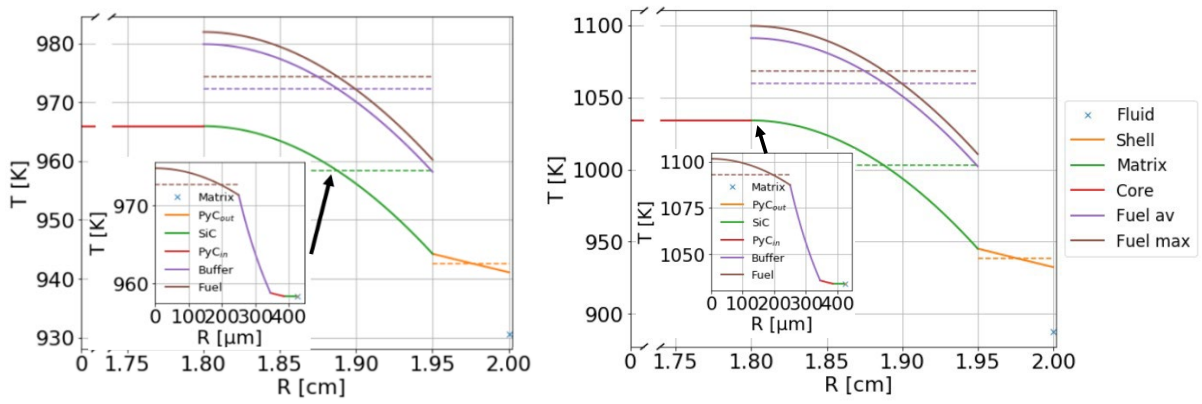

Figure 6-48: Temperature profiles in pebble with average fuel temperature and hottest fuel pebble as well as one TRISO particle of interest.

Neutronics response

In a comparable manner to Chapter 5.2, multiple coupling combinations between thermal components and neutronics are explored to assess the impact of one parameter on the overall behavior. They include matrix and coolant temperatures, fuel and coolant temperatures, fuel and matrix temperature, fuel, matrix and coolant temperatures, and all temperatures associated with coolant density. The combinations are then compared to the uncoupled case to derive the influence of the coupling on the simulation. The results are shown in Figure 6-49. The overall effect of the coupling is negative. However, it is worth decomposing each source individually. There is a difference between the coolant, matrix, and fuel obtained temperatures which are, on average, 880.6, 951.9, and 987.1K, and the initial temperature guess (900K). It can be observed by comparing the fully coupled temperature case with the case with matrix and coolant coupled temperatures only that the fuel temperature represents the main source of negative reactivity. Indeed, besides the Doppler effect, the difference between the first temperature guess and the fuel average value is the highest. The matrix temperature tends to cause a slight decrease in k_{eff}, whereas accounting for the coolant temperature leads to an increase due to the positive difference with the initial guess. Accounting for the density, contrary to the HTR-10 case, the coolant density changes reactivity. When the temperature of the coolant increases, its density decreases, leading to less moderation and absorption effects from the coolant, which leads to a decrease in the multiplication factor.

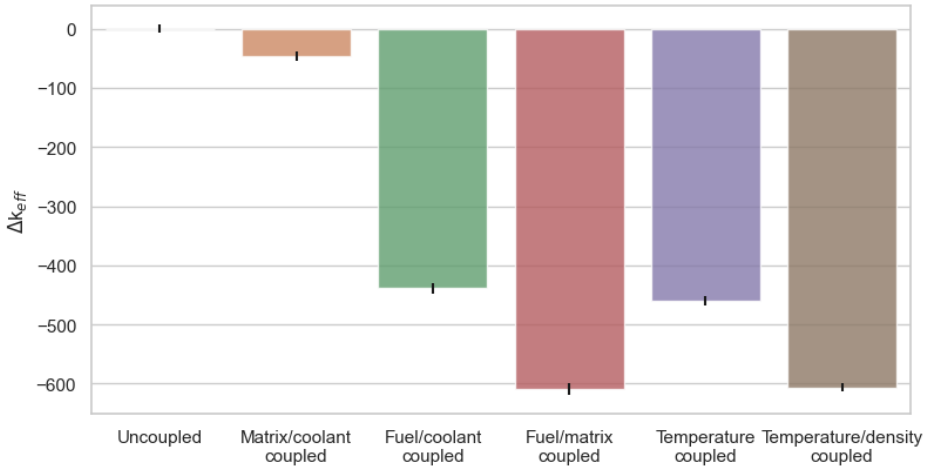

Figure 6-49: Effect of thermal coupling on the gFHR multiplication factor (in pcm) for different coupling combinations.

6.4 Conclusions

The HxF capabilities are applied to the gFHR model. First, the comparative analysis between KPACS and HxF provides valuable insights into the behavior of the gFHR case and the specificities of both approaches. While there are some differences between the two methodologies, their average results fall within an acceptable range, and the chosen method does not significantly

impact the overall equilibrium state. Indeed, although examining global core parameters, such as multiplication factors and conversion ratios, reveals slight discrepancies between KPACS and HxF, the differences are deemed reasonable. The reactivity coefficients derived from both methodologies show similar orders of magnitude and signs, indicating consistency in their predictions, although KPACS tends to underestimate them. The power and burnup distributions analysis highlights variations in the approach between KPACS and HxF, particularly in the axial profiles. Indeed, for KPACS, averaging compositions and fluxes over macrozones impacts local results and tends to dilute outlier pebbles. Averaging HxF results over KPACS-defined macrozones brings the distributions closer together, indicating that results are consistent and differences are attributable to the spectral zones. The examination of atomic densities of key nuclides further reveals differences in fission rates and the generation of fission products. The study highlights the benchmarking potential of HxF while demonstrating the consistent behavior of the KPACS tool. It further increases confidence in the code to perform rapid iterations for core design. In the future, both approaches should be used on a more realistic geometry and motion model, such as Discrete Element Methods, to draw further conclusions concerning the validity of KPACS.

Second, in assessing the behavior of the gFHR benchmark model with respect to discrete motion and DEM, notable differences and insights emerge. Compared to discrete motion, DEM allows for a more realistic representation of pebble movement, especially when integrated with varied geometries like fueling and defueling chutes. The packing of pebbles in the core varies between the methods. Discrete motion, with its structured lattice, demonstrates irregular radial packing and more proximity to the reflector, although it has roughly the same number of pebbles. In contrast, the DEM models, especially the full DEM, showed effects of shear stress, which was particularly pronounced in the active region where the defueling chute influences packing. While trajectories are relatively uniform in both the discrete motion and cylindrical DEM models, wall effects in the DEM models, especially the full DEM version, cause higher residence times. The flux distribution, whether thermal or fast and the pebble powers show distinct profiles depending on the modeling method. The discrete motion model demonstrated higher peaking factors, influenced by the fact that pebbles are closer to the bottom reflector. When analyzing burnup, the DEM models highlight the impact of higher residence times near the core edges, especially with the full version. This results in higher outlier fuel utilizations. Overall, the discrete motion yields satisfactory results for a simplified geometry such as the gFHR or when modeling the active region of the core only. This is especially true because the wall effect can be modeled by applying a different motion step by radial channel in the motion sequence, thus replicating the behavior observed with the DEM. However, for more realistic geometries, the DEM models, despite their additional computational cost, are to be used.

On the thermal front, a preliminary coupling of the gFHR equilibrium is performed. This coupling uses a shared mesh, with GeN-Foam applying a porous media model to determine thermal parameters. After two iterations, thermal equilibrium is achieved. The multiplication factor drops when actual temperatures are considered, a difference of -465 pcm, attributed to the reactor's global negative reactivity coefficient. While pebbles experience considerable differences in power when accounting for temperature variations, no clear spatial trend appears except for a minor power

increase at the core's bottom. The effect of coupling is negative overall, although it has different components. The fuel temperature stands out as the leading cause for negative reactivity, while the matrix temperature leads to a minor decrease in keff. As coolant temperature rises and its density falls, there is a resultant decrease in the multiplication factor due to diminished moderation and absorption effects. These phenomena are mainly due to the difference between the first temperature guess and the final average values in pebbles.

Chapter 7
Use cases for HxF and beyond

As Chapter 6 demonstrated, applications to full-scale models and search for equilibrium are made possible with HxF. This method proves to be particularly useful in providing verification for existing approaches, with benchmarking potential. On the other hand, it provides an accurate individual representation of the pebbles, in which outliers and average data are easily identifiable. This applies to in-core, discharged, and discarded pebbles. Therefore, the HxF approach improves the overall understanding of pebble bed reactors operation. In addition to these direct applications, HxF opens numerous possibilities. This Chapter summarizes some related applications in which HxF thrives, including ongoing and potential future work.

7.1 Potential uses of HxF

Given its flexibility, additional simulations with the HxF tool can be performed by incorporating novel designs or changing operational conditions to study how the PBR reacts or to find the proper parameters to use.

Slow transients, run-in phase, loading phase

HxF is able to run slow transients. Indeed, once an equilibrium is obtained, one can modify the operational conditions and simulate the system's response to this change. Such conditions include the reactor power, discarding condition, change in fuel-to-moderator ratio, change of fuel enrichment, or insertion of different fuel types. For instance, Figure 7-1 provides an example with the HTR-10 filled with 27,000 pebbles. The core is initially entirely fresh, and an approach to equilibrium with a discard threshold on burnup of 72 MWd/kg$_{HM}$ is performed. In this example, fresh fuel is initialized with a virtual burnup between 0 and 72 MWd/kg$_{HM}$ to converge faster. Indeed, if the fuel were entirely at zero burnups initially, the operation would follow a batch-like behavior in which pebbles are discarded/inserted around the same time.

To obtain an equilibrium state with that initial configuration, the calculation would be prohibitively slow to converge. Nevertheless, neither of these initializations, or even any initial guess is realistic and is only chosen in the context of an approach to equilibrium. However, the obtained equilibrium can be considered an initial condition for future operation calculations. After around 20 passes, the multiplication factor oscillates around 0.97077 ± 29 pcm. Then, the threshold is modified to 64.8 MWd/kg$_{HM}$. The multiplication factor then becomes 0.98122 ± 29 pcm. Therefore, a 10% decrease in threshold in this core represents a 1045 ± 58 pcm reactivity insertion.

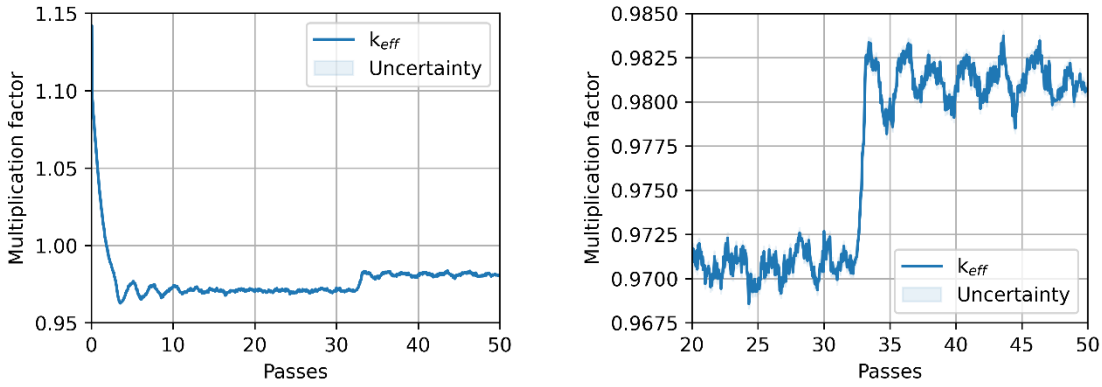

Figure 7-1: Global (left) and zoomed (right) evolution of the multiplication factor for an approach to equilibrium with HTR-10 (27,000 pebbles), and after a 10% decrease in threshold.

Furthermore, fuel loading with approach to criticality, power ascension, and a physical approach to equilibrium can be obtained with HxF. The fuel-to-moderator ratio can be modified by changing the compositions of some of the pebbles to only include graphite, replicating dummy pebbles initially filling the core. Therefore, the approach can finely analyze these crucial steps for the operation of the pebble bed reactor.

Exploring fuel cycles

Another benefit of HxF is that one can simultaneously simulate different fuel types, pebble geometries, and enrichments. This flexibility allows the opportunity to explore different fuel cycles than previously presented. Notably, HxF opens doors to investigating deep-burn strategies [93, 39, 94] and integrating PBRs within a thorium cycle [39, 95, 96], which have been explored, to provide more granular data. A particularly interesting possibility is to employ PBRs as waste burners by replacing a fraction of the fuel pebbles with pebbles containing long-lived fission products (LLFPs) generated by other reactors. The radiotoxicity of LLFPs is a crucial factor in designing nuclear waste storage sites, making their transmutation into stable elements or elements with significantly shorter half-lives an appealing prospect for fuel cycle management.

Using HxF can help determine the feasibility of transmuting LLFPs in PBRs and quantify its impact on neutronics parameters. Work is currently focusing on the gFHR model, replacing fuel kernels with relevant LLFPs (^{79}Se, ^{99}Tc, ^{107}Pd, ^{127}I, and ^{135}Cs) in the TRISO particles of a portion of the core pebbles. For instance, starting from the equilibrium state obtained in Chapter 6.1, 5% of fuel pebbles are replaced with pebbles containing LLFP TRISO particles made from spent PWR fuel after 10 years of cooling [94]. As no isotopic separation is assumed, the LLFP is blended with the element's other isotopes.

Removing fuel from the pebbles and replacing it with graphite already impacts the neutronics. Table 7-1 shows that a 5% replacement yields a positive difference of 969 pcm. This reactivity increase suggests that the initial reactor, entirely filled with fuel pebbles, is under-moderated. The subsequent impact of adding LLFPs varies, resulting in reactivity changes ranging from -5493 to +707 pcm. While most LLFPs negatively affect the reactivity due to their neutron poison effect

during transmutation, replacing fuel with Al2Se3 compound, used for selenium transmutation, acts as a moderator, increasing keff. In a reactor at the optimum of moderation, the impact of fission products replacing fuel would be solely negative [95].

Table 7-1: List of LLFPs of interest and impact of replacing 5% of the pebbles on the multiplication factor.

Element/Nuclide	Chemical form	k_{eff} at t=0	Impact on k_{eff} (pcm)	Natural half-life (years)	Transmutation half-life (years)
Equilibrium	-	1.02119	0	-	-
Graphite	-	1.03088	+969	-	-
^{79}Se	Al_2Se_3	1.02826	+707	327,000	4.7
^{129}I	CaI_2	1.01982	-137	15,700,000	8.4
^{135}Cs	CsF	1.01494	-625	2,300,000	21.6
^{107}Pd	Pd (metal)	0.99727	-2392	6,500,000	7.7
^{99}Tc	Tc (metal)	0.96626	-5493	211,000	5.0

The transmutation half-life of the LLFPs is estimated. LLFPs naturally decay with a half-life ranging from 105 to 107 years. In contrast, as shown in Figure 1, linear extrapolation of those decays yields transmutation half-lives of the order of years: 4.7 years for ^{79}Se, 5.0 years for ^{99}Tc, 7.7 years for ^{107}Pd, 8.4 years for ^{129}I and 48 years for ^{135}Cs. These values are comparable to those observed in fast breeder reactors [96, 97] and demonstrate the great LLFP burning potential of PBRs. Nonetheless, it is worth noting that the extrapolation method underestimates the actual transmutation half-life, as the long-term decrease follows a sublinear trend, as seen with ^{135}Cs. Further research will be conducted to assess these transmutation half-lives accurately.

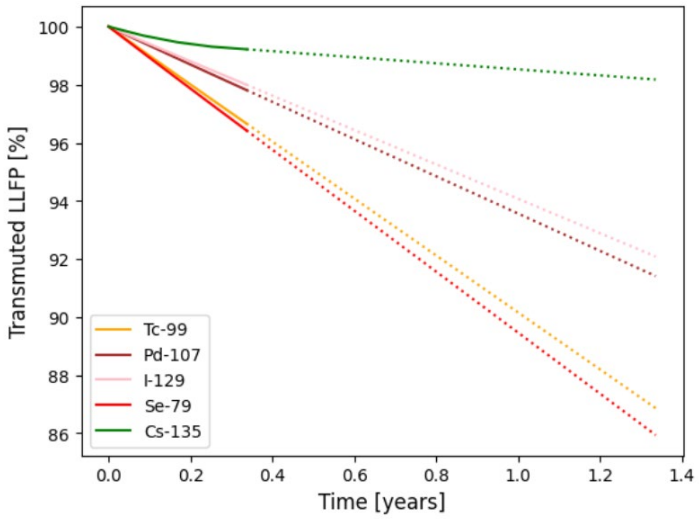

Figure 7-2 Proportion of transmuted LLFP as a function of time

Effect of inspection time on pebble bed reactor operation

Decay, cooling, or inspection time refers to the time spent by pebbles out of the irradiation zone between two passes through the core. Indeed, a pebble cannot be reinserted directly after discharge, as its temperature is too high to handle and measure for burnup. Burnup is generally estimated from gamma spectroscopy. Therefore, the cooling period must be long enough for short-lived isotopes to decay, thus ensuring accurate measurement. Typical inspection times are of the order of a few days.

This delay drives a change in the isotopic composition of discharged pebbles. The impact of this change needs to be assessed to determine to what extent it influences the performance of the reactor. The HxF tool is one of the only codes that accounts for the decay process of discharged pebbles while they are out of the core during their cooling-off period.

Therefore, the operation of a pebble bed reactor, here using the gFHR model, is simulated with HxF and discrete motion with different decay times. Using the equilibrium obtained in Chapter 6.1, where an instantaneous re-insertion of discharged pebbles is assumed, simulations with various decay times are performed with a shorter time step of 3.8 days (5.9% core discharge per step) to capture fission products' behavior accurately. With a decay time superior to 2 days, an immediate increase of the order of 100 pcm in k_{eff} is observed as soon as the decayed pebbles are reinserted (Figure 7-3). With a shorter decay time of 1 day, the multiplication factor increase is not immediately more limited. After 3 passes, the increase is about half of the one obtained by applying a more extended decay period.

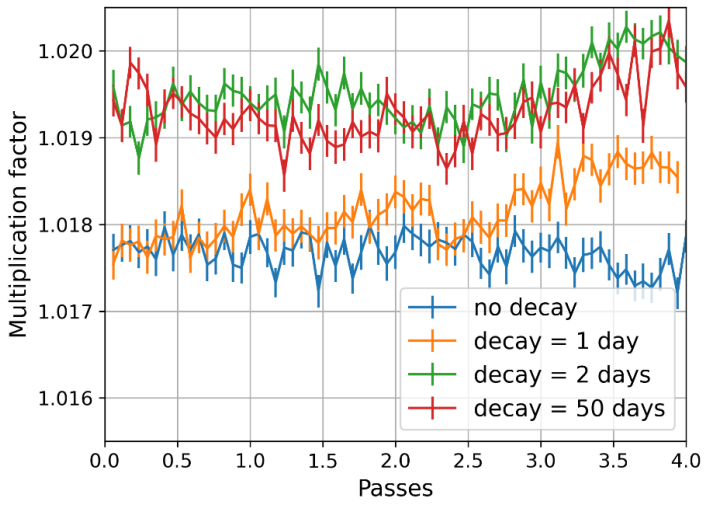

Figure 7-3: Evolution of the multiplication factor on the gFHR at equilibrium applying various out-of-core decay times.

This phenomenon is explained by the change in the macroscopic capture cross-section during cooling time, particularly due to the decrease in ^{135}Xe concentration by radioactive decay. Indeed, by comparing the composition of the pebbles before and after cooling, the effective capture cross-section of the fuel decreases by an average of 9.8% after two days and 12.6% after 5 days. This

effect is dominated by the decay of ^{135}Xe (-0.099877 cm^{-1} after 5 days), which more than offsets the production of ^{149}Sm (+0.012401 cm^{-1}). This also explains why the multiplication factor is less affected by a decay time of only 1 day since all the ^{135}Xe produced by the xenon effect does not have time to decay. This change also has spatial consequences, as only the reinserted pebbles are affected by the drop in ^{135}Xe concentration, which rapidly returns to equilibrium under irradiation. Therefore, a change in the power shape within the core occurs in favor of the bottom of the vessel, where the pebbles are reinserted (Figure 7-4).

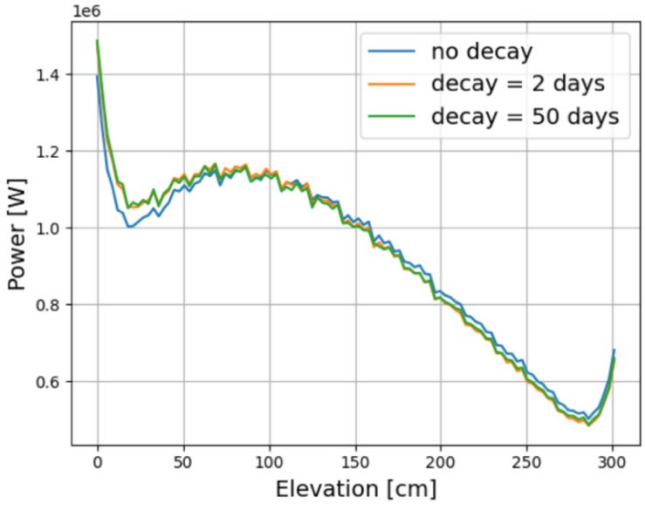

Figure 7-4: Axial power distributions on the gFHR at equilibrium applying various out-of-core decay times.

Find the right operational conditions

An additional foreseen application of HxF is the fine-tuning of operational parameters. For instance, the discard threshold is crucial to ensure criticality. In this context, the threshold can be modified with time manually. However, an adjustable threshold capability is integrated into the HxF tool to find the right value for the considered design. In this capability, for a given fuel material, the discard threshold is automatically adjusted given a target quantity and an associated value. The feature utilizes gradient descent with a decaying learning rate to converge to the proper value as fast as possible. The small-scale core (6,468 pebbles) represented in Figure 7-5 is used as an example case. It is worth noting that such a design is unrealistic regarding materials compositions and pebble bed velocity and is solely used as proof of concept.

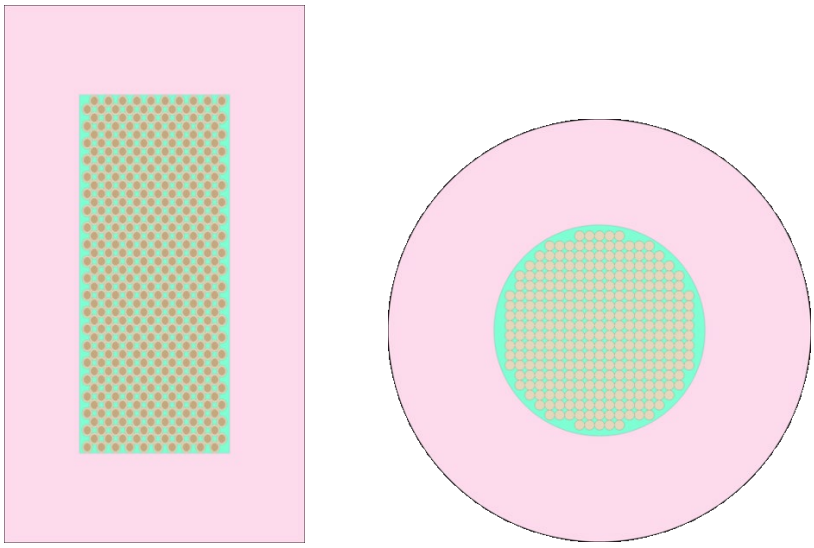

Figure 7-5: Small-scale test FHR used with adjustable threshold.

Starting from an entirely fresh core, a search for equilibrium is performed, adjusting the discarding threshold based on burnup. Initialized with a 120 MWd/kg$_{HM}$ value, it is adjusted at every step using a gradient descent approach. The initial learning rate is 200 and decreases by 1% every time the threshold value is adjusted. A maximum variation of 5 MWd/kg$_{HM}$ is set to limit overcompensation. In this example, the target variable is the multiplication factor, and the target value is 1.00. The threshold value is not adjusted until the discrepancy between the multiplication factor and the target value is below 1.04 to avoid unnecessary adjustments. Figure 7-6 shows that the entirely fresh core yields a multiplication factor of 1.08935 ± 133 pcm.

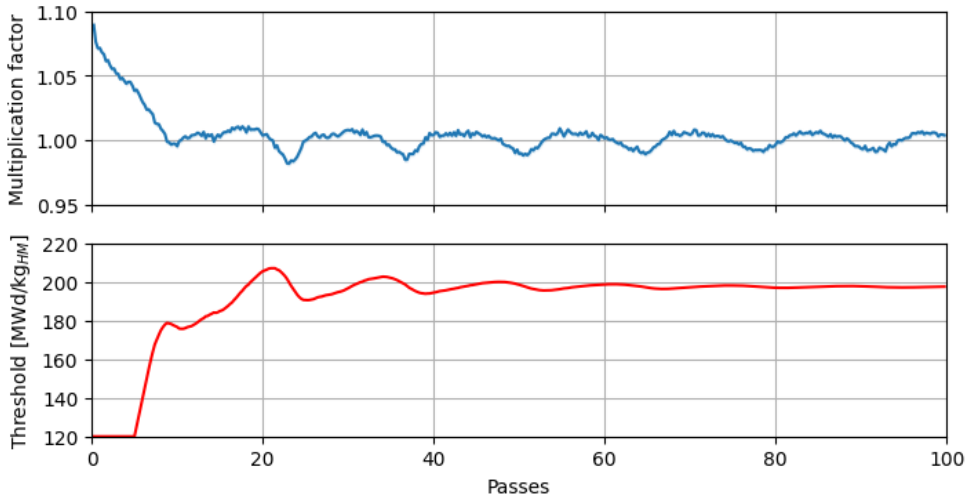

Figure 7-6: Approach to equilibrium on small-scale core model with adjustable threshold.

The fuel starts being consumed, and the multiplication factor decreases despite the relatively low threshold value. The threshold starts being adjusted once the value reaches 1.04 (5 passes).

Given the high learning rate and deviation to the target value of 1.00, the adjusted value increases by 5 MWd/kg$_{HM}$ at every step until the deviation is low enough not to be saturated to this value (6.5 passes). Then, the adjustment becomes finer with time, given that the core approaches an equilibrium state, that the k_{eff} becomes closer to the target, and that the learning rate slowly decreases. After around 20 passes, the values start oscillating around 200 MWd/kg$_{HM}$, and after 60 passes, the value stabilizes around 197.45 ± 0.26 MWd/kg, and the multiplication factor oscillates around 0.99989 ± 127 pcm, with a standard deviation of 379 pcm. This example, although non-realistic, shows that this tool could be used on large-scale reactors to adjust the threshold based on a target value.

Probabilistic threshold

In reality, the burnup measurement, performed with gamma spectrometry to quantify the ^{137}Cs content from the associated emission of 662 keV gamma rays, has uncertainties. Indeed, the value is influenced by external factors such as the background radiation and gamma self-attenuation in the pebble, but it also depends on the detector itself, usually a High Purity Germanium (HPGe) gamma detector. It was found that a Gaussian can represent the probability of discarding a pebble and that the standard deviation depends on the burnup itself [98]. Accounting for this uncertainty can lead to mis-discarded pebbles and impact the reactor operation [81]. Taking a representative standard deviation behavior [81], which yields an uncertainty of 5% at 90 MWd/kg$_{HM}$, the discard probabilities of pebbles with a given burnup as a function of the threshold value can be determined. An example is shown for burnup values of up to 140 MWd/kg$_{HM}$ with thresholds from 40 MWd/kg$_{HM}$ to 110 MWd/kg$_{HM}$ in Figure 7-7.

The capability of HxF to input a probability function as a threshold can be used to replicate that behavior, quantify the number of wrongly discarded pebbles, and determine the impact of such measurement uncertainty on the PBR operation.

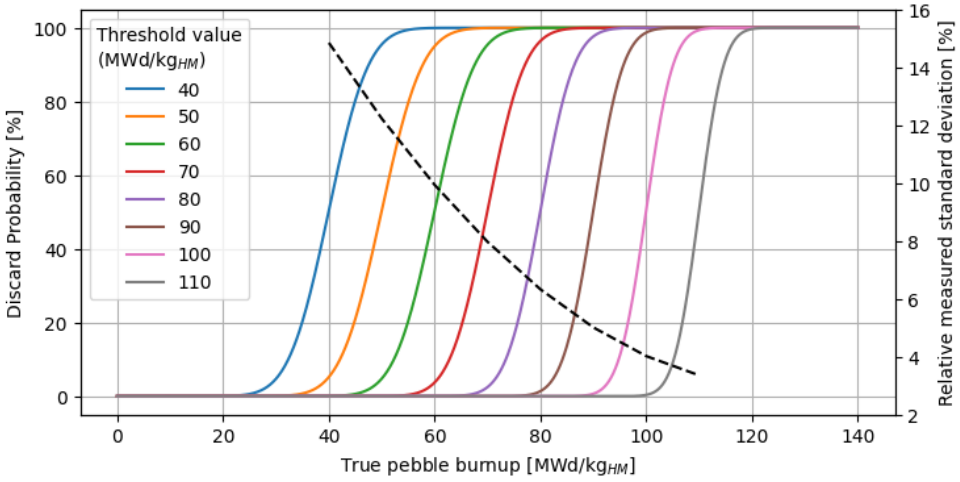

Figure 7-7: Discard probability as a function of the true pebble burnup for various threshold values. The associated measured standard deviation is displayed as a dashed line.

7.2 Applications beyond HxF

The significant amount of high-fidelity data produced during HxF simulations can be used for feeding models or analyzing specific characteristics of the pebbles in other key fields, such as waste management, non-proliferation, or fuel performance. Using machine learning, utilizing the generated data, is another foreseen application in which HxF can be involved.

Waste management

Since HxF records each pebble's discarded content, waste management analyses can use this data as input. For instance, some of the discarded data from the gFHR equilibrium obtained with HxF and discrete motion in Chapter 6.1 is compiled, and a Serpent 2 decay calculation up to 100,000 years is performed with each considered pebble. Serpent 2 automatically computes each pebble's total activity and decay heat. The evolution of these two quantities is given in Figure 7-8 on the pebble level. As an example, a group of 5,000 pebbles to put in a canister would have a decay heat of 16.3 kW (22.0 kW in the worst case scenario) a day after discarding, 10 kW after a week, 5.5 kW after a month, would reach 1kW after 15 months, and would decay to 110 W after 10 years, 25 W after 100 years. The difference between activities and decay heat lies in the fact that nuclides do not decay with the same energy.

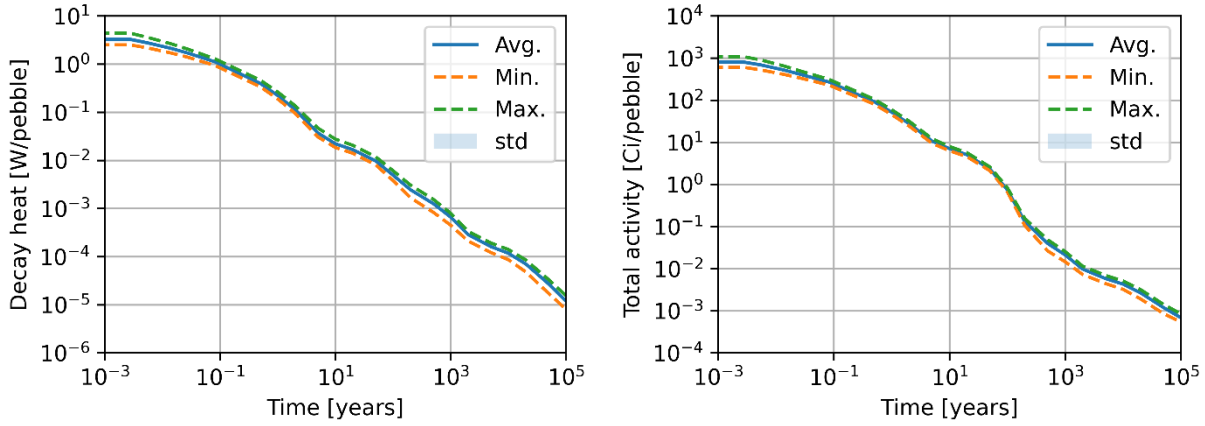

Figure 7-8: Evolution of minimum, average, and maximum decay heat (left) and activity (right) per discarded pebble in the gFHR at equilibrium.

One can identify key nuclides for multiple time scales by breaking down the main activity sources at several time steps. Figure 7-9 shows that the nuclides responsible for the total activity vary depending on the decay time. For instance, ^{95}Nb is responsible for 10.2% of the total activity in an average pebble after 10 days, but given its half-life of 35 days, after a year, it accounts for only 3.0%, whereas ^{144}Ce and ^{144}Pr are each responsible for 23.5% of the total activity, ^{144}Pr (17.3 min) being produced by the decay of ^{144}Ce (285 days). Similarly, after 100 years, ^{137}Cs (30.1 years) and ^{137m}Ba (2.5 min) are produced. Finally, in the long term, after 1000 years, transuranics, particularly 241Am (432.9 years), dominate until it disappears. The remaining radioactive sources

after 100,000 years are long-lived fission products (LLFP) dominated by ^{99}Tc (2.1×10^5 years) and plutonium isotopes. This data will be subject to further investigation in the future. More comprehensive data with activities of an average discarded pebble and with maximum discarded values are available in Appendix D.

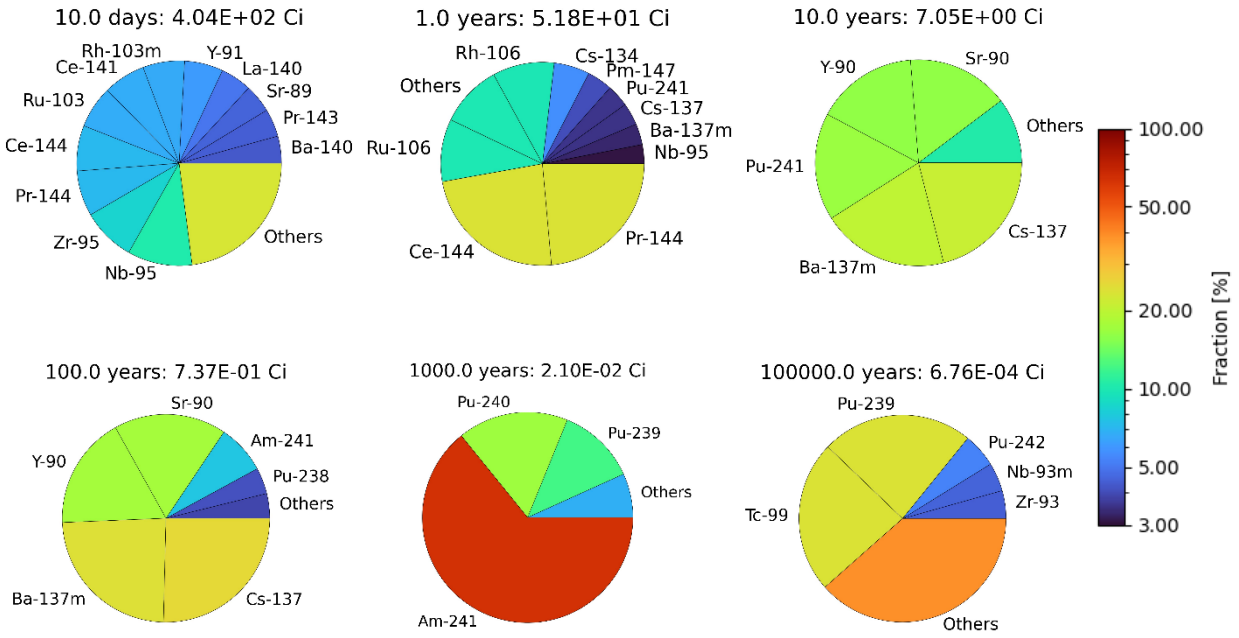

Figure 7-9: Proportions of activity by nuclide for chosen decay times in an average discarded pebble (threshold at 3%).

Fuel performance and non-proliferation

Discharged data can also be analyzed to provide further details and feed other models. A first example is TRISO fuel performance, which typically uses burnup, composition, and/or power/particle to derive the behavior and failure rate of the fuel. HxF can provide all this information on a pebble level. The distributions of the mass per particle for identified important isotopes for fuel performance or fission products release are quantified and summarized in Figure 7-10 for the gFHR.

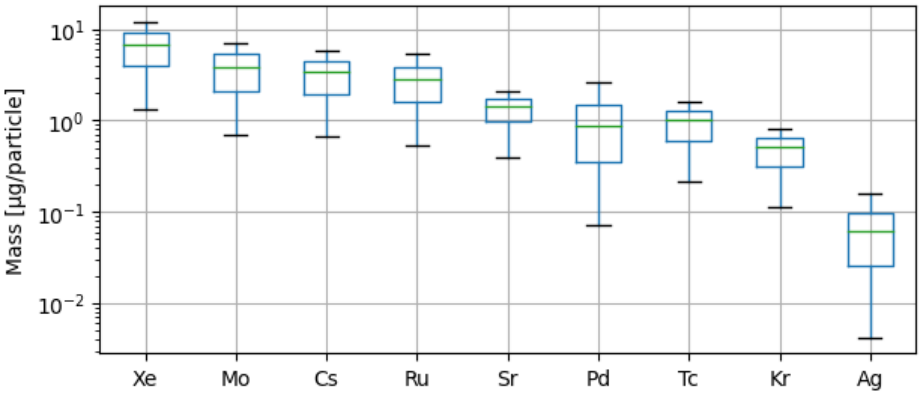

Figure 7-10: Key fuel performance/source term element masses per particle in equilibrium gFHR discharged pebbles.

These quantities can be separated per pass number, which provides more details about the build-up of hazardous or important fission products in the fuel elements. An example is given in Figure 7-11 for xenon and krypton, which are both responsible for increasing the internal pressure within TRISO particles.

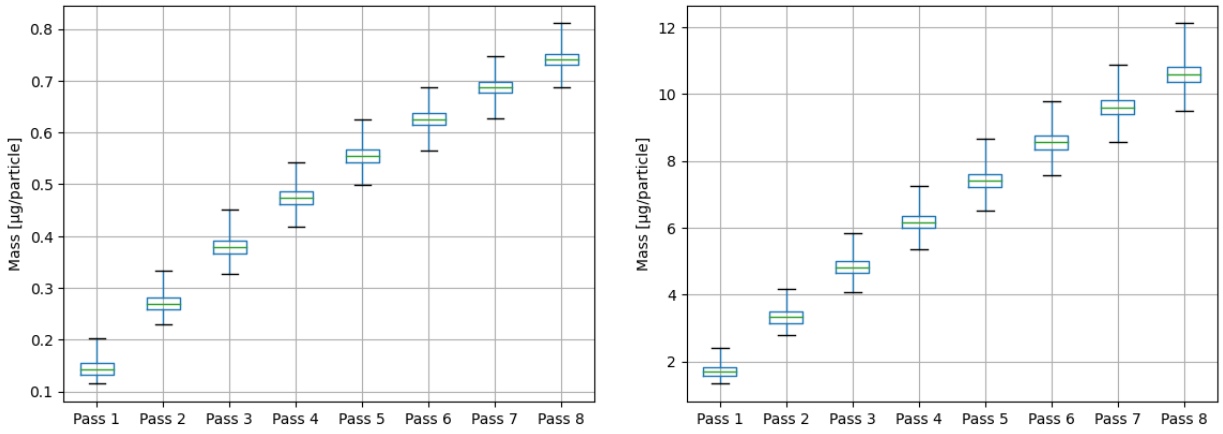

(a) Kr (b) Xe

Figure 7-11: Mass build-up per particle for krypton and xenon for each pass.

Another use of the discharged data is for non-proliferation. The plutonium vector at the first and last pass, as well as over the entire core, are shown in Figure 7-12. Assuming the highest contents in pebbles and that TRISO particle reprocessing is possible and ideal, one can determine worst-case scenarios for non-proliferation matters. The highest plutonium content is found for last-pass pebbles. Taking a critical mass of 10 kg for ^{239}Pu and 12 kg for ^{241}Pu, the number of pebbles to divert to obtain these quantities would be 1.90×10^5 and 5.02×10^5, which corresponds to almost 1 to 2 entire cores to divert. However, this estimate only represents a lower bound, and TRISO reprocessing is complex.

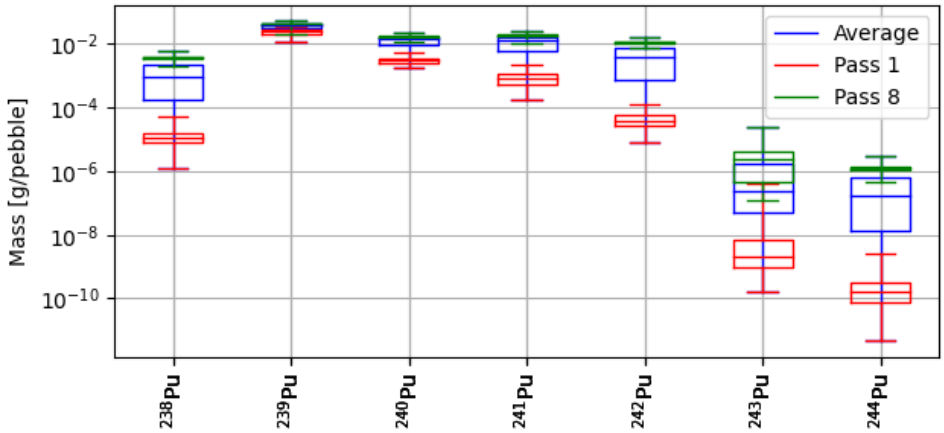

Figure 7-12: Plutonium vector for discharged pebbles at equilibrium in the gFHR.

Machine learning applications

HxF can be used to emulate a real reactor operation. With the lack of experimental data and the difficulty in obtaining detailed in-core operational parameters, this approach can potentially train machine learning models that could otherwise be trained with real data. In that context, two paths have been taken.

First, a long short-term memory (LSTM) model is being developed to predict the future multiplication factor from discharged pebbles data. LSTMs are a type of recurrent neural network specifically designed to learn long-term dependency by selectively retaining or forgetting information over time. This is done through a set of specialized gates that control the flow of information through the network. LSTMs have been successfully applied to a wide range of tasks, including natural language processing and time series prediction. Using a model with two LSTM layers, a dropout as a regularization layer, and an output layer, and optimizing hyperparameters with a grid search, the model is trained on HTR-10 equilibrium states, varying power, and threshold values. The input variables can be isotope concentrations histograms or, more realistically, gamma spectroscopy count rates distributions accounting for all discharged pebbles, and the target variable is the multiplication factor.

Using the gamma emission tool developed with HxF, one can extract the gamma spectrum emitted by each discharged pebble and convert it to a gamma spectroscopy measurement. This can be achieved by applying geometrical, detector absorption, and detector resolution transformations, which account for changes occurring between a gamma emission and absorption. The obtained spectrum, such as the one shown in Figure 7-13 for an average discharged HTR-10 pebble, can then be used as an input for machine learning. Hundreds of spectra are obtained for each depletion step, for which a multiplication factor is associated. A shift in spectra distribution indicates a shift in operating conditions, such as the multiplication factor. Given a training set, the LSTM should then be capable of estimating the following multiplication factors.

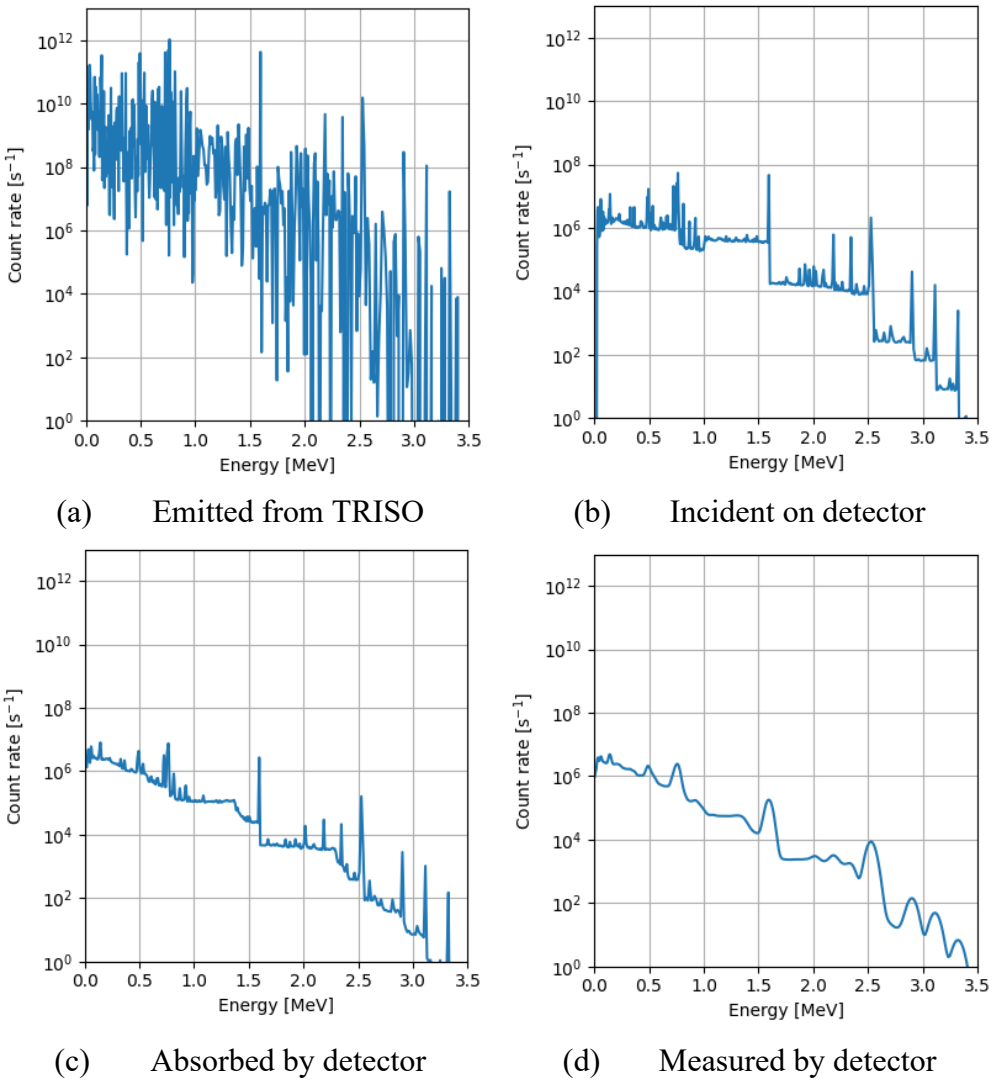

Figure 7-13: Gamma spectra from emission to detection in an average HTR-10 discharged pebble (NaI detector case, 3 days decay before measurement).

In addition, the opposite path can be taken, and given a pebble gamma spectrum, its history can be estimated. Indeed, another neural network can be trained to determine relevant tracked quantities (thermal/fast fluence, burnup, number of passes, average radial position in the core, residence time) for discharged pebbles. For instance, this technique could help estimate in a reactor the number of passes a pebble went through the core without adding any extra measurement on the discharged pebbles. For both approaches, preliminary results are encouraging, and work is currently being pursued.

Short transients and accident scenarios

Another application of the high-resolution data is to use it as an input for high-fidelity neutronics/thermal-hydraulics coupled transient analyses. An ongoing project aims to use the HxF-

obtained equilibrium states to evaluate normal and off-normal operating conditions. In particular, a framework, represented in Figure 7-14, is being implemented.

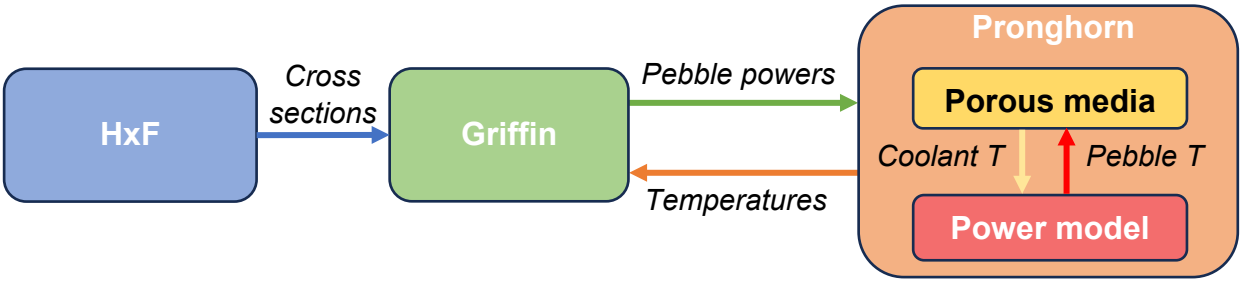

Figure 7-14: Framework for HxF/Pronghorn coupling through Griffin. T designates temperatures.

The multi-group cross-sections are calculated within HxF using the restart capability and fed into Griffin [44]. This finite-element-based neutronics code can efficiently perform transient scenarios, allowing for tight coupling with the porous-media solver Pronghorn [92], which adjusts the pebble temperatures from the obtained pebble-wise powers under transient conditions. Thus, Griffin serves as an intermediary tool between Serpent 2 and Pronghorn to run transient analyses. Pronghorn, like GeN-Foam, embeds a porous media solver and a power model linking coolant temperatures, pebble powers, and materials temperatures. Picard fixed-point iterations are performed until convergence. Three cases will be studied: the gFHR, the HTR-10, and a more realistic large-scale FHR model. In addition to steady-state verifications, loss of coolant flow, control rod malfunction, loss of heat sink, and reactivity insertion will be explored.

7.3 Conclusions

The HxF approach and tool present many opportunities for enhancing the study of PBRs operation and beyond. Its adaptability allows for in-depth investigations into various reactor designs and operating conditions, providing crucial insights into their behavior. By allowing the simulation of slow transients and other critical operational phases, HxF offers a comprehensive view of how the reactor responds to different scenarios and parameter changes. For instance, one can explore altering reactor power, adjusting discarding conditions, changing fuel-to-moderator ratios, changing fuel enrichment levels, and introducing different fuel types. It also allows exploring various fuel compositions, pebble geometries, cooling-off times, and enrichment levels. These capabilities allow for better identification of optimal reactor operational parameters and exploration of alternative fuel cycles.

Beyond its direct applications, HxF's high-fidelity data holds the potential to address challenges in waste management, non-proliferation efforts, fuel performance analysis, and machine learning. The detailed information about in-core and discharged pebbles enables the evaluation of waste disposal strategies, assessment of plutonium content for non-proliferation considerations, a better understanding of TRISO particles' behavior for fuel performance, and the development of machine learning algorithms for predicting/assessing the reactor behavior.

Conclusions

The development and application of the HxF approach and tool have proven promising in advancing the study of PBRs operation. HxF represents a significant leap in simulation fidelity, enabling the individual depletion of pebbles and tracking their composition, trajectory, and temperature over time. This approach has been made possible by integrating state-of-the-art codes and methods, such as Serpent 2, Cerberus, and GeN-Foam, through the Cerberus Python library. HxF's capabilities extend beyond conventional methodologies, providing detailed pebble-wise data on parameters like power, burnup, and fission product concentration, which are essential for fuel performance analysis, safety assessments, and core optimization. Chapter 2 introduced the HxF tool, highlighting its structure and integrated tools, which enable high-fidelity simulations of PBRs. It performs individual pebble depletion, motion, fuel handling, and thermal-hydraulic calculations with porous media.

Chapter 3 focused on demonstrating individual pebble depletion using Serpent 2, which is crucial for the HxF approach. Serpent 2 features enable individual depletion, such as delta-tracking, cartesian search mesh, explicit stochastic geometry for feasibility and time requirements, and, most importantly, domain decomposition for memory. These features collectively enable the analysis of each pebble's individual history. The performance of individual pebble depletion was quantified on a static full-scale core containing up to half a million burnable materials. The computational feasibility of simulating such a complex system was demonstrated without a supercomputer, making it practical for use on modest computing clusters. A first comparison between a macrozones approach and static individual depletion highlighted the latter's superiority, displaying its accuracy in capturing detailed distributions for important parameters within the core.

In Chapter 4, the HxF tool's capabilities were extended to incorporate pebble motion and fuel handling, representing a significant step towards more realistic and dynamic PBR simulations. Two distinct methods for pebble motion were explored: the discrete motion method and the Discrete Element Method (DEM). The discrete motion method involves representing pebble movement using an ordered bed, simplifying the simulation process and resulting in faster computation times. However, it has limitations in handling complex geometries and cannot accurately account for radial motion or varying pebble speeds, making it less suitable for detailed analyses of intricate reactor designs. In contrast, the DEM approach provided a more realistic representation of pebble trajectories, offering greater flexibility in handling geometries with conic regions and fueling/defueling chutes. This method employs a spring-dashpot model to simulate mechanical interactions between pebbles, providing a more granular view of pebble motion and behavior. While DEM requires higher computational resources than the discrete motion method, it offers a superior level of accuracy and is better suited for complex geometries. Fuel handling in HxF (discharge, discarding, reinsertion, insertion of fresh fuel) enables the simulation of the dynamic PBR operation and allows for performing an approach to equilibrium. Discharged pebbles are identified, and used pebbles are replaced with fresh fuel, facilitating a more realistic simulation of reactor behavior during transient scenarios.

Chapter 5 introduced the thermal aspects of the simulations in the HxF tool with the

implementation of thermal-hydraulics coupling using the GeN-Foam solver. This was achieved by employing a porous media solver and a novel double-heterogeneous power model to describe the pebbles' behavior under thermal conditions. The thermal-hydraulics coupling was carried out using an iterative process, where transport power distribution and porous media temperatures influenced each other through an external process loop. This integration allowed a deeper understanding of the complex interactions between temperature and density distributions and neutronics within the PBR core. By considering the mutual relation of these factors, HxF can achieve a new level of accuracy in simulating PBR behavior. An HTR-10-like model was used as a test case to demonstrate this coupling's capabilities. The results revealed the importance of considering thermal distributions to obtain accurate core behavior. The interaction between the neutronics and thermal-hydraulic aspects is shown through the variation in the multiplication factor caused by changes in temperature. The differences between the initial temperature guess and the final average values considerably impacted the core's reactivity, leading to a decrease in k_{eff}. Incorporating thermal-hydraulics coupling within HxF could represent a major step in achieving hyper-fidelity in PBR simulations. This advancement allows for a more comprehensive analysis of reactor behavior under various operational conditions, including transient scenarios and power excursions. Furthermore, it sets the stage for future improvements, such as exploring local packing fraction calculations and developing porosity-dependent porous media solvers to enhance further the accuracy and applicability of HxF in simulating PBRs.

The HxF tool was applied to the test in Chapter 6 to the gFHR model. The goal was first to benchmark the HxF results against those obtained from the KPACS code, a macrozones tool for PBR analysis developed and used by Kairos Power. The comparison showed that KPACS results are satisfactory for the equilibrium core on a zone basis, while HxF provides a sharper understanding of the parameter distributions within the core and temporal variations during equilibrium. Then, the gFHR was simulated using a DEM for pebble motion on the same geometry and adding fueling and defueling chutes. The results demonstrated that discrete motion yields mostly comparable results to DEM, but its capability for a more realistic representation of pebble trajectories offers clear advantages over discrete motion, particularly when dealing with complex geometries. Indeed, the DEM provided more accurate velocity profiles and allowed for greater flexibility in handling fueling and defueling chutes, significantly impacting the reactor's behavior. Its consideration of wall effects resulted in higher residence times near the core edges, increasing outlier fuel utilizations. The study further explored the potential for coupling GeN-Foam with HxF to analyze the thermal-hydraulic impact on reactor behavior.

Chapter 7 of this thesis delves into the potential applications of the HxF tool, leveraging its flexibility in simulation. The chapter explores how HxF's unique features can be leveraged to explore a wide range of scenarios and parameters. Among the key applications discussed is exploring slow transients, which involves studying the reactor's response to changes in operational conditions. HxF's high-fidelity data and accurate simulations enable us to analyze how the reactor adapts to varying power levels, fuel natures and cycles, and other parameters. In addition, one can explore different fueling strategies, adjust discarding conditions, and analyze the impact of various parameters on fuel utilization and overall reactor performance. The HxF tool's potential extends beyond reactor design to waste management, fuel performance, and non-proliferation efforts.

Detailed data on in-core and discharged pebbles enable an accurate assessment for waste disposal, while accurate predictions of plutonium content support non-proliferation considerations. The high-fidelity data generated by HxF can be used to understand TRISO particles' behavior better, leading to improved fuel performance modeling. The high-quality data produced by HxF can also be used as training data for machine learning algorithms, allowing for predictions and assessments of reactor behavior under various conditions.

Despite the significant advancements achieved, several important aspects remain to be addressed to enhance the HxF approach's capabilities further. These areas of development hold the potential to improve the accuracy, efficiency, and applicability of HxF. One crucial aspect not yet comprehensively explored in the current work is modifying the carbon-to-heavy metal (C/HM) ratio, a key parameter in PBR design. The C/HM ratio, dictated by the number of moderator pebbles in the core, significantly influences the reactor's neutronics and coolant void reactivity feedback. Incorporating the ability to vary the C/HM ratio within the HxF tool would allow reaching the adequate excess reactivity, given a set discard threshold. Associated with that point, another area that requires further development is threshold tuning. The discard threshold also plays a crucial role in the reactor's behavior and fuel utilization. Control rod modeling to assess the regulation of the reactivity in the reactor is another aspect being pursued that can be provided with HxF.

Calculations burnup steps are made large to balance the large computational burden of HxF calculations. The implementation of a motion-enabled predictor-corrector method has the potential to enhance the tool's accuracy and computational efficiency. One could use a predictor step before motion, move pebbles, and apply a corrector step with the new positions. This process would account for the variation of macroscopic cross sections with time and the spatial variation in the flux seen by the pebble due to its movement. However, no predictor-corrector method was applied to the dynamic simulations because a special treatment must be implemented within the Serpent/Cerberus source code to handle the fresh pebbles case. Indeed, a discarded pebble at a predictor step would be replaced at the corrector step, which would provide wrong results.

As Chapter 5 confirmed, continued development on the thermal-hydraulics side is also essential for improving HxF's accuracy. As it is, Serpent 2 (version 2.0) does not have a TMS treatment compatible with domain decomposition. In addition, Cerberus is not fully compatible with OpenFOAM using MPI and parallel nodes, which requires external resources to run a non-domain decomposed case so far. By addressing these aspects, the HxF tool will continue to evolve as a state-of-the-art tool for PBR design, benchmarking, analysis, and optimization.

Bibliography

[1] F. Daniels, "Suggestions for a High Temperature Pebble Pile," Chicago. Univ. Metallurgical Lab., Chicago, 1944.

[2] R. Moormann, "A safety re-evaluation of the AVR pebble bed reactor operation and its consequences for future HTR concepts," in *International Topical Meeting on High Temperature Reactor Technology*, Washington, DC , 2008.

[3] H. Gottaut and K. Krüger, "Results of experiments at the AVR reactor," *Nuclear Engineering and Design,* vol. 121, no. 2, pp. 143-153, 1990.

[4] R. Baumer and I. Kalinowski, "THTR commissioning and operating experience," *Energy,* vol. 16, no. 1-2, pp. 59-70, 1991.

[5] F. Reitsma, "Technical achievements of the PBMR project in South Africa," in *HTR2010*, Prague, 2010.

[6] A. Koster, H. D. Matzner and D. R. Nicholsi, "PBMR design for the future," *Nuclear Engineering and Design,* vol. 222, no. 2-3, pp. 231-245, 2003.

[7] S. Thomas, " The pebble bed modular reactor: an obituary," *Energy Policy,* vol. 39, no. 5, pp. 2431-2440, 2011.

[8] W. Z, L. D and D. Zhong, "The design features of the HTR-10," *Nuclear Engineering and Design,* vol. 218, no. 1-3, pp. 25-32, 2002.

[9] Z. Zhang, Z. Wu, D. Wang, Y. Xu, Y. Sun, F. Li and Y. Dong, "Current status and technical description of Chinese 2× 250 MWth HTR-PM demonstration plant," *Nuclear Engineering and Design,* vol. 239, no. 7, pp. 1212-1219, 2009.

[10] S. Alshehri, I. A. Said and S. Usman, "A review and safety aspects of modular high-temperature gas-cooled reactors," *International Journal of Energy Research,* vol. 45, no. 596, 2020.

[11] N. R. Brown, "Engineering demonstration reactors: A stepping stone on the path to deployment of advanced nuclear energy in the United States," *Energy,* Vols. Volume 238, Part A, no. 121750, 2022.

[12] E. Mulder and W. Boyes, "Neutronics characteristics of a 165 MWth Xe-100 reactor," *Nuclear Engineering and Design,* vol. 357, no. 110415, 2020.

[13] P. N. Haubenreich, J. R. Engel, B. E. Prince and H. C. Claiborne, "MSRE design and operations report. Part III. Nuclear analysis (No. ORNL-TM-730)," Oak Ridge National Lab.(ORNL), Oak Ridge, TN, 1964.

[14] C. Andreades, A. T. Cisneros, J. K. Choi, A. Y. K. Chong, M. Fratoni, S. Hong, L. R. Huddar, K. D. Huff, J. Kendrick and D. L. Krumwiede, "Design summary of the Mark-I pebble-bed, fluoride salt–cooled, high-temperature reactor commercial power plant.," *Nuclear Technology,* vol. 195, no. 3, pp. 223-238, 2016.

[15] A. T. Cisneros, J. K. Choi, A. Y. Chong, M. Fratoni and S. Hong, "Technical Description of the "Mark 1" Pebble-Bed Fluoride-Salt-Cooled High-Temperature Reactor (PB-FHR) Power Plant," Tech. Rep.. Department of Nuclear Engineering, University of California Berkeley, 2014.

[16] C. W. Forsberg, P. F. Peterson and P. S. Pickard, "Molten-salt-cooled advanced high-temperature reactor for production of hydrogen and electricity," *Nuclear Technology,* vol. 144, no. 3, pp. 289-302, 2003.

[17] S. Greene, J. Gehin, D. Holcomb, J. Carbajo, D. Ilas, A. Cisneros, V. Varma, W. Corwin, D. Wilson, G. Yoder Jr and A. Qualls, "Pre-conceptual design of a fluoride-salt-cooled small modular advanced high-temperature reactor (SmAHTR)," Oak Ridge National Laboratory, ORNL/TM-2010/199, Oak Ridge, Tennessee, 2010.

[18] R. Scarlat, M. Laufer, E. Blandford, N. Zweibaum, D. Krumwiede, A. Cisneros, C. Andreades, C. Forsberg, E. Greenspan, L. Hu and P. Peterson, "Design and licensing strategies for the fluoride-salt-cooled, high-temperature reactor (FHR) technology," *Progress in Nuclear Energy,* vol. 77, pp. 406-420, 2014.

[19] N. Rohbeck and P. Xiao, "Evaluation of the mechanical performance of silicon carbide in TRISO fuel at high temperatures," *Nuclear Engineering and Design,* vol. 306 , pp. 52-58, 2016.

[20] N. R. Brown, "A review of in-pile fuel safety tests of TRISO fuel forms and future testing opportunities in non-HTGR applications," *Journal of Nuclear Materials,* vol. 534 , no. 152139, 2020.

[21] General Atomics, "General Atomic's Prismatic Modular High Temperature Gas Cooled Reactor," International Atomic Energy Agency, Advanced Reactors Information System (IAEA, ARIS), Technical Data on Gas Cooled Reactors (GCR)., 2014.

[22] S. Gosse, C. Guéneau, F. Boinski, T. Alpettaz, S. Chatain and C. Chatillon, "High Temperature Interaction Between UO2 and Carbon: Application to TRISO Particles for Very High Temperature Reactors," *High Temperature Reactor Technology,* vol. 48548, pp. 317-327, 2008.

[23] Z. Zhang, Y. Dong, F. Li, Z. Zhang, H. Wang, X. Huang, H. Li, B. Liu, X. Wu, H. Wang and X. Diao, "The Shandong Shidao Bay 200 MWe high-temperature gas-cooled reactor pebble-bed module (HTR-PM) demonstration power plant: an engineering and technological innovation," *Engineering,* vol. 2, no. 1, pp. 112-118, 2016.

[24] U. Cleve, H. Handel and U. Scholz, "On-load fueling of pebble-bed high temperature reactors," *Proc. Inst. Mech. Eng. (London),* vol. 183, no. 124-30, 1968.

[25] A. G, R. R, D. V. E and C. R., "Process heat cogeneration using a high temperature reactor," *Nuclear Engineering and Design,* vol. 280, pp. 137-143, 2014.

[26] W. Yan, L. Zhang, Z. Zhang, Y. Zhang and Z. Xiao, "Prototype studies on the nondestructive online burnup determination for the modular pebble bed reactors," *Nuclear Engineering and Design,* vol. 267, pp. 172-179, 2014.

[27] E. Teuchert and H. Rütten, "Core physics and fuel cycles of the pebble bed reactor," *Nuclear Engineering and Design,* vol. 34, no. 1, pp. 109-118, 1975.

[28] S. Boarin and M. Ricotti, "An evaluation of SMR economic attractiveness," *Science and Technology of Nuclear Installations,* 2014.

[29] E. Teuchert, U. Hansen and K.-A. Haas, "VSOP-Computer code system for reactor physics and fuel cycle simulation," Kernforschungsanlage Juelich GmbH, Germany, 1980.

[30] W. Feltes, "HTR-Program Description of ZIRKUS, Report Nr. KWU BT71/93/0009.," Siemens, 1993.

[31] D. She, J. Guo, Z. Liu and L. Shi, "PANGU code for pebble-bed HTGR reactor physics and fuel cycle simulations," *Annals of Nuclear Energy,* vol. 126, pp. 48-58, 2019.

[32] P. Liem, "BATAN-MPASS: a general fuel management code for pebble-bed high-temperature reactors," *Annals of Nuclear Energy,* vol. 21, no. 5, pp. 281-290, 1994.

[33] W. K. Terry, H. D. Gougar and A. Ougouag, "Direct deterministic method for neutronics analysis and computation of asymptotic burnup distribution in a recirculating pebble-bed reactor," *Annals of Nuclear Energy,* vol. 29, pp. 1345-1364, 2001.

[34] H. D. Gougar, Advanced Core Design and Fuel Management for Pebble-Bed Reactors, The Pennsylvania State University, United States - Pennsylvania, 2004.

[35] W. L. Thompson, "MCNP, a general Monte Carlo code for neutron and photon transport: A summary.," No. LA-8176-MS. Los Alamos Scientific Lab., NM (USA), 1979.

[36] A. G. Croff, "ORIGEN2: a versatile computer code for calculating the nuclide compositions and characteristics of nuclear materials," *Nuclear Technology,* vol. 62, no. 3, pp. 335-352, 1983.

[37] M. Fratoni and E. Greenspan, "Equilibrium core composition search methodologies for pebble bed reactors.," *Nuclear science and engineering,* vol. 166, no. 1, pp. 1-16,

2010.

[38] M. Fratoni, Development and applications of methodologies for the neutronic design of the Pebble Bed Advanced High Temperature Reactor (PB-AHTR), University of California, Berkeley, 2008.

[39] A. T. Cisneros Jr, "Pebble Bed Reactors Design Optimization Methods and their Application to the Pebble Bed Fluoride Salt Cooled High Temperature Reactor (PB-FHR)," University of California, Berkeley, 2013.

[40] N. Satvat, F. Sarikurt, K. Johnson, I. Kolaja, M. Fratoni, B. Haugh and E. Blandford, "Neutronics, thermal-hydraulics, and multi-physics benchmark models for a generic pebble-bed fluoride-salt-cooled high temperature reactor (FHR)," *Nuclear Engineering and Design,* vol. 384, p. 111461, 2021.

[41] R. Kile, F. Bostelmann, S. Skutnik, W. Wieselquist and N. Brown, "Assessment of SCALE and MELCOR for a generic pebble bed fluoride high-temperature reactor," *Annals of Nuclear Energy,* vol. 173, no. 109107, 2022.

[42] P. K. Romano, N. E. Horelik, B. R. Herman, A. G. Nelson, B. Forget and K. Smith, "OpenMC: A state-of-the-art Monte Carlo code for research and development," *Annals of Nuclear Energy,* vol. 82, pp. 90-97, 2015.

[43] J. Leppänen, "Serpent–a continuous-energy Monte Carlo reactor physics burnup calculation code," VTT Technical Research Centre of Finland, 2013.

[44] S. Schunert, J. Ortensi, Y. Wang, P. Balestra, M. Jaradat, O. Calvin, J. Hanophy and L. Harbour, "An equilibrium core depletion algorithm for pebble-bed reactors in the Griffin code," *Annals of Nuclear Energy,* vol. 192, p. 109980, 2023.

[45] D. Hollenbach, L. Petrie and N. Landers, "KENO-VI: A general quadratic version of the keno program. vol. II, sect. f17 of scale: A modular code system for performing standard computer analysis for licensing evaluation," Technical Report NUREG/CR-0200, Rev. 7, Oak Ridge National Laboratory, 2004.

[46] Y. Robert, "HxF," 2023. [Online]. Available: https://github.com/yvrob/HxF.git.

[47] V. Valtavirta, "Python level introduction to coupled calculations with Kraken using Cerberus," in *Serpent User Group Meeting 2022*, Munich, 2022.

[48] Y. Robert and M. Fratoni, "Evaluation of Serpent Capabilities for Hyperfidelity Depletion of Pebble Bed Cores," in *International Conference on Nuclear Engineering*, 2021.

[49] H. G. Weller, G. Tabor, H. Jasak and C. Fureby, "A tensorial approach to computational continuum mechanics using object-oriented techniques," *Computers in physics,* vol. 12, no. 6, p. 620, 1998.

[50] M. Aufiero and M. Fratoni, "Development of multiphysics tools for fluoride-cooled high-temperature reactors," in *PHYSOR*, 2016.

[51] J. Ge, C. Wang, Y. Xiao, W. Tian, S. Qiu, G. Su, D. Zhang and Y. Wu, "Thermal-hydraulic analysis of a fluoride-salt-cooled pebble-bed reactor with CFD methodology," *Progress in Nuclear Energy,* vol. 91, pp. 83-96, 2016.

[52] C. Fiorina, I. Clifford, M. Aufiero and K. Mikityuk, "GeN-Foam: a novel OpenFOAM® based multi-physics solver for 2D/3D transient analysis of nuclear reactors," *Nuclear Engineering and Design,* vol. 294, pp. 24-37, 2015.

[53] Y. Robert, L. Jantzen, T. Siaraferas, C. Fiorina and M. Fratoni, "Impact Of Thermal Coupling On A Pebble Bed Reactor From Hyper-Fidelity Depletion," in *ICONE30*, Kyoto, Japan, 2023.

[54] Y. Robert and V. Valtavirta, "New features for pebble bed reactors simulations with Cerberus/Serpent," in *Serpent Users Group Meeting* , Garching, Germany, 2022.

[55] Y. Robert, M. Fratoni and T. Siaraferas, "Proof of Concept for Hyper-Fidelity Depletion of Full-Scale Pebble Bed Reactors," *Annals of Nuclear Energy,* 2022.

[56] V. Rintala, H. Suikkanen, J. Leppänen and R. Kyrki-Rajamäki, "Modeling of realistic pebble bed reactor geometries using the Serpent Monte Carlo code," *Annals of Nuclear Energy,* vol. 77, pp. 223-230, 2015.

[57] E. Woodcock, T. Murphy, P. Hemmings and S. Longworth, "Techniques used in the GEM code for Monte Carlo neutronics calculations in reactors and other systems of complex geometry," in *Proc. Conf. Applications of Computing Methods to Reactor Problems*, 1965.

[58] J. Leppänen, "Serpent 2 – Status and future plans," VTT Technical Research Centre of Finland, 2011.

[59] R. Chandra, R. Menon, L. Dagum and D. 2. Kohr, Parallel Programming in OpenMP., 2001.

[60] University of Tennessee, "MPI: A Message-Passing Interface Standard," 1994.

[61] M. Chadwick, P. Obložinský, M. Herman, N. Greene, R. McKnight, D. Smith, P. Young, R. MacFarlane, G. Hale, S. Frankle, A. Kahler, T. Kawano, R. Little, D. Madland, P. Moller, R. Mosteller, P. Page, P. Talou, H. Trellue and M. Whit, "ENDF/B-VII.0: Next Generation Evaluated Nuclear Data Library for Nuclear Science and Technology," *Nuclear Data Sheets,* vol. 107, no. 12, pp. 2931-3060, 2006.

[62] C. H. Rycroft, G. S. Grest, J. W. Landry and M. Z. Bazant, "Analysis of granular flow in a pebble-bed nuclear reactor," *Physical review E,* vol. 74, no. 2, p. 021306, 2006.

[63] D. Reger, E. Merzari, P. Balestra, S. Schunert, Y. Hassan, H. Yuan, Y.-H. Lan, P. Fischer and M. Min, "Pressure Drop Correlation Improvement for the Near-Wall Region of Pebble-Bed Reactors," *Nuclear Technology,* pp. 1-15, 2022.

[64] A. Tasora, R. Serban, H. Mazhar, A. Pazouki, D. Melanz, J. Fleischmann, M. Taylor, H. Sugiyama and D. Negrut, "Chrono: An open source multi-physics dynamics engine," in *International Conference on High Performance Computing in Science and Engineering*, Springer, Cham, 2015.

[65] Y. Robert, M. Fratoni and T. Siaraferas, "Hyper-fidelity depletion with discrete motion for pebble bed reactors (under review)," *Scientific Reports,* vol. 13, no. 1, p. 12711, 2023.

[66] Y. Robert and M. Fratoni, "Hyper-Fidelity Depletion Coupled with Discrete Pebble Motion in Pebble Bed Reactors," in *PHYSOR 2022*, Pittsburgh, PA, 2022.

[67] H. Suikkanen, J. Ritvanen, P. Jalali and R. Kyrki-Rajamäki, "Discrete element modelling of pebble packing in pebble bed reactors," *Nuclear Engineering and Design,* vol. 273, pp. 24-32, 2014.

[68] Y. Li, N. Gui, X. Yang, J. Tu and S. Jiang, "Effect of wall structure on pebble stagnation behavior in pebble bed reactor," *Annals of Nuclear Energy,* vol. 80, pp. 195-202, 2015.

[69] R. Mardus-Hall, M. Ho, G. Yeoh and V. Timchenko, "Coupled CFD-DEM Analysis of Molten Salt-Cooled Pebble-Bed Reactor Experiment," *Transactions of the American Nuclear Society,* vol. 116, pp. 1506-1509, 2017.

[70] F. Putra, "HTR-10 OTTO Cycle Depletion Simulation Using Discrete Element Method Coupled Monte Carlo," in *International Conference on High-Temperature Reactor Technology, HTR 2021*, Virtual Conference - Yogyakarta, Indonesia, 2021.

[71] Y.-s. Tang, Z.-z. Yin, L.-g. Zhang, Q.-j. Guo, J.-z. Cao and J.-j. Tong, "The application of the DEM-based burnup construction method in the pebble burnup history analysis in HTR-10," *Nuclear Engineering and Design,* vol. 349, pp. 1-7, 2019.

[72] F. Vitullo, J. Krepel, J. Kalilainen, H.-M. Prasser and A. Pautz, "Statistical Burnup Distribution of Moving Pebbles in the High-Temperature Reactor HTR-PM," *ASME J. of Nuclear Rad Sci.,* vol. 6, no. 2, 2020.

[73] M. R. Laufer, Granular dynamics in pebble bed reactor cores, University of California, Berkeley, 2013.

[74] L. Vergari and M. Fratoni, "Spent fuel management strategies for fluoride-cooled pebble bed reactors," *Nuclear Engineering and Design,* vol. 378, no. 111189, 2021.

[75] J. J. Powers and B. D. Wirth, "A review of TRISO fuel performance models,"

Journal of Nuclear Materials, vol. 405, no. 1, pp. 74-82, 2010.

[76] F. Reitsma, K. Ivanov, E. Sartori, H. C. Lee, A. Daavittila, J. Leppanen and E. Girardi, PBMR Coupled Neutronics/Thermal-hydraulics Transient Benchmark. The PBMR-400 Core Design-Volume 1 The Benchmark Definition., Organisation for Economic Co-Operation and Development, 2013.

[77] C. Rycroft, Multiscale modeling in granular flow, Boston, MA: Massachusetts Institute of Technology, Department of Mathematics, 2007.

[78] Y. Li, Y. Xu and S. Jiang, "DEM simulations and experiments of pebble flow with monosized spheres," *Powder technology,* vol. 193, no. 3, pp. 312-318, 2009.

[79] A. Thompson, H. Aktulga, R. Berger, D. Bolintineanu, W. Brown, P. Crozier, P. Veld, A. Kohlmeyer, S. Moore, T. Nguyen and R. Shan, "LAMMPS-a flexible simulation tool for particle-based materials modeling at the atomic, meso, and continuum scales," *Computer Physics Communications,* vol. 271, pp. 108-171, 2022.

[80] R. Li, Z. Liu, Z. Feng, J. Liang and L. Zhang, "High-Fidelity MC-DEM Modeling and Uncertainty Analysis of HTR-PM First Criticality," *Frontiers in Energy Research,* vol. 9, p. 822780, 2022.

[81] Y. Tang, L. Zhang, Q. Guo, B. Xia, Z. Yin, J. Cao, J. Tong and C. Rycroft, "Analysis of the pebble burnup profile in a pebble-bed nuclear reactor," *Nuclear Engineering and Design,* vol. 345, pp. 233-251, 2019.

[82] C. Kloss, C. Goniva, A. Amberger and S. Pirker, "Models, algorithms and validation for opensource CFD-DEM," *Progress in Computational Fluid Dynamics,* vol. 12, pp. 140-152, 2012.

[83] D. Reger, E. Merzari, P. Balestra, R. Stewart and G. Strydom, "Discrete element simulation of Pebble Bed Reactors on graphics processing units," *Annals of Nuclear Energy,* vol. 190, p. 109896, 2023.

[84] L. Halla-aho, "Development of an HTR-10 model in the Serpent reactor physics code," Lappeenranta University of Technology, Lappeenranta, 2014.

[85] D. She, F. Chen, B. Xia and L. Shi, "Simulation of the HTR-10 Operation History With the PANGU Code," *Frontiers in Energy Research,* vol. 9, 2021.

[86] J. Ortensi, S. Schunert, Y. Wang, V. Labouré, F. Gleicher and R. C. Martineau, "Benchmark Analysis of the HTR-10 with the MAMMOTH Reactor Physics Application," Idaho National Laboratory, Idaho Falls, 2018.

[87] H. D. Gougar, F. Reitsma and W. Joubert, "A comparison of pebble mixing and depletion algorithms used in pebble-bed reactor equilibrium cycle simulation.," No. INL/CON-09-15510. Idaho National Lab.(INL), Idaho Falls, ID (United States), 2009.

[88] L. Zou, G. Hu, D. O'Grady and R. Hu., "Explicit modeling of pebble temperature in the porous-media model for pebble-bed reactors," *Progress in Nuclear Energy,* vol. 146, p. 104175, 2022.

[89] A. Novak, "Multiscale Thermal-Hydraulic Methods for Pebble Bed Reactors," PhD Thesis, University of California, Berkeley, 2020.

[90] V. Valtavirta, "Coupled calculations with Serpent 2.1.29," in *Serpent UGM*, Gainesville, Florida, 2017.

[91] T. Viitanen and J. Leppänen, "Effect of the Target Motion Sampling temperature treatment method on the statistics and performance," *Annals of Nuclear Energy,* vol. 82, pp. 217-225, 2015.

[92] A. Novak, L. Zou, J. Peterson, R. Martineau and R. Slaybaugh, Pronghorn: Porous media thermal-hydraulics for reactor applications., Berkeley, California: University of California, Berkeley, 2018.

[93] Kairos Power LLC, "Generic FHR Core Model," [Online]. Available: https://kairospower.com/generic-fhr-core-model/.

[94] B. Dsouza, Neutronic analysis of light water Small Modular Reactor with flexible fuel configurations., Missouri University of Science and Technology., 2015.

[95] B. P. Bromley and A. V. Colton, "Reactor Physics Analysis Assessment of Feasibility of Using Advanced, Nonconventional Fuels in a Pressure Tube Heavy Water Reactor to Destroy Long-Lived Fission Products," *Nuclear Technology,* vol. 207, no. 8, pp. 1182-1192, 2021.

[96] S. Chiba, T. Wakabayashi, Y. Tachi, N. Takaki, A. Terashima, S. Okumura and T. Yoshida, "Method to reduce long-lived fission products by nuclear transmutations with fast spectrum reactors," *Scientific reports,* vol. 7, no. 1, p. 13961, 2017.

[97] X. Sun, W. Luo, H. Lan, Y. Song, Q. Gao, Z. Zhu, J. Chen and X. Cai, " Transmutation of long-lived fission products in an advanced nuclear energy system," *Scientific Reports,* vol. 12, no. 1, p. 2240, 2022.

[98] W.-H. Yan, L.-G. Zhang, Z. Zhang and Z.-G. Xiao, "Feasibility studies on the burnup measurement of fuel pebbles with HPGe gamma spectrometer," *Nuclear Instruments and Methods in Physics Research Section A: Accelerators, Spectrometers, Detectors and Associated Equipment,* vol. 712, pp. 130-136, 2013.

[99] D. E. Serfontein, F. Reitsma and E. Mulder, Deep burn strategy for the optimized incineration of reactor waste plutonium in pebble bed high temperature gas–cooled reactors, Potchefstroom Campus: North-West University, 2012.

[100] E. Greenspan, P. Peterson, M. Fratoni and A. Cisneros, "Deep Burn Modular High

Temperature Reactors," University of California, Berkeley, Berkeley, CA, 2007.

[101] E. Teuchert, H. J. Ruetten, H. Werner, K. A. Haas and R. Schulten, "Closed thorium cycles in the pebble bed HTR," 1979.

[102] F. Wols, J. Kloosterman, D. Lathouwers and T. Van der Hagen, "Conceptual design of a passively safe thorium breeder Pebble Bed Reactor," *Annals of Nuclear Energy,* vol. 75, pp. 542-558, 2015.

Appendices

A. Pebble power model thermal derivations

This appendix details the derivation of the two double-heterogeneous power models developed in GeN-Foam.

Pebble power and fluid-pebble interface

- Cell-wise power densities $\dot{q}_c$ are tallied
- Representative pebble (subscript p) power and matrix density. All the tallied power is produced within pebbles:

$$\dot{Q}_p = \dot{q}_c \times V_c$$

$$\dot{q}_p = \frac{\dot{Q}_p}{V_p} = \frac{\dot{Q}_p}{\frac{4}{3}\pi R_p^3}$$

- Fuel kernel (subscript f) power and density. All pebble power is generated within fuel kernels in the N_T TRISO particles (subscript T):

$$\dot{Q}_f = \dot{Q}_T = \frac{\dot{Q}_p}{N_T}$$

$$\dot{q}_f = \frac{\dot{Q}_f}{V_f} = \frac{\dot{Q}_f}{\frac{4}{3}\pi R_f^3}$$

- Convection boundary condition between the fluid (subscript F) T_F and representative pebble surface $T_{p,S}$ (for coupling). The pebble's outer surface corresponds to the interface surface:

$$q''_{p\to F} = \frac{\dot{Q}_p}{S_p} = \frac{\dot{Q}_p}{4\pi R_p^2}$$

$$q''_{p\to F} = h\left(T_F - T_{p,S}\right) \to T_{p,S} = \frac{\dot{q}''}{h} + T_F = \frac{q''_{p\to F} + hT_F}{h}$$

Pebble temperatures

- The pebble has three zones: core, matrix, and shell (subscripts c, m, s, respectively).
- R represents the outer radius of each zone.
- 1D conduction in each layer, with power generation only in the matrix layer.

<u>Shell</u>

- The pebble surface temperature corresponds to the outer shell temperature:

$$T_s(R_s) = T_{p,S}$$

- Profile temperature in the shell with the conductivity of graphite k_g:

$$T_s(r) = T_{p,S} + \frac{\dot{Q}_p}{4\pi\lambda_g} \times \left(\frac{1}{r} - \frac{1}{R_s}\right), r \in [R_m, R_s]$$

This can be rewritten as:

$$\dot{Q}_p = H_{shell}(T_m - T_s)$$

where H_{shell} is the conductance associated with the shell.

$$H_{shell} = \left(\frac{1}{4\pi\lambda_g} \times \left(\frac{1}{R_m} - \frac{1}{R_s}\right)\right)^{-1}$$

Matrix

- Matrix power density:

$$\dot{q}_m = \frac{\dot{Q}_p}{V_p} = \frac{\dot{Q}_p}{\frac{4}{3}\pi(R_m^3 - R_c^3)}$$

- Temperature profile:

$$\begin{cases} \lambda_{eff}\Delta T_m = \dot{q}_m \\ \frac{1}{r^2}\frac{d}{dr}\left(r^2\frac{dT_m}{dr}\right) = \frac{\dot{q}_m}{\lambda_{eff}} \end{cases}$$

  - Solving with flux $\psi = \frac{dT}{dr}$, the solution is of the form:

$$\psi = \frac{-r\dot{q}_m}{3\lambda_{eff}} + \frac{C_1}{r^2}$$

  - **Boundary condition 1**:

$$T_m(R_m) = T_s(R_m) = T_{p,S} + \frac{\dot{Q}_p}{4\pi\lambda_g} \times \left(\frac{1}{R_m} - \frac{1}{R_s}\right)$$

    - Case 1: $R_c = 0$ (no graphite core, HTGR)
      Boundary condition 2: zero flux

$$\frac{dT_m}{dr}(0) = 0$$

      Then, $C_1 = 0$:

$$T_m(r) = T_m(R_m) + \frac{\dot{q}_m}{6\lambda_{eff}}(R_m^2 - r^2), r \in [0, R_m]$$

    - Case 2: $R_c > 0$
      Boundary condition 2: continuity of the flux (unheated core).

$$-\lambda_{eff}\left(\frac{dT_m}{dr}\right)(R_{core}) = 0$$

      Then, $C_1 = \frac{R_{core}^3}{3\lambda_{eff}}$:

$$T_m(r) = T_m(R_m) + \frac{\dot{q}_m}{6\lambda_{eff}}(R_m^2 - r^2) + \frac{R_c^3}{3\lambda_{eff}}\left(\frac{1}{R_m} - \frac{1}{r}\right)$$

- Average value:

$$\bar{T}_m = \frac{\int_{R_c}^{R_m} T_m(r) r^2 dr}{\int_{R_c}^{R_m} r^2 dr}$$

$$\bar{T}_m = T_m(R_m) + \frac{\dot{q}_m}{6\lambda_{eff}}\left(R_m^2 - \frac{3}{5} \times \frac{R_m^5 - R_c^5}{R_m^3 - R_c^3}\right) + \dot{q}_m \frac{R_c^3}{3\lambda_{eff}}\left(\frac{1}{R_m} - \frac{2}{3}\frac{R_m^3 - R_c^3}{R_m^2 - R_c^2}\right)$$

This can be rewritten as :

$$\bar{T}_m = T_m(R_m) + \frac{\dot{Q}_p}{V_p}\frac{1}{6\lambda_{eff}}\left(R_m^2 - \frac{3}{5} \times \frac{R_m^5 - R_c^5}{R_m^3 - R_c^3}\right) + \frac{\dot{Q}_p}{V_p}\frac{R_c^3}{3\lambda_{eff}}\left(\frac{1}{R_m} - \frac{2}{3}\frac{R_m^3 - R_c^3}{R_m^2 - R_c^2}\right)$$

and:

$$\dot{Q}_p = H_{sToM}\left(T_{m,AV} - T_m\right)$$

where

$$H_{sToM} = \left(\frac{1}{V_p}\frac{1}{6\lambda_{eff}}\left(R_m^2 - \frac{3}{5} \times \frac{R_m^5 - R_c^5}{R_m^3 - R_c^3}\right) + \frac{1}{V_p}\frac{R_c^3}{3\lambda_{eff}}\left(\frac{1}{R_m} - \frac{2}{3}\frac{R_m^3 - R_c^3}{R_m^2 - R_c^2}\right)\right)^{-1}$$

This is the heat conductance between the matrix-shell interface and the average matrix temperature.

Fuel temperatures

- TRISO particle: 5 layers (inner to outer): fuel kernel, graphite buffer, inner Peek, SiC, outer PyC (subscripts f, b, Pin, Sick, Pout, respectively).
- The surface temperature of the TRISO is the matrix temperature at which TRISO is (r_p):

$$T_{T,S} = T_m\left(r_p\right)$$

- 1D conduction in the TRISO particle, with power generation only in the fuel kernel.
- Surface temperature of the fuel:

$$T_{f,S} = T_{T,S} + \frac{\dot{Q}_T}{4\pi} \times \left[\frac{1}{\lambda_b}\left(\frac{1}{R_f} - \frac{1}{R_b}\right) + \frac{1}{\lambda_{Pin}}\left(\frac{1}{R_b} - \frac{1}{R_{Pin}}\right) + \frac{1}{\lambda_{SiC}}\left(\frac{1}{R_{Pin}} - \frac{1}{R_{SiC}}\right) + \frac{1}{\lambda_{Pout}}\left(\frac{1}{R_{SiC}} - \frac{1}{R_{Pout}}\right)\right]$$

This can be rewritten as

$$T_{f,S} = T_{T,S} + \frac{\dot{Q}_p}{4\pi N_T} \times \left[\frac{1}{\lambda_b}\left(\frac{1}{R_f} - \frac{1}{R_b}\right) + \frac{1}{\lambda_{Pin}}\left(\frac{1}{R_b} - \frac{1}{R_{Pin}}\right) + \frac{1}{\lambda_{SiC}}\left(\frac{1}{R_{Pin}} - \frac{1}{R_{SiC}}\right) + \frac{1}{\lambda_{Pout}}\left(\frac{1}{R_{SiC}} - \frac{1}{R_{Pout}}\right)\right]$$

and:

$$\dot{Q}_p = H_{mToSf}\left(T_{f,S} - T_{m,AV}\right)$$

where

$$H_{mToSf} = \left(\frac{1}{4\pi N_T} \times \left[\frac{1}{\lambda_b}\left(\frac{1}{R_f} - \frac{1}{R_b}\right) + \frac{1}{\lambda_{Pin}}\left(\frac{1}{R_b} - \frac{1}{R_{Pin}}\right) + \frac{1}{\lambda_{SiC}}\left(\frac{1}{R_{Pin}} - \frac{1}{R_{SiC}}\right) + \frac{1}{\lambda_{Pout}}\left(\frac{1}{R_{SiC}} - \frac{1}{R_{Pout}}\right)\right]\right)^{-1}$$

This is the heat conductance TRISO surface and average matrix temperature. Please notice that we are neglecting the heat resistance between average matrix temperature and surface of the TRISO.

- Profile in the fuel is 1D conduction with heat generation in a sphere:

$$T_f(r) = T_{f,S} + \frac{\dot{q}_f}{6\lambda_f}\left(R_f^2 - r^2\right)$$

- Maximum fuel temperature: r=0

$$T_{f,max} = T_f(0) = T_f(r) = T_{f,S} + \frac{\dot{q}_f R_f^2}{6\lambda_f}$$

- Average fuel temperature:

$$\bar{T}_f = \frac{\int_0^{R_f} T_f(r) r^2 dr}{\int_0^{R_f} r^2 dr}$$

$$\bar{T}_f = T_{f,S} + \frac{\dot{q}_f R_f^2}{15\lambda_f}$$

This can be rewritten as:

$$\bar{T}_f = T_{f,S} + \frac{\dot{Q}_p}{4\pi R_f^3 N_T}\frac{R_f^2}{15\lambda_f}$$

and:

$$\dot{Q}_p = H\left(T_{f,av} - T_{f,S}\right)$$

where

$$H_{SmToSf} = \left(\frac{1}{4\pi R_f^3 N_T}\frac{R_f^2}{15\lambda_f}\right)^{-1}$$

This is the heat conductance between the fuel average and the fuel surface.

Lumped parameter model

The heat transfer in the pebble and fuel can be modeled as an electric equivalent with 2 nodes:

- 1 node for the graphite average temperature
- 1 node for the fuel average temperature

This requires at least 2 heat conductance.

1. The heat conductance between the pebble surface and graphite average temperature, which is the harmonic mean of H_{shell} and H_{sToM}
2. The heat conductance between graphite average temperature and fuel average temperature, which is the harmonic mean of H_{mToSf} and H_{SmToSf}

One can also add a third conductance between fuel average and maximum temperatures. GeN-Foam requires this third resistance, although one can give any value if the maximum temperature is not of interest.

Effective conductivity

The matrix, considered homogeneous, has an effective matrix conductivity denoted by λ_{eff}

- Packing fraction of TRISO in the matrix:

$$\phi = \frac{N_T V_T}{V_m} = N_T \frac{\frac{4}{3}\pi R_T^3}{\frac{4}{3}\pi (R_m^3 - R_c^3)} = \frac{N_T R_{Pout}^3}{R_m^3 - R_c^3}$$

- Average conductivity of the TRISO particles:

$$\lambda_T = \frac{\frac{1}{2R_{Pout}}}{\frac{1}{2k_f}\frac{1}{R_f} + \frac{1}{\lambda_b}\left(\frac{1}{R_f} - \frac{1}{R_b}\right) + \frac{1}{\lambda_{Pin}}\left(\frac{1}{R_b} - \frac{1}{R_{Pin}}\right) + \frac{1}{\lambda_{SiC}}\left(\frac{1}{R_{Pin}} - \frac{1}{R_{SiC}}\right) + \frac{1}{\lambda_{Pout}}\left(\frac{1}{R_{SiC}} - \frac{1}{R_{Pout}}\right)}$$

- Maxwell equation with the TRISO conductivity λ_T, the conductivity of the graphite in the matrix λ_g, and the packing fraction of TRISO in the matrix ϕ.

$$\kappa = \frac{\lambda_T}{\lambda_g}$$

$$\beta = \frac{\kappa - 1}{\kappa + 2}$$

$$\lambda_{eff} = \lambda_g \times \frac{1 + 2\beta\phi}{1 - \beta\phi}$$

B. In-core gFHR pebble content

The equilibrium in-core data for 10^7 pebbles from the gFHR model with discrete motion in Chapter 6.1 is compiled in this appendix. The minimum, average, and maximum values are calculated per pass, along with a global average for each field. Please note that the minimum and maximum values are not derived from a single pebble but are extracted from all pebbles.

Minimum content

General fields

Pass #	1	2	3	4	5	6	7	8	Avg
Residence time [days]	3.84	69.09	134.34	199.59	264.84	330.09	395.34	460.59	231.67
Pass burnup [MWd/kg$_{HM}$]	1.16	1.11	0.95	0.84	0.68	0.56	0.6	0.57	0.9
Burnup [MWd/kg$_{HM}$]	1.16	24.66	48.06	69.86	90.59	109.37	126.31	142.93	77.15
Thermal fluence [n/cm^2]	3.20E+19	5.91E+20	1.17E+21	1.75E+21	2.33E+21	2.91E+21	3.50E+21	4.09E+21	2.07E+21
Thermal fluence uncertainty	1.8%	2.4%	2.5%	2.5%	2.5%	2.5%	2.6%	2.6%	2.4%
Fast fluence [n/cm^2]	1.13E+19	3.03E+20	5.97E+20	8.93E+20	1.28E+21	1.68E+21	2.04E+21	2.52E+21	1.22E+21
Fast fluence uncertainty	2.6%	3.1%	3.1%	3.2%	3.2%	3.2%	3.3%	3.3%	3.1%
Power [W]	4.55E+02	4.02E+02	3.63E+02	3.33E+02	3.10E+02	2.81E+02	2.35E+02	1.74E+02	3.60E+02
Power uncertainty	4.7%	4.6%	4.8%	4.9%	4.9%	5.0%	5.1%	5.1%	5.1%

Atomic densities [at/b.cm]

Pass #	1	2	3	4	5	6	7	8	Avg
He-4	3.24E-13	3.66E-09	3.00E-08	7.60E-08	1.43E-07	2.39E-07	4.23E-07	6.65E-07	2.13E-07
C-12	1.17E-02	1.17E-02	1.17E-02	1.17E-02	1.17E-02	1.17E-02	1.17E-02	1.17E-02	1.17E-02
C-13	1.25E-04	1.25E-04	1.25E-04	1.25E-04	1.25E-04	1.25E-04	1.25E-04	1.25E-04	1.25E-04
O-16	3.55E-02	3.55E-02	3.55E-02	3.55E-02	3.55E-02	3.55E-02	3.55E-02	3.55E-02	3.55E-02
O-17	7.51E-11	1.64E-09	3.27E-09	4.92E-09	6.55E-09	8.23E-09	9.91E-09	1.17E-08	5.88E-09
Zn-70	1.25E-12	3.36E-11	7.35E-11	1.15E-10	1.55E-10	1.96E-10	2.35E-10	2.71E-10	1.37E-10
Ga-69	5.35E-13	1.42E-11	3.00E-11	4.58E-11	6.06E-11	7.59E-11	8.86E-11	1.01E-10	5.28E-11
Ga-71	2.86E-12	7.11E-11	1.53E-10	2.41E-10	3.23E-10	4.11E-10	4.93E-10	5.70E-10	2.87E-10
Ge-72	2.70E-12	2.01E-10	4.43E-10	7.02E-10	9.41E-10	1.18E-09	1.41E-09	1.61E-09	8.19E-10
Ge-73	2.92E-11	7.12E-10	1.44E-09	2.19E-09	2.86E-09	3.47E-09	4.04E-09	4.59E-09	2.44E-09
Ge-74	1.02E-10	2.27E-09	4.52E-09	6.76E-09	8.82E-09	1.07E-08	1.24E-08	1.41E-08	7.54E-09
Ge-76	9.12E-10	1.93E-08	3.73E-08	5.38E-08	6.91E-08	8.27E-08	9.49E-08	1.06E-07	5.85E-08
Ge-77	1.79E-10	1.57E-10	1.35E-10	1.22E-10	1.10E-10	9.66E-11	7.77E-11	5.86E-11	1.31E-10
As-75	3.07E-10	6.71E-09	1.31E-08	1.91E-08	2.46E-08	2.94E-08	3.37E-08	3.78E-08	2.07E-08
As-77	7.61E-10	6.67E-10	5.27E-10	4.83E-10	4.40E-10	3.90E-10	3.29E-10	2.72E-10	5.26E-10
Se-76	4.00E-14	1.50E-11	6.59E-11	1.49E-10	2.79E-10	4.62E-10	6.61E-10	8.41E-10	3.27E-10
Se-77	8.84E-10	4.66E-08	9.12E-08	1.32E-07	1.69E-07	2.01E-07	2.29E-07	2.55E-07	1.41E-07
Se-78	5.78E-09	1.28E-07	2.48E-07	3.59E-07	4.63E-07	5.56E-07	6.41E-07	7.21E-07	3.93E-07
Se-79	1.28E-08	2.72E-07	5.22E-07	7.47E-07	9.50E-07	1.13E-06	1.28E-06	1.43E-06	8.00E-07
Se-80	3.70E-08	7.76E-07	1.49E-06	2.14E-06	2.74E-06	3.28E-06	3.75E-06	4.20E-06	2.33E-06
Se-81	1.24E-10	1.07E-10	9.35E-11	8.55E-11	7.72E-11	6.80E-11	5.55E-11	4.15E-11	9.18E-11
Se-82	9.31E-08	1.94E-06	3.73E-06	5.33E-06	6.81E-06	8.13E-06	9.29E-06	1.04E-05	5.77E-06
Se-83	3.47E-10	2.91E-10	2.45E-10	2.21E-10	1.98E-10	1.67E-10	1.36E-10	1.03E-10	2.41E-10
Br-79	6.77E-12	1.43E-10	2.76E-10	3.94E-10	5.01E-10	5.96E-10	6.79E-10	7.55E-10	4.22E-10
Br-81	5.81E-08	1.23E-06	2.37E-06	3.41E-06	4.35E-06	5.18E-06	5.92E-06	6.62E-06	3.67E-06
Br-82	8.93E-12	5.41E-11	7.86E-11	9.12E-11	1.09E-10	1.20E-10	1.29E-10	1.33E-10	9.83E-11
Br-83	2.50E-09	2.10E-09	1.77E-09	1.61E-09	1.44E-09	1.22E-09	9.97E-10	7.53E-10	1.75E-09
Br-84	9.62E-10	8.04E-10	6.71E-10	6.07E-10	5.41E-10	4.52E-10	3.69E-10	2.79E-10	6.60E-10
Br-85	1.27E-10	1.05E-10	8.69E-11	7.85E-11	6.97E-11	5.75E-11	4.67E-11	3.57E-11	8.53E-11
Kr-82	9.86E-12	2.00E-09	8.62E-09	1.99E-08	3.50E-08	5.80E-08	8.28E-08	1.11E-07	4.24E-08

Kr-83	1.45E-07	3.13E-06	5.78E-06	7.97E-06	9.77E-06	1.12E-05	1.24E-05	1.32E-05	8.00E-06
Kr-83m	1.88E-09	1.58E-09	1.33E-09	1.21E-09	1.08E-09	9.19E-10	7.50E-10	5.67E-10	1.32E-09
Kr-84	2.78E-07	5.87E-06	1.14E-05	1.63E-05	2.10E-05	2.53E-05	2.92E-05	3.31E-05	1.80E-05
Kr-85	9.98E-08	2.15E-06	4.04E-06	5.66E-06	7.11E-06	8.35E-06	9.41E-06	1.04E-05	5.96E-06
Kr-85m	1.13E-08	9.37E-09	7.80E-09	7.02E-09	6.23E-09	5.15E-09	4.18E-09	3.19E-09	7.62E-09
Kr-86	5.31E-07	1.09E-05	2.06E-05	2.91E-05	3.68E-05	4.36E-05	4.95E-05	5.51E-05	3.11E-05
Kr-87	6.19E-09	5.12E-09	4.23E-09	3.82E-09	3.39E-09	2.79E-09	2.26E-09	1.73E-09	4.15E-09
Kr-88	1.87E-08	1.54E-08	1.27E-08	1.15E-08	1.02E-08	8.32E-09	6.74E-09	5.17E-09	1.24E-08
Kr-89	4.40E-10	3.62E-10	2.97E-10	2.68E-10	2.36E-10	1.92E-10	1.55E-10	1.20E-10	2.90E-10
Rb-85	2.82E-07	6.21E-06	1.18E-05	1.66E-05	2.11E-05	2.50E-05	2.85E-05	3.17E-05	1.78E-05
Rb-86	4.12E-12	7.35E-10	1.79E-09	2.61E-09	3.72E-09	4.44E-09	5.30E-09	5.52E-09	3.25E-09
Rb-87	7.30E-07	1.52E-05	2.88E-05	4.06E-05	5.13E-05	6.07E-05	6.88E-05	7.65E-05	4.33E-05
Rb-88	1.96E-09	1.62E-09	1.34E-09	1.21E-09	1.07E-09	8.81E-10	7.19E-10	5.62E-10	1.32E-09
Rb-89	2.22E-09	1.84E-09	1.51E-09	1.37E-09	1.21E-09	9.89E-10	8.01E-10	6.14E-10	1.48E-09
Rb-90	4.08E-10	3.34E-10	2.73E-10	2.46E-10	2.16E-10	1.75E-10	1.41E-10	1.09E-10	2.66E-10
Rb-91	1.69E-10	1.40E-10	1.16E-10	1.05E-10	9.28E-11	7.65E-11	6.22E-11	4.75E-11	1.14E-10
Sr-86	2.48E-13	1.09E-09	5.96E-09	1.41E-08	2.84E-08	4.73E-08	6.90E-08	9.60E-08	3.42E-08
Sr-87	3.91E-13	1.80E-11	4.87E-11	8.84E-11	1.35E-10	1.98E-10	2.70E-10	3.83E-10	1.47E-10
Sr-88	9.65E-07	2.07E-05	3.92E-05	5.52E-05	6.98E-05	8.26E-05	9.36E-05	1.04E-04	5.89E-05
Sr-89	1.31E-06	1.69E-05	2.19E-05	1.97E-05	1.71E-05	1.48E-05	1.25E-05	1.08E-05	1.45E-05
Sr-90	1.65E-06	3.38E-05	6.36E-05	8.93E-05	1.12E-04	1.33E-04	1.50E-04	1.66E-04	9.47E-05
Sr-91	1.06E-07	8.78E-08	7.31E-08	6.60E-08	5.88E-08	4.88E-08	3.97E-08	3.02E-08	7.18E-08
Sr-92	3.00E-08	2.51E-08	2.11E-08	1.92E-08	1.71E-08	1.45E-08	1.18E-08	8.93E-09	2.09E-08
Sr-93	1.48E-09	1.25E-09	1.06E-09	9.64E-10	8.68E-10	7.44E-10	6.09E-10	4.59E-10	1.05E-09
Sr-94	2.43E-10	2.06E-10	1.76E-10	1.60E-10	1.45E-10	1.25E-10	1.02E-10	7.68E-11	1.74E-10
Y-89	3.48E-08	1.07E-05	3.02E-05	5.15E-05	7.22E-05	9.08E-05	1.08E-04	1.23E-04	6.13E-05
Y-90	1.56E-10	8.33E-09	1.63E-08	2.32E-08	2.94E-08	3.50E-08	3.97E-08	4.43E-08	2.48E-08
Y-91	1.38E-06	2.21E-05	3.02E-05	2.91E-05	2.59E-05	2.26E-05	1.93E-05	1.68E-05	2.12E-05
Y-91m	5.20E-09	4.33E-09	3.60E-09	3.25E-09	2.89E-09	2.40E-09	1.96E-09	1.49E-09	3.53E-09
Y-92	4.04E-08	3.39E-08	2.85E-08	2.58E-08	2.31E-08	1.95E-08	1.59E-08	1.20E-08	2.81E-08
Y-93	1.24E-07	1.05E-07	8.95E-08	8.12E-08	7.33E-08	6.29E-08	5.14E-08	3.88E-08	8.85E-08
Y-94	3.89E-09	3.31E-09	2.85E-09	2.59E-09	2.35E-09	2.04E-09	1.67E-09	1.25E-09	2.82E-09
Y-95	2.13E-09	1.83E-09	1.59E-09	1.45E-09	1.32E-09	1.16E-09	9.50E-10	7.12E-10	1.57E-09
Zr-90	5.62E-11	7.76E-08	2.97E-07	6.46E-07	1.10E-06	1.66E-06	2.31E-06	3.06E-06	1.15E-06
Zr-91	2.74E-08	1.16E-05	3.41E-05	5.98E-05	8.52E-05	1.08E-04	1.30E-04	1.50E-04	7.31E-05
Zr-92	1.56E-06	3.54E-05	6.76E-05	9.58E-05	1.22E-04	1.45E-04	1.65E-04	1.84E-04	1.03E-04
Zr-93	1.52E-06	3.74E-05	7.15E-05	1.02E-04	1.30E-04	1.54E-04	1.76E-04	1.97E-04	1.10E-04
Zr-94	1.85E-06	3.87E-05	7.44E-05	1.06E-04	1.36E-04	1.63E-04	1.86E-04	2.08E-04	1.15E-04
Zr-95	1.82E-06	2.64E-05	3.74E-05	3.85E-05	3.55E-05	3.19E-05	2.80E-05	2.49E-05	2.84E-05
Zr-96	1.82E-06	3.82E-05	7.35E-05	1.05E-04	1.35E-04	1.62E-04	1.86E-04	2.09E-04	1.15E-04
Zr-97	2.04E-07	1.79E-07	1.58E-07	1.42E-07	1.33E-07	1.19E-07	9.89E-08	7.38E-08	1.55E-07
Nb-94	8.32E-14	6.64E-12	1.89E-11	3.41E-11	5.08E-11	6.77E-11	8.52E-11	1.03E-10	4.73E-11
Nb-95	3.68E-08	7.96E-06	1.63E-05	2.08E-05	2.14E-05	1.99E-05	1.76E-05	1.57E-05	1.52E-05
Nb-95m	3.31E-10	1.54E-08	2.25E-08	2.40E-08	2.20E-08	1.99E-08	1.74E-08	1.56E-08	1.74E-08
Nb-96	5.49E-11	4.38E-10	5.90E-10	5.89E-10	6.05E-10	5.82E-10	5.32E-10	4.90E-10	5.35E-10
Nb-97	1.47E-08	1.29E-08	1.14E-08	1.03E-08	9.59E-09	8.59E-09	7.15E-09	5.34E-09	1.12E-08
Mo-95	9.43E-10	4.50E-06	2.07E-05	4.50E-05	7.28E-05	9.99E-05	1.26E-04	1.52E-04	6.56E-05
Mo-96	1.04E-10	2.23E-08	1.65E-07	5.26E-07	1.21E-06	2.25E-06	3.69E-06	5.60E-06	1.75E-06
Mo-97	1.26E-06	3.60E-05	7.02E-05	1.02E-04	1.31E-04	1.58E-04	1.82E-04	2.04E-04	1.11E-04
Mo-98	1.65E-06	3.52E-05	6.86E-05	9.96E-05	1.29E-04	1.56E-04	1.79E-04	2.03E-04	1.10E-04
Mo-99	1.08E-06	9.54E-07	7.81E-07	7.30E-07	6.86E-07	6.15E-07	5.39E-07	4.74E-07	7.92E-07
Mo-100	1.80E-06	3.86E-05	7.54E-05	1.10E-04	1.42E-04	1.72E-04	1.98E-04	2.24E-04	1.21E-04
Mo-101	2.58E-09	2.34E-09	2.11E-09	1.94E-09	1.82E-09	1.67E-09	1.42E-09	1.05E-09	2.10E-09
Mo-102	1.69E-09	1.55E-09	1.45E-09	1.34E-09	1.26E-09	1.18E-09	1.02E-09	7.50E-10	1.44E-09
Mo-103	1.27E-10	1.23E-10	1.22E-10	1.14E-10	1.08E-10	1.05E-10	9.41E-11	6.84E-11	1.21E-10
Tc-99	5.45E-07	3.46E-05	6.78E-05	9.81E-05	1.25E-04	1.48E-04	1.68E-04	1.87E-04	1.04E-04
Tc-99m	8.43E-08	7.80E-08	6.35E-08	5.97E-08	5.59E-08	5.01E-08	4.41E-08	3.93E-08	6.39E-08
Tc-101	2.51E-09	2.28E-09	2.06E-09	1.89E-09	1.77E-09	1.63E-09	1.38E-09	1.02E-09	2.04E-09
Tc-103	1.05E-10	1.02E-10	1.00E-10	9.46E-11	8.95E-11	8.63E-11	7.76E-11	5.65E-11	1.00E-10

Tc-104	1.43E-09	1.48E-09	1.47E-09	1.46E-09	1.41E-09	1.38E-09	1.29E-09	9.46E-10	1.54E-09
Tc-105	3.65E-10	4.16E-10	4.25E-10	4.42E-10	4.47E-10	4.45E-10	4.23E-10	3.17E-10	4.75E-10
Ru-99	1.73E-11	1.14E-09	2.29E-09	3.37E-09	4.36E-09	5.26E-09	6.09E-09	6.90E-09	3.71E-09
Ru-100	9.25E-11	2.82E-07	1.63E-06	3.88E-06	7.17E-06	1.17E-05	1.69E-05	2.25E-05	8.27E-06
Ru-101	1.47E-06	3.18E-05	6.18E-05	9.00E-05	1.16E-04	1.40E-04	1.61E-04	1.81E-04	9.84E-05
Ru-102	1.23E-06	2.71E-05	5.41E-05	8.05E-05	1.06E-04	1.30E-04	1.53E-04	1.75E-04	9.16E-05
Ru-103	8.43E-07	1.11E-05	1.47E-05	1.47E-05	1.37E-05	1.29E-05	1.22E-05	1.17E-05	1.18E-05
Ru-104	5.39E-07	1.32E-05	2.75E-05	4.32E-05	5.80E-05	7.23E-05	8.68E-05	1.01E-04	5.09E-05
Ru-105	1.29E-08	1.47E-08	1.50E-08	1.56E-08	1.58E-08	1.59E-08	1.51E-08	1.24E-08	1.68E-08
Ru-106	1.17E-07	3.59E-06	8.36E-06	1.33E-05	1.83E-05	2.30E-05	2.76E-05	3.14E-05	1.60E-05
Ru-107	4.44E-11	8.02E-11	8.91E-11	1.03E-10	1.13E-10	1.17E-10	1.17E-10	9.01E-11	1.09E-10
Rh-103	2.80E-08	8.55E-06	2.34E-05	3.87E-05	5.25E-05	6.45E-05	7.37E-05	8.02E-05	4.32E-05
Rh-103m	8.14E-10	1.08E-08	1.44E-08	1.44E-08	1.34E-08	1.26E-08	1.19E-08	1.14E-08	1.15E-08
Rh-105	1.10E-07	1.21E-07	1.23E-07	1.27E-07	1.32E-07	1.28E-07	1.22E-07	1.14E-07	1.36E-07
Rh-107	2.57E-10	4.72E-10	5.24E-10	6.05E-10	6.65E-10	6.89E-10	6.87E-10	5.28E-10	6.42E-10
Pd-104	2.65E-11	2.51E-07	1.77E-06	5.13E-06	1.01E-05	1.79E-05	2.63E-05	3.61E-05	1.26E-05
Pd-105	1.28E-07	6.34E-06	1.44E-05	2.31E-05	3.16E-05	4.03E-05	4.88E-05	5.66E-05	2.80E-05
Pd-106	1.36E-08	1.18E-06	3.32E-06	6.47E-06	1.04E-05	1.53E-05	2.06E-05	2.71E-05	1.07E-05
Pd-107	4.37E-08	1.96E-06	5.29E-06	9.32E-06	1.39E-05	1.89E-05	2.44E-05	2.98E-05	1.32E-05
Pd-108	1.68E-08	1.04E-06	2.94E-06	5.51E-06	8.44E-06	1.19E-05	1.55E-05	1.91E-05	8.23E-06
Pd-109	2.16E-09	7.36E-09	8.59E-09	1.03E-08	1.20E-08	1.27E-08	1.29E-08	9.94E-09	1.10E-08
Pd-110	7.92E-09	3.70E-07	1.02E-06	1.85E-06	2.82E-06	3.93E-06	5.14E-06	6.36E-06	2.75E-06
Pd-112	1.10E-09	1.39E-09	1.49E-09	1.64E-09	1.78E-09	1.81E-09	1.80E-09	1.44E-09	1.82E-09
Ag-109	7.63E-09	6.22E-07	1.76E-06	3.23E-06	4.88E-06	6.47E-06	8.32E-06	1.02E-05	4.59E-06
Ag-110m	2.53E-13	6.82E-10	4.84E-09	1.45E-08	2.92E-08	5.28E-08	8.27E-08	1.13E-07	3.96E-08
Ag-111	4.50E-09	3.10E-08	4.10E-08	4.84E-08	5.32E-08	5.55E-08	5.89E-08	5.99E-08	4.72E-08
Ag-112	1.66E-10	2.08E-10	2.23E-10	2.47E-10	2.67E-10	2.71E-10	2.69E-10	2.18E-10	2.73E-10
Ag-113	1.54E-10	1.80E-10	1.86E-10	2.00E-10	2.07E-10	2.12E-10	2.07E-10	1.57E-10	2.20E-10
Cd-110	5.23E-12	1.52E-08	1.15E-07	3.65E-07	7.75E-07	1.48E-06	2.45E-06	3.55E-06	1.16E-06
Cd-111	8.75E-10	1.71E-07	4.82E-07	8.83E-07	1.34E-06	1.86E-06	2.41E-06	2.99E-06	1.29E-06
Cd-112	2.60E-09	1.21E-07	2.97E-07	5.06E-07	7.31E-07	9.82E-07	1.25E-06	1.50E-06	6.86E-07
Cd-113	3.06E-09	6.31E-09	6.82E-09	7.25E-09	7.22E-09	7.64E-09	7.72E-09	7.73E-09	7.03E-09
Cd-113m	4.52E-11	1.30E-09	2.97E-09	4.86E-09	6.83E-09	8.94E-09	1.12E-08	1.34E-08	6.30E-09
Cd-114	4.47E-09	1.97E-07	4.51E-07	7.36E-07	1.02E-06	1.32E-06	1.62E-06	1.91E-06	9.21E-07
Cd-115	2.09E-09	2.12E-09	2.01E-09	1.94E-09	2.02E-09	1.84E-09	1.70E-09	1.54E-09	2.08E-09
Cd-115m	2.20E-10	3.19E-09	4.64E-09	5.04E-09	4.80E-09	4.65E-09	4.64E-09	4.47E-09	4.05E-09
Cd-116	4.06E-09	9.83E-08	2.08E-07	3.25E-07	4.35E-07	5.39E-07	6.45E-07	7.45E-07	3.80E-07
In-113	1.07E-14	6.16E-12	2.51E-11	5.97E-11	1.11E-10	1.78E-10	2.59E-10	3.60E-10	1.27E-10
In-115	1.26E-09	6.28E-08	1.18E-07	1.55E-07	1.79E-07	1.89E-07	1.90E-07	2.01E-07	1.43E-07
In-115m	1.71E-10	1.80E-10	1.70E-10	1.64E-10	1.71E-10	1.57E-10	1.45E-10	1.33E-10	1.76E-10
Sn-115	6.68E-11	4.08E-09	8.76E-09	1.37E-08	1.83E-08	2.27E-08	2.70E-08	3.10E-08	1.59E-08
Sn-116	1.73E-12	5.94E-09	2.89E-08	7.22E-08	1.27E-07	2.08E-07	2.80E-07	3.66E-07	1.41E-07
Sn-117	3.64E-09	9.28E-08	1.94E-07	3.02E-07	4.03E-07	4.99E-07	5.93E-07	6.84E-07	3.50E-07
Sn-118	3.47E-09	8.15E-08	1.68E-07	2.58E-07	3.44E-07	4.23E-07	5.03E-07	5.80E-07	2.99E-07
Sn-119	3.94E-09	8.98E-08	1.83E-07	2.79E-07	3.70E-07	4.53E-07	5.34E-07	6.13E-07	3.19E-07
Sn-120	3.88E-09	8.78E-08	1.79E-07	2.73E-07	3.62E-07	4.44E-07	5.24E-07	6.03E-07	3.13E-07
Sn-121	8.85E-10	8.91E-10	8.47E-10	8.04E-10	7.96E-10	7.44E-10	6.62E-10	5.20E-10	8.63E-10
Sn-121m	2.11E-10	5.07E-09	1.06E-08	1.66E-08	2.21E-08	2.74E-08	3.27E-08	3.77E-08	1.93E-08
Sn-122	4.74E-09	1.10E-07	2.26E-07	3.47E-07	4.62E-07	5.67E-07	6.71E-07	7.72E-07	4.00E-07
Sn-123	2.16E-09	4.12E-08	7.16E-08	9.34E-08	1.05E-07	1.10E-07	1.09E-07	1.08E-07	8.11E-08
Sn-124	8.08E-09	1.89E-07	3.88E-07	5.95E-07	7.90E-07	9.69E-07	1.14E-06	1.31E-06	6.83E-07
Sn-125	4.36E-09	2.11E-08	2.05E-08	1.96E-08	1.87E-08	1.78E-08	1.71E-08	1.65E-08	1.77E-08
Sn-126	1.66E-08	4.01E-07	8.39E-07	1.31E-06	1.74E-06	2.15E-06	2.56E-06	2.96E-06	1.52E-06
Sn-127	6.95E-10	6.79E-10	6.54E-10	6.10E-10	5.75E-10	5.42E-10	4.78E-10	3.50E-10	6.44E-10
Sn-128	7.16E-10	6.73E-10	6.37E-10	5.89E-10	5.49E-10	5.12E-10	4.42E-10	3.25E-10	6.23E-10
Sb-121	2.34E-09	8.49E-08	1.75E-07	2.66E-07	3.53E-07	4.35E-07	5.07E-07	5.79E-07	3.04E-07
Sb-123	2.62E-09	6.93E-08	1.54E-07	2.51E-07	3.49E-07	4.46E-07	5.39E-07	6.32E-07	3.08E-07
Sb-124	3.61E-12	1.86E-10	6.27E-10	1.29E-09	2.12E-09	3.05E-09	4.03E-09	4.75E-09	2.13E-09
Sb-125	5.82E-09	2.14E-07	4.54E-07	6.99E-07	9.14E-07	1.10E-06	1.28E-06	1.44E-06	7.70E-07

Sb-126	4.32E-10	2.38E-09	2.45E-09	2.49E-09	2.48E-09	2.40E-09	2.47E-09	2.47E-09	2.29E-09
Sb-127	3.24E-08	5.21E-08	4.60E-08	4.66E-08	4.41E-08	4.07E-08	3.89E-08	3.63E-08	4.50E-08
Sb-128	6.86E-09	6.49E-09	6.18E-09	5.71E-09	5.33E-09	4.98E-09	4.31E-09	3.17E-09	6.03E-09
Sb-129	5.62E-09	5.50E-09	5.34E-09	5.00E-09	4.72E-09	4.48E-09	3.98E-09	2.91E-09	5.27E-09
Sb-130	1.10E-09	1.00E-09	9.24E-10	8.52E-10	7.93E-10	7.32E-10	6.21E-10	4.58E-10	9.12E-10
Sb-130m	2.02E-10	1.80E-10	1.63E-10	1.50E-10	1.39E-10	1.27E-10	1.06E-10	7.87E-11	1.61E-10
Sb-131	1.97E-09	1.74E-09	1.57E-09	1.44E-09	1.34E-09	1.22E-09	1.02E-09	7.57E-10	1.56E-09
Sb-132	1.82E-10	1.64E-10	1.50E-10	1.38E-10	1.28E-10	1.18E-10	9.93E-11	7.33E-11	1.48E-10
Sb-132m	1.14E-10	9.89E-11	8.69E-11	7.90E-11	7.36E-11	6.64E-11	5.49E-11	4.11E-11	8.70E-11
Sb-133	1.90E-10	1.62E-10	1.40E-10	1.27E-10	1.17E-10	1.04E-10	8.56E-11	6.45E-11	1.40E-10
Te-122	8.64E-14	3.26E-10	1.88E-09	4.44E-09	9.28E-09	1.37E-08	2.26E-08	3.17E-08	1.13E-08
Te-123	2.53E-16	3.32E-13	2.85E-12	9.01E-12	2.69E-11	5.54E-11	9.01E-11	1.43E-10	4.40E-11
Te-124	3.25E-13	8.48E-11	4.80E-10	1.55E-09	2.94E-09	6.09E-09	9.43E-09	1.49E-08	4.78E-09
Te-125	5.72E-12	4.08E-09	1.75E-08	4.14E-08	7.55E-08	1.19E-07	1.72E-07	2.32E-07	8.32E-08
Te-125m	1.71E-12	9.01E-10	3.01E-09	5.76E-09	8.64E-09	1.14E-08	1.39E-08	1.64E-08	7.56E-09
Te-126	2.62E-10	1.32E-08	2.96E-08	4.69E-08	6.49E-08	8.29E-08	1.02E-07	1.21E-07	5.84E-08
Te-127	2.75E-09	5.32E-09	4.69E-09	4.72E-09	4.43E-09	4.09E-09	3.96E-09	3.66E-09	4.48E-09
Te-127m	5.89E-10	2.94E-08	3.90E-08	3.72E-08	3.46E-08	3.23E-08	3.02E-08	2.87E-08	2.96E-08
Te-128	8.54E-08	2.28E-06	4.63E-06	7.02E-06	9.22E-06	1.13E-05	1.32E-05	1.51E-05	7.94E-06
Te-129	1.48E-09	1.45E-09	1.41E-09	1.32E-09	1.25E-09	1.18E-09	1.05E-09	7.68E-10	1.39E-09
Te-129m	5.08E-12	2.04E-10	3.00E-10	3.45E-10	3.63E-10	3.59E-10	3.80E-10	3.73E-10	3.03E-10
Te-130	5.16E-07	1.13E-05	2.22E-05	3.25E-05	4.23E-05	5.13E-05	5.95E-05	6.75E-05	3.61E-05
Te-131	2.31E-09	2.07E-09	1.89E-09	1.73E-09	1.62E-09	1.48E-09	1.25E-09	9.27E-10	1.87E-09
Te-131m	1.98E-08	2.04E-08	1.82E-08	1.79E-08	1.75E-08	1.60E-08	1.44E-08	1.15E-08	1.86E-08
Te-132	8.37E-07	8.40E-07	6.92E-07	6.58E-07	6.14E-07	5.58E-07	4.94E-07	4.37E-07	6.89E-07
Te-133	1.68E-09	1.47E-09	1.31E-09	1.19E-09	1.11E-09	1.01E-09	8.34E-10	6.20E-10	1.30E-09
Te-133m	5.51E-09	4.83E-09	4.33E-09	3.97E-09	3.69E-09	3.35E-09	2.77E-09	2.06E-09	4.29E-09
Te-134	9.42E-09	8.10E-09	7.09E-09	6.46E-09	5.96E-09	5.31E-09	4.38E-09	3.28E-09	7.07E-09
I-127	8.72E-09	9.57E-07	2.06E-06	3.20E-06	4.28E-06	5.28E-06	6.19E-06	7.10E-06	3.68E-06
I-129	1.44E-07	3.63E-06	7.39E-06	1.13E-05	1.48E-05	1.81E-05	2.11E-05	2.42E-05	1.27E-05
I-130	2.08E-11	2.39E-10	3.73E-10	5.04E-10	5.73E-10	6.79E-10	7.37E-10	8.40E-10	5.37E-10
I-131	6.77E-07	1.90E-06	1.68E-06	1.52E-06	1.36E-06	1.24E-06	1.12E-06	1.06E-06	1.39E-06
I-132	2.46E-08	2.55E-08	2.10E-08	2.01E-08	1.87E-08	1.70E-08	1.51E-08	1.34E-08	2.09E-08
I-133	2.92E-07	2.61E-07	2.33E-07	2.09E-07	1.98E-07	1.78E-07	1.51E-07	1.14E-07	2.27E-07
I-134	1.37E-08	1.20E-08	1.07E-08	9.84E-09	9.15E-09	8.32E-09	6.89E-09	5.13E-09	1.07E-08
I-135	8.32E-08	7.37E-08	6.67E-08	6.12E-08	5.71E-08	5.22E-08	4.36E-08	3.24E-08	6.62E-08
I-136	1.19E-10	1.04E-10	9.21E-11	8.38E-11	7.86E-11	7.16E-11	5.94E-11	4.43E-11	9.23E-11
Xe-128	8.00E-13	3.47E-09	1.77E-08	4.46E-08	8.92E-08	1.56E-07	2.32E-07	3.44E-07	1.17E-07
Xe-129	1.02E-16	2.19E-12	2.40E-11	1.00E-10	2.76E-10	5.19E-10	1.11E-09	1.79E-09	5.09E-10
Xe-130	7.41E-11	1.80E-08	7.15E-08	1.60E-07	2.88E-07	4.51E-07	6.41E-07	8.77E-07	3.18E-07
Xe-131	1.14E-07	1.47E-05	2.94E-05	4.13E-05	5.22E-05	5.97E-05	6.68E-05	6.94E-05	4.23E-05
Xe-131m	1.26E-09	4.40E-08	3.89E-08	3.56E-08	3.25E-08	2.91E-08	2.64E-08	2.46E-08	2.99E-08
Xe-132	3.76E-07	2.57E-05	5.36E-05	8.22E-05	1.10E-04	1.36E-04	1.63E-04	1.89E-04	9.56E-05
Xe-133	1.07E-06	2.50E-06	2.15E-06	1.95E-06	1.74E-06	1.57E-06	1.41E-06	1.35E-06	1.82E-06
Xe-133m	9.13E-09	9.88E-09	8.10E-09	7.84E-09	7.40E-09	6.62E-09	6.02E-09	5.64E-09	8.15E-09
Xe-134	2.20E-06	4.81E-05	9.36E-05	1.36E-04	1.76E-04	2.12E-04	2.45E-04	2.76E-04	1.50E-04
Xe-135	3.64E-08	3.25E-08	2.89E-08	2.44E-08	2.20E-08	1.94E-08	1.73E-08	1.62E-08	2.61E-08
Xe-135m	4.40E-10	4.08E-10	3.85E-10	3.58E-10	3.32E-10	3.09E-10	2.66E-10	1.96E-10	3.78E-10
Xe-136	3.07E-06	7.10E-05	1.40E-04	2.04E-04	2.66E-04	3.23E-04	3.75E-04	4.25E-04	2.28E-04
Xe-137	7.81E-10	6.88E-10	6.19E-10	5.68E-10	5.30E-10	4.83E-10	4.02E-10	2.99E-10	6.15E-10
Xe-138	2.91E-09	2.53E-09	2.24E-09	2.05E-09	1.90E-09	1.72E-09	1.42E-09	1.06E-09	2.23E-09
Xe-139	1.07E-10	9.13E-11	7.95E-11	7.23E-11	6.67E-11	5.92E-11	4.87E-11	3.66E-11	7.94E-11
Cs-133	2.28E-07	3.58E-05	7.19E-05	1.05E-04	1.34E-04	1.55E-04	1.78E-04	1.98E-04	1.11E-04
Cs-134	4.07E-11	3.03E-07	1.72E-06	3.74E-06	7.87E-06	1.24E-05	1.66E-05	2.24E-05	8.49E-06
Cs-134m	5.94E-13	7.41E-11	1.06E-10	1.23E-10	1.69E-10	1.88E-10	2.02E-10	2.17E-10	1.48E-10
Cs-135	2.99E-07	6.44E-06	1.19E-05	1.68E-05	2.11E-05	2.63E-05	3.00E-05	3.43E-05	1.88E-05
Cs-136	7.74E-10	1.34E-08	2.23E-08	2.86E-08	3.73E-08	4.16E-08	4.48E-08	5.37E-08	3.24E-08
Cs-137	1.77E-06	3.79E-05	7.37E-05	1.07E-04	1.39E-04	1.67E-04	1.93E-04	2.18E-04	1.18E-04
Cs-138	7.42E-09	6.48E-09	5.77E-09	5.28E-09	4.91E-09	4.45E-09	3.67E-09	2.74E-09	5.73E-09

Cs-139	1.94E-09	1.69E-09	1.50E-09	1.37E-09	1.27E-09	1.15E-09	9.48E-10	7.07E-10	1.49E-09
Cs-140	1.96E-10	1.69E-10	1.48E-10	1.34E-10	1.24E-10	1.11E-10	9.15E-11	6.84E-11	1.47E-10
Ba-134	3.53E-14	7.54E-09	7.89E-08	2.63E-07	7.05E-07	1.38E-06	2.35E-06	3.65E-06	1.09E-06
Ba-135	2.51E-14	6.87E-12	6.54E-11	3.26E-10	1.05E-09	2.50E-09	5.64E-09	1.21E-08	2.96E-09
Ba-136	9.03E-10	6.55E-08	2.04E-07	3.98E-07	6.27E-07	8.92E-07	1.21E-06	1.55E-06	6.38E-07
Ba-137	2.72E-10	9.33E-08	3.41E-07	7.32E-07	1.26E-06	1.89E-06	2.67E-06	3.54E-06	1.33E-06
Ba-138	1.92E-06	4.11E-05	7.96E-05	1.15E-04	1.49E-04	1.79E-04	2.06E-04	2.33E-04	1.27E-04
Ba-139	1.76E-08	1.54E-08	1.37E-08	1.25E-08	1.16E-08	1.05E-08	8.72E-09	6.47E-09	1.36E-08
Ba-140	1.61E-06	6.83E-06	6.00E-06	5.37E-06	4.72E-06	4.20E-06	3.66E-06	3.35E-06	4.65E-06
Ba-141	3.52E-09	3.07E-09	2.72E-09	2.49E-09	2.29E-09	2.07E-09	1.70E-09	1.27E-09	2.69E-09
Ba-142	2.00E-09	1.73E-09	1.52E-09	1.39E-09	1.28E-09	1.15E-09	9.41E-10	7.03E-10	1.51E-09
La-138	9.15E-12	2.02E-10	3.94E-10	5.69E-10	7.32E-10	8.56E-10	9.76E-10	1.08E-09	6.10E-10
La-139	1.79E-06	3.87E-05	7.50E-05	1.08E-04	1.39E-04	1.68E-04	1.93E-04	2.17E-04	1.18E-04
La-140	1.09E-07	9.42E-07	8.20E-07	7.37E-07	6.64E-07	5.86E-07	5.20E-07	4.70E-07	6.28E-07
La-141	4.55E-08	3.97E-08	3.52E-08	3.22E-08	2.97E-08	2.69E-08	2.21E-08	1.64E-08	3.49E-08
La-142	1.75E-08	1.52E-08	1.34E-08	1.23E-08	1.13E-08	1.01E-08	8.33E-09	6.22E-09	1.33E-08
La-143	2.73E-09	2.35E-09	2.05E-09	1.87E-09	1.72E-09	1.53E-09	1.25E-09	9.39E-10	2.04E-09
La-144	1.20E-10	1.02E-10	8.88E-11	8.09E-11	7.41E-11	6.53E-11	5.36E-11	4.02E-11	8.83E-11
Ce-140	6.61E-08	2.83E-05	6.34E-05	9.70E-05	1.28E-04	1.56E-04	1.82E-04	2.07E-04	1.09E-04
Ce-141	1.51E-06	1.70E-05	1.82E-05	1.64E-05	1.46E-05	1.30E-05	1.14E-05	1.04E-05	1.31E-05
Ce-142	1.63E-06	3.56E-05	6.89E-05	9.95E-05	1.28E-04	1.54E-04	1.78E-04	2.00E-04	1.09E-04
Ce-143	4.34E-07	3.84E-07	3.15E-07	2.81E-07	2.63E-07	2.34E-07	1.94E-07	1.56E-07	3.09E-07
Ce-144	1.57E-06	3.00E-05	5.32E-05	7.01E-05	8.28E-05	9.13E-05	9.64E-05	9.82E-05	6.60E-05
Ce-145	3.86E-10	3.33E-10	2.92E-10	2.66E-10	2.45E-10	2.19E-10	1.80E-10	1.42E-10	2.90E-10
Ce-146	1.33E-09	1.15E-09	1.02E-09	9.31E-10	8.60E-10	7.76E-10	6.39E-10	4.76E-10	1.01E-09
Pr-141	5.85E-08	1.79E-05	4.72E-05	7.79E-05	1.07E-04	1.32E-04	1.57E-04	1.79E-04	9.05E-05
Pr-142	1.53E-12	7.59E-10	1.66E-09	2.27E-09	2.73E-09	3.48E-09	3.58E-09	4.18E-09	2.58E-09
Pr-143	8.79E-07	7.14E-06	6.14E-06	5.44E-06	4.81E-06	4.25E-06	3.71E-06	3.31E-06	4.62E-06
Pr-144	7.02E-11	1.31E-09	2.30E-09	3.02E-09	3.54E-09	3.89E-09	4.10E-09	4.16E-09	2.82E-09
Pr-145	4.60E-08	3.97E-08	3.49E-08	3.18E-08	2.93E-08	2.61E-08	2.15E-08	1.69E-08	3.46E-08
Pr-146	2.37E-09	2.06E-09	1.82E-09	1.67E-09	1.54E-09	1.39E-09	1.14E-09	8.53E-10	1.81E-09
Pr-147	9.95E-10	8.71E-10	7.77E-10	7.11E-10	6.60E-10	6.00E-10	4.96E-10	3.69E-10	7.72E-10
Pr-148	1.23E-10	1.07E-10	9.53E-11	8.70E-11	8.12E-11	7.39E-11	6.12E-11	4.55E-11	9.51E-11
Nd-142	1.35E-12	1.98E-08	1.35E-07	3.83E-07	7.56E-07	1.26E-06	1.89E-06	2.60E-06	9.03E-07
Nd-143	6.65E-08	2.56E-05	5.53E-05	8.10E-05	1.02E-04	1.18E-04	1.31E-04	1.39E-04	8.20E-05
Nd-144	7.73E-09	3.79E-06	1.41E-05	2.97E-05	4.97E-05	7.26E-05	9.74E-05	1.25E-04	4.97E-05
Nd-145	1.02E-06	2.31E-05	4.40E-05	6.23E-05	7.82E-05	9.23E-05	1.04E-04	1.15E-04	6.54E-05
Nd-146	8.51E-07	1.85E-05	3.63E-05	5.33E-05	7.03E-05	8.58E-05	1.01E-04	1.16E-04	6.08E-05
Nd-147	5.68E-07	1.99E-06	1.76E-06	1.57E-06	1.39E-06	1.25E-06	1.09E-06	1.01E-06	1.38E-06
Nd-148	4.81E-07	1.05E-05	2.06E-05	2.99E-05	3.87E-05	4.67E-05	5.39E-05	6.10E-05	3.30E-05
Nd-149	3.86E-09	3.43E-09	3.16E-09	2.93E-09	2.74E-09	2.54E-09	2.18E-09	1.61E-09	3.19E-09
Nd-150	1.88E-07	4.12E-06	8.15E-06	1.21E-05	1.58E-05	1.94E-05	2.25E-05	2.58E-05	1.36E-05
Nd-151	1.88E-10	1.78E-10	1.75E-10	1.61E-10	1.53E-10	1.46E-10	1.30E-10	9.64E-11	1.74E-10
Nd-152	1.12E-10	1.09E-10	1.08E-10	1.01E-10	9.62E-11	9.34E-11	8.44E-11	6.14E-11	1.08E-10
Pm-147	7.13E-08	9.41E-06	1.75E-05	2.29E-05	2.61E-05	2.68E-05	2.72E-05	2.65E-05	1.99E-05
Pm-148	3.92E-11	3.22E-08	7.85E-08	1.03E-07	1.18E-07	1.12E-07	1.20E-07	1.14E-07	8.96E-08
Pm-148m	3.42E-11	2.57E-08	5.14E-08	6.87E-08	7.37E-08	7.75E-08	8.20E-08	7.59E-08	6.17E-08
Pm-149	1.62E-07	1.69E-07	1.60E-07	1.61E-07	1.55E-07	1.41E-07	1.38E-07	1.18E-07	1.61E-07
Pm-151	2.83E-08	2.73E-08	2.43E-08	2.30E-08	2.27E-08	2.10E-08	1.91E-08	1.51E-08	2.51E-08
Sm-147	6.71E-11	2.12E-07	8.19E-07	1.68E-06	2.61E-06	3.56E-06	4.51E-06	5.25E-06	2.37E-06
Sm-148	5.62E-12	2.20E-07	1.40E-06	3.52E-06	6.19E-06	9.71E-06	1.35E-05	1.75E-05	6.68E-06
Sm-149	9.42E-08	2.09E-07	2.05E-07	2.00E-07	1.76E-07	1.66E-07	1.66E-07	1.60E-07	1.86E-07
Sm-150	2.81E-08	6.18E-06	1.33E-05	2.05E-05	2.74E-05	3.43E-05	4.08E-05	4.64E-05	2.38E-05
Sm-151	6.99E-08	1.21E-06	1.30E-06	1.32E-06	1.29E-06	1.41E-06	1.43E-06	1.50E-06	1.23E-06
Sm-152	7.86E-08	2.61E-06	5.40E-06	7.55E-06	9.34E-06	1.08E-05	1.19E-05	1.24E-05	7.73E-06
Sm-153	2.46E-08	3.05E-08	3.70E-08	3.82E-08	4.06E-08	4.63E-08	4.73E-08	4.55E-08	4.23E-08
Sm-154	2.19E-08	5.54E-07	1.19E-06	1.87E-06	2.56E-06	3.25E-06	3.93E-06	4.68E-06	2.31E-06
Sm-156	4.80E-10	5.94E-10	6.23E-10	6.77E-10	7.11E-10	7.22E-10	7.04E-10	5.34E-10	7.38E-10
Eu-151	2.13E-12	4.11E-10	4.48E-10	4.57E-10	4.70E-10	4.81E-10	5.15E-10	5.10E-10	4.35E-10

Eu-152	5.83E-14	3.75E-10	6.63E-10	7.17E-10	6.93E-10	7.62E-10	8.14E-10	8.06E-10	6.27E-10
Eu-153	2.07E-08	1.11E-06	2.75E-06	5.08E-06	7.67E-06	1.03E-05	1.29E-05	1.53E-05	7.06E-06
Eu-154	4.61E-11	6.02E-08	2.41E-07	5.35E-07	8.99E-07	1.25E-06	1.67E-06	2.09E-06	8.87E-07
Eu-155	8.62E-09	7.69E-08	1.33E-07	2.13E-07	3.08E-07	4.30E-07	5.11E-07	6.00E-07	3.05E-07
Eu-156	3.92E-09	8.43E-08	1.42E-07	2.05E-07	2.91E-07	3.75E-07	5.09E-07	6.29E-07	2.94E-07
Eu-157	4.20E-10	6.00E-10	7.03E-10	7.49E-10	8.89E-10	9.23E-10	9.76E-10	9.90E-10	8.79E-10
Gd-154	1.05E-14	3.64E-10	2.59E-09	8.46E-09	1.96E-08	3.67E-08	6.05E-08	8.88E-08	2.79E-08
Gd-155	6.24E-12	2.70E-10	4.57E-10	7.51E-10	1.06E-09	1.41E-09	1.97E-09	2.42E-09	1.12E-09
Gd-156	3.00E-10	1.80E-07	6.34E-07	1.35E-06	2.36E-06	3.79E-06	5.57E-06	7.90E-06	2.78E-06
Gd-157	9.18E-10	1.97E-09	2.68E-09	3.11E-09	3.53E-09	3.96E-09	4.46E-09	4.11E-09	3.33E-09
Gd-158	1.40E-09	9.73E-08	2.57E-07	4.74E-07	7.41E-07	1.04E-06	1.41E-06	1.84E-06	7.58E-07
Gd-159	8.71E-11	1.75E-10	1.94E-10	2.28E-10	2.62E-10	3.00E-10	3.18E-10	2.77E-10	2.67E-10
Gd-160	1.00E-10	5.16E-09	1.45E-08	2.68E-08	4.12E-08	5.77E-08	7.58E-08	9.41E-08	4.03E-08
Tb-159	2.18E-10	1.27E-08	3.47E-08	6.19E-08	9.64E-08	1.35E-07	1.77E-07	2.19E-07	9.45E-08
Tb-160	7.02E-14	1.03E-10	4.77E-10	1.14E-09	2.00E-09	3.00E-09	4.18E-09	5.73E-09	2.26E-09
Tb-161	2.38E-11	3.37E-10	5.14E-10	6.87E-10	8.42E-10	8.79E-10	1.06E-09	1.17E-09	7.39E-10
Dy-160	8.53E-16	2.55E-11	2.31E-10	7.82E-10	1.88E-09	3.58E-09	6.07E-09	9.32E-09	2.90E-09
Dy-161	4.70E-12	1.61E-09	4.87E-09	9.27E-09	1.42E-08	1.90E-08	2.46E-08	3.01E-08	1.32E-08
Dy-162	6.07E-12	8.47E-10	2.69E-09	5.18E-09	8.32E-09	1.20E-08	1.56E-08	1.97E-08	8.31E-09
Dy-163	2.38E-12	3.70E-10	1.21E-09	2.72E-09	4.52E-09	7.26E-09	1.04E-08	1.39E-08	5.20E-09
Dy-164	7.56E-13	1.09E-10	3.00E-10	5.19E-10	8.62E-10	1.22E-09	1.73E-09	2.31E-09	9.34E-10
Ho-165	3.74E-13	7.23E-11	2.86E-10	6.63E-10	1.19E-09	2.05E-09	3.02E-09	4.37E-09	1.52E-09
Er-166	2.11E-14	2.31E-11	8.10E-11	1.72E-10	3.08E-10	4.84E-10	7.12E-10	1.03E-09	3.64E-10
Er-168	2.32E-14	4.48E-12	1.66E-11	3.53E-11	6.02E-11	9.24E-11	1.31E-10	1.73E-10	6.59E-11
U-234	1.32E-15	4.87E-12	2.32E-10	1.39E-09	5.69E-09	1.19E-08	2.43E-08	3.78E-08	1.14E-08
U-235	3.61E-03	2.84E-03	2.26E-03	1.81E-03	1.41E-03	1.12E-03	9.00E-04	7.54E-04	1.88E-03
U-236	6.44E-06	1.39E-04	2.50E-04	3.43E-04	4.19E-04	4.78E-04	5.23E-04	5.58E-04	3.42E-04
U-237	3.57E-10	7.01E-08	1.51E-07	2.42E-07	3.22E-07	3.66E-07	4.24E-07	3.89E-07	3.02E-07
U-238	1.86E-02	1.83E-02	1.80E-02	1.77E-02	1.74E-02	1.72E-02	1.69E-02	1.66E-02	1.76E-02
U-239	7.23E-09	7.49E-09	6.06E-09	7.05E-09	6.52E-09	5.93E-09	6.46E-09	5.03E-09	8.60E-09
Np-237	4.84E-11	5.26E-07	3.14E-06	8.37E-06	1.43E-05	2.26E-05	3.01E-05	3.74E-05	1.54E-05
Np-238	3.87E-14	1.97E-09	1.28E-08	2.96E-08	4.25E-08	5.88E-08	7.78E-08	8.93E-08	4.46E-08
Np-239	1.99E-06	2.07E-06	1.88E-06	1.97E-06	1.81E-06	1.98E-06	2.00E-06	1.85E-06	2.14E-06
Pu-238	1.02E-14	1.25E-08	2.02E-07	9.04E-07	2.08E-06	4.13E-06	6.86E-06	9.99E-06	3.20E-06
Pu-239	1.30E-06	8.48E-05	1.20E-04	1.34E-04	1.33E-04	1.40E-04	1.41E-04	1.42E-04	1.16E-04
Pu-240	1.19E-08	1.35E-05	3.55E-05	5.24E-05	6.31E-05	7.11E-05	7.56E-05	7.83E-05	5.04E-05
Pu-241	2.67E-11	1.76E-06	1.15E-05	2.63E-05	4.09E-05	5.25E-05	6.05E-05	7.02E-05	3.53E-05
Pu-242	6.64E-14	9.62E-08	1.31E-06	4.78E-06	1.06E-05	1.95E-05	2.96E-05	3.88E-05	1.36E-05
Pu-243	1.79E-18	4.09E-12	4.81E-11	1.63E-10	3.14E-10	4.61E-10	5.96E-10	7.81E-10	3.27E-10
Pu-244	5.09E-22	6.87E-14	3.38E-12	3.14E-11	1.42E-10	3.90E-10	9.61E-10	2.03E-09	4.85E-10
Am-241	3.00E-15	4.96E-09	5.91E-08	1.83E-07	3.65E-07	5.56E-07	7.31E-07	9.33E-07	3.73E-07
Am-242	8.00E-18	2.70E-11	3.16E-10	9.04E-10	1.58E-09	1.84E-09	2.49E-09	2.58E-09	1.40E-09
Am-242m	1.15E-18	2.50E-11	4.67E-10	1.79E-09	3.88E-09	6.29E-09	8.78E-09	1.17E-08	4.29E-09
Am-243	3.99E-18	3.77E-10	1.47E-08	1.24E-07	5.17E-07	1.41E-06	3.15E-06	5.52E-06	1.44E-06
Am-244	4.91E-23	1.21E-14	4.74E-13	5.16E-12	1.88E-11	4.14E-11	7.13E-11	1.14E-10	3.68E-11
Cm-242	4.42E-18	3.08E-10	7.96E-09	4.45E-08	1.24E-07	2.51E-07	4.10E-07	5.82E-07	1.86E-07
Cm-243	1.99E-22	3.76E-13	2.71E-11	2.35E-10	9.05E-10	2.42E-09	5.12E-09	9.02E-09	2.36E-09
Cm-244	1.35E-21	5.73E-12	7.71E-10	1.29E-08	7.55E-08	2.28E-07	6.28E-07	1.37E-06	3.12E-07
Cm-245	2.15E-25	2.77E-14	5.24E-12	1.61E-10	1.00E-09	4.61E-09	1.65E-08	4.25E-08	9.26E-09
Cm-246	8.81E-29	2.52E-16	1.15E-13	6.26E-12	4.24E-11	3.00E-10	1.18E-09	3.85E-09	7.54E-10

Average content

General fields

Pass #	1	2	3	4	5	6	7	8	Avg
Residence time [days]	34.54	99.78	165.04	230.29	295.54	360.8	426.11	491.83	262.96
Pass burnup [MWd/kg$_{HM}$]	16.58	15.62	14.38	13.13	11.98	10.94	10.04	9.22	12.74
Burnup [MWd/kg$_{HM}$]	16.58	43.79	68.99	92.06	113.09	132.3	149.89	166.19	97.84
Thermal fluence [n/cm^2]	3.89E+20	1.05E+21	1.72E+21	2.38E+21	3.05E+21	3.71E+21	4.38E+21	5.05E+21	2.72E+21
Thermal fluence uncertainty	2.67%	2.77%	2.78%	2.79%	2.79%	2.80%	2.80%	2.80%	2.78%
Fast fluence [n/cm^2]	2.86E+20	7.73E+20	1.26E+21	1.74E+21	2.22E+21	2.70E+21	3.18E+21	3.66E+21	1.98E+21
Fast fluence uncertainty	3.46%	3.55%	3.56%	3.57%	3.57%	3.58%	3.58%	3.59%	3.56%
Power [W]	1.46E+03	1.37E+03	1.26E+03	1.15E+03	1.05E+03	9.57E+02	8.78E+02	8.08E+02	1.12E+03
Power uncertainty	7.44%	7.49%	7.64%	7.82%	8.01%	8.21%	8.40%	8.60%	7.95%

Atomic densities [at/b.cm]

Pass #	1	2	3	4	5	6	7	8	Avg
H-1	1.12E-10	3.06E-10	5.15E-10	7.18E-10	9.20E-10	1.12E-09	1.32E-09	1.53E-09	8.18E-10
H-2	1.25E-11	3.41E-11	5.64E-11	7.80E-11	9.99E-11	1.21E-10	1.42E-10	1.64E-10	8.86E-11
He-4	3.25E-08	8.97E-08	1.56E-07	2.47E-07	3.89E-07	6.05E-07	9.15E-07	1.34E-06	4.72E-07
C-12	1.17E-02	1.17E-02	1.17E-02	1.17E-02	1.17E-02	1.17E-02	1.17E-02	1.17E-02	1.17E-02
C-13	1.25E-04	1.25E-04	1.25E-04	1.25E-04	1.25E-04	1.25E-04	1.25E-04	1.25E-04	1.25E-04
N-15	1.42E-11	3.88E-11	6.40E-11	8.85E-11	1.13E-10	1.37E-10	1.60E-10	1.85E-10	1.00E-10
O-16	3.55E-02	3.55E-02	3.55E-02	3.55E-02	3.55E-02	3.55E-02	3.55E-02	3.55E-02	3.55E-02
O-17	1.11E-09	3.02E-09	4.93E-09	6.84E-09	8.76E-09	1.07E-08	1.26E-08	1.46E-08	7.82E-09
Zn-70	2.20E-11	6.69E-11	1.17E-10	1.68E-10	2.19E-10	2.70E-10	3.19E-10	3.68E-10	1.94E-10
Ga-69	9.57E-12	2.75E-11	4.61E-11	6.45E-11	8.25E-11	9.97E-11	1.16E-10	1.33E-10	7.23E-11
Ga-71	4.66E-11	1.39E-10	2.40E-10	3.46E-10	4.54E-10	5.61E-10	6.67E-10	7.71E-10	4.03E-10
Ge-72	1.25E-10	3.99E-10	6.97E-10	9.95E-10	1.29E-09	1.56E-09	1.83E-09	2.10E-09	1.12E-09
Ge-73	4.68E-10	1.31E-09	2.15E-09	2.94E-09	3.68E-09	4.35E-09	4.98E-09	5.56E-09	3.18E-09
Ge-74	1.50E-09	4.11E-09	6.64E-09	9.00E-09	1.12E-08	1.32E-08	1.51E-08	1.68E-08	9.69E-09
Ge-76	1.30E-08	3.40E-08	5.31E-08	7.01E-08	8.53E-08	9.88E-08	1.11E-07	1.22E-07	7.34E-08
Ge-77	5.73E-10	5.24E-10	4.68E-10	4.15E-10	3.67E-10	3.26E-10	2.91E-10	2.62E-10	4.03E-10
Ge-78	1.95E-10	1.79E-10	1.61E-10	1.43E-10	1.28E-10	1.15E-10	1.03E-10	9.34E-11	1.40E-10
As-75	4.49E-09	1.19E-08	1.88E-08	2.49E-08	3.04E-08	3.53E-08	3.96E-08	4.36E-08	2.61E-08
As-77	1.97E-09	1.83E-09	1.64E-09	1.46E-09	1.30E-09	1.15E-09	1.03E-09	9.29E-10	1.42E-09
As-78	2.03E-10	1.87E-10	1.68E-10	1.51E-10	1.35E-10	1.21E-10	1.09E-10	9.89E-11	1.47E-10
Se-76	1.64E-11	9.55E-11	2.41E-10	4.43E-10	6.94E-10	9.87E-10	1.32E-09	1.68E-09	6.84E-10
Se-77	3.02E-08	8.29E-08	1.30E-07	1.71E-07	2.07E-07	2.38E-07	2.65E-07	2.88E-07	1.76E-07
Se-78	8.60E-08	2.26E-07	3.54E-07	4.70E-07	5.74E-07	6.68E-07	7.53E-07	8.31E-07	4.95E-07
Se-79	1.83E-07	4.76E-07	7.38E-07	9.66E-07	1.16E-06	1.34E-06	1.48E-06	1.61E-06	9.95E-07
Se-80	5.24E-07	1.36E-06	2.12E-06	2.79E-06	3.38E-06	3.91E-06	4.39E-06	4.82E-06	2.91E-06
Se-81	3.99E-10	3.66E-10	3.28E-10	2.92E-10	2.59E-10	2.31E-10	2.07E-10	1.86E-10	2.83E-10
Se-82	1.31E-06	3.41E-06	5.28E-06	6.93E-06	8.39E-06	9.69E-06	1.08E-05	1.19E-05	7.21E-06
Se-83	1.13E-09	9.98E-10	8.71E-10	7.59E-10	6.63E-10	5.80E-10	5.10E-10	4.50E-10	7.46E-10
Se-84	3.01E-10	2.63E-10	2.28E-10	1.98E-10	1.72E-10	1.50E-10	1.31E-10	1.15E-10	1.95E-10
Br-79	9.64E-11	2.51E-10	3.90E-10	5.11E-10	6.16E-10	7.07E-10	7.86E-10	8.56E-10	5.26E-10
Br-81	8.29E-07	2.17E-06	3.36E-06	4.43E-06	5.36E-06	6.18E-06	6.90E-06	7.54E-06	4.59E-06
Br-82	1.92E-10	5.18E-10	7.99E-10	1.05E-09	1.26E-09	1.44E-09	1.61E-09	1.76E-09	1.08E-09
Br-83	8.14E-09	7.20E-09	6.31E-09	5.52E-09	4.83E-09	4.24E-09	3.74E-09	3.31E-09	5.41E-09

Br-84	3.15E-09	2.76E-09	2.40E-09	2.08E-09	1.81E-09	1.58E-09	1.38E-09	1.22E-09	2.05E-09
Br-85	4.14E-10	3.61E-10	3.12E-10	2.70E-10	2.33E-10	2.02E-10	1.76E-10	1.54E-10	2.66E-10
Br-86	1.61E-10	1.40E-10	1.21E-10	1.05E-10	9.09E-11	7.89E-11	6.88E-11	6.02E-11	1.03E-10
Br-87	1.96E-10	1.70E-10	1.46E-10	1.26E-10	1.08E-10	9.36E-11	8.12E-11	7.07E-11	1.24E-10
Kr-82	2.49E-09	1.41E-08	3.48E-08	6.32E-08	9.81E-08	1.38E-07	1.83E-07	2.32E-07	9.58E-08
Kr-83	2.12E-06	5.32E-06	7.91E-06	9.96E-06	1.16E-05	1.28E-05	1.37E-05	1.43E-05	9.70E-06
Kr-83m	6.12E-09	5.42E-09	4.75E-09	4.15E-09	3.64E-09	3.19E-09	2.82E-09	2.50E-09	4.07E-09
Kr-84	3.98E-06	1.04E-05	1.62E-05	2.15E-05	2.63E-05	3.07E-05	3.47E-05	3.85E-05	2.28E-05
Kr-85	1.46E-06	3.71E-06	5.64E-06	7.28E-06	8.66E-06	9.83E-06	1.08E-05	1.17E-05	7.38E-06
Kr-85m	3.71E-08	3.23E-08	2.79E-08	2.41E-08	2.09E-08	1.81E-08	1.58E-08	1.38E-08	2.38E-08
Kr-86	7.40E-06	1.89E-05	2.89E-05	3.76E-05	4.51E-05	5.16E-05	5.73E-05	6.23E-05	3.86E-05
Kr-87	2.03E-08	1.76E-08	1.52E-08	1.31E-08	1.14E-08	9.83E-09	8.55E-09	7.47E-09	1.29E-08
Kr-88	6.13E-08	5.31E-08	4.58E-08	3.94E-08	3.40E-08	2.94E-08	2.55E-08	2.22E-08	3.89E-08
Kr-89	1.45E-09	1.25E-09	1.07E-09	9.20E-10	7.92E-10	6.82E-10	5.90E-10	5.12E-10	9.08E-10
Kr-90	2.66E-10	2.27E-10	1.94E-10	1.66E-10	1.42E-10	1.22E-10	1.05E-10	9.04E-11	1.64E-10
Rb-85	4.20E-06	1.08E-05	1.65E-05	2.15E-05	2.58E-05	2.96E-05	3.29E-05	3.58E-05	2.21E-05
Rb-86	1.09E-09	4.07E-09	7.01E-09	9.58E-09	1.18E-08	1.37E-08	1.54E-08	1.69E-08	9.96E-09
Rb-87	1.04E-05	2.64E-05	4.03E-05	5.24E-05	6.27E-05	7.17E-05	7.95E-05	8.63E-05	5.37E-05
Rb-88	6.44E-09	5.59E-09	4.83E-09	4.16E-09	3.60E-09	3.12E-09	2.71E-09	2.37E-09	4.10E-09
Rb-89	7.30E-09	6.33E-09	5.45E-09	4.69E-09	4.05E-09	3.50E-09	3.03E-09	2.64E-09	4.63E-09
Rb-90	1.34E-09	1.15E-09	9.87E-10	8.44E-10	7.24E-10	6.22E-10	5.36E-10	4.64E-10	8.34E-10
Rb-90m	3.21E-10	2.93E-10	2.62E-10	2.33E-10	2.07E-10	1.84E-10	1.65E-10	1.49E-10	2.27E-10
Rb-91	5.54E-10	4.81E-10	4.16E-10	3.59E-10	3.11E-10	2.70E-10	2.35E-10	2.05E-10	3.54E-10
Sr-86	8.48E-10	6.98E-09	2.05E-08	4.07E-08	6.66E-08	9.76E-08	1.33E-07	1.73E-07	6.73E-08
Sr-87	1.12E-11	4.78E-11	1.03E-10	1.78E-10	2.73E-10	3.94E-10	5.42E-10	7.23E-10	2.84E-10
Sr-88	1.41E-05	3.59E-05	5.49E-05	7.12E-05	8.53E-05	9.75E-05	1.08E-04	1.17E-04	7.30E-05
Sr-89	1.40E-05	2.48E-05	2.66E-05	2.50E-05	2.24E-05	1.97E-05	1.72E-05	1.50E-05	2.06E-05
Sr-90	2.30E-05	5.84E-05	8.89E-05	1.15E-04	1.37E-04	1.56E-04	1.73E-04	1.87E-04	1.17E-04
Sr-91	3.45E-07	3.02E-07	2.62E-07	2.27E-07	1.97E-07	1.71E-07	1.50E-07	1.31E-07	2.23E-07
Sr-92	9.79E-08	8.63E-08	7.54E-08	6.57E-08	5.74E-08	5.03E-08	4.43E-08	3.91E-08	6.46E-08
Sr-93	4.80E-09	4.27E-09	3.76E-09	3.30E-09	2.91E-09	2.57E-09	2.28E-09	2.03E-09	3.24E-09
Sr-94	7.91E-10	7.05E-10	6.23E-10	5.48E-10	4.84E-10	4.28E-10	3.81E-10	3.40E-10	5.38E-10
Sr-95	2.18E-10	1.94E-10	1.71E-10	1.51E-10	1.34E-10	1.19E-10	1.06E-10	9.44E-11	1.48E-10
Y-89	4.87E-06	2.32E-05	4.66E-05	6.99E-05	9.11E-05	1.10E-04	1.26E-04	1.41E-04	7.66E-05
Y-90	5.36E-09	1.48E-08	2.32E-08	3.04E-08	3.67E-08	4.20E-08	4.66E-08	5.06E-08	3.12E-08
Y-91	1.77E-05	3.31E-05	3.70E-05	3.59E-05	3.29E-05	2.94E-05	2.59E-05	2.28E-05	2.93E-05
Y-91m	1.70E-08	1.49E-08	1.29E-08	1.12E-08	9.70E-09	8.43E-09	7.37E-09	6.46E-09	1.10E-08
Y-92	1.32E-07	1.16E-07	1.02E-07	8.87E-08	7.75E-08	6.79E-08	5.97E-08	5.28E-08	8.71E-08
Y-93	4.03E-07	3.59E-07	3.17E-07	2.78E-07	2.45E-07	2.17E-07	1.92E-07	1.71E-07	2.73E-07
Y-94	1.26E-08	1.13E-08	1.00E-08	8.88E-09	7.86E-09	6.98E-09	6.22E-09	5.58E-09	8.69E-09
Y-95	6.89E-09	6.24E-09	5.57E-09	4.96E-09	4.42E-09	3.95E-09	3.54E-09	3.19E-09	4.85E-09
Zr-90	3.08E-08	2.04E-07	5.29E-07	9.86E-07	1.56E-06	2.23E-06	2.98E-06	3.81E-06	1.54E-06
Zr-91	5.20E-06	2.59E-05	5.35E-05	8.19E-05	1.08E-04	1.32E-04	1.54E-04	1.72E-04	9.16E-05
Zr-92	2.39E-05	6.18E-05	9.51E-05	1.24E-04	1.50E-04	1.72E-04	1.91E-04	2.09E-04	1.28E-04
Zr-93	2.51E-05	6.54E-05	1.01E-04	1.32E-04	1.60E-04	1.84E-04	2.05E-04	2.24E-04	1.37E-04
Zr-94	2.62E-05	6.79E-05	1.05E-04	1.38E-04	1.68E-04	1.94E-04	2.17E-04	2.39E-04	1.44E-04
Zr-95	2.08E-05	4.03E-05	4.68E-05	4.71E-05	4.46E-05	4.11E-05	3.73E-05	3.38E-05	3.90E-05
Zr-96	2.58E-05	6.71E-05	1.04E-04	1.38E-04	1.68E-04	1.94E-04	2.18E-04	2.40E-04	1.44E-04
Zr-97	6.43E-07	5.94E-07	5.38E-07	4.86E-07	4.39E-07	3.97E-07	3.61E-07	3.29E-07	4.73E-07
Zr-98	3.07E-10	2.86E-10	2.61E-10	2.37E-10	2.15E-10	1.96E-10	1.79E-10	1.64E-10	2.31E-10
Nb-94	4.51E-12	2.29E-11	5.02E-11	8.09E-11	1.12E-10	1.43E-10	1.73E-10	2.01E-10	9.85E-11

Nb-95	4.05E-06	1.45E-05	2.17E-05	2.46E-05	2.48E-05	2.36E-05	2.18E-05	1.98E-05	1.94E-05
Nb-95m	1.12E-08	2.39E-08	2.84E-08	2.88E-08	2.73E-08	2.52E-08	2.29E-08	2.07E-08	2.36E-08
Nb-96	6.04E-10	2.23E-09	3.41E-09	3.91E-09	3.99E-09	3.83E-09	3.58E-09	3.29E-09	3.10E-09
Nb-97	4.63E-08	4.28E-08	3.88E-08	3.51E-08	3.17E-08	2.87E-08	2.61E-08	2.38E-08	3.41E-08
Nb-98m	2.12E-10	2.00E-10	1.81E-10	1.63E-10	1.46E-10	1.31E-10	1.18E-10	1.08E-10	1.57E-10
Nb-99	1.51E-10	1.40E-10	1.28E-10	1.16E-10	1.06E-10	9.61E-11	8.78E-11	8.06E-11	1.13E-10
Nb-99m	1.21E-10	1.25E-10	1.19E-10	1.12E-10	1.04E-10	9.67E-11	9.02E-11	8.45E-11	1.07E-10
Mo-94	1.46E-13	3.04E-12	1.40E-11	3.62E-11	7.10E-11	1.17E-10	1.76E-10	2.44E-10	8.27E-11
Mo-95	1.51E-06	1.35E-05	3.70E-05	6.66E-05	9.74E-05	1.27E-04	1.54E-04	1.78E-04	8.44E-05
Mo-96	1.56E-08	1.93E-07	7.41E-07	1.78E-06	3.33E-06	5.38E-06	7.89E-06	1.08E-05	3.77E-06
Mo-97	2.40E-05	6.40E-05	1.00E-04	1.33E-04	1.63E-04	1.90E-04	2.14E-04	2.36E-04	1.40E-04
Mo-98	2.37E-05	6.25E-05	9.83E-05	1.31E-04	1.61E-04	1.88E-04	2.13E-04	2.36E-04	1.39E-04
Mo-99	2.53E-06	2.43E-06	2.23E-06	2.03E-06	1.85E-06	1.69E-06	1.55E-06	1.43E-06	1.97E-06
Mo-100	2.60E-05	6.87E-05	1.08E-04	1.44E-04	1.78E-04	2.08E-04	2.35E-04	2.61E-04	1.54E-04
Mo-101	8.18E-09	7.78E-09	7.22E-09	6.65E-09	6.13E-09	5.65E-09	5.22E-09	4.85E-09	6.46E-09
Mo-102	5.31E-09	5.18E-09	4.90E-09	4.59E-09	4.29E-09	4.00E-09	3.74E-09	3.51E-09	4.44E-09
Mo-103	3.87E-10	4.06E-10	4.02E-10	3.90E-10	3.75E-10	3.59E-10	3.44E-10	3.29E-10	3.74E-10
Mo-104	2.19E-10	2.46E-10	2.54E-10	2.56E-10	2.54E-10	2.49E-10	2.43E-10	2.36E-10	2.45E-10
Mo-105	7.23E-11	8.77E-11	9.51E-11	9.88E-11	1.00E-10	1.00E-10	9.94E-11	9.80E-11	9.40E-11
Tc-98	5.12E-12	1.93E-11	4.05E-11	6.67E-11	9.75E-11	1.32E-10	1.70E-10	2.11E-10	9.28E-11
Tc-99	2.20E-05	6.15E-05	9.65E-05	1.27E-04	1.53E-04	1.76E-04	1.95E-04	2.11E-04	1.30E-04
Tc-99m	2.02E-07	1.95E-07	1.79E-07	1.63E-07	1.49E-07	1.36E-07	1.24E-07	1.14E-07	1.58E-07
Tc-101	7.97E-09	7.57E-09	7.03E-09	6.48E-09	5.97E-09	5.50E-09	5.09E-09	4.72E-09	6.29E-09
Tc-103	3.20E-10	3.36E-10	3.33E-10	3.23E-10	3.10E-10	2.97E-10	2.84E-10	2.71E-10	3.09E-10
Tc-104	4.25E-09	4.80E-09	4.98E-09	5.01E-09	4.97E-09	4.87E-09	4.75E-09	4.62E-09	4.78E-09
Tc-105	1.05E-09	1.36E-09	1.50E-09	1.57E-09	1.60E-09	1.61E-09	1.60E-09	1.58E-09	1.48E-09
Ru-99	7.25E-10	2.06E-09	3.29E-09	4.41E-09	5.43E-09	6.34E-09	7.17E-09	7.93E-09	4.67E-09
Ru-100	3.20E-07	2.04E-06	5.25E-06	9.75E-06	1.53E-05	2.19E-05	2.92E-05	3.73E-05	1.51E-05
Ru-101	2.13E-05	5.63E-05	8.86E-05	1.18E-04	1.45E-04	1.68E-04	1.90E-04	2.10E-04	1.25E-04
Ru-102	1.81E-05	4.91E-05	7.93E-05	1.08E-04	1.36E-04	1.62E-04	1.87E-04	2.11E-04	1.19E-04
Ru-103	9.14E-06	1.71E-05	1.97E-05	2.02E-05	1.99E-05	1.92E-05	1.85E-05	1.77E-05	1.77E-05
Ru-104	8.57E-06	2.50E-05	4.27E-05	6.07E-05	7.86E-05	9.63E-05	1.13E-04	1.30E-04	6.95E-05
Ru-105	3.69E-08	4.78E-08	5.30E-08	5.56E-08	5.68E-08	5.71E-08	5.68E-08	5.63E-08	5.25E-08
Ru-106	2.33E-06	7.97E-06	1.47E-05	2.18E-05	2.87E-05	3.52E-05	4.12E-05	4.66E-05	2.48E-05
Ru-107	1.46E-10	2.66E-10	3.39E-10	3.88E-10	4.20E-10	4.40E-10	4.52E-10	4.59E-10	3.64E-10
Ru-108	9.74E-11	1.98E-10	2.63E-10	3.09E-10	3.40E-10	3.61E-10	3.74E-10	3.81E-10	2.90E-10
Rh-103	3.91E-06	1.82E-05	3.58E-05	5.25E-05	6.70E-05	7.89E-05	8.85E-05	9.60E-05	5.51E-05
Rh-103m	8.95E-09	1.67E-08	1.93E-08	1.98E-08	1.95E-08	1.88E-08	1.81E-08	1.73E-08	1.73E-08
Rh-104	5.21E-12	2.73E-11	5.48E-11	8.11E-11	1.04E-10	1.23E-10	1.38E-10	1.50E-10	8.53E-11
Rh-105	2.46E-07	3.23E-07	3.58E-07	3.76E-07	3.84E-07	3.86E-07	3.84E-07	3.80E-07	3.55E-07
Rh-106m	2.54E-10	3.37E-10	3.77E-10	3.97E-10	4.07E-10	4.10E-10	4.10E-10	4.06E-10	3.75E-10
Rh-107	8.59E-10	1.56E-09	1.99E-09	2.28E-09	2.47E-09	2.58E-09	2.65E-09	2.69E-09	2.14E-09
Pd-104	1.55E-07	1.69E-06	5.59E-06	1.20E-05	2.06E-05	3.11E-05	4.31E-05	5.63E-05	2.13E-05
Pd-105	3.86E-06	1.27E-05	2.30E-05	3.39E-05	4.50E-05	5.61E-05	6.70E-05	7.78E-05	3.99E-05
Pd-106	8.49E-07	3.18E-06	6.70E-06	1.14E-05	1.72E-05	2.40E-05	3.17E-05	4.04E-05	1.69E-05
Pd-107	1.22E-06	5.02E-06	1.04E-05	1.67E-05	2.36E-05	3.08E-05	3.83E-05	4.58E-05	2.15E-05
Pd-108	6.35E-07	2.91E-06	6.31E-06	1.05E-05	1.51E-05	2.01E-05	2.52E-05	3.05E-05	1.39E-05
Pd-109	1.17E-08	2.53E-08	3.49E-08	4.23E-08	4.81E-08	5.27E-08	5.64E-08	5.95E-08	4.13E-08
Pd-110	2.28E-07	9.75E-07	2.08E-06	3.43E-06	4.96E-06	6.61E-06	8.35E-06	1.01E-05	4.60E-06
Pd-111	9.42E-11	1.64E-10	2.10E-10	2.43E-10	2.66E-10	2.81E-10	2.91E-10	2.98E-10	2.31E-10
Pd-112	2.91E-09	4.39E-09	5.29E-09	5.89E-09	6.30E-09	6.54E-09	6.69E-09	6.79E-09	5.60E-09

Ag-109	3.85E-07	1.78E-06	3.78E-06	6.10E-06	8.55E-06	1.10E-05	1.34E-05	1.57E-05	7.59E-06
Ag-110m	8.37E-10	7.74E-09	2.50E-08	5.34E-08	9.23E-08	1.40E-07	1.95E-07	2.55E-07	9.62E-08
Ag-111	3.60E-08	7.11E-08	9.32E-08	1.09E-07	1.20E-07	1.28E-07	1.33E-07	1.36E-07	1.03E-07
Ag-112	4.33E-10	6.55E-10	7.91E-10	8.81E-10	9.42E-10	9.79E-10	1.00E-09	1.02E-09	8.37E-10
Ag-113	4.42E-10	5.79E-10	6.62E-10	7.16E-10	7.50E-10	7.69E-10	7.79E-10	7.84E-10	6.85E-10
Cd-110	1.82E-08	1.76E-07	5.99E-07	1.35E-06	2.47E-06	3.95E-06	5.81E-06	8.03E-06	2.80E-06
Cd-111	9.18E-08	4.32E-07	9.38E-07	1.56E-06	2.26E-06	3.03E-06	3.84E-06	4.69E-06	2.11E-06
Cd-112	7.59E-08	2.74E-07	5.33E-07	8.34E-07	1.17E-06	1.52E-06	1.88E-06	2.27E-06	1.07E-06
Cd-113	8.87E-09	1.19E-08	1.37E-08	1.48E-08	1.55E-08	1.59E-08	1.61E-08	1.62E-08	1.41E-08
Cd-113m	8.35E-10	2.69E-09	4.96E-09	7.52E-09	1.03E-08	1.32E-08	1.63E-08	1.95E-08	9.41E-09
Cd-114	1.24E-07	4.08E-07	7.41E-07	1.10E-06	1.49E-06	1.88E-06	2.27E-06	2.67E-06	1.33E-06
Cd-115	4.84E-09	5.57E-09	5.77E-09	5.78E-09	5.71E-09	5.60E-09	5.49E-09	5.38E-09	5.52E-09
Cd-115m	2.59E-09	5.28E-09	6.49E-09	6.98E-09	7.13E-09	7.13E-09	7.05E-09	6.96E-09	6.20E-09
Cd-116	6.39E-08	1.89E-07	3.22E-07	4.56E-07	5.87E-07	7.14E-07	8.37E-07	9.57E-07	5.16E-07
Cd-117	2.40E-10	2.69E-10	2.74E-10	2.69E-10	2.61E-10	2.51E-10	2.42E-10	2.33E-10	2.55E-10
In-113	2.46E-12	1.72E-11	4.93E-11	1.01E-10	1.74E-10	2.68E-10	3.85E-10	5.26E-10	1.91E-10
In-115	4.39E-08	1.20E-07	1.79E-07	2.22E-07	2.51E-07	2.70E-07	2.81E-07	2.86E-07	2.06E-07
In-115m	4.05E-10	4.68E-10	4.84E-10	4.85E-10	4.80E-10	4.70E-10	4.61E-10	4.51E-10	4.63E-10
In-117m	1.45E-10	1.63E-10	1.66E-10	1.63E-10	1.58E-10	1.52E-10	1.46E-10	1.41E-10	1.54E-10
Sn-115	2.56E-09	7.88E-09	1.35E-08	1.91E-08	2.46E-08	3.00E-08	3.51E-08	4.00E-08	2.16E-08
Sn-116	5.90E-09	3.71E-08	9.38E-08	1.70E-07	2.59E-07	3.57E-07	4.60E-07	5.67E-07	2.44E-07
Sn-117	6.03E-08	1.77E-07	2.99E-07	4.21E-07	5.39E-07	6.53E-07	7.62E-07	8.68E-07	4.72E-07
Sn-118	5.34E-08	1.53E-07	2.55E-07	3.56E-07	4.55E-07	5.49E-07	6.41E-07	7.29E-07	3.99E-07
Sn-119	5.91E-08	1.66E-07	2.75E-07	3.81E-07	4.82E-07	5.79E-07	6.71E-07	7.59E-07	4.22E-07
Sn-120	5.79E-08	1.63E-07	2.69E-07	3.73E-07	4.73E-07	5.69E-07	6.60E-07	7.49E-07	4.14E-07
Sn-121	2.51E-09	2.73E-09	2.74E-09	2.67E-09	2.57E-09	2.47E-09	2.36E-09	2.27E-09	2.54E-09
Sn-121m	3.30E-09	9.69E-09	1.65E-08	2.32E-08	2.98E-08	3.61E-08	4.22E-08	4.81E-08	2.61E-08
Sn-122	7.20E-08	2.06E-07	3.43E-07	4.78E-07	6.08E-07	7.32E-07	8.51E-07	9.66E-07	5.32E-07
Sn-123	2.91E-08	7.11E-08	1.01E-07	1.21E-07	1.33E-07	1.39E-07	1.41E-07	1.40E-07	1.09E-07
Sn-124	1.23E-07	3.52E-07	5.88E-07	8.17E-07	1.04E-06	1.25E-06	1.44E-06	1.63E-06	9.05E-07
Sn-125	2.62E-08	3.66E-08	3.88E-08	3.89E-08	3.82E-08	3.71E-08	3.59E-08	3.48E-08	3.58E-08
Sn-126	2.61E-07	7.63E-07	1.29E-06	1.82E-06	2.33E-06	2.82E-06	3.29E-06	3.74E-06	2.04E-06
Sn-127	2.12E-09	2.23E-09	2.19E-09	2.09E-09	1.98E-09	1.87E-09	1.77E-09	1.68E-09	1.99E-09
Sn-128	2.22E-09	2.24E-09	2.14E-09	2.01E-09	1.87E-09	1.75E-09	1.64E-09	1.54E-09	1.92E-09
Sn-129m	1.51E-10	1.47E-10	1.38E-10	1.28E-10	1.18E-10	1.09E-10	1.01E-10	9.41E-11	1.23E-10
Sn-130	2.50E-10	2.29E-10	2.07E-10	1.87E-10	1.69E-10	1.53E-10	1.39E-10	1.27E-10	1.82E-10
Sb-121	5.47E-08	1.59E-07	2.64E-07	3.66E-07	4.62E-07	5.51E-07	6.35E-07	7.13E-07	4.00E-07
Sb-122	6.37E-11	2.08E-10	3.54E-10	4.95E-10	6.28E-10	7.53E-10	8.70E-10	9.79E-10	5.44E-10
Sb-123	4.33E-08	1.34E-07	2.39E-07	3.49E-07	4.61E-07	5.71E-07	6.78E-07	7.81E-07	4.07E-07
Sb-124	2.40E-10	1.18E-09	2.65E-09	4.46E-09	6.46E-09	8.52E-09	1.06E-08	1.27E-08	5.85E-09
Sb-125	1.30E-07	4.06E-07	6.88E-07	9.53E-07	1.20E-06	1.41E-06	1.61E-06	1.78E-06	1.02E-06
Sb-126	2.80E-09	3.93E-09	4.37E-09	4.71E-09	5.01E-09	5.27E-09	5.52E-09	5.74E-09	4.67E-09
Sb-127	1.03E-07	1.19E-07	1.21E-07	1.17E-07	1.13E-07	1.08E-07	1.03E-07	9.89E-08	1.10E-07
Sb-128	2.12E-08	2.15E-08	2.07E-08	1.95E-08	1.83E-08	1.71E-08	1.60E-08	1.51E-08	1.87E-08
Sb-129	1.71E-08	1.81E-08	1.78E-08	1.71E-08	1.63E-08	1.55E-08	1.47E-08	1.40E-08	1.63E-08
Sb-130	3.48E-09	3.36E-09	3.14E-09	2.91E-09	2.68E-09	2.48E-09	2.29E-09	2.13E-09	2.81E-09
Sb-130m	6.43E-10	6.07E-10	5.59E-10	5.11E-10	4.68E-10	4.28E-10	3.93E-10	3.62E-10	4.96E-10
Sb-131	6.30E-09	5.87E-09	5.39E-09	4.92E-09	4.49E-09	4.11E-09	3.77E-09	3.47E-09	4.79E-09
Sb-132	5.77E-10	5.50E-10	5.11E-10	4.70E-10	4.32E-10	3.97E-10	3.67E-10	3.40E-10	4.56E-10
Sb-132m	3.70E-10	3.34E-10	3.01E-10	2.72E-10	2.46E-10	2.23E-10	2.03E-10	1.85E-10	2.67E-10
Sb-133	6.19E-10	5.51E-10	4.90E-10	4.38E-10	3.93E-10	3.53E-10	3.18E-10	2.88E-10	4.31E-10

Te-122	3.89E-10	2.65E-09	7.24E-09	1.41E-08	2.31E-08	3.41E-08	4.69E-08	6.15E-08	2.38E-08
Te-123	7.08E-13	8.85E-12	3.45E-11	8.46E-11	1.63E-10	2.72E-10	4.12E-10	5.83E-10	1.95E-10
Te-123m	5.30E-13	5.63E-12	2.08E-11	5.02E-11	9.64E-11	1.60E-10	2.43E-10	3.45E-10	1.15E-10
Te-124	5.99E-11	5.64E-10	2.00E-09	4.71E-09	8.90E-09	1.47E-08	2.21E-08	3.12E-08	1.05E-08
Te-125	1.55E-09	1.16E-08	3.32E-08	6.68E-08	1.12E-07	1.67E-07	2.31E-07	3.04E-07	1.16E-07
Te-125m	3.71E-10	2.21E-09	5.08E-09	8.36E-09	1.17E-08	1.48E-08	1.77E-08	2.04E-08	1.01E-08
Te-126	7.62E-09	2.57E-08	4.59E-08	6.70E-08	8.90E-08	1.12E-07	1.35E-07	1.60E-07	8.03E-08
Te-127	9.91E-09	1.16E-08	1.18E-08	1.15E-08	1.10E-08	1.06E-08	1.01E-08	9.67E-09	1.08E-08
Te-127m	2.06E-08	4.27E-08	5.00E-08	5.12E-08	5.01E-08	4.82E-08	4.61E-08	4.40E-08	4.41E-08
Te-128	1.50E-06	4.20E-06	6.90E-06	9.47E-06	1.19E-05	1.42E-05	1.63E-05	1.83E-05	1.03E-05
Te-129	4.50E-09	4.77E-09	4.70E-09	4.52E-09	4.31E-09	4.09E-09	3.89E-09	3.70E-09	4.31E-09
Te-129m	2.13E-10	4.58E-10	5.79E-10	6.36E-10	6.64E-10	6.81E-10	6.93E-10	7.05E-10	5.79E-10
Te-130	7.53E-06	2.01E-05	3.20E-05	4.30E-05	5.32E-05	6.25E-05	7.10E-05	7.90E-05	4.60E-05
Te-131	7.32E-09	6.95E-09	6.43E-09	5.91E-09	5.43E-09	4.99E-09	4.60E-09	4.26E-09	5.74E-09
Te-131m	5.25E-08	6.02E-08	6.08E-08	5.89E-08	5.63E-08	5.35E-08	5.10E-08	4.87E-08	5.52E-08
Te-132	2.09E-06	2.05E-06	1.90E-06	1.75E-06	1.60E-06	1.47E-06	1.36E-06	1.26E-06	1.68E-06
Te-133	5.39E-09	4.96E-09	4.51E-09	4.09E-09	3.71E-09	3.38E-09	3.08E-09	2.82E-09	3.99E-09
Te-133m	1.76E-08	1.64E-08	1.50E-08	1.36E-08	1.24E-08	1.12E-08	1.03E-08	9.42E-09	1.32E-08
Te-134	3.05E-08	2.76E-08	2.47E-08	2.22E-08	1.99E-08	1.80E-08	1.62E-08	1.47E-08	2.17E-08
Te-135	1.11E-10	1.00E-10	9.03E-11	8.14E-11	7.37E-11	6.68E-11	6.07E-11	5.54E-11	7.99E-11
I-127	5.71E-07	1.84E-06	3.15E-06	4.42E-06	5.63E-06	6.75E-06	7.80E-06	8.78E-06	4.86E-06
I-129	2.38E-06	6.72E-06	1.11E-05	1.53E-05	1.92E-05	2.29E-05	2.64E-05	2.96E-05	1.67E-05
I-130	2.69E-10	7.67E-10	1.25E-09	1.72E-09	2.16E-09	2.57E-09	2.96E-09	3.32E-09	1.88E-09
I-131	3.23E-06	3.53E-06	3.30E-06	3.05E-06	2.82E-06	2.60E-06	2.40E-06	2.23E-06	2.89E-06
I-132	6.29E-08	6.22E-08	5.78E-08	5.33E-08	4.90E-08	4.50E-08	4.16E-08	3.85E-08	5.13E-08
I-132m	1.58E-10	2.48E-10	2.84E-10	2.97E-10	3.01E-10	3.00E-10	2.97E-10	2.94E-10	2.72E-10
I-133	8.95E-07	8.41E-07	7.72E-07	7.04E-07	6.43E-07	5.87E-07	5.38E-07	4.95E-07	6.84E-07
I-134	4.38E-08	4.07E-08	3.71E-08	3.37E-08	3.07E-08	2.79E-08	2.55E-08	2.34E-08	3.28E-08
I-134m	1.58E-10	1.76E-10	1.77E-10	1.73E-10	1.66E-10	1.59E-10	1.52E-10	1.46E-10	1.63E-10
I-135	2.66E-07	2.49E-07	2.29E-07	2.10E-07	1.92E-07	1.76E-07	1.61E-07	1.49E-07	2.04E-07
I-136	3.87E-10	3.51E-10	3.18E-10	2.89E-10	2.63E-10	2.39E-10	2.19E-10	2.01E-10	2.83E-10
I-136m	1.07E-10	1.03E-10	9.73E-11	9.10E-11	8.49E-11	7.91E-11	7.39E-11	6.92E-11	8.82E-11
I-137	1.32E-10	1.21E-10	1.10E-10	1.00E-10	9.17E-11	8.37E-11	7.67E-11	7.06E-11	9.83E-11
Xe-128	3.72E-09	2.70E-08	7.56E-08	1.49E-07	2.47E-07	3.67E-07	5.09E-07	6.71E-07	2.56E-07
Xe-129	2.52E-12	3.89E-11	1.73E-10	4.74E-10	1.00E-09	1.82E-09	2.98E-09	4.54E-09	1.38E-09
Xe-130	1.06E-08	6.32E-08	1.64E-07	3.10E-07	4.99E-07	7.30E-07	9.98E-07	1.31E-06	5.10E-07
Xe-131	8.36E-06	2.62E-05	4.15E-05	5.39E-05	6.36E-05	7.11E-05	7.67E-05	8.07E-05	5.27E-05
Xe-131m	4.20E-08	6.12E-08	5.84E-08	5.41E-08	5.00E-08	4.61E-08	4.26E-08	3.95E-08	4.92E-08
Xe-132	1.61E-05	4.82E-05	8.05E-05	1.12E-04	1.43E-04	1.73E-04	2.02E-04	2.30E-04	1.26E-04
Xe-133	5.02E-06	5.10E-06	4.69E-06	4.29E-06	3.91E-06	3.58E-06	3.28E-06	3.02E-06	4.11E-06
Xe-133m	2.44E-08	2.46E-08	2.33E-08	2.17E-08	2.03E-08	1.89E-08	1.77E-08	1.67E-08	2.09E-08
Xe-134	3.24E-05	8.54E-05	1.34E-04	1.79E-04	2.19E-04	2.56E-04	2.90E-04	3.21E-04	1.90E-04
Xe-135	6.39E-08	6.04E-08	5.57E-08	5.10E-08	4.66E-08	4.27E-08	3.93E-08	3.63E-08	4.95E-08
Xe-135m	1.37E-09	1.37E-09	1.30E-09	1.22E-09	1.13E-09	1.05E-09	9.85E-10	9.22E-10	1.17E-09
Xe-136	4.87E-05	1.29E-04	2.05E-04	2.74E-04	3.38E-04	3.96E-04	4.50E-04	5.00E-04	2.92E-04
Xe-137	2.50E-09	2.33E-09	2.13E-09	1.94E-09	1.77E-09	1.62E-09	1.49E-09	1.37E-09	1.89E-09
Xe-138	9.36E-09	8.59E-09	7.78E-09	7.03E-09	6.36E-09	5.76E-09	5.24E-09	4.79E-09	6.86E-09
Xe-139	3.47E-10	3.11E-10	2.78E-10	2.49E-10	2.23E-10	2.00E-10	1.81E-10	1.64E-10	2.44E-10
Cs-133	2.11E-05	6.40E-05	1.02E-04	1.35E-04	1.63E-04	1.87E-04	2.07E-04	2.23E-04	1.38E-04
Cs-134	3.33E-07	2.32E-06	6.00E-06	1.10E-05	1.68E-05	2.33E-05	3.01E-05	3.71E-05	1.59E-05
Cs-134m	2.29E-10	7.58E-10	1.23E-09	1.63E-09	1.97E-09	2.26E-09	2.50E-09	2.70E-09	1.66E-09

Cs-135	4.08E-06	1.15E-05	1.85E-05	2.50E-05	3.12E-05	3.72E-05	4.29E-05	4.86E-05	2.74E-05
Cs-136	1.43E-08	4.03E-08	6.10E-08	7.84E-08	9.37E-08	1.08E-07	1.22E-07	1.35E-07	8.16E-08
Cs-137	2.54E-05	6.72E-05	1.06E-04	1.41E-04	1.73E-04	2.02E-04	2.29E-04	2.53E-04	1.50E-04
Cs-138	2.38E-08	2.20E-08	2.00E-08	1.81E-08	1.64E-08	1.49E-08	1.36E-08	1.24E-08	1.77E-08
Cs-139	6.22E-09	5.73E-09	5.19E-09	4.70E-09	4.25E-09	3.86E-09	3.51E-09	3.21E-09	4.58E-09
Cs-140	6.35E-10	5.74E-10	5.15E-10	4.62E-10	4.16E-10	3.74E-10	3.39E-10	3.08E-10	4.53E-10
Cs-141	1.82E-10	1.67E-10	1.51E-10	1.36E-10	1.23E-10	1.12E-10	1.02E-10	9.30E-11	1.33E-10
Ba-134	5.12E-09	7.45E-08	3.16E-07	8.17E-07	1.64E-06	2.83E-06	4.42E-06	6.43E-06	2.07E-06
Ba-135	5.90E-12	1.16E-10	7.15E-10	2.51E-09	6.45E-09	1.36E-08	2.53E-08	4.29E-08	1.15E-08
Ba-136	3.83E-08	1.92E-07	4.44E-07	7.68E-07	1.15E-06	1.59E-06	2.07E-06	2.60E-06	1.11E-06
Ba-137	3.93E-08	2.37E-07	6.03E-07	1.12E-06	1.78E-06	2.56E-06	3.46E-06	4.46E-06	1.78E-06
Ba-138	2.76E-05	7.26E-05	1.14E-04	1.51E-04	1.85E-04	2.16E-04	2.44E-04	2.70E-04	1.60E-04
Ba-139	5.65E-08	5.21E-08	4.73E-08	4.28E-08	3.88E-08	3.52E-08	3.21E-08	2.94E-08	4.18E-08
Ba-140	9.74E-06	1.13E-05	1.03E-05	9.33E-06	8.43E-06	7.64E-06	6.94E-06	6.33E-06	8.75E-06
Ba-141	1.13E-08	1.04E-08	9.44E-09	8.51E-09	7.69E-09	6.96E-09	6.32E-09	5.77E-09	8.30E-09
Ba-142	6.43E-09	5.88E-09	5.30E-09	4.76E-09	4.28E-09	3.86E-09	3.49E-09	3.17E-09	4.65E-09
Ba-143	1.40E-10	1.26E-10	1.12E-10	9.97E-11	8.90E-11	7.96E-11	7.15E-11	6.45E-11	9.77E-11
La-138	1.36E-10	3.72E-10	5.98E-10	8.05E-10	9.90E-10	1.16E-09	1.31E-09	1.44E-09	8.50E-10
La-139	2.61E-05	6.84E-05	1.07E-04	1.42E-04	1.73E-04	2.01E-04	2.27E-04	2.50E-04	1.49E-04
La-140	1.24E-06	1.50E-06	1.38E-06	1.25E-06	1.14E-06	1.03E-06	9.46E-07	8.68E-07	1.17E-06
La-141	1.46E-07	1.35E-07	1.22E-07	1.10E-07	9.97E-08	9.02E-08	8.20E-08	7.48E-08	1.08E-07
La-142	5.63E-08	5.17E-08	4.67E-08	4.20E-08	3.78E-08	3.41E-08	3.09E-08	2.82E-08	4.10E-08
La-143	8.83E-09	8.02E-09	7.19E-09	6.43E-09	5.76E-09	5.17E-09	4.66E-09	4.22E-09	6.28E-09
La-144	3.88E-10	3.49E-10	3.12E-10	2.78E-10	2.48E-10	2.22E-10	1.99E-10	1.80E-10	2.72E-10
La-145	1.66E-10	1.49E-10	1.33E-10	1.19E-10	1.07E-10	9.54E-11	8.59E-11	7.76E-11	1.17E-10
Ce-140	1.44E-05	5.38E-05	9.26E-05	1.28E-04	1.60E-04	1.89E-04	2.16E-04	2.41E-04	1.37E-04
Ce-141	1.52E-05	2.42E-05	2.46E-05	2.29E-05	2.08E-05	1.89E-05	1.71E-05	1.56E-05	1.99E-05
Ce-142	2.39E-05	6.30E-05	9.86E-05	1.31E-04	1.60E-04	1.86E-04	2.09E-04	2.31E-04	1.38E-04
Ce-143	1.23E-06	1.13E-06	1.01E-06	9.06E-07	8.12E-07	7.29E-07	6.58E-07	5.96E-07	8.85E-07
Ce-144	2.10E-05	5.06E-05	7.25E-05	8.80E-05	9.84E-05	1.05E-04	1.08E-04	1.09E-04	8.16E-05
Ce-145	1.24E-09	1.13E-09	1.02E-09	9.15E-10	8.22E-10	7.40E-10	6.70E-10	6.08E-10	8.94E-10
Ce-146	4.27E-09	3.92E-09	3.54E-09	3.19E-09	2.88E-09	2.60E-09	2.37E-09	2.16E-09	3.12E-09
Ce-147	1.90E-10	1.77E-10	1.63E-10	1.49E-10	1.36E-10	1.25E-10	1.15E-10	1.06E-10	1.45E-10
Ce-148	1.55E-10	1.40E-10	1.26E-10	1.13E-10	1.02E-10	9.26E-11	8.41E-11	7.66E-11	1.11E-10
Pr-141	8.41E-06	3.75E-05	7.17E-05	1.04E-04	1.34E-04	1.61E-04	1.85E-04	2.07E-04	1.14E-04
Pr-142	5.89E-10	3.05E-09	6.04E-09	8.92E-09	1.16E-08	1.40E-08	1.61E-08	1.81E-08	9.80E-09
Pr-143	9.33E-06	1.12E-05	1.01E-05	9.08E-06	8.14E-06	7.30E-06	6.58E-06	5.95E-06	8.46E-06
Pr-144	9.75E-10	2.24E-09	3.16E-09	3.80E-09	4.23E-09	4.49E-09	4.62E-09	4.65E-09	3.52E-09
Pr-145	1.49E-07	1.35E-07	1.22E-07	1.09E-07	9.82E-08	8.84E-08	8.00E-08	7.26E-08	1.07E-07
Pr-146	7.65E-09	7.01E-09	6.34E-09	5.71E-09	5.16E-09	4.67E-09	4.24E-09	3.87E-09	5.58E-09
Pr-147	3.19E-09	2.95E-09	2.69E-09	2.44E-09	2.21E-09	2.01E-09	1.84E-09	1.68E-09	2.38E-09
Pr-148	3.95E-10	3.63E-10	3.29E-10	2.99E-10	2.72E-10	2.47E-10	2.26E-10	2.07E-10	2.92E-10
Pr-149	2.62E-10	2.47E-10	2.29E-10	2.11E-10	1.95E-10	1.80E-10	1.66E-10	1.54E-10	2.06E-10
Nd-142	1.08E-08	1.17E-07	3.83E-07	8.16E-07	1.40E-06	2.13E-06	2.98E-06	3.95E-06	1.47E-06
Nd-143	1.31E-05	4.70E-05	7.71E-05	1.01E-04	1.20E-04	1.34E-04	1.45E-04	1.53E-04	9.88E-05
Nd-144	1.70E-06	1.05E-05	2.63E-05	4.74E-05	7.23E-05	1.00E-04	1.30E-04	1.61E-04	6.86E-05
Nd-145	1.56E-05	4.02E-05	6.15E-05	7.98E-05	9.53E-05	1.08E-04	1.19E-04	1.29E-04	8.11E-05
Nd-146	1.24E-05	3.32E-05	5.30E-05	7.18E-05	8.96E-05	1.07E-04	1.23E-04	1.38E-04	7.84E-05
Nd-147	3.07E-06	3.41E-06	3.12E-06	2.83E-06	2.57E-06	2.34E-06	2.14E-06	1.97E-06	2.68E-06
Nd-148	7.11E-06	1.89E-05	2.97E-05	3.96E-05	4.86E-05	5.68E-05	6.43E-05	7.12E-05	4.20E-05
Nd-149	1.21E-08	1.16E-08	1.08E-08	1.00E-08	9.30E-09	8.64E-09	8.05E-09	7.53E-09	9.75E-09

Nd-150	2.75E-06	7.42E-06	1.19E-05	1.62E-05	2.02E-05	2.39E-05	2.74E-05	3.07E-05	1.76E-05
Nd-151	5.87E-10	5.93E-10	5.77E-10	5.55E-10	5.30E-10	5.05E-10	4.82E-10	4.60E-10	5.36E-10
Nd-152	3.46E-10	3.59E-10	3.55E-10	3.45E-10	3.33E-10	3.20E-10	3.07E-10	2.94E-10	3.32E-10
Pm-146	1.40E-12	1.05E-11	2.69E-11	4.71E-11	6.93E-11	9.18E-11	1.14E-10	1.36E-10	6.21E-11
Pm-147	5.37E-06	1.62E-05	2.38E-05	2.85E-05	3.11E-05	3.22E-05	3.23E-05	3.17E-05	2.51E-05
Pm-148	5.59E-08	2.10E-07	3.20E-07	3.87E-07	4.24E-07	4.40E-07	4.42E-07	4.34E-07	3.39E-07
Pm-148m	4.32E-08	1.48E-07	2.21E-07	2.65E-07	2.89E-07	2.99E-07	2.99E-07	2.93E-07	2.32E-07
Pm-149	3.77E-07	4.26E-07	4.46E-07	4.50E-07	4.43E-07	4.30E-07	4.13E-07	3.94E-07	4.22E-07
Pm-150	4.88E-10	5.56E-10	5.85E-10	5.93E-10	5.86E-10	5.70E-10	5.50E-10	5.26E-10	5.57E-10
Pm-151	7.95E-08	8.09E-08	7.89E-08	7.59E-08	7.26E-08	6.92E-08	6.60E-08	6.30E-08	7.32E-08
Pm-152	1.28E-10	1.32E-10	1.31E-10	1.28E-10	1.23E-10	1.18E-10	1.14E-10	1.09E-10	1.23E-10
Pm-153	9.70E-11	1.03E-10	1.03E-10	1.02E-10	1.00E-10	9.71E-11	9.40E-11	9.09E-11	9.84E-11
Sm-147	7.64E-08	5.67E-07	1.43E-06	2.48E-06	3.59E-06	4.67E-06	5.68E-06	6.58E-06	3.13E-06
Sm-148	1.67E-07	1.45E-06	4.02E-06	7.46E-06	1.14E-05	1.58E-05	2.02E-05	2.48E-05	1.07E-05
Sm-149	3.97E-07	4.58E-07	4.79E-07	4.83E-07	4.74E-07	4.60E-07	4.43E-07	4.23E-07	4.52E-07
Sm-150	3.78E-06	1.19E-05	2.02E-05	2.85E-05	3.62E-05	4.34E-05	5.00E-05	5.59E-05	3.12E-05
Sm-151	9.51E-07	1.61E-06	1.85E-06	2.00E-06	2.13E-06	2.25E-06	2.35E-06	2.44E-06	1.95E-06
Sm-152	1.75E-06	5.38E-06	8.60E-06	1.12E-05	1.31E-05	1.47E-05	1.59E-05	1.69E-05	1.09E-05
Sm-153	7.14E-08	1.29E-07	1.79E-07	2.17E-07	2.46E-07	2.68E-07	2.85E-07	2.98E-07	2.12E-07
Sm-154	3.65E-07	1.09E-06	1.91E-06	2.78E-06	3.68E-06	4.58E-06	5.48E-06	6.38E-06	3.28E-06
Sm-155	1.00E-10	1.28E-10	1.44E-10	1.54E-10	1.60E-10	1.64E-10	1.66E-10	1.67E-10	1.48E-10
Sm-156	1.35E-09	1.93E-09	2.26E-09	2.46E-09	2.59E-09	2.65E-09	2.68E-09	2.69E-09	2.33E-09
Eu-151	2.74E-10	6.95E-10	8.61E-10	9.48E-10	1.01E-09	1.07E-09	1.12E-09	1.16E-09	8.92E-10
Eu-152	1.61E-10	7.91E-10	1.23E-09	1.45E-09	1.58E-09	1.68E-09	1.76E-09	1.83E-09	1.31E-09
Eu-153	7.66E-07	2.83E-06	5.62E-06	8.79E-06	1.20E-05	1.52E-05	1.81E-05	2.09E-05	1.05E-05
Eu-154	4.35E-08	2.76E-07	7.12E-07	1.30E-06	1.97E-06	2.66E-06	3.34E-06	3.99E-06	1.79E-06
Eu-155	7.09E-08	1.60E-07	2.82E-07	4.45E-07	6.34E-07	8.33E-07	1.03E-06	1.22E-06	5.84E-07
Eu-156	8.19E-08	2.02E-07	3.30E-07	4.97E-07	6.92E-07	9.01E-07	1.11E-06	1.31E-06	6.41E-07
Eu-157	1.28E-09	2.28E-09	3.06E-09	3.83E-09	4.59E-09	5.32E-09	6.01E-09	6.64E-09	4.13E-09
Gd-154	1.68E-10	2.15E-09	8.80E-09	2.25E-08	4.44E-08	7.50E-08	1.14E-07	1.61E-07	5.36E-08
Gd-155	2.60E-10	6.86E-10	1.26E-09	2.07E-09	3.06E-09	4.16E-09	5.33E-09	6.52E-09	2.92E-09
Gd-156	9.11E-08	5.20E-07	1.30E-06	2.51E-06	4.25E-06	6.57E-06	9.49E-06	1.30E-05	4.72E-06
Gd-157	3.96E-09	7.19E-09	9.94E-09	1.29E-08	1.60E-08	1.94E-08	2.31E-08	2.69E-08	1.49E-08
Gd-158	6.17E-08	2.53E-07	5.33E-07	8.96E-07	1.34E-06	1.87E-06	2.49E-06	3.20E-06	1.33E-06
Gd-159	2.90E-10	5.62E-10	7.74E-10	9.55E-10	1.11E-09	1.25E-09	1.38E-09	1.51E-09	9.80E-10
Gd-160	3.18E-09	1.40E-08	3.03E-08	5.04E-08	7.34E-08	9.82E-08	1.24E-07	1.52E-07	6.82E-08
Tb-159	7.83E-09	3.31E-08	7.05E-08	1.17E-07	1.71E-07	2.31E-07	2.95E-07	3.63E-07	1.61E-07
Tb-160	1.04E-10	7.36E-10	2.01E-09	3.83E-09	6.10E-09	8.72E-09	1.16E-08	1.48E-08	5.99E-09
Tb-161	3.76E-10	9.52E-10	1.38E-09	1.75E-09	2.07E-09	2.37E-09	2.65E-09	2.93E-09	1.81E-09
Dy-160	1.70E-11	2.32E-10	9.85E-10	2.56E-09	5.15E-09	8.87E-09	1.38E-08	1.99E-08	6.43E-09
Dy-161	8.77E-10	4.80E-09	1.08E-08	1.79E-08	2.57E-08	3.40E-08	4.27E-08	5.18E-08	2.36E-08
Dy-162	5.06E-10	2.67E-09	6.05E-09	1.03E-08	1.51E-08	2.05E-08	2.64E-08	3.28E-08	1.43E-08
Dy-163	2.37E-10	1.36E-09	3.38E-09	6.20E-09	9.80E-09	1.42E-08	1.93E-08	2.53E-08	9.97E-09
Dy-164	7.49E-11	3.83E-10	8.72E-10	1.53E-09	2.36E-09	3.39E-09	4.64E-09	6.12E-09	2.42E-09
Ho-165	4.27E-11	2.77E-10	7.66E-10	1.56E-09	2.72E-09	4.32E-09	6.44E-09	9.19E-09	3.16E-09
Er-166	1.33E-11	8.10E-11	2.04E-10	3.90E-10	6.59E-10	1.04E-09	1.57E-09	2.30E-09	7.83E-10
Er-168	2.89E-12	1.64E-11	4.15E-11	7.67E-11	1.21E-10	1.76E-10	2.45E-10	3.32E-10	1.27E-10
U-234	5.40E-09	1.31E-08	1.96E-08	2.66E-08	3.56E-08	4.83E-08	6.59E-08	8.96E-08	3.80E-08
U-235	4.18E-03	3.46E-03	2.85E-03	2.35E-03	1.94E-03	1.60E-03	1.32E-03	1.08E-03	2.35E-03
U-236	9.49E-05	2.33E-04	3.42E-04	4.28E-04	4.94E-04	5.45E-04	5.82E-04	6.09E-04	4.16E-04
U-237	3.72E-07	1.05E-06	1.58E-06	1.98E-06	2.28E-06	2.51E-06	2.68E-06	2.80E-06	1.91E-06

U-238	1.88E-02	1.86E-02	1.83E-02	1.81E-02	1.79E-02	1.76E-02	1.74E-02	1.72E-02	1.80E-02
U-239	8.78E-08	8.72E-08	8.66E-08	8.60E-08	8.53E-08	8.47E-08	8.42E-08	8.34E-08	8.57E-08
Np-237	8.79E-07	5.39E-06	1.30E-05	2.25E-05	3.29E-05	4.36E-05	5.40E-05	6.40E-05	2.95E-05
Np-238	4.26E-09	3.12E-08	7.92E-08	1.40E-07	2.06E-07	2.75E-07	3.43E-07	4.08E-07	1.86E-07
Np-239	1.25E-05	1.26E-05	1.25E-05	1.24E-05	1.23E-05	1.22E-05	1.21E-05	1.20E-05	1.23E-05
Np-240	3.20E-10	3.22E-10	3.20E-10	3.18E-10	3.16E-10	3.14E-10	3.13E-10	3.10E-10	3.17E-10
Pu-238	2.53E-08	3.70E-07	1.48E-06	3.61E-06	6.85E-06	1.12E-05	1.65E-05	2.26E-05	7.83E-06
Pu-239	9.93E-05	2.07E-04	2.53E-04	2.72E-04	2.79E-04	2.81E-04	2.81E-04	2.80E-04	2.44E-04
Pu-240	9.48E-06	4.00E-05	6.85E-05	8.85E-05	1.01E-04	1.08E-04	1.12E-04	1.14E-04	8.00E-05
Pu-241	2.15E-06	1.76E-05	4.37E-05	7.04E-05	9.24E-05	1.09E-04	1.19E-04	1.26E-04	7.25E-05
Pu-242	8.31E-08	1.52E-06	6.41E-06	1.53E-05	2.72E-05	4.11E-05	5.56E-05	7.01E-05	2.72E-05
Pu-243	3.80E-11	7.82E-10	3.47E-09	8.43E-09	1.51E-08	2.28E-08	3.10E-08	3.89E-08	1.51E-08
Pu-244	4.49E-13	1.96E-11	1.43E-10	5.17E-10	1.30E-09	2.63E-09	4.60E-09	7.29E-09	2.06E-09
Am-241	4.14E-09	6.39E-08	2.47E-07	5.36E-07	8.69E-07	1.19E-06	1.46E-06	1.68E-06	7.56E-07
Am-242	2.13E-11	3.94E-10	1.63E-09	3.66E-09	6.03E-09	8.34E-09	1.03E-08	1.19E-08	5.30E-09
Am-242m	2.09E-11	5.55E-10	2.73E-09	6.71E-09	1.17E-08	1.68E-08	2.13E-08	2.50E-08	1.06E-08
Am-243	1.96E-09	7.26E-08	4.86E-07	1.62E-06	3.73E-06	6.91E-06	1.11E-05	1.61E-05	5.01E-06
Am-244	1.77E-13	7.48E-12	5.30E-11	1.81E-10	4.24E-10	7.91E-10	1.28E-09	1.86E-09	5.75E-10
Am-244m	1.19E-13	4.95E-12	3.48E-11	1.19E-10	2.76E-10	5.15E-10	8.31E-10	1.21E-09	3.74E-10
Cm-242	2.43E-10	9.08E-09	5.76E-08	1.78E-07	3.77E-07	6.39E-07	9.39E-07	1.25E-06	4.31E-07
Cm-243	5.93E-13	4.87E-11	4.69E-10	1.98E-09	5.37E-09	1.11E-08	1.92E-08	2.92E-08	8.42E-09
Cm-244	6.65E-11	4.95E-09	5.20E-08	2.44E-07	7.38E-07	1.71E-06	3.33E-06	5.75E-06	1.48E-06
Cm-245	7.21E-13	1.00E-10	1.53E-09	9.42E-09	3.50E-08	9.56E-08	2.12E-07	4.07E-07	9.53E-08
Cm-246	5.26E-15	1.48E-12	3.59E-11	3.12E-10	1.54E-09	5.29E-09	1.44E-08	3.30E-08	6.83E-09
Cm-247	7.78E-18	4.20E-15	1.52E-13	1.77E-12	1.09E-11	4.55E-11	1.45E-10	3.84E-10	7.36E-11

Maximum content

General fields

Pass #	1	2	3	4	5	6	7	8	Avg
Residence time [days]	65.25	130.5	195.75	261	326.25	391.5	460.59	525.84	294.5
Pass burnup [MWd/kg$_{HM}$]	37.09	34.22	31.79	29.43	26.97	24.57	22.75	20.83	27.84
Burnup [MWd/kg$_{HM}$]	37.09	66.24	93.86	117.35	137.98	157.26	177.29	192.46	121
Thermal fluence [n/cm^2]	8.52E+20	1.68E+21	2.49E+21	3.23E+21	4.05E+21	4.84E+21	5.58E+21	6.32E+21	3.53E+21
Thermal fluence uncertainty	3.66%	3.12%	3.07%	3.07%	3.04%	3.04%	3.02%	3.02%	3.12%
Fast fluence [n/cm^2]	6.33E+20	1.23E+21	1.82E+21	2.39E+21	2.94E+21	3.49E+21	4.05E+21	4.55E+21	2.61E+21
Fast fluence uncertainty	6.53%	4.81%	4.73%	4.66%	4.44%	4.37%	4.35%	4.23%	4.66%
Power [W]	3.30E+03	3.11E+03	2.94E+03	2.77E+03	2.54E+03	2.40E+03	2.14E+03	1.93E+03	2.52E+03
Power uncertainty	13.3%	13.6%	14.5%	14.6%	15.3%	16.2%	17.5%	17.4	14.4%

Atomic densities [at/b.cm]

Pass #	1	2	3	4	5	6	7	8	Avg
H-1	1.79E-08	1.99E-08	1.99E-08	1.99E-08	2.19E-08	2.02E-08	2.36E-08	2.68E-08	1.89E-08
H-2	3.65E-09	4.58E-09	4.58E-09	4.58E-09	5.05E-09	5.87E-09	5.87E-09	7.25E-09	4.91E-09
H-3	1.82E-10	2.25E-10	2.79E-10	2.79E-10	2.99E-10	2.98E-10	3.00E-10	2.99E-10	2.56E-10
He-4	1.65E-07	2.52E-07	3.84E-07	5.21E-07	7.52E-07	1.10E-06	1.60E-06	2.25E-06	8.48E-07
Be-9	1.11E-10	1.11E-10	1.11E-10	1.11E-10	1.11E-10	1.11E-10	1.11E-10	2.20E-10	1.24E-10
C-12	1.17E-02	1.17E-02	1.17E-02	1.17E-02	1.17E-02	1.17E-02	1.17E-02	1.17E-02	1.17E-02
C-13	1.25E-04	1.25E-04	1.25E-04	1.25E-04	1.26E-04	1.26E-04	1.26E-04	1.26E-04	1.25E-04
N-14	1.76E-10	2.12E-10	2.71E-10	2.71E-10	2.71E-10	2.71E-10	2.59E-10	2.58E-10	2.37E-10
N-15	7.84E-09	8.79E-09	8.79E-09	8.79E-09	9.61E-09	9.67E-09	9.67E-09	1.55E-08	9.39E-09
O-16	3.55E-02	3.55E-02	3.55E-02	3.55E-02	3.55E-02	3.55E-02	3.55E-02	3.55E-02	3.55E-02
O-17	2.69E-09	5.21E-09	7.64E-09	9.79E-09	1.24E-08	1.47E-08	1.68E-08	1.85E-08	1.06E-08
Zn-70	5.20E-11	1.13E-10	1.75E-10	2.38E-10	2.96E-10	3.54E-10	4.12E-10	4.62E-10	2.59E-10
Ga-69	2.22E-11	4.52E-11	6.71E-11	8.88E-11	1.08E-10	1.28E-10	1.47E-10	1.63E-10	9.47E-11
Ga-71	1.07E-10	2.32E-10	3.59E-10	4.91E-10	6.16E-10	7.39E-10	8.62E-10	9.70E-10	5.39E-10
Ge-72	3.05E-10	6.73E-10	1.03E-09	1.39E-09	1.71E-09	2.01E-09	2.34E-09	2.58E-09	1.48E-09
Ge-73	1.02E-09	2.06E-09	2.98E-09	3.88E-09	4.63E-09	5.33E-09	6.04E-09	6.57E-09	4.02E-09
Ge-74	3.30E-09	6.31E-09	9.09E-09	1.17E-08	1.39E-08	1.60E-08	1.81E-08	1.97E-08	1.21E-08
Ge-76	2.86E-08	5.09E-08	7.12E-08	8.80E-08	1.02E-07	1.16E-07	1.29E-07	1.39E-07	8.96E-08
Ge-77	1.28E-09	1.17E-09	1.08E-09	9.82E-10	8.68E-10	7.94E-10	6.88E-10	6.04E-10	8.94E-10
Ge-78	4.38E-10	4.00E-10	3.71E-10	3.39E-10	3.02E-10	2.79E-10	2.44E-10	2.16E-10	3.10E-10
As-75	9.94E-09	1.79E-08	2.54E-08	3.15E-08	3.68E-08	4.16E-08	4.62E-08	5.00E-08	3.21E-08
As-77	3.64E-09	3.56E-09	3.04E-09	2.79E-09	2.46E-09	2.27E-09	2.00E-09	1.75E-09	2.59E-09
As-78	4.55E-10	4.18E-10	3.88E-10	3.56E-10	3.18E-10	2.94E-10	2.58E-10	2.29E-10	3.25E-10
Se-76	1.02E-10	3.15E-10	6.25E-10	9.54E-10	1.37E-09	1.88E-09	2.32E-09	2.78E-09	1.25E-09
Se-77	7.07E-08	1.26E-07	1.75E-07	2.14E-07	2.46E-07	2.76E-07	3.04E-07	3.24E-07	2.15E-07
Se-78	1.92E-07	3.43E-07	4.79E-07	5.94E-07	6.94E-07	7.86E-07	8.81E-07	9.52E-07	6.08E-07
Se-79	4.05E-07	7.12E-07	9.86E-07	1.20E-06	1.38E-06	1.54E-06	1.70E-06	1.81E-06	1.20E-06
Se-80	1.17E-06	2.08E-06	2.84E-06	3.49E-06	4.07E-06	4.55E-06	5.08E-06	5.45E-06	3.55E-06
Se-81	8.96E-10	8.20E-10	7.60E-10	6.92E-10	6.14E-10	5.65E-10	4.91E-10	4.31E-10	6.30E-10
Se-81m	1.13E-10	1.30E-10	1.30E-10	1.28E-10	1.21E-10	1.15E-10	1.08E-10	9.90E-11	1.12E-10
Se-82	2.93E-06	5.18E-06	7.07E-06	8.65E-06	1.01E-05	1.12E-05	1.25E-05	1.34E-05	8.77E-06
Se-83	2.61E-09	2.28E-09	2.05E-09	1.81E-09	1.57E-09	1.43E-09	1.21E-09	1.06E-09	1.68E-09
Se-84	6.95E-10	6.02E-10	5.39E-10	4.73E-10	4.08E-10	3.70E-10	3.10E-10	2.71E-10	4.39E-10
Se-85	1.46E-10	1.25E-10	1.11E-10	9.68E-11	8.26E-11	7.44E-11	6.15E-11	5.34E-11	8.96E-11
Br-79	2.14E-10	3.79E-10	5.26E-10	6.40E-10	7.42E-10	8.20E-10	9.06E-10	9.66E-10	6.40E-10
Br-81	1.85E-06	3.28E-06	4.54E-06	5.55E-06	6.43E-06	7.18E-06	7.95E-06	8.55E-06	5.59E-06
Br-82	3.00E-09	5.95E-09	8.16E-09	1.09E-08	1.46E-08	1.83E-08	1.94E-08	1.95E-08	1.05E-08
Br-83	1.87E-08	1.64E-08	1.49E-08	1.32E-08	1.15E-08	1.05E-08	8.85E-09	7.76E-09	1.22E-08
Br-84	7.28E-09	6.32E-09	5.67E-09	4.98E-09	4.30E-09	3.90E-09	3.27E-09	2.86E-09	4.61E-09

Br-85	9.61E-10	8.31E-10	7.40E-10	6.48E-10	5.56E-10	5.02E-10	4.18E-10	3.64E-10	6.00E-10
Br-86	3.74E-10	3.23E-10	2.88E-10	2.52E-10	2.16E-10	1.96E-10	1.63E-10	1.42E-10	2.33E-10
Br-87	4.57E-10	3.93E-10	3.47E-10	3.03E-10	2.58E-10	2.32E-10	1.92E-10	1.67E-10	2.81E-10
Br-88	1.13E-10	9.67E-11	8.51E-11	7.40E-11	6.28E-11	5.65E-11	4.68E-11	4.05E-11	6.86E-11
Kr-80	7.55E-12	2.11E-11	3.55E-11	5.48E-11	7.43E-11	9.65E-11	1.19E-10	1.44E-10	6.44E-11
Kr-82	1.75E-08	5.46E-08	9.42E-08	1.64E-07	2.16E-07	2.72E-07	3.37E-07	4.00E-07	1.85E-07
Kr-83	4.66E-06	7.86E-06	1.02E-05	1.19E-05	1.32E-05	1.41E-05	1.50E-05	1.55E-05	1.14E-05
Kr-83m	1.41E-08	1.23E-08	1.12E-08	9.91E-09	8.64E-09	7.87E-09	6.67E-09	5.84E-09	9.15E-09
Kr-84	9.00E-06	1.61E-05	2.21E-05	2.72E-05	3.21E-05	3.62E-05	4.04E-05	4.39E-05	2.80E-05
Kr-85	3.27E-06	5.68E-06	7.53E-06	9.01E-06	1.03E-05	1.13E-05	1.22E-05	1.29E-05	8.91E-06
Kr-85m	8.60E-08	7.44E-08	6.63E-08	5.80E-08	4.98E-08	4.50E-08	3.75E-08	3.26E-08	5.37E-08
Kr-86	1.65E-05	2.90E-05	3.87E-05	4.67E-05	5.38E-05	5.95E-05	6.52E-05	6.92E-05	4.67E-05
Kr-87	4.71E-08	4.07E-08	3.61E-08	3.16E-08	2.70E-08	2.44E-08	2.03E-08	1.76E-08	2.92E-08
Kr-88	1.43E-07	1.23E-07	1.09E-07	9.50E-08	8.11E-08	7.31E-08	6.06E-08	5.26E-08	8.80E-08
Kr-89	3.38E-09	2.90E-09	2.56E-09	2.22E-09	1.89E-09	1.70E-09	1.40E-09	1.21E-09	2.06E-09
Kr-90	6.22E-10	5.30E-10	4.64E-10	4.02E-10	3.39E-10	3.04E-10	2.51E-10	2.15E-10	3.73E-10
Kr-91	1.13E-10	9.63E-11	8.40E-11	7.26E-11	6.10E-11	5.46E-11	4.51E-11	3.86E-11	6.74E-11
Rb-84	1.93E-11	4.90E-11	7.37E-11	9.32E-11	1.23E-10	1.32E-10	1.53E-10	1.25E-10	7.83E-11
Rb-85	9.45E-06	1.66E-05	2.22E-05	2.68E-05	3.09E-05	3.42E-05	3.74E-05	3.98E-05	2.68E-05
Rb-86	6.34E-09	1.47E-08	2.06E-08	2.86E-08	4.47E-08	3.55E-08	4.14E-08	4.66E-08	2.67E-08
Rb-87	2.32E-05	4.06E-05	5.41E-05	6.51E-05	7.50E-05	8.28E-05	9.04E-05	9.58E-05	6.50E-05
Rb-88	1.50E-08	1.29E-08	1.15E-08	1.00E-08	8.57E-09	7.73E-09	6.44E-09	5.57E-09	9.28E-09
Rb-89	1.70E-08	1.46E-08	1.30E-08	1.13E-08	9.65E-09	8.69E-09	7.19E-09	6.24E-09	1.05E-08
Rb-90	3.14E-09	2.68E-09	2.36E-09	2.04E-09	1.73E-09	1.55E-09	1.28E-09	1.10E-09	1.89E-09
Rb-90m	7.24E-10	6.58E-10	6.09E-10	5.54E-10	4.91E-10	4.52E-10	3.92E-10	3.44E-10	5.05E-10
Rb-91	1.29E-09	1.11E-09	9.87E-10	8.63E-10	7.40E-10	6.68E-10	5.56E-10	4.84E-10	8.00E-10
Sr-86	6.78E-09	2.56E-08	5.30E-08	8.90E-08	1.32E-07	1.81E-07	2.31E-07	2.83E-07	1.20E-07
Sr-87	9.11E-11	2.19E-10	3.96E-10	5.13E-10	8.26E-10	1.02E-09	1.20E-09	1.51E-09	6.74E-10
Sr-88	3.15E-05	5.52E-05	7.36E-05	8.86E-05	1.02E-04	1.13E-04	1.23E-04	1.30E-04	8.84E-05
Sr-89	2.63E-05	3.29E-05	3.29E-05	3.03E-05	2.75E-05	2.46E-05	2.16E-05	1.88E-05	2.66E-05
Sr-90	5.14E-05	8.96E-05	1.19E-04	1.43E-04	1.64E-04	1.80E-04	1.96E-04	2.06E-04	1.42E-04
Sr-91	8.00E-07	6.94E-07	6.21E-07	5.44E-07	4.69E-07	4.25E-07	3.55E-07	3.10E-07	5.04E-07
Sr-92	2.26E-07	1.97E-07	1.78E-07	1.57E-07	1.37E-07	1.24E-07	1.05E-07	9.19E-08	1.45E-07
Sr-93	1.10E-08	9.67E-09	8.82E-09	7.86E-09	6.90E-09	6.31E-09	5.38E-09	4.74E-09	7.26E-09
Sr-94	1.81E-09	1.59E-09	1.46E-09	1.30E-09	1.15E-09	1.05E-09	9.01E-10	7.95E-10	1.20E-09
Sr-95	4.99E-10	4.39E-10	4.01E-10	3.59E-10	3.16E-10	2.91E-10	2.49E-10	2.21E-10	3.32E-10
Y-88	2.68E-11	1.14E-10	2.28E-10	2.65E-10	4.87E-10	5.45E-10	5.18E-10	5.54E-10	2.90E-10
Y-89	1.60E-05	4.29E-05	6.93E-05	9.28E-05	1.14E-04	1.32E-04	1.47E-04	1.60E-04	9.57E-05
Y-90	1.29E-08	2.31E-08	3.18E-08	3.85E-08	4.55E-08	5.08E-08	5.55E-08	6.23E-08	3.89E-08
Y-91	3.45E-05	4.41E-05	4.55E-05	4.30E-05	3.96E-05	3.58E-05	3.20E-05	2.81E-05	3.74E-05
Y-91m	3.94E-08	3.42E-08	3.06E-08	2.68E-08	2.31E-08	2.09E-08	1.75E-08	1.53E-08	2.48E-08
Y-92	3.04E-07	2.66E-07	2.40E-07	2.12E-07	1.84E-07	1.68E-07	1.42E-07	1.24E-07	1.96E-07
Y-93	9.22E-07	8.12E-07	7.43E-07	6.64E-07	5.83E-07	5.34E-07	4.56E-07	4.02E-07	6.12E-07
Y-94	2.87E-08	2.55E-08	2.34E-08	2.11E-08	1.86E-08	1.71E-08	1.47E-08	1.30E-08	1.94E-08
Y-95	1.56E-08	1.40E-08	1.29E-08	1.17E-08	1.04E-08	9.65E-09	8.37E-09	7.43E-09	1.08E-08
Zr-90	1.15E-07	4.26E-07	8.93E-07	1.47E-06	2.19E-06	3.00E-06	3.87E-06	4.76E-06	2.06E-06
Zr-91	1.74E-05	4.84E-05	8.03E-05	1.09E-04	1.37E-04	1.60E-04	1.81E-04	1.97E-04	1.15E-04
Zr-92	5.39E-05	9.48E-05	1.27E-04	1.54E-04	1.79E-04	1.98E-04	2.19E-04	2.34E-04	1.56E-04
Zr-93	5.68E-05	1.00E-04	1.36E-04	1.65E-04	1.91E-04	2.12E-04	2.36E-04	2.51E-04	1.66E-04
Zr-94	5.85E-05	1.03E-04	1.41E-04	1.73E-04	2.01E-04	2.25E-04	2.51E-04	2.70E-04	1.76E-04
Zr-95	4.04E-05	5.37E-05	5.82E-05	5.67E-05	5.37E-05	4.97E-05	4.51E-05	4.13E-05	4.93E-05
Zr-96	5.75E-05	1.02E-04	1.40E-04	1.73E-04	2.02E-04	2.27E-04	2.53E-04	2.73E-04	1.76E-04
Zr-97	1.42E-06	1.31E-06	1.22E-06	1.13E-06	1.02E-06	9.52E-07	8.39E-07	7.51E-07	1.03E-06
Zr-98	6.84E-10	6.38E-10	5.98E-10	5.57E-10	5.06E-10	4.74E-10	4.22E-10	3.79E-10	5.09E-10
Zr-100	1.58E-10	1.45E-10	1.36E-10	1.26E-10	1.15E-10	1.07E-10	9.52E-11	8.57E-11	1.16E-10
Nb-94	4.77E-11	1.46E-10	2.39E-10	3.33E-10	4.00E-10	4.24E-10	4.44E-10	4.87E-10	2.97E-10
Nb-95	1.20E-05	2.30E-05	2.80E-05	2.89E-05	2.88E-05	2.78E-05	2.61E-05	2.40E-05	2.45E-05
Nb-95m	2.44E-08	3.25E-08	3.53E-08	3.43E-08	3.26E-08	3.01E-08	2.78E-08	2.51E-08	3.00E-08
Nb-96	1.10E-08	2.67E-08	3.50E-08	4.70E-08	5.53E-08	3.89E-08	4.69E-08	4.03E-08	2.83E-08

Nb-97	1.02E-07	9.45E-08	8.80E-08	8.14E-08	7.34E-08	6.87E-08	6.06E-08	5.42E-08	7.45E-08
Nb-98m	4.71E-10	4.46E-10	4.18E-10	3.87E-10	3.47E-10	3.20E-10	2.83E-10	2.47E-10	3.49E-10
Nb-99	3.38E-10	3.12E-10	2.93E-10	2.73E-10	2.48E-10	2.33E-10	2.07E-10	1.87E-10	2.50E-10
Nb-99m	2.54E-10	2.74E-10	2.69E-10	2.62E-10	2.45E-10	2.32E-10	2.15E-10	1.95E-10	2.32E-10
Nb-101	1.41E-10	1.35E-10	1.28E-10	1.22E-10	1.12E-10	1.07E-10	9.62E-11	8.74E-11	1.11E-10
Mo-94	1.74E-11	1.12E-10	2.77E-10	6.75E-10	9.72E-10	1.32E-09	1.41E-09	1.75E-09	7.62E-10
Mo-95	6.48E-06	2.92E-05	6.15E-05	9.46E-05	1.28E-04	1.59E-04	1.88E-04	2.10E-04	1.08E-04
Mo-96	1.17E-07	8.04E-07	2.12E-06	4.08E-06	7.38E-06	1.02E-05	1.41E-05	1.75E-05	6.82E-06
Mo-97	5.46E-05	9.74E-05	1.36E-04	1.69E-04	1.97E-04	2.23E-04	2.50E-04	2.70E-04	1.73E-04
Mo-98	5.28E-05	9.43E-05	1.33E-04	1.66E-04	1.96E-04	2.23E-04	2.51E-04	2.72E-04	1.71E-04
Mo-99	4.61E-06	4.58E-06	3.95E-06	3.68E-06	3.34E-06	3.07E-06	2.83E-06	2.60E-06	3.49E-06
Mo-100	5.79E-05	1.03E-04	1.47E-04	1.84E-04	2.17E-04	2.47E-04	2.78E-04	3.02E-04	1.90E-04
Mo-101	1.81E-08	1.73E-08	1.63E-08	1.56E-08	1.43E-08	1.36E-08	1.23E-08	1.12E-08	1.41E-08
Mo-102	1.15E-08	1.14E-08	1.10E-08	1.07E-08	1.00E-08	9.59E-09	8.80E-09	8.06E-09	9.68E-09
Mo-103	7.99E-10	8.86E-10	8.97E-10	8.96E-10	8.70E-10	8.50E-10	8.07E-10	7.54E-10	8.04E-10
Mo-104	4.32E-10	5.29E-10	5.64E-10	5.79E-10	5.83E-10	5.82E-10	5.67E-10	5.42E-10	5.22E-10
Mo-105	1.33E-10	1.86E-10	2.09E-10	2.24E-10	2.29E-10	2.33E-10	2.32E-10	2.25E-10	2.00E-10
Tc-97	3.61E-11	8.22E-11	1.32E-10	1.60E-10	1.80E-10	2.07E-10	2.30E-10	2.48E-10	1.47E-10
Tc-98	1.89E-10	4.44E-10	6.78E-10	1.04E-09	1.44E-09	1.62E-09	1.73E-09	1.95E-09	1.04E-09
Tc-99	5.32E-05	9.53E-05	1.32E-04	1.61E-04	1.85E-04	2.06E-04	2.25E-04	2.39E-04	1.60E-04
Tc-99m	3.68E-07	3.65E-07	3.16E-07	2.94E-07	2.67E-07	2.45E-07	2.25E-07	2.07E-07	2.79E-07
Tc-100	3.12E-11	5.49E-11	6.94E-11	8.93E-11	1.07E-10	1.17E-10	1.45E-10	1.32E-10	8.22E-11
Tc-101	1.76E-08	1.68E-08	1.59E-08	1.52E-08	1.40E-08	1.33E-08	1.19E-08	1.09E-08	1.38E-08
Tc-103	6.59E-10	7.33E-10	7.42E-10	7.41E-10	7.19E-10	7.02E-10	6.66E-10	6.23E-10	6.64E-10
Tc-104	8.33E-09	1.03E-08	1.10E-08	1.14E-08	1.14E-08	1.14E-08	1.11E-08	1.06E-08	1.02E-08
Tc-105	1.91E-09	2.86E-09	3.30E-09	3.58E-09	3.67E-09	3.73E-09	3.74E-09	3.64E-09	3.16E-09
Tc-106	8.10E-11	1.29E-10	1.65E-10	1.89E-10	2.02E-10	2.09E-10	2.15E-10	2.14E-10	1.68E-10
Ru-99	1.76E-09	3.20E-09	4.52E-09	5.62E-09	6.66E-09	7.49E-09	8.44E-09	9.18E-09	5.78E-09
Ru-100	1.74E-06	5.83E-06	1.14E-05	1.85E-05	2.69E-05	3.48E-05	4.66E-05	5.54E-05	2.45E-05
Ru-101	4.75E-05	8.49E-05	1.21E-04	1.50E-04	1.76E-04	2.00E-04	2.24E-04	2.42E-04	1.54E-04
Ru-102	4.03E-05	7.51E-05	1.09E-04	1.42E-04	1.72E-04	1.99E-04	2.28E-04	2.50E-04	1.50E-04
Ru-103	1.64E-05	2.34E-05	2.59E-05	2.63E-05	2.57E-05	2.52E-05	2.41E-05	2.35E-05	2.35E-05
Ru-104	1.92E-05	4.09E-05	6.23E-05	8.42E-05	1.05E-04	1.24E-04	1.45E-04	1.61E-04	9.16E-05
Ru-105	6.71E-08	1.01E-07	1.17E-07	1.27E-07	1.30E-07	1.32E-07	1.33E-07	1.29E-07	1.12E-07
Ru-106	6.01E-06	1.47E-05	2.36E-05	3.26E-05	4.10E-05	4.83E-05	5.49E-05	6.03E-05	3.45E-05
Ru-107	3.21E-10	5.42E-10	7.48E-10	8.83E-10	9.65E-10	1.00E-09	1.05E-09	1.05E-09	7.85E-10
Ru-108	2.30E-10	4.09E-10	5.79E-10	7.03E-10	7.87E-10	8.27E-10	8.67E-10	8.77E-10	6.31E-10
Rh-102	3.26E-11	1.15E-10	2.14E-10	3.85E-10	5.27E-10	5.77E-10	6.08E-10	6.33E-10	3.39E-10
Rh-103	1.25E-05	3.29E-05	5.39E-05	7.24E-05	8.67E-05	9.79E-05	1.09E-04	1.14E-04	7.14E-05
Rh-103m	1.61E-08	2.29E-08	2.54E-08	2.57E-08	2.52E-08	2.47E-08	2.37E-08	2.31E-08	2.30E-08
Rh-104	3.69E-11	1.13E-10	2.14E-10	2.76E-10	3.74E-10	4.12E-10	4.65E-10	5.52E-10	2.67E-10
Rh-104m	1.73E-11	5.29E-11	1.00E-10	1.29E-10	1.75E-10	1.93E-10	2.17E-10	2.58E-10	1.25E-10
Rh-105	4.18E-07	5.61E-07	6.58E-07	7.13E-07	7.38E-07	7.42E-07	7.51E-07	7.29E-07	6.41E-07
Rh-105m	5.08E-11	7.64E-11	8.82E-11	9.61E-11	9.83E-11	1.00E-10	1.00E-10	9.78E-11	8.46E-11
Rh-106m	8.20E-10	1.20E-09	1.35E-09	1.46E-09	1.61E-09	1.61E-09	1.49E-09	1.45E-09	1.27E-09
Rh-107	1.89E-09	3.19E-09	4.40E-09	5.19E-09	5.67E-09	5.89E-09	6.17E-09	6.19E-09	4.61E-09
Rh-109	4.56E-11	8.20E-11	1.16E-10	1.42E-10	1.59E-10	1.67E-10	1.75E-10	1.78E-10	1.27E-10
Pd-103	2.06E-12	9.98E-12	3.90E-11	7.77E-11	1.09E-10	1.93E-10	2.61E-10	2.72E-10	1.02E-10
Pd-104	9.01E-07	4.85E-06	1.23E-05	2.23E-05	3.51E-05	5.10E-05	6.67E-05	8.24E-05	3.37E-05
Pd-105	9.32E-06	2.18E-05	3.45E-05	4.78E-05	6.12E-05	7.33E-05	8.66E-05	9.74E-05	5.32E-05
Pd-106	2.51E-06	6.63E-06	1.22E-05	1.94E-05	2.73E-05	3.65E-05	4.74E-05	5.77E-05	2.56E-05
Pd-107	3.61E-06	1.02E-05	1.78E-05	2.65E-05	3.54E-05	4.38E-05	5.33E-05	6.11E-05	3.10E-05
Pd-108	2.04E-06	6.27E-06	1.13E-05	1.72E-05	2.38E-05	2.98E-05	3.61E-05	4.24E-05	2.05E-05
Pd-109	2.92E-08	5.92E-08	9.02E-08	1.17E-07	1.41E-07	1.63E-07	1.88E-07	2.01E-07	1.12E-07
Pd-110	6.90E-07	2.04E-06	3.67E-06	5.61E-06	7.67E-06	9.69E-06	1.20E-05	1.38E-05	6.76E-06
Pd-111	1.99E-10	3.32E-10	4.59E-10	5.50E-10	6.10E-10	6.42E-10	6.69E-10	6.78E-10	4.95E-10
Pd-112	5.60E-09	8.83E-09	1.13E-08	1.31E-08	1.40E-08	1.46E-08	1.50E-08	1.51E-08	1.16E-08
Ag-109	1.28E-06	3.75E-06	6.77E-06	9.73E-06	1.28E-05	1.61E-05	1.87E-05	2.16E-05	1.11E-05
Ag-109m	2.34E-11	4.75E-11	7.23E-11	9.42E-11	1.13E-10	1.31E-10	1.51E-10	1.61E-10	8.98E-11

Ag-110m	6.50E-09	3.07E-08	8.05E-08	1.38E-07	2.10E-07	2.80E-07	3.75E-07	4.55E-07	1.86E-07
Ag-111	7.13E-08	1.25E-07	1.62E-07	1.90E-07	1.99E-07	2.14E-07	2.22E-07	2.26E-07	1.70E-07
Ag-112	8.37E-10	1.31E-09	1.68E-09	1.94E-09	2.09E-09	2.17E-09	2.24E-09	2.24E-09	1.73E-09
Ag-113	7.94E-10	1.22E-09	1.45E-09	1.62E-09	1.71E-09	1.76E-09	1.79E-09	1.78E-09	1.45E-09
Cd-108	3.40E-12	1.22E-11	2.60E-11	5.10E-11	7.23E-11	8.86E-11	1.00E-10	1.24E-10	5.45E-11
Cd-110	1.44E-07	7.09E-07	1.93E-06	3.56E-06	5.78E-06	7.97E-06	1.16E-05	1.46E-05	5.42E-06
Cd-111	3.01E-07	9.22E-07	1.67E-06	2.57E-06	3.52E-06	4.48E-06	5.59E-06	6.49E-06	3.13E-06
Cd-112	2.01E-07	5.20E-07	8.81E-07	1.30E-06	1.73E-06	2.16E-06	2.66E-06	3.05E-06	1.53E-06
Cd-113	1.49E-08	1.81E-08	2.06E-08	2.23E-08	2.32E-08	2.32E-08	2.43E-08	2.40E-08	2.07E-08
Cd-113m	2.01E-09	4.77E-09	7.91E-09	1.14E-08	1.51E-08	1.86E-08	2.28E-08	2.62E-08	1.33E-08
Cd-114	3.04E-07	7.14E-07	1.15E-06	1.62E-06	2.09E-06	2.54E-06	3.05E-06	3.44E-06	1.83E-06
Cd-115	8.45E-09	1.03E-08	1.02E-08	1.06E-08	1.04E-08	1.04E-08	1.07E-08	1.10E-08	9.81E-09
Cd-115m	4.89E-09	7.50E-09	8.86E-09	9.39E-09	9.51E-09	9.70E-09	9.58E-09	9.60E-09	8.46E-09
Cd-116	1.45E-07	3.09E-07	4.68E-07	6.29E-07	7.76E-07	9.14E-07	1.06E-06	1.17E-06	6.76E-07
Cd-117	4.55E-10	5.87E-10	6.04E-10	6.12E-10	5.96E-10	5.80E-10	5.60E-10	5.33E-10	5.43E-10
Cd-118	1.42E-10	1.72E-10	1.72E-10	1.73E-10	1.67E-10	1.62E-10	1.55E-10	1.48E-10	1.55E-10
In-113	8.86E-12	3.84E-11	9.11E-11	1.71E-10	2.74E-10	4.07E-10	5.81E-10	7.63E-10	2.87E-10
In-115	1.04E-07	2.04E-07	2.67E-07	3.16E-07	3.49E-07	3.71E-07	3.81E-07	3.92E-07	2.90E-07
In-115m	7.05E-10	8.59E-10	8.53E-10	8.74E-10	8.69E-10	8.57E-10	8.92E-10	9.15E-10	8.16E-10
In-117	8.13E-11	1.05E-10	1.08E-10	1.10E-10	1.07E-10	1.04E-10	1.00E-10	9.54E-11	9.73E-11
In-117m	2.75E-10	3.55E-10	3.66E-10	3.71E-10	3.61E-10	3.52E-10	3.40E-10	3.23E-10	3.29E-10
Sn-115	6.05E-09	1.30E-08	1.97E-08	2.66E-08	3.27E-08	3.86E-08	4.47E-08	4.97E-08	2.85E-08
Sn-116	3.14E-08	1.06E-07	2.03E-07	3.08E-07	4.27E-07	5.49E-07	6.80E-07	7.91E-07	3.76E-07
Sn-117	1.36E-07	2.87E-07	4.30E-07	5.76E-07	7.07E-07	8.28E-07	9.60E-07	1.06E-06	6.15E-07
Sn-117m	4.27E-11	5.56E-11	6.39E-11	7.28E-11	8.05E-11	8.91E-11	9.66E-11	1.25E-10	7.31E-11
Sn-118	1.18E-07	2.44E-07	3.63E-07	4.84E-07	5.91E-07	6.97E-07	8.05E-07	8.86E-07	5.16E-07
Sn-119	1.29E-07	2.62E-07	3.87E-07	5.11E-07	6.20E-07	7.24E-07	8.33E-07	9.15E-07	5.41E-07
Sn-120	1.26E-07	2.57E-07	3.79E-07	5.01E-07	6.09E-07	7.13E-07	8.21E-07	9.05E-07	5.32E-07
Sn-121	4.54E-09	5.63E-09	5.67E-09	5.70E-09	5.50E-09	5.37E-09	5.15E-09	4.90E-09	5.08E-09
Sn-121m	7.43E-09	1.58E-08	2.38E-08	3.19E-08	3.92E-08	4.60E-08	5.33E-08	5.88E-08	3.41E-08
Sn-122	1.59E-07	3.28E-07	4.87E-07	6.46E-07	7.88E-07	9.21E-07	1.06E-06	1.17E-06	6.86E-07
Sn-123	5.96E-08	1.04E-07	1.34E-07	1.53E-07	1.62E-07	1.69E-07	1.69E-07	1.68E-07	1.39E-07
Sn-123m	8.38E-11	1.02E-10	1.02E-10	1.03E-10	9.94E-11	9.63E-11	9.21E-11	8.73E-11	9.18E-11
Sn-124	2.72E-07	5.62E-07	8.33E-07	1.10E-06	1.34E-06	1.56E-06	1.80E-06	1.97E-06	1.16E-06
Sn-125	4.40E-08	5.65E-08	5.97E-08	6.03E-08	5.82E-08	5.76E-08	5.55E-08	5.47E-08	5.45E-08
Sn-126	5.86E-07	1.24E-06	1.86E-06	2.49E-06	3.05E-06	3.57E-06	4.14E-06	4.56E-06	2.65E-06
Sn-127	4.32E-09	4.89E-09	4.89E-09	4.85E-09	4.63E-09	4.45E-09	4.19E-09	3.87E-09	4.30E-09
Sn-128	4.71E-09	4.93E-09	4.79E-09	4.67E-09	4.38E-09	4.18E-09	3.86E-09	3.52E-09	4.18E-09
Sn-129	1.53E-10	1.73E-10	1.75E-10	1.74E-10	1.68E-10	1.63E-10	1.54E-10	1.44E-10	1.55E-10
Sn-129m	3.29E-10	3.26E-10	3.11E-10	2.99E-10	2.77E-10	2.62E-10	2.39E-10	2.16E-10	2.70E-10
Sn-130	5.64E-10	5.11E-10	4.76E-10	4.39E-10	3.96E-10	3.71E-10	3.26E-10	2.95E-10	4.04E-10
Sn-130m	2.20E-10	2.02E-10	1.89E-10	1.75E-10	1.60E-10	1.50E-10	1.34E-10	1.21E-10	1.61E-10
Sn-131	1.03E-10	9.24E-11	8.59E-11	7.90E-11	7.16E-11	6.72E-11	5.92E-11	5.40E-11	7.33E-11
Sn-131m	1.02E-10	9.16E-11	8.52E-11	7.84E-11	7.11E-11	6.68E-11	5.89E-11	5.38E-11	7.27E-11
Sb-121	1.23E-07	2.53E-07	3.76E-07	4.88E-07	5.91E-07	6.83E-07	7.75E-07	8.56E-07	5.12E-07
Sb-122	4.29E-10	1.02E-09	1.67E-09	2.21E-09	3.18E-09	3.37E-09	4.43E-09	4.22E-09	2.22E-09
Sb-123	9.91E-08	2.21E-07	3.48E-07	4.80E-07	6.01E-07	7.22E-07	8.48E-07	9.50E-07	5.28E-07
Sb-124	1.41E-09	3.82E-09	6.99E-09	1.02E-08	1.44E-08	1.88E-08	2.20E-08	2.53E-08	1.24E-08
Sb-125	3.10E-07	6.66E-07	9.87E-07	1.29E-06	1.55E-06	1.77E-06	1.98E-06	2.15E-06	1.32E-06
Sb-126	4.81E-09	6.91E-09	8.63E-09	1.02E-08	1.29E-08	1.31E-08	1.40E-08	1.50E-08	9.70E-09
Sb-127	1.73E-07	2.08E-07	2.05E-07	2.02E-07	1.91E-07	1.84E-07	1.80E-07	1.77E-07	1.85E-07
Sb-128	4.45E-08	4.75E-08	4.65E-08	4.55E-08	4.28E-08	4.09E-08	3.80E-08	3.47E-08	4.06E-08
Sb-129	3.48E-08	3.96E-08	3.99E-08	3.97E-08	3.81E-08	3.68E-08	3.48E-08	3.22E-08	3.52E-08
Sb-130	7.59E-09	7.45E-09	7.09E-09	6.79E-09	6.29E-09	5.96E-09	5.41E-09	4.89E-09	6.14E-09
Sb-130m	1.42E-09	1.35E-09	1.27E-09	1.20E-09	1.10E-09	1.03E-09	9.27E-10	8.35E-10	1.09E-09
Sb-131	1.40E-08	1.31E-08	1.23E-08	1.15E-08	1.05E-08	9.93E-09	8.87E-09	8.03E-09	1.06E-08
Sb-132	1.27E-09	1.22E-09	1.16E-09	1.10E-09	1.01E-09	9.57E-10	8.64E-10	7.81E-10	9.98E-10
Sb-132m	8.43E-10	7.48E-10	6.94E-10	6.37E-10	5.76E-10	5.41E-10	4.75E-10	4.33E-10	5.92E-10
Sb-133	1.43E-09	1.25E-09	1.14E-09	1.03E-09	9.23E-10	8.61E-10	7.46E-10	6.77E-10	9.63E-10

Te-122	2.28E-09	8.53E-09	1.88E-08	3.05E-08	4.54E-08	6.33E-08	8.20E-08	1.04E-07	4.27E-08
Te-123	1.22E-11	7.15E-11	1.77E-10	3.66E-10	5.61E-10	8.83E-10	1.19E-09	1.70E-09	5.87E-10
Te-123m	7.30E-12	3.81E-11	1.08E-10	2.02E-10	3.33E-10	5.10E-10	6.85E-10	1.01E-09	3.40E-10
Te-124	4.31E-10	2.18E-09	5.75E-09	1.13E-08	1.95E-08	3.01E-08	4.34E-08	5.91E-08	2.07E-08
Te-125	5.69E-09	2.48E-08	5.80E-08	1.05E-07	1.63E-07	2.32E-07	3.20E-07	4.07E-07	1.62E-07
Te-125m	1.27E-09	4.33E-09	8.10E-09	1.20E-08	1.57E-08	1.93E-08	2.26E-08	2.51E-08	1.34E-08
Te-126	1.95E-08	4.35E-08	7.08E-08	9.67E-08	1.26E-07	1.56E-07	1.83E-07	2.19E-07	1.12E-07
Te-127	1.65E-08	1.99E-08	1.98E-08	1.95E-08	1.86E-08	1.78E-08	1.73E-08	1.70E-08	1.79E-08
Te-127m	4.15E-08	5.61E-08	6.08E-08	6.03E-08	5.92E-08	5.74E-08	5.52E-08	5.31E-08	5.50E-08
Te-128	3.36E-06	6.57E-06	9.61E-06	1.25E-05	1.51E-05	1.74E-05	2.00E-05	2.19E-05	1.31E-05
Te-129	9.18E-09	1.04E-08	1.05E-08	1.05E-08	1.01E-08	9.71E-09	9.19E-09	8.51E-09	9.29E-09
Te-129m	4.94E-10	7.45E-10	9.32E-10	1.00E-09	1.07E-09	1.14E-09	1.23E-09	1.26E-09	9.43E-10
Te-130	1.68E-05	3.04E-05	4.37E-05	5.53E-05	6.55E-05	7.49E-05	8.48E-05	9.21E-05	5.73E-05
Te-131	1.61E-08	1.54E-08	1.46E-08	1.38E-08	1.27E-08	1.20E-08	1.08E-08	9.78E-09	1.26E-08
Te-131m	9.21E-08	1.21E-07	1.26E-07	1.26E-07	1.21E-07	1.18E-07	1.13E-07	1.06E-07	1.10E-07
Te-132	3.76E-06	3.80E-06	3.33E-06	3.13E-06	2.85E-06	2.64E-06	2.43E-06	2.26E-06	2.95E-06
Te-133	1.21E-08	1.11E-08	1.04E-08	9.61E-09	8.73E-09	8.19E-09	7.25E-09	6.55E-09	8.83E-09
Te-133m	3.94E-08	3.66E-08	3.43E-08	3.20E-08	2.91E-08	2.73E-08	2.42E-08	2.18E-08	2.92E-08
Te-134	6.94E-08	6.18E-08	5.73E-08	5.23E-08	4.70E-08	4.38E-08	3.82E-08	3.44E-08	4.83E-08
Te-135	2.52E-10	2.24E-10	2.08E-10	1.91E-10	1.73E-10	1.62E-10	1.42E-10	1.29E-10	1.77E-10
I-127	1.42E-06	3.02E-06	4.56E-06	6.00E-06	7.29E-06	8.45E-06	9.64E-06	1.06E-05	6.30E-06
I-128	6.14E-11	1.37E-10	2.00E-10	2.98E-10	3.67E-10	4.35E-10	5.24E-10	5.66E-10	2.79E-10
I-129	5.29E-06	1.06E-05	1.55E-05	2.03E-05	2.45E-05	2.84E-05	3.24E-05	3.53E-05	2.13E-05
I-130	1.09E-09	2.51E-09	3.87E-09	5.39E-09	6.40E-09	7.82E-09	8.83E-09	1.04E-08	5.23E-09
I-131	5.51E-06	5.68E-06	5.14E-06	4.91E-06	4.46E-06	4.18E-06	3.82E-06	3.54E-06	4.56E-06
I-132	1.13E-07	1.15E-07	1.01E-07	9.53E-08	8.71E-08	8.07E-08	7.45E-08	6.93E-08	8.98E-08
I-132m	3.25E-10	5.18E-10	6.41E-10	6.89E-10	6.96E-10	6.94E-10	7.08E-10	6.86E-10	5.95E-10
I-133	1.91E-06	1.82E-06	1.71E-06	1.61E-06	1.46E-06	1.38E-06	1.24E-06	1.11E-06	1.46E-06
I-134	9.80E-08	9.07E-08	8.50E-08	7.92E-08	7.21E-08	6.77E-08	6.02E-08	5.42E-08	7.25E-08
I-134m	3.10E-10	3.81E-10	3.95E-10	3.98E-10	3.87E-10	3.76E-10	3.61E-10	3.36E-10	3.51E-10
I-135	5.92E-07	5.56E-07	5.24E-07	4.93E-07	4.51E-07	4.26E-07	3.81E-07	3.45E-07	4.50E-07
I-136	8.81E-10	7.86E-10	7.32E-10	6.75E-10	6.15E-10	5.80E-10	5.12E-10	4.70E-10	6.28E-10
I-136m	2.34E-10	2.29E-10	2.19E-10	2.11E-10	1.98E-10	1.90E-10	1.74E-10	1.59E-10	1.92E-10
I-137	2.98E-10	2.70E-10	2.53E-10	2.35E-10	2.15E-10	2.03E-10	1.80E-10	1.64E-10	2.17E-10
Xe-128	2.46E-08	9.20E-08	1.95E-07	3.34E-07	5.17E-07	6.86E-07	9.18E-07	1.16E-06	4.74E-07
Xe-129	3.03E-11	1.97E-10	6.42E-10	1.52E-09	2.63E-09	4.43E-09	6.79E-09	9.26E-09	3.06E-09
Xe-129m	1.47E-12	7.69E-12	2.00E-11	3.49E-11	5.24E-11	7.66E-11	1.03E-10	1.41E-10	4.66E-11
Xe-130	4.05E-08	1.50E-07	3.15E-07	5.52E-07	8.07E-07	1.13E-06	1.53E-06	1.93E-06	7.86E-07
Xe-131	2.25E-05	4.20E-05	5.84E-05	7.01E-05	7.89E-05	8.53E-05	9.08E-05	9.30E-05	6.66E-05
Xe-131m	7.94E-08	8.64E-08	8.08E-08	7.63E-08	6.99E-08	6.48E-08	6.03E-08	5.62E-08	7.07E-08
Xe-132	3.92E-05	7.70E-05	1.15E-04	1.51E-04	1.85E-04	2.17E-04	2.53E-04	2.78E-04	1.62E-04
Xe-133	8.82E-06	8.75E-06	7.68E-06	7.22E-06	6.52E-06	6.08E-06	5.50E-06	5.01E-06	6.81E-06
Xe-133m	4.33E-08	4.53E-08	4.05E-08	4.02E-08	3.78E-08	3.87E-08	3.73E-08	3.96E-08	3.85E-08
Xe-134	7.25E-05	1.29E-04	1.82E-04	2.27E-04	2.67E-04	3.04E-04	3.42E-04	3.71E-04	2.34E-04
Xe-135	9.68E-08	9.04E-08	8.66E-08	7.97E-08	7.54E-08	7.22E-08	6.71E-08	6.30E-08	7.63E-08
Xe-135m	2.93E-09	3.02E-09	2.92E-09	2.84E-09	2.66E-09	2.53E-09	2.33E-09	2.12E-09	2.55E-09
Xe-136	1.12E-04	2.00E-04	2.83E-04	3.54E-04	4.16E-04	4.75E-04	5.37E-04	5.85E-04	3.66E-04
Xe-137	5.58E-09	5.19E-09	4.88E-09	4.56E-09	4.17E-09	3.92E-09	3.50E-09	3.16E-09	4.18E-09
Xe-138	2.11E-08	1.92E-08	1.79E-08	1.65E-08	1.50E-08	1.40E-08	1.24E-08	1.11E-08	1.52E-08
Xe-139	7.93E-10	7.00E-10	6.46E-10	5.87E-10	5.25E-10	4.89E-10	4.26E-10	3.83E-10	5.44E-10
Xe-140	1.97E-10	1.71E-10	1.55E-10	1.38E-10	1.22E-10	1.13E-10	9.68E-11	8.69E-11	1.29E-10
Cs-131	3.08E-11	7.55E-11	1.24E-10	1.49E-10	1.68E-10	1.95E-10	2.15E-10	2.20E-10	1.01E-10
Cs-132	1.46E-10	3.75E-10	5.58E-10	8.25E-10	7.80E-10	9.80E-10	1.12E-09	1.00E-09	5.63E-10
Cs-133	5.51E-05	1.01E-04	1.42E-04	1.73E-04	1.98E-04	2.20E-04	2.40E-04	2.55E-04	1.71E-04
Cs-134	2.12E-06	6.95E-06	1.32E-05	2.29E-05	3.00E-05	3.82E-05	4.80E-05	5.54E-05	2.60E-05
Cs-134m	2.64E-09	5.26E-09	7.20E-09	8.29E-09	1.02E-08	1.11E-08	1.26E-08	1.34E-08	7.91E-09
Cs-135	8.66E-06	1.65E-05	2.40E-05	3.12E-05	3.80E-05	4.48E-05	5.12E-05	5.78E-05	3.37E-05
Cs-136	4.70E-08	9.83E-08	1.34E-07	1.75E-07	2.18E-07	2.43E-07	2.83E-07	3.08E-07	1.82E-07
Cs-137	5.67E-05	1.01E-04	1.44E-04	1.80E-04	2.11E-04	2.40E-04	2.71E-04	2.93E-04	1.85E-04

Cs-138	5.35E-08	4.91E-08	4.59E-08	4.26E-08	3.86E-08	3.62E-08	3.20E-08	2.88E-08	3.90E-08
Cs-138m	1.57E-10	1.80E-10	1.81E-10	1.80E-10	1.71E-10	1.65E-10	1.55E-10	1.43E-10	1.58E-10
Cs-139	1.40E-08	1.28E-08	1.19E-08	1.10E-08	1.00E-08	9.37E-09	8.27E-09	7.45E-09	1.01E-08
Cs-140	1.45E-09	1.29E-09	1.19E-09	1.09E-09	9.79E-10	9.13E-10	7.97E-10	7.18E-10	1.01E-09
Cs-141	4.11E-10	3.73E-10	3.48E-10	3.21E-10	2.90E-10	2.72E-10	2.40E-10	2.16E-10	2.95E-10
Ba-134	4.64E-08	2.93E-07	8.69E-07	1.87E-06	3.44E-06	5.36E-06	7.69E-06	1.07E-05	3.66E-06
Ba-135	9.42E-11	9.72E-10	3.96E-09	1.05E-08	2.41E-08	4.51E-08	6.97E-08	1.17E-07	3.24E-08
Ba-135m	1.97E-12	1.14E-11	3.54E-11	8.80E-11	1.62E-10	2.42E-10	3.71E-10	6.28E-10	1.66E-10
Ba-136	1.31E-07	4.28E-07	8.38E-07	1.33E-06	1.85E-06	2.49E-06	3.13E-06	3.84E-06	1.71E-06
Ba-137	1.35E-07	4.70E-07	9.86E-07	1.66E-06	2.47E-06	3.39E-06	4.56E-06	5.71E-06	2.38E-06
Ba-138	6.17E-05	1.10E-04	1.54E-04	1.91E-04	2.24E-04	2.55E-04	2.86E-04	3.10E-04	1.97E-04
Ba-139	1.27E-07	1.16E-07	1.09E-07	1.01E-07	9.14E-08	8.56E-08	7.57E-08	6.82E-08	9.25E-08
Ba-140	1.66E-05	1.68E-05	1.52E-05	1.40E-05	1.25E-05	1.15E-05	1.05E-05	9.58E-06	1.31E-05
Ba-141	2.54E-08	2.33E-08	2.17E-08	2.01E-08	1.81E-08	1.69E-08	1.49E-08	1.34E-08	1.84E-08
Ba-142	1.45E-08	1.32E-08	1.22E-08	1.12E-08	1.01E-08	9.40E-09	8.24E-09	7.38E-09	1.03E-08
Ba-143	3.19E-10	2.82E-10	2.60E-10	2.36E-10	2.10E-10	1.95E-10	1.69E-10	1.51E-10	2.18E-10
Ba-144	2.00E-10	1.75E-10	1.60E-10	1.43E-10	1.27E-10	1.18E-10	1.01E-10	9.03E-11	1.33E-10
La-137	2.88E-11	6.12E-11	1.03E-10	1.30E-10	1.50E-10	1.77E-10	2.05E-10	2.10E-10	1.23E-10
La-138	5.09E-10	1.01E-09	1.41E-09	2.08E-09	2.58E-09	2.98E-09	3.16E-09	3.39E-09	2.03E-09
La-139	5.83E-05	1.03E-04	1.44E-04	1.79E-04	2.09E-04	2.37E-04	2.65E-04	2.87E-04	1.83E-04
La-140	2.16E-06	2.20E-06	2.00E-06	1.87E-06	1.71E-06	1.53E-06	1.41E-06	1.32E-06	1.75E-06
La-141	3.28E-07	3.01E-07	2.81E-07	2.60E-07	2.35E-07	2.20E-07	1.94E-07	1.73E-07	2.38E-07
La-142	1.27E-07	1.16E-07	1.08E-07	9.91E-08	8.92E-08	8.32E-08	7.31E-08	6.54E-08	9.09E-08
La-143	2.00E-08	1.80E-08	1.67E-08	1.52E-08	1.36E-08	1.26E-08	1.10E-08	9.83E-09	1.40E-08
La-144	8.84E-10	7.85E-10	7.24E-10	6.57E-10	5.85E-10	5.42E-10	4.70E-10	4.20E-10	6.06E-10
La-145	3.79E-10	3.36E-10	3.10E-10	2.81E-10	2.51E-10	2.33E-10	2.02E-10	1.81E-10	2.60E-10
Ce-138	2.81E-11	8.38E-11	1.47E-10	1.79E-10	2.11E-10	2.53E-10	2.93E-10	3.03E-10	1.73E-10
Ce-139	1.55E-10	4.30E-10	7.00E-10	1.21E-09	1.52E-09	1.67E-09	1.93E-09	1.90E-09	1.03E-09
Ce-140	4.28E-05	8.92E-05	1.30E-04	1.66E-04	1.97E-04	2.27E-04	2.57E-04	2.80E-04	1.72E-04
Ce-141	2.70E-05	3.27E-05	3.18E-05	2.98E-05	2.69E-05	2.50E-05	2.24E-05	2.08E-05	2.67E-05
Ce-142	5.36E-05	9.53E-05	1.34E-04	1.65E-04	1.93E-04	2.19E-04	2.45E-04	2.65E-04	1.69E-04
Ce-143	2.42E-06	2.28E-06	2.10E-06	1.92E-06	1.71E-06	1.60E-06	1.41E-06	1.25E-06	1.76E-06
Ce-144	4.55E-05	7.39E-05	9.38E-05	1.06E-04	1.14E-04	1.19E-04	1.21E-04	1.21E-04	9.84E-05
Ce-145	2.82E-09	2.54E-09	2.36E-09	2.16E-09	1.94E-09	1.81E-09	1.58E-09	1.41E-09	1.98E-09
Ce-146	9.65E-09	8.76E-09	8.16E-09	7.51E-09	6.78E-09	6.33E-09	5.57E-09	5.01E-09	6.91E-09
Ce-147	4.23E-10	3.95E-10	3.71E-10	3.49E-10	3.20E-10	3.02E-10	2.70E-10	2.45E-10	3.19E-10
Ce-148	3.54E-10	3.14E-10	2.91E-10	2.66E-10	2.40E-10	2.25E-10	1.97E-10	1.79E-10	2.47E-10
Pr-141	2.67E-05	6.62E-05	1.03E-04	1.38E-04	1.67E-04	1.93E-04	2.20E-04	2.40E-04	1.43E-04
Pr-142	5.57E-09	1.39E-08	2.39E-08	3.15E-08	4.02E-08	4.69E-08	5.21E-08	5.94E-08	3.08E-08
Pr-142m	2.59E-11	6.38E-11	1.09E-10	1.43E-10	1.83E-10	2.13E-10	2.37E-10	2.69E-10	1.40E-10
Pr-143	1.62E-05	1.63E-05	1.47E-05	1.35E-05	1.19E-05	1.08E-05	9.81E-06	8.89E-06	1.25E-05
Pr-144	2.11E-09	3.22E-09	4.07E-09	4.61E-09	4.94E-09	5.19E-09	5.28E-09	5.28E-09	4.26E-09
Pr-144m	1.55E-10	1.74E-10	1.69E-10	1.52E-10	1.45E-10	1.25E-10	1.29E-10	1.05E-10	1.23E-10
Pr-145	3.37E-07	3.04E-07	2.82E-07	2.58E-07	2.32E-07	2.16E-07	1.89E-07	1.69E-07	2.37E-07
Pr-146	1.73E-08	1.57E-08	1.46E-08	1.35E-08	1.21E-08	1.13E-08	9.99E-09	8.98E-09	1.24E-08
Pr-147	7.18E-09	6.59E-09	6.16E-09	5.72E-09	5.20E-09	4.88E-09	4.32E-09	3.90E-09	5.25E-09
Pr-148	8.92E-10	8.10E-10	7.57E-10	7.01E-10	6.37E-10	5.99E-10	5.31E-10	4.81E-10	6.46E-10
Pr-149	5.80E-10	5.49E-10	5.19E-10	4.93E-10	4.56E-10	4.33E-10	3.91E-10	3.57E-10	4.51E-10
Nd-142	6.51E-08	3.39E-07	8.36E-07	1.53E-06	2.36E-06	3.35E-06	4.48E-06	5.78E-06	2.29E-06
Nd-143	3.81E-05	7.49E-05	1.02E-04	1.24E-04	1.40E-04	1.53E-04	1.61E-04	1.67E-04	1.19E-04
Nd-144	6.36E-06	2.30E-05	4.60E-05	7.26E-05	1.05E-04	1.37E-04	1.74E-04	2.06E-04	9.39E-05
Nd-145	3.50E-05	6.09E-05	8.27E-05	9.90E-05	1.14E-04	1.25E-04	1.36E-04	1.44E-04	9.83E-05
Nd-146	2.78E-05	5.06E-05	7.24E-05	9.24E-05	1.12E-04	1.30E-04	1.49E-04	1.64E-04	9.85E-05
Nd-147	5.18E-06	5.19E-06	4.64E-06	4.33E-06	3.92E-06	3.60E-06	3.28E-06	3.01E-06	4.06E-06
Nd-148	1.61E-05	2.87E-05	4.07E-05	5.07E-05	5.95E-05	6.77E-05	7.63E-05	8.25E-05	5.22E-05
Nd-149	2.68E-08	2.56E-08	2.42E-08	2.31E-08	2.17E-08	2.06E-08	1.85E-08	1.73E-08	2.12E-08
Nd-150	6.11E-06	1.13E-05	1.64E-05	2.11E-05	2.53E-05	2.92E-05	3.31E-05	3.64E-05	2.21E-05
Nd-151	1.25E-09	1.30E-09	1.28E-09	1.26E-09	1.21E-09	1.18E-09	1.16E-09	1.05E-09	1.15E-09
Nd-152	7.24E-10	7.83E-10	7.91E-10	7.90E-10	7.71E-10	7.57E-10	7.19E-10	6.74E-10	7.15E-10

Pm-145	2.14E-11	4.44E-11	6.32E-11	7.94E-11	8.77E-11	9.30E-11	9.29E-11	1.17E-10	7.02E-11
Pm-146	7.75E-11	1.91E-10	3.34E-10	4.31E-10	6.03E-10	6.29E-10	6.46E-10	6.55E-10	4.14E-10
Pm-147	1.49E-05	2.68E-05	3.40E-05	3.74E-05	3.91E-05	3.99E-05	3.98E-05	3.87E-05	3.32E-05
Pm-148	3.35E-07	6.42E-07	8.94E-07	1.02E-06	1.07E-06	1.15E-06	1.09E-06	1.03E-06	8.35E-07
Pm-148m	2.73E-07	4.90E-07	6.43E-07	6.98E-07	7.34E-07	7.79E-07	7.53E-07	6.98E-07	5.85E-07
Pm-149	6.66E-07	7.64E-07	8.32E-07	8.70E-07	8.76E-07	8.19E-07	7.98E-07	7.72E-07	7.68E-07
Pm-150	2.13E-09	2.44E-09	2.63E-09	2.68E-09	2.98E-09	2.75E-09	2.56E-09	2.58E-09	2.21E-09
Pm-151	1.50E-07	1.66E-07	1.62E-07	1.62E-07	1.55E-07	1.50E-07	1.47E-07	1.35E-07	1.47E-07
Pm-152	2.77E-10	2.88E-10	2.97E-10	2.91E-10	2.84E-10	2.84E-10	2.64E-10	2.48E-10	2.63E-10
Pm-153	2.00E-10	2.23E-10	2.30E-10	2.32E-10	2.30E-10	2.29E-10	2.19E-10	2.08E-10	2.11E-10
Sm-146	1.38E-12	7.67E-12	1.97E-11	3.73E-11	6.28E-11	8.06E-11	9.47E-11	1.16E-10	4.80E-11
Sm-147	3.19E-07	1.23E-06	2.47E-06	3.83E-06	5.17E-06	6.43E-06	7.59E-06	8.68E-06	4.35E-06
Sm-148	1.07E-06	4.14E-06	8.33E-06	1.28E-05	1.78E-05	2.29E-05	2.89E-05	3.31E-05	1.56E-05
Sm-149	7.13E-07	7.85E-07	8.59E-07	8.51E-07	8.72E-07	8.29E-07	8.86E-07	7.92E-07	7.85E-07
Sm-150	9.48E-06	1.96E-05	2.94E-05	3.89E-05	4.67E-05	5.42E-05	6.14E-05	6.62E-05	4.00E-05
Sm-151	1.64E-06	2.11E-06	2.39E-06	2.63E-06	2.86E-06	3.22E-06	3.22E-06	3.35E-06	2.61E-06
Sm-152	4.86E-06	9.82E-06	1.35E-05	1.65E-05	1.83E-05	2.02E-05	2.21E-05	2.28E-05	1.58E-05
Sm-153	2.61E-07	5.02E-07	6.55E-07	8.11E-07	9.10E-07	9.36E-07	9.75E-07	1.03E-06	7.02E-07
Sm-154	8.51E-07	1.88E-06	3.00E-06	4.10E-06	5.13E-06	6.30E-06	7.34E-06	8.31E-06	4.54E-06
Sm-155	1.79E-10	2.81E-10	3.10E-10	3.53E-10	3.63E-10	4.01E-10	4.25E-10	4.55E-10	3.24E-10
Sm-156	2.54E-09	4.03E-09	4.99E-09	5.64E-09	5.94E-09	6.14E-09	6.27E-09	6.21E-09	4.99E-09
Eu-151	7.33E-10	1.20E-09	1.41E-09	1.58E-09	1.69E-09	1.78E-09	1.88E-09	1.93E-09	1.48E-09
Eu-152	5.41E-10	1.28E-09	1.70E-09	2.00E-09	2.17E-09	2.32E-09	2.49E-09	2.61E-09	1.85E-09
Eu-153	2.40E-06	5.92E-06	9.90E-06	1.38E-05	1.72E-05	2.08E-05	2.37E-05	2.66E-05	1.47E-05
Eu-154	2.05E-07	7.94E-07	1.60E-06	2.48E-06	3.48E-06	4.45E-06	5.22E-06	5.94E-06	2.95E-06
Eu-154m	9.16E-12	2.94E-11	5.60E-11	6.67E-11	9.06E-11	1.09E-10	1.42E-10	1.65E-10	7.50E-11
Eu-155	1.54E-07	3.15E-07	5.81E-07	8.44E-07	1.14E-06	1.41E-06	1.74E-06	2.09E-06	9.95E-07
Eu-156	1.88E-07	3.81E-07	6.38E-07	9.79E-07	1.34E-06	1.73E-06	1.94E-06	2.27E-06	1.13E-06
Eu-157	7.70E-09	1.58E-08	2.05E-08	3.30E-08	4.18E-08	4.99E-08	5.95E-08	6.71E-08	3.17E-08
Eu-158	5.97E-11	9.80E-11	1.34E-10	1.62E-10	1.79E-10	1.88E-10	1.96E-10	1.98E-10	1.45E-10
Gd-154	1.08E-09	7.77E-09	2.28E-08	5.03E-08	8.55E-08	1.33E-07	1.91E-07	2.55E-07	9.07E-08
Gd-155	7.88E-10	1.84E-09	3.38E-09	5.35E-09	7.44E-09	9.50E-09	1.21E-08	1.45E-08	6.40E-09
Gd-156	3.39E-07	1.19E-06	2.64E-06	4.75E-06	7.61E-06	1.12E-05	1.63E-05	2.04E-05	7.81E-06
Gd-157	2.07E-08	4.01E-08	5.95E-08	7.19E-08	9.87E-08	1.16E-07	1.24E-07	1.81E-07	7.55E-08
Gd-158	2.01E-07	5.52E-07	1.06E-06	1.66E-06	2.34E-06	3.22E-06	4.31E-06	5.31E-06	2.26E-06
Gd-159	6.59E-10	1.35E-09	2.03E-09	2.90E-09	3.69E-09	4.46E-09	6.11E-09	6.67E-09	3.12E-09
Gd-160	9.87E-09	2.98E-08	5.41E-08	8.31E-08	1.14E-07	1.45E-07	1.80E-07	2.07E-07	1.01E-07
Tb-159	2.35E-08	7.07E-08	1.29E-07	1.99E-07	2.74E-07	3.57E-07	4.55E-07	5.34E-07	2.48E-07
Tb-160	6.51E-10	2.60E-09	5.52E-09	9.58E-09	1.40E-08	1.84E-08	2.35E-08	2.91E-08	1.23E-08
Tb-161	8.95E-10	1.78E-09	2.60E-09	3.24E-09	3.92E-09	4.63E-09	5.50E-09	5.90E-09	3.40E-09
Dy-160	1.53E-10	1.00E-09	3.01E-09	6.60E-09	1.16E-08	1.83E-08	2.88E-08	3.72E-08	1.29E-08
Dy-161	3.37E-09	1.09E-08	2.01E-08	3.05E-08	4.16E-08	5.40E-08	6.70E-08	7.89E-08	3.75E-08
Dy-162	1.86E-09	5.87E-09	1.13E-08	1.76E-08	2.49E-08	3.24E-08	4.10E-08	4.98E-08	2.25E-08
Dy-163	9.53E-10	3.42E-09	7.24E-09	1.23E-08	1.77E-08	2.52E-08	3.18E-08	4.16E-08	1.71E-08
Dy-164	2.92E-10	9.82E-10	1.99E-09	3.18E-09	4.96E-09	6.83E-09	9.11E-09	1.19E-08	4.75E-09
Ho-165	1.68E-10	7.19E-10	1.69E-09	3.21E-09	5.37E-09	8.48E-09	1.24E-08	1.76E-08	6.02E-09
Ho-166	2.46E-12	6.81E-12	1.32E-11	2.27E-11	3.67E-11	5.55E-11	7.59E-11	1.17E-10	3.60E-11
Er-166	5.41E-11	2.02E-10	4.40E-10	8.16E-10	1.32E-09	2.21E-09	3.20E-09	4.69E-09	1.56E-09
Er-167	1.10E-11	2.37E-11	3.56E-11	4.79E-11	6.31E-11	9.32E-11	1.25E-10	1.71E-10	6.79E-11
Er-168	1.09E-11	3.99E-11	8.34E-11	1.42E-10	2.15E-10	3.03E-10	4.39E-10	5.72E-10	2.19E-10
U-233	3.65E-09	2.80E-09	2.33E-09	2.48E-09	2.21E-09	1.82E-09	1.60E-09	1.35E-09	2.07E-09
U-234	4.66E-08	5.90E-08	6.69E-08	7.46E-08	8.36E-08	9.85E-08	1.24E-07	1.60E-07	8.59E-08
U-235	4.63E-03	3.96E-03	3.35E-03	2.85E-03	2.40E-03	2.03E-03	1.71E-03	1.43E-03	2.78E-03
U-236	1.95E-04	3.36E-04	4.39E-04	5.14E-04	5.70E-04	6.11E-04	6.42E-04	6.62E-04	4.91E-04
U-237	2.18E-06	3.57E-06	5.07E-06	5.58E-06	6.05E-06	6.64E-06	6.93E-06	7.31E-06	5.00E-06
U-238	1.90E-02	1.88E-02	1.87E-02	1.85E-02	1.83E-02	1.82E-02	1.80E-02	1.78E-02	1.84E-02
U-239	2.12E-07	2.17E-07	2.08E-07	2.15E-07	2.07E-07	1.99E-07	2.06E-07	2.03E-07	1.96E-07
U-240	2.91E-10	3.15E-10	2.57E-10	2.41E-10	2.75E-10	2.71E-10	2.44E-10	2.64E-10	2.40E-10
Np-236	8.91E-12	2.47E-11	6.12E-11	1.05E-10	1.54E-10	1.77E-10	2.21E-10	2.62E-10	1.03E-10

Np-237	5.88E-06	1.74E-05	2.93E-05	4.40E-05	5.61E-05	6.88E-05	7.98E-05	9.01E-05	4.74E-05
Np-238	3.56E-08	1.34E-07	2.43E-07	4.16E-07	5.62E-07	7.06E-07	9.00E-07	1.05E-06	4.82E-07
Np-239	2.81E-05	2.76E-05	2.71E-05	2.70E-05	2.74E-05	2.57E-05	2.71E-05	2.58E-05	2.57E-05
Np-240	1.19E-09	1.24E-09	1.19E-09	1.16E-09	1.15E-09	1.12E-09	1.27E-09	1.13E-09	1.08E-09
Np-240m	2.47E-10	2.57E-10	2.46E-10	2.41E-10	2.37E-10	2.32E-10	2.64E-10	2.34E-10	2.24E-10
Pu-237	1.15E-10	1.52E-10	1.94E-10	1.94E-10	2.04E-10	2.25E-10	2.18E-10	2.36E-10	1.62E-10
Pu-238	2.65E-07	1.81E-06	4.80E-06	9.15E-06	1.52E-05	2.21E-05	3.26E-05	4.00E-05	1.50E-05
Pu-239	2.29E-04	3.09E-04	3.44E-04	3.51E-04	3.63E-04	3.57E-04	3.58E-04	3.55E-04	3.28E-04
Pu-240	3.42E-05	7.95E-05	1.14E-04	1.32E-04	1.49E-04	1.52E-04	1.54E-04	1.54E-04	1.18E-04
Pu-241	1.33E-05	5.11E-05	8.54E-05	1.16E-04	1.38E-04	1.51E-04	1.61E-04	1.63E-04	1.07E-04
Pu-242	7.51E-07	6.56E-06	1.73E-05	3.37E-05	5.17E-05	6.90E-05	9.06E-05	1.07E-04	4.56E-05
Pu-243	2.53E-09	2.10E-08	5.56E-08	1.01E-07	1.50E-07	1.81E-07	2.39E-07	2.55E-07	1.12E-07
Pu-244	1.31E-11	2.41E-10	9.58E-10	2.33E-09	5.85E-09	9.49E-09	1.29E-08	1.74E-08	5.63E-09
Am-241	3.66E-08	2.40E-07	5.94E-07	1.04E-06	1.45E-06	1.85E-06	2.13E-06	2.36E-06	1.19E-06
Am-242	2.35E-10	1.61E-09	4.28E-09	9.13E-09	1.41E-08	1.98E-08	2.38E-08	2.65E-08	1.16E-08
Am-242m	2.29E-10	2.36E-09	7.20E-09	1.40E-08	2.07E-08	2.72E-08	3.24E-08	3.67E-08	1.72E-08
Am-243	5.24E-08	6.94E-07	2.71E-06	6.46E-06	1.33E-05	1.77E-05	2.38E-05	3.02E-05	1.12E-05
Am-244	1.02E-11	1.94E-10	7.06E-10	1.82E-09	3.15E-09	5.21E-09	8.15E-09	1.04E-08	3.18E-09
Am-244m	6.77E-12	1.27E-10	4.59E-10	1.18E-09	2.06E-09	3.36E-09	5.30E-09	6.73E-09	2.07E-09
Cm-242	2.87E-09	4.35E-08	1.74E-07	4.10E-07	7.41E-07	1.09E-06	1.47E-06	1.83E-06	7.09E-07
Cm-243	1.57E-11	4.32E-10	2.60E-09	9.43E-09	1.67E-08	3.01E-08	4.49E-08	6.11E-08	1.96E-08
Cm-244	2.96E-09	7.07E-08	4.09E-07	1.46E-06	3.37E-06	7.26E-06	1.00E-05	1.46E-05	4.16E-06
Cm-245	5.84E-11	3.44E-09	2.45E-08	8.31E-08	2.80E-07	5.38E-07	9.26E-07	1.53E-06	3.98E-07
Cm-246	4.05E-13	4.52E-11	5.54E-10	3.27E-09	1.24E-08	3.21E-08	7.76E-08	1.48E-07	3.15E-08
Cm-247	1.16E-15	2.16E-13	3.97E-12	2.69E-11	1.19E-10	3.94E-10	9.30E-10	2.42E-09	4.57E-10
Cm-248	1.11E-17	3.85E-15	1.10E-13	1.05E-12	6.38E-12	2.59E-11	7.03E-11	1.93E-10	3.47E-11

C.Discharged gFHR pebble content

The equilibrium discharged data for $1.5x10^6$ pebbles from the gFHR model with discrete motion in Chapter 6.1 is compiled in this appendix. The minimum, average, and maximum values are calculated per pass, along with a global average for each field. Please note that the minimum and maximum values are not derived from a single pebble but are extracted from all pebbles. The pass 8 data can be considered as spent fuel composition.

Minimum content

General fields

Pass #	1	2	3	4	5	6	7	8	Avg
Residence time [days]	65.25	130.5	195.75	261	326.25	391.5	456.75	522	291.17
Pass burnup [MWd/kg$_{HM}$]	23.15	20.33	17.77	16.04	14.26	12.75	10.94	10.52	16.19
Burnup [MWd/kg$_{HM}$]	23.15	46.3	68.49	89.22	107.94	124.6	141.35	155.94	95.18
Thermal fluence [n/cm^2]	5.55E+20	1.13E+21	1.70E+21	2.29E+21	2.87E+21	3.46E+21	4.05E+21	4.64E+21	2.61E+21
Thermal fluence uncertainty	2.43%	2.48%	2.53%	2.54%	2.52%	2.56%	2.57%	2.56%	2.57%
Fast fluence [n/cm^2]	2.76E+20	5.73E+20	8.72E+20	1.20E+21	1.64E+21	2.01E+21	2.44E+21	2.90E+21	1.55E+21
Fast fluence uncertainty	3.05%	3.14%	3.18%	3.21%	3.22%	3.26%	3.27%	3.29%	3.24%

Atomic densities [at/b.cm]

Pass #	1	2	3	4	5	6	7	8	Avg
He-4	2.93E-09	2.26E-08	6.37E-08	1.39E-07	2.34E-07	4.12E-07	6.52E-07	9.45E-07	3.29E-07
C-12	1.17E-02	1.17E-02	1.17E-02	1.17E-02	1.17E-02	1.17E-02	1.17E-02	1.17E-02	1.17E-02
C-13	1.25E-04	1.25E-04	1.25E-04	1.25E-04	1.25E-04	1.25E-04	1.25E-04	1.25E-04	1.25E-04
O-16	3.55E-02	3.55E-02	3.55E-02	3.55E-02	3.55E-02	3.55E-02	3.55E-02	3.55E-02	3.55E-02
O-17	1.53E-09	3.16E-09	4.80E-09	6.46E-09	8.13E-09	9.81E-09	1.15E-08	1.33E-08	7.43E-09
Zn-70	3.04E-11	7.01E-11	1.11E-10	1.52E-10	1.93E-10	2.32E-10	2.68E-10	3.08E-10	1.73E-10
Ga-69	1.29E-11	2.86E-11	4.47E-11	5.95E-11	7.45E-11	8.75E-11	1.00E-10	1.14E-10	6.64E-11
Ga-71	6.49E-11	1.47E-10	2.33E-10	3.18E-10	4.00E-10	4.87E-10	5.65E-10	6.49E-10	3.64E-10
Ge-72	1.89E-10	4.31E-10	6.86E-10	9.27E-10	1.16E-09	1.39E-09	1.60E-09	1.82E-09	1.04E-09
Ge-73	6.69E-10	1.40E-09	2.13E-09	2.81E-09	3.43E-09	4.00E-09	4.55E-09	5.03E-09	3.03E-09
Ge-74	2.13E-09	4.37E-09	6.58E-09	8.65E-09	1.06E-08	1.23E-08	1.40E-08	1.55E-08	9.35E-09
Ge-76	1.81E-08	3.60E-08	5.28E-08	6.82E-08	8.18E-08	9.37E-08	1.05E-07	1.16E-07	7.19E-08
Ge-77	1.87E-10	1.58E-10	1.35E-10	1.22E-10	1.07E-10	9.48E-11	7.77E-11	5.86E-11	1.35E-10
As-75	6.31E-09	1.27E-08	1.86E-08	2.42E-08	2.90E-08	3.34E-08	3.73E-08	4.10E-08	2.55E-08
As-77	7.63E-10	6.58E-10	5.27E-10	4.83E-10	4.40E-10	3.90E-10	3.29E-10	2.72E-10	5.37E-10
Se-76	1.21E-11	5.97E-11	1.45E-10	2.60E-10	4.46E-10	6.47E-10	8.29E-10	1.05E-09	4.66E-10
Se-77	4.44E-08	8.89E-08	1.30E-07	1.67E-07	1.99E-07	2.27E-07	2.52E-07	2.75E-07	1.74E-07
Se-78	1.20E-07	2.40E-07	3.52E-07	4.57E-07	5.50E-07	6.32E-07	7.14E-07	7.86E-07	4.84E-07
Se-79	2.55E-07	5.04E-07	7.34E-07	9.40E-07	1.12E-06	1.27E-06	1.41E-06	1.53E-06	9.77E-07
Se-80	7.29E-07	1.44E-06	2.10E-06	2.71E-06	3.24E-06	3.72E-06	4.16E-06	4.57E-06	2.85E-06
Se-81	1.30E-10	1.10E-10	9.35E-11	8.55E-11	7.52E-11	6.67E-11	5.55E-11	4.15E-11	9.40E-11
Se-82	1.83E-06	3.60E-06	5.24E-06	6.73E-06	8.05E-06	9.21E-06	1.03E-05	1.13E-05	7.07E-06
Se-83	3.62E-10	2.97E-10	2.45E-10	2.21E-10	1.91E-10	1.63E-10	1.36E-10	1.03E-10	2.46E-10
Br-79	1.34E-10	2.66E-10	3.86E-10	4.95E-10	5.90E-10	6.71E-10	7.49E-10	8.10E-10	5.17E-10
Br-81	1.16E-06	2.29E-06	3.34E-06	4.30E-06	5.12E-06	5.86E-06	6.55E-06	7.18E-06	4.51E-06
Br-82	3.48E-11	5.41E-11	7.44E-11	9.12E-11	1.07E-10	1.16E-10	1.29E-10	1.32E-10	1.02E-10
Br-83	2.60E-09	2.15E-09	1.77E-09	1.61E-09	1.40E-09	1.20E-09	9.97E-10	7.53E-10	1.79E-09
Br-84	1.00E-09	8.20E-10	6.71E-10	6.07E-10	5.21E-10	4.43E-10	3.69E-10	2.79E-10	6.75E-10

Br-85	1.32E-10	1.07E-10	8.69E-11	7.85E-11	6.67E-11	5.64E-11	4.67E-11	3.57E-11	8.71E-11
Kr-82	1.79E-09	7.32E-09	1.93E-08	3.43E-08	5.31E-08	7.90E-08	1.11E-07	1.43E-07	5.88E-08
Kr-83	2.96E-06	5.59E-06	7.82E-06	9.67E-06	1.11E-05	1.23E-05	1.31E-05	1.37E-05	9.57E-06
Kr-83m	1.96E-09	1.61E-09	1.33E-09	1.21E-09	1.05E-09	9.01E-10	7.50E-10	5.67E-10	1.34E-09
Kr-84	5.52E-06	1.10E-05	1.60E-05	2.07E-05	2.51E-05	2.90E-05	3.27E-05	3.63E-05	2.22E-05
Kr-85	2.02E-06	3.91E-06	5.57E-06	7.03E-06	8.29E-06	9.35E-06	1.03E-05	1.11E-05	7.24E-06
Kr-85m	1.18E-08	9.59E-09	7.80E-09	7.02E-09	5.99E-09	5.04E-09	4.18E-09	3.19E-09	7.81E-09
Kr-86	1.03E-05	1.99E-05	2.86E-05	3.64E-05	4.32E-05	4.92E-05	5.44E-05	5.95E-05	3.79E-05
Kr-87	6.43E-09	5.23E-09	4.23E-09	3.82E-09	3.24E-09	2.73E-09	2.26E-09	1.73E-09	4.24E-09
Kr-88	1.94E-08	1.58E-08	1.27E-08	1.15E-08	9.67E-09	8.16E-09	6.74E-09	5.17E-09	1.27E-08
Kr-89	4.57E-10	3.70E-10	2.97E-10	2.68E-10	2.24E-10	1.88E-10	1.55E-10	1.20E-10	2.97E-10
Rb-85	5.85E-06	1.14E-05	1.64E-05	2.09E-05	2.48E-05	2.83E-05	3.13E-05	3.43E-05	2.18E-05
Rb-86	6.72E-10	1.68E-09	2.61E-09	3.28E-09	4.14E-09	4.77E-09	5.43E-09	5.52E-09	3.81E-09
Rb-87	1.44E-05	2.79E-05	3.99E-05	5.08E-05	6.02E-05	6.83E-05	7.56E-05	8.25E-05	5.28E-05
Rb-88	2.04E-09	1.66E-09	1.34E-09	1.21E-09	1.02E-09	8.63E-10	7.19E-10	5.62E-10	1.35E-09
Rb-89	2.31E-09	1.88E-09	1.51E-09	1.37E-09	1.15E-09	9.70E-10	8.01E-10	6.14E-10	1.51E-09
Rb-90	4.23E-10	3.42E-10	2.73E-10	2.46E-10	2.04E-10	1.71E-10	1.41E-10	1.09E-10	2.72E-10
Rb-90m	1.04E-10	8.80E-11	7.46E-11	6.82E-11	6.01E-11	5.30E-11	4.41E-11	3.31E-11	7.51E-11
Rb-91	1.76E-10	1.43E-10	1.16E-10	1.05E-10	8.86E-11	7.50E-11	6.22E-11	4.75E-11	1.16E-10
Sr-86	9.17E-10	5.39E-09	1.36E-08	2.57E-08	4.64E-08	6.81E-08	9.44E-08	1.27E-07	4.98E-08
Sr-87	1.62E-11	4.63E-11	8.53E-11	1.32E-10	1.92E-10	2.65E-10	3.64E-10	4.79E-10	2.08E-10
Sr-88	1.95E-05	3.79E-05	5.43E-05	6.90E-05	8.19E-05	9.30E-05	1.03E-04	1.12E-04	7.17E-05
Sr-89	1.62E-05	2.14E-05	2.19E-05	1.97E-05	1.71E-05	1.45E-05	1.25E-05	1.08E-05	1.70E-05
Sr-90	3.18E-05	6.15E-05	8.79E-05	1.11E-04	1.32E-04	1.49E-04	1.64E-04	1.79E-04	1.15E-04
Sr-91	1.10E-07	8.97E-08	7.31E-08	6.60E-08	5.64E-08	4.78E-08	3.97E-08	3.02E-08	7.33E-08
Sr-92	3.12E-08	2.57E-08	2.11E-08	1.92E-08	1.66E-08	1.42E-08	1.18E-08	8.93E-09	2.13E-08
Sr-93	1.54E-09	1.27E-09	1.06E-09	9.64E-10	8.45E-10	7.28E-10	6.09E-10	4.59E-10	1.07E-09
Sr-94	2.54E-10	2.11E-10	1.76E-10	1.60E-10	1.41E-10	1.22E-10	1.02E-10	7.68E-11	1.78E-10
Y-89	9.68E-06	2.90E-05	5.01E-05	7.10E-05	8.98E-05	1.07E-04	1.22E-04	1.35E-04	7.71E-05
Y-90	7.89E-09	1.57E-08	2.27E-08	2.89E-08	3.43E-08	3.91E-08	4.34E-08	4.71E-08	3.00E-08
Y-91	2.13E-05	2.96E-05	3.13E-05	2.91E-05	2.58E-05	2.23E-05	1.93E-05	1.68E-05	2.48E-05
Y-91m	5.41E-09	4.42E-09	3.60E-09	3.25E-09	2.78E-09	2.36E-09	1.96E-09	1.49E-09	3.61E-09
Y-92	4.21E-08	3.46E-08	2.85E-08	2.58E-08	2.23E-08	1.91E-08	1.59E-08	1.20E-08	2.87E-08
Y-93	1.29E-07	1.07E-07	8.95E-08	8.12E-08	7.13E-08	6.15E-08	5.14E-08	3.88E-08	9.02E-08
Y-94	4.06E-09	3.38E-09	2.85E-09	2.59E-09	2.30E-09	1.99E-09	1.67E-09	1.25E-09	2.87E-09
Y-95	2.23E-09	1.87E-09	1.59E-09	1.45E-09	1.29E-09	1.13E-09	9.50E-10	7.12E-10	1.61E-09
Zr-90	6.85E-08	2.80E-07	6.19E-07	1.07E-06	1.63E-06	2.27E-06	2.98E-06	3.77E-06	1.60E-06
Zr-91	1.05E-05	3.27E-05	5.81E-05	8.37E-05	1.07E-04	1.29E-04	1.48E-04	1.66E-04	9.24E-05
Zr-92	3.34E-05	6.53E-05	9.43E-05	1.20E-04	1.44E-04	1.64E-04	1.82E-04	1.99E-04	1.26E-04
Zr-93	3.53E-05	6.91E-05	1.00E-04	1.28E-04	1.53E-04	1.75E-04	1.95E-04	2.13E-04	1.34E-04
Zr-94	3.64E-05	7.18E-05	1.04E-04	1.34E-04	1.61E-04	1.84E-04	2.06E-04	2.26E-04	1.41E-04
Zr-95	2.52E-05	3.65E-05	4.00E-05	3.85E-05	3.53E-05	3.14E-05	2.80E-05	2.49E-05	3.30E-05
Zr-96	3.59E-05	7.09E-05	1.04E-04	1.34E-04	1.60E-04	1.84E-04	2.07E-04	2.27E-04	1.41E-04
Zr-97	2.12E-07	1.81E-07	1.58E-07	1.42E-07	1.30E-07	1.16E-07	9.89E-08	7.38E-08	1.59E-07
Zr-98	1.00E-10	8.62E-11	7.56E-11	6.93E-11	6.33E-11	5.72E-11	4.82E-11	3.59E-11	7.68E-11
Nb-94	5.91E-12	1.76E-11	3.29E-11	4.88E-11	6.45E-11	8.38E-11	1.02E-10	1.19E-10	6.21E-11
Nb-95	7.41E-06	1.60E-05	2.07E-05	2.22E-05	2.14E-05	1.97E-05	1.76E-05	1.57E-05	1.79E-05
Nb-95m	1.50E-08	2.24E-08	2.47E-08	2.40E-08	2.20E-08	1.97E-08	1.74E-08	1.56E-08	2.04E-08
Nb-96	2.30E-10	4.38E-10	5.90E-10	5.89E-10	6.05E-10	5.82E-10	4.90E-10	4.48E-10	5.47E-10
Nb-97	1.53E-08	1.31E-08	1.14E-08	1.03E-08	9.40E-09	8.39E-09	7.15E-09	5.34E-09	1.14E-08
Mo-95	3.86E-06	1.95E-05	4.32E-05	7.10E-05	9.83E-05	1.25E-04	1.50E-04	1.72E-04	8.56E-05
Mo-96	1.90E-08	1.50E-07	4.93E-07	1.12E-06	2.21E-06	3.52E-06	5.34E-06	7.75E-06	2.74E-06
Mo-97	3.41E-05	6.80E-05	1.00E-04	1.30E-04	1.56E-04	1.80E-04	2.03E-04	2.22E-04	1.37E-04

Mo-98	3.31E-05	6.61E-05	9.77E-05	1.27E-04	1.54E-04	1.77E-04	2.01E-04	2.21E-04	1.35E-04
Mo-99	1.08E-06	9.54E-07	7.81E-07	7.30E-07	6.85E-07	6.15E-07	5.39E-07	4.74E-07	7.97E-07
Mo-100	3.63E-05	7.26E-05	1.08E-04	1.40E-04	1.70E-04	1.96E-04	2.22E-04	2.45E-04	1.49E-04
Mo-101	2.70E-09	2.35E-09	2.11E-09	1.94E-09	1.81E-09	1.66E-09	1.42E-09	1.05E-09	2.16E-09
Mo-102	1.77E-09	1.57E-09	1.45E-09	1.34E-09	1.27E-09	1.18E-09	1.02E-09	7.50E-10	1.48E-09
Mo-103	1.34E-10	1.25E-10	1.21E-10	1.14E-10	1.12E-10	1.05E-10	9.41E-11	6.84E-11	1.24E-10
Tc-99	3.30E-05	6.61E-05	9.65E-05	1.23E-04	1.47E-04	1.67E-04	1.86E-04	2.01E-04	1.28E-04
Tc-99m	8.74E-08	7.80E-08	6.35E-08	5.97E-08	5.58E-08	5.01E-08	4.41E-08	3.93E-08	6.47E-08
Tc-101	2.63E-09	2.29E-09	2.06E-09	1.89E-09	1.76E-09	1.62E-09	1.38E-09	1.02E-09	2.10E-09
Tc-103	1.11E-10	1.03E-10	9.98E-11	9.46E-11	9.22E-11	8.68E-11	7.76E-11	5.65E-11	1.02E-10
Tc-104	1.52E-09	1.50E-09	1.49E-09	1.46E-09	1.46E-09	1.41E-09	1.29E-09	9.46E-10	1.57E-09
Tc-105	3.90E-10	4.26E-10	4.40E-10	4.50E-10	4.62E-10	4.59E-10	4.23E-10	3.17E-10	4.81E-10
Ru-99	1.09E-09	2.24E-09	3.31E-09	4.31E-09	5.21E-09	6.05E-09	6.85E-09	7.51E-09	4.61E-09
Ru-100	2.53E-07	1.48E-06	3.77E-06	6.98E-06	1.12E-05	1.61E-05	2.15E-05	2.83E-05	1.18E-05
Ru-101	2.99E-05	5.95E-05	8.79E-05	1.14E-04	1.38E-04	1.59E-04	1.80E-04	1.96E-04	1.21E-04
Ru-102	2.54E-05	5.22E-05	7.87E-05	1.04E-04	1.28E-04	1.51E-04	1.73E-04	1.93E-04	1.14E-04
Ru-103	1.05E-05	1.43E-05	1.48E-05	1.46E-05	1.37E-05	1.29E-05	1.22E-05	1.17E-05	1.35E-05
Ru-104	1.23E-05	2.66E-05	4.20E-05	5.67E-05	7.10E-05	8.56E-05	1.00E-04	1.14E-04	6.41E-05
Ru-105	1.37E-08	1.51E-08	1.55E-08	1.59E-08	1.63E-08	1.62E-08	1.51E-08	1.24E-08	1.70E-08
Ru-106	3.32E-06	7.95E-06	1.30E-05	1.79E-05	2.25E-05	2.72E-05	3.10E-05	3.50E-05	2.03E-05
Ru-107	5.94E-11	8.47E-11	9.31E-11	1.05E-10	1.19E-10	1.24E-10	1.17E-10	9.01E-11	1.14E-10
Ru-108	3.88E-11	6.20E-11	7.06E-11	8.32E-11	9.62E-11	1.01E-10	9.68E-11	7.47E-11	9.06E-11
Rh-103	7.83E-06	2.26E-05	3.78E-05	5.17E-05	6.30E-05	7.30E-05	7.96E-05	8.62E-05	5.36E-05
Rh-103m	1.03E-08	1.41E-08	1.45E-08	1.43E-08	1.34E-08	1.26E-08	1.19E-08	1.14E-08	1.32E-08
Rh-105	1.10E-07	1.21E-07	1.23E-07	1.31E-07	1.30E-07	1.34E-07	1.22E-07	1.14E-07	1.38E-07
Rh-107	3.48E-10	4.98E-10	5.46E-10	6.18E-10	6.97E-10	7.28E-10	6.87E-10	5.28E-10	6.69E-10
Pd-104	2.08E-07	1.50E-06	4.91E-06	9.55E-06	1.70E-05	2.53E-05	3.52E-05	4.67E-05	1.82E-05
Pd-105	5.97E-06	1.39E-05	2.26E-05	3.12E-05	3.95E-05	4.81E-05	5.61E-05	6.47E-05	3.57E-05
Pd-106	1.07E-06	3.16E-06	6.22E-06	9.94E-06	1.48E-05	2.02E-05	2.67E-05	3.34E-05	1.46E-05
Pd-107	1.78E-06	4.97E-06	9.04E-06	1.35E-05	1.84E-05	2.39E-05	2.94E-05	3.49E-05	1.75E-05
Pd-108	9.29E-07	2.73E-06	5.35E-06	8.15E-06	1.13E-05	1.52E-05	1.89E-05	2.29E-05	1.10E-05
Pd-109	4.68E-09	7.65E-09	8.90E-09	1.06E-08	1.23E-08	1.29E-08	1.29E-08	9.94E-09	1.18E-08
Pd-110	3.34E-07	9.52E-07	1.80E-06	2.74E-06	3.80E-06	5.05E-06	6.27E-06	7.57E-06	3.67E-06
Pd-112	1.16E-09	1.44E-09	1.62E-09	1.72E-09	1.84E-09	1.90E-09	1.80E-09	1.44E-09	1.86E-09
Ag-109	5.62E-07	1.63E-06	3.09E-06	4.76E-06	6.33E-06	8.06E-06	1.00E-05	1.19E-05	6.03E-06
Ag-110m	5.23E-10	3.99E-09	1.25E-08	2.80E-08	4.95E-08	8.03E-08	1.12E-07	1.46E-07	5.92E-08
Ag-111	2.68E-08	3.64E-08	4.47E-08	4.84E-08	5.32E-08	5.53E-08	5.89E-08	5.99E-08	5.11E-08
Ag-112	1.74E-10	2.15E-10	2.42E-10	2.58E-10	2.74E-10	2.84E-10	2.69E-10	2.18E-10	2.78E-10
Ag-113	1.64E-10	1.83E-10	1.98E-10	2.05E-10	2.19E-10	2.20E-10	2.07E-10	1.57E-10	2.24E-10
Cd-110	1.17E-08	9.44E-08	3.18E-07	7.42E-07	1.41E-06	2.38E-06	3.46E-06	4.90E-06	1.80E-06
Cd-111	1.59E-07	4.65E-07	8.63E-07	1.31E-06	1.80E-06	2.38E-06	2.96E-06	3.56E-06	1.73E-06
Cd-112	1.13E-07	2.85E-07	4.93E-07	7.20E-07	9.62E-07	1.22E-06	1.49E-06	1.77E-06	9.00E-07
Cd-113	6.11E-09	6.54E-09	7.17E-09	7.62E-09	7.73E-09	7.95E-09	7.72E-09	7.90E-09	7.70E-09
Cd-113m	1.20E-09	2.84E-09	4.72E-09	6.70E-09	8.80E-09	1.09E-08	1.33E-08	1.57E-08	8.13E-09
Cd-114	1.82E-07	4.33E-07	7.13E-07	9.99E-07	1.28E-06	1.60E-06	1.89E-06	2.19E-06	1.18E-06
Cd-115	2.09E-09	2.08E-09	2.01E-09	1.94E-09	1.98E-09	1.90E-09	1.70E-09	1.54E-09	2.12E-09
Cd-115m	3.01E-09	4.49E-09	4.95E-09	4.99E-09	4.80E-09	4.65E-09	4.64E-09	4.47E-09	4.67E-09
Cd-116	9.15E-08	2.01E-07	3.17E-07	4.26E-07	5.30E-07	6.37E-07	7.38E-07	8.35E-07	4.77E-07
In-113	5.44E-12	2.37E-11	5.72E-11	1.07E-10	1.73E-10	2.54E-10	3.54E-10	4.75E-10	1.83E-10
In-115	6.25E-08	1.15E-07	1.55E-07	1.83E-07	1.95E-07	1.94E-07	2.13E-07	2.15E-07	1.74E-07
In-115m	1.77E-10	1.77E-10	1.70E-10	1.64E-10	1.68E-10	1.62E-10	1.45E-10	1.33E-10	1.80E-10
Sn-115	3.87E-09	8.51E-09	1.34E-08	1.80E-08	2.23E-08	2.68E-08	3.08E-08	3.48E-08	2.01E-08
Sn-116	4.94E-09	2.59E-08	6.98E-08	1.26E-07	1.96E-07	2.72E-07	3.54E-07	4.40E-07	1.93E-07

Sn-117	8.66E-08	1.88E-07	2.95E-07	3.95E-07	4.90E-07	5.86E-07	6.77E-07	7.63E-07	4.40E-07
Sn-118	7.61E-08	1.62E-07	2.52E-07	3.37E-07	4.17E-07	4.96E-07	5.75E-07	6.46E-07	3.74E-07
Sn-119	8.42E-08	1.77E-07	2.72E-07	3.62E-07	4.47E-07	5.28E-07	6.08E-07	6.79E-07	3.98E-07
Sn-120	8.24E-08	1.73E-07	2.66E-07	3.54E-07	4.38E-07	5.18E-07	5.98E-07	6.69E-07	3.91E-07
Sn-121	9.30E-10	8.80E-10	8.47E-10	8.04E-10	7.77E-10	7.61E-10	6.62E-10	5.20E-10	8.85E-10
Sn-121m	4.72E-09	1.03E-08	1.62E-08	2.17E-08	2.69E-08	3.22E-08	3.73E-08	4.21E-08	2.42E-08
Sn-122	1.03E-07	2.19E-07	3.39E-07	4.52E-07	5.59E-07	6.63E-07	7.66E-07	8.58E-07	4.99E-07
Sn-123	3.87E-08	6.99E-08	9.15E-08	1.04E-07	1.10E-07	1.11E-07	1.09E-07	1.08E-07	9.45E-08
Sn-124	1.76E-07	3.75E-07	5.80E-07	7.73E-07	9.54E-07	1.13E-06	1.30E-06	1.46E-06	8.51E-07
Sn-125	1.94E-08	2.10E-08	2.05E-08	1.96E-08	1.87E-08	1.78E-08	1.71E-08	1.65E-08	1.97E-08
Sn-126	3.73E-07	8.12E-07	1.27E-06	1.71E-06	2.12E-06	2.53E-06	2.93E-06	3.30E-06	1.90E-06
Sn-127	7.39E-10	6.87E-10	6.50E-10	6.10E-10	5.82E-10	5.43E-10	4.78E-10	3.50E-10	6.61E-10
Sn-128	7.58E-10	6.83E-10	6.37E-10	5.89E-10	5.50E-10	5.12E-10	4.42E-10	3.25E-10	6.41E-10
Sb-121	8.02E-08	1.70E-07	2.61E-07	3.48E-07	4.27E-07	5.03E-07	5.74E-07	6.40E-07	3.79E-07
Sb-123	6.46E-08	1.48E-07	2.43E-07	3.40E-07	4.39E-07	5.31E-07	6.25E-07	7.12E-07	3.90E-07
Sb-124	1.72E-10	5.93E-10	1.16E-09	1.88E-09	2.93E-09	3.69E-09	4.43E-09	5.49E-09	2.91E-09
Sb-125	2.01E-07	4.41E-07	6.82E-07	8.96E-07	1.09E-06	1.27E-06	1.43E-06	1.56E-06	9.55E-07
Sb-126	2.19E-09	2.35E-09	2.41E-09	2.45E-09	2.48E-09	2.40E-09	2.45E-09	2.47E-09	2.52E-09
Sb-127	5.22E-08	5.21E-08	4.60E-08	4.66E-08	4.34E-08	4.07E-08	3.89E-08	3.63E-08	4.81E-08
Sb-128	7.26E-09	6.59E-09	6.18E-09	5.71E-09	5.35E-09	4.98E-09	4.31E-09	3.17E-09	6.20E-09
Sb-129	5.97E-09	5.57E-09	5.30E-09	5.00E-09	4.80E-09	4.51E-09	3.98E-09	2.91E-09	5.41E-09
Sb-130	1.16E-09	1.02E-09	9.24E-10	8.52E-10	7.90E-10	7.32E-10	6.21E-10	4.58E-10	9.39E-10
Sb-130m	2.12E-10	1.83E-10	1.63E-10	1.50E-10	1.38E-10	1.26E-10	1.06E-10	7.87E-11	1.66E-10
Sb-131	2.06E-09	1.77E-09	1.57E-09	1.44E-09	1.33E-09	1.20E-09	1.02E-09	7.57E-10	1.60E-09
Sb-132	1.91E-10	1.67E-10	1.50E-10	1.38E-10	1.27E-10	1.18E-10	9.93E-11	7.33E-11	1.52E-10
Sb-132m	1.19E-10	1.00E-10	8.69E-11	7.90E-11	7.18E-11	6.43E-11	5.49E-11	4.11E-11	8.89E-11
Sb-133	1.98E-10	1.64E-10	1.40E-10	1.27E-10	1.13E-10	1.01E-10	8.56E-11	6.45E-11	1.43E-10
Te-122	2.98E-10	1.77E-09	4.35E-09	8.79E-09	1.32E-08	2.23E-08	3.08E-08	4.12E-08	1.66E-08
Te-123	2.66E-13	2.51E-12	8.30E-12	2.51E-11	5.19E-11	8.71E-11	1.36E-10	2.01E-10	7.37E-11
Te-123m	3.31E-13	1.90E-12	5.38E-12	1.33E-11	2.76E-11	4.52E-11	6.85E-11	1.11E-10	3.93E-11
Te-124	7.55E-11	4.32E-10	1.40E-09	2.76E-09	5.95E-09	9.17E-09	1.47E-08	1.98E-08	7.32E-09
Te-125	3.59E-09	1.65E-08	3.95E-08	7.29E-08	1.16E-07	1.68E-07	2.27E-07	2.94E-07	1.18E-07
Te-125m	8.10E-10	2.87E-09	5.53E-09	8.43E-09	1.13E-08	1.38E-08	1.62E-08	1.83E-08	9.70E-09
Te-126	1.24E-08	2.86E-08	4.59E-08	6.41E-08	8.18E-08	9.96E-08	1.18E-07	1.38E-07	7.44E-08
Te-127	5.25E-09	5.32E-09	4.69E-09	4.72E-09	4.43E-09	4.09E-09	3.96E-09	3.66E-09	4.84E-09
Te-127m	2.93E-08	4.07E-08	4.01E-08	3.71E-08	3.46E-08	3.23E-08	3.08E-08	2.86E-08	3.53E-08
Te-128	2.14E-06	4.48E-06	6.82E-06	9.04E-06	1.12E-05	1.31E-05	1.50E-05	1.67E-05	9.89E-06
Te-129	1.57E-09	1.47E-09	1.40E-09	1.32E-09	1.27E-09	1.19E-09	1.05E-09	7.68E-10	1.43E-09
Te-129m	1.89E-10	2.98E-10	3.31E-10	3.45E-10	3.60E-10	3.76E-10	3.75E-10	3.73E-10	3.50E-10
Te-130	1.06E-05	2.13E-05	3.18E-05	4.16E-05	5.07E-05	5.87E-05	6.67E-05	7.36E-05	4.47E-05
Te-131	2.42E-09	2.10E-09	1.89E-09	1.73E-09	1.61E-09	1.48E-09	1.25E-09	9.27E-10	1.92E-09
Te-131m	2.00E-08	2.01E-08	1.82E-08	1.81E-08	1.69E-08	1.62E-08	1.44E-08	1.15E-08	1.93E-08
Te-132	9.36E-07	8.40E-07	6.92E-07	6.58E-07	6.03E-07	5.58E-07	4.94E-07	4.37E-07	7.06E-07
Te-133	1.75E-09	1.49E-09	1.31E-09	1.19E-09	1.10E-09	9.81E-10	8.34E-10	6.20E-10	1.33E-09
Te-133m	5.76E-09	4.94E-09	4.33E-09	3.97E-09	3.64E-09	3.27E-09	2.77E-09	2.06E-09	4.40E-09
Te-134	9.83E-09	8.26E-09	7.09E-09	6.46E-09	5.82E-09	5.16E-09	4.38E-09	3.28E-09	7.22E-09
I-127	9.05E-07	2.01E-06	3.15E-06	4.21E-06	5.24E-06	6.15E-06	7.06E-06	7.87E-06	4.61E-06
I-129	3.41E-06	7.17E-06	1.10E-05	1.45E-05	1.78E-05	2.09E-05	2.40E-05	2.66E-05	1.58E-05
I-130	1.27E-10	2.60E-10	3.50E-10	4.94E-10	5.65E-10	6.98E-10	7.37E-10	8.40E-10	5.66E-10
I-131	2.07E-06	1.90E-06	1.68E-06	1.52E-06	1.36E-06	1.24E-06	1.12E-06	1.06E-06	1.57E-06
I-132	2.84E-08	2.55E-08	2.10E-08	2.01E-08	1.84E-08	1.70E-08	1.51E-08	1.34E-08	2.15E-08
I-133	3.03E-07	2.61E-07	2.33E-07	2.09E-07	1.95E-07	1.77E-07	1.51E-07	1.14E-07	2.34E-07
I-134	1.43E-08	1.22E-08	1.07E-08	9.84E-09	9.04E-09	8.13E-09	6.89E-09	5.13E-09	1.09E-08

I-135	8.71E-08	7.52E-08	6.67E-08	6.12E-08	5.66E-08	5.14E-08	4.36E-08	3.24E-08	6.80E-08
I-136	1.25E-10	1.05E-10	9.21E-11	8.38E-11	7.67E-11	6.93E-11	5.94E-11	4.43E-11	9.44E-11
Xe-128	2.89E-09	1.65E-08	4.03E-08	8.75E-08	1.50E-07	2.26E-07	3.25E-07	4.16E-07	1.71E-07
Xe-129	1.82E-12	2.20E-11	9.27E-11	2.66E-10	5.01E-10	9.89E-10	1.71E-09	2.76E-09	8.80E-10
Xe-130	1.52E-08	6.57E-08	1.50E-07	2.75E-07	4.31E-07	6.27E-07	8.51E-07	1.11E-06	4.48E-07
Xe-131	1.39E-05	2.88E-05	4.09E-05	5.20E-05	5.93E-05	6.67E-05	7.02E-05	7.38E-05	5.14E-05
Xe-131m	4.50E-08	4.40E-08	3.89E-08	3.56E-08	3.25E-08	2.91E-08	2.52E-08	2.46E-08	3.55E-08
Xe-132	2.44E-05	5.22E-05	8.07E-05	1.08E-04	1.35E-04	1.61E-04	1.86E-04	2.09E-04	1.21E-04
Xe-133	2.78E-06	2.50E-06	2.15E-06	1.95E-06	1.74E-06	1.57E-06	1.41E-06	1.31E-06	2.04E-06
Xe-133m	1.07E-08	9.88E-09	8.10E-09	7.80E-09	7.21E-09	6.62E-09	6.02E-09	5.64E-09	8.36E-09
Xe-134	4.52E-05	9.03E-05	1.33E-04	1.73E-04	2.09E-04	2.41E-04	2.74E-04	3.02E-04	1.85E-04
Xe-135	3.64E-08	3.25E-08	2.84E-08	2.44E-08	2.20E-08	1.86E-08	1.72E-08	1.49E-08	2.62E-08
Xe-135m	4.64E-10	4.17E-10	3.85E-10	3.58E-10	3.32E-10	3.09E-10	2.66E-10	1.96E-10	3.88E-10
Xe-136	6.67E-05	1.35E-04	2.01E-04	2.62E-04	3.19E-04	3.69E-04	4.20E-04	4.65E-04	2.82E-04
Xe-137	8.17E-10	7.02E-10	6.19E-10	5.68E-10	5.24E-10	4.73E-10	4.02E-10	2.99E-10	6.31E-10
Xe-138	3.04E-09	2.58E-09	2.24E-09	2.05E-09	1.87E-09	1.67E-09	1.42E-09	1.06E-09	2.28E-09
Xe-139	1.11E-10	9.31E-11	7.95E-11	7.23E-11	6.48E-11	5.74E-11	4.87E-11	3.66E-11	8.10E-11
Cs-133	3.42E-05	7.04E-05	1.03E-04	1.32E-04	1.55E-04	1.76E-04	1.96E-04	2.09E-04	1.36E-04
Cs-134	2.65E-07	1.60E-06	3.61E-06	7.54E-06	1.17E-05	1.61E-05	2.12E-05	2.66E-05	1.17E-05
Cs-134m	3.75E-11	7.49E-11	1.08E-10	1.23E-10	1.69E-10	1.93E-10	2.08E-10	2.17E-10	1.53E-10
Cs-135	6.10E-06	1.16E-05	1.65E-05	2.09E-05	2.52E-05	2.98E-05	3.41E-05	3.85E-05	2.38E-05
Cs-136	1.17E-08	2.00E-08	2.54E-08	3.17E-08	3.66E-08	4.44E-08	5.15E-08	5.26E-08	3.83E-08
Cs-137	3.56E-05	7.10E-05	1.05E-04	1.37E-04	1.65E-04	1.90E-04	2.15E-04	2.37E-04	1.45E-04
Cs-138	7.75E-09	6.61E-09	5.77E-09	5.28E-09	4.84E-09	4.33E-09	3.67E-09	2.74E-09	5.87E-09
Cs-139	2.02E-09	1.72E-09	1.50E-09	1.37E-09	1.25E-09	1.12E-09	9.48E-10	7.07E-10	1.52E-09
Cs-140	2.05E-10	1.72E-10	1.48E-10	1.34E-10	1.21E-10	1.08E-10	9.15E-11	6.84E-11	1.50E-10
Ba-134	5.92E-09	6.59E-08	2.50E-07	6.11E-07	1.31E-06	2.24E-06	3.50E-06	4.98E-06	1.68E-06
Ba-135	5.81E-12	5.39E-11	2.62E-10	9.80E-10	2.40E-09	5.43E-09	1.18E-08	1.87E-08	5.46E-09
Ba-136	5.96E-08	1.95E-07	3.86E-07	6.14E-07	8.78E-07	1.20E-06	1.52E-06	1.90E-06	8.72E-07
Ba-137	8.32E-08	3.22E-07	7.06E-07	1.22E-06	1.85E-06	2.62E-06	3.48E-06	4.43E-06	1.84E-06
Ba-138	3.86E-05	7.67E-05	1.13E-04	1.47E-04	1.77E-04	2.04E-04	2.31E-04	2.54E-04	1.56E-04
Ba-139	1.84E-08	1.57E-08	1.37E-08	1.25E-08	1.15E-08	1.02E-08	8.72E-09	6.47E-09	1.39E-08
Ba-140	7.52E-06	6.83E-06	6.00E-06	5.37E-06	4.72E-06	4.20E-06	3.64E-06	3.35E-06	5.39E-06
Ba-141	3.68E-09	3.13E-09	2.72E-09	2.49E-09	2.26E-09	2.02E-09	1.70E-09	1.27E-09	2.76E-09
Ba-142	2.09E-09	1.76E-09	1.52E-09	1.39E-09	1.26E-09	1.11E-09	9.41E-10	7.03E-10	1.54E-09
La-138	1.89E-10	3.81E-10	5.57E-10	7.18E-10	8.50E-10	9.68E-10	1.07E-09	1.15E-09	7.43E-10
La-139	3.64E-05	7.23E-05	1.06E-04	1.38E-04	1.66E-04	1.90E-04	2.15E-04	2.36E-04	1.46E-04
La-140	1.03E-06	9.42E-07	8.20E-07	7.37E-07	6.64E-07	5.86E-07	5.05E-07	4.70E-07	7.44E-07
La-141	4.76E-08	4.05E-08	3.52E-08	3.22E-08	2.93E-08	2.61E-08	2.21E-08	1.64E-08	3.57E-08
La-142	1.83E-08	1.55E-08	1.34E-08	1.23E-08	1.11E-08	9.87E-09	8.33E-09	6.22E-09	1.36E-08
La-143	2.85E-09	2.40E-09	2.05E-09	1.87E-09	1.69E-09	1.49E-09	1.25E-09	9.39E-10	2.08E-09
La-144	1.25E-10	1.05E-10	8.88E-11	8.09E-11	7.23E-11	6.35E-11	5.36E-11	4.02E-11	9.01E-11
Ce-140	2.64E-05	6.17E-05	9.52E-05	1.27E-04	1.55E-04	1.81E-04	2.06E-04	2.29E-04	1.36E-04
Ce-141	1.64E-05	1.95E-05	1.82E-05	1.64E-05	1.44E-05	1.29E-05	1.13E-05	1.04E-05	1.53E-05
Ce-142	3.34E-05	6.65E-05	9.77E-05	1.27E-04	1.52E-04	1.75E-04	1.98E-04	2.17E-04	1.34E-04
Ce-143	4.40E-07	3.73E-07	3.15E-07	2.81E-07	2.63E-07	2.30E-07	1.94E-07	1.56E-07	3.17E-07
Ce-144	2.83E-05	5.15E-05	6.92E-05	8.22E-05	9.06E-05	9.54E-05	9.83E-05	9.82E-05	7.73E-05
Ce-145	4.03E-10	3.40E-10	2.92E-10	2.66E-10	2.41E-10	2.14E-10	1.80E-10	1.42E-10	2.97E-10
Ce-146	1.39E-09	1.18E-09	1.02E-09	9.31E-10	8.49E-10	7.54E-10	6.39E-10	4.76E-10	1.04E-09
Pr-141	1.64E-05	4.56E-05	7.60E-05	1.05E-04	1.31E-04	1.56E-04	1.78E-04	1.98E-04	1.14E-04
Pr-142	3.77E-10	1.00E-09	1.66E-09	2.30E-09	3.00E-09	3.46E-09	4.02E-09	4.47E-09	2.80E-09
Pr-143	7.79E-06	7.14E-06	6.14E-06	5.44E-06	4.81E-06	4.25E-06	3.59E-06	3.31E-06	5.49E-06
Pr-144	1.23E-09	2.21E-09	2.94E-09	3.49E-09	3.84E-09	4.04E-09	4.16E-09	4.15E-09	3.28E-09

Pr-145	4.81E-08	4.06E-08	3.49E-08	3.18E-08	2.88E-08	2.55E-08	2.15E-08	1.69E-08	3.55E-08
Pr-146	2.48E-09	2.10E-09	1.82E-09	1.67E-09	1.52E-09	1.35E-09	1.14E-09	8.53E-10	1.86E-09
Pr-147	1.04E-09	8.88E-10	7.77E-10	7.11E-10	6.53E-10	5.85E-10	4.96E-10	3.69E-10	7.91E-10
Pr-148	1.28E-10	1.09E-10	9.53E-11	8.70E-11	8.00E-11	7.18E-11	6.12E-11	4.55E-11	9.73E-11
Nd-142	1.63E-08	1.24E-07	3.64E-07	7.21E-07	1.21E-06	1.82E-06	2.56E-06	3.34E-06	1.31E-06
Nd-143	2.40E-05	5.40E-05	7.95E-05	1.01E-04	1.18E-04	1.31E-04	1.40E-04	1.43E-04	9.91E-05
Nd-144	3.36E-06	1.33E-05	2.86E-05	4.84E-05	7.08E-05	9.59E-05	1.22E-04	1.51E-04	6.74E-05
Nd-145	2.18E-05	4.26E-05	6.11E-05	7.71E-05	9.10E-05	1.03E-04	1.14E-04	1.22E-04	7.95E-05
Nd-146	1.74E-05	3.50E-05	5.23E-05	6.91E-05	8.49E-05	9.92E-05	1.15E-04	1.28E-04	7.57E-05
Nd-147	2.22E-06	1.99E-06	1.76E-06	1.57E-06	1.39E-06	1.25E-06	1.09E-06	1.01E-06	1.59E-06
Nd-148	9.90E-06	1.99E-05	2.93E-05	3.82E-05	4.61E-05	5.32E-05	6.04E-05	6.65E-05	4.07E-05
Nd-149	4.00E-09	3.48E-09	3.16E-09	2.93E-09	2.74E-09	2.51E-09	2.18E-09	1.61E-09	3.24E-09
Nd-150	3.86E-06	7.86E-06	1.18E-05	1.55E-05	1.91E-05	2.23E-05	2.55E-05	2.83E-05	1.69E-05
Nd-151	1.99E-10	1.83E-10	1.75E-10	1.61E-10	1.57E-10	1.46E-10	1.30E-10	9.64E-11	1.79E-10
Nd-152	1.19E-10	1.10E-10	1.07E-10	1.01E-10	1.00E-10	9.35E-11	8.44E-11	6.14E-11	1.10E-10
Pm-147	8.96E-06	1.70E-05	2.28E-05	2.62E-05	2.74E-05	2.83E-05	2.76E-05	2.68E-05	2.37E-05
Pm-148	2.63E-08	5.89E-08	8.33E-08	1.03E-07	1.15E-07	1.12E-07	1.20E-07	1.08E-07	9.75E-08
Pm-148m	2.30E-08	4.70E-08	6.09E-08	7.34E-08	7.47E-08	7.75E-08	8.09E-08	7.59E-08	7.25E-08
Pm-149	1.62E-07	1.64E-07	1.60E-07	1.61E-07	1.55E-07	1.38E-07	1.29E-07	1.18E-07	1.60E-07
Pm-151	2.91E-08	2.71E-08	2.43E-08	2.30E-08	2.25E-08	2.12E-08	1.91E-08	1.51E-08	2.60E-08
Sm-147	1.86E-07	7.74E-07	1.60E-06	2.55E-06	3.49E-06	4.40E-06	5.21E-06	5.83E-06	3.06E-06
Sm-148	1.71E-07	1.29E-06	3.38E-06	5.98E-06	9.54E-06	1.31E-05	1.71E-05	2.07E-05	9.23E-06
Sm-149	2.48E-07	2.36E-07	2.33E-07	2.08E-07	2.20E-07	1.97E-07	1.82E-07	1.73E-07	2.40E-07
Sm-150	5.76E-06	1.29E-05	2.01E-05	2.69E-05	3.36E-05	3.97E-05	4.61E-05	5.15E-05	3.00E-05
Sm-151	1.23E-06	1.32E-06	1.36E-06	1.37E-06	1.40E-06	1.44E-06	1.48E-06	1.51E-06	1.45E-06
Sm-152	2.36E-06	5.13E-06	7.34E-06	9.13E-06	1.06E-05	1.17E-05	1.25E-05	1.29E-05	9.34E-06
Sm-153	2.53E-08	3.23E-08	3.54E-08	3.68E-08	4.06E-08	4.39E-08	4.59E-08	4.61E-08	4.25E-08
Sm-154	5.13E-07	1.14E-06	1.81E-06	2.51E-06	3.20E-06	3.87E-06	4.62E-06	5.33E-06	2.93E-06
Sm-156	5.17E-10	6.14E-10	6.64E-10	6.93E-10	7.43E-10	7.54E-10	7.04E-10	5.34E-10	7.46E-10
Eu-151	4.88E-10	5.88E-10	6.33E-10	6.39E-10	6.42E-10	6.51E-10	6.93E-10	6.90E-10	6.64E-10
Eu-152	3.19E-10	6.37E-10	6.95E-10	7.47E-10	7.59E-10	7.88E-10	8.20E-10	8.14E-10	7.47E-10
Eu-153	1.02E-06	2.67E-06	4.74E-06	7.51E-06	1.02E-05	1.28E-05	1.54E-05	1.76E-05	9.31E-06
Eu-154	5.18E-08	2.25E-07	4.97E-07	8.47E-07	1.20E-06	1.59E-06	2.05E-06	2.40E-06	1.19E-06
Eu-155	7.00E-08	1.30E-07	2.02E-07	3.05E-07	4.32E-07	5.41E-07	6.47E-07	7.60E-07	4.12E-07
Eu-156	7.43E-08	1.27E-07	1.90E-07	2.68E-07	3.61E-07	4.53E-07	5.67E-07	6.71E-07	3.61E-07
Eu-157	4.53E-10	5.91E-10	7.00E-10	7.69E-10	8.89E-10	9.23E-10	9.45E-10	9.74E-10	8.98E-10
Gd-154	3.10E-10	2.39E-09	8.04E-09	1.88E-08	3.56E-08	5.89E-08	8.67E-08	1.23E-07	4.29E-08
Gd-155	3.71E-10	6.27E-10	1.03E-09	1.53E-09	1.90E-09	2.76E-09	3.38E-09	4.16E-09	2.14E-09
Gd-156	1.65E-07	6.08E-07	1.30E-06	2.31E-06	3.71E-06	5.48E-06	7.80E-06	1.05E-05	4.09E-06
Gd-157	1.98E-09	2.52E-09	2.96E-09	3.22E-09	3.86E-09	4.29E-09	4.30E-09	4.11E-09	3.73E-09
Gd-158	8.89E-08	2.49E-07	4.55E-07	7.16E-07	1.02E-06	1.38E-06	1.81E-06	2.27E-06	1.04E-06
Gd-159	1.21E-10	1.79E-10	2.13E-10	2.43E-10	2.78E-10	3.12E-10	3.18E-10	2.77E-10	2.79E-10
Gd-160	4.64E-09	1.35E-08	2.59E-08	4.00E-08	5.57E-08	7.45E-08	9.27E-08	1.12E-07	5.40E-08
Tb-159	1.17E-08	3.31E-08	6.01E-08	9.42E-08	1.34E-07	1.74E-07	2.17E-07	2.75E-07	1.28E-07
Tb-160	8.69E-11	4.25E-10	1.06E-09	1.88E-09	2.95E-09	4.04E-09	5.60E-09	7.38E-09	3.25E-09
Tb-161	2.88E-10	4.67E-10	6.19E-10	7.05E-10	8.63E-10	9.67E-10	1.06E-09	1.17E-09	8.16E-10
Dy-160	2.18E-11	2.14E-10	7.46E-10	1.80E-09	3.46E-09	5.60E-09	8.28E-09	1.32E-08	4.62E-09
Dy-161	1.50E-09	4.70E-09	9.09E-09	1.35E-08	1.85E-08	2.44E-08	2.98E-08	3.48E-08	1.77E-08
Dy-162	7.40E-10	2.48E-09	4.96E-09	8.07E-09	1.17E-08	1.52E-08	1.94E-08	2.40E-08	1.12E-08
Dy-163	3.26E-10	1.15E-09	2.60E-09	4.36E-09	6.94E-09	1.00E-08	1.36E-08	1.73E-08	7.39E-09
Dy-164	9.84E-11	2.88E-10	5.09E-10	7.88E-10	1.16E-09	1.64E-09	2.14E-09	2.87E-09	1.31E-09
Ho-165	6.31E-11	2.62E-10	6.20E-10	1.16E-09	1.91E-09	2.93E-09	4.27E-09	5.86E-09	2.26E-09
Er-166	2.12E-11	7.69E-11	1.67E-10	2.83E-10	4.31E-10	6.97E-10	1.01E-09	1.40E-09	5.46E-10

Er-168	3.91E-12	1.55E-11	3.43E-11	5.77E-11	8.75E-11	1.27E-10	1.70E-10	2.28E-10	9.41E-11
U-234	3.92E-12	2.07E-10	1.28E-09	5.38E-09	1.15E-08	2.27E-08	3.68E-08	5.57E-08	1.94E-08
U-235	3.61E-03	2.84E-03	2.26E-03	1.79E-03	1.41E-03	1.12E-03	9.00E-04	7.11E-04	1.89E-03
U-236	1.30E-04	2.41E-04	3.35E-04	4.11E-04	4.74E-04	5.20E-04	5.56E-04	5.76E-04	4.08E-04
U-237	5.07E-08	1.43E-07	2.08E-07	2.66E-07	3.44E-07	3.66E-07	4.24E-07	3.89E-07	3.40E-07
U-238	1.86E-02	1.83E-02	1.80E-02	1.77E-02	1.74E-02	1.71E-02	1.69E-02	1.66E-02	1.76E-02
U-239	7.23E-09	6.10E-09	6.06E-09	6.23E-09	6.52E-09	5.93E-09	6.43E-09	4.66E-09	8.37E-09
Np-237	4.35E-07	2.93E-06	8.07E-06	1.32E-05	2.25E-05	2.84E-05	3.57E-05	4.40E-05	2.10E-05
Np-238	9.90E-10	6.66E-09	1.79E-08	2.85E-08	4.25E-08	5.88E-08	7.69E-08	8.93E-08	4.44E-08
Np-239	2.06E-06	2.03E-06	1.88E-06	1.87E-06	1.81E-06	1.85E-06	2.00E-06	1.85E-06	2.16E-06
Pu-238	9.86E-09	1.89E-07	8.30E-07	1.95E-06	3.97E-06	6.68E-06	9.88E-06	1.35E-05	4.95E-06
Pu-239	8.21E-05	1.20E-04	1.30E-04	1.35E-04	1.40E-04	1.45E-04	1.42E-04	1.42E-04	1.37E-04
Pu-240	1.26E-05	3.28E-05	5.01E-05	6.11E-05	7.04E-05	7.61E-05	7.69E-05	8.20E-05	6.02E-05
Pu-241	1.41E-06	9.99E-06	2.60E-05	4.02E-05	4.76E-05	5.96E-05	6.86E-05	7.11E-05	4.51E-05
Pu-242	7.08E-08	1.12E-06	4.42E-06	1.01E-05	1.81E-05	2.83E-05	3.83E-05	4.76E-05	1.97E-05
Pu-243	1.21E-12	1.93E-11	6.75E-11	1.63E-10	3.20E-10	4.84E-10	5.96E-10	7.74E-10	3.46E-10
Pu-244	2.72E-14	2.31E-12	2.42E-11	1.20E-10	3.81E-10	8.53E-10	1.84E-09	3.10E-09	8.89E-10
Am-241	4.15E-09	5.64E-08	1.75E-07	3.59E-07	5.23E-07	7.32E-07	9.32E-07	1.08E-06	5.18E-07
Am-242	1.05E-11	1.25E-10	4.48E-10	9.36E-10	1.55E-09	1.84E-09	2.25E-09	2.58E-09	1.44E-09
Am-242m	1.69E-11	3.81E-10	1.56E-09	3.60E-09	5.86E-09	8.41E-09	1.08E-08	1.26E-08	5.92E-09
Am-243	1.91E-10	1.16E-08	9.24E-08	5.02E-07	1.18E-06	2.64E-06	5.25E-06	8.28E-06	2.53E-06
Am-244	2.66E-15	1.90E-13	1.80E-12	5.72E-12	1.88E-11	4.14E-11	7.13E-11	1.14E-10	3.73E-11
Cm-242	2.13E-10	6.57E-09	4.08E-08	1.16E-07	2.25E-07	4.00E-07	5.66E-07	7.72E-07	2.80E-07
Cm-243	2.59E-13	1.74E-11	2.10E-10	8.50E-10	2.36E-09	4.93E-09	8.90E-09	1.49E-08	4.43E-09
Cm-244	3.14E-12	6.28E-10	9.20E-09	6.02E-08	1.97E-07	5.64E-07	1.06E-06	2.21E-06	6.05E-07
Cm-245	1.22E-14	3.67E-12	1.27E-10	8.31E-10	3.29E-09	1.49E-08	3.62E-08	6.04E-08	1.93E-08
Cm-246	1.39E-16	9.76E-14	4.25E-12	3.78E-11	2.34E-10	7.14E-10	3.38E-09	7.21E-09	1.63E-09

Average content

General fields

Pass #	1	2	3	4	5	6	7	8	Avg
Residence time [days]	65.25	130.5	195.75	261	326.25	391.5	456.89	522.55	293.62
Pass burnup [MWd/kg$_{HM}$]	28.16	26.42	24.27	22.16	20.23	18.47	16.95	15.59	21.53
Burnup [MWd/kg$_{HM}$]	28.16	54.58	78.88	101.06	121.31	139.81	156.85	172.54	106.61
Thermal fluence [n/cm^2]	6.64E+20	1.33E+21	1.99E+21	2.65E+21	3.32E+21	3.99E+21	4.66E+21	5.33E+21	2.99E+21
Thermal fluence uncertainty	2.82%	2.81%	2.81%	2.81%	2.81%	2.81%	2.81%	2.81%	2.81%
Fast fluence [n/cm^2]	4.88E+20	9.73E+20	1.46E+21	1.94E+21	2.42E+21	2.90E+21	3.37E+21	3.85E+21	2.17E+21
Fast fluence uncertainty	3.62%	3.60%	3.60%	3.59%	3.59%	3.60%	3.60%	3.60%	3.60%

Atomic densities [at/b.cm]

Pass #	1	2	3	4	5	6	7	8	Avg
H-1	1.94E-10	3.91E-10	5.98E-10	7.98E-10	1.00E-09	1.21E-09	1.41E-09	1.61E-09	9.01E-10
H-2	2.18E-11	4.33E-11	6.54E-11	8.65E-11	1.08E-10	1.30E-10	1.52E-10	1.72E-10	9.74E-11
He-4	5.56E-08	1.15E-07	1.90E-07	3.01E-07	4.74E-07	7.32E-07	1.09E-06	1.56E-06	5.65E-07
C-12	1.17E-02	1.17E-02	1.17E-02	1.17E-02	1.17E-02	1.17E-02	1.17E-02	1.17E-02	1.17E-02
C-13	1.25E-04	1.25E-04	1.25E-04	1.25E-04	1.25E-04	1.25E-04	1.25E-04	1.25E-04	1.25E-04
N-15	2.47E-11	4.92E-11	7.41E-11	9.77E-11	1.23E-10	1.47E-10	1.71E-10	1.93E-10	1.10E-10
O-16	3.55E-02	3.55E-02	3.55E-02	3.55E-02	3.55E-02	3.55E-02	3.55E-02	3.55E-02	3.55E-02
O-17	1.90E-09	3.81E-09	5.72E-09	7.63E-09	9.56E-09	1.15E-08	1.34E-08	1.54E-08	8.61E-09
Zn-70	3.94E-11	8.70E-11	1.38E-10	1.89E-10	2.40E-10	2.90E-10	3.40E-10	3.88E-10	2.14E-10
Ga-69	1.68E-11	3.52E-11	5.38E-11	7.21E-11	8.97E-11	1.07E-10	1.23E-10	1.39E-10	7.95E-11
Ga-71	8.27E-11	1.80E-10	2.84E-10	3.91E-10	4.98E-10	6.05E-10	7.11E-10	8.14E-10	4.46E-10
Ge-72	2.37E-10	5.27E-10	8.27E-10	1.12E-09	1.41E-09	1.68E-09	1.95E-09	2.21E-09	1.24E-09
Ge-73	8.16E-10	1.67E-09	2.49E-09	3.26E-09	3.97E-09	4.62E-09	5.23E-09	5.79E-09	3.48E-09
Ge-74	2.59E-09	5.18E-09	7.65E-09	9.93E-09	1.20E-08	1.40E-08	1.58E-08	1.75E-08	1.06E-08
Ge-76	2.20E-08	4.22E-08	6.04E-08	7.67E-08	9.12E-08	1.04E-07	1.16E-07	1.26E-07	7.98E-08
Ge-77	3.50E-10	3.16E-10	2.81E-10	2.49E-10	2.21E-10	1.97E-10	1.76E-10	1.59E-10	2.44E-10
Ge-78	1.20E-10	1.08E-10	9.69E-11	8.66E-11	7.75E-11	6.96E-11	6.29E-11	5.71E-11	8.48E-11
As-75	7.65E-09	1.49E-08	2.14E-08	2.73E-08	3.25E-08	3.72E-08	4.13E-08	4.51E-08	2.84E-08
As-77	1.21E-09	1.10E-09	9.78E-10	8.68E-10	7.72E-10	6.89E-10	6.19E-10	5.59E-10	8.49E-10
As-78	1.25E-10	1.13E-10	1.02E-10	9.10E-11	8.17E-11	7.35E-11	6.65E-11	6.05E-11	8.91E-11
Se-76	3.82E-11	1.47E-10	3.18E-10	5.43E-10	8.13E-10	1.12E-09	1.47E-09	1.84E-09	7.85E-10
Se-77	5.39E-08	1.04E-07	1.49E-07	1.87E-07	2.21E-07	2.50E-07	2.76E-07	2.98E-07	1.92E-07
Se-78	1.46E-07	2.82E-07	4.04E-07	5.15E-07	6.15E-07	7.05E-07	7.87E-07	8.62E-07	5.39E-07
Se-79	3.09E-07	5.90E-07	8.38E-07	1.05E-06	1.24E-06	1.40E-06	1.54E-06	1.66E-06	1.08E-06
Se-80	8.86E-07	1.69E-06	2.41E-06	3.05E-06	3.61E-06	4.12E-06	4.57E-06	4.98E-06	3.16E-06
Se-81	2.45E-10	2.22E-10	1.98E-10	1.76E-10	1.57E-10	1.40E-10	1.26E-10	1.14E-10	1.72E-10
Se-82	2.22E-06	4.22E-06	6.00E-06	7.57E-06	8.96E-06	1.02E-05	1.13E-05	1.23E-05	7.83E-06
Se-83	6.79E-10	5.95E-10	5.19E-10	4.53E-10	3.96E-10	3.47E-10	3.07E-10	2.72E-10	4.46E-10
Se-84	1.79E-10	1.56E-10	1.35E-10	1.18E-10	1.02E-10	8.94E-11	7.85E-11	6.92E-11	1.16E-10
Br-79	1.63E-10	3.11E-10	4.42E-10	5.57E-10	6.56E-10	7.42E-10	8.17E-10	8.82E-10	5.71E-10
Br-81	1.40E-06	2.69E-06	3.83E-06	4.83E-06	5.71E-06	6.49E-06	7.18E-06	7.79E-06	4.99E-06
Br-82	1.78E-10	3.25E-10	4.53E-10	5.62E-10	6.59E-10	7.44E-10	8.18E-10	8.85E-10	5.78E-10
Br-83	4.89E-09	4.30E-09	3.77E-09	3.30E-09	2.89E-09	2.54E-09	2.25E-09	2.00E-09	3.24E-09
Br-84	1.88E-09	1.64E-09	1.43E-09	1.24E-09	1.08E-09	9.45E-10	8.30E-10	7.33E-10	1.22E-09
Br-85	2.47E-10	2.14E-10	1.85E-10	1.60E-10	1.39E-10	1.21E-10	1.06E-10	9.26E-11	1.58E-10
Br-87	1.16E-10	1.00E-10	8.64E-11	7.44E-11	6.43E-11	5.57E-11	4.84E-11	4.23E-11	7.35E-11
Kr-82	5.78E-09	2.16E-08	4.58E-08	7.72E-08	1.15E-07	1.57E-07	2.04E-07	2.54E-07	1.10E-07
Kr-83	3.56E-06	6.49E-06	8.85E-06	1.07E-05	1.21E-05	1.32E-05	1.40E-05	1.45E-05	1.04E-05

Kr-83m	3.68E-09	3.24E-09	2.83E-09	2.48E-09	2.18E-09	1.92E-09	1.70E-09	1.51E-09	2.44E-09
Kr-84	6.73E-06	1.29E-05	1.85E-05	2.36E-05	2.82E-05	3.24E-05	3.63E-05	3.99E-05	2.48E-05
Kr-85	2.45E-06	4.56E-06	6.36E-06	7.88E-06	9.17E-06	1.03E-05	1.12E-05	1.20E-05	7.98E-06
Kr-85m	2.21E-08	1.91E-08	1.66E-08	1.43E-08	1.24E-08	1.08E-08	9.45E-09	8.30E-09	1.41E-08
Kr-86	1.24E-05	2.33E-05	3.27E-05	4.08E-05	4.79E-05	5.40E-05	5.94E-05	6.41E-05	4.18E-05
Kr-87	1.21E-08	1.04E-08	9.02E-09	7.79E-09	6.75E-09	5.86E-09	5.11E-09	4.48E-09	7.69E-09
Kr-88	3.64E-08	3.14E-08	2.71E-08	2.34E-08	2.02E-08	1.75E-08	1.52E-08	1.33E-08	2.31E-08
Kr-89	8.57E-10	7.38E-10	6.34E-10	5.45E-10	4.69E-10	4.05E-10	3.51E-10	3.06E-10	5.38E-10
Kr-90	1.57E-10	1.34E-10	1.14E-10	9.79E-11	8.40E-11	7.21E-11	6.22E-11	5.39E-11	9.69E-11
Rb-85	7.09E-06	1.33E-05	1.87E-05	2.34E-05	2.75E-05	3.10E-05	3.42E-05	3.69E-05	2.40E-05
Rb-86	1.88E-09	4.52E-09	6.90E-09	8.95E-09	1.07E-08	1.23E-08	1.37E-08	1.49E-08	9.23E-09
Rb-87	1.74E-05	3.25E-05	4.56E-05	5.69E-05	6.67E-05	7.51E-05	8.25E-05	8.89E-05	5.82E-05
Rb-88	3.83E-09	3.31E-09	2.86E-09	2.47E-09	2.14E-09	1.85E-09	1.62E-09	1.42E-09	2.44E-09
Rb-89	4.33E-09	3.74E-09	3.23E-09	2.78E-09	2.40E-09	2.08E-09	1.81E-09	1.58E-09	2.75E-09
Rb-90	7.92E-10	6.79E-10	5.82E-10	4.99E-10	4.28E-10	3.69E-10	3.19E-10	2.77E-10	4.93E-10
Rb-90m	1.97E-10	1.77E-10	1.58E-10	1.41E-10	1.25E-10	1.12E-10	1.00E-10	9.08E-11	1.38E-10
Rb-91	3.29E-10	2.85E-10	2.47E-10	2.13E-10	1.85E-10	1.61E-10	1.40E-10	1.23E-10	2.10E-10
Sr-86	2.51E-09	1.22E-08	2.90E-08	5.21E-08	8.06E-08	1.14E-07	1.51E-07	1.92E-07	7.91E-08
Sr-87	2.30E-11	6.79E-11	1.31E-10	2.14E-10	3.19E-10	4.50E-10	6.11E-10	8.05E-10	3.27E-10
Sr-88	2.37E-05	4.43E-05	6.21E-05	7.74E-05	9.07E-05	1.02E-04	1.12E-04	1.21E-04	7.91E-05
Sr-89	1.96E-05	2.50E-05	2.49E-05	2.28E-05	2.02E-05	1.77E-05	1.54E-05	1.34E-05	1.99E-05
Sr-90	3.85E-05	7.18E-05	1.00E-04	1.25E-04	1.46E-04	1.63E-04	1.79E-04	1.92E-04	1.27E-04
Sr-91	2.06E-07	1.79E-07	1.55E-07	1.35E-07	1.17E-07	1.02E-07	8.96E-08	7.89E-08	1.33E-07
Sr-92	5.86E-08	5.14E-08	4.49E-08	3.92E-08	3.44E-08	3.02E-08	2.66E-08	2.36E-08	3.86E-08
Sr-93	2.89E-09	2.56E-09	2.25E-09	1.98E-09	1.75E-09	1.55E-09	1.38E-09	1.23E-09	1.95E-09
Sr-94	4.77E-10	4.23E-10	3.73E-10	3.29E-10	2.91E-10	2.58E-10	2.31E-10	2.07E-10	3.24E-10
Sr-95	1.31E-10	1.16E-10	1.03E-10	9.08E-11	8.05E-11	7.15E-11	6.39E-11	5.74E-11	8.93E-11
Y-89	1.20E-05	3.40E-05	5.78E-05	8.03E-05	1.00E-04	1.18E-04	1.34E-04	1.47E-04	8.54E-05
Y-90	9.60E-09	1.84E-08	2.61E-08	3.26E-08	3.83E-08	4.31E-08	4.73E-08	5.09E-08	3.33E-08
Y-91	2.57E-05	3.45E-05	3.55E-05	3.33E-05	3.01E-05	2.67E-05	2.35E-05	2.07E-05	2.88E-05
Y-91m	1.01E-08	8.82E-09	7.66E-09	6.64E-09	5.77E-09	5.03E-09	4.41E-09	3.89E-09	6.55E-09
Y-92	7.91E-08	6.93E-08	6.06E-08	5.29E-08	4.63E-08	4.07E-08	3.59E-08	3.19E-08	5.21E-08
Y-93	2.43E-07	2.15E-07	1.90E-07	1.67E-07	1.47E-07	1.30E-07	1.16E-07	1.04E-07	1.64E-07
Y-94	7.64E-09	6.81E-09	6.03E-09	5.34E-09	4.74E-09	4.22E-09	3.77E-09	3.40E-09	5.24E-09
Y-95	4.19E-09	3.77E-09	3.36E-09	2.99E-09	2.67E-09	2.39E-09	2.16E-09	1.95E-09	2.94E-09
Zr-90	8.61E-08	3.33E-07	7.23E-07	1.24E-06	1.86E-06	2.57E-06	3.36E-06	4.22E-06	1.80E-06
Zr-91	1.31E-05	3.85E-05	6.70E-05	9.48E-05	1.20E-04	1.43E-04	1.63E-04	1.80E-04	1.02E-04
Zr-92	4.05E-05	7.64E-05	1.08E-04	1.35E-04	1.59E-04	1.80E-04	1.99E-04	2.15E-04	1.39E-04
Zr-93	4.27E-05	8.10E-05	1.15E-04	1.44E-04	1.70E-04	1.93E-04	2.13E-04	2.31E-04	1.49E-04
Zr-94	4.42E-05	8.41E-05	1.20E-04	1.51E-04	1.79E-04	2.04E-04	2.27E-04	2.47E-04	1.57E-04
Zr-95	3.05E-05	4.26E-05	4.57E-05	4.45E-05	4.15E-05	3.79E-05	3.44E-05	3.11E-05	3.85E-05
Zr-96	4.35E-05	8.32E-05	1.19E-04	1.51E-04	1.79E-04	2.04E-04	2.27E-04	2.48E-04	1.57E-04
Zr-97	3.95E-07	3.61E-07	3.26E-07	2.95E-07	2.66E-07	2.42E-07	2.20E-07	2.02E-07	2.88E-07
Zr-98	1.90E-10	1.75E-10	1.59E-10	1.45E-10	1.31E-10	1.20E-10	1.10E-10	1.01E-10	1.41E-10
Nb-94	1.01E-11	3.32E-11	6.26E-11	9.40E-11	1.25E-10	1.56E-10	1.85E-10	2.13E-10	1.10E-10
Nb-95	9.10E-06	1.88E-05	2.37E-05	2.51E-05	2.44E-05	2.28E-05	2.09E-05	1.89E-05	2.05E-05
Nb-95m	1.83E-08	2.62E-08	2.84E-08	2.77E-08	2.59E-08	2.37E-08	2.15E-08	1.94E-08	2.39E-08
Nb-96	7.58E-10	1.52E-09	1.92E-09	2.05E-09	2.01E-09	1.91E-09	1.77E-09	1.63E-09	1.70E-09
Nb-97	2.85E-08	2.60E-08	2.35E-08	2.13E-08	1.92E-08	1.74E-08	1.59E-08	1.46E-08	2.08E-08
Nb-98m	1.33E-10	1.22E-10	1.10E-10	9.89E-11	8.89E-11	8.00E-11	7.26E-11	6.62E-11	9.65E-11
Mo-94	4.94E-13	5.81E-12	2.11E-11	4.85E-11	8.83E-11	1.40E-10	2.02E-10	2.73E-10	9.75E-11
Mo-95	4.88E-06	2.31E-05	5.05E-05	8.12E-05	1.12E-04	1.40E-04	1.66E-04	1.89E-04	9.58E-05
Mo-96	4.43E-08	3.45E-07	1.08E-06	2.33E-06	4.10E-06	6.35E-06	9.04E-06	1.21E-05	4.43E-06

Mo-97	4.14E-05	7.99E-05	1.15E-04	1.46E-04	1.75E-04	2.00E-04	2.23E-04	2.44E-04	1.53E-04
Mo-98	4.02E-05	7.79E-05	1.12E-04	1.44E-04	1.72E-04	1.98E-04	2.22E-04	2.44E-04	1.51E-04
Mo-99	1.61E-06	1.49E-06	1.36E-06	1.24E-06	1.13E-06	1.04E-06	9.53E-07	8.79E-07	1.21E-06
Mo-100	4.41E-05	8.56E-05	1.24E-04	1.59E-04	1.90E-04	2.19E-04	2.46E-04	2.71E-04	1.67E-04
Mo-101	5.12E-09	4.79E-09	4.43E-09	4.08E-09	3.77E-09	3.48E-09	3.22E-09	3.00E-09	3.99E-09
Mo-102	3.37E-09	3.23E-09	3.04E-09	2.84E-09	2.66E-09	2.48E-09	2.33E-09	2.19E-09	2.77E-09
Mo-103	2.57E-10	2.60E-10	2.55E-10	2.46E-10	2.36E-10	2.26E-10	2.16E-10	2.07E-10	2.38E-10
Mo-104	1.52E-10	1.61E-10	1.64E-10	1.64E-10	1.62E-10	1.58E-10	1.54E-10	1.50E-10	1.58E-10
Tc-98	9.76E-12	2.69E-11	5.05E-11	7.88E-11	1.11E-10	1.48E-10	1.87E-10	2.28E-10	1.05E-10
Tc-99	4.01E-05	7.77E-05	1.11E-04	1.39E-04	1.64E-04	1.85E-04	2.03E-04	2.18E-04	1.42E-04
Tc-99m	1.29E-07	1.19E-07	1.09E-07	9.96E-08	9.09E-08	8.31E-08	7.64E-08	7.06E-08	9.73E-08
Tc-101	4.99E-09	4.67E-09	4.32E-09	3.98E-09	3.67E-09	3.39E-09	3.14E-09	2.92E-09	3.88E-09
Tc-103	2.13E-10	2.15E-10	2.11E-10	2.03E-10	1.95E-10	1.86E-10	1.78E-10	1.71E-10	1.97E-10
Tc-104	2.96E-09	3.16E-09	3.22E-09	3.21E-09	3.16E-09	3.09E-09	3.02E-09	2.94E-09	3.09E-09
Tc-105	7.97E-10	9.27E-10	9.94E-10	1.02E-09	1.04E-09	1.03E-09	1.03E-09	1.01E-09	9.81E-10
Ru-99	1.33E-09	2.62E-09	3.81E-09	4.88E-09	5.85E-09	6.73E-09	7.53E-09	8.25E-09	5.12E-09
Ru-100	7.65E-07	3.14E-06	6.91E-06	1.19E-05	1.79E-05	2.48E-05	3.24E-05	4.07E-05	1.73E-05
Ru-101	3.62E-05	7.02E-05	1.01E-04	1.29E-04	1.55E-04	1.78E-04	1.99E-04	2.17E-04	1.36E-04
Ru-102	3.10E-05	6.18E-05	9.15E-05	1.20E-04	1.47E-04	1.72E-04	1.97E-04	2.20E-04	1.30E-04
Ru-103	1.28E-05	1.75E-05	1.88E-05	1.88E-05	1.83E-05	1.77E-05	1.69E-05	1.62E-05	1.71E-05
Ru-104	1.51E-05	3.23E-05	5.01E-05	6.82E-05	8.60E-05	1.03E-04	1.21E-04	1.37E-04	7.66E-05
Ru-105	2.81E-08	3.27E-08	3.51E-08	3.62E-08	3.67E-08	3.66E-08	3.64E-08	3.60E-08	3.47E-08
Ru-106	4.36E-06	1.06E-05	1.75E-05	2.45E-05	3.12E-05	3.75E-05	4.32E-05	4.83E-05	2.71E-05
Ru-107	1.40E-10	1.98E-10	2.36E-10	2.61E-10	2.78E-10	2.88E-10	2.94E-10	2.97E-10	2.49E-10
Ru-108	1.01E-10	1.51E-10	1.86E-10	2.10E-10	2.27E-10	2.37E-10	2.44E-10	2.47E-10	2.00E-10
Rh-103	9.64E-06	2.67E-05	4.44E-05	6.03E-05	7.36E-05	8.45E-05	9.31E-05	9.97E-05	6.15E-05
Rh-103m	1.26E-08	1.71E-08	1.84E-08	1.84E-08	1.80E-08	1.73E-08	1.66E-08	1.59E-08	1.68E-08
Rh-105	2.00E-07	2.34E-07	2.51E-07	2.59E-07	2.62E-07	2.62E-07	2.60E-07	2.57E-07	2.48E-07
Rh-106m	1.25E-10	1.46E-10	1.57E-10	1.63E-10	1.66E-10	1.66E-10	1.65E-10	1.64E-10	1.57E-10
Rh-107	8.24E-10	1.16E-09	1.39E-09	1.53E-09	1.63E-09	1.69E-09	1.73E-09	1.74E-09	1.46E-09
Pd-104	4.39E-07	2.87E-06	7.83E-06	1.52E-05	2.46E-05	3.58E-05	4.84E-05	6.20E-05	2.46E-05
Pd-105	7.35E-06	1.70E-05	2.77E-05	3.87E-05	4.98E-05	6.09E-05	7.18E-05	8.24E-05	4.44E-05
Pd-106	1.60E-06	4.47E-06	8.53E-06	1.37E-05	2.00E-05	2.72E-05	3.54E-05	4.44E-05	1.94E-05
Pd-107	2.47E-06	7.05E-06	1.29E-05	1.95E-05	2.66E-05	3.39E-05	4.14E-05	4.89E-05	2.41E-05
Pd-108	1.35E-06	4.18E-06	7.93E-06	1.23E-05	1.71E-05	2.22E-05	2.74E-05	3.27E-05	1.56E-05
Pd-109	1.25E-08	1.94E-08	2.45E-08	2.83E-08	3.13E-08	3.35E-08	3.53E-08	3.67E-08	2.77E-08
Pd-110	4.69E-07	1.38E-06	2.60E-06	4.04E-06	5.63E-06	7.32E-06	9.08E-06	1.09E-05	5.17E-06
Pd-111	8.65E-11	1.22E-10	1.47E-10	1.64E-10	1.77E-10	1.84E-10	1.90E-10	1.93E-10	1.58E-10
Pd-112	2.43E-09	3.14E-09	3.61E-09	3.92E-09	4.13E-09	4.25E-09	4.33E-09	4.38E-09	3.77E-09
Ag-109	8.37E-07	2.55E-06	4.72E-06	7.12E-06	9.59E-06	1.20E-05	1.44E-05	1.66E-05	8.48E-06
Ag-110m	2.18E-09	1.28E-08	3.45E-08	6.71E-08	1.10E-07	1.60E-07	2.17E-07	2.78E-07	1.10E-07
Ag-111	4.08E-08	6.03E-08	7.40E-08	8.38E-08	9.06E-08	9.51E-08	9.81E-08	1.00E-07	8.03E-08
Ag-112	3.62E-10	4.67E-10	5.38E-10	5.85E-10	6.16E-10	6.34E-10	6.46E-10	6.54E-10	5.63E-10
Ag-113	3.35E-10	4.00E-10	4.44E-10	4.72E-10	4.89E-10	4.97E-10	5.02E-10	5.05E-10	4.55E-10
Cd-110	4.84E-08	3.01E-07	8.54E-07	1.75E-06	3.02E-06	4.66E-06	6.67E-06	9.03E-06	3.29E-06
Cd-111	2.13E-07	6.42E-07	1.21E-06	1.87E-06	2.61E-06	3.39E-06	4.22E-06	5.08E-06	2.40E-06
Cd-112	1.47E-07	3.75E-07	6.55E-07	9.70E-07	1.31E-06	1.67E-06	2.04E-06	2.43E-06	1.20E-06
Cd-113	1.04E-08	1.26E-08	1.40E-08	1.49E-08	1.54E-08	1.57E-08	1.59E-08	1.59E-08	1.43E-08
Cd-113m	1.53E-09	3.58E-09	5.98E-09	8.64E-09	1.15E-08	1.45E-08	1.76E-08	2.08E-08	1.05E-08
Cd-114	2.31E-07	5.40E-07	8.89E-07	1.26E-06	1.65E-06	2.04E-06	2.43E-06	2.83E-06	1.48E-06
Cd-115	3.40E-09	3.63E-09	3.68E-09	3.65E-09	3.59E-09	3.51E-09	3.44E-09	3.37E-09	3.54E-09
Cd-115m	3.80E-09	5.60E-09	6.38E-09	6.67E-09	6.73E-09	6.69E-09	6.61E-09	6.52E-09	6.12E-09
Cd-116	1.13E-07	2.44E-07	3.78E-07	5.11E-07	6.40E-07	7.66E-07	8.87E-07	1.00E-06	5.68E-07

Cd-117	1.66E-10	1.75E-10	1.74E-10	1.70E-10	1.64E-10	1.58E-10	1.52E-10	1.47E-10	1.63E-10
In-113	6.85E-12	2.94E-11	7.05E-11	1.32E-10	2.15E-10	3.20E-10	4.49E-10	6.00E-10	2.28E-10
In-115	7.98E-08	1.50E-07	2.02E-07	2.39E-07	2.63E-07	2.78E-07	2.86E-07	2.90E-07	2.23E-07
In-115m	2.85E-10	3.05E-10	3.09E-10	3.07E-10	3.01E-10	2.95E-10	2.89E-10	2.83E-10	2.97E-10
In-117m	1.01E-10	1.06E-10	1.05E-10	1.03E-10	9.92E-11	9.54E-11	9.20E-11	8.88E-11	9.88E-11
Sn-115	4.77E-09	1.03E-08	1.60E-08	2.16E-08	2.70E-08	3.22E-08	3.73E-08	4.21E-08	2.39E-08
Sn-116	1.41E-08	5.69E-08	1.23E-07	2.05E-07	2.98E-07	3.99E-07	5.04E-07	6.11E-07	2.76E-07
Sn-117	1.07E-07	2.27E-07	3.50E-07	4.70E-07	5.87E-07	6.99E-07	8.07E-07	9.11E-07	5.20E-07
Sn-118	9.34E-08	1.95E-07	2.97E-07	3.98E-07	4.94E-07	5.88E-07	6.78E-07	7.65E-07	4.38E-07
Sn-119	1.03E-07	2.12E-07	3.19E-07	4.24E-07	5.23E-07	6.18E-07	7.08E-07	7.95E-07	4.63E-07
Sn-120	1.01E-07	2.07E-07	3.12E-07	4.15E-07	5.13E-07	6.07E-07	6.97E-07	7.84E-07	4.54E-07
Sn-121	1.70E-09	1.75E-09	1.72E-09	1.67E-09	1.60E-09	1.54E-09	1.48E-09	1.42E-09	1.61E-09
Sn-121m	5.83E-09	1.25E-08	1.93E-08	2.59E-08	3.24E-08	3.86E-08	4.47E-08	5.04E-08	2.87E-08
Sn-122	1.26E-07	2.63E-07	4.00E-07	5.33E-07	6.60E-07	7.82E-07	8.99E-07	1.01E-06	5.84E-07
Sn-123	4.74E-08	8.38E-08	1.09E-07	1.25E-07	1.33E-07	1.37E-07	1.38E-07	1.36E-07	1.14E-07
Sn-124	2.16E-07	4.50E-07	6.84E-07	9.10E-07	1.12E-06	1.33E-06	1.52E-06	1.71E-06	9.93E-07
Sn-125	2.57E-08	2.92E-08	3.00E-08	2.96E-08	2.89E-08	2.80E-08	2.72E-08	2.64E-08	2.81E-08
Sn-126	4.60E-07	9.82E-07	1.51E-06	2.03E-06	2.54E-06	3.02E-06	3.48E-06	3.92E-06	2.24E-06
Sn-127	1.42E-09	1.42E-09	1.38E-09	1.31E-09	1.24E-09	1.17E-09	1.11E-09	1.06E-09	1.26E-09
Sn-128	1.44E-09	1.40E-09	1.33E-09	1.24E-09	1.16E-09	1.09E-09	1.02E-09	9.60E-10	1.21E-09
Sn-130	1.53E-10	1.39E-10	1.25E-10	1.13E-10	1.03E-10	9.31E-11	8.50E-11	7.78E-11	1.11E-10
Sb-121	9.81E-08	2.04E-07	3.08E-07	4.08E-07	5.01E-07	5.88E-07	6.69E-07	7.44E-07	4.40E-07
Sb-122	6.92E-11	1.46E-10	2.22E-10	2.93E-10	3.62E-10	4.24E-10	4.84E-10	5.40E-10	3.17E-10
Sb-123	7.90E-08	1.78E-07	2.86E-07	3.98E-07	5.10E-07	6.19E-07	7.24E-07	8.26E-07	4.52E-07
Sb-124	4.88E-10	1.63E-09	3.20E-09	5.02E-09	6.97E-09	8.95E-09	1.09E-08	1.29E-08	6.26E-09
Sb-125	2.46E-07	5.32E-07	8.08E-07	1.06E-06	1.30E-06	1.50E-06	1.69E-06	1.85E-06	1.12E-06
Sb-126	2.86E-09	3.30E-09	3.60E-09	3.84E-09	4.06E-09	4.25E-09	4.44E-09	4.61E-09	3.87E-09
Sb-127	7.61E-08	7.96E-08	7.87E-08	7.60E-08	7.29E-08	6.97E-08	6.68E-08	6.40E-08	7.30E-08
Sb-128	1.38E-08	1.36E-08	1.29E-08	1.21E-08	1.13E-08	1.06E-08	9.98E-09	9.42E-09	1.17E-08
Sb-129	1.14E-08	1.16E-08	1.12E-08	1.07E-08	1.02E-08	9.71E-09	9.24E-09	8.82E-09	1.04E-08
Sb-130	2.20E-09	2.08E-09	1.94E-09	1.79E-09	1.65E-09	1.53E-09	1.42E-09	1.32E-09	1.74E-09
Sb-130m	4.01E-10	3.73E-10	3.42E-10	3.13E-10	2.87E-10	2.63E-10	2.42E-10	2.24E-10	3.06E-10
Sb-131	3.90E-09	3.59E-09	3.29E-09	3.01E-09	2.75E-09	2.52E-09	2.32E-09	2.14E-09	2.94E-09
Sb-132	3.62E-10	3.40E-10	3.14E-10	2.89E-10	2.66E-10	2.45E-10	2.26E-10	2.10E-10	2.81E-10
Sb-132m	2.24E-10	2.02E-10	1.82E-10	1.65E-10	1.50E-10	1.36E-10	1.24E-10	1.14E-10	1.62E-10
Sb-133	3.72E-10	3.31E-10	2.96E-10	2.65E-10	2.38E-10	2.14E-10	1.94E-10	1.76E-10	2.61E-10
Te-122	9.90E-10	4.29E-09	9.91E-09	1.77E-08	2.77E-08	3.95E-08	5.31E-08	6.84E-08	2.77E-08
Te-123	2.10E-12	1.63E-11	5.16E-11	1.14E-10	2.06E-10	3.30E-10	4.85E-10	6.70E-10	2.34E-10
Te-123m	1.43E-12	9.70E-12	2.98E-11	6.49E-11	1.17E-10	1.87E-10	2.76E-10	3.82E-10	1.34E-10
Te-124	1.80E-10	1.06E-09	3.05E-09	6.43E-09	1.14E-08	1.79E-08	2.61E-08	3.59E-08	1.27E-08
Te-125	4.48E-09	1.98E-08	4.71E-08	8.60E-08	1.36E-07	1.95E-07	2.64E-07	3.41E-07	1.37E-07
Te-125m	1.00E-09	3.46E-09	6.60E-09	9.94E-09	1.32E-08	1.62E-08	1.90E-08	2.15E-08	1.14E-08
Te-126	1.53E-08	3.47E-08	5.54E-08	7.70E-08	9.94E-08	1.22E-07	1.46E-07	1.71E-07	9.02E-08
Te-127	7.46E-09	7.85E-09	7.77E-09	7.51E-09	7.21E-09	6.89E-09	6.60E-09	6.33E-09	7.20E-09
Te-127m	3.44E-08	4.80E-08	5.18E-08	5.16E-08	5.00E-08	4.79E-08	4.58E-08	4.38E-08	4.66E-08
Te-128	2.62E-06	5.34E-06	7.99E-06	1.05E-05	1.29E-05	1.51E-05	1.72E-05	1.92E-05	1.13E-05
Te-129	3.02E-09	3.05E-09	2.97E-09	2.84E-09	2.70E-09	2.56E-09	2.44E-09	2.33E-09	2.74E-09
Te-129m	3.14E-10	4.82E-10	5.61E-10	5.99E-10	6.19E-10	6.32E-10	6.43E-10	6.54E-10	5.63E-10
Te-130	1.29E-05	2.52E-05	3.67E-05	4.74E-05	5.71E-05	6.61E-05	7.44E-05	8.22E-05	5.02E-05
Te-131	4.58E-09	4.28E-09	3.95E-09	3.63E-09	3.33E-09	3.07E-09	2.84E-09	2.64E-09	3.54E-09
Te-131m	3.71E-08	3.91E-08	3.85E-08	3.69E-08	3.52E-08	3.35E-08	3.20E-08	3.06E-08	3.53E-08
Te-132	1.36E-06	1.28E-06	1.18E-06	1.08E-06	9.95E-07	9.15E-07	8.46E-07	7.85E-07	1.06E-06
Te-133	3.31E-09	3.02E-09	2.75E-09	2.49E-09	2.27E-09	2.06E-09	1.89E-09	1.74E-09	2.44E-09

Te-133m	1.09E-08	1.00E-08	9.13E-09	8.29E-09	7.55E-09	6.88E-09	6.31E-09	5.81E-09	8.11E-09
Te-134	1.85E-08	1.67E-08	1.50E-08	1.34E-08	1.21E-08	1.09E-08	9.91E-09	9.03E-09	1.32E-08
I-127	1.12E-06	2.43E-06	3.73E-06	4.98E-06	6.15E-06	7.23E-06	8.25E-06	9.20E-06	5.38E-06
I-129	4.16E-06	8.56E-06	1.29E-05	1.69E-05	2.08E-05	2.44E-05	2.78E-05	3.09E-05	1.83E-05
I-130	3.07E-10	6.05E-10	8.92E-10	1.16E-09	1.42E-09	1.66E-09	1.89E-09	2.10E-09	1.25E-09
I-131	2.66E-06	2.54E-06	2.36E-06	2.18E-06	2.01E-06	1.85E-06	1.72E-06	1.60E-06	2.11E-06
I-132	4.13E-08	3.88E-08	3.59E-08	3.30E-08	3.04E-08	2.80E-08	2.59E-08	2.41E-08	3.22E-08
I-132m	1.39E-10	1.75E-10	1.89E-10	1.94E-10	1.94E-10	1.93E-10	1.91E-10	1.89E-10	1.83E-10
I-133	5.55E-07	5.14E-07	4.70E-07	4.29E-07	3.92E-07	3.59E-07	3.30E-07	3.05E-07	4.19E-07
I-134	2.70E-08	2.48E-08	2.26E-08	2.06E-08	1.87E-08	1.71E-08	1.57E-08	1.44E-08	2.01E-08
I-134m	1.09E-10	1.14E-10	1.13E-10	1.09E-10	1.05E-10	1.00E-10	9.62E-11	9.24E-11	1.05E-10
I-135	1.65E-07	1.53E-07	1.40E-07	1.28E-07	1.18E-07	1.08E-07	9.94E-08	9.20E-08	1.25E-07
I-136	2.35E-10	2.13E-10	1.93E-10	1.76E-10	1.60E-10	1.46E-10	1.34E-10	1.24E-10	1.73E-10
Xe-128	9.26E-09	4.29E-08	1.02E-07	1.86E-07	2.93E-07	4.22E-07	5.73E-07	7.41E-07	2.96E-07
Xe-129	7.76E-12	7.39E-11	2.67E-10	6.54E-10	1.30E-09	2.25E-09	3.57E-09	5.29E-09	1.68E-09
Xe-130	2.47E-08	9.74E-08	2.17E-07	3.82E-07	5.89E-07	8.35E-07	1.12E-06	1.44E-06	5.88E-07
Xe-131	1.70E-05	3.40E-05	4.80E-05	5.91E-05	6.78E-05	7.44E-05	7.92E-05	8.26E-05	5.77E-05
Xe-131m	5.54E-08	5.61E-08	5.24E-08	4.85E-08	4.47E-08	4.12E-08	3.82E-08	3.55E-08	4.65E-08
Xe-132	3.01E-05	6.24E-05	9.44E-05	1.26E-04	1.56E-04	1.86E-04	2.14E-04	2.42E-04	1.39E-04
Xe-133	3.66E-06	3.39E-06	3.11E-06	2.84E-06	2.59E-06	2.38E-06	2.19E-06	2.02E-06	2.77E-06
Xe-133m	1.59E-08	1.52E-08	1.43E-08	1.33E-08	1.24E-08	1.15E-08	1.08E-08	1.02E-08	1.29E-08
Xe-134	5.50E-05	1.06E-04	1.53E-04	1.96E-04	2.35E-04	2.71E-04	3.03E-04	3.33E-04	2.07E-04
Xe-135	5.32E-08	4.95E-08	4.55E-08	4.16E-08	3.81E-08	3.50E-08	3.23E-08	2.99E-08	4.07E-08
Xe-135m	8.85E-10	8.57E-10	8.08E-10	7.54E-10	7.02E-10	6.54E-10	6.13E-10	5.76E-10	7.31E-10
Xe-136	8.27E-05	1.61E-04	2.34E-04	3.01E-04	3.62E-04	4.19E-04	4.71E-04	5.19E-04	3.19E-04
Xe-137	1.55E-09	1.42E-09	1.30E-09	1.19E-09	1.09E-09	9.94E-10	9.14E-10	8.44E-10	1.16E-09
Xe-138	5.74E-09	5.22E-09	4.73E-09	4.27E-09	3.87E-09	3.52E-09	3.21E-09	2.95E-09	4.19E-09
Xe-139	2.10E-10	1.88E-10	1.68E-10	1.50E-10	1.35E-10	1.22E-10	1.10E-10	1.00E-10	1.48E-10
Cs-133	4.15E-05	8.26E-05	1.18E-04	1.49E-04	1.75E-04	1.97E-04	2.15E-04	2.31E-04	1.51E-04
Cs-134	8.31E-07	3.58E-06	7.85E-06	1.32E-05	1.93E-05	2.59E-05	3.29E-05	3.98E-05	1.79E-05
Cs-134m	2.42E-10	4.76E-10	6.85E-10	8.59E-10	1.01E-09	1.13E-09	1.24E-09	1.33E-09	8.71E-10
Cs-135	7.57E-06	1.48E-05	2.15E-05	2.79E-05	3.40E-05	3.98E-05	4.55E-05	5.11E-05	3.03E-05
Cs-136	2.10E-08	4.00E-08	5.51E-08	6.81E-08	8.00E-08	9.11E-08	1.02E-07	1.13E-07	7.12E-08
Cs-137	4.32E-05	8.37E-05	1.21E-04	1.55E-04	1.86E-04	2.13E-04	2.39E-04	2.63E-04	1.63E-04
Cs-138	1.47E-08	1.34E-08	1.22E-08	1.10E-08	1.00E-08	9.11E-09	8.34E-09	7.66E-09	1.08E-08
Cs-139	3.82E-09	3.48E-09	3.16E-09	2.86E-09	2.59E-09	2.36E-09	2.15E-09	1.97E-09	2.80E-09
Cs-140	3.86E-10	3.47E-10	3.12E-10	2.80E-10	2.52E-10	2.28E-10	2.07E-10	1.89E-10	2.75E-10
Cs-141	1.11E-10	1.01E-10	9.17E-11	8.29E-11	7.52E-11	6.83E-11	6.24E-11	5.72E-11	8.13E-11
Ba-134	1.84E-08	1.52E-07	5.04E-07	1.15E-06	2.14E-06	3.52E-06	5.30E-06	7.50E-06	2.53E-06
Ba-135	1.79E-11	2.38E-10	1.19E-09	3.70E-09	8.79E-09	1.76E-08	3.15E-08	5.18E-08	1.44E-08
Ba-136	8.78E-08	2.93E-07	5.81E-07	9.34E-07	1.34E-06	1.80E-06	2.31E-06	2.86E-06	1.28E-06
Ba-137	1.04E-07	3.83E-07	8.23E-07	1.41E-06	2.13E-06	2.96E-06	3.91E-06	4.96E-06	2.08E-06
Ba-138	4.69E-05	9.03E-05	1.30E-04	1.66E-04	1.98E-04	2.28E-04	2.55E-04	2.80E-04	1.74E-04
Ba-139	3.47E-08	3.17E-08	2.88E-08	2.61E-08	2.37E-08	2.15E-08	1.97E-08	1.81E-08	2.56E-08
Ba-140	9.31E-06	8.80E-06	7.98E-06	7.21E-06	6.53E-06	5.92E-06	5.39E-06	4.93E-06	7.01E-06
Ba-141	6.94E-09	6.33E-09	5.73E-09	5.17E-09	4.68E-09	4.24E-09	3.87E-09	3.54E-09	5.07E-09
Ba-142	3.93E-09	3.56E-09	3.21E-09	2.89E-09	2.60E-09	2.35E-09	2.13E-09	1.95E-09	2.83E-09
La-138	2.34E-10	4.69E-10	6.87E-10	8.85E-10	1.06E-09	1.22E-09	1.36E-09	1.49E-09	9.27E-10
La-139	4.42E-05	8.50E-05	1.22E-04	1.55E-04	1.85E-04	2.12E-04	2.37E-04	2.59E-04	1.62E-04
La-140	1.27E-06	1.21E-06	1.10E-06	9.95E-07	9.04E-07	8.23E-07	7.53E-07	6.92E-07	9.68E-07
La-141	8.98E-08	8.20E-08	7.42E-08	6.70E-08	6.07E-08	5.50E-08	5.02E-08	4.60E-08	6.56E-08
La-142	3.46E-08	3.14E-08	2.83E-08	2.55E-08	2.30E-08	2.08E-08	1.89E-08	1.73E-08	2.50E-08
La-143	5.38E-09	4.85E-09	4.34E-09	3.89E-09	3.49E-09	3.14E-09	2.84E-09	2.58E-09	3.82E-09

La-144	2.35E-10	2.11E-10	1.88E-10	1.68E-10	1.50E-10	1.35E-10	1.21E-10	1.10E-10	1.65E-10
La-145	1.01E-10	9.01E-11	8.05E-11	7.19E-11	6.45E-11	5.79E-11	5.23E-11	4.75E-11	7.07E-11
Ce-140	3.24E-05	7.28E-05	1.10E-04	1.44E-04	1.74E-04	2.02E-04	2.28E-04	2.52E-04	1.52E-04
Ce-141	1.98E-05	2.30E-05	2.21E-05	2.03E-05	1.84E-05	1.67E-05	1.52E-05	1.38E-05	1.87E-05
Ce-142	4.07E-05	7.83E-05	1.12E-04	1.43E-04	1.71E-04	1.96E-04	2.18E-04	2.39E-04	1.50E-04
Ce-143	7.51E-07	6.77E-07	6.07E-07	5.44E-07	4.88E-07	4.40E-07	3.98E-07	3.62E-07	5.34E-07
Ce-144	3.44E-05	6.03E-05	7.91E-05	9.22E-05	1.01E-04	1.06E-04	1.08E-04	1.08E-04	8.60E-05
Ce-145	7.60E-10	6.86E-10	6.17E-10	5.54E-10	4.99E-10	4.50E-10	4.09E-10	3.72E-10	5.44E-10
Ce-146	2.62E-09	2.38E-09	2.15E-09	1.94E-09	1.75E-09	1.59E-09	1.45E-09	1.33E-09	1.90E-09
Ce-147	1.17E-10	1.09E-10	9.96E-11	9.12E-11	8.36E-11	7.67E-11	7.08E-11	6.55E-11	8.92E-11
Pr-141	2.03E-05	5.37E-05	8.76E-05	1.19E-04	1.48E-04	1.73E-04	1.96E-04	2.17E-04	1.27E-04
Pr-142	9.87E-10	2.64E-09	4.34E-09	5.93E-09	7.35E-09	8.64E-09	9.84E-09	1.09E-08	6.33E-09
Pr-143	9.58E-06	9.03E-06	8.11E-06	7.26E-06	6.51E-06	5.85E-06	5.28E-06	4.79E-06	7.05E-06
Pr-144	1.50E-09	2.59E-09	3.38E-09	3.92E-09	4.28E-09	4.48E-09	4.57E-09	4.58E-09	3.66E-09
Pr-145	9.07E-08	8.19E-08	7.37E-08	6.62E-08	5.96E-08	5.38E-08	4.88E-08	4.45E-08	6.49E-08
Pr-146	4.68E-09	4.26E-09	3.85E-09	3.47E-09	3.14E-09	2.85E-09	2.60E-09	2.38E-09	3.40E-09
Pr-147	1.97E-09	1.80E-09	1.64E-09	1.48E-09	1.35E-09	1.23E-09	1.13E-09	1.04E-09	1.45E-09
Pr-148	2.42E-10	2.21E-10	2.00E-10	1.82E-10	1.66E-10	1.51E-10	1.39E-10	1.27E-10	1.79E-10
Pr-149	1.63E-10	1.52E-10	1.41E-10	1.30E-10	1.20E-10	1.11E-10	1.03E-10	9.57E-11	1.27E-10
Nd-142	3.12E-08	2.00E-07	5.38E-07	1.04E-06	1.68E-06	2.47E-06	3.37E-06	4.38E-06	1.71E-06
Nd-143	2.92E-05	6.27E-05	9.00E-05	1.12E-04	1.28E-04	1.41E-04	1.50E-04	1.56E-04	1.09E-04
Nd-144	4.41E-06	1.66E-05	3.50E-05	5.80E-05	8.43E-05	1.13E-04	1.43E-04	1.74E-04	7.86E-05
Nd-145	2.64E-05	4.96E-05	6.96E-05	8.66E-05	1.01E-04	1.13E-04	1.24E-04	1.32E-04	8.78E-05
Nd-146	2.12E-05	4.15E-05	6.09E-05	7.93E-05	9.67E-05	1.13E-04	1.29E-04	1.44E-04	8.58E-05
Nd-147	2.76E-06	2.58E-06	2.35E-06	2.13E-06	1.94E-06	1.77E-06	1.62E-06	1.49E-06	2.08E-06
Nd-148	1.21E-05	2.35E-05	3.40E-05	4.35E-05	5.21E-05	6.00E-05	6.72E-05	7.39E-05	4.58E-05
Nd-149	7.59E-09	7.12E-09	6.63E-09	6.15E-09	5.71E-09	5.30E-09	4.95E-09	4.64E-09	6.01E-09
Nd-150	4.70E-06	9.32E-06	1.37E-05	1.79E-05	2.18E-05	2.54E-05	2.88E-05	3.21E-05	1.92E-05
Nd-151	3.80E-10	3.74E-10	3.62E-10	3.46E-10	3.30E-10	3.15E-10	3.00E-10	2.87E-10	3.37E-10
Nd-152	2.28E-10	2.29E-10	2.25E-10	2.18E-10	2.10E-10	2.01E-10	1.93E-10	1.85E-10	2.11E-10
Pm-146	3.61E-12	1.62E-11	3.47E-11	5.60E-11	7.86E-11	1.01E-10	1.23E-10	1.44E-10	6.97E-11
Pm-147	1.10E-05	2.06E-05	2.68E-05	3.04E-05	3.22E-05	3.28E-05	3.25E-05	3.16E-05	2.72E-05
Pm-148	8.55E-08	1.73E-07	2.28E-07	2.61E-07	2.77E-07	2.83E-07	2.81E-07	2.73E-07	2.33E-07
Pm-148m	7.96E-08	1.61E-07	2.12E-07	2.42E-07	2.56E-07	2.61E-07	2.58E-07	2.51E-07	2.15E-07
Pm-149	2.59E-07	2.77E-07	2.83E-07	2.80E-07	2.73E-07	2.63E-07	2.52E-07	2.40E-07	2.66E-07
Pm-150	1.96E-10	2.11E-10	2.16E-10	2.15E-10	2.11E-10	2.04E-10	1.96E-10	1.87E-10	2.05E-10
Pm-151	5.18E-08	5.11E-08	4.94E-08	4.74E-08	4.52E-08	4.31E-08	4.11E-08	3.93E-08	4.61E-08
Sm-147	2.33E-07	9.35E-07	1.92E-06	3.02E-06	4.13E-06	5.19E-06	6.15E-06	7.00E-06	3.57E-06
Sm-148	4.95E-07	2.44E-06	5.47E-06	9.20E-06	1.34E-05	1.78E-05	2.23E-05	2.68E-05	1.22E-05
Sm-149	4.28E-07	4.61E-07	4.72E-07	4.69E-07	4.58E-07	4.42E-07	4.23E-07	4.04E-07	4.45E-07
Sm-150	7.19E-06	1.55E-05	2.39E-05	3.20E-05	3.95E-05	4.64E-05	5.27E-05	5.83E-05	3.44E-05
Sm-151	1.40E-06	1.76E-06	1.94E-06	2.08E-06	2.20E-06	2.31E-06	2.40E-06	2.49E-06	2.07E-06
Sm-152	3.26E-06	6.84E-06	9.77E-06	1.21E-05	1.39E-05	1.53E-05	1.64E-05	1.73E-05	1.18E-05
Sm-153	5.77E-08	8.60E-08	1.08E-07	1.25E-07	1.38E-07	1.48E-07	1.55E-07	1.61E-07	1.22E-07
Sm-154	6.45E-07	1.42E-06	2.26E-06	3.15E-06	4.05E-06	4.95E-06	5.85E-06	6.74E-06	3.63E-06
Sm-155	7.49E-11	8.76E-11	9.55E-11	1.00E-10	1.03E-10	1.05E-10	1.05E-10	1.05E-10	9.71E-11
Sm-156	1.10E-09	1.37E-09	1.53E-09	1.63E-09	1.69E-09	1.72E-09	1.73E-09	1.73E-09	1.56E-09
Eu-151	6.33E-10	9.45E-10	1.07E-09	1.16E-09	1.23E-09	1.30E-09	1.35E-09	1.40E-09	1.14E-09
Eu-152	4.09E-10	1.02E-09	1.34E-09	1.51E-09	1.62E-09	1.71E-09	1.79E-09	1.86E-09	1.41E-09
Eu-153	1.50E-06	3.95E-06	6.99E-06	1.02E-05	1.35E-05	1.66E-05	1.94E-05	2.20E-05	1.18E-05
Eu-154	1.03E-07	4.25E-07	9.34E-07	1.56E-06	2.25E-06	2.95E-06	3.62E-06	4.24E-06	2.01E-06
Eu-155	1.09E-07	2.06E-07	3.49E-07	5.27E-07	7.25E-07	9.26E-07	1.12E-06	1.31E-06	6.59E-07
Eu-156	1.14E-07	2.07E-07	3.25E-07	4.73E-07	6.40E-07	8.13E-07	9.84E-07	1.14E-06	5.87E-07

Eu-157	1.08E-09	1.53E-09	1.91E-09	2.27E-09	2.60E-09	2.90E-09	3.17E-09	3.40E-09	2.36E-09
Gd-154	5.77E-10	4.33E-09	1.40E-08	3.15E-08	5.76E-08	9.24E-08	1.35E-07	1.86E-07	6.52E-08
Gd-155	5.69E-10	1.13E-09	1.98E-09	3.09E-09	4.38E-09	5.76E-09	7.17E-09	8.57E-09	4.08E-09
Gd-156	2.34E-07	8.24E-07	1.79E-06	3.23E-06	5.24E-06	7.84E-06	1.11E-05	1.48E-05	5.63E-06
Gd-157	4.91E-09	7.25E-09	9.46E-09	1.18E-08	1.43E-08	1.69E-08	1.96E-08	2.24E-08	1.33E-08
Gd-158	1.26E-07	3.58E-07	6.73E-07	1.07E-06	1.55E-06	2.12E-06	2.78E-06	3.53E-06	1.52E-06
Gd-159	2.81E-10	4.23E-10	5.39E-10	6.36E-10	7.17E-10	7.88E-10	8.52E-10	9.16E-10	6.44E-10
Gd-160	6.63E-09	2.00E-08	3.81E-08	5.96E-08	8.34E-08	1.09E-07	1.35E-07	1.63E-07	7.68E-08
Tb-159	1.61E-08	4.72E-08	8.89E-08	1.39E-07	1.95E-07	2.57E-07	3.23E-07	3.93E-07	1.82E-07
Tb-160	2.44E-10	1.11E-09	2.57E-09	4.51E-09	6.85E-09	9.49E-09	1.24E-08	1.55E-08	6.59E-09
Tb-161	4.93E-10	8.35E-10	1.11E-09	1.35E-09	1.57E-09	1.76E-09	1.95E-09	2.14E-09	1.40E-09
Dy-160	5.89E-11	4.78E-10	1.59E-09	3.64E-09	6.77E-09	1.11E-08	1.66E-08	2.33E-08	7.93E-09
Dy-161	2.20E-09	7.35E-09	1.40E-08	2.16E-08	2.97E-08	3.83E-08	4.73E-08	5.66E-08	2.71E-08
Dy-162	1.16E-09	3.92E-09	7.68E-09	1.22E-08	1.73E-08	2.29E-08	2.90E-08	3.56E-08	1.62E-08
Dy-163	5.49E-10	2.06E-09	4.41E-09	7.56E-09	1.15E-08	1.62E-08	2.17E-08	2.79E-08	1.15E-08
Dy-164	1.68E-10	5.59E-10	1.12E-09	1.84E-09	2.75E-09	3.87E-09	5.22E-09	6.79E-09	2.79E-09
Ho-165	1.02E-10	4.35E-10	1.04E-09	1.97E-09	3.30E-09	5.10E-09	7.47E-09	1.05E-08	3.74E-09
Er-166	3.36E-11	1.26E-10	2.74E-10	4.91E-10	8.02E-10	1.24E-09	1.85E-09	2.67E-09	9.35E-10
Er-168	6.48E-12	2.50E-11	5.45E-11	9.35E-11	1.42E-10	2.02E-10	2.77E-10	3.73E-10	1.47E-10
U-234	8.88E-09	1.59E-08	2.25E-08	3.03E-08	4.09E-08	5.58E-08	7.62E-08	1.03E-07	4.42E-08
U-235	3.86E-03	3.19E-03	2.63E-03	2.17E-03	1.79E-03	1.47E-03	1.21E-03	9.97E-04	2.17E-03
U-236	1.57E-04	2.83E-04	3.81E-04	4.58E-04	5.18E-04	5.62E-04	5.95E-04	6.18E-04	4.47E-04
U-237	4.60E-07	8.62E-07	1.17E-06	1.40E-06	1.57E-06	1.71E-06	1.80E-06	1.87E-06	1.35E-06
U-238	1.87E-02	1.85E-02	1.82E-02	1.80E-02	1.78E-02	1.75E-02	1.73E-02	1.71E-02	1.79E-02
U-239	3.94E-08	3.91E-08	3.88E-08	3.85E-08	3.82E-08	3.79E-08	3.77E-08	3.74E-08	3.84E-08
Np-237	2.30E-06	8.59E-06	1.74E-05	2.75E-05	3.81E-05	4.88E-05	5.92E-05	6.89E-05	3.38E-05
Np-238	7.96E-09	3.03E-08	6.18E-08	9.80E-08	1.37E-07	1.75E-07	2.13E-07	2.48E-07	1.21E-07
Np-239	6.43E-06	6.39E-06	6.34E-06	6.30E-06	6.25E-06	6.20E-06	6.17E-06	6.11E-06	6.27E-06
Pu-238	8.33E-08	6.99E-07	2.23E-06	4.85E-06	8.58E-06	1.34E-05	1.91E-05	2.56E-05	9.30E-06
Pu-239	1.65E-04	2.39E-04	2.70E-04	2.83E-04	2.87E-04	2.87E-04	2.86E-04	2.85E-04	2.63E-04
Pu-240	2.10E-05	5.34E-05	7.85E-05	9.49E-05	1.05E-04	1.10E-04	1.13E-04	1.14E-04	8.62E-05
Pu-241	5.71E-06	2.73E-05	5.50E-05	8.03E-05	9.99E-05	1.14E-04	1.23E-04	1.28E-04	7.90E-05
Pu-242	2.75E-07	2.89E-06	9.48E-06	1.98E-05	3.28E-05	4.70E-05	6.17E-05	7.59E-05	3.12E-05
Pu-243	7.56E-11	7.69E-10	2.48E-09	5.14E-09	8.45E-09	1.20E-08	1.56E-08	1.92E-08	7.96E-09
Pu-244	1.46E-12	3.99E-11	2.32E-10	7.38E-10	1.71E-09	3.28E-09	5.53E-09	8.49E-09	2.50E-09
Am-241	1.57E-08	1.34E-07	3.84E-07	7.15E-07	1.06E-06	1.37E-06	1.63E-06	1.82E-06	8.90E-07
Am-242	6.55E-11	5.54E-10	1.59E-09	2.97E-09	4.41E-09	5.72E-09	6.81E-09	7.63E-09	3.72E-09
Am-242m	8.24E-11	1.13E-09	4.08E-09	8.60E-09	1.37E-08	1.86E-08	2.28E-08	2.61E-08	1.19E-08
Am-243	7.18E-09	1.58E-07	8.10E-07	2.32E-06	4.88E-06	8.49E-06	1.31E-05	1.84E-05	6.01E-06
Am-244	4.33E-13	9.10E-12	4.60E-11	1.31E-10	2.73E-10	4.74E-10	7.29E-10	1.02E-09	3.35E-10
Am-244m	2.85E-13	5.93E-12	2.98E-11	8.45E-11	1.77E-10	3.07E-10	4.71E-10	6.58E-10	2.17E-10
Cm-242	9.97E-10	1.95E-08	9.25E-08	2.44E-07	4.70E-07	7.48E-07	1.05E-06	1.35E-06	4.97E-07
Cm-243	2.57E-12	1.16E-10	8.47E-10	3.02E-09	7.33E-09	1.40E-08	2.30E-08	3.37E-08	1.03E-08
Cm-244	2.74E-10	1.22E-08	9.73E-08	3.85E-07	1.05E-06	2.27E-06	4.20E-06	6.95E-06	1.87E-06
Cm-245	3.21E-12	2.71E-10	3.11E-09	1.60E-08	5.29E-08	1.33E-07	2.79E-07	5.11E-07	1.24E-07
Cm-246	2.75E-14	4.56E-12	8.16E-11	5.82E-10	2.52E-09	7.93E-09	2.02E-08	4.40E-08	9.41E-09
Cm-247	4.10E-17	1.35E-14	3.64E-13	3.48E-12	1.89E-11	7.16E-11	2.14E-10	5.32E-10	1.05E-10

Maximum content

General fields

Pass #	1	2	3	4	5	6	7	8	Avg
Residence time [days]	65.25	130.5	195.75	261	326.25	391.5	460.59	525.84	296.91
Pass burnup [MWd/kg$_{HM}$]	37.09	34.52	31.92	29.43	27.05	24.57	22.75	21.08	27.84
Burnup [MWd/kg$_{HM}$]	37.09	66.24	93.86	117.35	138.54	158.26	177.29	192.46	121.84
Thermal fluence [n/cm^2]	8.52E+20	1.68E+21	2.49E+21	3.24E+21	4.07E+21	4.84E+21	5.58E+21	6.36E+21	3.52E+21
Thermal fluence uncertainty	3.14%	3.10%	3.07%	3.05%	3.04%	3.03%	3.02%	3.02%	3.04%
Fast fluence [n/cm^2]	6.33E+20	1.23E+21	1.82E+21	2.40E+21	2.95E+21	3.50E+21	4.05E+21	4.59E+21	2.62E+21
Fast fluence uncertainty	4.93%	4.76%	4.71%	4.56%	4.40%	4.37%	4.23%	4.15%	4.39%

Atomic densities [at/b.cm]

Pass #	1	2	3	4	5	6	7	8	Avg
H-1	1.79E-08	1.99E-08	1.99E-08	1.99E-08	2.19E-08	2.19E-08	2.36E-08	2.68E-08	1.63E-08
H-2	4.77E-09	4.93E-09	4.58E-09	4.58E-09	5.05E-09	5.87E-09	6.77E-09	7.25E-09	4.00E-09
H-3	2.32E-10	2.25E-10	2.79E-10	2.83E-10	2.98E-10	3.07E-10	2.99E-10	2.99E-10	2.02E-10
He-4	1.70E-07	2.57E-07	3.84E-07	5.36E-07	8.01E-07	1.11E-06	1.60E-06	2.25E-06	8.46E-07
Be-9	1.11E-10	1.11E-10	1.11E-10	1.11E-10	1.11E-10	1.11E-10	1.11E-10	2.20E-10	1.10E-10
C-12	1.17E-02	1.17E-02	1.17E-02	1.17E-02	1.17E-02	1.17E-02	1.17E-02	1.17E-02	1.17E-02
C-13	1.25E-04	1.25E-04	1.25E-04	1.25E-04	1.26E-04	1.26E-04	1.26E-04	1.26E-04	1.25E-04
N-14	2.30E-10	2.12E-10	2.71E-10	2.71E-10	2.71E-10	2.71E-10	2.71E-10	2.59E-10	1.84E-10
N-15	9.02E-09	9.18E-09	8.79E-09	8.79E-09	9.61E-09	9.67E-09	1.12E-08	1.55E-08	8.33E-09
O-16	3.55E-02	3.55E-02	3.55E-02	3.55E-02	3.55E-02	3.55E-02	3.55E-02	3.55E-02	3.55E-02
O-17	2.69E-09	5.21E-09	7.64E-09	9.86E-09	1.24E-08	1.47E-08	1.68E-08	1.91E-08	1.06E-08
Zn-70	5.32E-11	1.13E-10	1.75E-10	2.38E-10	2.99E-10	3.56E-10	4.14E-10	4.62E-10	2.60E-10
Ga-69	2.27E-11	4.52E-11	6.71E-11	8.88E-11	1.10E-10	1.29E-10	1.47E-10	1.63E-10	9.50E-11
Ga-71	1.09E-10	2.32E-10	3.59E-10	4.91E-10	6.21E-10	7.43E-10	8.70E-10	9.70E-10	5.43E-10
Ge-72	3.08E-10	6.73E-10	1.03E-09	1.39E-09	1.71E-09	2.03E-09	2.34E-09	2.58E-09	1.49E-09
Ge-73	1.02E-09	2.06E-09	2.98E-09	3.88E-09	4.63E-09	5.36E-09	6.04E-09	6.57E-09	4.04E-09
Ge-74	3.30E-09	6.31E-09	9.09E-09	1.17E-08	1.40E-08	1.61E-08	1.81E-08	1.97E-08	1.22E-08
Ge-76	2.86E-08	5.09E-08	7.12E-08	8.80E-08	1.03E-07	1.16E-07	1.29E-07	1.39E-07	9.02E-08
Ge-77	6.42E-10	5.80E-10	5.34E-10	4.59E-10	4.08E-10	3.71E-10	3.43E-10	3.24E-10	4.35E-10
Ge-78	2.20E-10	2.00E-10	1.84E-10	1.61E-10	1.43E-10	1.31E-10	1.23E-10	1.16E-10	1.52E-10
As-75	9.94E-09	1.80E-08	2.54E-08	3.15E-08	3.70E-08	4.17E-08	4.62E-08	5.00E-08	3.22E-08
As-77	2.02E-09	1.81E-09	1.65E-09	1.46E-09	1.33E-09	1.20E-09	1.09E-09	1.02E-09	1.38E-09
As-78	2.29E-10	2.09E-10	1.93E-10	1.69E-10	1.51E-10	1.39E-10	1.30E-10	1.23E-10	1.60E-10
Se-76	1.02E-10	3.15E-10	6.67E-10	9.78E-10	1.37E-09	1.88E-09	2.32E-09	2.78E-09	1.22E-09
Se-77	7.07E-08	1.26E-07	1.75E-07	2.14E-07	2.47E-07	2.77E-07	3.04E-07	3.24E-07	2.16E-07
Se-78	1.92E-07	3.43E-07	4.79E-07	5.94E-07	6.97E-07	7.89E-07	8.81E-07	9.52E-07	6.12E-07
Se-79	4.05E-07	7.12E-07	9.86E-07	1.20E-06	1.39E-06	1.55E-06	1.70E-06	1.81E-06	1.21E-06
Se-80	1.17E-06	2.08E-06	2.84E-06	3.49E-06	4.08E-06	4.58E-06	5.08E-06	5.45E-06	3.56E-06
Se-81	4.51E-10	4.09E-10	3.77E-10	3.26E-10	2.90E-10	2.66E-10	2.46E-10	2.32E-10	3.09E-10
Se-82	2.93E-06	5.18E-06	7.07E-06	8.65E-06	1.01E-05	1.13E-05	1.25E-05	1.34E-05	8.82E-06
Se-83	1.24E-09	1.08E-09	9.89E-10	8.37E-10	7.33E-10	6.57E-10	6.02E-10	5.57E-10	7.94E-10
Se-84	3.26E-10	2.83E-10	2.58E-10	2.17E-10	1.89E-10	1.69E-10	1.54E-10	1.42E-10	2.06E-10
Br-79	2.14E-10	3.79E-10	5.26E-10	6.40E-10	7.42E-10	8.27E-10	9.06E-10	9.66E-10	6.43E-10
Br-81	1.85E-06	3.28E-06	4.54E-06	5.55E-06	6.45E-06	7.19E-06	7.95E-06	8.55E-06	5.62E-06
Br-82	2.87E-09	5.21E-09	7.04E-09	8.25E-09	1.02E-08	1.28E-08	1.20E-08	1.33E-08	6.79E-09
Br-83	8.93E-09	7.84E-09	7.18E-09	6.09E-09	5.35E-09	4.82E-09	4.42E-09	4.10E-09	5.78E-09
Br-84	3.43E-09	2.97E-09	2.72E-09	2.29E-09	2.00E-09	1.79E-09	1.63E-09	1.51E-09	2.17E-09
Br-85	4.49E-10	3.87E-10	3.53E-10	2.96E-10	2.57E-10	2.29E-10	2.08E-10	1.90E-10	2.81E-10
Br-86	1.75E-10	1.50E-10	1.37E-10	1.15E-10	1.00E-10	8.91E-11	8.12E-11	7.44E-11	1.09E-10
Br-87	2.12E-10	1.81E-10	1.65E-10	1.38E-10	1.19E-10	1.05E-10	9.59E-11	8.71E-11	1.31E-10
Kr-80	9.09E-12	2.11E-11	3.55E-11	5.48E-11	7.56E-11	1.02E-10	1.24E-10	1.44E-10	6.31E-11

Kr-82	1.75E-08	5.46E-08	1.08E-07	1.64E-07	2.16E-07	2.72E-07	3.48E-07	4.00E-07	1.82E-07
Kr-83	4.66E-06	7.86E-06	1.02E-05	1.20E-05	1.32E-05	1.42E-05	1.50E-05	1.55E-05	1.15E-05
Kr-83m	6.72E-09	5.90E-09	5.40E-09	4.58E-09	4.03E-09	3.62E-09	3.33E-09	3.09E-09	4.35E-09
Kr-84	9.00E-06	1.61E-05	2.21E-05	2.75E-05	3.23E-05	3.64E-05	4.04E-05	4.39E-05	2.82E-05
Kr-85	3.27E-06	5.68E-06	7.53E-06	9.10E-06	1.04E-05	1.13E-05	1.22E-05	1.29E-05	8.93E-06
Kr-85m	4.02E-08	3.46E-08	3.16E-08	2.65E-08	2.30E-08	2.05E-08	1.86E-08	1.70E-08	2.51E-08
Kr-86	1.65E-05	2.90E-05	3.87E-05	4.71E-05	5.42E-05	5.96E-05	6.52E-05	6.92E-05	4.68E-05
Kr-87	2.20E-08	1.89E-08	1.72E-08	1.44E-08	1.25E-08	1.11E-08	1.01E-08	9.22E-09	1.37E-08
Kr-88	6.62E-08	5.68E-08	5.18E-08	4.32E-08	3.74E-08	3.32E-08	3.02E-08	2.74E-08	4.10E-08
Kr-89	1.56E-09	1.33E-09	1.21E-09	1.01E-09	8.69E-10	7.68E-10	6.97E-10	6.30E-10	9.56E-10
Kr-90	2.84E-10	2.42E-10	2.19E-10	1.81E-10	1.55E-10	1.37E-10	1.24E-10	1.11E-10	1.72E-10
Rb-84	2.41E-11	3.04E-11	5.84E-11	7.15E-11	1.09E-10	1.22E-10	1.35E-10	1.25E-10	5.48E-11
Rb-85	9.45E-06	1.66E-05	2.22E-05	2.70E-05	3.11E-05	3.42E-05	3.74E-05	3.98E-05	2.69E-05
Rb-86	5.82E-09	1.34E-08	1.86E-08	2.25E-08	3.39E-08	3.07E-08	3.74E-08	3.35E-08	2.11E-08
Rb-87	2.32E-05	4.06E-05	5.41E-05	6.57E-05	7.54E-05	8.28E-05	9.04E-05	9.58E-05	6.51E-05
Rb-88	6.97E-09	5.99E-09	5.46E-09	4.56E-09	3.95E-09	3.52E-09	3.19E-09	2.91E-09	4.33E-09
Rb-89	7.89E-09	6.77E-09	6.16E-09	5.14E-09	4.45E-09	3.94E-09	3.58E-09	3.26E-09	4.88E-09
Rb-90	1.44E-09	1.23E-09	1.11E-09	9.23E-10	7.93E-10	7.00E-10	6.34E-10	5.71E-10	8.75E-10
Rb-90m	3.62E-10	3.28E-10	3.02E-10	2.61E-10	2.32E-10	2.12E-10	1.97E-10	1.85E-10	2.47E-10
Rb-91	6.00E-10	5.16E-10	4.70E-10	3.94E-10	3.42E-10	3.04E-10	2.77E-10	2.53E-10	3.74E-10
Sr-86	6.78E-09	2.56E-08	5.30E-08	8.90E-08	1.32E-07	1.81E-07	2.31E-07	2.83E-07	1.19E-07
Sr-87	1.12E-10	2.19E-10	3.96E-10	5.13E-10	8.26E-10	1.02E-09	1.20E-09	1.51E-09	6.16E-10
Sr-88	3.15E-05	5.52E-05	7.36E-05	8.94E-05	1.03E-04	1.13E-04	1.23E-04	1.30E-04	8.86E-05
Sr-89	2.63E-05	3.09E-05	3.00E-05	2.73E-05	2.43E-05	2.16E-05	1.88E-05	1.64E-05	2.40E-05
Sr-90	5.14E-05	8.96E-05	1.19E-04	1.44E-04	1.65E-04	1.80E-04	1.96E-04	2.07E-04	1.42E-04
Sr-91	3.75E-07	3.25E-07	2.97E-07	2.49E-07	2.17E-07	1.94E-07	1.77E-07	1.62E-07	2.37E-07
Sr-92	1.07E-07	9.36E-08	8.57E-08	7.25E-08	6.36E-08	5.71E-08	5.24E-08	4.85E-08	6.89E-08
Sr-93	5.29E-09	4.67E-09	4.29E-09	3.66E-09	3.23E-09	2.93E-09	2.70E-09	2.52E-09	3.48E-09
Sr-94	8.73E-10	7.74E-10	7.11E-10	6.09E-10	5.39E-10	4.89E-10	4.52E-10	4.23E-10	5.78E-10
Sr-95	2.40E-10	2.13E-10	1.95E-10	1.68E-10	1.49E-10	1.35E-10	1.25E-10	1.17E-10	1.59E-10
Y-88	3.57E-11	9.84E-11	2.06E-10	2.23E-10	4.30E-10	5.31E-10	5.42E-10	5.14E-10	2.10E-10
Y-89	1.60E-05	4.29E-05	6.98E-05	9.35E-05	1.15E-04	1.32E-04	1.47E-04	1.60E-04	9.59E-05
Y-90	1.29E-08	2.31E-08	3.18E-08	3.83E-08	4.41E-08	4.97E-08	5.43E-08	5.74E-08	3.79E-08
Y-91	3.45E-05	4.24E-05	4.24E-05	3.94E-05	3.57E-05	3.21E-05	2.81E-05	2.49E-05	3.44E-05
Y-91m	1.85E-08	1.60E-08	1.46E-08	1.23E-08	1.07E-08	9.54E-09	8.70E-09	7.99E-09	1.17E-08
Y-92	1.44E-07	1.26E-07	1.16E-07	9.79E-08	8.58E-08	7.71E-08	7.06E-08	6.54E-08	9.29E-08
Y-93	4.45E-07	3.94E-07	3.61E-07	3.09E-07	2.73E-07	2.47E-07	2.28E-07	2.13E-07	2.93E-07
Y-94	1.40E-08	1.25E-08	1.15E-08	9.87E-09	8.77E-09	7.98E-09	7.40E-09	6.94E-09	9.37E-09
Y-95	7.70E-09	6.94E-09	6.39E-09	5.54E-09	4.95E-09	4.53E-09	4.22E-09	3.98E-09	5.26E-09
Zr-90	1.15E-07	4.26E-07	8.95E-07	1.47E-06	2.19E-06	3.00E-06	3.87E-06	4.81E-06	2.07E-06
Zr-91	1.74E-05	4.84E-05	8.08E-05	1.10E-04	1.38E-04	1.60E-04	1.81E-04	1.97E-04	1.15E-04
Zr-92	5.39E-05	9.48E-05	1.27E-04	1.56E-04	1.80E-04	1.99E-04	2.19E-04	2.34E-04	1.56E-04
Zr-93	5.68E-05	1.00E-04	1.36E-04	1.66E-04	1.92E-04	2.14E-04	2.36E-04	2.51E-04	1.67E-04
Zr-94	5.85E-05	1.03E-04	1.41E-04	1.73E-04	2.01E-04	2.27E-04	2.51E-04	2.70E-04	1.77E-04
Zr-95	4.04E-05	5.22E-05	5.47E-05	5.25E-05	4.88E-05	4.50E-05	4.06E-05	3.71E-05	4.58E-05
Zr-96	5.75E-05	1.02E-04	1.40E-04	1.73E-04	2.02E-04	2.28E-04	2.53E-04	2.73E-04	1.77E-04
Zr-97	7.23E-07	6.65E-07	6.15E-07	5.46E-07	4.91E-07	4.53E-07	4.33E-07	4.16E-07	5.16E-07
Zr-98	3.51E-10	3.26E-10	3.02E-10	2.71E-10	2.46E-10	2.27E-10	2.14E-10	2.05E-10	2.54E-10
Nb-94	5.91E-11	1.47E-10	2.63E-10	3.33E-10	4.00E-10	4.36E-10	4.87E-10	4.87E-10	2.74E-10
Nb-95	1.20E-05	2.30E-05	2.80E-05	2.88E-05	2.80E-05	2.62E-05	2.41E-05	2.22E-05	2.37E-05
Nb-95m	2.44E-08	3.20E-08	3.41E-08	3.28E-08	3.05E-08	2.81E-08	2.54E-08	2.33E-08	2.84E-08
Nb-96	1.02E-08	2.37E-08	2.78E-08	2.88E-08	2.97E-08	2.45E-08	2.50E-08	2.17E-08	1.75E-08
Nb-97	5.21E-08	4.80E-08	4.43E-08	3.94E-08	3.55E-08	3.27E-08	3.12E-08	3.01E-08	3.72E-08
Nb-98m	2.45E-10	2.28E-10	2.11E-10	1.85E-10	1.65E-10	1.52E-10	1.42E-10	1.35E-10	1.74E-10
Nb-99	1.72E-10	1.59E-10	1.48E-10	1.33E-10	1.20E-10	1.11E-10	1.05E-10	1.01E-10	1.25E-10
Nb-99m	1.51E-10	1.51E-10	1.42E-10	1.35E-10	1.24E-10	1.17E-10	1.12E-10	1.08E-10	1.23E-10
Mo-94	2.59E-11	1.30E-10	3.19E-10	6.75E-10	1.05E-09	1.32E-09	1.51E-09	2.15E-09	6.92E-10
Mo-95	6.48E-06	2.92E-05	6.16E-05	9.59E-05	1.29E-04	1.59E-04	1.88E-04	2.10E-04	1.09E-04
Mo-96	1.23E-07	8.04E-07	2.12E-06	4.12E-06	7.38E-06	1.02E-05	1.44E-05	1.75E-05	6.69E-06

Mo-97	5.46E-05	9.74E-05	1.36E-04	1.69E-04	1.98E-04	2.24E-04	2.50E-04	2.70E-04	1.74E-04
Mo-98	5.28E-05	9.43E-05	1.33E-04	1.66E-04	1.96E-04	2.24E-04	2.51E-04	2.72E-04	1.73E-04
Mo-99	2.57E-06	2.35E-06	2.17E-06	2.02E-06	1.85E-06	1.70E-06	1.59E-06	1.50E-06	1.89E-06
Mo-100	5.79E-05	1.03E-04	1.47E-04	1.84E-04	2.17E-04	2.49E-04	2.78E-04	3.02E-04	1.91E-04
Mo-101	9.48E-09	9.02E-09	8.39E-09	7.77E-09	7.09E-09	6.61E-09	6.29E-09	6.06E-09	7.20E-09
Mo-102	6.28E-09	6.14E-09	5.75E-09	5.44E-09	5.07E-09	4.76E-09	4.58E-09	4.44E-09	5.03E-09
Mo-103	4.85E-10	5.07E-10	4.87E-10	4.82E-10	4.61E-10	4.40E-10	4.30E-10	4.23E-10	4.38E-10
Mo-104	2.90E-10	3.22E-10	3.20E-10	3.27E-10	3.21E-10	3.11E-10	3.08E-10	3.08E-10	2.95E-10
Mo-105	1.02E-10	1.21E-10	1.24E-10	1.30E-10	1.30E-10	1.28E-10	1.28E-10	1.29E-10	1.17E-10
Tc-97	4.39E-11	8.22E-11	1.32E-10	1.60E-10	1.83E-10	2.07E-10	2.87E-10	2.48E-10	1.22E-10
Tc-98	2.26E-10	4.44E-10	6.84E-10	1.04E-09	1.46E-09	1.62E-09	1.73E-09	2.02E-09	8.87E-10
Tc-99	5.32E-05	9.53E-05	1.32E-04	1.61E-04	1.86E-04	2.07E-04	2.25E-04	2.39E-04	1.61E-04
Tc-99m	2.03E-07	1.85E-07	1.72E-07	1.59E-07	1.46E-07	1.35E-07	1.26E-07	1.18E-07	1.49E-07
Tc-101	9.23E-09	8.78E-09	8.17E-09	7.56E-09	6.90E-09	6.44E-09	6.13E-09	5.91E-09	7.02E-09
Tc-103	4.01E-10	4.20E-10	4.03E-10	3.98E-10	3.80E-10	3.64E-10	3.55E-10	3.49E-10	3.62E-10
Tc-104	5.66E-09	6.31E-09	6.28E-09	6.42E-09	6.28E-09	6.11E-09	6.04E-09	6.04E-09	5.79E-09
Tc-105	1.57E-09	1.92E-09	1.99E-09	2.10E-09	2.11E-09	2.08E-09	2.07E-09	2.10E-09	1.87E-09
Tc-106	7.22E-11	9.62E-11	1.05E-10	1.16E-10	1.20E-10	1.21E-10	1.21E-10	1.25E-10	1.03E-10
Ru-99	1.76E-09	3.20E-09	4.52E-09	5.64E-09	6.66E-09	7.53E-09	8.44E-09	9.18E-09	5.78E-09
Ru-100	1.94E-06	5.84E-06	1.14E-05	1.85E-05	2.69E-05	3.60E-05	4.66E-05	5.54E-05	2.44E-05
Ru-101	4.75E-05	8.52E-05	1.21E-04	1.50E-04	1.77E-04	2.01E-04	2.24E-04	2.42E-04	1.55E-04
Ru-102	4.03E-05	7.51E-05	1.09E-04	1.42E-04	1.72E-04	2.00E-04	2.29E-04	2.51E-04	1.51E-04
Ru-103	1.64E-05	2.17E-05	2.35E-05	2.33E-05	2.28E-05	2.21E-05	2.12E-05	2.06E-05	2.10E-05
Ru-104	1.92E-05	4.09E-05	6.23E-05	8.42E-05	1.05E-04	1.26E-04	1.46E-04	1.61E-04	9.21E-05
Ru-105	5.55E-08	6.76E-08	7.03E-08	7.42E-08	7.46E-08	7.38E-08	7.32E-08	7.46E-08	6.63E-08
Ru-106	6.01E-06	1.47E-05	2.38E-05	3.26E-05	4.10E-05	4.84E-05	5.54E-05	6.03E-05	3.45E-05
Ru-107	3.06E-10	4.36E-10	5.02E-10	5.54E-10	5.86E-10	5.96E-10	5.97E-10	6.19E-10	4.90E-10
Ru-108	2.26E-10	3.38E-10	4.03E-10	4.49E-10	4.80E-10	4.91E-10	4.96E-10	5.18E-10	3.96E-10
Rh-102	4.55E-11	1.07E-10	2.19E-10	3.66E-10	5.74E-10	5.69E-10	5.49E-10	5.86E-10	2.83E-10
Rh-103	1.25E-05	3.30E-05	5.40E-05	7.24E-05	8.72E-05	9.79E-05	1.09E-04	1.14E-04	7.11E-05
Rh-103m	1.61E-08	2.12E-08	2.30E-08	2.28E-08	2.23E-08	2.17E-08	2.07E-08	2.02E-08	2.06E-08
Rh-104	3.53E-11	9.62E-11	1.45E-10	1.72E-10	2.34E-10	2.31E-10	2.87E-10	3.00E-10	1.56E-10
Rh-104m	1.65E-11	4.50E-11	6.78E-11	8.05E-11	1.09E-10	1.08E-10	1.34E-10	1.40E-10	7.28E-11
Rh-105	3.62E-07	4.35E-07	4.60E-07	4.79E-07	4.83E-07	4.89E-07	4.71E-07	4.80E-07	4.33E-07
Rh-106m	4.45E-10	4.99E-10	5.77E-10	5.49E-10	5.99E-10	5.79E-10	6.03E-10	5.79E-10	4.80E-10
Rh-107	1.80E-09	2.56E-09	2.96E-09	3.26E-09	3.44E-09	3.50E-09	3.51E-09	3.64E-09	2.88E-09
Rh-109	4.52E-11	6.81E-11	8.15E-11	9.07E-11	9.72E-11	9.94E-11	1.00E-10	1.05E-10	8.00E-11
Pd-103	2.88E-12	9.59E-12	2.68E-11	5.70E-11	1.12E-10	1.65E-10	2.11E-10	2.72E-10	6.75E-11
Pd-104	9.01E-07	4.85E-06	1.23E-05	2.33E-05	3.51E-05	5.10E-05	6.67E-05	8.24E-05	3.40E-05
Pd-105	9.36E-06	2.18E-05	3.49E-05	4.81E-05	6.12E-05	7.41E-05	8.66E-05	9.74E-05	5.36E-05
Pd-106	2.51E-06	6.63E-06	1.22E-05	1.94E-05	2.74E-05	3.68E-05	4.78E-05	5.77E-05	2.58E-05
Pd-107	3.61E-06	1.02E-05	1.81E-05	2.66E-05	3.54E-05	4.44E-05	5.36E-05	6.11E-05	3.11E-05
Pd-108	2.04E-06	6.27E-06	1.15E-05	1.73E-05	2.38E-05	3.01E-05	3.66E-05	4.24E-05	2.06E-05
Pd-109	2.92E-08	4.83E-08	7.15E-08	8.21E-08	1.02E-07	1.00E-07	1.18E-07	1.23E-07	7.18E-08
Pd-110	6.90E-07	2.04E-06	3.72E-06	5.64E-06	7.67E-06	9.82E-06	1.21E-05	1.38E-05	6.81E-06
Pd-111	1.86E-10	2.68E-10	3.12E-10	3.48E-10	3.71E-10	3.81E-10	3.85E-10	4.00E-10	3.09E-10
Pd-112	4.93E-09	6.62E-09	7.35E-09	8.06E-09	8.45E-09	8.61E-09	8.59E-09	8.96E-09	7.22E-09
Ag-109	1.28E-06	3.83E-06	6.77E-06	9.74E-06	1.32E-05	1.61E-05	1.90E-05	2.18E-05	1.11E-05
Ag-110m	6.96E-09	3.07E-08	8.01E-08	1.38E-07	2.10E-07	2.81E-07	3.73E-07	4.55E-07	1.82E-07
Ag-111	6.47E-08	9.66E-08	1.17E-07	1.28E-07	1.35E-07	1.44E-07	1.49E-07	1.48E-07	1.18E-07
Ag-112	7.33E-10	9.83E-10	1.10E-09	1.20E-09	1.26E-09	1.28E-09	1.28E-09	1.34E-09	1.08E-09
Ag-113	6.63E-10	8.34E-10	8.95E-10	9.71E-10	1.00E-09	1.01E-09	1.01E-09	1.04E-09	8.70E-10
Cd-108	4.66E-12	1.22E-11	2.72E-11	5.10E-11	8.18E-11	8.86E-11	1.00E-10	1.24E-10	4.77E-11
Cd-110	1.53E-07	7.09E-07	1.93E-06	3.56E-06	5.78E-06	8.03E-06	1.16E-05	1.46E-05	5.38E-06
Cd-111	3.01E-07	9.22E-07	1.70E-06	2.57E-06	3.52E-06	4.53E-06	5.60E-06	6.49E-06	3.15E-06
Cd-112	2.01E-07	5.20E-07	8.87E-07	1.30E-06	1.73E-06	2.18E-06	2.66E-06	3.07E-06	1.54E-06
Cd-113	1.46E-08	1.79E-08	2.04E-08	2.11E-08	2.17E-08	2.30E-08	2.26E-08	2.29E-08	1.97E-08
Cd-113m	2.01E-09	4.77E-09	7.91E-09	1.14E-08	1.51E-08	1.88E-08	2.29E-08	2.63E-08	1.34E-08
Cd-114	3.04E-07	7.14E-07	1.15E-06	1.62E-06	2.09E-06	2.57E-06	3.06E-06	3.44E-06	1.84E-06

Cd-115	5.83E-09	6.30E-09	6.43E-09	6.39E-09	6.35E-09	6.22E-09	6.54E-09	6.35E-09	5.91E-09
Cd-115m	4.94E-09	7.14E-09	8.30E-09	8.56E-09	8.62E-09	8.72E-09	8.69E-09	8.91E-09	7.80E-09
Cd-116	1.45E-07	3.09E-07	4.68E-07	6.29E-07	7.76E-07	9.22E-07	1.06E-06	1.17E-06	6.79E-07
Cd-117	3.17E-10	3.43E-10	3.40E-10	3.36E-10	3.26E-10	3.15E-10	3.03E-10	3.02E-10	3.04E-10
In-113	8.98E-12	3.84E-11	9.11E-11	1.71E-10	2.76E-10	4.09E-10	5.81E-10	7.63E-10	2.89E-10
In-115	1.04E-07	2.04E-07	2.70E-07	3.17E-07	3.62E-07	3.71E-07	3.92E-07	3.92E-07	2.87E-07
In-115m	4.84E-10	5.22E-10	5.34E-10	5.31E-10	5.26E-10	5.18E-10	5.41E-10	5.27E-10	4.91E-10
In-117m	1.92E-10	2.08E-10	2.06E-10	2.04E-10	1.97E-10	1.91E-10	1.84E-10	1.83E-10	1.84E-10
Sn-115	6.08E-09	1.30E-08	1.97E-08	2.66E-08	3.27E-08	3.89E-08	4.50E-08	4.97E-08	2.86E-08
Sn-116	3.20E-08	1.06E-07	2.11E-07	3.08E-07	4.32E-07	5.49E-07	6.83E-07	7.97E-07	3.77E-07
Sn-117	1.36E-07	2.87E-07	4.31E-07	5.76E-07	7.07E-07	8.37E-07	9.62E-07	1.06E-06	6.19E-07
Sn-118	1.18E-07	2.44E-07	3.63E-07	4.84E-07	5.94E-07	7.00E-07	8.06E-07	8.86E-07	5.19E-07
Sn-119	1.29E-07	2.62E-07	3.87E-07	5.11E-07	6.21E-07	7.29E-07	8.34E-07	9.15E-07	5.44E-07
Sn-120	1.26E-07	2.57E-07	3.79E-07	5.01E-07	6.10E-07	7.17E-07	8.22E-07	9.05E-07	5.35E-07
Sn-121	3.12E-09	3.28E-09	3.23E-09	3.15E-09	3.08E-09	2.96E-09	2.83E-09	2.82E-09	2.90E-09
Sn-121m	7.43E-09	1.58E-08	2.38E-08	3.19E-08	3.92E-08	4.64E-08	5.34E-08	5.88E-08	3.43E-08
Sn-122	1.59E-07	3.28E-07	4.87E-07	6.46E-07	7.88E-07	9.28E-07	1.06E-06	1.17E-06	6.90E-07
Sn-123	5.96E-08	1.04E-07	1.33E-07	1.51E-07	1.59E-07	1.64E-07	1.64E-07	1.62E-07	1.35E-07
Sn-124	2.72E-07	5.62E-07	8.33E-07	1.10E-06	1.34E-06	1.57E-06	1.80E-06	1.97E-06	1.17E-06
Sn-125	3.54E-08	4.03E-08	4.24E-08	4.09E-08	3.99E-08	3.97E-08	3.84E-08	3.74E-08	3.79E-08
Sn-126	5.86E-07	1.24E-06	1.86E-06	2.49E-06	3.05E-06	3.61E-06	4.15E-06	4.56E-06	2.67E-06
Sn-127	2.67E-09	2.77E-09	2.63E-09	2.56E-09	2.41E-09	2.29E-09	2.21E-09	2.16E-09	2.33E-09
Sn-128	2.70E-09	2.69E-09	2.52E-09	2.40E-09	2.23E-09	2.10E-09	2.01E-09	1.95E-09	2.20E-09
Sn-129m	1.79E-10	1.73E-10	1.62E-10	1.50E-10	1.38E-10	1.29E-10	1.23E-10	1.19E-10	1.39E-10
Sn-130	2.81E-10	2.57E-10	2.38E-10	2.11E-10	1.90E-10	1.76E-10	1.66E-10	1.58E-10	1.99E-10
Sn-130m	1.11E-10	1.02E-10	9.51E-11	8.56E-11	7.77E-11	7.20E-11	6.82E-11	6.54E-11	8.04E-11
Sb-121	1.23E-07	2.53E-07	3.76E-07	4.88E-07	5.94E-07	6.86E-07	7.76E-07	8.56E-07	5.14E-07
Sb-122	3.83E-10	8.18E-10	1.08E-09	1.48E-09	1.99E-09	2.02E-09	2.82E-09	2.83E-09	1.37E-09
Sb-123	9.98E-08	2.21E-07	3.48E-07	4.80E-07	6.01E-07	7.26E-07	8.48E-07	9.50E-07	5.32E-07
Sb-124	1.41E-09	3.75E-09	6.78E-09	1.02E-08	1.36E-08	1.84E-08	2.12E-08	2.39E-08	1.13E-08
Sb-125	3.12E-07	6.66E-07	9.89E-07	1.29E-06	1.55E-06	1.79E-06	2.00E-06	2.15E-06	1.33E-06
Sb-126	4.18E-09	5.54E-09	7.14E-09	8.95E-09	9.19E-09	9.63E-09	1.12E-08	1.26E-08	7.65E-09
Sb-127	1.18E-07	1.24E-07	1.24E-07	1.21E-07	1.14E-07	1.12E-07	1.07E-07	1.06E-07	1.10E-07
Sb-128	2.60E-08	2.61E-08	2.45E-08	2.35E-08	2.19E-08	2.06E-08	1.98E-08	1.92E-08	2.15E-08
Sb-129	2.16E-08	2.26E-08	2.15E-08	2.11E-08	2.00E-08	1.90E-08	1.84E-08	1.80E-08	1.92E-08
Sb-130	4.09E-09	3.94E-09	3.67E-09	3.40E-09	3.13E-09	2.92E-09	2.79E-09	2.68E-09	3.16E-09
Sb-130m	7.42E-10	6.99E-10	6.50E-10	5.90E-10	5.38E-10	4.99E-10	4.73E-10	4.55E-10	5.52E-10
Sb-131	7.19E-09	6.72E-09	6.24E-09	5.65E-09	5.15E-09	4.78E-09	4.53E-09	4.35E-09	5.30E-09
Sb-132	6.71E-10	6.39E-10	5.95E-10	5.46E-10	5.01E-10	4.66E-10	4.43E-10	4.27E-10	5.09E-10
Sb-132m	4.11E-10	3.73E-10	3.45E-10	3.07E-10	2.77E-10	2.57E-10	2.43E-10	2.32E-10	2.90E-10
Sb-133	6.80E-10	6.08E-10	5.60E-10	4.90E-10	4.40E-10	4.06E-10	3.80E-10	3.59E-10	4.66E-10
Te-122	2.39E-09	8.53E-09	1.99E-08	3.12E-08	4.54E-08	6.36E-08	8.20E-08	1.04E-07	4.33E-08
Te-123	1.40E-11	7.15E-11	1.77E-10	3.66E-10	5.61E-10	8.83E-10	1.19E-09	1.66E-09	5.63E-10
Te-123m	8.16E-12	3.81E-11	1.08E-10	1.98E-10	3.22E-10	5.10E-10	6.80E-10	9.87E-10	3.24E-10
Te-124	4.31E-10	2.18E-09	5.75E-09	1.16E-08	1.99E-08	3.01E-08	4.34E-08	5.91E-08	2.03E-08
Te-125	5.74E-09	2.49E-08	5.80E-08	1.05E-07	1.63E-07	2.32E-07	3.20E-07	4.07E-07	1.63E-07
Te-125m	1.28E-09	4.33E-09	8.10E-09	1.20E-08	1.58E-08	1.94E-08	2.26E-08	2.51E-08	1.35E-08
Te-126	1.95E-08	4.47E-08	7.08E-08	9.73E-08	1.29E-07	1.56E-07	1.88E-07	2.19E-07	1.12E-07
Te-127	1.12E-08	1.19E-08	1.19E-08	1.15E-08	1.10E-08	1.07E-08	1.03E-08	1.01E-08	1.06E-08
Te-127m	4.15E-08	5.61E-08	5.99E-08	5.99E-08	5.86E-08	5.61E-08	5.43E-08	5.23E-08	5.41E-08
Te-128	3.36E-06	6.57E-06	9.61E-06	1.25E-05	1.51E-05	1.76E-05	2.00E-05	2.19E-05	1.32E-05
Te-129	5.71E-09	5.95E-09	5.69E-09	5.56E-09	5.26E-09	5.01E-09	4.86E-09	4.76E-09	5.06E-09
Te-129m	5.08E-10	7.29E-10	8.65E-10	9.00E-10	9.97E-10	1.07E-09	1.12E-09	1.13E-09	8.33E-10
Te-130	1.68E-05	3.05E-05	4.37E-05	5.53E-05	6.56E-05	7.54E-05	8.48E-05	9.21E-05	5.77E-05
Te-131	8.47E-09	8.04E-09	7.48E-09	6.85E-09	6.28E-09	5.84E-09	5.55E-09	5.34E-09	6.39E-09
Te-131m	6.86E-08	7.41E-08	7.20E-08	7.00E-08	6.66E-08	6.42E-08	6.16E-08	6.09E-08	6.39E-08
Te-132	2.13E-06	1.97E-06	1.84E-06	1.71E-06	1.58E-06	1.47E-06	1.38E-06	1.31E-06	1.60E-06
Te-133	6.09E-09	5.62E-09	5.21E-09	4.67E-09	4.22E-09	3.90E-09	3.70E-09	3.53E-09	4.39E-09
Te-133m	2.01E-08	1.87E-08	1.73E-08	1.56E-08	1.41E-08	1.30E-08	1.23E-08	1.18E-08	1.46E-08

Te-134	3.40E-08	3.08E-08	2.84E-08	2.50E-08	2.24E-08	2.07E-08	1.94E-08	1.84E-08	2.37E-08
Te-135	1.23E-10	1.12E-10	1.04E-10	9.22E-11	8.30E-11	7.71E-11	7.28E-11	6.93E-11	8.71E-11
I-127	1.42E-06	3.02E-06	4.56E-06	6.00E-06	7.29E-06	8.54E-06	9.65E-06	1.06E-05	6.33E-06
I-128	4.64E-11	1.04E-10	1.73E-10	2.37E-10	3.04E-10	2.85E-10	3.39E-10	4.86E-10	1.76E-10
I-129	5.29E-06	1.06E-05	1.55E-05	2.03E-05	2.45E-05	2.86E-05	3.25E-05	3.53E-05	2.14E-05
I-130	9.80E-10	1.95E-09	3.01E-09	3.98E-09	4.23E-09	5.44E-09	5.72E-09	5.93E-09	3.35E-09
I-131	3.49E-06	3.30E-06	3.17E-06	2.90E-06	2.71E-06	2.55E-06	2.37E-06	2.24E-06	2.78E-06
I-132	6.42E-08	5.99E-08	5.61E-08	5.23E-08	4.83E-08	4.51E-08	4.22E-08	4.03E-08	4.89E-08
I-132m	2.93E-10	3.69E-10	3.89E-10	4.06E-10	4.05E-10	4.06E-10	3.91E-10	3.99E-10	3.60E-10
I-133	1.01E-06	9.47E-07	8.77E-07	7.97E-07	7.26E-07	6.70E-07	6.36E-07	6.09E-07	7.45E-07
I-134	4.99E-08	4.63E-08	4.29E-08	3.86E-08	3.50E-08	3.24E-08	3.06E-08	2.93E-08	3.62E-08
I-134m	2.09E-10	2.25E-10	2.19E-10	2.17E-10	2.06E-10	1.98E-10	1.93E-10	1.90E-10	1.96E-10
I-135	3.05E-07	2.87E-07	2.66E-07	2.42E-07	2.21E-07	2.05E-07	1.94E-07	1.87E-07	2.26E-07
I-136	4.31E-10	3.94E-10	3.66E-10	3.28E-10	2.98E-10	2.77E-10	2.63E-10	2.51E-10	3.10E-10
I-136m	1.25E-10	1.22E-10	1.14E-10	1.07E-10	1.00E-10	9.39E-11	9.02E-11	8.74E-11	9.96E-11
I-137	1.49E-10	1.37E-10	1.27E-10	1.15E-10	1.05E-10	9.70E-11	9.22E-11	8.84E-11	1.08E-10
Xe-128	2.46E-08	9.20E-08	1.95E-07	3.34E-07	5.17E-07	6.94E-07	9.28E-07	1.16E-06	4.61E-07
Xe-129	3.03E-11	2.02E-10	7.00E-10	1.52E-09	2.70E-09	4.43E-09	6.79E-09	9.62E-09	3.02E-09
Xe-129m	1.50E-12	7.69E-12	1.55E-11	2.74E-11	4.08E-11	5.20E-11	8.28E-11	1.00E-10	3.46E-11
Xe-130	4.05E-08	1.50E-07	3.19E-07	5.55E-07	8.18E-07	1.13E-06	1.53E-06	1.93E-06	7.93E-07
Xe-131	2.25E-05	4.23E-05	5.85E-05	7.01E-05	7.90E-05	8.55E-05	9.08E-05	9.30E-05	6.67E-05
Xe-131m	7.36E-08	7.23E-08	6.80E-08	6.22E-08	5.81E-08	5.34E-08	4.93E-08	4.59E-08	5.91E-08
Xe-132	3.92E-05	7.70E-05	1.15E-04	1.51E-04	1.85E-04	2.19E-04	2.53E-04	2.78E-04	1.63E-04
Xe-133	4.88E-06	4.50E-06	4.23E-06	3.84E-06	3.58E-06	3.33E-06	3.08E-06	2.91E-06	3.72E-06
Xe-133m	2.48E-08	2.42E-08	2.32E-08	2.27E-08	2.43E-08	2.26E-08	2.20E-08	2.32E-08	2.15E-08
Xe-134	7.25E-05	1.29E-04	1.82E-04	2.27E-04	2.68E-04	3.06E-04	3.42E-04	3.71E-04	2.36E-04
Xe-135	7.49E-08	7.53E-08	6.89E-08	6.65E-08	5.92E-08	5.75E-08	5.20E-08	5.15E-08	5.91E-08
Xe-135m	1.66E-09	1.64E-09	1.53E-09	1.45E-09	1.35E-09	1.26E-09	1.21E-09	1.17E-09	1.33E-09
Xe-136	1.12E-04	2.00E-04	2.83E-04	3.54E-04	4.19E-04	4.79E-04	5.37E-04	5.85E-04	3.68E-04
Xe-137	2.85E-09	2.66E-09	2.47E-09	2.23E-09	2.03E-09	1.88E-09	1.79E-09	1.71E-09	2.09E-09
Xe-138	1.06E-08	9.69E-09	8.97E-09	7.99E-09	7.19E-09	6.65E-09	6.29E-09	5.99E-09	7.52E-09
Xe-139	3.84E-10	3.46E-10	3.19E-10	2.79E-10	2.50E-10	2.31E-10	2.16E-10	2.04E-10	2.65E-10
Cs-131	3.01E-11	5.74E-11	9.44E-11	1.09E-10	7.57E-11	1.53E-10	2.74E-10	1.60E-10	3.74E-11
Cs-132	1.32E-10	2.37E-10	4.84E-10	4.27E-10	7.81E-10	8.29E-10	8.03E-10	1.00E-09	3.56E-10
Cs-133	5.51E-05	1.01E-04	1.42E-04	1.73E-04	1.99E-04	2.20E-04	2.40E-04	2.55E-04	1.71E-04
Cs-134	2.14E-06	6.95E-06	1.35E-05	2.29E-05	3.00E-05	3.82E-05	4.80E-05	5.54E-05	2.57E-05
Cs-134m	2.45E-09	3.62E-09	4.42E-09	5.79E-09	6.13E-09	6.52E-09	6.46E-09	7.31E-09	4.44E-09
Cs-135	8.66E-06	1.65E-05	2.40E-05	3.12E-05	3.80E-05	4.48E-05	5.12E-05	5.78E-05	3.40E-05
Cs-136	4.46E-08	8.29E-08	1.10E-07	1.39E-07	1.62E-07	1.91E-07	2.14E-07	2.30E-07	1.35E-07
Cs-137	5.67E-05	1.01E-04	1.44E-04	1.80E-04	2.12E-04	2.42E-04	2.71E-04	2.93E-04	1.86E-04
Cs-138	2.70E-08	2.49E-08	2.31E-08	2.06E-08	1.86E-08	1.72E-08	1.63E-08	1.56E-08	1.94E-08
Cs-138m	9.85E-11	1.03E-10	9.77E-11	9.50E-11	8.91E-11	8.50E-11	8.18E-11	8.00E-11	8.65E-11
Cs-139	7.03E-09	6.47E-09	5.99E-09	5.34E-09	4.82E-09	4.45E-09	4.21E-09	4.02E-09	5.03E-09
Cs-140	7.08E-10	6.41E-10	5.92E-10	5.21E-10	4.67E-10	4.31E-10	4.05E-10	3.84E-10	4.93E-10
Cs-141	2.05E-10	1.88E-10	1.74E-10	1.55E-10	1.40E-10	1.29E-10	1.22E-10	1.16E-10	1.46E-10
Ba-134	4.64E-08	2.93E-07	8.69E-07	1.87E-06	3.44E-06	5.36E-06	7.69E-06	1.07E-05	3.65E-06
Ba-135	9.42E-11	1.13E-09	3.96E-09	1.05E-08	2.41E-08	4.51E-08	7.47E-08	1.17E-07	3.23E-08
Ba-135m	1.65E-12	1.04E-11	4.03E-11	8.80E-11	1.25E-10	2.28E-10	3.11E-10	5.16E-10	1.34E-10
Ba-136	1.31E-07	4.28E-07	8.38E-07	1.33E-06	1.85E-06	2.49E-06	3.13E-06	3.84E-06	1.71E-06
Ba-137	1.35E-07	4.70E-07	9.86E-07	1.66E-06	2.47E-06	3.39E-06	4.56E-06	5.71E-06	2.41E-06
Ba-138	6.17E-05	1.10E-04	1.54E-04	1.91E-04	2.25E-04	2.56E-04	2.86E-04	3.10E-04	1.98E-04
Ba-139	6.40E-08	5.90E-08	5.47E-08	4.88E-08	4.41E-08	4.08E-08	3.85E-08	3.68E-08	4.59E-08
Ba-140	1.24E-05	1.15E-05	1.05E-05	9.36E-06	8.41E-06	7.74E-06	7.13E-06	6.53E-06	8.98E-06
Ba-141	1.28E-08	1.18E-08	1.09E-08	9.67E-09	8.70E-09	8.03E-09	7.57E-09	7.21E-09	9.10E-09
Ba-142	7.24E-09	6.60E-09	6.10E-09	5.38E-09	4.82E-09	4.45E-09	4.18E-09	3.97E-09	5.08E-09
Ba-143	1.55E-10	1.39E-10	1.28E-10	1.11E-10	9.97E-11	9.13E-11	8.53E-11	8.04E-11	1.06E-10
La-137	3.29E-11	6.12E-11	1.03E-10	1.30E-10	1.50E-10	1.77E-10	2.16E-10	2.10E-10	1.01E-10
La-138	5.20E-10	1.01E-09	1.44E-09	2.08E-09	2.70E-09	2.98E-09	3.16E-09	3.50E-09	1.86E-09
La-139	5.83E-05	1.03E-04	1.44E-04	1.79E-04	2.10E-04	2.38E-04	2.65E-04	2.87E-04	1.84E-04

La-140	1.69E-06	1.60E-06	1.45E-06	1.31E-06	1.18E-06	1.11E-06	9.86E-07	9.26E-07	1.25E-06
La-141	1.66E-07	1.52E-07	1.41E-07	1.25E-07	1.13E-07	1.04E-07	9.82E-08	9.36E-08	1.18E-07
La-142	6.36E-08	5.82E-08	5.38E-08	4.76E-08	4.27E-08	3.94E-08	3.70E-08	3.52E-08	4.49E-08
La-143	9.88E-09	8.95E-09	8.26E-09	7.22E-09	6.46E-09	5.94E-09	5.57E-09	5.27E-09	6.84E-09
La-144	4.31E-10	3.88E-10	3.57E-10	3.10E-10	2.78E-10	2.54E-10	2.38E-10	2.24E-10	2.95E-10
La-145	1.84E-10	1.66E-10	1.53E-10	1.33E-10	1.19E-10	1.09E-10	1.03E-10	9.68E-11	1.27E-10
Ce-138	3.86E-11	8.38E-11	1.47E-10	1.79E-10	2.13E-10	2.53E-10	3.44E-10	3.03E-10	1.41E-10
Ce-139	2.07E-10	3.75E-10	6.79E-10	1.10E-09	1.62E-09	1.64E-09	1.57E-09	1.64E-09	8.35E-10
Ce-140	4.28E-05	8.92E-05	1.30E-04	1.66E-04	1.98E-04	2.28E-04	2.57E-04	2.80E-04	1.73E-04
Ce-141	2.62E-05	2.90E-05	2.73E-05	2.52E-05	2.30E-05	2.10E-05	1.88E-05	1.73E-05	2.30E-05
Ce-142	5.36E-05	9.53E-05	1.34E-04	1.65E-04	1.94E-04	2.20E-04	2.45E-04	2.65E-04	1.70E-04
Ce-143	1.31E-06	1.18E-06	1.08E-06	9.63E-07	8.73E-07	7.91E-07	7.41E-07	6.96E-07	9.08E-07
Ce-144	4.55E-05	7.39E-05	9.38E-05	1.06E-04	1.13E-04	1.18E-04	1.20E-04	1.20E-04	9.74E-05
Ce-145	1.40E-09	1.27E-09	1.17E-09	1.03E-09	9.23E-10	8.52E-10	7.99E-10	7.58E-10	9.74E-10
Ce-146	4.81E-09	4.41E-09	4.08E-09	3.62E-09	3.25E-09	3.00E-09	2.83E-09	2.70E-09	3.41E-09
Ce-147	2.17E-10	2.03E-10	1.89E-10	1.72E-10	1.57E-10	1.46E-10	1.38E-10	1.33E-10	1.61E-10
Ce-148	1.73E-10	1.56E-10	1.45E-10	1.28E-10	1.15E-10	1.07E-10	1.01E-10	9.58E-11	1.21E-10
Pr-141	2.67E-05	6.62E-05	1.03E-04	1.38E-04	1.67E-04	1.94E-04	2.20E-04	2.40E-04	1.44E-04
Pr-142	5.57E-09	1.23E-08	1.81E-08	2.38E-08	2.71E-08	2.90E-08	3.47E-08	3.99E-08	1.92E-08
Pr-142m	2.59E-11	5.64E-11	8.32E-11	1.09E-10	1.22E-10	1.32E-10	1.57E-10	1.82E-10	8.72E-11
Pr-143	1.28E-05	1.20E-05	1.07E-05	9.60E-06	8.52E-06	7.77E-06	6.93E-06	6.20E-06	9.06E-06
Pr-144	2.11E-09	3.22E-09	4.01E-09	4.51E-09	4.84E-09	5.02E-09	5.07E-09	5.11E-09	4.16E-09
Pr-145	1.67E-07	1.52E-07	1.40E-07	1.23E-07	1.10E-07	1.02E-07	9.55E-08	9.06E-08	1.16E-07
Pr-146	8.62E-09	7.90E-09	7.30E-09	6.48E-09	5.83E-09	5.38E-09	5.08E-09	4.84E-09	6.11E-09
Pr-147	3.62E-09	3.35E-09	3.10E-09	2.78E-09	2.52E-09	2.33E-09	2.20E-09	2.11E-09	2.61E-09
Pr-148	4.45E-10	4.10E-10	3.80E-10	3.41E-10	3.09E-10	2.86E-10	2.71E-10	2.59E-10	3.21E-10
Pr-149	3.01E-10	2.86E-10	2.66E-10	2.46E-10	2.26E-10	2.11E-10	2.01E-10	1.94E-10	2.29E-10
Nd-142	6.51E-08	3.39E-07	8.36E-07	1.55E-06	2.36E-06	3.41E-06	4.50E-06	5.78E-06	2.30E-06
Nd-143	3.81E-05	7.49E-05	1.02E-04	1.24E-04	1.40E-04	1.53E-04	1.61E-04	1.67E-04	1.20E-04
Nd-144	6.36E-06	2.30E-05	4.60E-05	7.49E-05	1.06E-04	1.37E-04	1.74E-04	2.06E-04	9.40E-05
Nd-145	3.50E-05	6.09E-05	8.27E-05	9.96E-05	1.14E-04	1.25E-04	1.36E-04	1.44E-04	9.83E-05
Nd-146	2.78E-05	5.06E-05	7.24E-05	9.24E-05	1.12E-04	1.31E-04	1.49E-04	1.64E-04	9.90E-05
Nd-147	3.65E-06	3.37E-06	3.07E-06	2.75E-06	2.51E-06	2.33E-06	2.15E-06	2.00E-06	2.66E-06
Nd-148	1.61E-05	2.87E-05	4.07E-05	5.07E-05	5.98E-05	6.82E-05	7.63E-05	8.25E-05	5.25E-05
Nd-149	1.40E-08	1.34E-08	1.25E-08	1.16E-08	1.07E-08	1.01E-08	9.58E-09	9.57E-09	1.08E-08
Nd-150	6.11E-06	1.13E-05	1.64E-05	2.11E-05	2.53E-05	2.95E-05	3.33E-05	3.64E-05	2.23E-05
Nd-151	7.10E-10	7.19E-10	6.94E-10	6.65E-10	6.32E-10	6.38E-10	6.15E-10	5.99E-10	6.22E-10
Nd-152	4.29E-10	4.46E-10	4.28E-10	4.26E-10	4.09E-10	3.91E-10	3.83E-10	3.78E-10	3.88E-10
Pm-145	2.35E-11	4.43E-11	6.32E-11	7.91E-11	8.77E-11	9.29E-11	1.30E-10	1.17E-10	6.06E-11
Pm-146	8.40E-11	2.05E-10	3.47E-10	4.30E-10	5.99E-10	6.17E-10	6.50E-10	7.23E-10	3.85E-10
Pm-147	1.49E-05	2.68E-05	3.40E-05	3.74E-05	3.91E-05	3.99E-05	3.93E-05	3.81E-05	3.30E-05
Pm-148	2.92E-07	4.82E-07	5.80E-07	6.11E-07	6.79E-07	6.59E-07	6.62E-07	6.32E-07	5.18E-07
Pm-148m	2.58E-07	4.75E-07	5.33E-07	6.02E-07	6.45E-07	6.46E-07	6.48E-07	5.74E-07	4.85E-07
Pm-149	4.40E-07	4.76E-07	5.03E-07	5.12E-07	5.00E-07	4.94E-07	4.76E-07	4.51E-07	4.44E-07
Pm-150	8.65E-10	9.46E-10	1.08E-09	1.13E-09	1.08E-09	9.37E-10	8.87E-10	8.47E-10	7.40E-10
Pm-151	9.37E-08	9.46E-08	9.20E-08	8.80E-08	8.36E-08	8.45E-08	8.15E-08	7.96E-08	8.22E-08
Pm-152	1.57E-10	1.64E-10	1.58E-10	1.56E-10	1.50E-10	1.44E-10	1.43E-10	1.40E-10	1.43E-10
Pm-153	1.22E-10	1.30E-10	1.27E-10	1.28E-10	1.24E-10	1.20E-10	1.18E-10	1.17E-10	1.16E-10
Sm-146	1.82E-12	8.30E-12	1.97E-11	3.73E-11	6.28E-11	8.06E-11	9.79E-11	1.42E-10	4.48E-11
Sm-147	3.19E-07	1.23E-06	2.47E-06	3.85E-06	5.17E-06	6.43E-06	7.59E-06	8.68E-06	4.38E-06
Sm-148	1.07E-06	4.14E-06	8.33E-06	1.28E-05	1.79E-05	2.29E-05	2.89E-05	3.31E-05	1.56E-05
Sm-149	6.57E-07	7.48E-07	7.98E-07	7.96E-07	7.71E-07	7.54E-07	7.47E-07	7.43E-07	7.13E-07
Sm-150	9.48E-06	1.96E-05	2.94E-05	3.89E-05	4.67E-05	5.42E-05	6.14E-05	6.63E-05	4.02E-05
Sm-151	1.64E-06	2.11E-06	2.39E-06	2.60E-06	2.82E-06	3.15E-06	3.16E-06	3.35E-06	2.57E-06
Sm-152	4.86E-06	9.82E-06	1.35E-05	1.65E-05	1.85E-05	2.04E-05	2.21E-05	2.28E-05	1.56E-05
Sm-153	2.23E-07	3.22E-07	4.16E-07	4.43E-07	5.33E-07	5.62E-07	5.76E-07	6.44E-07	3.98E-07
Sm-154	8.51E-07	1.89E-06	3.00E-06	4.10E-06	5.16E-06	6.32E-06	7.50E-06	8.33E-06	4.55E-06
Sm-155	1.48E-10	1.84E-10	2.09E-10	2.18E-10	2.45E-10	2.71E-10	2.66E-10	3.16E-10	2.06E-10
Sm-156	2.24E-09	2.90E-09	3.12E-09	3.40E-09	3.50E-09	3.51E-09	3.51E-09	3.60E-09	3.02E-09

Eu-151	7.33E-10	1.22E-09	1.41E-09	1.58E-09	1.69E-09	1.78E-09	1.88E-09	2.03E-09	1.48E-09
Eu-152	5.41E-10	1.28E-09	1.73E-09	2.00E-09	2.17E-09	2.45E-09	2.46E-09	2.61E-09	1.84E-09
Eu-153	2.40E-06	5.92E-06	9.90E-06	1.38E-05	1.72E-05	2.08E-05	2.37E-05	2.66E-05	1.48E-05
Eu-154	2.05E-07	7.94E-07	1.62E-06	2.48E-06	3.47E-06	4.38E-06	5.17E-06	6.01E-06	2.88E-06
Eu-155	1.54E-07	3.16E-07	5.81E-07	8.63E-07	1.14E-06	1.44E-06	1.71E-06	2.02E-06	9.79E-07
Eu-156	1.76E-07	3.39E-07	5.87E-07	7.88E-07	1.07E-06	1.32E-06	1.59E-06	1.83E-06	9.17E-07
Eu-157	6.03E-09	1.03E-08	1.30E-08	1.61E-08	2.26E-08	2.96E-08	4.22E-08	3.94E-08	1.66E-08
Eu-158	5.49E-11	7.83E-11	9.06E-11	1.01E-10	1.08E-10	1.09E-10	1.12E-10	1.16E-10	9.02E-11
Gd-154	1.08E-09	7.77E-09	2.28E-08	5.03E-08	8.55E-08	1.33E-07	1.91E-07	2.55E-07	9.07E-08
Gd-155	7.95E-10	1.84E-09	3.38E-09	5.31E-09	7.44E-09	9.50E-09	1.27E-08	1.45E-08	6.39E-09
Gd-156	3.39E-07	1.19E-06	2.64E-06	4.75E-06	7.61E-06	1.16E-05	1.63E-05	2.04E-05	7.89E-06
Gd-157	1.63E-08	3.01E-08	4.65E-08	5.22E-08	7.63E-08	8.85E-08	1.18E-07	1.14E-07	5.27E-08
Gd-158	2.01E-07	5.52E-07	1.06E-06	1.66E-06	2.37E-06	3.27E-06	4.31E-06	5.31E-06	2.23E-06
Gd-159	6.21E-10	1.06E-09	1.57E-09	2.50E-09	2.70E-09	2.91E-09	3.55E-09	4.81E-09	2.07E-09
Gd-160	9.87E-09	2.98E-08	5.49E-08	8.36E-08	1.14E-07	1.47E-07	1.81E-07	2.07E-07	1.02E-07
Tb-159	2.35E-08	7.07E-08	1.29E-07	1.99E-07	2.75E-07	3.64E-07	4.55E-07	5.41E-07	2.48E-07
Tb-160	6.49E-10	2.60E-09	5.63E-09	9.35E-09	1.36E-08	1.75E-08	2.30E-08	2.80E-08	1.16E-08
Tb-161	8.39E-10	1.43E-09	1.89E-09	2.21E-09	2.70E-09	3.25E-09	3.42E-09	3.89E-09	2.29E-09
Dy-160	1.53E-10	1.00E-09	3.06E-09	6.60E-09	1.16E-08	1.87E-08	2.88E-08	3.72E-08	1.31E-08
Dy-161	3.37E-09	1.09E-08	2.02E-08	3.06E-08	4.16E-08	5.40E-08	6.70E-08	7.89E-08	3.76E-08
Dy-162	1.86E-09	5.98E-09	1.13E-08	1.76E-08	2.51E-08	3.24E-08	4.10E-08	4.98E-08	2.25E-08
Dy-163	9.86E-10	3.42E-09	7.24E-09	1.23E-08	1.77E-08	2.52E-08	3.22E-08	4.16E-08	1.69E-08
Dy-164	2.92E-10	9.82E-10	1.99E-09	3.44E-09	4.96E-09	6.83E-09	9.11E-09	1.18E-08	4.65E-09
Ho-165	1.68E-10	7.19E-10	1.69E-09	3.35E-09	5.54E-09	8.48E-09	1.24E-08	1.76E-08	5.98E-09
Er-166	5.58E-11	2.02E-10	4.44E-10	8.16E-10	1.36E-09	2.22E-09	3.20E-09	4.69E-09	1.55E-09
Er-167	1.10E-11	2.37E-11	3.56E-11	4.91E-11	6.60E-11	9.32E-11	1.25E-10	1.71E-10	6.81E-11
Er-168	1.09E-11	3.99E-11	8.34E-11	1.42E-10	2.15E-10	3.12E-10	4.39E-10	5.72E-10	2.20E-10
U-233	3.13E-09	2.54E-09	1.96E-09	2.24E-09	1.85E-09	1.62E-09	1.60E-09	1.18E-09	1.64E-09
U-234	4.66E-08	5.90E-08	6.69E-08	7.46E-08	8.36E-08	9.86E-08	1.24E-07	1.60E-07	8.30E-08
U-235	4.00E-03	3.39E-03	2.88E-03	2.42E-03	2.05E-03	1.73E-03	1.47E-03	1.22E-03	2.38E-03
U-236	1.97E-04	3.36E-04	4.39E-04	5.14E-04	5.70E-04	6.11E-04	6.42E-04	6.62E-04	4.92E-04
U-237	1.77E-06	2.78E-06	3.09E-06	3.64E-06	3.88E-06	4.35E-06	4.85E-06	4.45E-06	3.23E-06
U-238	1.88E-02	1.87E-02	1.85E-02	1.84E-02	1.82E-02	1.80E-02	1.78E-02	1.76E-02	1.82E-02
U-239	9.72E-08	9.77E-08	9.95E-08	9.50E-08	9.65E-08	9.56E-08	9.47E-08	9.78E-08	8.81E-08
Np-236	8.91E-12	2.53E-11	5.69E-11	9.79E-11	1.29E-10	1.77E-10	1.91E-10	3.15E-10	1.00E-10
Np-237	5.93E-06	1.74E-05	2.93E-05	4.40E-05	5.66E-05	6.88E-05	7.98E-05	9.35E-05	4.75E-05
Np-238	3.40E-08	1.03E-07	1.89E-07	2.72E-07	3.60E-07	4.33E-07	5.71E-07	6.53E-07	2.84E-07
Np-239	1.32E-05	1.36E-05	1.27E-05	1.25E-05	1.38E-05	1.25E-05	1.29E-05	1.29E-05	1.21E-05
Np-240	2.67E-10	2.58E-10	2.50E-10	2.35E-10	2.46E-10	2.44E-10	2.36E-10	2.53E-10	2.21E-10
Pu-237	1.12E-10	1.35E-10	1.68E-10	1.85E-10	1.81E-10	1.89E-10	3.64E-10	1.94E-10	1.25E-10
Pu-238	2.80E-07	1.81E-06	4.80E-06	9.43E-06	1.53E-05	2.31E-05	3.26E-05	4.00E-05	1.50E-05
Pu-239	2.29E-04	3.11E-04	3.47E-04	3.54E-04	3.63E-04	3.56E-04	3.57E-04	3.53E-04	3.26E-04
Pu-240	3.42E-05	7.95E-05	1.16E-04	1.34E-04	1.49E-04	1.57E-04	1.56E-04	1.55E-04	1.17E-04
Pu-241	1.42E-05	5.10E-05	8.63E-05	1.15E-04	1.38E-04	1.50E-04	1.58E-04	1.61E-04	1.06E-04
Pu-242	7.66E-07	6.56E-06	1.73E-05	3.37E-05	5.17E-05	6.92E-05	9.06E-05	1.07E-04	4.52E-05
Pu-243	2.73E-09	1.80E-08	5.25E-08	8.25E-08	1.04E-07	1.25E-07	1.88E-07	1.83E-07	7.12E-08
Pu-244	1.38E-11	2.53E-10	1.01E-09	2.37E-09	5.85E-09	9.73E-09	1.39E-08	1.74E-08	5.46E-09
Am-241	3.66E-08	2.40E-07	5.96E-07	1.04E-06	1.45E-06	1.86E-06	2.15E-06	2.36E-06	1.20E-06
Am-242	2.35E-10	1.74E-09	4.22E-09	6.92E-09	9.87E-09	1.22E-08	1.45E-08	1.55E-08	7.66E-09
Am-242m	2.29E-10	2.38E-09	7.22E-09	1.40E-08	2.07E-08	2.72E-08	3.29E-08	3.66E-08	1.71E-08
Am-243	6.07E-08	7.36E-07	3.06E-06	6.46E-06	1.33E-05	1.76E-05	2.59E-05	3.17E-05	1.12E-05
Am-244	1.07E-11	1.53E-10	5.49E-10	1.33E-09	2.25E-09	3.44E-09	5.78E-09	7.12E-09	2.02E-09
Am-244m	7.07E-12	9.86E-11	3.56E-10	8.60E-10	1.46E-09	2.23E-09	3.74E-09	4.61E-09	1.31E-09
Cm-242	2.89E-09	4.35E-08	1.74E-07	4.30E-07	7.41E-07	1.09E-06	1.48E-06	1.87E-06	7.09E-07
Cm-243	1.57E-11	4.68E-10	2.60E-09	9.39E-09	1.71E-08	3.30E-08	4.47E-08	6.11E-08	1.97E-08
Cm-244	3.27E-09	8.26E-08	4.18E-07	1.46E-06	3.37E-06	7.66E-06	1.18E-05	1.46E-05	4.31E-06
Cm-245	5.88E-11	3.44E-09	2.59E-08	9.59E-08	2.77E-07	5.45E-07	9.65E-07	1.65E-06	3.93E-07
Cm-246	4.78E-13	4.52E-11	5.92E-10	3.27E-09	1.24E-08	3.29E-08	7.76E-08	1.48E-07	3.08E-08
Cm-247	1.62E-15	2.16E-13	3.97E-12	2.69E-11	1.24E-10	4.00E-10	1.03E-09	2.42E-09	4.62E-10

Cm-248	1.16E-17	3.85E-15	1.36E-13	1.05E-12	6.38E-12	2.59E-11	7.78E-11	1.93E-10	3.40E-11

D. Spent fuel activity

The equilibrium discarded data activities (Ci) evolution for $2x10^5$ pebbles from the gFHR model with discrete motion in Chapter 6.1 is compiled in this appendix. The average and maximum compositions are decayed for each time step and activities for each nuclide, and the total activity and decay heat are computed. Please note that the maximum values are not derived from a single pebble but are extracted from all pebbles.

Average activities [Ci]

Decay time	0 d	1 d	10 d	1 m	1 y	10 y	100 y	1,000 y	10,000 y	100,000 y
H-3	6.24E-09	6.24E-09	6.23E-09	6.21E-09	5.90E-09	3.56E-09	2.26E-11	0	0	0
C-14	2.36E-10	2.36E-10	2.36E-10	2.36E-10	2.36E-10	2.36E-10	2.33E-10	2.09E-10	7.00E-11	0
N-16	1.76E-04	0	0	0	0	0	0	0	0	0
N-17	3.25E-11	0	0	0	0	0	0	0	0	0
O-15	4.41E-09	0	0	0	0	0	0	0	0	0
Mn-66	4.38E-09	0	0	0	0	0	0	0	0	0
Mn-67	1.60E-09	0	0	0	0	0	0	0	0	0
Mn-68	1.28E-10	0	0	0	0	0	0	0	0	0
Mn-69	1.38E-12	0	0	0	0	0	0	0	0	0
Fe-65	2.24E-09	0	0	0	0	0	0	0	0	0
Fe-66	2.69E-07	0	0	0	0	0	0	0	0	0
Fe-67	2.42E-07	0	0	0	0	0	0	0	0	0
Fe-68	1.47E-07	0	0	0	0	0	0	0	0	0
Fe-69	4.04E-08	0	0	0	0	0	0	0	0	0
Fe-70	1.58E-08	0	0	0	0	0	0	0	0	0
Fe-71	8.73E-09	0	0	0	0	0	0	0	0	0
Fe-72	1.54E-04	0	0	0	0	0	0	0	0	0
Co-65	1.48E-09	0	0	0	0	0	0	0	0	0
Co-66	8.33E-07	0	0	0	0	0	0	0	0	0
Co-67	1.49E-06	0	0	0	0	0	0	0	0	0
Co-68	1.55E-06	0	0	0	0	0	0	0	0	0
Co-69	1.68E-06	0	0	0	0	0	0	0	0	0
Co-70	1.05E-06	0	0	0	0	0	0	0	0	0
Co-71	3.80E-07	0	0	0	0	0	0	0	0	0
Co-72	9.68E-08	0	0	0	0	0	0	0	0	0
Co-73	1.65E-08	0	0	0	0	0	0	0	0	0
Co-74	2.11E-09	0	0	0	0	0	0	0	0	0
Co-75	2.53E-10	0	0	0	0	0	0	0	0	0
Ni-65	1.43E-09	1.92E-12	0	0	0	0	0	0	0	0
Ni-66	1.08E-06	7.95E-07	5.12E-08	1.16E-10	0	0	0	0	0	0
Ni-67	2.59E-06	0	0	0	0	0	0	0	0	0
Ni-68	5.96E-06	0	0	0	0	0	0	0	0	0
Ni-69	1.33E-05	0	0	0	0	0	0	0	0	0
Ni-70	2.86E-05	0	0	0	0	0	0	0	0	0
Ni-71	3.20E-05	0	0	0	0	0	0	0	0	0
Ni-72	3.05E-05	0	0	0	0	0	0	0	0	0
Ni-73	1.96E-05	0	0	0	0	0	0	0	0	0
Ni-74	1.04E-05	0	0	0	0	0	0	0	0	0

Ni-75	5.52E-06	0	0	0	0	0	0	0	0	0
Ni-76	7.83E-07	0	0	0	0	0	0	0	0	0
Ni-77	7.32E-08	0	0	0	0	0	0	0	0	0
Ni-78	8.34E-09	0	0	0	0	0	0	0	0	0
Cu-66	1.08E-06	7.96E-07	5.13E-08	1.16E-10	0	0	0	0	0	0
Cu-67	2.71E-06	2.07E-06	1.84E-07	8.45E-10	0	0	0	0	0	0
Cu-68	6.39E-06	0	0	0	0	0	0	0	0	0
Cu-68m	3.08E-07	0	0	0	0	0	0	0	0	0
Cu-69	1.71E-05	0	0	0	0	0	0	0	0	0
Cu-70	1.99E-05	0	0	0	0	0	0	0	0	0
Cu-70m	4.43E-06	0	0	0	0	0	0	0	0	0
Cu-71	9.80E-05	0	0	0	0	0	0	0	0	0
Cu-72	1.54E-04	0	0	0	0	0	0	0	0	0
Cu-73	2.42E-04	0	0	0	0	0	0	0	0	0
Cu-74	2.42E-04	0	0	0	0	0	0	0	0	0
Cu-75	2.59E-04	0	0	0	0	0	0	0	0	0
Cu-76	1.68E-04	0	0	0	0	0	0	0	0	0
Cu-77	7.96E-05	0	0	0	0	0	0	0	0	0
Cu-78	1.90E-05	0	0	0	0	0	0	0	0	0
Cu-79	3.89E-07	0	0	0	0	0	0	0	0	0
Cu-80	2.47E-09	0	0	0	0	0	0	0	0	0
Zn-69	1.73E-05	4.44E-08	0	0	0	0	0	0	0	0
Zn-69m	1.39E-07	4.14E-08	0	0	0	0	0	0	0	0
Zn-71	1.01E-04	0	0	0	0	0	0	0	0	0
Zn-71m	1.55E-05	2.33E-07	0	0	0	0	0	0	0	0
Zn-72	2.70E-04	1.89E-04	7.54E-06	5.89E-09	0	0	0	0	0	0
Zn-73	6.29E-04	0	0	0	0	0	0	0	0	0
Zn-74	1.50E-03	0	0	0	0	0	0	0	0	0
Zn-75	2.87E-03	0	0	0	0	0	0	0	0	0
Zn-76	5.09E-03	0	0	0	0	0	0	0	0	0
Zn-77	6.70E-03	0	0	0	0	0	0	0	0	0
Zn-78	6.95E-03	0	0	0	0	0	0	0	0	0
Zn-79	3.94E-03	0	0	0	0	0	0	0	0	0
Zn-80	4.28E-04	0	0	0	0	0	0	0	0	0
Zn-81	9.70E-06	0	0	0	0	0	0	0	0	0
Zn-82	1.92E-06	0	0	0	0	0	0	0	0	0
Zn-83	1.72E-08	0	0	0	0	0	0	0	0	0
Ga-68	8.94E-12	0	0	0	0	0	0	0	0	0
Ga-70	3.52E-07	0	0	0	0	0	0	0	0	0
Ga-72	2.77E-04	2.37E-04	1.08E-05	8.45E-09	0	0	0	0	0	0
Ga-73	6.72E-04	2.19E-05	0	0	0	0	0	0	0	0
Ga-74	1.69E-03	0	0	0	0	0	0	0	0	0
Ga-74m	1.21E-04	0	0	0	0	0	0	0	0	0
Ga-75	4.27E-03	0	0	0	0	0	0	0	0	0
Ga-76	9.91E-03	0	0	0	0	0	0	0	0	0
Ga-77	2.11E-02	0	0	0	0	0	0	0	0	0
Ga-78	3.74E-02	0	0	0	0	0	0	0	0	0
Ga-79	4.34E-02	0	0	0	0	0	0	0	0	0
Ga-80	2.42E-02	0	0	0	0	0	0	0	0	0
Ga-81	1.67E-02	0	0	0	0	0	0	0	0	0
Ga-82	1.03E-02	0	0	0	0	0	0	0	0	0

Ga-83	3.64E-04	0	0	0	0	0	0	0	0	0
Ga-84	8.42E-03	0	0	0	0	0	0	0	0	0
Ga-85	2.77E-07	0	0	0	0	0	0	0	0	0
Ga-86	3.48E-06	0	0	0	0	0	0	0	0	0
Ge-71	2.90E-09	2.73E-09	1.58E-09	4.70E-10	0	0	0	0	0	0
Ge-71m	6.26E-12	0	0	0	0	0	0	0	0	0
Ge-73m	4.74E-05	1.54E-06	0	0	0	0	0	0	0	0
Ge-75	4.39E-03	2.61E-08	0	0	0	0	0	0	0	0
Ge-75m	1.00E-04	0	0	0	0	0	0	0	0	0
Ge-77	2.68E-02	6.15E-03	1.08E-08	0	0	0	0	0	0	0
Ge-77m	7.78E-04	0	0	0	0	0	0	0	0	0
Ge-78	7.35E-02	8.72E-07	0	0	0	0	0	0	0	0
Ge-79	9.47E-02	0	0	0	0	0	0	0	0	0
Ge-79m	4.82E-02	0	0	0	0	0	0	0	0	0
Ge-80	3.10E-01	0	0	0	0	0	0	0	0	0
Ge-81	3.44E-01	0	0	0	0	0	0	0	0	0
Ge-82	2.89E-01	0	0	0	0	0	0	0	0	0
Ge-83	1.16E-01	0	0	0	0	0	0	0	0	0
Ge-84	4.20E-02	0	0	0	0	0	0	0	0	0
Ge-85	4.29E-03	0	0	0	0	0	0	0	0	0
Ge-86	1.80E-01	0	0	0	0	0	0	0	0	0
Ge-87	2.30E-03	0	0	0	0	0	0	0	0	0
Ge-88	6.92E+00	0	0	0	0	0	0	0	0	0
Ge-89	1.24E-03	0	0	0	0	0	0	0	0	0
As-72	2.87E-12	1.51E-12	0	0	0	0	0	0	0	0
As-73	3.58E-10	3.55E-10	3.28E-10	2.76E-10	1.53E-11	0	0	0	0	0
As-74	1.84E-08	1.77E-08	1.24E-08	5.70E-09	0	0	0	0	0	0
As-75m	1.35E-10	1.34E-10	1.28E-10	1.14E-10	1.64E-11	0	0	0	0	0
As-76	3.56E-04	1.89E-04	6.29E-07	1.96E-12	0	0	0	0	0	0
As-77	2.72E-02	2.23E-02	5.26E-04	9.99E-08	0	0	0	0	0	0
As-78	7.56E-02	1.27E-05	0	0	0	0	0	0	0	0
As-79	1.60E-01	0	0	0	0	0	0	0	0	0
As-80	3.92E-01	0	0	0	0	0	0	0	0	0
As-81	6.41E-01	0	0	0	0	0	0	0	0	0
As-82	6.36E-01	0	0	0	0	0	0	0	0	0
As-82m	1.68E-01	0	0	0	0	0	0	0	0	0
As-83	8.84E-01	0	0	0	0	0	0	0	0	0
As-84	4.23E-01	0	0	0	0	0	0	0	0	0
As-85	3.27E-01	0	0	0	0	0	0	0	0	0
As-86	1.05E+00	0	0	0	0	0	0	0	0	0
As-87	9.74E-02	0	0	0	0	0	0	0	0	0
As-88	6.46E-02	0	0	0	0	0	0	0	0	0
As-89	2.01E+01	0	0	0	0	0	0	0	0	0
As-90	3.53E-01	0	0	0	0	0	0	0	0	0
Se-75	2.09E-09	2.08E-09	1.97E-09	1.76E-09	2.53E-10	0	0	0	0	0
Se-77m	1.04E-04	7.42E-05	1.75E-06	3.32E-10	0	0	0	0	0	0
Se-79	1.09E-06	1.09E-06	1.09E-06	1.09E-06	1.09E-06	1.09E-06	1.09E-06	1.09E-06	1.07E-06	8.65E-07
Se-79m	1.51E-01	0	0	0	0	0	0	0	0	0
Se-81	6.99E-01	2.12E-09	0	0	0	0	0	0	0	0
Se-81m	5.31E-02	1.44E-09	0	0	0	0	0	0	0	0
Se-83	1.38E+00	0	0	0	0	0	0	0	0	0

Se-83m	1.30E-01	0	0	0	0	0	0	0	0	0
Se-84	2.40E+00	0	0	0	0	0	0	0	0	0
Se-85	2.79E+00	0	0	0	0	0	0	0	0	0
Se-86	3.05E+00	0	0	0	0	0	0	0	0	0
Se-87	1.73E+00	0	0	0	0	0	0	0	0	0
Se-88	7.23E-01	0	0	0	0	0	0	0	0	0
Se-89	8.80E-02	0	0	0	0	0	0	0	0	0
Se-90	1.69E-02	0	0	0	0	0	0	0	0	0
Se-91	1.18E-03	0	0	0	0	0	0	0	0	0
Se-94	5.83E-02	0	0	0	0	0	0	0	0	0
Br-77	5.51E-11	4.12E-11	2.98E-12	0	0	0	0	0	0	0
Br-77m	4.26E-11	0	0	0	0	0	0	0	0	0
Br-78	5.87E-09	0	0	0	0	0	0	0	0	0
Br-79m	3.17E-07	0	0	0	0	0	0	0	0	0
Br-80	1.72E-05	1.34E-07	0	0	0	0	0	0	0	0
Br-80m	5.38E-06	1.25E-07	0	0	0	0	0	0	0	0
Br-82	4.73E-02	2.96E-02	4.25E-04	3.41E-08	0	0	0	0	0	0
Br-82m	4.03E-02	0	0	0	0	0	0	0	0	0
Br-83	1.59E+00	1.81E-03	0	0	0	0	0	0	0	0
Br-84	2.61E+00	0	0	0	0	0	0	0	0	0
Br-84m	1.20E-01	0	0	0	0	0	0	0	0	0
Br-85	3.62E+00	0	0	0	0	0	0	0	0	0
Br-86	4.46E+00	0	0	0	0	0	0	0	0	0
Br-87	5.16E+00	0	0	0	0	0	0	0	0	0
Br-88	4.23E+00	0	0	0	0	0	0	0	0	0
Br-89	2.74E+00	0	0	0	0	0	0	0	0	0
Br-90	1.47E+00	0	0	0	0	0	0	0	0	0
Br-91	4.08E-01	0	0	0	0	0	0	0	0	0
Br-92	5.47E-02	0	0	0	0	0	0	0	0	0
Br-93	1.04E-02	0	0	0	0	0	0	0	0	0
Br-94	1.82E-03	0	0	0	0	0	0	0	0	0
Br-95	1.79E+00	0	0	0	0	0	0	0	0	0
Br-96	2.57E-01	0	0	0	0	0	0	0	0	0
Br-97	3.20E-03	0	0	0	0	0	0	0	0	0
Kr-79	3.44E-11	2.14E-11	0	0	0	0	0	0	0	0
Kr-79m	1.62E-11	0	0	0	0	0	0	0	0	0
Kr-81	5.06E-12	5.06E-12	5.06E-12	5.06E-12	5.06E-12	5.06E-12	5.06E-12	5.04E-12	4.91E-12	3.74E-12
Kr-81m	3.76E-07	0	0	0	0	0	0	0	0	0
Kr-83m	1.56E+00	6.73E-03	8.36E-08	7.12E-08	4.81E-09	0	0	0	0	0
Kr-85	2.40E-01	2.40E-01	2.40E-01	2.39E-01	2.25E-01	1.26E-01	3.83E-04	0	0	0
Kr-85m	3.50E+00	8.64E-02	0	0	0	0	0	0	0	0
Kr-87	6.65E+00	1.40E-05	0	0	0	0	0	0	0	0
Kr-88	8.90E+00	2.55E-02	0	0	0	0	0	0	0	0
Kr-89	1.10E+01	0	0	0	0	0	0	0	0	0
Kr-90	1.13E+01	0	0	0	0	0	0	0	0	0
Kr-91	7.58E+00	0	0	0	0	0	0	0	0	0
Kr-92	3.73E+00	0	0	0	0	0	0	0	0	0
Kr-93	1.05E+00	0	0	0	0	0	0	0	0	0
Kr-94	1.70E-01	0	0	0	0	0	0	0	0	0
Kr-95	1.21E-02	0	0	0	0	0	0	0	0	0
Kr-96	3.34E-02	0	0	0	0	0	0	0	0	0

Kr-97	9.14E-04	0	0	0	0	0	0	0	0	0
Kr-98	6.22E-04	0	0	0	0	0	0	0	0	0
Kr-99	1.49E-07	0	0	0	0	0	0	0	0	0
Kr-100	3.88E-06	0	0	0	0	0	0	0	0	0
Rb-81	1.14E-11	0	0	0	0	0	0	0	0	0
Rb-83	1.22E-07	1.21E-07	1.12E-07	9.57E-08	6.47E-09	0	0	0	0	0
Rb-84	3.07E-06	3.01E-06	2.49E-06	1.63E-06	1.36E-09	0	0	0	0	0
Rb-86	6.27E-02	6.05E-02	4.33E-02	2.06E-02	8.01E-08	0	0	0	0	0
Rb-86m	4.47E-03	0	0	0	0	0	0	0	0	0
Rb-87	3.85E-10	3.85E-10	3.85E-10	3.85E-10	3.85E-10	3.85E-10	3.85E-10	3.85E-10	3.85E-10	3.85E-10
Rb-88	9.03E+00	2.83E-02	0	0	0	0	0	0	0	0
Rb-89	1.17E+01	0	0	0	0	0	0	0	0	0
Rb-90	1.19E+01	0	0	0	0	0	0	0	0	0
Rb-90m	2.39E+00	0	0	0	0	0	0	0	0	0
Rb-91	1.44E+01	0	0	0	0	0	0	0	0	0
Rb-92	1.28E+01	0	0	0	0	0	0	0	0	0
Rb-93	9.56E+00	0	0	0	0	0	0	0	0	0
Rb-94	4.77E+00	0	0	0	0	0	0	0	0	0
Rb-95	2.03E+00	0	0	0	0	0	0	0	0	0
Rb-96	4.13E-01	0	0	0	0	0	0	0	0	0
Rb-97	6.84E-02	0	0	0	0	0	0	0	0	0
Rb-98	6.85E-03	0	0	0	0	0	0	0	0	0
Rb-99	9.10E-05	0	0	0	0	0	0	0	0	0
Rb-100	1.53E-02	0	0	0	0	0	0	0	0	0
Rb-101	4.90E-07	0	0	0	0	0	0	0	0	0
Rb-102	1.03E-08	0	0	0	0	0	0	0	0	0
Sr-83	1.94E-12	1.16E-12	0	0	0	0	0	0	0	0
Sr-85	3.30E-08	3.26E-08	2.96E-08	2.39E-08	6.66E-10	0	0	0	0	0
Sr-85m	9.89E-09	0	0	0	0	0	0	0	0	0
Sr-87m	1.33E-04	3.60E-07	0	0	0	0	0	0	0	0
Sr-89	2.08E+01	2.05E+01	1.82E+01	1.38E+01	1.39E-01	0	0	0	0	0
Sr-90	1.44E+00	1.44E+00	1.44E+00	1.43E+00	1.40E+00	1.13E+00	1.30E-01	5.11E-11	0	0
Sr-91	1.54E+01	2.75E+00	4.86E-07	0	0	0	0	0	0	0
Sr-92	1.71E+01	3.29E-02	0	0	0	0	0	0	0	0
Sr-93	1.87E+01	0	0	0	0	0	0	0	0	0
Sr-94	1.86E+01	0	0	0	0	0	0	0	0	0
Sr-95	1.63E+01	0	0	0	0	0	0	0	0	0
Sr-96	1.07E+01	0	0	0	0	0	0	0	0	0
Sr-97	4.59E+00	0	0	0	0	0	0	0	0	0
Sr-98	2.11E+00	0	0	0	0	0	0	0	0	0
Sr-99	3.19E-01	0	0	0	0	0	0	0	0	0
Sr-100	8.04E-02	0	0	0	0	0	0	0	0	0
Sr-101	5.76E-03	0	0	0	0	0	0	0	0	0
Sr-102	1.83E-04	0	0	0	0	0	0	0	0	0
Sr-103	8.75E-06	0	0	0	0	0	0	0	0	0
Sr-104	2.60E-07	0	0	0	0	0	0	0	0	0
Sr-105	1.99E-08	0	0	0	0	0	0	0	0	0
Y-87	4.90E-09	3.98E-09	6.10E-10	9.43E-12	0	0	0	0	0	0
Y-88	5.40E-06	5.36E-06	5.06E-06	4.44E-06	5.03E-07	0	0	0	0	0
Y-89m	2.02E-03	1.98E-03	1.75E-03	1.33E-03	1.34E-05	0	0	0	0	0
Y-90	1.50E+00	1.49E+00	1.44E+00	1.43E+00	1.40E+00	1.13E+00	1.30E-01	5.11E-11	0	0

Y-90m	3.07E-04	1.67E-06	0	0	0	0	0	0	0	0
Y-91	2.78E+01	2.75E+01	2.48E+01	1.95E+01	3.69E-01	0	0	0	0	0
Y-91m	8.85E+00	1.72E+00	3.05E-07	0	0	0	0	0	0	0
Y-92	1.70E+01	5.19E-01	0	0	0	0	0	0	0	0
Y-93	1.93E+01	3.81E+00	1.56E-06	0	0	0	0	0	0	0
Y-93m	1.22E+00	0	0	0	0	0	0	0	0	0
Y-94	2.06E+01	0	0	0	0	0	0	0	0	0
Y-95	2.14E+01	0	0	0	0	0	0	0	0	0
Y-96	1.23E+01	0	0	0	0	0	0	0	0	0
Y-96m	8.14E+00	0	0	0	0	0	0	0	0	0
Y-97	1.14E+01	0	0	0	0	0	0	0	0	0
Y-97m	5.73E+00	0	0	0	0	0	0	0	0	0
Y-98	7.57E+00	0	0	0	0	0	0	0	0	0
Y-98m	4.68E+00	0	0	0	0	0	0	0	0	0
Y-99	7.32E+00	0	0	0	0	0	0	0	0	0
Y-100	2.20E+00	0	0	0	0	0	0	0	0	0
Y-101	7.51E-01	0	0	0	0	0	0	0	0	0
Y-102	3.51E-01	0	0	0	0	0	0	0	0	0
Y-103	1.08E-02	0	0	0	0	0	0	0	0	0
Y-104	1.14E-03	0	0	0	0	0	0	0	0	0
Y-105	2.54E-05	0	0	0	0	0	0	0	0	0
Y-106	5.35E-07	0	0	0	0	0	0	0	0	0
Y-107	3.26E-09	0	0	0	0	0	0	0	0	0
Y-108	1.05E-10	0	0	0	0	0	0	0	0	0
Zr-88	1.29E-11	1.28E-11	1.19E-11	1.00E-11	0	0	0	0	0	0
Zr-89	6.84E-08	5.53E-08	8.19E-09	1.18E-10	0	0	0	0	0	0
Zr-90m	4.63E-08	0	0	0	0	0	0	0	0	0
Zr-93	3.09E-05	3.09E-05	3.09E-05	3.09E-05	3.09E-05	3.09E-05	3.09E-05	3.09E-05	3.08E-05	2.95E-05
Zr-95	3.82E+01	3.78E+01	3.42E+01	2.76E+01	7.34E-01	0	0	0	0	0
Zr-97	2.27E+01	8.42E+00	1.10E-03	2.58E-12	0	0	0	0	0	0
Zr-98	2.23E+01	0	0	0	0	0	0	0	0	0
Zr-99	2.17E+01	0	0	0	0	0	0	0	0	0
Zr-100	2.16E+01	0	0	0	0	0	0	0	0	0
Zr-101	1.18E+01	0	0	0	0	0	0	0	0	0
Zr-102	7.18E+00	0	0	0	0	0	0	0	0	0
Zr-103	1.87E+00	0	0	0	0	0	0	0	0	0
Zr-104	4.16E-01	0	0	0	0	0	0	0	0	0
Zr-105	1.90E-01	0	0	0	0	0	0	0	0	0
Zr-106	3.61E-03	0	0	0	0	0	0	0	0	0
Zr-107	5.56E-05	0	0	0	0	0	0	0	0	0
Zr-108	5.81E-06	0	0	0	0	0	0	0	0	0
Zr-109	1.14E-06	0	0	0	0	0	0	0	0	0
Zr-110	2.57E-08	0	0	0	0	0	0	0	0	0
Nb-93m	1.14E-06	1.14E-06	1.17E-06	1.25E-06	2.42E-06	1.18E-05	3.13E-05	3.17E-05	3.16E-05	3.03E-05
Nb-94	2.26E-09	2.26E-09	2.26E-09	2.26E-09	2.26E-09	2.25E-09	2.25E-09	2.18E-09	1.60E-09	7.44E-11
Nb-94m	1.13E-05	0	0	0	0	0	0	0	0	0
Nb-95	4.26E+01	4.25E+01	4.14E+01	3.79E+01	1.59E+00	0	0	0	0	0
Nb-95m	4.23E-01	4.20E-01	3.90E-01	3.16E-01	8.40E-03	0	0	0	0	0
Nb-96	1.31E-01	6.44E-02	1.06E-04	6.86E-11	0	0	0	0	0	0
Nb-97	2.29E+01	9.07E+00	1.19E-03	2.79E-12	0	0	0	0	0	0
Nb-97m	2.68E-02	0	0	0	0	0	0	0	0	0

Nb-98	2.28E+01	0	0	0	0	0	0	0	0	0
Nb-98m	1.46E-01	5.19E-10	0	0	0	0	0	0	0	0
Nb-99	2.25E+01	0	0	0	0	0	0	0	0	0
Nb-99m	2.39E+00	0	0	0	0	0	0	0	0	0
Nb-100	2.38E+01	0	0	0	0	0	0	0	0	0
Nb-100m	2.03E+00	0	0	0	0	0	0	0	0	0
Nb-101	2.24E+01	0	0	0	0	0	0	0	0	0
Nb-102	3.68E+00	0	0	0	0	0	0	0	0	0
Nb-102m	1.66E+01	0	0	0	0	0	0	0	0	0
Nb-103	1.12E+01	0	0	0	0	0	0	0	0	0
Nb-104	2.91E+00	0	0	0	0	0	0	0	0	0
Nb-104m	2.33E+00	0	0	0	0	0	0	0	0	0
Nb-105	2.14E+00	0	0	0	0	0	0	0	0	0
Nb-106	3.65E-01	0	0	0	0	0	0	0	0	0
Nb-107	6.82E-02	0	0	0	0	0	0	0	0	0
Nb-108	5.11E-03	0	0	0	0	0	0	0	0	0
Nb-109	1.42E-03	0	0	0	0	0	0	0	0	0
Nb-110	4.26E-05	0	0	0	0	0	0	0	0	0
Nb-111	3.44E-06	0	0	0	0	0	0	0	0	0
Nb-112	4.15E-08	0	0	0	0	0	0	0	0	0
Nb-113	8.06E-09	0	0	0	0	0	0	0	0	0
Mo-93m	1.06E-11	0	0	0	0	0	0	0	0	0
Mo-99	2.51E+01	1.95E+01	2.02E+00	1.30E-02	0	0	0	0	0	0
Mo-101	2.33E+01	0	0	0	0	0	0	0	0	0
Mo-102	2.19E+01	0	0	0	0	0	0	0	0	0
Mo-103	2.08E+01	0	0	0	0	0	0	0	0	0
Mo-104	1.70E+01	0	0	0	0	0	0	0	0	0
Mo-105	1.19E+01	0	0	0	0	0	0	0	0	0
Mo-106	6.89E+00	0	0	0	0	0	0	0	0	0
Mo-107	2.61E+00	0	0	0	0	0	0	0	0	0
Mo-108	8.26E-01	0	0	0	0	0	0	0	0	0
Mo-109	9.27E-02	0	0	0	0	0	0	0	0	0
Mo-110	5.49E-03	0	0	0	0	0	0	0	0	0
Mo-111	5.91E-04	0	0	0	0	0	0	0	0	0
Mo-112	9.51E-05	0	0	0	0	0	0	0	0	0
Mo-113	5.55E-06	0	0	0	0	0	0	0	0	0
Mo-114	1.70E-06	0	0	0	0	0	0	0	0	0
Mo-115	9.45E-08	0	0	0	0	0	0	0	0	0
Tc-97m	1.03E-08	1.02E-08	9.52E-09	8.17E-09	6.21E-10	0	0	0	0	0
Tc-98	1.17E-11	1.17E-11	1.17E-11	1.17E-11	1.17E-11	1.17E-11	1.17E-11	1.17E-11	1.17E-11	1.15E-11
Tc-99	2.22E-04	2.22E-04	2.23E-04	2.23E-04	2.23E-04	2.23E-04	2.23E-04	2.22E-04	2.16E-04	1.61E-04
Tc-99m	2.22E+01	1.88E+01	1.96E+00	1.26E-02	0	0	0	0	0	0
Tc-100	7.22E+00	0	0	0	0	0	0	0	0	0
Tc-101	2.33E+01	0	0	0	0	0	0	0	0	0
Tc-102	2.20E+01	0	0	0	0	0	0	0	0	0
Tc-102m	7.29E-02	0	0	0	0	0	0	0	0	0
Tc-103	2.14E+01	0	0	0	0	0	0	0	0	0
Tc-104	1.82E+01	0	0	0	0	0	0	0	0	0
Tc-105	1.51E+01	0	0	0	0	0	0	0	0	0
Tc-106	1.14E+01	0	0	0	0	0	0	0	0	0
Tc-107	7.34E+00	0	0	0	0	0	0	0	0	0

Tc-108	3.44E+00	0	0	0	0	0	0	0	0	0
Tc-109	1.41E+00	0	0	0	0	0	0	0	0	0
Tc-110	2.61E-01	0	0	0	0	0	0	0	0	0
Tc-111	3.79E-02	0	0	0	0	0	0	0	0	0
Tc-112	4.84E-03	0	0	0	0	0	0	0	0	0
Tc-113	7.04E-04	0	0	0	0	0	0	0	0	0
Tc-114	4.87E-04	0	0	0	0	0	0	0	0	0
Tc-115	1.85E-04	0	0	0	0	0	0	0	0	0
Tc-116	2.91E-06	0	0	0	0	0	0	0	0	0
Tc-117	8.37E-08	0	0	0	0	0	0	0	0	0
Tc-118	9.17E-09	0	0	0	0	0	0	0	0	0
Ru-103	3.25E+01	3.20E+01	2.73E+01	1.91E+01	5.17E-02	0	0	0	0	0
Ru-105	1.53E+01	3.72E-01	0	0	0	0	0	0	0	0
Ru-106	1.02E+01	1.02E+01	1.00E+01	9.67E+00	5.19E+00	1.17E-02	0	0	0	0
Ru-107	8.96E+00	0	0	0	0	0	0	0	0	0
Ru-108	6.15E+00	0	0	0	0	0	0	0	0	0
Ru-109	4.10E+00	0	0	0	0	0	0	0	0	0
Ru-110	1.87E+00	0	0	0	0	0	0	0	0	0
Ru-111	7.97E-01	0	0	0	0	0	0	0	0	0
Ru-112	2.85E-01	0	0	0	0	0	0	0	0	0
Ru-113	1.28E-01	0	0	0	0	0	0	0	0	0
Ru-114	4.20E-02	0	0	0	0	0	0	0	0	0
Ru-115	2.11E-02	0	0	0	0	0	0	0	0	0
Ru-116	2.88E-03	0	0	0	0	0	0	0	0	0
Ru-117	1.01E-04	0	0	0	0	0	0	0	0	0
Ru-118	1.72E-05	0	0	0	0	0	0	0	0	0
Ru-119	9.54E-07	0	0	0	0	0	0	0	0	0
Ru-120	1.24E-07	0	0	0	0	0	0	0	0	0
Rh-101	1.35E-09	1.35E-09	1.35E-09	1.33E-09	1.10E-09	1.66E-10	0	0	0	0
Rh-101m	8.92E-11	7.60E-11	1.81E-11	0	0	0	0	0	0	0
Rh-102	1.50E-05	1.49E-05	1.45E-05	1.35E-05	4.41E-06	7.42E-11	0	0	0	0
Rh-102m	1.78E-09	1.78E-09	1.77E-09	1.75E-09	1.40E-09	1.63E-10	0	0	0	0
Rh-103m	3.21E+01	3.16E+01	2.69E+01	1.89E+01	5.11E-02	0	0	0	0	0
Rh-104	1.28E+01	0	0	0	0	0	0	0	0	0
Rh-104m	9.76E-01	0	0	0	0	0	0	0	0	0
Rh-105	1.37E+01	9.94E+00	1.45E-01	1.19E-05	0	0	0	0	0	0
Rh-105m	4.31E+00	1.05E-01	0	0	0	0	0	0	0	0
Rh-106	1.14E+01	1.01E+01	9.90E+00	9.54E+00	5.12E+00	1.15E-02	0	0	0	0
Rh-106m	1.41E-01	6.94E-05	0	0	0	0	0	0	0	0
Rh-107	9.08E+00	0	0	0	0	0	0	0	0	0
Rh-108	6.19E+00	0	0	0	0	0	0	0	0	0
Rh-108m	3.70E-02	0	0	0	0	0	0	0	0	0
Rh-109	4.21E+00	0	0	0	0	0	0	0	0	0
Rh-110	1.90E+00	0	0	0	0	0	0	0	0	0
Rh-110m	3.46E-02	0	0	0	0	0	0	0	0	0
Rh-111	9.26E-01	0	0	0	0	0	0	0	0	0
Rh-112	3.72E-01	0	0	0	0	0	0	0	0	0
Rh-113	2.61E-01	0	0	0	0	0	0	0	0	0
Rh-114	1.38E-01	0	0	0	0	0	0	0	0	0
Rh-115	5.90E-02	0	0	0	0	0	0	0	0	0
Rh-116	2.07E-02	0	0	0	0	0	0	0	0	0

Rh-117	5.23E-03	0	0	0	0	0	0	0	0	0
Rh-118	8.95E-04	0	0	0	0	0	0	0	0	0
Rh-119	2.91E-04	0	0	0	0	0	0	0	0	0
Rh-120	2.25E-05	0	0	0	0	0	0	0	0	0
Rh-121	3.33E-06	0	0	0	0	0	0	0	0	0
Rh-122	1.66E-02	0	0	0	0	0	0	0	0	0
Pd-103	7.79E-06	7.48E-06	5.18E-06	2.29E-06	2.66E-12	0	0	0	0	0
Pd-107	1.62E-06	1.62E-06	1.62E-06	1.62E-06	1.62E-06	1.62E-06	1.62E-06	1.62E-06	1.62E-06	1.60E-06
Pd-107m	1.93E-03	0	0	0	0	0	0	0	0	0
Pd-109	5.09E+00	1.52E+00	2.72E-05	0	0	0	0	0	0	0
Pd-109m	1.77E-02	0	0	0	0	0	0	0	0	0
Pd-111	9.32E-01	4.59E-05	0	0	0	0	0	0	0	0
Pd-111m	1.20E-03	5.84E-05	0	0	0	0	0	0	0	0
Pd-112	3.93E-01	1.78E-01	1.44E-04	1.94E-11	0	0	0	0	0	0
Pd-113	2.70E-01	0	0	0	0	0	0	0	0	0
Pd-114	1.71E-01	0	0	0	0	0	0	0	0	0
Pd-115	1.17E-01	0	0	0	0	0	0	0	0	0
Pd-116	1.05E-01	0	0	0	0	0	0	0	0	0
Pd-117	6.94E-02	0	0	0	0	0	0	0	0	0
Pd-118	2.93E-02	0	0	0	0	0	0	0	0	0
Pd-119	7.43E-03	0	0	0	0	0	0	0	0	0
Pd-120	5.69E-03	0	0	0	0	0	0	0	0	0
Pd-121	5.56E-04	0	0	0	0	0	0	0	0	0
Pd-122	2.17E-04	0	0	0	0	0	0	0	0	0
Pd-123	2.46E-05	0	0	0	0	0	0	0	0	0
Pd-124	1.00E-05	0	0	0	0	0	0	0	0	0
Ag-105	1.62E-12	1.59E-12	1.37E-12	0	0	0	0	0	0	0
Ag-106	1.22E-11	0	0	0	0	0	0	0	0	0
Ag-106m	4.96E-11	4.56E-11	2.15E-11	4.02E-12	0	0	0	0	0	0
Ag-107m	2.02E-09	0	0	0	0	0	0	0	0	0
Ag-108	2.61E-06	1.02E-11	1.02E-11	1.02E-11	1.02E-11	1.01E-11	8.68E-12	1.95E-12	0	0
Ag-108m	1.13E-10	1.13E-10	1.13E-10	1.13E-10	1.13E-10	1.11E-10	9.57E-11	2.15E-11	0	0
Ag-109m	5.02E+00	1.50E+00	2.71E-05	2.75E-07	1.66E-07	1.20E-09	0	0	0	0
Ag-110	2.08E+00	1.19E-03	1.16E-03	1.10E-03	4.33E-04	4.75E-08	0	0	0	0
Ag-110m	8.75E-02	8.72E-02	8.51E-02	8.05E-02	3.18E-02	3.49E-06	0	0	0	0
Ag-111	1.06E+00	9.64E-01	4.17E-01	6.49E-02	0	0	0	0	0	0
Ag-111m	9.04E-01	4.47E-05	0	0	0	0	0	0	0	0
Ag-112	3.94E-01	2.09E-01	1.69E-04	2.28E-11	0	0	0	0	0	0
Ag-113	1.77E-01	8.07E-03	0	0	0	0	0	0	0	0
Ag-113m	2.58E-01	0	0	0	0	0	0	0	0	0
Ag-114	1.73E-01	0	0	0	0	0	0	0	0	0
Ag-115	1.19E-01	0	0	0	0	0	0	0	0	0
Ag-115m	3.65E-03	0	0	0	0	0	0	0	0	0
Ag-116	8.42E-02	0	0	0	0	0	0	0	0	0
Ag-116m	3.44E-03	0	0	0	0	0	0	0	0	0
Ag-117	9.22E-02	0	0	0	0	0	0	0	0	0
Ag-117m	1.96E-02	0	0	0	0	0	0	0	0	0
Ag-118	6.63E-02	0	0	0	0	0	0	0	0	0
Ag-118m	2.45E-02	0	0	0	0	0	0	0	0	0
Ag-119	5.34E-02	0	0	0	0	0	0	0	0	0
Ag-120	1.98E-02	0	0	0	0	0	0	0	0	0

Ag-120m	1.07E-02	0	0	0	0	0	0	0	0	0
Ag-121	1.29E-02	0	0	0	0	0	0	0	0	0
Ag-122	1.59E-03	0	0	0	0	0	0	0	0	0
Ag-122m	5.03E-03	0	0	0	0	0	0	0	0	0
Ag-123	9.59E-04	0	0	0	0	0	0	0	0	0
Ag-124	6.87E-04	0	0	0	0	0	0	0	0	0
Ag-125	3.46E-05	0	0	0	0	0	0	0	0	0
Ag-126	1.12E-05	0	0	0	0	0	0	0	0	0
Ag-127	4.76E-07	0	0	0	0	0	0	0	0	0
Ag-128	6.68E-08	0	0	0	0	0	0	0	0	0
Ag-129	7.78E-09	0	0	0	0	0	0	0	0	0
Ag-130	3.41E-06	0	0	0	0	0	0	0	0	0
Cd-107	2.10E-12	0	0	0	0	0	0	0	0	0
Cd-109	2.89E-07	2.89E-07	2.85E-07	2.76E-07	1.67E-07	1.20E-09	0	0	0	0
Cd-111m	3.43E-04	0	0	0	0	0	0	0	0	0
Cd-113m	3.18E-04	3.18E-04	3.17E-04	3.17E-04	3.03E-04	1.95E-04	2.34E-06	0	0	0
Cd-115	1.19E-01	8.77E-02	5.33E-03	1.06E-05	0	0	0	0	0	0
Cd-115m	1.15E-02	1.13E-02	9.85E-03	7.22E-03	3.94E-05	0	0	0	0	0
Cd-117	1.11E-01	1.41E-04	0	0	0	0	0	0	0	0
Cd-117m	3.31E-03	2.34E-05	0	0	0	0	0	0	0	0
Cd-118	9.20E-02	2.22E-10	0	0	0	0	0	0	0	0
Cd-119	7.35E-02	0	0	0	0	0	0	0	0	0
Cd-119m	1.82E-02	0	0	0	0	0	0	0	0	0
Cd-120	8.55E-02	0	0	0	0	0	0	0	0	0
Cd-121	4.37E-02	0	0	0	0	0	0	0	0	0
Cd-121m	3.25E-02	0	0	0	0	0	0	0	0	0
Cd-122	6.42E-02	0	0	0	0	0	0	0	0	0
Cd-123	3.40E-02	0	0	0	0	0	0	0	0	0
Cd-123m	1.50E-04	0	0	0	0	0	0	0	0	0
Cd-124	2.49E-02	0	0	0	0	0	0	0	0	0
Cd-125	9.32E-03	0	0	0	0	0	0	0	0	0
Cd-126	1.26E-02	0	0	0	0	0	0	0	0	0
Cd-127	1.18E-02	0	0	0	0	0	0	0	0	0
Cd-128	4.82E-03	0	0	0	0	0	0	0	0	0
Cd-129	2.88E-05	0	0	0	0	0	0	0	0	0
Cd-130	9.85E-02	0	0	0	0	0	0	0	0	0
Cd-131	8.56E-03	0	0	0	0	0	0	0	0	0
Cd-132	1.98E-06	0	0	0	0	0	0	0	0	0
In-111	3.60E-12	2.81E-12	0	0	0	0	0	0	0	0
In-112	1.11E-10	0	0	0	0	0	0	0	0	0
In-112m	3.17E-11	0	0	0	0	0	0	0	0	0
In-113m	1.09E-10	4.83E-12	4.58E-12	4.06E-12	0	0	0	0	0	0
In-114	2.35E-05	1.55E-05	1.37E-05	1.03E-05	9.48E-08	0	0	0	0	0
In-114m	1.62E-05	1.60E-05	1.41E-05	1.07E-05	9.80E-08	0	0	0	0	0
In-115m	1.19E-01	9.54E-02	5.82E-03	1.23E-05	4.18E-09	0	0	0	0	0
In-116	8.94E-02	0	0	0	0	0	0	0	0	0
In-116m	1.20E-10	0	0	0	0	0	0	0	0	0
In-117	6.88E-02	3.57E-04	0	0	0	0	0	0	0	0
In-117m	8.66E-02	4.35E-04	0	0	0	0	0	0	0	0
In-118	9.21E-02	2.22E-10	0	0	0	0	0	0	0	0
In-118m	5.76E-07	0	0	0	0	0	0	0	0	0

In-119	4.87E-02	0	0	0	0	0	0	0	0	0
In-119m	4.80E-02	0	0	0	0	0	0	0	0	0
In-120	8.78E-02	0	0	0	0	0	0	0	0	0
In-120m	2.23E-03	0	0	0	0	0	0	0	0	0
In-121	7.62E-02	0	0	0	0	0	0	0	0	0
In-121m	2.76E-02	0	0	0	0	0	0	0	0	0
In-122	7.99E-02	0	0	0	0	0	0	0	0	0
In-122m	1.61E-02	0	0	0	0	0	0	0	0	0
In-123	6.41E-02	0	0	0	0	0	0	0	0	0
In-123m	2.83E-02	0	0	0	0	0	0	0	0	0
In-124	6.39E-02	0	0	0	0	0	0	0	0	0
In-124m	3.79E-02	0	0	0	0	0	0	0	0	0
In-125	5.60E-02	0	0	0	0	0	0	0	0	0
In-125m	4.69E-02	0	0	0	0	0	0	0	0	0
In-126	5.22E-02	0	0	0	0	0	0	0	0	0
In-126m	3.79E-02	0	0	0	0	0	0	0	0	0
In-127	1.34E-01	0	0	0	0	0	0	0	0	0
In-127m	6.67E-02	0	0	0	0	0	0	0	0	0
In-128	9.00E-02	0	0	0	0	0	0	0	0	0
In-129	6.27E-02	0	0	0	0	0	0	0	0	0
In-129m	5.74E-02	0	0	0	0	0	0	0	0	0
In-130	1.61E-01	0	0	0	0	0	0	0	0	0
In-130m	2.34E-02	0	0	0	0	0	0	0	0	0
In-131	4.19E-02	0	0	0	0	0	0	0	0	0
In-131m	2.20E-02	0	0	0	0	0	0	0	0	0
In-132	1.19E-02	0	0	0	0	0	0	0	0	0
In-133	4.32E-04	0	0	0	0	0	0	0	0	0
In-134	1.12E-05	0	0	0	0	0	0	0	0	0
In-135	9.58E-08	0	0	0	0	0	0	0	0	0
Sn-113	4.86E-12	4.83E-12	4.57E-12	4.05E-12	0	0	0	0	0	0
Sn-117m	2.06E-04	1.97E-04	1.25E-04	4.57E-05	2.14E-12	0	0	0	0	0
Sn-119m	1.37E-05	1.37E-05	1.34E-05	1.28E-05	5.78E-06	2.45E-09	0	0	0	0
Sn-121	9.91E-02	5.37E-02	3.63E-04	1.53E-04	1.51E-04	1.35E-04	4.35E-05	5.20E-10	0	0
Sn-121m	2.47E-04	2.47E-04	2.47E-04	2.47E-04	2.44E-04	2.18E-04	7.02E-05	8.39E-10	0	0
Sn-123	8.30E-02	8.25E-02	7.86E-02	7.06E-02	1.17E-02	2.60E-10	0	0	0	0
Sn-123m	6.80E-02	1.03E-12	0	0	0	0	0	0	0	0
Sn-125	2.15E-01	2.00E-01	1.05E-01	2.49E-02	0	0	0	0	0	0
Sn-125m	1.01E-01	0	0	0	0	0	0	0	0	0
Sn-126	3.67E-06	3.67E-06	3.67E-06	3.67E-06	3.67E-06	3.67E-06	3.67E-06	3.66E-06	3.56E-06	2.72E-06
Sn-127	9.51E-01	3.45E-04	0	0	0	0	0	0	0	0
Sn-127m	2.60E-01	0	0	0	0	0	0	0	0	0
Sn-128	1.84E+00	8.45E-08	0	0	0	0	0	0	0	0
Sn-129	2.00E+00	0	0	0	0	0	0	0	0	0
Sn-129m	9.60E-01	0	0	0	0	0	0	0	0	0
Sn-130	2.37E+00	0	0	0	0	0	0	0	0	0
Sn-130m	2.14E+00	0	0	0	0	0	0	0	0	0
Sn-131	1.72E+00	0	0	0	0	0	0	0	0	0
Sn-131m	1.65E+00	0	0	0	0	0	0	0	0	0
Sn-132	2.20E+00	0	0	0	0	0	0	0	0	0
Sn-133	3.87E-01	0	0	0	0	0	0	0	0	0
Sn-134	4.75E-02	0	0	0	0	0	0	0	0	0

Sn-135	1.95E-03	0	0	0	0	0	0	0	0	0
Sn-136	4.40E-05	0	0	0	0	0	0	0	0	0
Sn-137	2.31E-05	0	0	0	0	0	0	0	0	0
Sb-117	1.06E-12	0	0	0	0	0	0	0	0	0
Sb-118	1.18E-11	0	0	0	0	0	0	0	0	0
Sb-118m	2.56E-11	0	0	0	0	0	0	0	0	0
Sb-119	2.17E-09	1.40E-09	2.78E-11	0	0	0	0	0	0	0
Sb-120	1.33E-07	0	0	0	0	0	0	0	0	0
Sb-120m	5.42E-08	4.81E-08	1.63E-08	1.47E-09	0	0	0	0	0	0
Sb-122	1.56E-02	1.21E-02	1.22E-03	7.53E-06	0	0	0	0	0	0
Sb-122m	4.20E+02	0	0	0	0	0	0	0	0	0
Sb-124	1.68E-02	1.66E-02	1.50E-02	1.19E-02	2.52E-04	0	0	0	0	0
Sb-124m	1.57E-03	0	0	0	0	0	0	0	0	0
Sb-125	1.45E-01	1.45E-01	1.45E-01	1.43E-01	1.14E-01	1.19E-02	1.83E-12	0	0	0
Sb-126	2.93E-02	2.77E-02	1.67E-02	5.45E-03	5.14E-07	5.14E-07	5.14E-07	5.13E-07	4.99E-07	3.80E-07
Sb-126m	3.32E-05	0	0	0	0	0	0	0	0	0
Sb-127	1.31E+00	1.11E+00	2.20E-01	6.00E-03	0	0	0	0	0	0
Sb-128	1.96E+00	3.45E-01	2.10E-08	0	0	0	0	0	0	0
Sb-128m	1.14E-01	0	0	0	0	0	0	0	0	0
Sb-129	3.81E+00	8.79E-02	0	0	0	0	0	0	0	0
Sb-130	3.80E+00	4.15E-11	0	0	0	0	0	0	0	0
Sb-130m	4.03E+00	0	0	0	0	0	0	0	0	0
Sb-131	1.05E+01	0	0	0	0	0	0	0	0	0
Sb-132	8.54E+00	0	0	0	0	0	0	0	0	0
Sb-132m	3.14E+00	0	0	0	0	0	0	0	0	0
Sb-133	8.51E+00	0	0	0	0	0	0	0	0	0
Sb-134	1.25E+00	0	0	0	0	0	0	0	0	0
Sb-134m	1.31E+00	0	0	0	0	0	0	0	0	0
Sb-135	4.99E-01	0	0	0	0	0	0	0	0	0
Sb-136	4.35E-02	0	0	0	0	0	0	0	0	0
Sb-137	4.07E-02	0	0	0	0	0	0	0	0	0
Sb-138	7.54E-05	0	0	0	0	0	0	0	0	0
Sb-139	9.48E-06	0	0	0	0	0	0	0	0	0
Te-121	1.02E-08	9.90E-09	7.27E-09	3.74E-09	9.87E-11	0	0	0	0	0
Te-121m	4.73E-10	4.71E-10	4.52E-10	4.13E-10	9.15E-11	0	0	0	0	0
Te-123m	2.52E-04	2.51E-04	2.38E-04	2.12E-04	3.02E-05	0	0	0	0	0
Te-125m	2.95E-02	2.96E-02	3.00E-02	3.07E-02	2.80E-02	2.93E-03	0	0	0	0
Te-127	1.28E+00	1.18E+00	2.63E-01	3.38E-02	3.27E-03	2.77E-12	0	0	0	0
Te-127m	3.24E-02	3.26E-02	3.23E-02	2.88E-02	3.43E-03	2.90E-12	0	0	0	0
Te-129	3.79E+00	1.19E-01	7.86E-04	5.20E-04	5.18E-07	0	0	0	0	0
Te-129m	1.53E-03	1.50E-03	1.25E-03	8.24E-04	8.22E-07	0	0	0	0	0
Te-131	1.19E+01	2.49E-01	1.69E-03	2.58E-08	0	0	0	0	0	0
Te-131m	1.74E+00	9.98E-01	6.78E-03	1.04E-07	0	0	0	0	0	0
Te-132	1.93E+01	1.55E+01	2.21E+00	2.93E-02	0	0	0	0	0	0
Te-133	1.57E+01	4.02E-08	0	0	0	0	0	0	0	0
Te-133m	1.19E+01	1.78E-07	0	0	0	0	0	0	0	0
Te-134	2.45E+01	1.04E-09	0	0	0	0	0	0	0	0
Te-135	1.21E+01	0	0	0	0	0	0	0	0	0
Te-136	4.34E+00	0	0	0	0	0	0	0	0	0
Te-137	1.31E+00	0	0	0	0	0	0	0	0	0
Te-138	2.01E-01	0	0	0	0	0	0	0	0	0

Te-139	4.75E-03	0	0	0	0	0	0	0	0	0
I-123	2.03E-10	5.78E-11	0	0	0	0	0	0	0	0
I-125	6.87E-09	6.79E-09	6.11E-09	4.84E-09	9.71E-11	0	0	0	0	0
I-126	2.44E-06	2.31E-06	1.43E-06	4.88E-07	0	0	0	0	0	0
I-128	1.51E-01	0	0	0	0	0	0	0	0	0
I-129	4.24E-07	4.24E-07	4.24E-07	4.24E-07	4.24E-07	4.24E-07	4.24E-07	4.24E-07	4.24E-07	4.22E-07
I-130	3.20E-01	8.39E-02	4.60E-07	0	0	0	0	0	0	0
I-130m	2.05E-01	0	0	0	0	0	0	0	0	0
I-131	1.57E+01	1.45E+01	6.78E+00	1.20E+00	0	0	0	0	0	0
I-132	1.98E+01	1.60E+01	2.28E+00	3.02E-02	0	0	0	0	0	0
I-132m	2.57E-01	1.59E-06	0	0	0	0	0	0	0	0
I-133	2.76E+01	1.27E+01	9.53E-03	1.08E-09	0	0	0	0	0	0
I-133m	1.06E+00	0	0	0	0	0	0	0	0	0
I-134	3.11E+01	6.98E-07	0	0	0	0	0	0	0	0
I-134m	2.97E+00	0	0	0	0	0	0	0	0	0
I-135	2.64E+01	2.10E+00	2.66E-10	0	0	0	0	0	0	0
I-136	1.01E+01	0	0	0	0	0	0	0	0	0
I-136m	6.24E+00	0	0	0	0	0	0	0	0	0
I-137	1.20E+01	0	0	0	0	0	0	0	0	0
I-138	6.16E+00	0	0	0	0	0	0	0	0	0
I-139	2.43E+00	0	0	0	0	0	0	0	0	0
I-140	4.75E-01	0	0	0	0	0	0	0	0	0
I-141	9.13E-02	0	0	0	0	0	0	0	0	0
I-142	1.30E-02	0	0	0	0	0	0	0	0	0
I-143	2.96E-04	0	0	0	0	0	0	0	0	0
I-144	4.65E+00	0	0	0	0	0	0	0	0	0
Xe-125	1.48E-12	0	0	0	0	0	0	0	0	0
Xe-127	1.55E-07	1.52E-07	1.28E-07	8.77E-08	1.49E-10	0	0	0	0	0
Xe-127m	3.15E-09	0	0	0	0	0	0	0	0	0
Xe-129m	2.78E-04	2.57E-04	1.28E-04	2.68E-05	0	0	0	0	0	0
Xe-131m	2.36E-01	2.32E-01	1.85E-01	7.96E-02	3.32E-10	0	0	0	0	0
Xe-133	3.03E+01	2.89E+01	9.62E+00	6.85E-01	0	0	0	0	0	0
Xe-133m	3.65E-01	3.19E-01	2.35E-02	4.19E-05	0	0	0	0	0	0
Xe-134m	3.41E-01	0	0	0	0	0	0	0	0	0
Xe-135	6.18E+00	6.61E+00	9.22E-07	0	0	0	0	0	0	0
Xe-135m	4.26E+00	2.15E-01	2.73E-11	0	0	0	0	0	0	0
Xe-137	2.50E+01	0	0	0	0	0	0	0	0	0
Xe-138	2.37E+01	0	0	0	0	0	0	0	0	0
Xe-139	1.71E+01	0	0	0	0	0	0	0	0	0
Xe-140	1.12E+01	0	0	0	0	0	0	0	0	0
Xe-141	3.84E+00	0	0	0	0	0	0	0	0	0
Xe-142	1.33E+00	0	0	0	0	0	0	0	0	0
Xe-143	1.63E-01	0	0	0	0	0	0	0	0	0
Xe-144	6.16E-03	0	0	0	0	0	0	0	0	0
Xe-145	6.41E-04	0	0	0	0	0	0	0	0	0
Xe-146	3.59E-05	0	0	0	0	0	0	0	0	0
Xe-147	4.04E-06	0	0	0	0	0	0	0	0	0
Cs-129	1.16E-11	6.92E-12	0	0	0	0	0	0	0	0
Cs-131	6.50E-08	6.06E-08	3.18E-08	7.61E-09	0	0	0	0	0	0
Cs-132	4.26E-05	3.83E-05	1.46E-05	1.72E-06	0	0	0	0	0	0
Cs-134	4.15E+00	4.15E+00	4.11E+00	4.04E+00	2.97E+00	1.45E-01	0	0	0	0

Cs-134m	8.60E-01	2.84E-03	0	0	0	0	0	0	0	0
Cs-135	4.79E-06	4.79E-06	4.80E-06	4.80E-06	4.80E-06	4.80E-06	4.80E-06	4.80E-06	4.78E-06	4.66E-06
Cs-135m	1.89E-02	1.25E-10	0	0	0	0	0	0	0	0
Cs-136	6.73E-01	6.38E-01	3.97E-01	1.39E-01	3.01E-09	0	0	0	0	0
Cs-136m	9.58E-02	0	0	0	0	0	0	0	0	0
Cs-137	1.88E+00	1.88E+00	1.88E+00	1.88E+00	1.84E+00	1.49E+00	1.88E-01	1.86E-10	0	0
Cs-138	2.60E+01	4.60E-12	0	0	0	0	0	0	0	0
Cs-138m	1.52E+00	0	0	0	0	0	0	0	0	0
Cs-139	2.41E+01	0	0	0	0	0	0	0	0	0
Cs-140	2.01E+01	0	0	0	0	0	0	0	0	0
Cs-141	1.56E+01	0	0	0	0	0	0	0	0	0
Cs-142	9.13E+00	0	0	0	0	0	0	0	0	0
Cs-143	4.66E+00	0	0	0	0	0	0	0	0	0
Cs-144	1.36E+00	0	0	0	0	0	0	0	0	0
Cs-145	2.52E-01	0	0	0	0	0	0	0	0	0
Cs-146	2.69E-02	0	0	0	0	0	0	0	0	0
Cs-147	5.06E-03	0	0	0	0	0	0	0	0	0
Cs-148	7.93E-05	0	0	0	0	0	0	0	0	0
Cs-149	3.96E-06	0	0	0	0	0	0	0	0	0
Cs-150	6.81E-08	0	0	0	0	0	0	0	0	0
Cs-151	9.49E-09	0	0	0	0	0	0	0	0	0
Ba-131	3.09E-12	2.91E-12	1.69E-12	0	0	0	0	0	0	0
Ba-133	4.51E-08	4.51E-08	4.50E-08	4.48E-08	4.22E-08	2.33E-08	6.19E-11	0	0	0
Ba-133m	2.04E-09	1.33E-09	2.84E-11	0	0	0	0	0	0	0
Ba-135m	1.52E-03	8.53E-04	4.63E-06	4.27E-11	0	0	0	0	0	0
Ba-136m	7.51E-02	7.09E-02	4.41E-02	1.54E-02	3.34E-10	0	0	0	0	0
Ba-137m	1.78E+00	1.77E+00	1.77E+00	1.77E+00	1.73E+00	1.41E+00	1.77E-01	1.76E-10	0	0
Ba-139	2.47E+01	1.69E-04	0	0	0	0	0	0	0	0
Ba-140	3.04E+01	2.88E+01	1.77E+01	5.95E+00	7.35E-08	0	0	0	0	0
Ba-141	2.20E+01	0	0	0	0	0	0	0	0	0
Ba-142	2.08E+01	0	0	0	0	0	0	0	0	0
Ba-143	1.84E+01	0	0	0	0	0	0	0	0	0
Ba-144	1.38E+01	0	0	0	0	0	0	0	0	0
Ba-145	5.97E+00	0	0	0	0	0	0	0	0	0
Ba-146	2.56E+00	0	0	0	0	0	0	0	0	0
Ba-147	6.30E-01	0	0	0	0	0	0	0	0	0
Ba-148	7.07E-02	0	0	0	0	0	0	0	0	0
Ba-149	5.06E-03	0	0	0	0	0	0	0	0	0
Ba-150	3.24E-04	0	0	0	0	0	0	0	0	0
Ba-151	1.09E+01	0	0	0	0	0	0	0	0	0
Ba-152	6.06E-02	0	0	0	0	0	0	0	0	0
La-135	1.23E-09	5.24E-10	0	0	0	0	0	0	0	0
La-137	1.08E-10	1.08E-10	1.08E-10	1.08E-10	1.08E-10	1.08E-10	1.08E-10	1.07E-10	9.64E-11	3.41E-11
La-140	3.24E+01	3.14E+01	2.03E+01	6.85E+00	8.47E-08	0	0	0	0	0
La-141	2.21E+01	3.45E-01	0	0	0	0	0	0	0	0
La-142	2.15E+01	4.23E-04	0	0	0	0	0	0	0	0
La-143	2.06E+01	0	0	0	0	0	0	0	0	0
La-144	1.83E+01	0	0	0	0	0	0	0	0	0
La-145	1.30E+01	0	0	0	0	0	0	0	0	0
La-146	5.52E+00	0	0	0	0	0	0	0	0	0
La-146m	2.81E+00	0	0	0	0	0	0	0	0	0

La-147	3.62E+00	0	0	0	0	0	0	0	0	0
La-148	1.29E+00	0	0	0	0	0	0	0	0	0
La-149	3.53E-01	0	0	0	0	0	0	0	0	0
La-150	5.13E-02	0	0	0	0	0	0	0	0	0
La-151	2.01E+04	0	0	0	0	0	0	0	0	0
La-152	9.45E-04	0	0	0	0	0	0	0	0	0
La-153	4.79E-05	0	0	0	0	0	0	0	0	0
La-154	4.39E-07	0	0	0	0	0	0	0	0	0
La-155	1.25E-08	0	0	0	0	0	0	0	0	0
Ce-137	2.88E-10	4.54E-11	0	0	0	0	0	0	0	0
Ce-139	4.62E-05	4.60E-05	4.40E-05	3.98E-05	7.36E-06	0	0	0	0	0
Ce-139m	4.09E-07	0	0	0	0	0	0	0	0	0
Ce-141	3.35E+01	3.29E+01	2.71E+01	1.77E+01	1.40E-02	0	0	0	0	0
Ce-143	2.07E+01	1.26E+01	1.36E-01	5.74E-06	0	0	0	0	0	0
Ce-144	2.98E+01	2.97E+01	2.91E+01	2.77E+01	1.23E+01	4.15E-03	0	0	0	0
Ce-145	1.40E+01	0	0	0	0	0	0	0	0	0
Ce-146	1.11E+01	0	0	0	0	0	0	0	0	0
Ce-147	7.89E+00	0	0	0	0	0	0	0	0	0
Ce-148	5.61E+00	0	0	0	0	0	0	0	0	0
Ce-149	3.17E+00	0	0	0	0	0	0	0	0	0
Ce-150	1.66E+00	0	0	0	0	0	0	0	0	0
Ce-151	2.67E-01	0	0	0	0	0	0	0	0	0
Ce-152	1.15E-01	0	0	0	0	0	0	0	0	0
Ce-153	1.56E+05	0	0	0	0	0	0	0	0	0
Ce-154	1.21E+04	0	0	0	0	0	0	0	0	0
Ce-155	1.55E+02	0	0	0	0	0	0	0	0	0
Pr-139	8.91E-11	2.05E-12	0	0	0	0	0	0	0	0
Pr-140	2.25E-05	7.07E-11	1.11E-11	0	0	0	0	0	0	0
Pr-142	1.08E+00	4.53E-01	1.80E-04	4.99E-12	0	0	0	0	0	0
Pr-142m	3.75E-01	0	0	0	0	0	0	0	0	0
Pr-143	2.78E+01	2.72E+01	1.81E+01	6.51E+00	2.41E-07	0	0	0	0	0
Pr-144	3.00E+01	2.97E+01	2.91E+01	2.77E+01	1.23E+01	4.15E-03	0	0	0	0
Pr-144m	4.09E-01	2.83E-01	2.77E-01	2.64E-01	1.17E-01	3.95E-05	0	0	0	0
Pr-145	1.40E+01	8.79E-01	1.20E-11	0	0	0	0	0	0	0
Pr-146	1.12E+01	0	0	0	0	0	0	0	0	0
Pr-147	8.75E+00	0	0	0	0	0	0	0	0	0
Pr-148	6.30E+00	0	0	0	0	0	0	0	0	0
Pr-148m	5.29E-01	0	0	0	0	0	0	0	0	0
Pr-149	4.79E+00	0	0	0	0	0	0	0	0	0
Pr-150	3.18E+00	0	0	0	0	0	0	0	0	0
Pr-151	1.87E+00	0	0	0	0	0	0	0	0	0
Pr-152	8.48E-01	0	0	0	0	0	0	0	0	0
Pr-153	3.08E-01	0	0	0	0	0	0	0	0	0
Pr-154	7.50E-02	0	0	0	0	0	0	0	0	0
Pr-155	7.97E-03	0	0	0	0	0	0	0	0	0
Pr-156	3.29E-03	0	0	0	0	0	0	0	0	0
Pr-157	1.88E-04	0	0	0	0	0	0	0	0	0
Pr-158	1.14E-05	0	0	0	0	0	0	0	0	0
Pr-159	1.81E-07	0	0	0	0	0	0	0	0	0
Nd-140	8.67E-11	7.06E-11	1.11E-11	0	0	0	0	0	0	0
Nd-141	4.99E-07	6.26E-10	0	0	0	0	0	0	0	0

Nd-147	1.07E+01	1.00E+01	5.69E+00	1.61E+00	1.05E-09	0	0	0	0	0
Nd-149	5.07E+00	3.41E-04	0	0	0	0	0	0	0	0
Nd-151	2.61E+00	0	0	0	0	0	0	0	0	0
Nd-152	1.84E+00	0	0	0	0	0	0	0	0	0
Nd-153	1.10E+00	0	0	0	0	0	0	0	0	0
Nd-154	6.01E-01	0	0	0	0	0	0	0	0	0
Nd-155	2.31E-01	0	0	0	0	0	0	0	0	0
Nd-156	8.87E-02	0	0	0	0	0	0	0	0	0
Nd-157	3.49E-02	0	0	0	0	0	0	0	0	0
Nd-158	6.03E-03	0	0	0	0	0	0	0	0	0
Nd-159	4.88E-04	0	0	0	0	0	0	0	0	0
Nd-160	1.12E-05	0	0	0	0	0	0	0	0	0
Nd-161	4.83E-07	0	0	0	0	0	0	0	0	0
Pm-144	1.74E-11	1.74E-11	1.71E-11	1.65E-11	8.68E-12	0	0	0	0	0
Pm-145	7.21E-09	7.21E-09	7.21E-09	7.19E-09	6.98E-09	4.94E-09	1.46E-10	0	0	0
Pm-146	5.61E-06	5.61E-06	5.59E-06	5.55E-06	4.95E-06	1.60E-06	2.04E-11	0	0	0
Pm-147	2.59E+00	2.60E+00	2.63E+00	2.64E+00	2.09E+00	1.94E-01	9.27E-12	0	0	0
Pm-148	4.00E+00	3.52E+00	1.11E+00	9.65E-02	5.03E-05	0	0	0	0	0
Pm-149	8.52E+00	6.36E+00	3.79E-01	7.18E-04	0	0	0	0	0	0
Pm-150	1.31E-01	2.64E-04	0	0	0	0	0	0	0	0
Pm-151	2.61E+00	1.46E+00	7.52E-03	6.14E-08	0	0	0	0	0	0
Pm-152	1.87E+00	0	0	0	0	0	0	0	0	0
Pm-152m	3.86E-02	0	0	0	0	0	0	0	0	0
Pm-153	1.24E+00	0	0	0	0	0	0	0	0	0
Pm-154	7.02E-01	0	0	0	0	0	0	0	0	0
Pm-154m	9.92E-02	0	0	0	0	0	0	0	0	0
Pm-155	4.55E-01	0	0	0	0	0	0	0	0	0
Pm-156	2.60E-01	0	0	0	0	0	0	0	0	0
Pm-157	1.27E-01	0	0	0	0	0	0	0	0	0
Pm-158	4.51E-02	0	0	0	0	0	0	0	0	0
Pm-159	1.06E-02	0	0	0	0	0	0	0	0	0
Pm-160	4.53E-03	0	0	0	0	0	0	0	0	0
Pm-161	1.12E-04	0	0	0	0	0	0	0	0	0
Pm-162	7.40E-07	0	0	0	0	0	0	0	0	0
Pm-163	1.65E-08	0	0	0	0	0	0	0	0	0
Sm-145	1.55E-09	1.55E-09	1.52E-09	1.46E-09	7.39E-10	0	0	0	0	0
Sm-147	1.42E-11	1.43E-11	1.47E-11	1.56E-11	2.98E-11	7.66E-11	8.14E-11	8.14E-11	8.14E-11	8.14E-11
Sm-151	5.95E-03	5.99E-03	6.05E-03	6.04E-03	6.00E-03	5.60E-03	2.80E-03	2.75E-06	0	0
Sm-153	6.58E+00	4.59E+00	1.81E-01	1.37E-04	0	0	0	0	0	0
Sm-155	5.36E-01	0	0	0	0	0	0	0	0	0
Sm-156	3.47E-01	5.92E-02	7.16E-09	0	0	0	0	0	0	0
Sm-157	2.20E-01	0	0	0	0	0	0	0	0	0
Sm-158	1.27E-01	0	0	0	0	0	0	0	0	0
Sm-159	5.37E-02	0	0	0	0	0	0	0	0	0
Sm-160	1.81E-02	0	0	0	0	0	0	0	0	0
Sm-161	4.44E-03	0	0	0	0	0	0	0	0	0
Sm-162	1.69E-04	0	0	0	0	0	0	0	0	0
Sm-163	1.29E-05	0	0	0	0	0	0	0	0	0
Sm-164	3.37E-07	0	0	0	0	0	0	0	0	0
Sm-165	8.68E-09	0	0	0	0	0	0	0	0	0
Eu-149	2.32E-11	2.30E-11	2.15E-11	1.86E-11	1.53E-12	0	0	0	0	0

Eu-150	1.78E-11	1.78E-11	1.78E-11	1.78E-11	1.75E-11	1.48E-11	2.73E-12	0	0	0
Eu-152	2.96E-05	2.96E-05	2.96E-05	2.95E-05	2.81E-05	1.78E-05	1.78E-07	0	0	0
Eu-152m	1.51E-08	0	0	0	0	0	0	0	0	0
Eu-154	1.06E-01	1.06E-01	1.06E-01	1.06E-01	9.80E-02	4.74E-02	3.35E-05	0	0	0
Eu-154m	6.79E-02	2.95E-11	0	0	0	0	0	0	0	0
Eu-155	5.92E-02	5.92E-02	5.90E-02	5.85E-02	5.12E-02	1.38E-02	2.78E-08	0	0	0
Eu-156	5.92E+00	5.67E+00	3.76E+00	1.51E+00	3.47E-07	0	0	0	0	0
Eu-157	4.23E-01	1.42E-01	7.40E-06	0	0	0	0	0	0	0
Eu-158	1.38E-01	5.55E-11	0	0	0	0	0	0	0	0
Eu-159	6.83E-02	0	0	0	0	0	0	0	0	0
Eu-160	2.92E-02	0	0	0	0	0	0	0	0	0
Eu-161	1.18E-02	0	0	0	0	0	0	0	0	0
Eu-162	1.76E-03	0	0	0	0	0	0	0	0	0
Eu-163	3.17E-04	0	0	0	0	0	0	0	0	0
Eu-164	2.45E-05	0	0	0	0	0	0	0	0	0
Eu-165	2.79E-06	0	0	0	0	0	0	0	0	0
Eu-166	1.32E-07	0	0	0	0	0	0	0	0	0
Eu-167	4.68E-02	0	0	0	0	0	0	0	0	0
Gd-151	8.82E-12	8.77E-12	8.34E-12	7.46E-12	1.15E-12	0	0	0	0	0
Gd-153	5.10E-07	5.08E-07	4.95E-07	4.68E-07	1.78E-07	1.37E-11	0	0	0	0
Gd-159	9.35E-02	3.85E-02	1.17E-05	0	0	0	0	0	0	0
Gd-161	1.44E-02	0	0	0	0	0	0	0	0	0
Gd-162	3.87E-03	0	0	0	0	0	0	0	0	0
Gd-163	1.51E-03	0	0	0	0	0	0	0	0	0
Gd-164	4.71E-04	0	0	0	0	0	0	0	0	0
Gd-165	1.22E-04	0	0	0	0	0	0	0	0	0
Gd-166	4.58E-05	0	0	0	0	0	0	0	0	0
Gd-167	5.41E+01	0	0	0	0	0	0	0	0	0
Gd-168	2.00E+00	0	0	0	0	0	0	0	0	0
Gd-169	9.48E-01	0	0	0	0	0	0	0	0	0
Tb-155	1.33E-10	1.17E-10	3.63E-11	2.68E-12	0	0	0	0	0	0
Tb-156	2.30E-09	2.03E-09	6.37E-10	4.78E-11	0	0	0	0	0	0
Tb-156m	1.41E-10	7.11E-11	0	0	0	0	0	0	0	0
Tb-157	4.47E-10	4.47E-10	4.46E-10	4.46E-10	4.42E-10	4.05E-10	1.68E-10	0	0	0
Tb-158	2.63E-09	2.63E-09	2.63E-09	2.63E-09	2.62E-09	2.53E-09	1.79E-09	5.62E-11	0	0
Tb-158m	2.17E-08	0	0	0	0	0	0	0	0	0
Tb-160	1.69E-02	1.67E-02	1.53E-02	1.27E-02	5.10E-04	0	0	0	0	0
Tb-161	2.44E-02	2.21E-02	8.95E-03	1.20E-03	0	0	0	0	0	0
Tb-162	3.98E-03	0	0	0	0	0	0	0	0	0
Tb-163	1.70E-03	0	0	0	0	0	0	0	0	0
Tb-164	6.20E-04	0	0	0	0	0	0	0	0	0
Tb-165	2.44E-04	0	0	0	0	0	0	0	0	0
Tb-166	8.29E-05	0	0	0	0	0	0	0	0	0
Tb-167	1.96E-05	0	0	0	0	0	0	0	0	0
Tb-168	8.45E-06	0	0	0	0	0	0	0	0	0
Tb-169	8.11E-07	0	0	0	0	0	0	0	0	0
Tb-170	1.17E-06	0	0	0	0	0	0	0	0	0
Tb-171	1.36E-08	0	0	0	0	0	0	0	0	0
Dy-157	1.24E-11	1.61E-12	0	0	0	0	0	0	0	0
Dy-159	1.01E-08	1.00E-08	9.60E-09	8.72E-09	1.75E-09	0	0	0	0	0
Dy-165	4.96E-03	4.01E-06	0	0	0	0	0	0	0	0

Dy-165m	3.17E-03	0	0	0	0	0	0	0	0	0
Dy-166	1.29E-04	1.05E-04	1.68E-05	2.85E-07	0	0	0	0	0	0
Dy-167	3.34E-05	0	0	0	0	0	0	0	0	0
Dy-168	1.74E-05	0	0	0	0	0	0	0	0	0
Dy-169	6.44E-06	0	0	0	0	0	0	0	0	0
Dy-171	1.59E+01	0	0	0	0	0	0	0	0	0
Dy-172	2.56E+00	0	0	0	0	0	0	0	0	0
Ho-159	1.06E-12	0	0	0	0	0	0	0	0	0
Ho-161	1.06E-10	0	0	0	0	0	0	0	0	0
Ho-161m	7.35E-12	0	0	0	0	0	0	0	0	0
Ho-162	4.66E-10	0	0	0	0	0	0	0	0	0
Ho-162m	5.22E-10	0	0	0	0	0	0	0	0	0
Ho-163	1.11E-12	1.11E-12	1.11E-12	1.11E-12	1.11E-12	1.11E-12	1.09E-12	0	0	0
Ho-163m	4.09E-10	0	0	0	0	0	0	0	0	0
Ho-164	2.70E-08	0	0	0	0	0	0	0	0	0
Ho-164m	1.56E-08	0	0	0	0	0	0	0	0	0
Ho-166	8.79E-04	5.26E-04	2.64E-05	4.24E-07	0	0	0	0	0	0
Ho-166m	1.68E-09	1.68E-09	1.68E-09	1.68E-09	1.68E-09	1.67E-09	1.59E-09	9.43E-10	5.23E-12	0
Ho-167	8.28E-05	3.92E-07	0	0	0	0	0	0	0	0
Ho-168	1.83E-05	0	0	0	0	0	0	0	0	0
Ho-169	7.54E-06	0	0	0	0	0	0	0	0	0
Ho-170	2.37E-06	0	0	0	0	0	0	0	0	0
Ho-170m	3.70E-07	0	0	0	0	0	0	0	0	0
Ho-171	9.71E-07	0	0	0	0	0	0	0	0	0
Ho-172	4.02E-07	0	0	0	0	0	0	0	0	0
Er-163	4.12E-12	0	0	0	0	0	0	0	0	0
Er-165	2.25E-09	4.52E-10	0	0	0	0	0	0	0	0
Er-167m	3.71E-05	4.67E-08	7.22E-12	1.61E-12	0	0	0	0	0	0
Er-169	1.14E-05	1.06E-05	5.47E-06	1.25E-06	0	0	0	0	0	0
Er-171	1.19E-06	1.30E-07	0	0	0	0	0	0	0	0
Er-172	5.62E-07	4.01E-07	1.92E-08	2.26E-11	0	0	0	0	0	0
Tm-166	1.74E-12	0	0	0	0	0	0	0	0	0
Tm-167	1.57E-11	1.45E-11	7.40E-12	1.65E-12	0	0	0	0	0	0
Tm-168	1.00E-10	9.96E-11	9.31E-11	8.02E-11	6.63E-12	0	0	0	0	0
Tm-170	1.45E-09	1.44E-09	1.38E-09	1.24E-09	2.03E-10	0	0	0	0	0
Tm-171	4.55E-07	4.55E-07	4.51E-07	4.42E-07	3.18E-07	1.24E-08	0	0	0	0
Tm-172	6.04E-07	5.74E-07	1.19E-07	9.16E-10	0	0	0	0	0	0
Yb-169	1.16E-12	1.14E-12	0	0	0	0	0	0	0	0
Tl-206	0	0	0	0	0	0	0	0	2.12E-12	1.63E-11
Tl-207	0	0	0	0	0	8.84E-12	4.55E-10	6.19E-09	6.01E-08	3.33E-07
Tl-208	2.98E-10	2.99E-10	3.12E-10	3.43E-10	8.05E-10	2.21E-09	9.72E-10	2.08E-12	2.92E-12	1.31E-11
Tl-209	0	0	0	0	0	0	0	4.97E-11	6.03E-09	1.35E-07
Tl-210	0	0	0	0	0	0	0	6.85E-12	3.34E-10	2.56E-09
Pb-209	0	0	0	0	0	0	1.55E-11	2.35E-09	2.85E-07	6.41E-06
Pb-210	0	0	0	0	0	0	4.99E-11	3.05E-08	1.59E-06	1.22E-05
Pb-211	0	0	0	0	0	8.86E-12	4.56E-10	6.21E-09	6.02E-08	3.34E-07
Pb-212	8.30E-10	8.33E-10	8.68E-10	9.55E-10	2.24E-09	6.15E-09	2.70E-09	5.92E-12	8.12E-12	3.63E-11
Pb-214	0	0	0	0	0	0	1.03E-10	3.23E-08	1.58E-06	1.21E-05
Bi-210	0	0	0	0	0	0	4.99E-11	3.05E-08	1.59E-06	1.22E-05
Bi-211	0	0	0	0	0	8.86E-12	4.56E-10	6.21E-09	6.02E-08	3.34E-07
Bi-212	8.30E-10	8.33E-10	8.68E-10	9.55E-10	2.24E-09	6.15E-09	2.70E-09	5.78E-12	8.12E-12	3.63E-11

Bi-213	0	0	0	0	0	0	1.55E-11	2.34E-09	2.83E-07	6.37E-06
Bi-214	0	0	0	0	0	0	1.04E-10	3.26E-08	1.59E-06	1.22E-05
Po-210	0	0	0	0	0	0	4.90E-11	3.04E-08	1.59E-06	1.22E-05
Po-211	0	0	0	0	0	0	1.26E-12	1.71E-11	1.66E-10	9.21E-10
Po-212	5.31E-10	5.34E-10	5.56E-10	6.12E-10	1.43E-09	3.94E-09	1.73E-09	3.70E-12	5.20E-12	2.33E-11
Po-213	0	0	0	0	0	0	1.71E-11	2.58E-09	3.13E-07	7.04E-06
Po-214	0	0	0	0	0	0	1.04E-10	3.26E-08	1.59E-06	1.22E-05
Po-215	0	0	0	0	0	8.86E-12	4.56E-10	6.21E-09	6.02E-08	3.34E-07
Po-216	8.32E-10	8.35E-10	8.71E-10	9.58E-10	2.24E-09	6.15E-09	2.70E-09	5.92E-12	8.12E-12	3.63E-11
Po-218	0	0	0	0	0	0	1.04E-10	3.26E-08	1.59E-06	1.22E-05
At-217	0	0	0	0	0	0	1.55E-11	2.34E-09	2.83E-07	6.37E-06
At-218	0	0	0	0	0	0	0	6.52E-12	3.18E-10	2.44E-09
Rn-217	0	0	0	0	0	0	0	0	1.98E-11	4.46E-10
Rn-218	0	0	0	0	0	0	0	0	0	2.44E-12
Rn-219	0	0	0	0	0	1.11E-11	4.56E-10	6.21E-09	6.02E-08	3.34E-07
Rn-220	8.32E-10	8.35E-10	8.71E-10	9.58E-10	2.24E-09	6.15E-09	2.70E-09	5.92E-12	8.12E-12	3.63E-11
Rn-222	0	0	0	0	0	0	1.04E-10	3.26E-08	1.59E-06	1.22E-05
Fr-221	0	0	0	0	0	0	1.56E-11	2.34E-09	2.83E-07	6.37E-06
Fr-223	0	0	0	0	0	0	6.30E-12	8.57E-11	8.31E-10	4.61E-09
Ra-223	0	0	0	0	0	1.11E-11	4.56E-10	6.21E-09	6.02E-08	3.34E-07
Ra-224	8.38E-10	8.42E-10	8.78E-10	9.65E-10	2.26E-09	6.20E-09	2.72E-09	5.97E-12	8.18E-12	3.66E-11
Ra-225	0	0	0	0	0	0	1.56E-11	2.34E-09	2.83E-07	6.37E-06
Ra-226	0	0	0	0	0	0	1.04E-10	3.26E-08	1.59E-06	1.22E-05
Ra-228	0	0	0	0	0	0	0	0	3.01E-12	3.29E-11
Ac-225	0	0	0	0	0	0	1.57E-11	2.36E-09	2.86E-07	6.42E-06
Ac-227	0	0	0	0	0	1.14E-11	4.57E-10	6.21E-09	6.02E-08	3.34E-07
Ac-228	0	0	0	0	0	0	0	0	3.01E-12	3.29E-11
Th-227	0	0	0	0	0	1.11E-11	4.50E-10	6.12E-09	5.94E-08	3.29E-07
Th-228	8.50E-10	8.54E-10	8.94E-10	9.81E-10	2.26E-09	6.15E-09	2.70E-09	5.92E-12	8.12E-12	3.63E-11
Th-229	0	0	0	0	0	0	1.46E-11	2.18E-09	2.64E-07	5.93E-06
Th-230	0	0	0	0	2.02E-12	9.24E-11	6.84E-09	1.91E-07	2.05E-06	1.23E-05
Th-231	3.15E-07	3.10E-07	3.05E-07	3.05E-07	3.05E-07	3.05E-07	3.05E-07	3.07E-07	3.28E-07	3.94E-07
Th-232	0	0	0	0	0	0	0	0	3.02E-12	3.30E-11
Th-233	1.68E-07	0	0	0	0	0	0	0	0	0
Th-234	8.22E-07	8.22E-07	8.22E-07	8.22E-07	8.22E-07	8.22E-07	8.22E-07	8.22E-07	8.22E-07	8.22E-07
Th-235	2.29E-09	0	0	0	0	0	0	0	0	0
Pa-230	1.19E-12	1.14E-12	0	0	0	0	0	0	0	0
Pa-231	6.98E-12	6.99E-12	7.15E-12	7.51E-12	1.34E-11	7.14E-11	6.51E-10	6.41E-09	6.04E-08	3.34E-07
Pa-232	2.77E-07	1.63E-07	1.40E-09	0	0	0	0	0	0	0
Pa-233	6.31E-06	6.33E-06	6.46E-06	6.71E-06	7.11E-06	7.15E-06	8.66E-06	1.74E-05	2.01E-05	1.96E-05
Pa-234	9.03E-07	8.29E-07	8.22E-07	8.22E-07	8.22E-07	8.22E-07	8.22E-07	8.22E-07	8.22E-07	8.22E-07
Pa-234m	8.54E-08	0	0	0	0	0	0	0	0	0
Pa-235	2.30E-09	0	0	0	0	0	0	0	0	0
U-232	5.29E-09	5.30E-09	5.31E-09	5.33E-09	5.63E-09	6.32E-09	2.63E-09	5.63E-12	5.11E-12	3.41E-12
U-233	2.52E-11	2.52E-11	2.59E-11	2.75E-11	5.57E-11	3.35E-10	3.41E-09	5.84E-08	8.22E-07	6.98E-06
U-234	9.03E-08	9.07E-08	9.51E-08	1.05E-07	2.73E-07	1.89E-06	1.31E-05	2.39E-05	2.33E-05	1.83E-05
U-235	3.05E-07	3.05E-07	3.05E-07	3.05E-07	3.05E-07	3.05E-07	3.05E-07	3.07E-07	3.28E-07	3.94E-07
U-235m	3.72E-03	0	0	0	0	0	0	0	0	0
U-236	5.68E-06	5.68E-06	5.68E-06	5.68E-06	5.68E-06	5.68E-06	5.69E-06	5.79E-06	6.41E-06	6.78E-06
U-237	2.18E+01	1.96E+01	7.79E+00	1.00E+00	4.51E-05	2.91E-05	3.72E-07	2.92E-10	1.40E-10	0
U-238	8.22E-07	8.22E-07	8.22E-07	8.22E-07	8.22E-07	8.22E-07	8.22E-07	8.22E-07	8.22E-07	8.22E-07

U-239	1.80E+02	0	0	0	0	0	0	0	0	0
U-240	1.16E-03	3.57E-04	8.76E-09	2.28E-11	2.28E-11	2.28E-11	2.28E-11	2.28E-11	2.28E-11	2.28E-11
U-242	6.44E-12	0	0	0	0	0	0	0	0	0
Np-235	1.97E-08	1.97E-08	1.94E-08	1.87E-08	1.04E-08	3.32E-11	0	0	0	0
Np-236	4.25E-11	4.25E-11	4.25E-11	4.25E-11	4.25E-11	4.25E-11	4.25E-11	4.23E-11	4.06E-11	2.71E-11
Np-236m	7.67E-09	3.66E-09	4.72E-12	0	0	0	0	0	0	0
Np-237	6.92E-06	6.94E-06	7.04E-06	7.10E-06	7.11E-06	7.15E-06	8.67E-06	1.74E-05	2.01E-05	1.96E-05
Np-238	9.29E+00	6.70E+00	3.52E-01	5.04E-04	1.80E-07	1.72E-07	1.11E-07	1.33E-09	0	0
Np-239	2.04E+02	1.53E+02	1.08E+01	3.07E-02	5.37E-04	5.37E-04	5.32E-04	4.89E-04	2.10E-04	4.45E-08
Np-240	1.38E-01	3.86E-04	9.45E-09	2.28E-11	2.28E-11	2.28E-11	2.28E-11	2.28E-11	2.28E-11	2.28E-11
Np-240m	2.46E-01	0	0	0	0	0	0	0	0	0
Np-241	9.16E-07	0	0	0	0	0	0	0	0	0
Np-242	6.44E-12	0	0	0	0	0	0	0	0	0
Pu-236	4.32E-08	4.32E-08	4.29E-08	4.24E-08	3.39E-08	3.84E-09	5.27E-12	5.25E-12	5.04E-12	3.37E-12
Pu-237	1.43E-05	1.41E-05	1.23E-05	9.03E-06	5.30E-08	0	0	0	0	0
Pu-237m	5.80E-09	2.33E-10	1.93E-10	1.26E-10	0	0	0	0	0	0
Pu-238	6.28E-02	6.30E-02	6.35E-02	6.37E-02	6.55E-02	6.17E-02	3.03E-02	2.54E-05	0	0
Pu-239	2.54E-03	2.56E-03	2.59E-03	2.60E-03	2.60E-03	2.60E-03	2.59E-03	2.54E-03	2.03E-03	1.60E-04
Pu-240	3.75E-03	3.75E-03	3.75E-03	3.75E-03	3.76E-03	3.82E-03	3.93E-03	3.58E-03	1.38E-03	1.03E-07
Pu-241	1.92E+00	1.92E+00	1.92E+00	1.92E+00	1.83E+00	1.18E+00	1.51E-02	1.19E-05	5.72E-06	3.73E-09
Pu-242	4.36E-05	4.36E-05	4.36E-05	4.36E-05	4.36E-05	4.36E-05	4.36E-05	4.35E-05	4.28E-05	3.62E-05
Pu-243	7.30E+00	2.54E-01	7.37E-12	7.35E-12	7.35E-12	7.35E-12	7.35E-12	7.35E-12	7.34E-12	7.31E-12
Pu-244	2.28E-11	2.29E-11	2.29E-11	2.29E-11	2.29E-11	2.29E-11	2.29E-11	2.29E-11	2.29E-11	2.28E-11
Pu-245	8.25E-05	1.69E-05	1.09E-11	0	0	0	0	0	0	0
Am-239	1.43E-09	3.53E-10	0	0	0	0	0	0	0	0
Am-240	2.96E-07	2.14E-07	1.12E-08	1.62E-11	0	0	0	0	0	0
Am-241	9.06E-04	9.15E-04	9.91E-04	1.16E-03	3.92E-03	2.52E-02	5.64E-02	1.35E-02	6.05E-06	3.94E-09
Am-242	8.99E-01	3.18E-01	6.74E-05	3.96E-05	3.94E-05	3.77E-05	2.42E-05	2.91E-07	0	0
Am-242m	3.98E-05	3.98E-05	3.98E-05	3.98E-05	3.96E-05	3.79E-05	2.44E-05	2.93E-07	0	0
Am-243	5.37E-04	5.38E-04	5.38E-04	5.38E-04	5.38E-04	5.37E-04	5.33E-04	4.89E-04	2.10E-04	4.45E-08
Am-244	1.90E-01	3.66E-02	1.34E-08	0	0	0	0	0	0	0
Am-244m	2.86E+00	0	0	0	0	0	0	0	0	0
Am-245	4.33E-04	2.11E-05	1.65E-11	2.89E-12	1.43E-12	0	0	0	0	0
Cm-240	9.46E-11	9.22E-11	7.31E-11	4.38E-11	0	0	0	0	0	0
Cm-241	3.46E-08	3.38E-08	2.80E-08	1.83E-08	1.54E-11	0	0	0	0	0
Cm-242	6.54E-01	6.53E-01	6.30E-01	5.78E-01	1.39E-01	3.14E-05	2.01E-05	2.42E-07	0	0
Cm-243	2.50E-04	2.49E-04	2.49E-04	2.49E-04	2.44E-04	1.97E-04	2.31E-05	0	0	0
Cm-244	8.26E-02	8.26E-02	8.26E-02	8.24E-02	7.95E-02	5.64E-02	1.80E-03	0	0	0
Cm-245	1.30E-05	1.30E-05	1.30E-05	1.30E-05	1.30E-05	1.30E-05	1.29E-05	1.20E-05	5.78E-06	3.77E-09
Cm-246	2.01E-06	2.01E-06	2.01E-06	2.01E-06	2.01E-06	2.01E-06	1.98E-06	1.74E-06	4.69E-07	0
Cm-247	7.35E-12	7.35E-12	7.35E-12	7.35E-12	7.35E-12	7.35E-12	7.35E-12	7.35E-12	7.34E-12	7.31E-12
Cm-248	2.35E-11	2.35E-11	2.35E-11	2.35E-11	2.35E-11	2.35E-11	2.35E-11	2.34E-11	2.30E-11	1.92E-11
Cm-249	8.76E-07	0	0	0	0	0	0	0	0	0
Bk-249	2.12E-07	2.12E-07	2.08E-07	1.99E-07	9.85E-08	9.93E-11	0	0	0	0
Cf-249	6.46E-11	6.57E-11	7.59E-11	9.79E-11	3.56E-10	5.99E-10	5.02E-10	8.50E-11	0	0
Total activity	1.92E+05	8.18E+02	4.08E+02	2.72E+02	5.21E+01	7.08E+00	7.39E-01	2.10E-02	4.28E-03	6.79E-04
Decay heat [W]	3.02E+01	3.35E+00	1.72E+00	1.12E+00	2.23E-01	2.22E-02	4.93E-03	6.59E-04	1.17E-04	1.20E-05

Maximum activities [Ci]

Decay time	0 d	1 d	10 d	1 m	1 y	10 y	100 y	1,000 y	10,000 y	100,000 y
H-3	5.22E-06	5.22E-06	5.22E-06	5.20E-06	4.94E-06	2.98E-06	1.89E-08	0	0	0
He-6	2.72E-09	0	0	0	0	0	0	0	0	0
Li-8	1.38E-12	0	0	0	0	0	0	0	0	0
B-12	5.95E-10	0	0	0	0	0	0	0	0	0
C-14	3.48E-10	3.48E-10	3.48E-10	3.48E-10	3.48E-10	3.47E-10	3.44E-10	3.08E-10	1.03E-10	0
C-15	4.41E-09	0	0	0	0	0	0	0	0	0
N-16	2.24E-01	0	0	0	0	0	0	0	0	0
N-17	7.18E-08	0	0	0	0	0	0	0	0	0
O-15	3.18E-04	0	0	0	0	0	0	0	0	0
Mn-66	3.16E-08	0	0	0	0	0	0	0	0	0
Mn-67	9.36E-09	0	0	0	0	0	0	0	0	0
Mn-68	8.77E-10	0	0	0	0	0	0	0	0	0
Mn-69	1.02E-11	0	0	0	0	0	0	0	0	0
Fe-65	1.62E-08	0	0	0	0	0	0	0	0	0
Fe-66	1.33E-06	0	0	0	0	0	0	0	0	0
Fe-67	1.00E-06	0	0	0	0	0	0	0	0	0
Fe-68	6.41E-07	0	0	0	0	0	0	0	0	0
Fe-69	1.89E-07	0	0	0	0	0	0	0	0	0
Fe-70	8.01E-08	0	0	0	0	0	0	0	0	0
Fe-71	5.30E-08	0	0	0	0	0	0	0	0	0
Fe-72	1.04E-03	0	0	0	0	0	0	0	0	0
Co-65	1.07E-08	0	0	0	0	0	0	0	0	0
Co-66	3.87E-06	0	0	0	0	0	0	0	0	0
Co-67	5.66E-06	0	0	0	0	0	0	0	0	0
Co-68	5.87E-06	0	0	0	0	0	0	0	0	0
Co-69	5.38E-06	0	0	0	0	0	0	0	0	0
Co-70	3.38E-06	0	0	0	0	0	0	0	0	0
Co-71	1.25E-06	0	0	0	0	0	0	0	0	0
Co-72	3.80E-07	0	0	0	0	0	0	0	0	0
Co-73	6.77E-08	0	0	0	0	0	0	0	0	0
Co-74	1.02E-08	0	0	0	0	0	0	0	0	0
Co-75	1.37E-09	0	0	0	0	0	0	0	0	0
Ni-65	1.03E-08	1.39E-11	0	0	0	0	0	0	0	0
Ni-66	3.41E-06	2.51E-06	1.62E-07	3.66E-10	0	0	0	0	0	0
Ni-67	8.75E-06	0	0	0	0	0	0	0	0	0
Ni-68	1.62E-05	0	0	0	0	0	0	0	0	0
Ni-69	2.98E-05	0	0	0	0	0	0	0	0	0
Ni-70	5.93E-05	0	0	0	0	0	0	0	0	0
Ni-71	6.55E-05	0	0	0	0	0	0	0	0	0
Ni-72	6.16E-05	0	0	0	0	0	0	0	0	0
Ni-73	4.12E-05	0	0	0	0	0	0	0	0	0
Ni-74	2.14E-05	0	0	0	0	0	0	0	0	0
Ni-75	1.18E-05	0	0	0	0	0	0	0	0	0
Ni-76	1.63E-06	0	0	0	0	0	0	0	0	0
Ni-77	1.60E-07	0	0	0	0	0	0	0	0	0
Ni-78	1.93E-08	0	0	0	0	0	0	0	0	0
Cu-66	3.42E-06	2.52E-06	1.62E-07	3.66E-10	0	0	0	0	0	0
Cu-67	6.60E-06	5.04E-06	4.48E-07	2.06E-09	0	0	0	0	0	0
Cu-68	1.71E-05	0	0	0	0	0	0	0	0	0
Cu-68m	7.15E-07	0	0	0	0	0	0	0	0	0
Cu-69	3.71E-05	0	0	0	0	0	0	0	0	0
Cu-70	4.17E-05	0	0	0	0	0	0	0	0	0
Cu-70m	9.18E-06	0	0	0	0	0	0	0	0	0
Cu-71	2.02E-04	0	0	0	0	0	0	0	0	0
Cu-72	3.18E-04	0	0	0	0	0	0	0	0	0
Cu-73	4.88E-04	0	0	0	0	0	0	0	0	0
Cu-74	4.88E-04	0	0	0	0	0	0	0	0	0
Cu-75	5.27E-04	0	0	0	0	0	0	0	0	0

Cu-76	3.45E-04	0	0	0	0	0	0	0	0	0
Cu-77	1.65E-04	0	0	0	0	0	0	0	0	0
Cu-78	3.95E-05	0	0	0	0	0	0	0	0	0
Cu-79	1.54E-06	0	0	0	0	0	0	0	0	0
Cu-80	6.38E-09	0	0	0	0	0	0	0	0	0
Zn-69	3.75E-05	9.49E-08	1.78E-12	0	0	0	0	0	0	0
Zn-69m	2.96E-07	8.84E-08	1.66E-12	0	0	0	0	0	0	0
Zn-71	2.09E-04	0	0	0	0	0	0	0	0	0
Zn-71m	3.25E-05	4.88E-07	0	0	0	0	0	0	0	0
Zn-72	5.11E-04	3.57E-04	1.43E-05	1.11E-08	0	0	0	0	0	0
Zn-73	1.28E-03	0	0	0	0	0	0	0	0	0
Zn-74	3.02E-03	0	0	0	0	0	0	0	0	0
Zn-75	5.84E-03	0	0	0	0	0	0	0	0	0
Zn-76	1.04E-02	0	0	0	0	0	0	0	0	0
Zn-77	1.38E-02	0	0	0	0	0	0	0	0	0
Zn-78	1.44E-02	0	0	0	0	0	0	0	0	0
Zn-79	8.19E-03	0	0	0	0	0	0	0	0	0
Zn-80	8.88E-04	0	0	0	0	0	0	0	0	0
Zn-81	2.45E-05	0	0	0	0	0	0	0	0	0
Zn-82	4.04E-06	0	0	0	0	0	0	0	0	0
Zn-83	4.70E-08	0	0	0	0	0	0	0	0	0
Ga-68	1.16E-08	0	0	0	0	0	0	0	0	0
Ga-70	4.79E-06	0	0	0	0	0	0	0	0	0
Ga-72	5.28E-04	4.50E-04	2.05E-05	1.60E-08	0	0	0	0	0	0
Ga-73	1.38E-03	4.50E-05	0	0	0	0	0	0	0	0
Ga-74	3.42E-03	0	0	0	0	0	0	0	0	0
Ga-74m	2.54E-04	0	0	0	0	0	0	0	0	0
Ga-75	8.64E-03	0	0	0	0	0	0	0	0	0
Ga-76	2.01E-02	0	0	0	0	0	0	0	0	0
Ga-77	4.31E-02	0	0	0	0	0	0	0	0	0
Ga-78	7.67E-02	0	0	0	0	0	0	0	0	0
Ga-79	8.95E-02	0	0	0	0	0	0	0	0	0
Ga-80	4.99E-02	0	0	0	0	0	0	0	0	0
Ga-81	3.46E-02	0	0	0	0	0	0	0	0	0
Ga-82	2.15E-02	0	0	0	0	0	0	0	0	0
Ga-83	7.57E-04	0	0	0	0	0	0	0	0	0
Ga-84	1.77E-02	0	0	0	0	0	0	0	0	0
Ga-85	7.72E-07	0	0	0	0	0	0	0	0	0
Ga-86	7.34E-06	0	0	0	0	0	0	0	0	0
Ge-69	7.35E-11	4.80E-11	1.04E-12	0	0	0	0	0	0	0
Ge-71	4.28E-08	4.02E-08	2.33E-08	6.93E-09	0	0	0	0	0	0
Ge-71m	1.33E-11	0	0	0	0	0	0	0	0	0
Ge-73m	9.70E-05	3.15E-06	0	0	0	0	0	0	0	0
Ge-75	8.88E-03	5.29E-08	0	0	0	0	0	0	0	0
Ge-75m	2.10E-04	0	0	0	0	0	0	0	0	0
Ge-77	5.45E-02	1.25E-02	2.20E-08	0	0	0	0	0	0	0
Ge-77m	1.99E-03	0	0	0	0	0	0	0	0	0
Ge-78	1.50E-01	1.77E-06	0	0	0	0	0	0	0	0
Ge-79	1.93E-01	0	0	0	0	0	0	0	0	0
Ge-79m	9.78E-02	0	0	0	0	0	0	0	0	0
Ge-80	6.35E-01	0	0	0	0	0	0	0	0	0
Ge-81	7.07E-01	0	0	0	0	0	0	0	0	0
Ge-82	5.97E-01	0	0	0	0	0	0	0	0	0
Ge-83	2.40E-01	0	0	0	0	0	0	0	0	0
Ge-84	8.74E-02	0	0	0	0	0	0	0	0	0
Ge-85	8.94E-03	0	0	0	0	0	0	0	0	0
Ge-86	3.78E-01	0	0	0	0	0	0	0	0	0
Ge-87	4.85E-03	0	0	0	0	0	0	0	0	0
Ge-88	1.46E+01	0	0	0	0	0	0	0	0	0

Ge-89	5.57E-03	0	0	0	0	0	0	0	0	0
As-72	5.99E-12	3.16E-12	0	0	0	0	0	0	0	0
As-73	1.99E-09	1.97E-09	1.82E-09	1.53E-09	8.51E-11	0	0	0	0	0
As-74	6.60E-07	6.34E-07	4.46E-07	2.05E-07	0	0	0	0	0	0
As-75m	7.76E-10	7.71E-10	7.32E-10	6.52E-10	9.39E-11	0	0	0	0	0
As-76	4.27E-03	2.27E-03	7.54E-06	2.35E-11	0	0	0	0	0	0
As-77	4.94E-02	4.16E-02	9.87E-04	1.88E-07	0	0	0	0	0	0
As-78	1.54E-01	2.58E-05	0	0	0	0	0	0	0	0
As-79	3.26E-01	0	0	0	0	0	0	0	0	0
As-80	8.01E-01	0	0	0	0	0	0	0	0	0
As-81	1.31E+00	0	0	0	0	0	0	0	0	0
As-82	1.31E+00	0	0	0	0	0	0	0	0	0
As-82m	3.42E-01	0	0	0	0	0	0	0	0	0
As-83	1.82E+00	0	0	0	0	0	0	0	0	0
As-84	8.71E-01	0	0	0	0	0	0	0	0	0
As-85	6.79E-01	0	0	0	0	0	0	0	0	0
As-86	2.20E+00	0	0	0	0	0	0	0	0	0
As-87	2.04E-01	0	0	0	0	0	0	0	0	0
As-88	1.36E-01	0	0	0	0	0	0	0	0	0
As-89	4.20E+01	0	0	0	0	0	0	0	0	0
As-90	7.22E-01	0	0	0	0	0	0	0	0	0
Se-75	1.20E-08	1.19E-08	1.13E-08	1.01E-08	1.45E-09	0	0	0	0	0
Se-77m	1.90E-04	1.38E-04	3.28E-06	6.23E-10	0	0	0	0	0	0
Se-79	1.19E-06	1.19E-06	1.19E-06	1.19E-06	1.19E-06	1.19E-06	1.19E-06	1.19E-06	1.17E-06	9.44E-07
Se-79m	3.07E-01	0	0	0	0	0	0	0	0	0
Se-81	1.43E+00	4.35E-09	0	0	0	0	0	0	0	0
Se-81m	1.09E-01	2.95E-09	0	0	0	0	0	0	0	0
Se-83	2.83E+00	0	0	0	0	0	0	0	0	0
Se-83m	2.64E-01	0	0	0	0	0	0	0	0	0
Se-84	4.94E+00	0	0	0	0	0	0	0	0	0
Se-85	5.75E+00	0	0	0	0	0	0	0	0	0
Se-86	6.31E+00	0	0	0	0	0	0	0	0	0
Se-87	3.58E+00	0	0	0	0	0	0	0	0	0
Se-88	1.50E+00	0	0	0	0	0	0	0	0	0
Se-89	1.82E-01	0	0	0	0	0	0	0	0	0
Se-90	3.50E-02	0	0	0	0	0	0	0	0	0
Se-91	2.46E-03	0	0	0	0	0	0	0	0	0
Se-94	1.19E-01	0	0	0	0	0	0	0	0	0
Br-77	1.37E-10	1.02E-10	7.39E-12	0	0	0	0	0	0	0
Br-77m	9.12E-11	0	0	0	0	0	0	0	0	0
Br-78	8.78E-08	0	0	0	0	0	0	0	0	0
Br-79m	6.79E-07	0	0	0	0	0	0	0	0	0
Br-80	8.55E-04	8.23E-07	0	0	0	0	0	0	0	0
Br-80m	3.31E-05	7.68E-07	0	0	0	0	0	0	0	0
Br-82	7.12E-01	4.46E-01	6.40E-03	5.14E-07	0	0	0	0	0	0
Br-82m	7.82E-01	0	0	0	0	0	0	0	0	0
Br-83	3.26E+00	3.70E-03	0	0	0	0	0	0	0	0
Br-84	5.37E+00	0	0	0	0	0	0	0	0	0
Br-84m	2.46E-01	0	0	0	0	0	0	0	0	0
Br-85	7.44E+00	0	0	0	0	0	0	0	0	0
Br-86	9.16E+00	0	0	0	0	0	0	0	0	0
Br-87	1.06E+01	0	0	0	0	0	0	0	0	0
Br-88	8.72E+00	0	0	0	0	0	0	0	0	0
Br-89	5.64E+00	0	0	0	0	0	0	0	0	0
Br-90	3.02E+00	0	0	0	0	0	0	0	0	0
Br-91	8.48E-01	0	0	0	0	0	0	0	0	0
Br-92	1.14E-01	0	0	0	0	0	0	0	0	0
Br-93	2.11E-02	0	0	0	0	0	0	0	0	0
Br-94	3.84E-03	0	0	0	0	0	0	0	0	0

Br-95	3.65E+00	0	0	0	0	0	0	0	0	0
Br-96	5.33E-01	0	0	0	0	0	0	0	0	0
Br-97	6.74E-03	0	0	0	0	0	0	0	0	0
Kr-79	6.58E-09	4.09E-09	5.71E-11	0	0	0	0	0	0	0
Kr-79m	3.48E-11	0	0	0	0	0	0	0	0	0
Kr-81	8.50E-12	8.50E-12	8.50E-12	8.50E-12	8.50E-12	8.50E-12	8.50E-12	8.48E-12	8.25E-12	6.28E-12
Kr-81m	5.64E-06	0	0	0	0	0	0	0	0	0
Kr-83m	3.19E+00	1.38E-02	1.18E-07	1.01E-07	6.81E-09	0	0	0	0	0
Kr-85	2.58E-01	2.58E-01	2.58E-01	2.57E-01	2.42E-01	1.36E-01	4.12E-04	0	0	0
Kr-85m	7.18E+00	1.77E-01	0	0	0	0	0	0	0	0
Kr-87	1.37E+01	2.88E-05	0	0	0	0	0	0	0	0
Kr-88	1.83E+01	5.24E-02	0	0	0	0	0	0	0	0
Kr-89	2.27E+01	0	0	0	0	0	0	0	0	0
Kr-90	2.33E+01	0	0	0	0	0	0	0	0	0
Kr-91	1.57E+01	0	0	0	0	0	0	0	0	0
Kr-92	7.70E+00	0	0	0	0	0	0	0	0	0
Kr-93	2.16E+00	0	0	0	0	0	0	0	0	0
Kr-94	3.50E-01	0	0	0	0	0	0	0	0	0
Kr-95	2.48E-02	0	0	0	0	0	0	0	0	0
Kr-96	6.92E-02	0	0	0	0	0	0	0	0	0
Kr-97	1.95E-03	0	0	0	0	0	0	0	0	0
Kr-98	1.31E-03	0	0	0	0	0	0	0	0	0
Kr-99	7.81E-07	0	0	0	0	0	0	0	0	0
Kr-100	8.17E-06	0	0	0	0	0	0	0	0	0
Rb-81	2.45E-11	0	0	0	0	0	0	0	0	0
Rb-83	1.72E-07	1.71E-07	1.59E-07	1.35E-07	9.16E-09	0	0	0	0	0
Rb-84	3.00E-04	2.94E-04	2.43E-04	1.59E-04	1.33E-07	0	0	0	0	0
Rb-86	1.41E-01	1.36E-01	9.75E-02	4.63E-02	1.80E-07	0	0	0	0	0
Rb-86m	5.76E-02	0	0	0	0	0	0	0	0	0
Rb-87	4.15E-10	4.15E-10	4.15E-10	4.15E-10	4.15E-10	4.15E-10	4.15E-10	4.15E-10	4.15E-10	4.15E-10
Rb-88	1.85E+01	5.82E-02	0	0	0	0	0	0	0	0
Rb-89	2.41E+01	0	0	0	0	0	0	0	0	0
Rb-90	2.45E+01	0	0	0	0	0	0	0	0	0
Rb-90m	4.87E+00	0	0	0	0	0	0	0	0	0
Rb-91	2.95E+01	0	0	0	0	0	0	0	0	0
Rb-92	2.62E+01	0	0	0	0	0	0	0	0	0
Rb-93	1.96E+01	0	0	0	0	0	0	0	0	0
Rb-94	9.78E+00	0	0	0	0	0	0	0	0	0
Rb-95	4.16E+00	0	0	0	0	0	0	0	0	0
Rb-96	8.51E-01	0	0	0	0	0	0	0	0	0
Rb-97	1.41E-01	0	0	0	0	0	0	0	0	0
Rb-98	1.42E-02	0	0	0	0	0	0	0	0	0
Rb-99	2.54E-04	0	0	0	0	0	0	0	0	0
Rb-100	3.23E-02	0	0	0	0	0	0	0	0	0
Rb-101	1.01E-06	0	0	0	0	0	0	0	0	0
Rb-102	4.70E-08	0	0	0	0	0	0	0	0	0
Sr-83	5.20E-11	3.11E-11	0	0	0	0	0	0	0	0
Sr-85	7.36E-07	7.28E-07	6.61E-07	5.34E-07	1.49E-08	0	0	0	0	0
Sr-85m	3.78E-08	0	0	0	0	0	0	0	0	0
Sr-87m	2.36E-03	6.42E-06	0	0	0	0	0	0	0	0
Sr-89	2.56E+01	2.52E+01	2.23E+01	1.69E+01	1.71E-01	0	0	0	0	0
Sr-90	1.55E+00	1.55E+00	1.54E+00	1.54E+00	1.51E+00	1.22E+00	1.39E-01	5.50E-11	0	0
Sr-91	3.17E+01	5.65E+00	1.00E-06	0	0	0	0	0	0	0
Sr-92	3.50E+01	6.74E-02	0	0	0	0	0	0	0	0
Sr-93	3.84E+01	0	0	0	0	0	0	0	0	0
Sr-94	3.81E+01	0	0	0	0	0	0	0	0	0
Sr-95	3.33E+01	0	0	0	0	0	0	0	0	0
Sr-96	2.19E+01	0	0	0	0	0	0	0	0	0
Sr-97	9.38E+00	0	0	0	0	0	0	0	0	0

Sr-98	4.33E+00	0	0	0	0	0	0	0	0	0
Sr-99	6.54E-01	0	0	0	0	0	0	0	0	0
Sr-100	1.67E-01	0	0	0	0	0	0	0	0	0
Sr-101	1.20E-02	0	0	0	0	0	0	0	0	0
Sr-102	3.81E-04	0	0	0	0	0	0	0	0	0
Sr-103	1.78E-05	0	0	0	0	0	0	0	0	0
Sr-104	6.61E-07	0	0	0	0	0	0	0	0	0
Sr-105	9.23E-08	0	0	0	0	0	0	0	0	0
Y-87	8.66E-09	7.03E-09	1.08E-09	1.67E-11	0	0	0	0	0	0
Y-88	3.79E-04	3.76E-04	3.55E-04	3.12E-04	3.53E-05	0	0	0	0	0
Y-89m	2.48E-03	2.43E-03	2.15E-03	1.63E-03	1.65E-05	0	0	0	0	0
Y-90	1.69E+00	1.66E+00	1.56E+00	1.54E+00	1.51E+00	1.22E+00	1.39E-01	5.50E-11	0	0
Y-90m	9.33E-04	5.07E-06	0	0	0	0	0	0	0	0
Y-91	3.35E+01	3.33E+01	3.00E+01	2.36E+01	4.47E-01	0	0	0	0	0
Y-91m	1.82E+01	3.54E+00	6.27E-07	0	0	0	0	0	0	0
Y-92	3.49E+01	1.06E+00	0	0	0	0	0	0	0	0
Y-93	3.95E+01	7.80E+00	3.20E-06	0	0	0	0	0	0	0
Y-93m	2.50E+00	0	0	0	0	0	0	0	0	0
Y-94	4.20E+01	0	0	0	0	0	0	0	0	0
Y-95	4.37E+01	0	0	0	0	0	0	0	0	0
Y-96	2.51E+01	0	0	0	0	0	0	0	0	0
Y-96m	1.65E+01	0	0	0	0	0	0	0	0	0
Y-97	2.32E+01	0	0	0	0	0	0	0	0	0
Y-97m	1.17E+01	0	0	0	0	0	0	0	0	0
Y-98	1.54E+01	0	0	0	0	0	0	0	0	0
Y-98m	9.48E+00	0	0	0	0	0	0	0	0	0
Y-99	1.49E+01	0	0	0	0	0	0	0	0	0
Y-100	4.48E+00	0	0	0	0	0	0	0	0	0
Y-101	1.54E+00	0	0	0	0	0	0	0	0	0
Y-102	7.31E-01	0	0	0	0	0	0	0	0	0
Y-103	2.20E-02	0	0	0	0	0	0	0	0	0
Y-104	2.35E-03	0	0	0	0	0	0	0	0	0
Y-105	8.20E-05	0	0	0	0	0	0	0	0	0
Y-106	1.17E-06	0	0	0	0	0	0	0	0	0
Y-107	3.40E-08	0	0	0	0	0	0	0	0	0
Y-108	6.39E-10	0	0	0	0	0	0	0	0	0
Zr-88	1.67E-11	1.65E-11	1.54E-11	1.30E-11	0	0	0	0	0	0
Zr-89	1.62E-04	1.31E-04	1.94E-05	2.78E-07	0	0	0	0	0	0
Zr-90m	9.91E-08	0	0	0	0	0	0	0	0	0
Zr-93	3.36E-05	3.36E-05	3.36E-05	3.36E-05	3.36E-05	3.36E-05	3.36E-05	3.36E-05	3.35E-05	3.22E-05
Zr-95	4.55E+01	4.51E+01	4.09E+01	3.29E+01	8.76E-01	0	0	0	0	0
Zr-97	4.69E+01	1.74E+01	2.27E-03	5.33E-12	0	0	0	0	0	0
Zr-98	4.54E+01	0	0	0	0	0	0	0	0	0
Zr-99	4.42E+01	0	0	0	0	0	0	0	0	0
Zr-100	4.40E+01	0	0	0	0	0	0	0	0	0
Zr-101	2.40E+01	0	0	0	0	0	0	0	0	0
Zr-102	1.46E+01	0	0	0	0	0	0	0	0	0
Zr-103	3.80E+00	0	0	0	0	0	0	0	0	0
Zr-104	8.43E-01	0	0	0	0	0	0	0	0	0
Zr-105	3.94E-01	0	0	0	0	0	0	0	0	0
Zr-106	7.50E-03	0	0	0	0	0	0	0	0	0
Zr-107	1.43E-04	0	0	0	0	0	0	0	0	0
Zr-108	1.38E-05	0	0	0	0	0	0	0	0	0
Zr-109	2.33E-06	0	0	0	0	0	0	0	0	0
Zr-110	6.78E-08	0	0	0	0	0	0	0	0	0
Nb-90	1.26E-12	0	0	0	0	0	0	0	0	0
Nb-93m	1.29E-06	1.29E-06	1.32E-06	1.40E-06	2.68E-06	1.29E-05	3.41E-05	3.45E-05	3.44E-05	3.30E-05
Nb-94	5.16E-09	5.16E-09	5.16E-09	5.16E-09	5.16E-09	5.16E-09	5.14E-09	4.99E-09	3.67E-09	1.70E-10
Nb-94m	2.40E-05	0	0	0	0	0	0	0	0	0

Nb-95	4.99E+01	4.98E+01	4.87E+01	4.47E+01	1.89E+00	0	0	0	0	0
Nb-95m	5.06E-01	5.03E-01	4.66E-01	3.77E-01	1.00E-02	0	0	0	0	0
Nb-96	1.75E+00	8.59E-01	1.41E-03	9.14E-10	0	0	0	0	0	0
Nb-97	4.72E+01	1.87E+01	2.45E-03	5.75E-12	0	0	0	0	0	0
Nb-97m	5.62E-02	0	0	0	0	0	0	0	0	0
Nb-98	4.63E+01	0	0	0	0	0	0	0	0	0
Nb-98m	2.97E-01	1.05E-09	0	0	0	0	0	0	0	0
Nb-99	4.57E+01	0	0	0	0	0	0	0	0	0
Nb-99m	4.89E+00	0	0	0	0	0	0	0	0	0
Nb-100	4.83E+01	0	0	0	0	0	0	0	0	0
Nb-100m	4.16E+00	0	0	0	0	0	0	0	0	0
Nb-101	4.54E+01	0	0	0	0	0	0	0	0	0
Nb-102	7.47E+00	0	0	0	0	0	0	0	0	0
Nb-102m	3.38E+01	0	0	0	0	0	0	0	0	0
Nb-103	2.26E+01	0	0	0	0	0	0	0	0	0
Nb-104	5.92E+00	0	0	0	0	0	0	0	0	0
Nb-104m	4.75E+00	0	0	0	0	0	0	0	0	0
Nb-105	4.36E+00	0	0	0	0	0	0	0	0	0
Nb-106	7.48E-01	0	0	0	0	0	0	0	0	0
Nb-107	1.39E-01	0	0	0	0	0	0	0	0	0
Nb-108	1.04E-02	0	0	0	0	0	0	0	0	0
Nb-109	2.93E-03	0	0	0	0	0	0	0	0	0
Nb-110	9.68E-05	0	0	0	0	0	0	0	0	0
Nb-111	1.56E-05	0	0	0	0	0	0	0	0	0
Nb-112	3.15E-07	0	0	0	0	0	0	0	0	0
Nb-113	8.17E-08	0	0	0	0	0	0	0	0	0
Mo-93	1.60E-09	1.60E-09	1.60E-09	1.60E-09	1.60E-09	1.60E-09	1.57E-09	1.34E-09	2.83E-10	0
Mo-93m	2.33E-11	2.05E-12	0	0	0	0	0	0	0	0
Mo-99	4.30E+01	3.34E+01	3.45E+00	2.22E-02	0	0	0	0	0	0
Mo-101	4.70E+01	0	0	0	0	0	0	0	0	0
Mo-102	4.45E+01	0	0	0	0	0	0	0	0	0
Mo-103	4.26E+01	0	0	0	0	0	0	0	0	0
Mo-104	3.49E+01	0	0	0	0	0	0	0	0	0
Mo-105	2.46E+01	0	0	0	0	0	0	0	0	0
Mo-106	1.43E+01	0	0	0	0	0	0	0	0	0
Mo-107	5.40E+00	0	0	0	0	0	0	0	0	0
Mo-108	1.71E+00	0	0	0	0	0	0	0	0	0
Mo-109	1.87E-01	0	0	0	0	0	0	0	0	0
Mo-110	1.15E-02	0	0	0	0	0	0	0	0	0
Mo-111	1.47E-03	0	0	0	0	0	0	0	0	0
Mo-112	3.96E-04	0	0	0	0	0	0	0	0	0
Mo-113	4.62E-05	0	0	0	0	0	0	0	0	0
Mo-114	3.99E-06	0	0	0	0	0	0	0	0	0
Mo-115	3.08E-07	0	0	0	0	0	0	0	0	0
Tc-95	3.42E-12	1.49E-12	0	0	0	0	0	0	0	0
Tc-97	1.27E-11	1.27E-11	1.27E-11	1.27E-11	1.27E-11	1.27E-11	1.27E-11	1.27E-11	1.26E-11	1.23E-11
Tc-97m	1.33E-08	1.32E-08	1.23E-08	1.05E-08	8.01E-10	0	0	0	0	0
Tc-98	1.04E-10	1.04E-10	1.04E-10	1.04E-10	1.04E-10	1.04E-10	1.03E-10	1.03E-10	1.03E-10	1.02E-10
Tc-99	2.44E-04	2.45E-04	2.46E-04	2.46E-04	2.46E-04	2.46E-04	2.46E-04	2.45E-04	2.38E-04	1.77E-04
Tc-99m	3.71E+01	3.21E+01	3.34E+00	2.15E-02	0	0	0	0	0	0
Tc-100	3.98E+01	0	0	0	0	0	0	0	0	0
Tc-101	4.70E+01	0	0	0	0	0	0	0	0	0
Tc-102	4.46E+01	0	0	0	0	0	0	0	0	0
Tc-102m	1.51E-01	0	0	0	0	0	0	0	0	0
Tc-103	4.38E+01	0	0	0	0	0	0	0	0	0
Tc-104	3.74E+01	0	0	0	0	0	0	0	0	0
Tc-105	3.13E+01	0	0	0	0	0	0	0	0	0
Tc-106	2.38E+01	0	0	0	0	0	0	0	0	0
Tc-107	1.53E+01	0	0	0	0	0	0	0	0	0

Tc-108	7.16E+00	0	0	0	0	0	0	0	0	0
Tc-109	2.94E+00	0	0	0	0	0	0	0	0	0
Tc-110	5.36E-01	0	0	0	0	0	0	0	0	0
Tc-111	7.62E-02	0	0	0	0	0	0	0	0	0
Tc-112	1.00E-02	0	0	0	0	0	0	0	0	0
Tc-113	1.77E-03	0	0	0	0	0	0	0	0	0
Tc-114	1.04E-03	0	0	0	0	0	0	0	0	0
Tc-115	4.03E-04	0	0	0	0	0	0	0	0	0
Tc-116	1.03E-05	0	0	0	0	0	0	0	0	0
Tc-117	5.70E-07	0	0	0	0	0	0	0	0	0
Tc-118	9.67E-08	0	0	0	0	0	0	0	0	0
Ru-97	1.93E-08	1.52E-08	1.77E-09	1.48E-11	0	0	0	0	0	0
Ru-103	4.12E+01	4.05E+01	3.45E+01	2.43E+01	6.55E-02	0	0	0	0	0
Ru-105	3.17E+01	7.71E-01	0	0	0	0	0	0	0	0
Ru-106	1.27E+01	1.27E+01	1.25E+01	1.21E+01	6.48E+00	1.46E-02	0	0	0	0
Ru-107	1.87E+01	0	0	0	0	0	0	0	0	0
Ru-108	1.29E+01	0	0	0	0	0	0	0	0	0
Ru-109	8.59E+00	0	0	0	0	0	0	0	0	0
Ru-110	3.91E+00	0	0	0	0	0	0	0	0	0
Ru-111	1.66E+00	0	0	0	0	0	0	0	0	0
Ru-112	5.91E-01	0	0	0	0	0	0	0	0	0
Ru-113	2.63E-01	0	0	0	0	0	0	0	0	0
Ru-114	8.66E-02	0	0	0	0	0	0	0	0	0
Ru-115	4.31E-02	0	0	0	0	0	0	0	0	0
Ru-116	6.01E-03	0	0	0	0	0	0	0	0	0
Ru-117	3.07E-04	0	0	0	0	0	0	0	0	0
Ru-118	1.18E-04	0	0	0	0	0	0	0	0	0
Ru-119	9.00E-06	0	0	0	0	0	0	0	0	0
Ru-120	1.32E-06	0	0	0	0	0	0	0	0	0
Rh-101	2.08E-06	2.08E-06	2.07E-06	2.04E-06	1.68E-06	2.55E-07	0	0	0	0
Rh-101m	1.62E-10	1.38E-10	3.28E-11	1.35E-12	0	0	0	0	0	0
Rh-102	2.22E-04	2.21E-04	2.15E-04	2.01E-04	6.54E-05	1.09E-09	0	0	0	0
Rh-102m	2.09E-09	2.09E-09	2.08E-09	2.05E-09	1.65E-09	1.92E-10	0	0	0	0
Rh-103m	4.07E+01	4.00E+01	3.41E+01	2.40E+01	6.47E-02	0	0	0	0	0
Rh-104	4.81E+01	0	0	0	0	0	0	0	0	0
Rh-104m	3.66E+00	0	0	0	0	0	0	0	0	0
Rh-105	2.56E+01	1.88E+01	2.75E-01	2.25E-05	0	0	0	0	0	0
Rh-105m	8.94E+00	2.18E-01	0	0	0	0	0	0	0	0
Rh-106	1.56E+01	1.25E+01	1.23E+01	1.19E+01	6.39E+00	1.44E-02	0	0	0	0
Rh-106m	5.01E-01	2.46E-04	0	0	0	0	0	0	0	0
Rh-107	1.90E+01	0	0	0	0	0	0	0	0	0
Rh-108	1.30E+01	0	0	0	0	0	0	0	0	0
Rh-108m	7.86E-02	0	0	0	0	0	0	0	0	0
Rh-109	8.82E+00	0	0	0	0	0	0	0	0	0
Rh-110	3.96E+00	0	0	0	0	0	0	0	0	0
Rh-110m	7.34E-02	0	0	0	0	0	0	0	0	0
Rh-111	1.93E+00	0	0	0	0	0	0	0	0	0
Rh-112	7.71E-01	0	0	0	0	0	0	0	0	0
Rh-113	5.39E-01	0	0	0	0	0	0	0	0	0
Rh-114	2.84E-01	0	0	0	0	0	0	0	0	0
Rh-115	1.22E-01	0	0	0	0	0	0	0	0	0
Rh-116	4.29E-02	0	0	0	0	0	0	0	0	0
Rh-117	1.08E-02	0	0	0	0	0	0	0	0	0
Rh-118	2.91E-03	0	0	0	0	0	0	0	0	0
Rh-119	1.60E-03	0	0	0	0	0	0	0	0	0
Rh-120	1.69E-04	0	0	0	0	0	0	0	0	0
Rh-121	3.44E-05	0	0	0	0	0	0	0	0	0
Rh-122	1.80E-01	0	0	0	0	0	0	0	0	0
Pd-101	1.59E-09	2.23E-10	0	0	0	0	0	0	0	0

Pd-103	1.26E-03	1.21E-03	8.38E-04	3.71E-04	4.30E-10	0	0	0	0	0
Pd-107	2.02E-06	2.02E-06	2.02E-06	2.02E-06	2.02E-06	2.02E-06	2.02E-06	2.02E-06	2.02E-06	2.00E-06
Pd-107m	4.20E-02	0	0	0	0	0	0	0	0	0
Pd-109	1.71E+01	5.09E+00	9.14E-05	0	0	0	0	0	0	0
Pd-109m	2.74E-01	0	0	0	0	0	0	0	0	0
Pd-111	1.93E+00	4.34E-04	0	0	0	0	0	0	0	0
Pd-111m	1.14E-02	5.52E-04	0	0	0	0	0	0	0	0
Pd-112	8.04E-01	3.64E-01	2.95E-04	3.97E-11	0	0	0	0	0	0
Pd-113	5.56E-01	0	0	0	0	0	0	0	0	0
Pd-114	3.54E-01	0	0	0	0	0	0	0	0	0
Pd-115	2.40E-01	0	0	0	0	0	0	0	0	0
Pd-116	2.17E-01	0	0	0	0	0	0	0	0	0
Pd-117	1.42E-01	0	0	0	0	0	0	0	0	0
Pd-118	6.01E-02	0	0	0	0	0	0	0	0	0
Pd-119	1.64E-02	0	0	0	0	0	0	0	0	0
Pd-120	1.20E-02	0	0	0	0	0	0	0	0	0
Pd-121	2.87E-03	0	0	0	0	0	0	0	0	0
Pd-122	1.75E-03	0	0	0	0	0	0	0	0	0
Pd-123	2.44E-04	0	0	0	0	0	0	0	0	0
Pd-124	9.15E-05	0	0	0	0	0	0	0	0	0
Ag-105	2.89E-12	2.85E-12	2.45E-12	1.75E-12	0	0	0	0	0	0
Ag-105m	7.02E-12	0	0	0	0	0	0	0	0	0
Ag-106	5.35E-10	0	0	0	0	0	0	0	0	0
Ag-106m	1.10E-10	1.01E-10	4.75E-11	8.90E-12	0	0	0	0	0	0
Ag-107m	1.16E-08	5.41E-10	0	0	0	0	0	0	0	0
Ag-108	2.18E-03	1.30E-11	1.30E-11	1.30E-11	1.30E-11	1.28E-11	1.10E-11	2.47E-12	0	0
Ag-108m	1.43E-10	1.43E-10	1.43E-10	1.43E-10	1.43E-10	1.41E-10	1.21E-10	2.73E-11	0	0
Ag-109m	1.69E+01	5.02E+00	9.82E-05	7.75E-06	4.69E-06	3.37E-08	0	0	0	0
Ag-110	1.45E+01	1.95E-03	1.90E-03	1.80E-03	7.09E-04	7.79E-08	0	0	0	0
Ag-110m	1.43E-01	1.43E-01	1.39E-01	1.32E-01	5.21E-02	5.72E-06	0	0	0	0
Ag-111	1.57E+00	1.43E+00	6.20E-01	9.64E-02	0	0	0	0	0	0
Ag-111m	1.88E+00	4.22E-04	0	0	0	0	0	0	0	0
Ag-112	8.06E-01	4.28E-01	3.47E-04	4.67E-11	0	0	0	0	0	0
Ag-113	3.66E-01	1.66E-02	0	0	0	0	0	0	0	0
Ag-113m	5.32E-01	0	0	0	0	0	0	0	0	0
Ag-114	3.57E-01	0	0	0	0	0	0	0	0	0
Ag-115	2.45E-01	0	0	0	0	0	0	0	0	0
Ag-115m	7.52E-03	0	0	0	0	0	0	0	0	0
Ag-116	1.74E-01	0	0	0	0	0	0	0	0	0
Ag-116m	7.17E-03	0	0	0	0	0	0	0	0	0
Ag-117	1.89E-01	0	0	0	0	0	0	0	0	0
Ag-117m	4.09E-02	0	0	0	0	0	0	0	0	0
Ag-118	1.36E-01	0	0	0	0	0	0	0	0	0
Ag-118m	5.04E-02	0	0	0	0	0	0	0	0	0
Ag-119	1.09E-01	0	0	0	0	0	0	0	0	0
Ag-120	4.02E-02	0	0	0	0	0	0	0	0	0
Ag-120m	2.23E-02	0	0	0	0	0	0	0	0	0
Ag-121	2.78E-02	0	0	0	0	0	0	0	0	0
Ag-122	4.90E-03	0	0	0	0	0	0	0	0	0
Ag-122m	1.43E-02	0	0	0	0	0	0	0	0	0
Ag-123	4.20E-03	0	0	0	0	0	0	0	0	0
Ag-124	1.74E-03	0	0	0	0	0	0	0	0	0
Ag-125	3.72E-04	0	0	0	0	0	0	0	0	0
Ag-126	1.23E-04	0	0	0	0	0	0	0	0	0
Ag-127	5.25E-06	0	0	0	0	0	0	0	0	0
Ag-128	7.33E-07	0	0	0	0	0	0	0	0	0
Ag-129	8.16E-08	0	0	0	0	0	0	0	0	0
Ag-130	7.19E-06	0	0	0	0	0	0	0	0	0
Cd-107	6.98E-09	5.40E-10	0	0	0	0	0	0	0	0

Cd-109	8.14E-06	8.13E-06	8.02E-06	7.78E-06	4.70E-06	3.38E-08	0	0	0	0
Cd-111m	7.22E-03	8.44E-12	0	0	0	0	0	0	0	0
Cd-113m	4.01E-04	4.01E-04	4.01E-04	4.00E-04	3.82E-04	2.46E-04	2.95E-06	0	0	0
Cd-115	2.24E-01	1.65E-01	1.01E-02	1.99E-05	0	0	0	0	0	0
Cd-115m	1.57E-02	1.55E-02	1.35E-02	9.86E-03	5.38E-05	0	0	0	0	0
Cd-117	2.29E-01	2.89E-04	0	0	0	0	0	0	0	0
Cd-117m	6.75E-03	4.78E-05	0	0	0	0	0	0	0	0
Cd-118	1.89E-01	4.55E-10	0	0	0	0	0	0	0	0
Cd-119	1.50E-01	0	0	0	0	0	0	0	0	0
Cd-119m	3.73E-02	0	0	0	0	0	0	0	0	0
Cd-120	1.74E-01	0	0	0	0	0	0	0	0	0
Cd-121	8.94E-02	0	0	0	0	0	0	0	0	0
Cd-121m	6.64E-02	0	0	0	0	0	0	0	0	0
Cd-122	1.29E-01	0	0	0	0	0	0	0	0	0
Cd-123	6.89E-02	0	0	0	0	0	0	0	0	0
Cd-123m	6.57E-04	0	0	0	0	0	0	0	0	0
Cd-124	5.14E-02	0	0	0	0	0	0	0	0	0
Cd-125	2.07E-02	0	0	0	0	0	0	0	0	0
Cd-126	2.65E-02	0	0	0	0	0	0	0	0	0
Cd-127	2.48E-02	0	0	0	0	0	0	0	0	0
Cd-128	1.01E-02	0	0	0	0	0	0	0	0	0
Cd-129	2.20E-04	0	0	0	0	0	0	0	0	0
Cd-130	2.07E-01	0	0	0	0	0	0	0	0	0
Cd-131	1.80E-02	0	0	0	0	0	0	0	0	0
Cd-132	5.41E-06	0	0	0	0	0	0	0	0	0
In-111	2.85E-09	2.22E-09	2.40E-10	1.72E-12	0	0	0	0	0	0
In-112	9.84E-08	0	0	0	0	0	0	0	0	0
In-112m	1.31E-10	0	0	0	0	0	0	0	0	0
In-113m	9.43E-09	9.27E-09	8.78E-09	7.78E-09	1.04E-09	0	0	0	0	0
In-114	6.98E-05	2.61E-05	2.30E-05	1.74E-05	1.59E-07	0	0	0	0	0
In-114m	2.73E-05	2.69E-05	2.37E-05	1.79E-05	1.65E-07	0	0	0	0	0
In-115m	2.22E-01	1.80E-01	1.10E-02	2.28E-05	5.72E-09	0	0	0	0	0
In-116	5.87E-01	0	0	0	0	0	0	0	0	0
In-116m	3.01E-10	0	0	0	0	0	0	0	0	0
In-117	1.42E-01	7.34E-04	0	0	0	0	0	0	0	0
In-117m	1.78E-01	8.96E-04	0	0	0	0	0	0	0	0
In-118	1.89E-01	4.56E-10	0	0	0	0	0	0	0	0
In-118m	1.21E-06	0	0	0	0	0	0	0	0	0
In-119	9.96E-02	0	0	0	0	0	0	0	0	0
In-119m	9.79E-02	0	0	0	0	0	0	0	0	0
In-120	1.79E-01	0	0	0	0	0	0	0	0	0
In-120m	4.64E-03	0	0	0	0	0	0	0	0	0
In-121	1.56E-01	0	0	0	0	0	0	0	0	0
In-121m	5.66E-02	0	0	0	0	0	0	0	0	0
In-122	1.62E-01	0	0	0	0	0	0	0	0	0
In-122m	3.38E-02	0	0	0	0	0	0	0	0	0
In-123	1.31E-01	0	0	0	0	0	0	0	0	0
In-123m	5.69E-02	0	0	0	0	0	0	0	0	0
In-124	1.29E-01	0	0	0	0	0	0	0	0	0
In-124m	7.94E-02	0	0	0	0	0	0	0	0	0
In-125	1.14E-01	0	0	0	0	0	0	0	0	0
In-125m	9.64E-02	0	0	0	0	0	0	0	0	0
In-126	1.05E-01	0	0	0	0	0	0	0	0	0
In-126m	7.87E-02	0	0	0	0	0	0	0	0	0
In-127	2.75E-01	0	0	0	0	0	0	0	0	0
In-127m	1.37E-01	0	0	0	0	0	0	0	0	0
In-128	1.82E-01	0	0	0	0	0	0	0	0	0
In-129	1.30E-01	0	0	0	0	0	0	0	0	0
In-129m	1.18E-01	0	0	0	0	0	0	0	0	0

In-130	3.37E-01	0	0	0	0	0	0	0	0	0
In-130m	4.80E-02	0	0	0	0	0	0	0	0	0
In-131	8.62E-02	0	0	0	0	0	0	0	0	0
In-131m	4.45E-02	0	0	0	0	0	0	0	0	0
In-132	2.46E-02	0	0	0	0	0	0	0	0	0
In-133	8.90E-04	0	0	0	0	0	0	0	0	0
In-134	2.42E-05	0	0	0	0	0	0	0	0	0
In-135	3.77E-07	0	0	0	0	0	0	0	0	0
Sn-113	9.32E-09	9.26E-09	8.78E-09	7.78E-09	1.03E-09	0	0	0	0	0
Sn-113m	1.35E-11	0	0	0	0	0	0	0	0	0
Sn-117m	4.92E-04	4.71E-04	2.99E-04	1.09E-04	5.12E-12	0	0	0	0	0
Sn-119m	2.00E-05	1.99E-05	1.95E-05	1.86E-05	8.42E-06	3.56E-09	0	0	0	0
Sn-121	1.97E-01	1.07E-01	5.98E-04	1.79E-04	1.76E-04	1.58E-04	5.07E-05	6.06E-10	0	0
Sn-121m	2.89E-04	2.89E-04	2.88E-04	2.88E-04	2.85E-04	2.54E-04	8.19E-05	9.79E-10	0	0
Sn-123	9.89E-02	9.83E-02	9.37E-02	8.42E-02	1.40E-02	3.10E-10	0	0	0	0
Sn-123m	1.39E-01	2.11E-12	0	0	0	0	0	0	0	0
Sn-125	3.05E-01	2.84E-01	1.49E-01	3.53E-02	1.22E-12	0	0	0	0	0
Sn-125m	2.27E-01	0	0	0	0	0	0	0	0	0
Sn-126	4.27E-06	4.27E-06	4.27E-06	4.27E-06	4.27E-06	4.27E-06	4.27E-06	4.26E-06	4.14E-06	3.16E-06
Sn-127	1.94E+00	7.04E-04	0	0	0	0	0	0	0	0
Sn-127m	5.47E-01	0	0	0	0	0	0	0	0	0
Sn-128	3.74E+00	1.72E-07	0	0	0	0	0	0	0	0
Sn-129	4.09E+00	0	0	0	0	0	0	0	0	0
Sn-129m	1.95E+00	0	0	0	0	0	0	0	0	0
Sn-130	4.82E+00	0	0	0	0	0	0	0	0	0
Sn-130m	4.35E+00	0	0	0	0	0	0	0	0	0
Sn-131	3.50E+00	0	0	0	0	0	0	0	0	0
Sn-131m	3.35E+00	0	0	0	0	0	0	0	0	0
Sn-132	4.49E+00	0	0	0	0	0	0	0	0	0
Sn-133	7.94E-01	0	0	0	0	0	0	0	0	0
Sn-134	9.78E-02	0	0	0	0	0	0	0	0	0
Sn-135	4.02E-03	0	0	0	0	0	0	0	0	0
Sn-136	9.16E-05	0	0	0	0	0	0	0	0	0
Sn-137	4.85E-05	0	0	0	0	0	0	0	0	0
Sb-117	8.08E-12	0	0	0	0	0	0	0	0	0
Sb-118	5.37E-11	0	0	0	0	0	0	0	0	0
Sb-118m	1.45E-10	5.19E-12	0	0	0	0	0	0	0	0
Sb-119	8.42E-07	5.45E-07	1.08E-08	1.78E-12	0	0	0	0	0	0
Sb-120	1.17E-04	0	0	0	0	0	0	0	0	0
Sb-120m	8.54E-08	7.57E-08	2.56E-08	2.31E-09	0	0	0	0	0	0
Sb-122	8.16E-02	6.33E-02	6.40E-03	3.95E-05	0	0	0	0	0	0
Sb-122m	2.99E+03	0	0	0	0	0	0	0	0	0
Sb-124	3.12E-02	3.09E-02	2.79E-02	2.21E-02	4.67E-04	0	0	0	0	0
Sb-124m	3.22E-03	0	0	0	0	0	0	0	0	0
Sb-125	1.68E-01	1.68E-01	1.68E-01	1.67E-01	1.33E-01	1.38E-02	2.12E-12	0	0	0
Sb-126	8.01E-02	7.57E-02	4.57E-02	1.49E-02	5.98E-07	5.98E-07	5.98E-07	5.96E-07	5.80E-07	4.42E-07
Sb-126m	6.74E-05	0	0	0	0	0	0	0	0	0
Sb-127	2.16E+00	1.84E+00	3.64E-01	9.94E-03	0	0	0	0	0	0
Sb-128	4.00E+00	7.04E-01	4.27E-08	0	0	0	0	0	0	0
Sb-128m	2.40E-01	0	0	0	0	0	0	0	0	0
Sb-129	7.79E+00	1.80E-01	0	0	0	0	0	0	0	0
Sb-130	7.69E+00	8.41E-11	0	0	0	0	0	0	0	0
Sb-130m	8.17E+00	0	0	0	0	0	0	0	0	0
Sb-131	2.14E+01	0	0	0	0	0	0	0	0	0
Sb-132	1.73E+01	0	0	0	0	0	0	0	0	0
Sb-132m	6.39E+00	0	0	0	0	0	0	0	0	0
Sb-133	1.74E+01	0	0	0	0	0	0	0	0	0
Sb-134	2.54E+00	0	0	0	0	0	0	0	0	0
Sb-134m	2.66E+00	0	0	0	0	0	0	0	0	0

Sb-135	1.02E+00	0	0	0	0	0	0	0	0	0
Sb-136	8.88E-02	0	0	0	0	0	0	0	0	0
Sb-137	8.55E-02	0	0	0	0	0	0	0	0	0
Sb-138	1.55E-04	0	0	0	0	0	0	0	0	0
Sb-139	2.07E-05	0	0	0	0	0	0	0	0	0
Te-121	1.27E-06	1.23E-06	8.86E-07	4.30E-07	1.32E-10	0	0	0	0	0
Te-121m	6.21E-10	6.18E-10	5.94E-10	5.43E-10	1.20E-10	0	0	0	0	0
Te-123m	6.51E-04	6.47E-04	6.14E-04	5.47E-04	7.79E-05	0	0	0	0	0
Te-125m	3.44E-02	3.45E-02	3.49E-02	3.57E-02	3.25E-02	3.40E-03	0	0	0	0
Te-127	2.03E+00	1.92E+00	4.23E-01	4.43E-02	4.01E-03	3.40E-12	0	0	0	0
Te-127m	3.87E-02	3.91E-02	3.95E-02	3.54E-02	4.21E-03	3.56E-12	0	0	0	0
Te-129	7.74E+00	2.44E-01	1.36E-03	8.99E-04	8.96E-07	0	0	0	0	0
Te-129m	2.65E-03	2.59E-03	2.15E-03	1.42E-03	1.42E-06	0	0	0	0	0
Te-131	2.42E+01	4.96E-01	3.37E-03	5.14E-08	0	0	0	0	0	0
Te-131m	3.46E+00	1.99E+00	1.35E-02	2.06E-07	0	0	0	0	0	0
Te-132	3.22E+01	2.59E+01	3.70E+00	4.89E-02	0	0	0	0	0	0
Te-133	3.20E+01	8.17E-08	0	0	0	0	0	0	0	0
Te-133m	2.41E+01	3.61E-07	0	0	0	0	0	0	0	0
Te-134	4.99E+01	2.12E-09	0	0	0	0	0	0	0	0
Te-135	2.47E+01	0	0	0	0	0	0	0	0	0
Te-136	8.87E+00	0	0	0	0	0	0	0	0	0
Te-137	2.69E+00	0	0	0	0	0	0	0	0	0
Te-138	4.12E-01	0	0	0	0	0	0	0	0	0
Te-139	9.70E-03	0	0	0	0	0	0	0	0	0
I-123	4.36E-10	1.24E-10	0	0	0	0	0	0	0	0
I-125	6.74E-06	6.66E-06	6.00E-06	4.75E-06	9.52E-08	0	0	0	0	0
I-126	2.50E-04	2.37E-04	1.46E-04	5.01E-05	0	0	0	0	0	0
I-128	2.20E+00	0	0	0	0	0	0	0	0	0
I-129	4.84E-07	4.85E-07	4.85E-07	4.85E-07	4.85E-07	4.85E-07	4.85E-07	4.85E-07	4.84E-07	4.82E-07
I-130	9.05E-01	2.37E-01	1.30E-06	0	0	0	0	0	0	0
I-130m	5.85E-01	0	0	0	0	0	0	0	0	0
I-131	2.19E+01	2.04E+01	9.57E+00	1.70E+00	0	0	0	0	0	0
I-132	3.31E+01	2.67E+01	3.81E+00	5.04E-02	0	0	0	0	0	0
I-132m	5.43E-01	3.35E-06	0	0	0	0	0	0	0	0
I-133	5.52E+01	2.55E+01	1.90E-02	2.15E-09	0	0	0	0	0	0
I-133m	2.23E+00	0	0	0	0	0	0	0	0	0
I-134	6.33E+01	1.42E-06	0	0	0	0	0	0	0	0
I-134m	6.11E+00	0	0	0	0	0	0	0	0	0
I-135	5.36E+01	4.26E+00	5.40E-10	0	0	0	0	0	0	0
I-136	2.05E+01	0	0	0	0	0	0	0	0	0
I-136m	1.26E+01	0	0	0	0	0	0	0	0	0
I-137	2.44E+01	0	0	0	0	0	0	0	0	0
I-138	1.25E+01	0	0	0	0	0	0	0	0	0
I-139	4.97E+00	0	0	0	0	0	0	0	0	0
I-140	9.71E-01	0	0	0	0	0	0	0	0	0
I-141	1.88E-01	0	0	0	0	0	0	0	0	0
I-142	2.66E-02	0	0	0	0	0	0	0	0	0
I-143	8.11E-04	0	0	0	0	0	0	0	0	0
I-144	9.46E+00	0	0	0	0	0	0	0	0	0
Xe-125	1.16E-09	4.32E-10	0	0	0	0	0	0	0	0
Xe-125m	4.97E-12	0	0	0	0	0	0	0	0	0
Xe-127	8.48E-06	8.32E-06	7.01E-06	4.79E-06	8.13E-09	0	0	0	0	0
Xe-127m	1.91E-07	0	0	0	0	0	0	0	0	0
Xe-129m	8.90E-04	8.23E-04	4.08E-04	8.56E-05	0	0	0	0	0	0
Xe-131m	3.05E-01	3.02E-01	2.45E-01	1.07E-01	4.54E-10	0	0	0	0	0
Xe-133	4.36E+01	4.31E+01	1.48E+01	1.05E+00	0	0	0	0	0	0
Xe-133m	8.29E-01	7.11E-01	5.11E-02	9.13E-05	0	0	0	0	0	0
Xe-134m	7.12E-01	0	0	0	0	0	0	0	0	0
Xe-135	1.06E+01	1.31E+01	1.85E-06	0	0	0	0	0	0	0

Xe-135m	8.69E+00	4.38E-01	5.55E-11	0	0	0	0	0	0	0
Xe-137	5.08E+01	0	0	0	0	0	0	0	0	0
Xe-138	4.82E+01	0	0	0	0	0	0	0	0	0
Xe-139	3.50E+01	0	0	0	0	0	0	0	0	0
Xe-140	2.28E+01	0	0	0	0	0	0	0	0	0
Xe-141	7.84E+00	0	0	0	0	0	0	0	0	0
Xe-142	2.73E+00	0	0	0	0	0	0	0	0	0
Xe-143	3.32E-01	0	0	0	0	0	0	0	0	0
Xe-144	1.26E-02	0	0	0	0	0	0	0	0	0
Xe-145	1.30E-03	0	0	0	0	0	0	0	0	0
Xe-146	7.40E-05	0	0	0	0	0	0	0	0	0
Xe-147	8.28E-06	0	0	0	0	0	0	0	0	0
Cs-129	8.33E-11	4.96E-11	0	0	0	0	0	0	0	0
Cs-131	1.30E-03	1.21E-03	6.35E-04	1.52E-04	0	0	0	0	0	0
Cs-132	1.21E-02	1.09E-02	4.17E-03	4.90E-04	0	0	0	0	0	0
Cs-134	5.78E+00	5.77E+00	5.72E+00	5.62E+00	4.13E+00	2.02E-01	0	0	0	0
Cs-134m	4.74E+00	1.56E-02	0	0	0	0	0	0	0	0
Cs-135	5.41E-06	5.43E-06	5.44E-06	5.44E-06	5.44E-06	5.44E-06	5.44E-06	5.43E-06	5.42E-06	5.27E-06
Cs-135m	3.87E-02	2.56E-10	0	0	0	0	0	0	0	0
Cs-136	1.38E+00	1.31E+00	8.13E-01	2.83E-01	6.16E-09	0	0	0	0	0
Cs-136m	2.06E-01	0	0	0	0	0	0	0	0	0
Cs-137	2.10E+00	2.10E+00	2.10E+00	2.09E+00	2.05E+00	1.67E+00	2.10E-01	2.08E-10	0	0
Cs-138	5.28E+01	9.35E-12	0	0	0	0	0	0	0	0
Cs-138m	3.11E+00	0	0	0	0	0	0	0	0	0
Cs-139	4.91E+01	0	0	0	0	0	0	0	0	0
Cs-140	4.10E+01	0	0	0	0	0	0	0	0	0
Cs-141	3.18E+01	0	0	0	0	0	0	0	0	0
Cs-142	1.86E+01	0	0	0	0	0	0	0	0	0
Cs-143	9.52E+00	0	0	0	0	0	0	0	0	0
Cs-144	2.79E+00	0	0	0	0	0	0	0	0	0
Cs-145	5.13E-01	0	0	0	0	0	0	0	0	0
Cs-146	5.47E-02	0	0	0	0	0	0	0	0	0
Cs-147	1.04E-02	0	0	0	0	0	0	0	0	0
Cs-148	1.63E-04	0	0	0	0	0	0	0	0	0
Cs-149	8.06E-06	0	0	0	0	0	0	0	0	0
Cs-150	2.02E-07	0	0	0	0	0	0	0	0	0
Cs-151	4.43E-08	0	0	0	0	0	0	0	0	0
Ba-131	2.88E-10	2.71E-10	1.58E-10	4.72E-11	0	0	0	0	0	0
Ba-133	9.09E-07	9.08E-07	9.07E-07	9.04E-07	8.51E-07	4.70E-07	1.25E-09	0	0	0
Ba-133m	1.28E-07	8.35E-08	1.78E-09	0	0	0	0	0	0	0
Ba-135m	3.39E-02	1.90E-02	1.03E-04	9.51E-10	0	0	0	0	0	0
Ba-136m	1.53E-01	1.45E-01	9.03E-02	3.15E-02	6.84E-10	0	0	0	0	0
Ba-137m	1.99E+00	1.98E+00	1.98E+00	1.98E+00	1.94E+00	1.57E+00	1.98E-01	1.96E-10	0	0
Ba-139	5.03E+01	3.43E-04	0	0	0	0	0	0	0	0
Ba-140	4.03E+01	3.82E+01	2.34E+01	7.89E+00	9.74E-08	0	0	0	0	0
Ba-141	4.47E+01	0	0	0	0	0	0	0	0	0
Ba-142	4.24E+01	0	0	0	0	0	0	0	0	0
Ba-143	3.76E+01	0	0	0	0	0	0	0	0	0
Ba-144	2.82E+01	0	0	0	0	0	0	0	0	0
Ba-145	1.22E+01	0	0	0	0	0	0	0	0	0
Ba-146	5.26E+00	0	0	0	0	0	0	0	0	0
Ba-147	1.29E+00	0	0	0	0	0	0	0	0	0
Ba-148	1.45E-01	0	0	0	0	0	0	0	0	0
Ba-149	1.03E-02	0	0	0	0	0	0	0	0	0
Ba-150	6.63E-04	0	0	0	0	0	0	0	0	0
Ba-151	3.45E+01	0	0	0	0	0	0	0	0	0
Ba-152	1.41E-01	0	0	0	0	0	0	0	0	0
La-133	3.59E-12	0	0	0	0	0	0	0	0	0
La-135	5.21E-09	2.22E-09	1.03E-12	0	0	0	0	0	0	0

La-136	4.75E-09	0	0	0	0	0	0	0	0	0
La-137	7.53E-10	7.53E-10	7.53E-10	7.53E-10	7.53E-10	7.53E-10	7.52E-10	7.44E-10	6.71E-10	2.37E-10
La-140	4.34E+01	4.19E+01	2.69E+01	9.08E+00	1.12E-07	0	0	0	0	0
La-141	4.51E+01	7.02E-01	0	0	0	0	0	0	0	0
La-142	4.38E+01	8.61E-04	0	0	0	0	0	0	0	0
La-143	4.20E+01	0	0	0	0	0	0	0	0	0
La-144	3.73E+01	0	0	0	0	0	0	0	0	0
La-145	2.65E+01	0	0	0	0	0	0	0	0	0
La-146	1.13E+01	0	0	0	0	0	0	0	0	0
La-146m	5.72E+00	0	0	0	0	0	0	0	0	0
La-147	7.36E+00	0	0	0	0	0	0	0	0	0
La-148	2.62E+00	0	0	0	0	0	0	0	0	0
La-149	7.17E-01	0	0	0	0	0	0	0	0	0
La-150	1.04E-01	0	0	0	0	0	0	0	0	0
La-151	4.07E+04	0	0	0	0	0	0	0	0	0
La-152	1.91E-03	0	0	0	0	0	0	0	0	0
La-153	9.76E-05	0	0	0	0	0	0	0	0	0
La-154	9.12E-07	0	0	0	0	0	0	0	0	0
La-155	2.54E-08	0	0	0	0	0	0	0	0	0
Ce-137	2.61E-07	4.11E-08	0	0	0	0	0	0	0	0
Ce-139	9.36E-04	9.31E-04	8.90E-04	8.05E-04	1.49E-04	9.74E-12	0	0	0	0
Ce-139m	8.73E-07	1.68E-11	0	0	0	0	0	0	0	0
Ce-141	4.18E+01	4.11E+01	3.40E+01	2.22E+01	1.75E-02	0	0	0	0	0
Ce-143	3.98E+01	2.42E+01	2.61E-01	1.10E-05	0	0	0	0	0	0
Ce-144	3.30E+01	3.30E+01	3.22E+01	3.07E+01	1.36E+01	4.60E-03	0	0	0	0
Ce-145	2.85E+01	0	0	0	0	0	0	0	0	0
Ce-146	2.26E+01	0	0	0	0	0	0	0	0	0
Ce-147	1.60E+01	0	0	0	0	0	0	0	0	0
Ce-148	1.14E+01	0	0	0	0	0	0	0	0	0
Ce-149	6.44E+00	0	0	0	0	0	0	0	0	0
Ce-150	3.37E+00	0	0	0	0	0	0	0	0	0
Ce-151	5.41E-01	0	0	0	0	0	0	0	0	0
Ce-152	2.33E-01	0	0	0	0	0	0	0	0	0
Ce-153	3.14E+05	0	0	0	0	0	0	0	0	0
Ce-154	2.43E+04	0	0	0	0	0	0	0	0	0
Ce-155	3.11E+02	0	0	0	0	0	0	0	0	0
Pr-139	5.76E-06	1.33E-07	0	0	0	0	0	0	0	0
Pr-140	3.24E-02	8.59E-06	1.35E-06	2.21E-08	0	0	0	0	0	0
Pr-142	3.94E+00	1.66E+00	6.59E-04	1.83E-11	0	0	0	0	0	0
Pr-142m	1.41E+00	0	0	0	0	0	0	0	0	0
Pr-143	3.59E+01	3.57E+01	2.42E+01	8.74E+00	3.24E-07	0	0	0	0	0
Pr-144	3.35E+01	3.30E+01	3.22E+01	3.07E+01	1.36E+01	4.60E-03	0	0	0	0
Pr-144m	9.51E-01	3.14E-01	3.07E-01	2.92E-01	1.29E-01	4.38E-05	0	0	0	0
Pr-145	2.86E+01	1.79E+00	2.44E-11	0	0	0	0	0	0	0
Pr-146	2.27E+01	0	0	0	0	0	0	0	0	0
Pr-147	1.78E+01	0	0	0	0	0	0	0	0	0
Pr-148	1.28E+01	0	0	0	0	0	0	0	0	0
Pr-148m	1.11E+00	0	0	0	0	0	0	0	0	0
Pr-149	9.72E+00	0	0	0	0	0	0	0	0	0
Pr-150	6.43E+00	0	0	0	0	0	0	0	0	0
Pr-151	3.78E+00	0	0	0	0	0	0	0	0	0
Pr-152	1.72E+00	0	0	0	0	0	0	0	0	0
Pr-153	6.26E-01	0	0	0	0	0	0	0	0	0
Pr-154	1.53E-01	0	0	0	0	0	0	0	0	0
Pr-155	1.62E-02	0	0	0	0	0	0	0	0	0
Pr-156	6.78E-03	0	0	0	0	0	0	0	0	0
Pr-157	3.88E-04	0	0	0	0	0	0	0	0	0
Pr-158	2.36E-05	0	0	0	0	0	0	0	0	0
Pr-159	3.67E-07	0	0	0	0	0	0	0	0	0

Nd-140	1.05E-05	8.59E-06	1.35E-06	2.20E-08	0	0	0	0	0	0
Nd-141	7.53E-04	9.45E-07	0	0	0	0	0	0	0	0
Nd-147	1.43E+01	1.34E+01	7.61E+00	2.15E+00	1.41E-09	0	0	0	0	0
Nd-149	1.05E+01	7.04E-04	0	0	0	0	0	0	0	0
Nd-151	5.45E+00	0	0	0	0	0	0	0	0	0
Nd-152	3.76E+00	0	0	0	0	0	0	0	0	0
Nd-153	2.24E+00	0	0	0	0	0	0	0	0	0
Nd-154	1.23E+00	0	0	0	0	0	0	0	0	0
Nd-155	4.75E-01	0	0	0	0	0	0	0	0	0
Nd-156	1.83E-01	0	0	0	0	0	0	0	0	0
Nd-157	7.23E-02	0	0	0	0	0	0	0	0	0
Nd-158	1.26E-02	0	0	0	0	0	0	0	0	0
Nd-159	1.02E-03	0	0	0	0	0	0	0	0	0
Nd-160	2.34E-05	0	0	0	0	0	0	0	0	0
Nd-161	1.00E-06	0	0	0	0	0	0	0	0	0
Pm-144	2.43E-11	2.42E-11	2.38E-11	2.29E-11	1.21E-11	0	0	0	0	0
Pm-145	1.42E-06	1.42E-06	1.42E-06	1.42E-06	1.41E-06	1.02E-06	3.01E-08	0	0	0
Pm-146	2.81E-05	2.81E-05	2.81E-05	2.79E-05	2.48E-05	8.04E-06	1.02E-10	0	0	0
Pm-147	3.13E+00	3.14E+00	3.18E+00	3.20E+00	2.53E+00	2.35E-01	1.12E-11	0	0	0
Pm-148	9.25E+00	8.14E+00	2.57E+00	2.23E-01	1.15E-04	0	0	0	0	0
Pm-149	1.60E+01	1.20E+01	7.13E-01	1.35E-03	0	0	0	0	0	0
Pm-150	5.92E-01	1.19E-03	0	0	0	0	0	0	0	0
Pm-151	5.29E+00	2.97E+00	1.52E-02	1.24E-07	0	0	0	0	0	0
Pm-152	3.86E+00	0	0	0	0	0	0	0	0	0
Pm-152m	8.14E-02	0	0	0	0	0	0	0	0	0
Pm-153	2.53E+00	0	0	0	0	0	0	0	0	0
Pm-154	1.44E+00	0	0	0	0	0	0	0	0	0
Pm-154m	2.07E-01	0	0	0	0	0	0	0	0	0
Pm-155	9.41E-01	0	0	0	0	0	0	0	0	0
Pm-156	5.38E-01	0	0	0	0	0	0	0	0	0
Pm-157	2.63E-01	0	0	0	0	0	0	0	0	0
Pm-158	9.36E-02	0	0	0	0	0	0	0	0	0
Pm-159	2.20E-02	0	0	0	0	0	0	0	0	0
Pm-160	9.48E-03	0	0	0	0	0	0	0	0	0
Pm-161	2.36E-04	0	0	0	0	0	0	0	0	0
Pm-162	1.78E-06	0	0	0	0	0	0	0	0	0
Pm-163	6.61E-08	0	0	0	0	0	0	0	0	0
Sm-145	1.59E-06	1.58E-06	1.55E-06	1.49E-06	7.53E-07	9.30E-10	0	0	0	0
Sm-146	0	0	0	0	0	1.01E-12	1.23E-12	1.23E-12	1.23E-12	1.23E-12
Sm-147	1.76E-11	1.77E-11	1.82E-11	1.93E-11	3.65E-11	9.33E-11	9.91E-11	9.91E-11	9.91E-11	9.91E-11
Sm-151	8.00E-03	8.09E-03	8.19E-03	8.19E-03	8.13E-03	7.59E-03	3.80E-03	3.72E-06	0	0
Sm-153	2.62E+01	1.83E+01	7.21E-01	5.45E-04	0	0	0	0	0	0
Sm-155	1.60E+00	0	0	0	0	0	0	0	0	0
Sm-156	7.23E-01	1.23E-01	1.49E-08	0	0	0	0	0	0	0
Sm-157	4.58E-01	0	0	0	0	0	0	0	0	0
Sm-158	2.64E-01	0	0	0	0	0	0	0	0	0
Sm-159	1.12E-01	0	0	0	0	0	0	0	0	0
Sm-160	3.76E-02	0	0	0	0	0	0	0	0	0
Sm-161	9.26E-03	0	0	0	0	0	0	0	0	0
Sm-162	3.59E-04	0	0	0	0	0	0	0	0	0
Sm-163	2.73E-05	0	0	0	0	0	0	0	0	0
Sm-164	8.06E-07	0	0	0	0	0	0	0	0	0
Sm-165	3.57E-08	0	0	0	0	0	0	0	0	0
Eu-149	1.98E-09	1.97E-09	1.84E-09	1.59E-09	1.31E-10	0	0	0	0	0
Eu-150	1.16E-10	1.16E-10	1.16E-10	1.16E-10	1.14E-10	9.64E-11	1.78E-11	0	0	0
Eu-152	4.16E-05	4.16E-05	4.15E-05	4.14E-05	3.95E-05	2.49E-05	2.49E-07	0	0	0
Eu-152m	3.33E-08	1.02E-12	0	0	0	0	0	0	0	0
Eu-154	1.50E-01	1.50E-01	1.50E-01	1.49E-01	1.39E-01	6.72E-02	4.75E-05	0	0	0
Eu-154m	2.31E-01	1.00E-10	0	0	0	0	0	0	0	0

Eu-155	9.13E-02	9.13E-02	9.10E-02	9.02E-02	7.89E-02	2.13E-02	4.28E-08	0	0	0
Eu-156	9.50E+00	9.09E+00	6.03E+00	2.42E+00	5.56E-07	0	0	0	0	0
Eu-157	4.89E+00	1.64E+00	8.52E-05	0	0	0	0	0	0	0
Eu-158	2.86E-01	1.15E-10	0	0	0	0	0	0	0	0
Eu-159	1.42E-01	0	0	0	0	0	0	0	0	0
Eu-160	6.08E-02	0	0	0	0	0	0	0	0	0
Eu-161	2.46E-02	0	0	0	0	0	0	0	0	0
Eu-162	3.76E-03	0	0	0	0	0	0	0	0	0
Eu-163	6.81E-04	0	0	0	0	0	0	0	0	0
Eu-164	5.23E-05	0	0	0	0	0	0	0	0	0
Eu-165	6.05E-06	0	0	0	0	0	0	0	0	0
Eu-166	3.60E-07	0	0	0	0	0	0	0	0	0
Eu-167	2.31E-01	0	0	0	0	0	0	0	0	0
Gd-151	8.41E-11	8.36E-11	7.95E-11	7.11E-11	1.09E-11	0	0	0	0	0
Gd-153	8.91E-07	8.89E-07	8.66E-07	8.17E-07	3.11E-07	2.40E-11	0	0	0	0
Gd-159	4.92E-01	2.01E-01	6.08E-05	0	0	0	0	0	0	0
Gd-161	3.00E-02	0	0	0	0	0	0	0	0	0
Gd-162	8.27E-03	0	0	0	0	0	0	0	0	0
Gd-163	3.25E-03	0	0	0	0	0	0	0	0	0
Gd-164	1.02E-03	0	0	0	0	0	0	0	0	0
Gd-165	2.62E-04	0	0	0	0	0	0	0	0	0
Gd-166	9.73E-05	0	0	0	0	0	0	0	0	0
Gd-167	1.23E+02	0	0	0	0	0	0	0	0	0
Gd-168	4.15E+00	0	0	0	0	0	0	0	0	0
Gd-169	2.15E+00	0	0	0	0	0	0	0	0	0
Tb-153	1.62E-12	1.20E-12	0	0	0	0	0	0	0	0
Tb-155	4.21E-10	3.70E-10	1.14E-10	8.45E-12	0	0	0	0	0	0
Tb-156	6.29E-09	5.58E-09	1.77E-09	1.32E-10	0	0	0	0	0	0
Tb-156m	7.05E-10	3.57E-10	0	0	0	0	0	0	0	0
Tb-157	3.71E-09	3.71E-09	3.70E-09	3.70E-09	3.67E-09	3.36E-09	1.40E-09	0	0	0
Tb-158	9.65E-09	9.65E-09	9.65E-09	9.64E-09	9.61E-09	9.28E-09	6.56E-09	2.06E-10	0	0
Tb-158m	4.70E-08	0	0	0	0	0	0	0	0	0
Tb-160	3.04E-02	3.01E-02	2.77E-02	2.28E-02	9.20E-04	0	0	0	0	0
Tb-161	4.44E-02	4.02E-02	1.63E-02	2.19E-03	0	0	0	0	0	0
Tb-162	8.51E-03	0	0	0	0	0	0	0	0	0
Tb-163	3.66E-03	0	0	0	0	0	0	0	0	0
Tb-164	1.34E-03	0	0	0	0	0	0	0	0	0
Tb-165	5.28E-04	0	0	0	0	0	0	0	0	0
Tb-166	1.77E-04	0	0	0	0	0	0	0	0	0
Tb-167	4.26E-05	0	0	0	0	0	0	0	0	0
Tb-168	1.84E-05	0	0	0	0	0	0	0	0	0
Tb-169	1.76E-06	0	0	0	0	0	0	0	0	0
Tb-170	2.63E-06	0	0	0	0	0	0	0	0	0
Tb-171	5.25E-08	0	0	0	0	0	0	0	0	0
Dy-157	9.79E-11	1.27E-11	0	0	0	0	0	0	0	0
Dy-159	1.19E-07	1.18E-07	1.13E-07	1.03E-07	2.06E-08	0	0	0	0	0
Dy-165	1.32E-02	1.07E-05	0	0	0	0	0	0	0	0
Dy-165m	8.43E-03	0	0	0	0	0	0	0	0	0
Dy-166	2.27E-04	1.85E-04	2.95E-05	5.00E-07	0	0	0	0	0	0
Dy-167	7.22E-05	0	0	0	0	0	0	0	0	0
Dy-168	3.90E-05	0	0	0	0	0	0	0	0	0
Dy-169	1.47E-05	0	0	0	0	0	0	0	0	0
Dy-171	4.21E+01	0	0	0	0	0	0	0	0	0
Dy-172	8.98E+00	0	0	0	0	0	0	0	0	0
Ho-159	8.72E-12	0	0	0	0	0	0	0	0	0
Ho-161	8.02E-10	0	0	0	0	0	0	0	0	0
Ho-161m	5.58E-11	0	0	0	0	0	0	0	0	0
Ho-162	2.85E-09	0	0	0	0	0	0	0	0	0
Ho-162m	3.35E-09	0	0	0	0	0	0	0	0	0

Ho-163	2.47E-12	2.47E-12	2.47E-12	2.47E-12	2.47E-12	2.47E-12	2.43E-12	2.12E-12	0	0
Ho-163m	1.09E-09	0	0	0	0	0	0	0	0	0
Ho-164	2.19E-06	0	0	0	0	0	0	0	0	0
Ho-164m	4.49E-08	0	0	0	0	0	0	0	0	0
Ho-166	5.14E-03	2.86E-03	5.37E-05	7.45E-07	0	0	0	0	0	0
Ho-166m	5.25E-09	5.25E-09	5.25E-09	5.25E-09	5.25E-09	5.22E-09	4.95E-09	2.95E-09	1.63E-11	0
Ho-167	2.28E-04	1.08E-06	0	0	0	0	0	0	0	0
Ho-168	4.12E-05	0	0	0	0	0	0	0	0	0
Ho-169	1.74E-05	0	0	0	0	0	0	0	0	0
Ho-170	5.79E-06	0	0	0	0	0	0	0	0	0
Ho-170m	1.02E-06	0	0	0	0	0	0	0	0	0
Ho-171	2.70E-06	0	0	0	0	0	0	0	0	0
Ho-172	1.31E-06	0	0	0	0	0	0	0	0	0
Er-163	3.96E-11	0	0	0	0	0	0	0	0	0
Er-165	6.38E-07	1.28E-07	0	0	0	0	0	0	0	0
Er-167m	3.29E-04	1.28E-07	1.84E-11	4.11E-12	0	0	0	0	0	0
Er-169	2.66E-05	2.47E-05	1.27E-05	2.91E-06	0	0	0	0	0	0
Er-171	3.21E-06	3.51E-07	0	0	0	0	0	0	0	0
Er-172	1.54E-06	1.10E-06	5.27E-08	6.18E-11	0	0	0	0	0	0
Tm-165	1.23E-12	0	0	0	0	0	0	0	0	0
Tm-166	1.39E-11	1.61E-12	0	0	0	0	0	0	0	0
Tm-167	3.99E-11	3.70E-11	1.88E-11	4.21E-12	0	0	0	0	0	0
Tm-168	1.47E-10	1.46E-10	1.36E-10	1.18E-10	9.71E-12	0	0	0	0	0
Tm-170	2.14E-09	2.12E-09	2.02E-09	1.82E-09	2.99E-10	0	0	0	0	0
Tm-171	6.77E-07	6.78E-07	6.72E-07	6.59E-07	4.73E-07	1.84E-08	0	0	0	0
Tm-172	1.46E-06	1.42E-06	3.13E-07	2.43E-09	0	0	0	0	0	0
Yb-169	2.11E-12	2.07E-12	1.70E-12	1.10E-12	0	0	0	0	0	0
Lu-172	1.84E-12	1.66E-12	0	0	0	0	0	0	0	0
Lu-172m	1.97E-12	0	0	0	0	0	0	0	0	0
Tl-206	0	0	0	0	0	0	0	0	3.32E-12	2.55E-11
Tl-207	1.74E-12	1.75E-12	1.69E-12	1.26E-12	0	1.09E-11	5.55E-10	7.56E-09	7.34E-08	4.10E-07
Tl-208	1.45E-08	1.45E-08	1.47E-08	1.54E-08	2.71E-08	1.11E-07	5.39E-08	2.64E-11	2.04E-11	2.61E-11
Tl-209	0	0	0	0	0	0	0	6.94E-11	7.91E-09	1.77E-07
Tl-210	0	0	0	0	0	0	0	1.07E-11	5.23E-10	4.00E-09
Pb-209	4.73E-12	4.74E-12	4.77E-12	4.80E-12	4.96E-12	6.46E-12	4.08E-11	3.28E-09	3.74E-07	8.39E-06
Pb-210	0	0	0	0	0	0	7.81E-11	4.77E-08	2.48E-06	1.91E-05
Pb-211	1.74E-12	1.75E-12	1.70E-12	1.26E-12	0	1.09E-11	5.57E-10	7.58E-09	7.36E-08	4.12E-07
Pb-212	4.04E-08	4.04E-08	4.10E-08	4.27E-08	7.53E-08	3.10E-07	1.50E-07	7.35E-11	5.67E-11	7.25E-11
Pb-214	0	0	0	0	0	0	1.61E-10	5.05E-08	2.47E-06	1.89E-05
Bi-210	0	0	0	0	0	0	7.81E-11	4.77E-08	2.48E-06	1.91E-05
Bi-211	1.74E-12	1.75E-12	1.70E-12	1.26E-12	0	1.09E-11	5.57E-10	7.58E-09	7.36E-08	4.12E-07
Bi-212	4.03E-08	4.04E-08	4.10E-08	4.27E-08	7.53E-08	3.10E-07	1.50E-07	7.34E-11	5.67E-11	7.25E-11
Bi-213	4.70E-12	4.71E-12	4.74E-12	4.77E-12	4.93E-12	6.43E-12	4.06E-11	3.27E-09	3.72E-07	8.34E-06
Bi-214	0	0	0	0	0	0	1.63E-10	5.10E-08	2.49E-06	1.91E-05
Po-210	0	0	0	0	0	0	7.67E-11	4.76E-08	2.48E-06	1.91E-05
Po-211	0	0	0	0	0	0	1.54E-12	2.09E-11	2.03E-10	1.14E-09
Po-212	2.58E-08	2.59E-08	2.63E-08	2.74E-08	4.82E-08	1.98E-07	9.60E-08	4.70E-11	3.63E-11	4.64E-11
Po-213	5.20E-12	5.21E-12	5.24E-12	5.27E-12	5.45E-12	7.10E-12	4.49E-11	3.61E-09	4.11E-07	9.22E-06
Po-214	1.56E-12	1.63E-12	1.62E-12	1.24E-12	0	0	1.63E-10	5.10E-08	2.49E-06	1.91E-05
Po-215	1.74E-12	1.75E-12	1.70E-12	1.26E-12	0	1.09E-11	5.57E-10	7.58E-09	7.36E-08	4.12E-07
Po-216	4.04E-08	4.04E-08	4.11E-08	4.28E-08	7.54E-08	3.10E-07	1.50E-07	7.35E-11	5.67E-11	7.25E-11
Po-218	0	0	0	0	0	0	1.63E-10	5.11E-08	2.49E-06	1.91E-05
At-217	4.70E-12	4.71E-12	4.74E-12	4.77E-12	4.93E-12	6.43E-12	4.06E-11	3.27E-09	3.72E-07	8.34E-06
At-218	0	0	0	0	0	0	0	1.02E-11	4.98E-10	3.81E-09
Rn-217	0	0	0	0	0	0	0	0	2.60E-11	5.84E-10
Rn-218	1.56E-12	1.63E-12	1.62E-12	1.24E-12	0	0	0	0	0	3.81E-12
Rn-219	1.74E-12	1.75E-12	1.70E-12	1.26E-12	0	1.37E-11	5.57E-10	7.58E-09	7.36E-08	4.12E-07
Rn-220	4.04E-08	4.04E-08	4.11E-08	4.28E-08	7.54E-08	3.10E-07	1.50E-07	7.35E-11	5.67E-11	7.25E-11
Rn-222	0	0	0	0	0	0	1.63E-10	5.10E-08	2.49E-06	1.91E-05

Fr-221	4.71E-12	4.71E-12	4.74E-12	4.77E-12	4.93E-12	6.43E-12	4.08E-11	3.27E-09	3.72E-07	8.34E-06
Fr-223	0	0	0	0	0	0	7.70E-12	1.05E-10	1.02E-09	5.68E-09
Ra-222	1.56E-12	1.63E-12	1.62E-12	1.24E-12	0	0	0	0	0	0
Ra-223	1.74E-12	1.75E-12	1.70E-12	1.26E-12	0	1.37E-11	5.57E-10	7.58E-09	7.36E-08	4.12E-07
Ra-224	4.07E-08	4.08E-08	4.14E-08	4.31E-08	7.60E-08	3.12E-07	1.51E-07	7.41E-11	5.71E-11	7.31E-11
Ra-225	4.75E-12	4.75E-12	4.76E-12	4.79E-12	4.94E-12	6.48E-12	4.08E-11	3.27E-09	3.72E-07	8.34E-06
Ra-226	0	0	0	0	0	0	1.63E-10	5.10E-08	2.49E-06	1.91E-05
Ra-228	0	0	0	0	0	0	0	0	3.29E-12	3.69E-11
Ra-229	2.15E-12	0	0	0	0	0	0	0	0	0
Ac-225	4.74E-12	4.75E-12	4.78E-12	4.81E-12	4.97E-12	6.53E-12	4.11E-11	3.29E-09	3.75E-07	8.40E-06
Ac-227	0	0	0	0	0	1.40E-11	5.58E-10	7.58E-09	7.36E-08	4.12E-07
Ac-228	0	0	0	0	0	0	0	0	3.29E-12	3.69E-11
Ac-229	2.15E-12	0	0	0	0	0	0	0	0	0
Ac-232	3.70E-12	0	0	0	0	0	0	0	0	0
Th-226	1.56E-12	1.63E-12	1.62E-12	1.24E-12	0	0	0	0	0	0
Th-227	1.92E-12	1.86E-12	1.43E-12	0	0	1.36E-11	5.49E-10	7.47E-09	7.25E-08	4.06E-07
Th-228	4.07E-08	4.08E-08	4.15E-08	4.33E-08	7.59E-08	3.10E-07	1.50E-07	7.35E-11	5.67E-11	7.25E-11
Th-229	4.46E-12	4.47E-12	4.47E-12	4.48E-12	4.61E-12	6.05E-12	3.80E-11	3.04E-09	3.46E-07	7.77E-06
Th-230	0	0	0	0	3.34E-12	1.45E-10	1.07E-08	2.99E-07	3.21E-06	1.93E-05
Th-231	4.07E-07	3.90E-07	3.72E-07	3.72E-07	3.72E-07	3.72E-07	3.72E-07	3.75E-07	4.01E-07	4.86E-07
Th-232	0	0	0	0	0	0	0	0	3.30E-12	3.70E-11
Th-233	1.82E-06	0	0	0	0	0	0	0	0	0
Th-234	8.49E-07	8.49E-07	8.49E-07	8.49E-07	8.49E-07	8.49E-07	8.49E-07	8.49E-07	8.49E-07	8.50E-07
Th-235	6.59E-09	0	0	0	0	0	0	0	0	0
Pa-229	2.20E-11	1.38E-11	0	0	0	0	0	0	0	0
Pa-230	2.27E-11	2.18E-11	1.53E-11	6.88E-12	0	0	0	0	0	0
Pa-231	8.95E-12	8.97E-12	9.17E-12	9.60E-12	1.68E-11	8.76E-11	7.95E-10	7.82E-09	7.38E-08	4.12E-07
Pa-232	7.07E-07	4.16E-07	3.56E-09	0	0	0	0	0	0	0
Pa-233	8.49E-06	8.51E-06	8.73E-06	9.15E-06	9.84E-06	9.89E-06	1.18E-05	2.29E-05	2.63E-05	2.56E-05
Pa-234	1.30E-06	8.86E-07	8.49E-07	8.49E-07	8.49E-07	8.49E-07	8.49E-07	8.49E-07	8.49E-07	8.50E-07
Pa-234m	5.15E-07	0	0	0	0	0	0	0	0	0
Pa-235	6.60E-09	0	0	0	0	0	0	0	0	0
U-230	1.61E-12	1.68E-12	1.66E-12	1.28E-12	0	0	0	0	0	0
U-231	1.25E-10	1.06E-10	2.39E-11	0	0	0	0	0	0	0
U-232	1.27E-07	1.27E-07	1.28E-07	1.32E-07	1.81E-07	3.36E-07	1.46E-07	7.27E-11	5.34E-11	3.56E-11
U-233	1.59E-09	1.59E-09	1.59E-09	1.60E-09	1.63E-09	2.02E-09	6.24E-09	7.90E-08	1.08E-06	9.14E-06
U-234	1.40E-07	1.41E-07	1.48E-07	1.64E-07	4.27E-07	2.97E-06	2.05E-05	3.74E-05	3.65E-05	2.85E-05
U-235	3.72E-07	3.72E-07	3.72E-07	3.72E-07	3.72E-07	3.72E-07	3.72E-07	3.75E-07	4.01E-07	4.86E-07
U-235m	3.73E-02	0	0	0	0	0	0	0	0	0
U-236	6.08E-06	6.08E-06	6.08E-06	6.08E-06	6.08E-06	6.08E-06	6.10E-06	6.24E-06	7.10E-06	7.62E-06
U-237	5.18E+01	4.67E+01	1.85E+01	2.38E+00	5.68E-05	3.67E-05	4.69E-07	9.44E-10	4.53E-10	0
U-238	8.49E-07	8.49E-07	8.49E-07	8.49E-07	8.49E-07	8.49E-07	8.49E-07	8.49E-07	8.49E-07	8.50E-07
U-239	4.72E+02	0	0	0	0	0	0	0	0	0
U-240	8.47E-03	2.60E-03	6.37E-08	4.69E-11	4.69E-11	4.69E-11	4.69E-11	4.69E-11	4.69E-11	4.69E-11
U-242	2.46E-10	0	0	0	0	0	0	0	0	0
Np-233	5.55E-12	0	0	0	0	0	0	0	0	0
Np-234	1.39E-09	1.19E-09	2.89E-10	1.24E-11	0	0	0	0	0	0
Np-235	8.01E-06	8.00E-06	7.87E-06	7.60E-06	4.23E-06	1.35E-08	0	0	0	0
Np-236	4.43E-10	4.43E-10	4.43E-10	4.43E-10	4.43E-10	4.43E-10	4.43E-10	4.41E-10	4.24E-10	2.83E-10
Np-236m	3.25E-06	1.55E-06	2.00E-09	0	0	0	0	0	0	0
Np-237	9.39E-06	9.43E-06	9.68E-06	9.82E-06	9.84E-06	9.89E-06	1.18E-05	2.29E-05	2.63E-05	2.56E-05
Np-238	2.45E+01	1.76E+01	9.26E-01	1.33E-03	2.52E-07	2.41E-07	1.55E-07	1.86E-09	0	0
Np-239	4.29E+02	3.22E+02	2.28E+01	6.44E-02	9.32E-04	9.31E-04	9.24E-04	8.49E-04	3.64E-04	7.73E-08
Np-240	4.62E-01	2.81E-03	6.88E-08	4.69E-11	4.69E-11	4.69E-11	4.69E-11	4.69E-11	4.69E-11	4.69E-11
Np-240m	8.22E-01	0	0	0	0	0	0	0	0	0
Np-241	2.33E-05	0	0	0	0	0	0	0	0	0
Np-242	2.46E-10	0	0	0	0	0	0	0	0	0
Pu-234	6.91E-11	1.04E-11	0	0	0	0	0	0	0	0
Pu-235	4.08E-09	0	0	0	0	0	0	0	0	0

Pu-236	6.27E-06	6.27E-06	6.23E-06	6.15E-06	4.93E-06	5.56E-07	5.51E-11	5.48E-11	5.27E-11	3.51E-11
Pu-237	3.34E-04	3.29E-04	2.86E-04	2.11E-04	1.24E-06	0	0	0	0	0
Pu-237m	2.09E-06	3.78E-09	3.12E-09	2.05E-09	1.72E-12	0	0	0	0	0
Pu-238	9.82E-02	9.87E-02	9.99E-02	1.00E-01	1.03E-01	9.65E-02	4.74E-02	3.97E-05	0	0
Pu-239	3.15E-03	3.18E-03	3.26E-03	3.27E-03	3.27E-03	3.27E-03	3.26E-03	3.20E-03	2.60E-03	2.08E-04
Pu-240	5.10E-03	5.10E-03	5.10E-03	5.10E-03	5.11E-03	5.24E-03	5.51E-03	5.02E-03	1.94E-03	1.45E-07
Pu-241	2.43E+00	2.43E+00	2.42E+00	2.42E+00	2.31E+00	1.49E+00	1.91E-02	3.84E-05	1.85E-05	1.20E-08
Pu-242	6.15E-05	6.15E-05	6.15E-05	6.15E-05	6.15E-05	6.15E-05	6.15E-05	6.14E-05	6.05E-05	5.12E-05
Pu-243	6.96E+01	2.43E+00	3.36E-11	3.34E-11	3.34E-11	3.34E-11	3.34E-11	3.34E-11	3.34E-11	3.33E-11
Pu-244	4.69E-11	4.69E-11	4.69E-11	4.69E-11	4.69E-11	4.69E-11	4.69E-11	4.69E-11	4.70E-11	4.70E-11
Pu-245	1.12E-03	2.30E-04	1.47E-10	0	0	0	0	0	0	0
Am-239	1.39E-05	3.45E-06	1.18E-11	0	0	0	0	0	0	0
Am-240	3.34E-05	2.41E-05	1.26E-06	1.87E-09	0	0	0	0	0	0
Am-241	1.17E-03	1.19E-03	1.28E-03	1.49E-03	4.97E-03	3.17E-02	7.11E-02	1.70E-02	1.95E-05	1.27E-08
Am-242	1.83E+00	6.46E-01	1.12E-04	5.56E-05	5.53E-05	5.29E-05	3.40E-05	4.09E-07	0	0
Am-242m	5.59E-05	5.59E-05	5.59E-05	5.58E-05	5.56E-05	5.32E-05	3.42E-05	4.11E-07	0	0
Am-243	9.28E-04	9.33E-04	9.33E-04	9.33E-04	9.33E-04	9.32E-04	9.24E-04	8.49E-04	3.65E-04	7.73E-08
Am-244	1.33E+00	2.56E-01	9.35E-08	0	0	0	0	0	0	0
Am-244m	2.01E+01	0	0	0	0	0	0	0	0	0
Am-245	2.95E-03	2.86E-04	2.07E-10	2.28E-11	1.13E-11	0	0	0	0	0
Cm-240	4.12E-08	4.02E-08	3.19E-08	1.91E-08	3.51E-12	0	0	0	0	0
Cm-241	5.60E-07	5.48E-07	4.53E-07	2.97E-07	2.50E-10	0	0	0	0	0
Cm-242	9.01E-01	9.01E-01	8.70E-01	7.99E-01	1.92E-01	4.41E-05	2.82E-05	3.39E-07	0	0
Cm-243	4.52E-04	4.52E-04	4.52E-04	4.51E-04	4.42E-04	3.56E-04	4.18E-05	0	0	0
Cm-244	1.74E-01	1.74E-01	1.74E-01	1.74E-01	1.68E-01	1.19E-01	3.79E-03	0	0	0
Cm-245	4.21E-05	4.21E-05	4.21E-05	4.21E-05	4.21E-05	4.21E-05	4.18E-05	3.88E-05	1.86E-05	1.22E-08
Cm-246	6.76E-06	6.76E-06	6.76E-06	6.76E-06	6.76E-06	6.75E-06	6.67E-06	5.85E-06	1.58E-06	3.24E-12
Cm-247	3.34E-11	3.34E-11	3.34E-11	3.34E-11	3.34E-11	3.34E-11	3.34E-11	3.34E-11	3.34E-11	3.33E-11
Cm-248	1.20E-10	1.20E-10	1.20E-10	1.20E-10	1.20E-10	1.20E-10	1.20E-10	1.19E-10	1.17E-10	9.81E-11
Cm-249	2.96E-05	5.17E-12	0	0	0	0	0	0	0	0
Cm-251	1.94E-11	0	0	0	0	0	0	0	0	0
Bk-249	1.67E-06	1.67E-06	1.64E-06	1.57E-06	7.77E-07	7.83E-10	0	0	0	0
Bk-251	1.94E-11	0	0	0	0	0	0	0	0	0
Cf-249	4.71E-10	4.80E-10	5.61E-10	7.34E-10	2.77E-09	4.69E-09	3.93E-09	6.65E-10	0	0
Total activity	3.89E+05	1.31E+03	5.32E+02	3.32E+02	6.09E+01	8.15E+00	8.43E-01	2.75E-02	5.84E-03	8.76E-04
Decay heat [W]	6.09E+01	5.26E+00	2.24E+00	1.38E+00	2.70E-01	2.81E-02	6.31E-03	8.57E-04	1.60E-04	1.63E-05